CEBAF-R-95-001

Workshop on CEBAF at Higher Energies

April 14 - 16, 1994

Chairpersons

Nathan Isgur and Paul Stoler

Organizing Committee

Ted Barnes - *ORNL & Tennessee*
Rolf Ent - *CEBAF*
Bernard Frois - *Saclay*
Roy Holt - *Illinois*
Richard Milner - *MIT*
Piet Mulders - *NIKHEF*
James Napolitano - *RPI*
Gerasimos Petratos - *Kent State*
Paul Stoler - *RPI*

DISTRIBUTION OF THIS DOCUMENT IS UNLIMITED

MASTER

CEBAF

The Continuous Electron Beam Accelerator Facility

The Southeastern Universities Research Association (SURA) operates the Continuous Electron Beam Accelerator Facility for the United States Department of Energy under contract DE-AC05-84ER40150

DISCLAIMER

This report was prepared as an account of work sponsored by the United States government. Neither the United States nor the United States Department of Energy, nor any of their employees, makes any warranty, express or implied, or assumes any legal liability or responsibility for the accuracy, completeness, or usefulness of any information, apparatus, product, or process disclosed, or represents that its use would not infringe privately owned rights. Reference herein to any specific commercial product, process, or service by trade name, mark, manufacturer, or otherwise, does not necessarily constitute or imply its endorsement, recommendation, or favoring by the United States government or any agency thereof. The views and opinions of authors expressed herein do not necessarily state or reflect those of the United States government or any agency thereof.

DISCLAIMER

Portions of this document may be illegible in electronic image products. Images are produced from the best available original document.

Table of Contents

Preface vi
Overview vii
Working Group on Hadron Spectroscopy and Production

Working Group Summary by T. Barnes and J. Napolitano 1

Plenary Talks

A. Dzierba "Photoproduction Opportunities at CEBAF: Meson Spectroscopy and the Physics of Flying ϕ's" 13

S. Godfrey "Issues in Light Meson Spectroscopy: The Case for Meson Spectroscopy at CEBAF" 41

Contributed Talks

G. Adams and J. Napolitano "Exotic Meson Spectroscopy with CLAS" 65

S. Capstick "Problems in Baryon Spectroscopy" 73

C. Carlson, M. Sher and L. Weinstein "Electromagnetic Production of Very Light Gluinos" 79

D. Coffman, "Solenoidal Detectors in Spectroscopy" 85

H. Funsten "Using Contour Plots in Electroproduction to Examine Regions in ε, Q^2, W Space" 91

H. Funsten and G. Gilfoyle "Spin 0 Decay Angular Distribution for Interfering Mesons in Electroproduction" 97

C. Meyer "New Results in Meson Spectroscopy from the Crystal Barrel Experiment" 103

N. Mukhopadhyay, J. Zhang, and M. Benmerrouche "Photo-production of the η' Meson in the Effective Lagrangian Approach" 109

Table of Contents

N. Mukhopadhyay and L. Zhang "Sensitivity to Properties of the ϕ Meson in the Nucleon Structure in the Chiral Soliton Model" 115

K. Seth "A τ -Charm Factory at CEBAF" 119

J. Weinstein "Spectroscopy, Scattering, and $K\overline{K}$ Molecules" 127

Working Group on Form Factors and Exclusive Reactions

Working Group Summary by P. Stoler and G. Petratos 135

Plenary Talks

S. Brodsky "Exclusive Processes: Tests of Coherent QCD Phenomena and Nucleon Substructure at CEBAF" 153

Contributed Talks

A. Afanasev "Form Factors of the Transitions $\gamma^* \pi^0 \to \gamma$ and $\gamma^* \eta \to \gamma$" 185

K. Baker "CEBAF at Higher Energies and the Kaon Electromagnetic Form Factor" 191

W. Brooks "Prospects for Measuring G_{M_N} in CLAS with Higher CEBAF Beam Energies" 197

F. Cardarelli, E. Pace, I. Grach, I. Narodetskii; G. Salmè, and S. Simula "The Charge Form Factor of Pseudoscalar Mesons in a Relativistic Constituent Quark Model" 203

C. Carlson and N. Mukhopadhyay "The Bloom-Gilman Duality and Leading Logarithms" 209

R. Eckhardt J. Hansper, and M. Gari "Death to Perturbative QCD in Exclusive Processes?" 215

R. Gilman, R. Holt, and P. Rutt "Measurement of $p(\gamma,\vec{p})\pi^0$ at Higher Energies" 221

C.-R. Ji, A. Pang, and A. Szczepaniak "Pion Form Factor" 231

Table of Contents

C. Keppel "Nucleon Resonance Electroproduction at High Momentum Transfers: Results from SLAC and Suggestions for CEBAF" 237

D. Mack "Measurement of the Pion Form Factor at Higher Energies" 243

B. Niczyporuk "Electroproduction of Pseudoscalar Mesons Above the Resonance Region" 249

G. Petratos "Elastic Form Factors at Higher CEBAF Energies" 263

D. Potterveld and R. Holt "Deuteron Photo-Disintegration at High Energies" 267

A. Radyushkin "Nonperturbative QCD and Elastic Processes at CEBAF Energies" 273

P. Stoler "Excited Baryon Form-Factors at High Momentum Transfer at CEBAF at Higher Energies" 289

E. Voutier, C. Furget, S. Kox and J. Réal "Helicity Non-Conserving Form Factor of the Proton" 295

Working Group on Inclusive and Semi-Inclusive Processes

Working Group Summary by B. Frois and P. Mulders 309

Plenary Talks

A. Mueller "Interactions of Quarks and Gluons with Nuclei at Intermediate Energies" 315

A. Schäfer "Measuring Spin-Dependent Structure Functions at CEBAF" 321

Contributed Talks

N. Bianchi "A Detailed Study of Nucleon Structure Function in Nuclei in the Valence Quark Region" 341

S. Kuhn and K. Griffioen "Inelastic Electron Scattering from a Moving Nucleon" 347

P. Markowitz "Kaon Electroproduction" 353

Table of Contents

W. Melnitchouk and A. Thomas "Pion Content of the Nucleon in Polarized Semi-Inclusive DIS" 359

J. Milana "On the A-dependence of σ_L / σ_T: Skeletons in the Shadow" 365

P. Mulders and J. Levelt "Time Reversal Odd Fragmentation Functions in Semi-Inclusive Deep Inelastic Lepton-Hadron Scattering" 371

S. Simula "Nucleon-Nucleon Correlations and Multiquark Cluster Effects in Semi-Inclusive Deep Inelastic Lepton Scattering Off Nuclei" 379

P. Souder "Parity Violation in Deep Inelastic Scattering at CEBAF" 385

Working Group on Hadrons in the Nuclear Medium

Working Group Summary by R. Ent and R. Milner 391

Plenary Talks

B. Filippone "Color Transparency Experiments at Higher Energies" 405

J. Nemchik, N. Nikolaev, and B. Zakharov "Color Transparency after the NE18 and E665 Experiments: Outlook and Perspectives at CEBAF" 415

Contributed Talks

D. Beck "Meson Exchange and Neutral Weak Currents" 465

O. Benhar, S. Fantoni, N. Nikolaev, and B. Zakharov "Diffractive Electroproduction of $s\bar{s}$ Mesons Off Nuclei at CEBAF Energies" 471

J. van den Brand and R. Ent "Medium Modifications with Recoil Polarization" 479

C. Carlson and K. Lassila "Signatures for Quark Clustering in Nuclei" 487

G. Fang "Measuring Nuclear Transparency from Exclusive Vector Meson Production in Lepton-Nucleus Scattering" 493

Table of Contents

L. Frankfurt, M. Sargsyan, and M. Strikman "Color Coherent Effects in (e, e´N) and (e, e´N, N(h)) Processes at CEBAF" 499

M. Kossov "Photoproduction of Vector Mesons Off Nuclei" 509

G. Miller "Color Transparency Effects in Quasi-Elastic Nuclear Reactions" 515

T. Saito and F. Takagi "Exclusive Experiment on Nuclei with Backward Emitted Particles by Electron-Nucleus Collision in ~10 GeV Energy Range" 523

M. Strikman, L. Frankfurt, D. Day, and M. Sargsyan "Evidence for Short Range Correlations from High Q^2 (e,e´) Reactions" 529

Appendix A: Capabilities of Current CEBAF Experimental Equipment at Higher Energies 535

Appendix B: Participants 543

PREFACE

Two important developments led to the organization of this Workshop on CEBAF at Higher Energies. First, almost a decade has passed since the current parameters of CEBAF were defined. During that period there has been a remarkably fruitful evolution of our picture of the behavior of strongly interacting matter which apparently could be addressed by CEBAF at higher energies. Second, favorable technical developments coupled with foresight in initial laboratory planning have now made it feasible to consider a significant energy upgrade to approximately double the current design value of 4 GeV at rather modest cost. This would enable the CEBAF community to greatly expand its physics horizons.

As CEBAF nears completion and the experimental program is about to begin, it is in any event appropriate to begin to develop the next phase of CEBAF's program. The purpose of the workshop, sponsored by the CEBAF User Group, was to begin this process by giving the entire community the opportunity to participate in defining the future of our field, and in particular the physics accessible with an upgraded CEBAF energy.

The workshop was held at CEBAF on 14-16 April, 1994. It was organized into four working groups centered around four main physics topics, by an organizing committee consisting of T. Barnes, R. Ent, B. Frois, R. Holt, R. Milner, P. Mulders, J. Napolitano, M. Petratos, and P. Stoler. Each working group was represented by one or two plenary speakers who were asked to summarize the outstanding physics issues which could be addressed by an upgrade, and many shorter parallel contributions dealing with specific issues. Members of the organizing committee then undertook to summarize the presentations as well as present their personal views on the physics case for an upgrade of CEBAF to higher energies.

It is intended that this report mark the first step toward an ultimate goal of defining a physics program that will form the basis of an upgrade of CEBAF.

The report begins with our brief overview of the conclusions of the Workshop. Its body consists of sections corresponding to the four Working Groups. Each section begins with the Working Group summaries, written by members of the organizing committee, followed by the associated plenary talks and then the individual contributions presenting specific physics programs.

The organizers thank the CEBAF user liaison staff, and in particular Karen Hokansson and Gladys Smith as well as students Katie Bevins and Rhonda Morrison, for their continuous organizational efforts which have made this workshop possible.

Paul Stoler, for the CEBAF User Group

Nathan Isgur, for CEBAF

July, 1994

OVERVIEW

The spectacular success of CEBAF's superconducting radiofrequency (SRF) accelerating cavity technology, and the imminent completion of CEBAF on time and on budget, created the opportunity for this Workshop on CEBAF at Higher Energies. By the Summer of 1994, CEBAF had installed the world's largest SRF accelerator, based on cavities which on average exceeded specifications by a factor of two in both parameters which are critical for accelerator applications: gradient and Q.

This technology opens up the possibility of a relatively simple and inexpensive upgrade of CEBAF's top energy. The "footprint" of the CEBAF accelerator was, with considerable foresight, layed out so that the magnetic arcs could accomodate an electron beam of up to 20 GeV. With the latent accelerating power of the CEBAF SRF cavities, the addition of a few cavities in the linacs, and a minor upgrade of the magnets in the arcs, it seems quite possible to attain energies that will at least double CEBAF's design energy from its present 4 GeV (a machine we might call "CEBAF I") to a machine with a top energy approaching 10 GeV ("CEBAF II").

The purpose of this Workshop was to assess the scientific case for pursuing such an upgrade. All indications going into the Workshop were that there was a very strong case. The most substantial such case is made in the documents arguing for a higher energy electron accelerator (ELFE) to be built in Europe. *The results of this Workshop, which we will briefly review here, indeed provide a very strong scientific justification for proceeding with all due speed to propose such an upgrade.* It is not just that with higher energy much of the research already planned can be done better and more efficiently. More important is that with higher energy qualitatively new areas of research vital to understanding the quark structure of matter would be opened. This vision of the importance of an energy upgrade to CEBAF's long-range scientific goals emerged as the common theme of all four of the Working Groups.

The results of the *Working Group on Hadron Spectroscopy and Production* provide a typical example. The 4 GeV "CEBAF I", coupled with the planned complement of detectors (especially CLAS), provides an almost ideal tool for studying baryon spectroscopy; an energy upgrade would provide additional power to this program, but not change its basic characteristics. In contrast, "CEBAF II" would open up the door to a completely new program of meson resonance studies, providing access to the most interesting domain from 1.5 to about 3 GeV in meson mass. Elements of this capability would be new not just at CEBAF, but on the world scene. In particular, such a program is expected to have very important leverage in certain key areas: a "photon beam" (real or virtual) is expected to produce ϕ-like mesons and exotic meson hybrid states more copiously than a hadron beam could. The relative production of $s\bar{s}$ mesons is enhanced simply because the pho-

ton produces all quark-antiquark flavors in proportion to the squares of their charges. The production of exotic hybrid mesons is expected to be enhanced (at least in some models) as a consequence of another unique feature of photon beams: their preference for producing $q\bar{q}$ systems with total quark spin 1. This Working Group was also enthusiastic about another potential advantage of CEBAF II related to strange particle production: the creation of a secondary beam of kaons for use in CP and CPT violation studies or the search for other rare processes associated with kaons.

The *Working Group on High Q^2 Form Factors and Exclusive Reactions* foresaw a dramatic improvement in the accessibility to reactions that would reveal the nature of the mechanisms underlying exclusive processes at moderate Q^2. At this time it is unclear whether such processes in the 10 GeV^2 range are controlled by the physics of confinement *via* the Feynman endpoint mechanism or by the physics of perturbative QCD *via* hard gluon exchanges. Resolving this issue is clearly important for understanding the physics underlying almost all of the important short-distance phenomena in nuclei and hadrons. Two classes of measurements can be be particularly helpful in this regard. Perturbatively controlled processes have amplitudes with strengths set by α_s^n, where n is the number of hard gluon exchanges. As a result, comparison of the amplitudes for processes proceeding without hard exchange ($\gamma^*\pi^0 \rightarrow \gamma$), with a single hard exchange (the pion form factor), with two hard exchanges (the proton form factor), *etc.*, should be very informative. Measurements of helicity amplitudes should be even more definitive. Hard gluon exchanges conserve helicity, while confinement generically breaks helicity conservation. If perturbative mechanisms are dominating exclusive processes at moderate Q^2, the associated helicity conservation laws should be observed independent of issues surrounding the absolute normalization of the amplitudes.

The *Working Group on Inclusive and Semi-inclusive Processes* concluded that an energy upgrade of CEBAF would have little impact on the study of the scaling region, where SLAC and HERA will be making major contributions. However, it appears that such an upgrade could provide information critical to physics that is central to one of CEBAF's present scientific goals: the transition from hadronic to quark degrees of freedom. CEBAF II would provide excellent measurements of structure functions in the medium to high x range as a function of Q^2 which, when coupled with exclusive measurements, would reveal how deep inelastic scattering off the valence quarks is built up out of specific final states. This issue is at the heart of understanding "quark-hadron duality", which should be perfect in the naive quark model and in various idealizations of QCD (like the large N_c limit), and so might form the basis of a systematic understanding of the transition from hadronic to quark variables.

The *Working Group on Hadrons in the Nuclear Medium* found some particularly compelling physics in CEBAF II. It appears that the 10 GeV^2 range

for Q^2 may be ideally suited for seeing the phenomenon of "color transparency". This is a phenomenon predicted by QCD which signals in a very beautiful way the presence of the nonabelian color degrees of freedom underlying strongly interacting matter. The basic idea is that a color singlet $q\bar{q}$ or qqq system produced in a small spatial region will have nearly cancelling color charges and therefore diminished strong interactions. Such a system would see the nucleus as transparent to its passage; hence the name. A similar phenomenon occurs in electrodynamics where an e^+e^- pair of small size has a small cross section determined by its electric dipole moment. In QCD a $q\bar{q}$ pair should have an analogous small color dipole moment. In addition, the qqq system should behave in a similar fashion since with nonabelian charges it will have zero monopole moment and therefore once again interactions proportional to its dipole moment. Measurements of vector meson production and of the $(e, e'p)$ reaction inside nuclei probe the transparency of these two simplest systems.

The plenary talks and working group summaries associated with the four areas mentioned here provide a much more substantial discussion of not only the very few topics we have chosen to highlight in this Overview, but also of an enormous range of other topics which might be addressed by CEBAF II. Many of the participants in the Workshop have joined together to continue exploring the most promising such measurements. We expect that a future Workshop will bring these and other people together to help create a proposal for an upgrade of CEBAF that can begin to move the laboratory along the path toward this new and very important physics.

Working Group on Hadron Spectroscopy and Production

T. Barnes & J. Napolitano

CEBAF AT HIGHER ENERGIES*

WORKING GROUP REPORT ON HADRON SPECTROSCOPY AND PRODUCTION

TED BARNES
Physics Division, Oak Ridge National Laboratory
Oak Ridge, TN, 37831-6373
and
Department of Physics and Astronomy, University of Tennessee
Knoxville, TN, 37996-1200

and

JIM NAPOLITANO
Department of Physics, Rensselaer Polytechnic Institute
Troy, NY, 12180-3590

ABSTRACT

This report summarizes topics in hadron spectroscopy and production which could be addressed at CEBAF with an energy upgrade to $E_\gamma = 8$ GeV and beyond. The topics discussed include conventional meson and baryon spectroscopy, spectroscopy of exotica (especially molecules and hybrids), CP and CPT tests using ϕ mesons, and new detector and accelerator options.

1. Overview

The photon, real or virtual, makes a unique particle beam. It has spin one, and selectively couples to different quark flavors according to their charges. As the beam energy increases, one can expect to see a transition from dynamics dominated by a few hadron resonances to a regime in which perturbative QED and QCD processes are evident.[1] In the resonance regime, the photon's polarization allows tests of many resonance form factors which have been studied theoretically but never adequately investigated experimentally. In addition to conventional hadronic resonances, unusual states such as glueballs, hybrids and molecules are anticipated in the 1-3 GeV region, and these may be identifiable through unusual photon couplings and decay modes. Obviously, the opportunities for spectroscopy with a sufficiently energetic and intense photon beam are enormous.

Despite these opportunities, experimental progress in resonance production by photons has been rather limited because high intensity, high energy CW electron accelerators have not been available. The initial program of experiments at CEBAF with a 4 GeV beam represents the first high-statistics experimental investigation of

*A Workshop held at CEBAF, Newport News, Virginia, 14-16 April 1994.

this field. However, most of these experiments are limited to baryon spectroscopy in s-channel photo- or electroproduction, because the beam energy is not high enough to reach the thresholds anticipated for photoproduction of interesting new meson resonances. Of course one should exceed these expected thresholds in the design beam energy, both for reasons of cross section and to insure that states somewhat above theoretical mass predictions are not missed.

For our quantitative discussion of energies we consider the photoproduction reaction

$$\gamma + P \rightarrow m + B$$

where m is a meson (of mass m) and B is a baryon (of mass M_B). The photon energy E_γ required to reach the threshold for this reaction is

$$E_\gamma = \frac{1}{2M_P}\left[(m + M_B)^2 - M_P^2\right] . \qquad (1)$$

The highest meson mass is produced against a final-state proton, in which case the beam energy required to reach a threshold m is

$$E_\gamma = m + \frac{m^2}{2M_P} . \qquad (2)$$

Electroproduction using spacelike photons requires higher photon energy than photoproduction to reach a given invariant mass. For an off-shell photon with $q^2 < 0$ the threshold energy required for the reaction

$$\gamma^* + P \rightarrow m + P$$

is given by

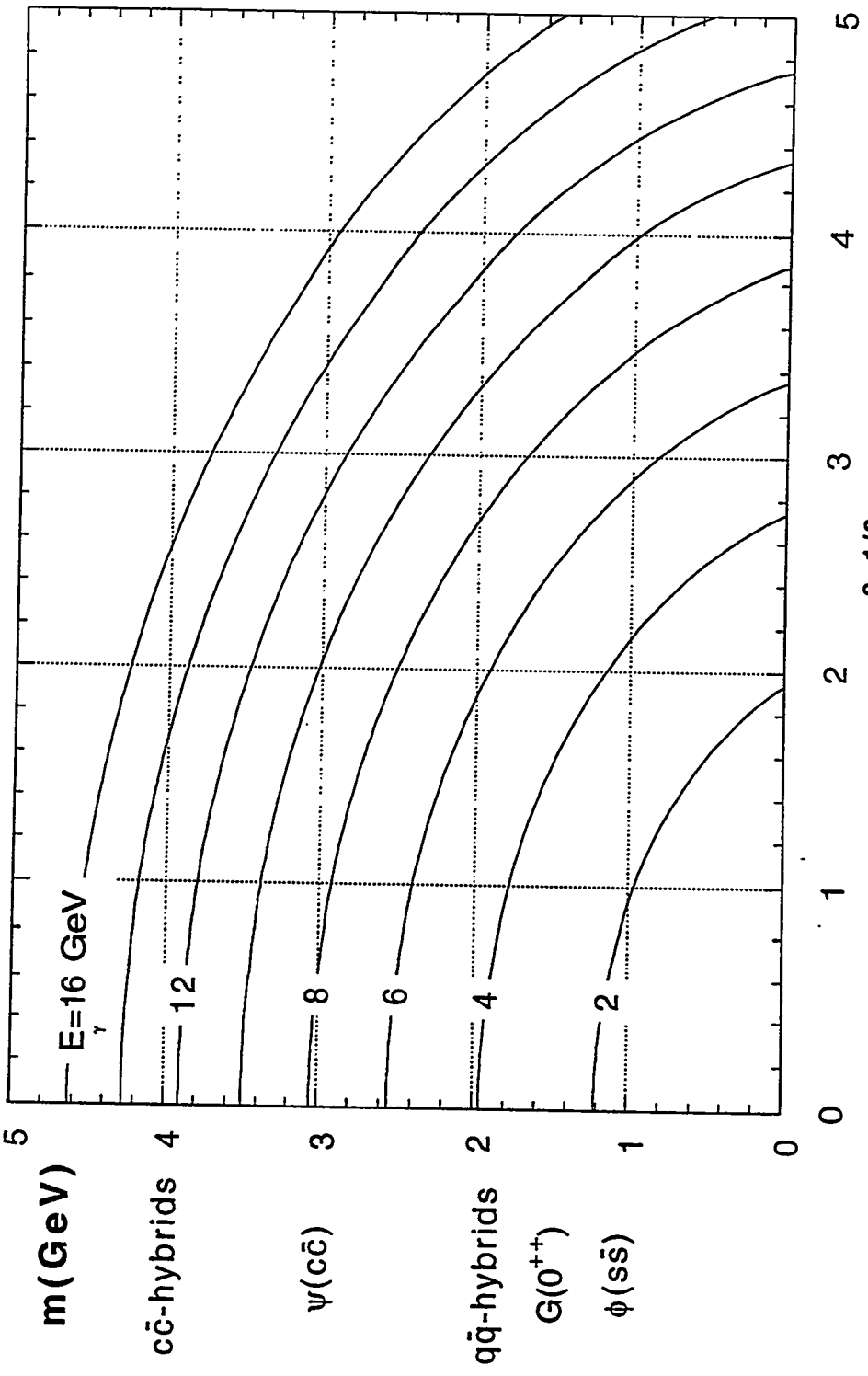
$$E_\gamma^* = \frac{1}{2M_P}\left[\, m^2 + 2mM_P + |q^2| \,\right] .$$

Thresholds associated with photo- and electroproduction from a proton are shown as a contour plot in figure 1. As examples, the threshold photon energy for photoproducing a 1.9 GeV light hybrid is $E_\gamma = 3.8$ GeV, which is just possible at CEBAF with $E_\gamma = 4$ GeV; photoproduction of a 2.5 GeV $s\bar{s}$ meson requires $E_\gamma = 5.8$ GeV; the ψ at 3.1 GeV requires $E_\gamma = 8.2$ GeV; and a charmonium hybrid at 4.1 GeV would require $E_\gamma = 13.1$ GeV.

Thus, with an upgrade of CEBAF to $E_\gamma = 8$ GeV one could use photoproduction to explore meson spectroscopy up to an invariant mass of about 3.0 GeV but no higher.

This should allow detailed photoproduction and electroproduction studies of u, d, s $q\bar{q}$ spectroscopy as well as searches for light hybrids. In order to produce the reaction products with sufficient phase space to be useful experimentally the beam energy should of course be somewhat higher than these threshold values.

Fig.1. Kinematic thresholds
in the electroproduction reaction $\gamma^* P \rightarrow m+P$.



Our working group considered both theoretical and experimental aspects of an energy upgrade. The preliminary organization was informal, and reserved many intervals for discussion and additional contributions; this proved to be a wise decision, since the talks generated extensive discussions. The topics considered were generally in the following categories:

- Conventional Meson and Baryon Spectroscopy
- Exotica: Molecules and Hybrid Mesons
- CP and CPT Violation in Flying ϕ Decay
- New Detectors and Accelerator Developments

We also had two contributions on specialized topics: Marc Sher described a possible experiment to search for low-mass gluinos[2] (a proposed spin-1/2, strongly interacting supersymmetric partner of the gluon) in a mass and lifetime "window" that has not been excluded experimentally. Kam Seth described the high-precision charmonium results from Fermilab Experiment E760, and discussed how charm and related physics could be addressed with a τ-charm factory at CEBAF.

A list of the speakers and topics is given in Table 1; the remainder of this report summarizes and expands on their comments. For additional details see the individual contributions to this report.

2. Conventional Spectroscopy

A variety of important problems in conventional $q\bar{q}$ meson spectroscopy ($q = u, d, s$) can be addressed at CEBAF using photon beams. Establishing $q\bar{q}$ spectroscopy is important both because anomalous states must be identified against a background of these conventional resonances (which are poorly known above about $1\frac{1}{2}$ GeV), and because there may yet be surprises in the conventional light meson spectrum, for example in configuration mixing, photon couplings or decay amplitudes. The production mechanism at CEBAF may be especially useful for distinguishing conventional $q\bar{q}$ mesons from unusual states, because their electroproduction amplitudes should be quite characteristic and can be studied using polarized and $q^2 < 0$ virtual photons.

One example of an interesting area in conventional mesons, $s\bar{s}$ spectroscopy, was discussed by Steve Godfrey in his plenary talk. Strangeonia are attractive in part because they are largely unexplored, and photoproduction at CEBAF should allow a detailed study of $s\bar{s}$ spectroscopy. The strange quark is sufficiently light so that one would naively expect $s\bar{s}$ spectroscopy to repeat $I = 0$ $(u\bar{u} + d\bar{d})$ spectroscopy, displaced upwards by $\approx$ 200-250 MeV, but surprises such as $\eta - \eta'$ flavor mixing may await experimental studies. The spectroscopy of radially-excited $^1S_0$ $q\bar{q}$ states is especially interesting because of the possibility of $\eta - \eta'$ type mixing and because several poorly understood 0^{-+} states reported in $\psi(3100)$ radiative decays, such as the $\eta(1440)$, may involve radially-excited $q\bar{q}$ states. The 0^{++} channel is interesting

because the lightest glueball is expected to be a scalar with a mass of ≈ 1.5 GeV, just where the $^3P_0$ $s\bar{s}$ scalar is expected. Strong mixing between these and the nonstrange $I = 0$ $^3P_0$ $q\bar{q}$ states may be present, or these may be relatively unmixed states. A comparison of $s\bar{s}$ and $(u\bar{u} \pm d\bar{d})$ spectroscopy may also be useful as an indication of the importance of mixing with two-meson continuua, since this effect is expected to split the $(u\bar{u} \pm d\bar{d})$ $I = 0, 1$ $^3D_1$ states near 1.6 GeV as well as the $(u\bar{u} \pm d\bar{d})$ $^3S_1'$ radials near 1.45 GeV,[3] and may induce important $s\bar{s}$ components in the $I = 0$ states. These predictions may be testable through the photoproduction amplitudes and branching fractions of these states.

The best experimental work to date on $s\bar{s}$ spectroscopy has been done by the SLAC E135 collaboration[4] using the reactions $K^-P \rightarrow K^-K^+\Lambda$, $K_S^0K_S^0\Lambda$ and $K_S^0K^\pm\pi^\mp\Lambda$. Photoproduction would add considerably to our knowledge since $s\bar{s}$ pairs are copiously produced. However, many of the interesting $s\bar{s}$ states are expected to lie near or above 2 GeV;[5] the $L = 2$ and $L = 3$ $s\bar{s}$ multiplets are expected at 1.9 and 2.2 GeV respectively, and the $L = 0$ $s\bar{s}$ radials are expected at 1.6-1.7 GeV. Producing states above 2 GeV would require higher beam energies than are currently available at CEBAF, particularly if virtual photons are used.

Simon Capstick discussed baryon spectroscopy, and noted that although a considerable program of baryon spectroscopy is planned for CEBAF with $E_\gamma \leq 4$ GeV (especially relating to photo- and electroproduction amplitudes), much more could be done with a higher beam energy. For example, the q^2-dependence of electroproduction amplitudes of problematical resonances such as the Roper could be measured usefully (from the quark model viewpoint) to ≈ 5 GeV^2 for comparison with theoretical predictions for q^3-radial, hybrid or other assignments for this and other controversial states. In addition, associated production of strange baryons with kaons could be useful for the study of strange baryon spectroscopy, which is much less well known than nonstrange spectroscopy. Here interesting topics include the $\Lambda(1405)$ (which is lighter than expected for a conventional uds baryon[6]) and the possible existence of Z^* flavor-exotic molecules.[7] Only moderate beam energies are required for strange baryon spectroscopy; to reach the photoproduction threshold of $K + \Lambda(1405)$ we require only $E_\gamma = 1.5$ GeV, and photoproduction of a $\bar{K}$ and a 2.1 GeV Z^* requires $E_\gamma = 3.1$ GeV.

Nimai Mukhopadhyay discussed new calculations of baryon resonance production in the $\gamma P \rightarrow \eta P$ and $\gamma P \rightarrow \eta' P$ reactions. The calculations indicate that the cross section for η' production, at least near threshold, depends on s—channel creation of the $N^*(2080)$. Again, the q^2 dependences of such reactions may provide new clues to baryon structure.

Stan Brodsky urged us to consider reactions which would produce charmonium, for example $\gamma P \rightarrow \eta_c P$ and $\gamma P \rightarrow \psi P$, to investigate the possibility that charmonium may bind to nuclei.[8] Since charmonium in flight may quickly dissociate in nuclei, open charm reactions such as $\gamma P \rightarrow \bar{D}^0\Lambda_c^+$ should also be studied. The threshold photon energies for these processes are rather high, $E_\gamma = 7.7$ GeV for $\eta_c P$, $E_\gamma = 8.2$ GeV for ψP and $E_\gamma = 8.7$ GeV for $\bar{D}\Lambda_c$. This provides a case for a 10 GeV capability.

3. Exotica: Molecules and Hybrid Mesons

A primary goal of modern meson spectroscopy is the identification of "exotica", which are mesons external to the $q\bar{q}$ quark model. The more restrictive term *exotic meson* is used to refer to a meson whose quantum numbers are inconsistent with *any* $q\bar{q}$ assignment, either because of flavor (for example $I = 2$) or J^{PC_n}; 0^{--}, 0^{+-}, 1^{-+}, 2^{+-}, 3^{-+}... are all forbidden to $q\bar{q}$ states. Exotica includes multiquark systems (such as weakly bound hadronic molecules) and states with gluonic excitation, generically called gluonic hadrons. Gluonic hadrons are referred to as hybrids if quarks and gluonic excitations are both present in the dominant basis state, and glueballs if they are relatively pure excited glue.

Much of the recent interest in multiquark systems has concentrated on molecules, which are weakly bound states of two or more conventional $q\bar{q}$ or qqq hadrons. Nuclei are the most familiar examples of these. Two meson resonances, the $f_0(975)$ and $a_0(980)$ have long been advocated by Weinstein and Isgur[9] as $K\bar{K}$ molecules. These resonances are a problem in the quark model if one tries to identify them as $^3P_0$ $q\bar{q}$ states, due to their low masses and anomalous strong and electromagnetic couplings. In our working group John Weinstein presented the theoretical case for identifying these states as $K\bar{K}$ molecules, and Alex Dzierba discussed an experiment[10] at CEBAF which can distinguish between $K\bar{K}$ and $q\bar{q}$ assignments by measuring the branching ratios[11] for $\phi \to \gamma f_0(975)$ and $\phi \to \gamma a_0(980)$. There are many other candidates for light molecules,[12] notably the $\Lambda(1405)$ baryon ($\bar{K}N$) and the mesons $f_1(1420)$ ($K^*\bar{K} + \bar{K}^*K$ enhancement), $f_0(1520)$ ($\rho\rho, \omega\omega$) and $f_0(1710)$ ($K^*\bar{K}^*, \omega\phi$), which CEBAF might also usefully study in photoproduction experiments.

Curtis Meyer summarized results from the Crystal Barrel $P\bar{P}$ experiment[13] at LEAR, including high-statistics results on the $f_0(1520)$ in $\pi^o\pi^o$ and $\eta\eta$. This state is interesting as a candidate ($\rho\rho, \omega\omega$) molecule and as a candidate scalar glueball. (A search for flavor-singlet couplings, indicated by the $\pi\pi$, $K\bar{K}$ and $\eta\eta$ branching fractions, may tell us if this state is indeed the anticipated 1.5 GeV scalar glueball; the $K\bar{K}$ analysis is in progress.) Meyer's talk emphasized the importance of correctly including interference effects and unitarity in extracting broad, overlapping resonances in the 1-2 GeV mass range.

Suh-Urk Chung discussed the status of J^{PC_n}-exotics, notably hybrids in the flux-tube model, and summarized current experiments and future experimental prospects. J^{PC_n}-exotic hybrids arise when the excited gluonic degree of freedom is combined with the $q\bar{q}$ system to make a hybrid meson with definite quantum numbers; these exotic states are predicted by all the theoretical models and approaches which have been applied to hybrids.[14] The quantum numbers 1^{-+} are often chosen for experimental searches because most models predict this to be the lightest exotic hybrid, and the flux tube model of decays predicts the $I = 1$ state to be relatively narrow.

Much of the current interest in hybrids is due to the flux tube model of Isgur, Kokoski, Merlin and Paton.[15] This model treats the confining $q\bar{q}$ interaction as a gluonic flux tube between the quarks, and makes quite specific predictions for the masses and partial widths of states with excited flux tubes, which are the hybrids of

this model. The mass of the lightest hybrid multiplet is predicted to be ≈ 1.9 GeV, and the anticipated dominant decay modes are quite characteristic. In the flux tube model a hybrid meson decays by $q\bar{q}$ pair production, which breaks the flux tube. Consideration of overlap integrals suggests that the orbital angular momentum of the flux tube in a decaying hybrid tends to be transferred to an internal L of a final $q\bar{q}$ meson, so the preferred decay modes of the lowest-lying hybrids are the little-explored S+P two-body systems. The constituent gluon model of hybrids also predicted this preferred mode.[16]

The low-lying exotic hybrids and their decays predicted by Isgur, Kokoski and Paton are listed in Table 2. The notation has been changed to conform to 1992 Particle Data Group useage.[17] In the table, $\Gamma_{H\to AB}$ is the partial width to the channel specified, which consists of a π or a K plus an excited meson. (For the strange particle decays, our notation implies the two charge conjugate combinations that give zero strangeness.) We also list the principal decay branches of the excited meson "B" in the two-body final state; Γ_B is the total width of the excited meson, and in the list of final states we abbreviate $K^*(892)$ by K^* and $K_0^*(1430)$ by K_0^*.

Chung noted that a persistent but controversial $I = 1, 1^{-+}$ signal has been reported in $\eta\pi$ and $\eta'\pi$ by several experiments.[18] He also presented new results from BNL[19] which appear consistent with a 1^{-+} exotic $\hat{\rho}(1900)$ decaying to $f_1(1285)\pi^-$ followed by $f_1 \to K^+K_S^0\pi^-$; an experiment in progress[20] will study this candidate exotic state with better statistics.

The flux tube model suggests that photoproduction should be an effective way to produce hybrids, since the transfer of momentum and angular momentum to a single struck quark may be an effective way to "pluck" (orbitally excite) a flux tube. There is some evidence for a 1^{-+} exotic, possibly a hybrid, near 1.8-1.9 GeV in photoproduction of $b_1\pi$ (Atkinson *et al.*[21]) and $\rho\pi$ (Condo *et al.*[22]) final states. Gary Adams discussed a proposal to study some of these final states at CEBAF using the CLAS spectrometer in Hall B.

In summary, there is an excellent opportunity for CEBAF to contribute to the spectroscopy of exotica through photoproduction studies if the beam energy is increased to ≈ 6 GeV or beyond.

4. CP and CPT Violation in ϕ Decay

One very exciting possibility for CEBAF is the study of CP and CPT violation in ϕ decay. This idea was originally developed[23] to take advantage of e^+e^- ϕ-factories such as those now under construction at Frascati and Novosibirsk. In these experiments one measures the decays $K^0 \to \pi^+\pi^-$ and $K^0 \to \pi^0\pi^0$ in the same apparatus (to reduce systematic errors) and determines the asymmetry between these two modes as a function of the separation of the K_L^0 and K_S^0 from the ϕ decay. Not only is this an intriguing way to measure the CP violation parameter ϵ'/ϵ from K^0 decay, it also provides a new test of CPT violation. This may be more than an exercise in improving lower limits, since some string theories predict CPT violation.[24]

To carry out these measurements at CEBAF, it is proposed to produce "flying" ϕ

mesons using the reaction $\gamma P \rightarrow \phi P$. This was the principal topic of a recent workshop at Indiana University; Alex Dzierba summarized the conclusions of that meeting and the status of this work in his plenary talk. CEBAF has a *potential* advantage in that it generates a much larger ϕ luminosity than the e^+e^- machines, although the associated problems of detector design and especially background rejection are nontrivial. Since the decay products are boosted forwards, particle identification is considerably easier than at an e^+e^--ϕ factory.

A possible problem with such an experiment at CEBAF is the presence of a substantial background from S-wave $K\bar{K}$ photoproduction.[25] This introduces a $K^0_S K^0_S$ signal which could obscure the CP-violating amplitude from the decay of a K^0_L from the ϕ. However, Nathan Isgur explained how the dominant S-wave might be used to advantage by observing the interference between the S-wave and P-wave (ϕ) amplitude. These ideas are still under development, but appear promising at present.

5. New Detectors

Our working group also discussed possible new detector systems that could be used for both spectroscopy and ϕ decay experiments. Of the existing CEBAF detectors, only CLAS appears to be appropriate for these studies, and Gary Adams discussed possible exotic meson signatures that could be measured in the CLAS. It appears unlikely, however, that this general purpose facility will prove suitable for the complete range of experiments we considered.

In his plenary talk Alex Dzierba discussed an experiment[10] using a new segmented lead glass calorimeter[26] to study ϕ radiative decays. This can be carried out on a relatively short time scale at CEBAF because the detector is currently available. Although this experiment is limited to all-neutral decay modes of the ϕ, produced with a real, tagged photon beam, it illustrates how impressive physics results may be forthcoming from a relatively simple apparatus.

Experience with facilities such as LEAR have made clear the importance of complete event reconstruction, so one should have charged particle detection and momentum measurement in addition to neutrals. Since many results will require relatively detailed partial wave analyses, it is important that a detector for spectroscopy approach 4π *cm* solid angle coverage with as little bias as possible. Experiments which would use an incident electron beam (as opposed to photons, in which case the primary electrons have been removed) face additional complications from luminosity limitations.

The traditional approach to high energy spectroscopy has been to use a dipole magnet spectrometer with a large magnetic field volume, equipped with tracking chambers, particle identification, and possibly neutral particle detection.[20] This approach has been applied to tagged photon spectroscopy with good results,[21,27,28,29] but in all cases the maximum allowed incident photon rate was limited to a few$\times 10^5$/sec. This limitation arises partly from e^+e^- pairs produced in the target by the incident photon beam; these pairs spread in the dipole field and are incident on the detectors at very high rates.

At CEBAF, the CLAS avoids this problem, while retaining the large bending power of a dipole spectrometer, by using a toroidal magnetic field. This essentially eliminates the problem of e^+e^- pair production, although as a result of this geometry the detector is insensitive in the forward region because the magnetic field is very low. Unfortunately, many of the high energy experiments of interest for spectroscopy, especially those using small-q^2 "diffractive" photon interactions, preferentially populate the extreme-forward region.

An alternative approach, followed by Crystal Barrel and LASS,[30,31] is to use a solenoidal magnetic field. Since particles are deflected only according to their transverse momentum, one can sacrifice some momentum resolution for the more forward-going particles, and LASS[31] augment their system with a dipole magnet far downstream. Advantages of solenoidal spectrometers include a large, flat acceptance over phase space, and the "trapping" of e^+e^- pairs along the axis of the solenoid. In our working group Dan Coffman discussed the state-of-the-art in solenoidal spectrometers, specifically the CLEO detector at Cornell/CESR which is used for high energy e^+e^- collision experiments.

Heavy quark spectroscopy, including charm and τ decays, would be difficult to pursue unless CEBAF extends well above 8 GeV. (See Figure 1.) Kam Seth proposed a different solution, namely an e^+e^- τ/charm factory using a 6 GeV electron beam incident on a 1 GeV positron beam in a storage ring. Center-of-mass energies up to 4.90 GeV are possible, and that would be extended to 5.66 GeV with an 8 GeV electron beam. What's more, the incident electron beam is used "non-destructively", and might be incident on fixed targets downstream. Similar designs have been studied previously, and luminosities approaching 10^{33}/cm^{2}sec may be possible, leading to orders of magnitude improvement in the present event sample.

Specific designs and cost estimates for these detector and accelerator developments are in preparation.

6. References

1. D.W.G.S. Leith, in *Electromagnetic Interactions of Hadrons*, Vol.I ed. A. Donnachie and G. Shaw (Plenum Press, New York, 1978).
2. C.E. Carlson and M. Sher, *Phys. Rev. Lett.* 72 (1994) 2686.
3. P. Geiger, *Phys. Rev.* D49 (1994) 6003.
4. D. Aston *et al.*, SLAC-PUB-5145; *Nucl. Phys. (Proc. Suppl.)* B8 (1989) 32.
5. S. Godfrey and N. Isgur, *Phys. Rev.* D32 (1985) 189.
6. S. Capstick and N. Isgur, *Phys. Rev.* D34 (1986) 2809.
7. K. Maltman and S. Godfrey, *Nucl. Phys.* A452 (1986) 669; T. Barnes and E.S. Swanson, *Phys. Rev.* C49 (1994) 1166.
8. S.J. Brodsky, I. Schmidt and G.F. de Téramond, *Phys. Rev. Lett.* 64 (1990) 1011.
9. J. Weinstein and N. Isgur, *Phys. Rev. Lett.* 48 (1982) 659; *Phys. Rev.* D27 (1983) 588; *Phys. Rev.* D41 (1990) 2236; J. Weinstein, *Phys. Rev.* D43 (1991)

95.
10. A. Dzierba, J. Napolitano *et al.*, CEBAF Experiment 94-016.
11. F.E. Close, Nathan Isgur, and S. Kumano, *Nucl. Phys.* B389 (1993) 513.
12. N. Törnqvist, *Phys. Rev. Lett.* 67 (1991) 556; K. Dooley, E.S. Swanson and T. Barnes, *Phys. Lett.* B275 (1992) 478; for recent reviews see N. Törnqvist, Helsinki report HU-SEFT-R-1993-13 and T. Barnes, RAL-94-056.
13. V.V. Anisovich *et al.*, *Phys. Lett.* B323 (1994) 233.
14. For recent reviews of hybrids see T. Barnes, RAL-93-069; F.E. Close, RAL-93-053; *Rep. Prog. Phys.* 51 (1988) 833; G. Karl, *Nucl. Phys.* A558 (1993) 113c; D. Hertzog, *Nucl. Phys.* A558 (1993) 499c; N. Isgur, CEBAF-TH-92-31;
15. N. Isgur, R. Kokoski, and J. Paton, *Phys. Rev. Lett.* 54 (1985) 869; N. Isgur and J. Paton, *Phys. Rev.* D31 (1985) 2910; J. Merlin and J. Paton, *J. Phys.* G11 (1985) 439; *Phys. Rev.* D35 (1987) 1668.
16. M. Tanimoto *et al.*, *Phys. Lett.* 116B (1982) 198; A. LeYaouanc *et al.*, *Z. Phys.* C28 (1985) 309; F. Iddir *et al* , *Phys. Lett.* B205 (1988) 564.
17. Particle Data Group, *Phys. Rev.* D45/II (1992).
18. G.M. Beladidze *et al.*, *Phys. Lett.* B313 (1993) 276, and references therein.
19. J.H. Lee *et al.*, *Phys. Lett.* B323 (1994) 227.
20. A. Dzierba, S.-U. Chung *et al.*, BNL Experiment E852.
21. M. Atkinson *et al.*, *Z. Phys.* C34 (1987) 157.
22. G. Condo *et al.*, *Phys. Rev.* D43 (1991) 2787.
23. C.D. Buchanan *et al.*, *Phys. Rev.* D45 (1992) 4088.
24. V. Alan Kostelecky and R. Potting, "CPT, Strings, and the $K\bar{K}$ System", in D. B. Cline, ed., "Gamma Ray Neutrino Cosmology and Planck Scale Physics", World Scientific, Singapore, 1993; V. Alan Kostelecky and R. Potting, *Nucl. Phys.* B359 (1991) 545.
25. D. P. Barber *et al.*, *Z. Phys.* C12 (1982) 1; D. Aston *et al.*, *Nucl. Phys.* B172 (1980) 1; D. C. Fries *et al.*, *Nucl. Phys.* B143 (1978) 408.
26. B.B. Brabson *et al.*, *Nucl. Inst. Meth. Phys. Res.* A332 (1993) 419.
27. D.P. Barber *et al.*, *Nucl. Inst. Meth.* 155 (1978) 353.
28. D. Aston *et al.*, *Nucl. Inst. Meth.* 197 (1982) 287;
W. Beusch, CERN/SPSC/77-10.
29. Rudolf J. Wedemeyer, "The SAPHIR Detector", in *Electron and Photon Interactions at Intermediate Energies*, Lecture Notes in Physics No.234, Springer-Verlag (1985).
30. E. Aker *et al.*, *Nucl. Inst. Meth. Phys. Res.* A321 (1992) 69.
31. D. Aston *et al.*, SLAC Report 298 (1986).

Table 1: Agenda for the Hadron Spectroscopy Working Group

Speaker	Topic
	Thursday 14 April
Simon Capstick (FSU)	Problems in Baryon Spectroscopy
Alex Dzierba* (IU)	Flying ϕs and High Energy Spectroscopy
John Weinstein (U.Miss.)	$K\bar{K}$ Molecules
	Friday 15 April
Steve Godfrey* (Carleton)	Issues in Light Hadron Spectroscopy
Suh-Urk Chung (BNL)	Exotic Meson Spectroscopy
Curtis Meyer (CMU)	Results from Crystal Barrel
Kamal Seth (Northwestern)	A τ-Charm Factory at CEBAF
Gary Adams (Rensselaer)	Exotic Meson Spectroscopy in CLAS
Dan Coffman (Cornell)	Solenoidal Detectors in Spectroscopy
	Saturday 16 April
Marc Sher (William and Mary)	Gluino Searches at CEBAF Energies
Nimai Mukhopadhyay (Rensselaer)	Photoproduction of η and η'
Nathan Isgur (CEBAF)	S-P Interference in $K\bar{K}$ Photoproduction and Searches for CP and CPT Violation

* Plenary Talk

Table 2: J^{PC_n}-Exotic Hybrid Mesons and Dominant Decays in the Flux Tube Model

Hybrid Meson					Secondary Decays		
State	IKP label	$J^{PC_n}(I^G)$	Decay	$\Gamma_{H\to AB}$ (MeV)	Γ_B (MeV)	Decay	b.f.
$\hat{a}_2(1900)$	x_2^{+-}	$2^{+-}(1^+)$	$[\pi a_2(1320)]_P$	450	103	$a_2 \to \rho\pi$	70%
						$\to \eta\pi$	15%
						$\to \omega\pi\pi$	11%
						$\to K\bar{K}$	5%
			$[\pi a_1(1260)]_P$	100	~400	$a_1 \to \rho\pi$	most
			$[\pi h_1(1170)]_P$	150	360	$h_1 \to \rho\pi$	seen
$\hat{f}_2(1900)$	y_2^{+-}	$2^{+-}(0^-)$	$[\pi b_1(1235)]_P$	500	155	$b_1 \to (\omega\pi)_{S,D}$	most
						$\to \eta\rho$	seen
$\hat{f}_2'(2100)$	z_2^{+-}	$2^{+-}(0^-)$	$[KK_2^*(1430)]_P$	250	98	$K_2^* \to K\pi$	50%
						$\to K^*\pi$	25%
						$\to K^*\pi\pi$	13%
			$[KK_1(1400)]_P$	200	174	$K_1 \to K^*\pi$	94%
$\hat{\rho}(1900)$	x_1^{-+}	$1^{-+}(1^-)$	$[\pi b_1(1235)]_{S,D}$	100,30	155	$b_1 \to (\omega\pi)_{S,D}$	most
						$\to \eta\rho$	seen
			$[\pi f_1(1285)]_{S,D}$	30,20	24	$f_1 \to \eta\pi\pi$	50%
						$\to 4\pi(\rho\pi\pi)$	38%
						$\to a_0(980)\pi$	37%
$\hat{\omega}(1900)$	y_1^{-+}	$1^{-+}(0^+)$	$[\pi a_1(1260)]_{S,D}$	100,70	~400	$a_1 \to \rho\pi$	most
			$[\pi\pi(1300)]_P$	100	200-600	$\pi(1300) \to \rho\pi$	seen
			$[KK_1(1400)]_S$	100	174	$K_1 \to K^*\pi$	94%
$\hat{\phi}(2100)$	z_1^{-+}	$1^{-+}(0^+)$	$[KK_1(1270)]_D$	80	90	$K_1 \to K\rho$	42%
						$\to K_0^*\pi$	28%
						$\to K^*\pi$	16%
						$\to K\omega$	11%
			$[KK_1(1400)]_S$	250	174	$K_1 \to K^*\pi$	94%
			$[KK(1460)]_P$	30	250	$K \to K\pi\pi$	seen
$\hat{a}_0(1900)$	x_0^{+-}	$0^{+-}(1^+)$	$[\pi a_1(1260)]_P$	800	~400	$a_1 \to \rho\pi$	most
			$[\pi h_1(1170)]_P$	100	360	$h_1 \to \rho\pi$	seen
			$[\pi\pi(1300)]_S$	900	200-600	$\pi(1300) \to \rho\pi$	seen
$\hat{f}_0(1900)$	y_0^{+-}	$0^{+-}(0^-)$	$[\pi b_1(1235)]_P$	250	155	$b_1 \to (\omega\pi)_{S,D}$	most
						$\to \eta\rho$	seen
$\hat{f}_0'(2100)$	z_0^{+-}	$0^{+-}(0^-)$	$[KK_1(1270)]_P$	800	90	See $\hat{\phi}(2100)$	
			$[KK_1(1400)]_P$	50	174	$K_1 \to K^*\pi$	94%
			$[KK(1460)]_S$	800	250	$K \to K\pi\pi$	seen

Photoproduction Opportunities at CEBAF: Meson Spectroscopy and The Physics of Flying ϕ's

Alex R. Dzierba
Department of Physics
Indiana University
Bloomington, IN 47405

ABSTRACT

The availability of high-intensity photon beams with an efficient duty-factor and with energies in the range 10 to 12 GeV makes possible studies in meson spectroscopy, rare decays and possibly symmetry tests such as CP and CPT. Indeed, with a 6 GeV tagged photon beam, realizable in the near future at CEBAF, measurements of rare radiative decays of the ϕ's will be made. At higher energies, a photon beam could be used to answer a number of questions in meson spectroscopy. An even more exciting possibility is the use of photon beams to produce an intense source of ϕ's. The physics contemplated at e^+e^- ϕ *factories*, such as CP and CPT tests, might be also studied at CEBAF with completely different and complementary systematics; e.g. having the ϕ's decay in flight may offer distinct advantages over ϕ's produced at rest.

1. Introduction

1.1 ϕ Photoproduction at CEBAF and Vector Meson Physics

Consider the photoproduction of the ϕ as shown in the diagram of Fig. 1. At CEBAF energies realizable in the near future, photon energies in the 4-6 GeV range are well above threshold for production of the ϕ. [1] In the vector dominance picture, which describes the data well, the photon ($J^{PC} = 1^{--}$) turns into a ϕ ($J^{PC} = 1^{--}$) which elastically scatters off the proton. The cross section ($\sim$ *0.5* μb) is approximately constant with energy and the ϕ is produced strongly peaked in the forward direction with a steeply falling t distribution:

---

[1] There are a number of references for the production of the ϕ on hydrogen at near-term and upgraded CEBAF energies. We list a few here: H. J. Behrend *et al,* Nucl Phys B144 (1978) 22, D. Aston *et al,* Nucl Phys B172 (1980) 1, and D. P. Barber *et al,* Z. Phys. C12 (1982) 1. These measurements span photon energies from 2.8 to 36 GeV.

$$\frac{d\sigma}{d|t|} \propto e^{-\alpha|t|} \qquad \textit{Eq. 1}$$

where t is the square of the momentum transferred from the incoming γ to the outgoing ϕ and $\alpha \approx 6$ *to* $8\ GeV^{-2}$. These remarks, which apply to the ϕ, also are applicable to the vector mesons ρ and ω.

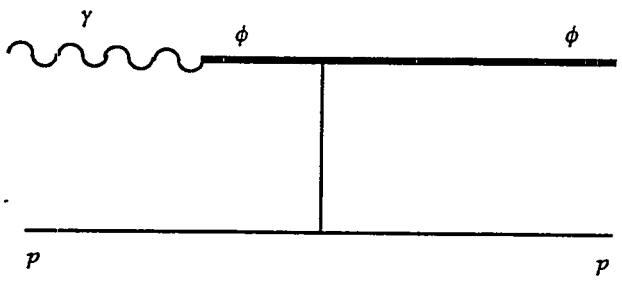


Fig. 1: *Photoproduction of the* ϕ

The vector mesons provide a splendid laboratory for the study of fundamental physics. Witness the factories being contemplated, planned or under construction to collide electrons and positrons at *cms* energies near or at the mass of the ϕ $(\phi - factory)$, the J/ψ $(\tau/charm - factory)$ and the Y $(B - factory)$. These projects are justified by the wealth of physics already uncovered by studying the decays of these vector mesons. Trying to understand the decays of the ϕ led to the OZI rule. Decays of the J/ψ and Y and their radial excitations have already provided important information about light-quark and heavy-quark spectroscopy and tests of the standard model. Prominent among the decays are the radiative decays of these states. Photoproduction of the $\rho,\ \omega,\ \phi,\ and\ J/\psi$ has also provided insight into the quark structure of matter and the nature of the coupling of the photon $(J^{PC} = 1^{--})$ to vectors $(J^{PC} = 1^{--})$. The suppression and/or enhancement of the ϕ and J/ψ are being suggested as possible signatures for the onset of the quark-gluon plasma in relativistic heavy-ion collisions.

1.2 Photoproduction of Other Mesons

Now consider the diagram of Fig. 2. CEBAF can be viewed as an $s\bar{s}$ *factory* for the production of states with $s\bar{s}$ content with decays into $K\bar{K}$ + *c.c.* or some energetically accessible quark rearrangements such as $\phi\omega$. This provides an opportunity to study, for example, $K\bar{K}$ molecules or $\phi\omega$ molecules (see T. Barnes [2]). The importance of studying $s\bar{s}$ states from the viewpoint of searching for exotics, hybrids and glueballs will be examined below. The photoproduction mechanism may also enhance production of spin 1, J^{PC} exotics, such as the $J^{PC} = 1^{-+}$ $\hat{\rho}(1405)$.

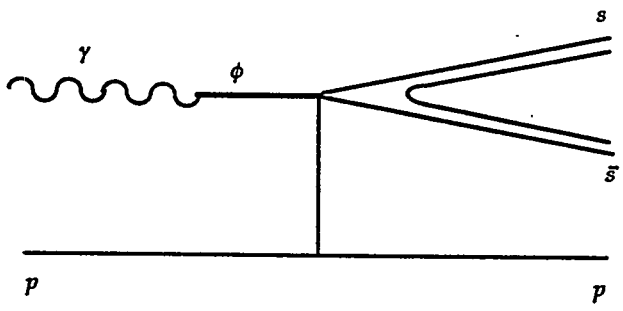


Fig. 2: *Photoproduction of mesons with strange quark content*

1.3 Organization

In Section 2, issues in light-quark meson spectroscopy will be briefly summarized along with a description of how some relevant measurements could be carried out at CEBAF. In Section 3, an experiment, planned for Hall B, to measure rare radiative decays of the ϕ will be described. Part of the interest in this experiment is the determination of a ϕ branching ratio critical to CP measurements at a *(ϕ – factory)*. Finally in Section 4, the possibility of a *flying ϕ – factory* at CEBAF will be examined. This could lead to an experimental program which is complementary to that planned for e^+e^- *ϕ – factories* at Frascati (DAΦNE) and at Novosibirsk.

2. Light-Quark Meson Spectroscopy

2.1 Introduction [2]

The conventional wisdom is that QCD, which has been with us now for approximately 20 years, describes the interactions of quarks and gluons. It has met with quantitative success in high energy processes, where perturbative techniques are applicable. In the non-perturbative regime, the situation is quite different. This is an area where light-quark meson spectroscopy has played, and will continue to play, an important role in understanding the spectrum of conventional $q\bar{q}$ mesons, as well as of other mesonic states. Qualitatively, QCD allows for mesons outside of the conventional $q\bar{q}$ mesons, including glueballs (gg or ggg), hybrids ($q\bar{q}g$) and multi-quark states ($q\bar{q}q\bar{q}$). For theoretical guidance on the properties of such states, we have to rely on models which are only approximations to QCD [3]. It is encouraging that results from different models differ appreciably since experiments can then serve as a guide as to which models can be discarded and which might provide further insight into QCD.

2.2 The Naive Quark Model

The naive quark model of light quark mesons is straightforward. If we form $q\bar{q}$ states from u, d and s quarks, we expect to find mesons to be grouped in nonets, with wave functions as shown in Fig. 3. Each member of a nonet has the same J^{PC}, with these quantum numbers following the restrictions expected of a non-relativistic fermion-antifermion system, as shown in Fig. 3. In this scheme, $J^{PC} = 0^{+-}$, 0^{--}, 1^{-+},...are not allowed and are called *exotic*. In addition to orbital excita-

---

[2] T. Barnes, Workshop Proceedings: *Future Directions in Particle and Nuclear Physics at Multi-GeV Hadron Facilities*, BNL-52389 (1993) 300; A. R. Dzierba, *ibid*, 311 and also Workshop Proceedings: DPF QCD Working Group Meeting, April 9-10, 1994 in Madison, WI.

[3] T. H. Burnnett and S. R. Sharpe, Ann. Rev. Nucl. Part. Sci. 40 (1990) 327. See also S. Godfrey's contribution to these Proceedings.

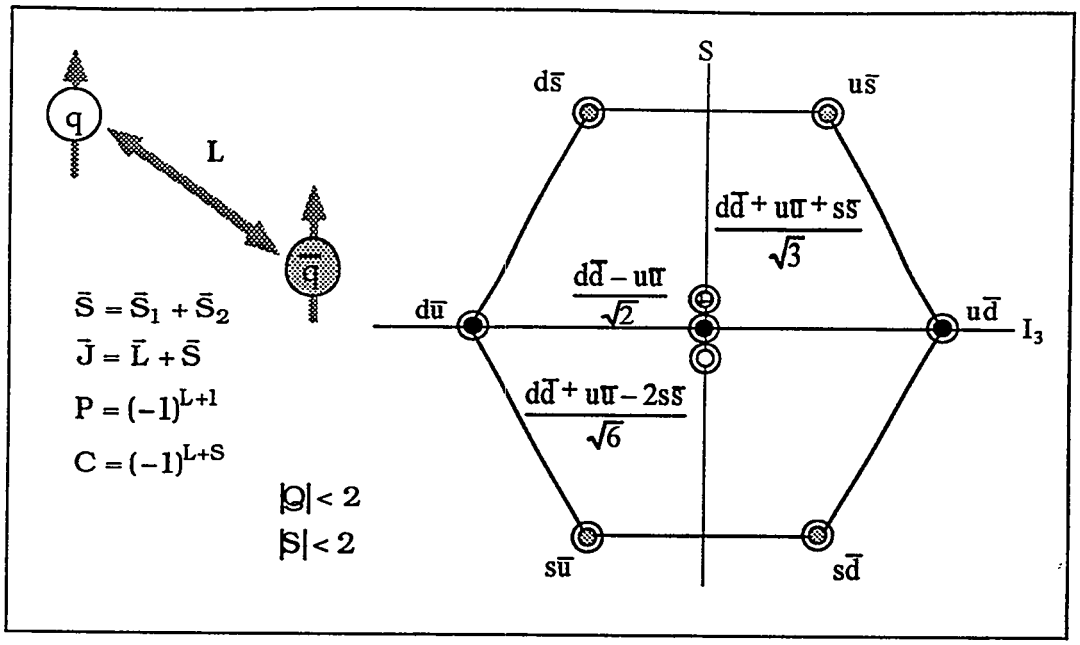


Fig. 3: *A light quark $q\bar{q}$ nonet with no mixing*

tions, we also expect to find radial excitations. It is also interesting that the observed nonets, except for the pseudoscalar nonet, exhibit nearly ideal mixing, that is, the physical realization of the two I = 0 members are linear combinations of the octet and singlet states such that one of the physical states is approximately pure $s\bar{s}$, while the other is $(u\bar{u} + d\bar{d})/\sqrt{2}$.

The naive quark model provides a template against which experiments search for other mesonic states. Since glueball, hybrid and multi-quark states have no J^{PC} restrictions, a state with exotic quantum numbers would be *prima facie* evidence for a non-$q\bar{q}$ meson. Since glueballs are expected to be flavorless, the I = 0 sector of the conventional $q\bar{q}$ nonets deserves close scrutiny. In particular, candidate states with I = 0 should be examined with regard to their production and decay to see if they can be identified as $q\bar{q}$ states. For example, if ideal or nearly ideal mixing obtains, one should expect to see one of the I = 0 members with production and decays expected for that of a $s\bar{s}$ meson while the other should have production and decays associated with a $(u\bar{u} + d\bar{d})/\sqrt{2}$ state. The current assignment of known mesons to nonets needs to be examined since possible non-$q\bar{q}$ states can show up where nonets are over-booked with extraneous states. In Fig. 4 the current assignments of meson sates to the conventional $q\bar{q}$ nonets including radial excitations is summarized [4]. Fig. 5. is a cartoon illustrating where to look for non-conventional mesons. It is clearly important to determine whether or not a meson has $s\bar{s}$ content.

---

[4] The presentation in Fig 4 originates from S. Godfrey, Z. Phys. C46 (1990) S93 and has been updated to show where some possible non-conventional states might exist.

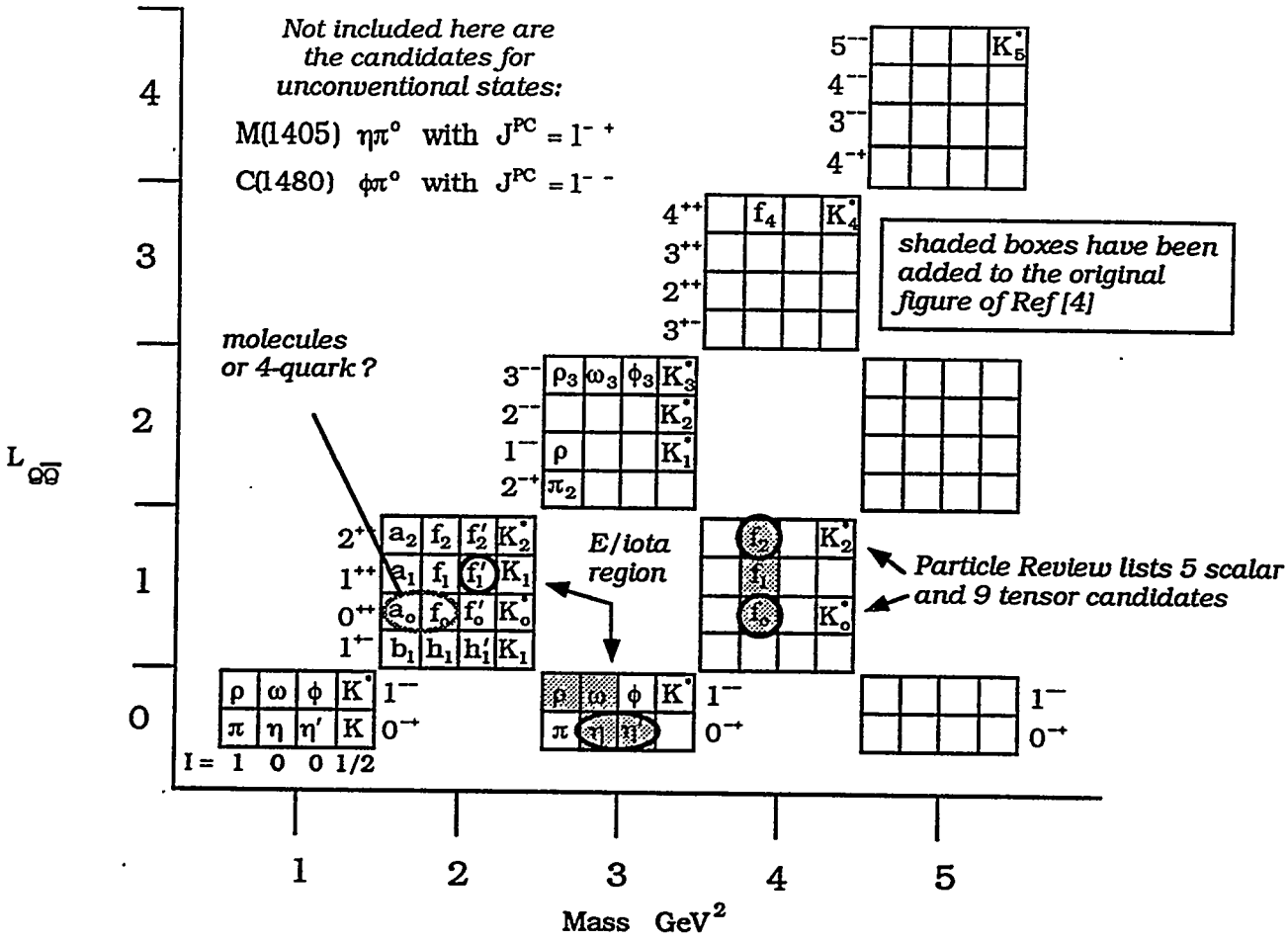


Fig. 4: *Population of light quark nonets*

- ✓ *states with exotic quantum numbers*
- ✓ *extraneous states - especially in I = 0, S = 0 sector*
- ✓ *states with peculiar decays properties*
- ✓ *states with peculiar production properties*

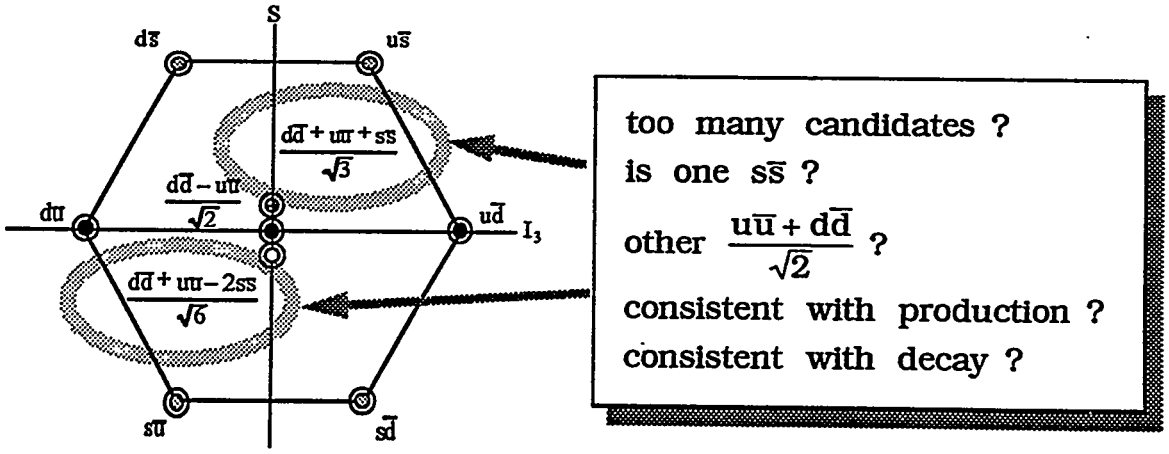


Fig. 5: *Where to look for non-$q\bar{q}$ candidates*

2.3 Searches for Non-Conventional Mesons

Fig. 4 includes a number of non-$q\bar{q}$ candidate states. We will consider some of these states.

Isovector and Isoscalar Scalar States. The $a_o(980)$ and the $f_o(980)$ are almost certainly not conventional $q\bar{q}$ states although they originally were assigned to the scalar nonet. Their masses and widths are too low to be $q\bar{q}$ states. There is also recent experimental evidence from the Crystal Barrel [5] to now jettison these states since they do have higher mass candidate isovector and isoscalar states to fill these positions in the scalar nonet. Section 3 shows how measurements of rare radiative decays of the ϕ can shed light on the substructure of these mesons.

States in the I = S = 0 Sector. The presence or absence of states in photoproduction (where $s\bar{s}$ should be enhanced) which occupy slots in the I = S = 0 sector of the various nonets could provide important information on the nature of various candidates.

Spin 1 Exotics. Spin 1 states might be enhanced in photoproduction. One such state is the $J^{PC} = 1^{-+}$ exotic $\hat{\rho}(1405)$. This state has been seen by the GAMS group [6] operating at CERN and Serpukhov decaying into $\eta\pi^o$. One advantage of looking at $\eta\pi^o$ is that if this system resonates in a P-wave, it is manifestly exotic, i.e. $J^{PC} = 1^{-+}$.

Flux-Tube Model Predictions for Spin 1 Exotics. In the flux tube model of Isgur *et al* [7], string states define adiabatic quark potentials and one expects towers of quark states built on each adiabatic surface. The conventional $q\bar{q}$ mesons correspond to the ground state of gluonic fields. Hybrids correspond to excitation of the quantum string into higher normal modes. In considering the decays of hybrids, there is a selection rule which prevents gluonic excitations from transferring angular momentum to final state pairs of mesons as relative orbital angular momentum but rather to internal orbital angular momentum. This would inhibit decays into phase-space favored systems such as $\pi\eta$ or $\pi\rho$ or $K^*\bar{K}$. The model also predicts decays into final states with one ground state S-wave $q\bar{q}$ and one excited P-wave $q\bar{q}$. The model predict that the lowest lying exotic $J^{PC} = 1^{-+}$ hybrid has a mass of 1900 MeV and decays into $b_1(1235)\pi$ or $f_1(1285)\pi$. This may explain why hybrids have not yet been observed - the final states are quite complicated and would not have been observed in earlier experiments with limited detection capability. For example, the $b_1(1235)\pi$ decays into $\omega\pi\pi \rightarrow 5\pi$!

---

[5] See the talk by C. Meyer in these Proceedings.

[6] D. Alde *et al*, Phys Lett. B205 (1988) 397 and references therein.

[7] N. Isgur *et al*, Phys Lett B124 (1983) 247, Phys Rev D31 (1985) 2910 and Phys Rev Lett 54 (1985) 869.

The $\phi\pi^\circ$ State at 1480 MeV. The C(1480) has been observed by only one group [8] as a $\phi\pi^\circ$ resonance with a likely $J^{PC} = 1^{--}$ assignment. Its OZI-violating branching ratio of $\phi\pi : \omega\pi$ makes it unlikely that it is a I = 1 $(u\bar{u} - d\bar{d})/\sqrt{2}$ state. It has been pointed out by Kopeliovich and Predazzi [9] that under the assumption of vector dominance and one pion exchange, if the C(1480) is a diquark-diquark state, the cross-section for $\gamma p \to Cp \to \phi\pi^\circ p$ is about 1/5 of the ϕ photoproduction cross section at 4 GeV, quite a substantial cross-section.

Other Possible non-$q\bar{q}$ States. The table in Fig. 7 lists other non-$q\bar{q}$ candidate states which have been seen in peripheral charge exchange production with incident pions. Many of these states have been observed by the GAMS group and need confirmation. For the reasons referred to above, it is also important to look for such sates in reactions initiated by incident photons.

P_{Lab} (GeV)	State and Mass	J^{PC}	Decays	Comments on Production and Decay
38, 100	M(1405)	1^{-+}	$\pi^\circ\eta$ ✓	PWA - some questions
38, 100, 230, 300	G(1590)/ f_0(1590)	0^{++}	$\eta\eta, \eta\eta', 4\pi^\circ$ ✓	*Peculiar BR for $q\bar{q}$* $2\pi^\circ$ $K\bar{K}$ $\eta\eta$ $\eta\eta'$ $4\pi^\circ$ <0.3 <1 1 3 0.8 *seen at LEAR $p\bar{p} \to \pi^\circ\eta\eta$ and in central production*
38	X(1740)	0^{++} 2^{++}	$\eta\eta$ ✓	*no $\eta\eta'$ or $2\pi^\circ$* *no OPE prod., produced with Δ(1236)*
100	X(1810)	2^{++}	$\eta\eta, 4\pi^\circ$ ✓	*$BR(2\pi^\circ)/BR(4\pi^\circ) < 1/4$* *indicates little $(\rho\rho)^\circ$*
38	X(1910)	1^{-+}	$\eta\eta'$ ✓	*no $\pi^\circ\pi^\circ$, $\eta\eta$, $K_s^\circ K_s^\circ$* *flat t-dependence*
38, 100	X(2210)	2^{++} 4^{++}	$\eta\eta'$	
38	f_6(2510)	6^{++}	$2\pi^\circ$	

***Fig. 6:** Peripheral charge exchange production of meson states. Possible non-$q\bar{q}$ states are indicated with a ✓ and need confirmation*

---

[8] Bityukov *et al*, Phys Lett B188 (1987) 383.

[9] B. Kopeliovich and E. Predazzi, Indiana University preprint IUHET-271 (1994) and private communication with the authors.

2.4 Doing the Experiment with a Neutral Detector

All of the states mentioned in the previous Section have decay modes which eventually lead to all photons in the final state. For example: $\pi^o \to \gamma\gamma$ *(99 %)*, $\eta \to \gamma\gamma$ *(40 %)*, $\eta' \to \gamma\gamma$ *(2 %)*, $\eta' \to \eta\pi^o\pi^o \to 6\gamma$ *(8 %)*, $\omega \to \pi^o\gamma \to 3\gamma$ *(9 %)*, $\phi \to \eta\gamma \to 3\gamma$ *(0.4 %)*, and so on. Looking at states with two body decays into combinations of π^o, η and η' provides some nice constraints. Since all these have spin zero, the spin, J, and relative orbital angular momentum, L, are simply related, $J = L$. Since the parity is given by $P = (-1)^L$, we have $J^P = (even)^+$ or $J^P = (odd)^-$. The charge conjugation, C, of the pseudoscalars is even so the two-meson system also has $C = +$. If $\pi^o\eta$, $\pi^o\eta'$ or $\eta\eta'$ resonate in a P-wave then the decaying state has manifestly exotic $J^{PC} = 1^{-+}$. The first two combinations have $I = 1$ while the last has $I = 0$. The latter may correspond to a glueball (completely flavorless) while the other two cannot. Seeing a resonant state decaying into $\pi^o\pi^o$, $\eta\eta$ or $\eta'\eta'$ requires $I = 0$ and $J^P = (even)^+$.

An all-neutral detector, for example a lead-glass detector (LGD) has many virtues for a photoproduction experiment. First of all, the states accessible are large indeed. Secondly, an all neutral detector removes the need for a magnetic field which is particularly important for a tagged bremsstrahlung photon beam to avoid problems with electron-positron pairs associated with the electromagnetic background inherent in such a tagged photon beam. (This issue is discussed further in Section 3 where the experiment to measure rare radiative decys of the ϕ is presented). A possible arrangement is shown in Fig. 7. A 30 cm-long LH_2 target is surrounded by cylindrical charged particle detector (circular drift chamber) and a cylindrical photon detec-

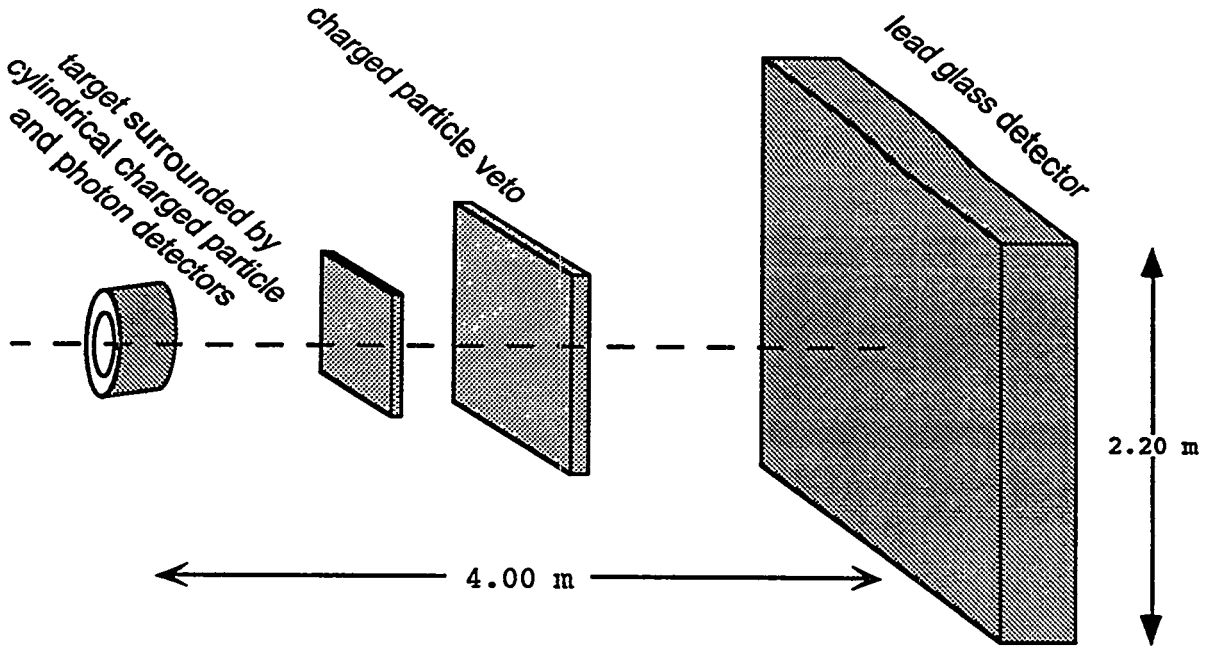


***Fig. 7:** A possible all-neutral deterctor arrangement to study meson production in a tagged photon beam at CEBAF*

tor (Cs I crystals). The detectors around the target would be used in the overall event reconstruction, requiring the recoil proton, rejecting soft photons and providing azimuthal information about the forward-going system. Charged particle veto counters would define a first-level trigger requiring no charged particles in the forward direction. A 55 x 55 element (3025 blocks) lead glass detector, with the glass stacked in a square or circular geometry would provide the photon detection.

The target-to-detector distance of 4 meters represents a compromise for incident photons of 10 GeV; close enough to have good acceptance for all photons and yet far enough so that the photons from the most energetic π^0's are resolvable. The acceptance (requiring all photons to strike the glass, exceed 250 MeV of energy and be separated by 6 cm from the nearest neighbor) ranges from about 60 % for 4 photon decays to 20 % for 7 or 8 photon states for meson masses of order 1.5 GeV.

2.5 Performance of the AGS E852 Lead Glass Detector

A lead glass detector has been built for Brookhaven AGS E852: *A Search for Mesons with Unsusual Quantum Numbers* [10]. That stack is 43 x 71 blocks (3053 blocks), each block is 4 cm x 4 cm x 45 cm in overall dimensions. A schematic of that detector is shown in Fig. 8. The stack

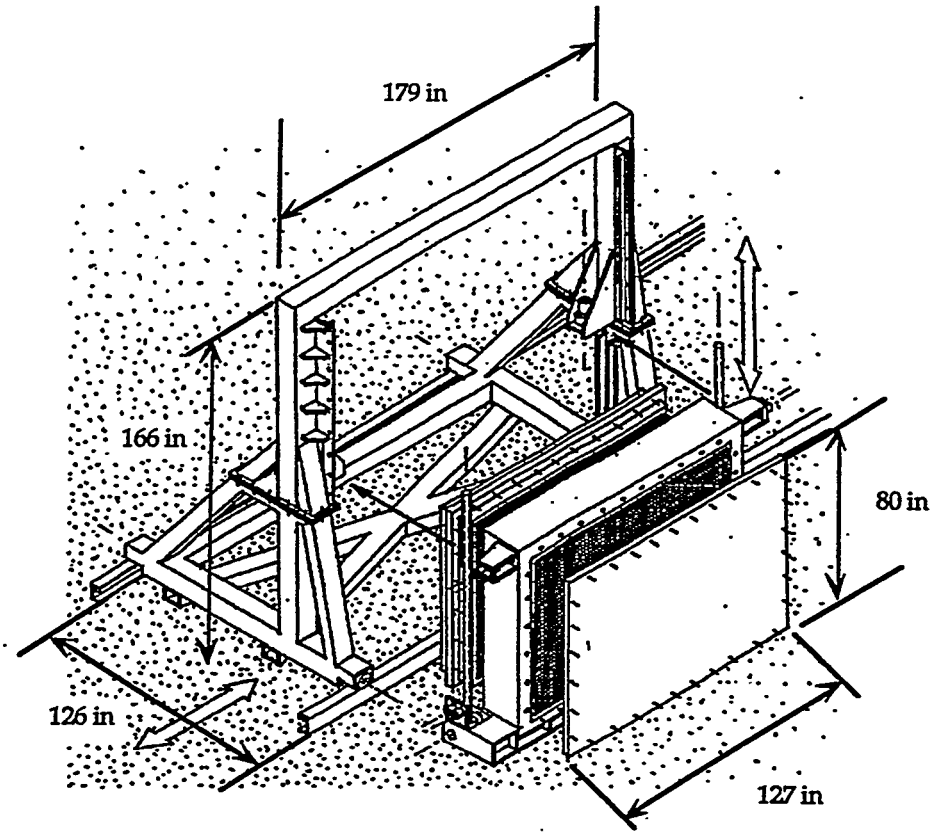


Fig. 8: *A schematic of the lead glass detector (3053 elements) used in Brookhaven AGS Experiment E852*

can be moved horizontally and vertically under computer control to position each block in an electron beam for calibration purposes. The E852 LGD comes equipped with custom-built ADC's and a trigger processor which provides the possibility of triggering on essentially any kinematic function based on the 4-vectors of the photons striking the LGD, e.g. total energy, effective mass, momentum transfer squared, as well as other variables. The calculation time is about $4-5\ \mu sec$.

In a recent data run at the AGS, the LGD has been used to trigger on energy and effective mass. A result of all-neutral forward triggers collected with an incident $18\ GeV\ \pi^-$ beam on a hydrogen target is shown in Figs. 9 through 14. The data set shown represents 12 hours of data-taking.

Fig. 9:

This plot is the diphoton effective mass spectrum for events in which two photon clusters were identified. Peaks are clearly seen at the π^o, η, ω and η' mass regions. The structure just above the π^o is not fully understood at this preliminary stage of the analysis but is thought to be an artifact of the cluster finder in the beam region.

The ω shows up in this plot due to photons coalescing in the LGD from the $\pi^o\gamma$ decay of the ω.

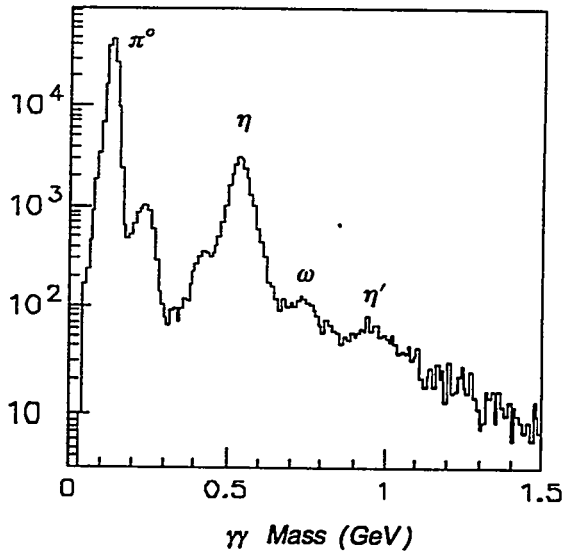
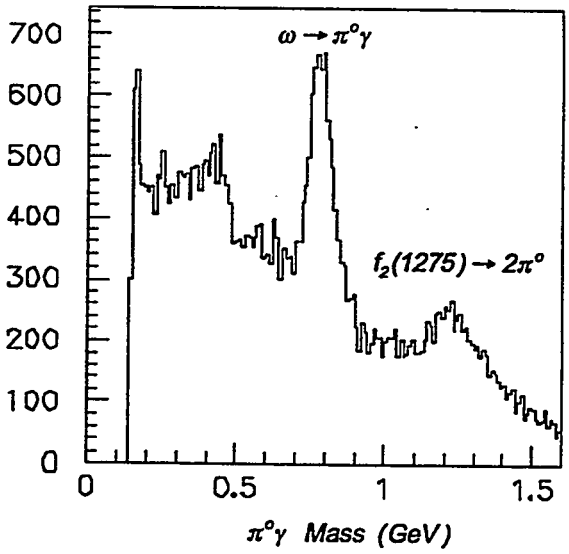


Fig. 10:

This plot shows the $\pi^o\gamma$ effective mass distribution for three-cluster events in which two of the photons satisfied the constrained fit to the π^o mass. The $\omega \to \pi^o\gamma$ is clearly seen. There also is a peak at the $f_2(1275) \to \pi^o\pi^o \to 4\gamma$. In some cases the photons from one of the π^o coalesce at the LGD and appear as a single photon. This resonance is also seen in Fig. 11.



[10] See AGS Proposal E852 and Brabson *et al*, Nucl Instr & Meth A332 (1993) 419 for a description of tests of lead glass detector prototypes.

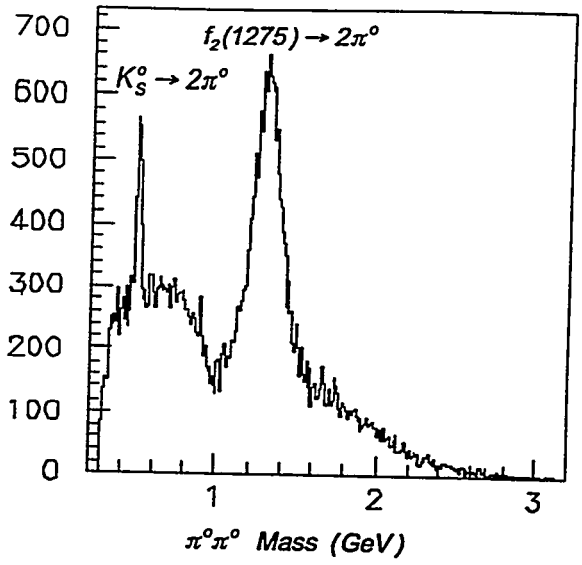


Fig. 11:

This plot shows the $\pi^o\pi^o$ effective mass distribution for four-cluster events satisfying constrained fits to $\pi^o\pi^o$. The $f_2(1275)$ is observed as well as $K_S^o \rightarrow \pi^o\pi^o \rightarrow 4\gamma$.

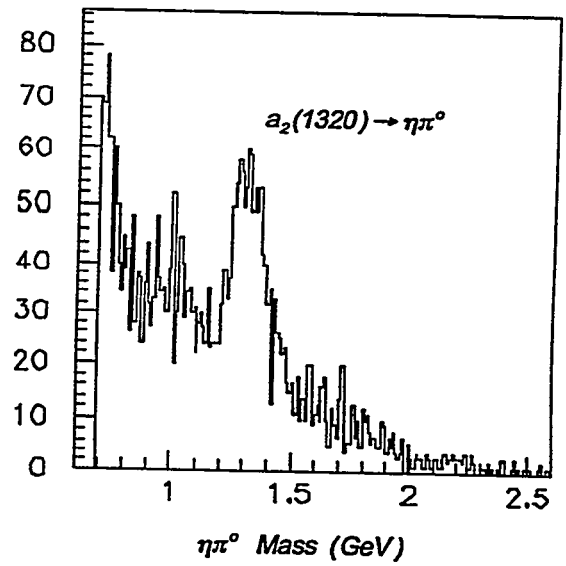


Fig. 12:

This plot shows the $\pi^o\eta$ effective mass distribution for four-cluster events satisfying constrained fits to $\pi^o\eta$. The $a_2(1320) \rightarrow \pi^o\eta \rightarrow 4\gamma$ is observed. This plot is very relevant to one of the E852 physics goals. The only reported sighting to date of a J^{PC} exotic meson is the $J^{PC} = 1^{-+}$ reported by GAMS with a mass of 1405 MeV decaying into $\pi^o\eta$. It manifests itself in their data as a odd-wave/even-wave interference with the D-wave $a_2(1320)$.

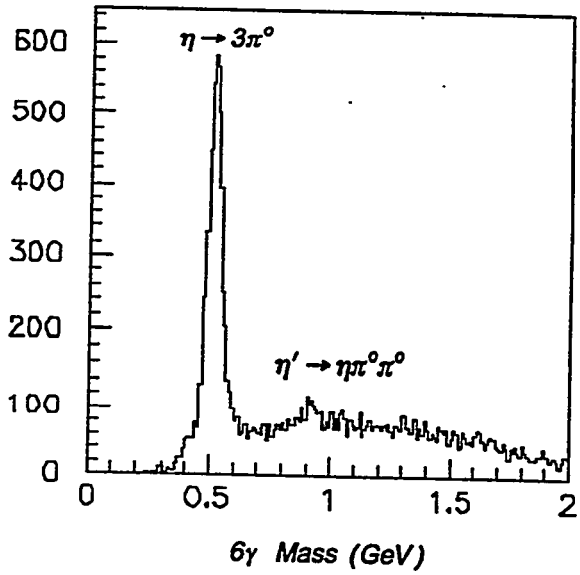


Fig. 13:

This plot shows the 6γ effective mass distribution for 6-cluster events. The $\eta \rightarrow 3\pi^o \rightarrow 6\gamma$ decay is clearly observed. In this distribution there is no requirement that the photons come from π^o decays. The width of the η peak is 40 MeV in this plot. If we require a constrained fit to $3\pi^o$, the resulting mass distribution shows an η peak with a width of 18 MeV.

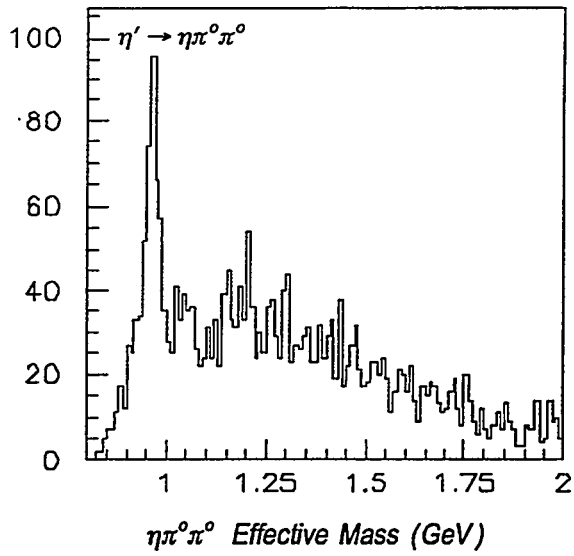


Fig. 14:

This plot shows the $\eta\pi^o\pi^o$ effective mass distribution for 6-cluster events satisfying constrained fits to $\eta\pi^o\pi^o$. The $\eta' \to \eta\pi^o\pi^o$ decay is observed.

3. Rare Radiative Decays of the ϕ Meson

3.1 Introduction

A proposal to measure rare radiative decays of the ϕ meson was presented to CEBAF as a letter of intent in January, 1994 and to the PAC-8 as a formal proposal in June, 1994. That experiment would use the tagged photon beam in Hall B and would set up a 25 x 25 element lead glass detector in front of the CLAS detector.

3.2 Radiative Decays of the ϕ

There is still physics to be uncovered in the study of radiative decays of the ϕ. It is interesting that although there are a number of mesons which are energetically accessible through the radiative decay of the ϕ, only *two* radiative modes have been observed. The decay $\phi \to \eta\gamma$ occurs with a branching ratio of 1.3 % and $\phi \to \pi^o\gamma$ has a branching ratio about a factor of 10 smaller. This already is an interesting result which points to the $s\bar{s}$ content of the η.

The paucity of other observed modes is due in some cases to conservation principles; for example the decays $\phi \to \rho\gamma$ and $\phi \to \omega\gamma$ are C-violating. For decays which are otherwise allowed, the kinematics of the decay, to a large extent, explains why some decays have not yet been observed. Before discussing explicit decays of the ϕ, a review of the decay kinematics is in order. Consider the decay $\phi \to X\gamma$ in the rest frame of the ϕ. The energy of the photon, E_γ, is given by

$$E_\gamma = \frac{m_\phi^2 - m_X^2}{2m_\phi} \qquad \text{Eq. 2}$$

If $m_X \sim m_\phi$ then $E_\gamma \sim m_\phi - m_X$. As we will see below, many of the interesting decays correspond to masses, m_X, which are of order 1 GeV. In these cases, the radiated photon has just several tens of MeV of energy, which makes experimental detection difficult. A way to circumvent this problem is to produce boosted ϕ's. For example, in the photoproduction process $\gamma p \to \phi p$, the ϕ is produced in the very forward direction with essentially the beam momentum. The boost factor for the radiated photon can be as high as $2 \cdot E_{beam}/m_\phi$. For a 6 GeV tagged photon beam at initial CEBAF energies, this factor is as high as 12.

The small values of E_γ also damp rates for $\phi \to scalar + \gamma$ and $\phi \to pseudoscalar + \gamma$ since these proceed through electric and magnetic dipole transitions respectively and involve E_γ^3 in the final rate, apart from any matrix element contributions. To appreciate the effect of this strong dependence on E_γ, consider the expected ratio of the branching ratios of $\phi \to \eta'\gamma$ relative to $\phi \to \eta\gamma$ ignoring any difference in the quark or gluon content of the final state mesons:

$$\frac{BR(\phi \to \eta'\gamma)}{BR(\phi \to \eta\gamma)} = \left[\frac{m_\phi^2 - m_{\eta'}^2}{m_\phi^2 - m_\eta^2}\right]^3 = 4 \times 10^{-3} \qquad Eq.\ 3$$

We will now consider a number of ϕ radiative decay modes.

3.3 $\phi \to a_o\gamma$ and $\phi \to f_o\gamma$

These are decays of the ϕ into a scalar meson state and a photon and therefore their rates suffer from the E_γ^3 dampening. The first of these scalar states is an isovector and the second is an isoscalar. They are nearly degenerate in mass. For completeness their properties are:

$$\begin{aligned} a_o &: \ I^G = 1^- \quad J^{PC} = 0^{++} \quad m = 980\ MeV \quad \Gamma = 57\ MeV \\ f_o &: \ I^G = 0^+ \quad J^{PC} = 0^{++} \quad m = 975\ MeV \quad \Gamma = 47\ MeV \end{aligned} \qquad Eq.\ 4$$

The isoscalar state decays into $\pi\pi$ while the isovector state decays into $\eta\pi$. Both states also decay into $K\bar{K}$. The question of the interpretation of these states as $q\bar{q}$ states is an intriguing one and has attracted much theoretical attention [11]. For example the masses and widths are inconsistent for a P-wave $q\bar{q}$ nonet. The proximity of these states to the $K\bar{K}$ threshold complicates the picture. Moreover the $q\bar{q}$ nonet is oversubscribed adding to the real possibility that these may be $non-q\bar{q}$ states, for example $qq\bar{q}\bar{q}$ or $K\bar{K}$ molecules.

---

[11] See the discussion of these states and other candidates in the Review of Particle Properties (1992).

The authors of ref [12] show how a measurement of the ratio of branching ratios of ϕ radiative decays can provide information on the makeup of these scalar states. In the conventional ^3P_o $q\bar{q}$ picture we expect $(\phi \to a_o\gamma)/(\phi \to f_o\gamma) = 0$ because of OZI suppression. The $K\bar{K}$ *molecule vs* $qq\bar{q}\bar{q}$ pictures can be distinguished by the electric dipole nature of these decays (which probes the electric charges of the constituents weighted by the distance from the overall cm) through the relative phases in I = 0 and I = 1 wavefunctions and through the relative spatial distributions of quarks and antiquarks. To summarize:

$$^3P_o \; q\bar{q} \; nonet:$$
$$\left.\begin{array}{l} a_o = (u\bar{u} - d\bar{d})/\sqrt{2} \\ f_o = some \;\; s\bar{s} \end{array}\right\} \Rightarrow \frac{\phi \to a_o\gamma}{\phi \to f_o\gamma} = 0 \qquad \text{Eq. 5}$$

$$K\bar{K} \; molecule:$$
$$\left.\begin{array}{l} a_o \\ f_o \end{array}\right\} = \frac{1}{\sqrt{2}}\left[(u\bar{s})(\bar{u}s) \mp (d\bar{s})(\bar{d}s)\right] \Rightarrow \frac{\phi \to a_o\gamma}{\phi \to f_o\gamma} = 1 \qquad \text{Eq. 6}$$

$$qq\bar{q}\bar{q}:$$
$$\left.\begin{array}{l} a_o \\ f_o \end{array}\right\} = \frac{1}{\sqrt{2}}\left[(us)(\bar{u}\bar{s}) \pm (ds)(\bar{d}\bar{s})\right] \Rightarrow \frac{\phi \to a_o\gamma}{\phi \to f_o\gamma} = 9 \qquad \text{Eq. 7}$$

3.4 $\phi \to$ scalar + γ and implications for CP studies at a ϕ – factory

The measurements of the branching ratios discussed above is important information for CP studies at a ϕ – *factory*. The decay sequence $\phi \to K^o\bar{K}^o \to K_L^oK_S^o$ occurs because the spin of the ϕ requires the antisymmetric $K_L^oK_s^o$. This means that CP-studies can be performed at a ϕ – *factory* by tagging the K_s^o which thereby tags the K_L^o. However, the presence of the radiative decay

$$\phi \to (K_S^oK_S^o \;\; or \;\; K_L^oK_L^o)\gamma$$

will complicate or possibly destroy CP studies at a e^+e^- ϕ – *factory* if the branching ratio is higher than 10^{-4} since at a ϕ – *factory* [13] the radiated photon, which has at most $m_\phi - 2 \cdot m_K = 24$ *MeV* of energy, will escape detection. The measurement of the radiative decays into scalars will provide information on this potentially insidious background to CP

---

[12] F. Close, N. Isgur and S. Kumano, Nucl. Phys. B389 (1993) 513

[13] G. Barbiellini *et al*, Particle World, 1 (1990) 138.

studies. At the current measured limits (which do not provide the guarantee that CP physics can be done at a ϕ – *factory*), we will observe a few tens of thousands of decays into scalar states. Ref [12] includes a discussion of how the explicit rate for $\phi \to K_s^o K_s^o \gamma$ can by extracted from a measurement of $\phi \to \pi^o \pi^o \gamma$ and $\phi \to \eta \pi^o \gamma$.

3.5 $\phi \to \eta' \gamma$

This decay mode is strongly damped because of the mass of the η' relative to the ϕ. The measurement of this branching ratio is important in providing information on the gluonic and $s\bar{s}$ content of the η' [14, 15].

3.6 $\phi \to \eta\gamma$ *and* $\phi \to \pi^o\gamma$

These modes have already been observed and are well measured. Although the proposed experiment will not contribute new information about these modes, a measurement of these decays and their ratio will be an important monitor in this proposed experiment. As we show in Section 4, we expect to see about 150,000 $\phi \to \eta\gamma$ decays.

3.7 $\phi \to \rho\gamma$ *and* $\phi \to \omega\gamma$

These modes are C-violating but the current limits on them are very imprecise and of order several percent. The sensitivity of the proposed experiment is such that the limit on $\phi \to \omega\gamma$ should be improved by 3 to 4 orders of magnitude.

3.8 Other physics

i) $\phi \to \omega\pi^o$ is an isospin violating decay which has not been observed. From the measured branching ratio of $\phi \to \rho\pi^o$ we expect the branching ratio for the isospin violating decay to be of order 10^{-4}. We will search for this mode in this proposed experiment.

ii) Radiative decays of the ρ *and* ω. In a photoproduction experiment, we expect a rich sample of ρ *and* ω. This experiment provides an opportunity to improve the measurement of the branching ratios of $\rho \to \pi^o\gamma$ and $\omega \to \eta\gamma$. The isospin-violating decay $\omega \to \eta\pi^o$ has not been observed.

---

[14] F. Lenz, Nucl. Phys B279 (1987) 119. This paper also treats the structure of the f_o.

[15] J. L. Rosner, Phys Rev D27 (1983) 1101.

3.9 Brief outline of the Experiment and Yields

The proposal is to install a 25×25 element lead glass detector (LGD) in the Hall B tagged photon beam in front of the CLAS detector. A similar detector is shown in Fig. 15 and the placement in Hall B is shown in Fig. 16. The proposal assumes 5×10^7 *tagged 4 GeV photons/sec* although a photon beam may be available fairly soon after this experiment is ready to run. The beam will be incident on a 1-in thick Be target which will be followed by a charged particle veto (CPV) downstream of the target. The CPV will be used to veto on the presence of charged particles in the final state. The array will be large enough to match the transverse dimensions of the lead glass array but will not intercept recoil protons from the ϕ production reaction: $\gamma p \rightarrow \phi p$.

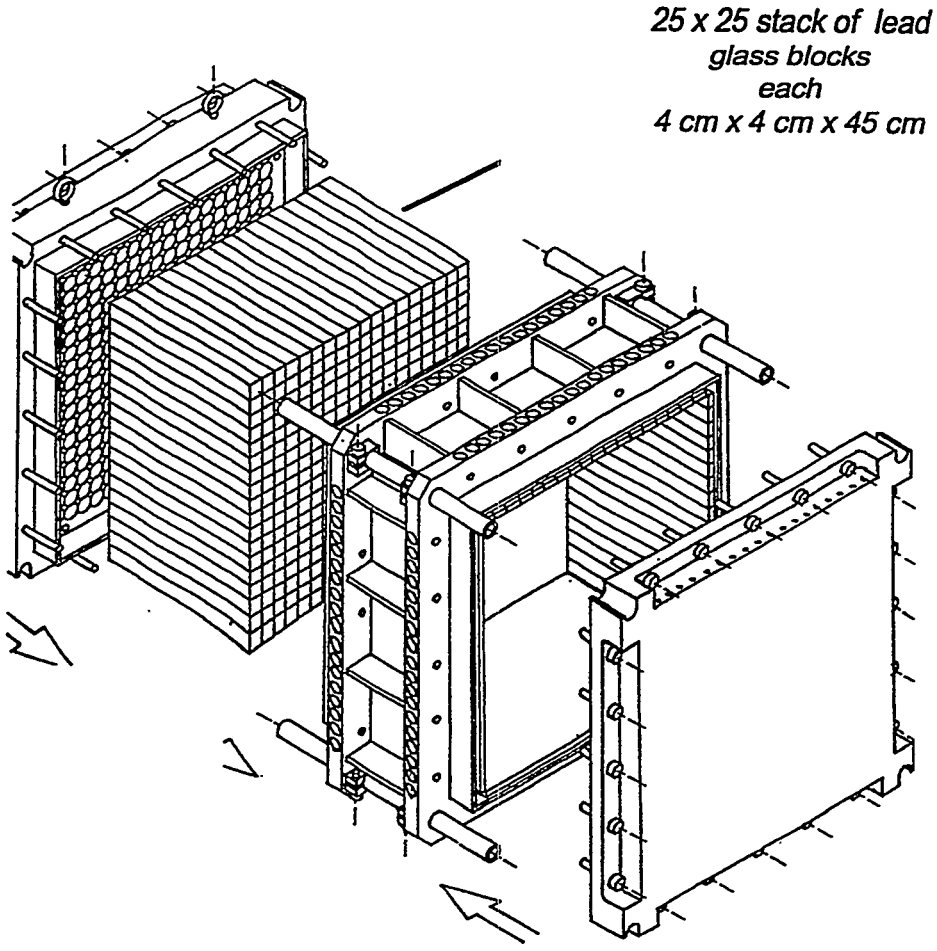


***Fig. 15:** Schematic of the lead glass detector (LGD)*

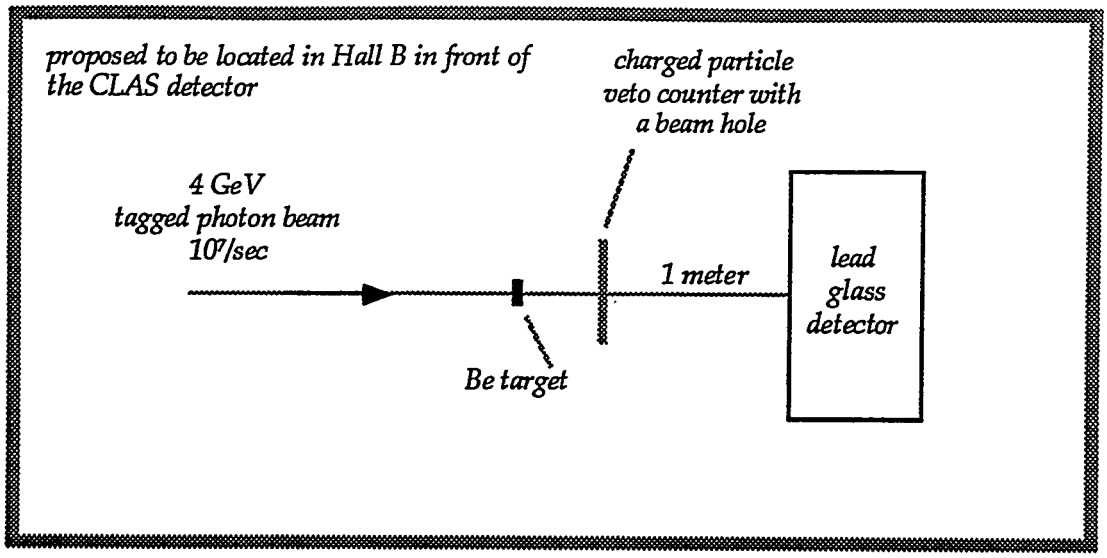


Fig. 16: *Installation of the LGD in Hall B*

It may be that the optimal place for the charged particle veto is just upstream of the LGD. This is being studied. The lead glass detector and the CPV will have holes for passage of the non-interacting photon beam. A *4-cm* diameter vacuum pipe will be used between the target and the LGD to minimize material presented to the non-interacting photon beam between the target and LGD.

In order to understand the acceptance of this experiment, a hybrid Monte Carlo simulation was employed. The four-vectors of the ϕ and its decay products were generated to the photon level. The ϕ's were produced with a t distribution following:

$$\frac{d\sigma}{d|t|} = const \cdot e^{-8|t|} \qquad Eq.\ 8$$

and the decay angular distribution of the $\phi \rightarrow (spin\ 0) + \gamma$ in the ϕ rest frame was chosen to follow:

$$\frac{dN}{d\cos\theta} = const \cdot (1 + \cos^2\theta) \qquad Eq.\ 9$$

The photons were tracked to the LGD. The response of the detector to photons of various energies, striking the LGD at various angles was not simulated. Rather, data collected during a test run of an *18 x 18* lead glass array [10] were used to estimate the detector response. Files of real shower data, indexed by energy and position, were used. The detector response was fed to the pattern recognition program of E852. Fig. 17 shows the reconstructed ϕ mass from the decay $\phi \rightarrow \eta\gamma$. The acceptance, as a function of photon energy and convoluted with the bremsstrahlung spectrum, is shown in Fig. 18 for *4 GeV* electrons and in Fig. 19 for *6 GeV* electrons. These curves require that all photons at the LGD face be separated by at least *6 cm*

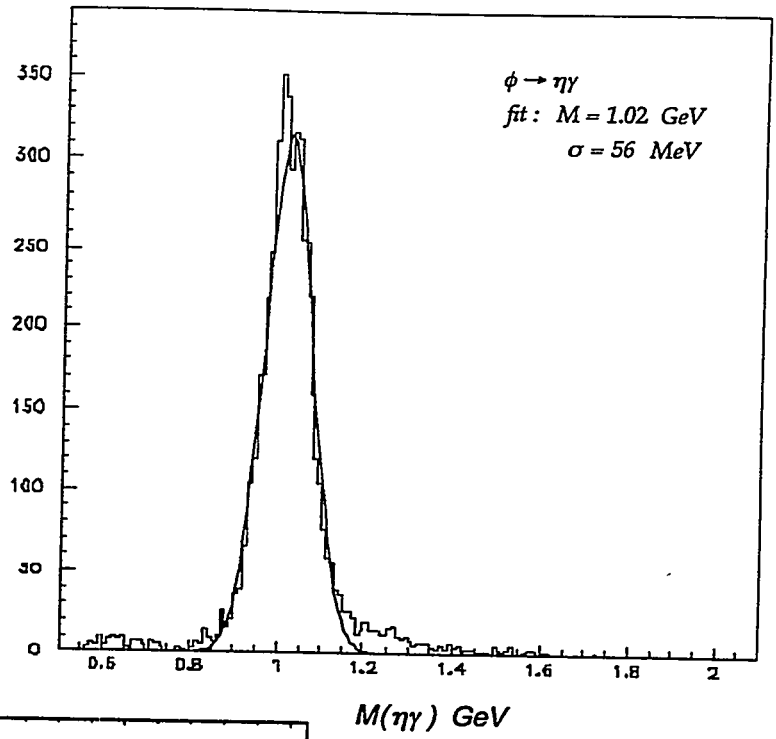


Fig. 17: Reconstructed $\eta\gamma$ mass from ϕ decays using a hybrid Monte Carlo for the CEBAF geometry and the E852 pattern recognition. Details are given in the text.

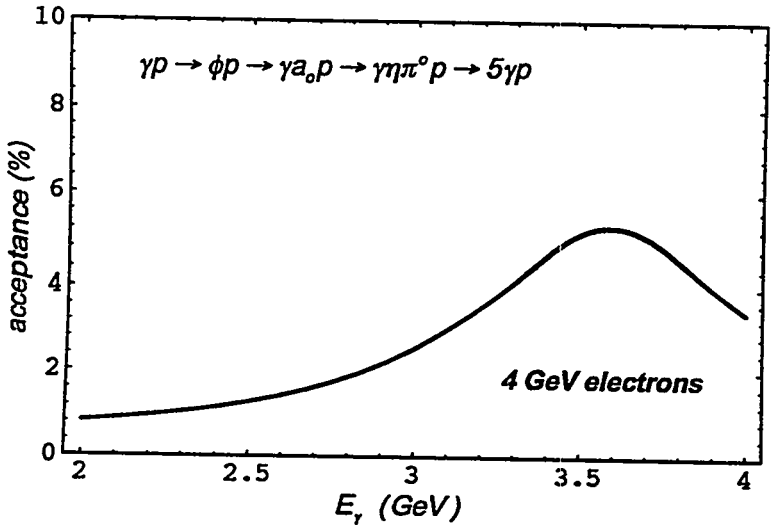


Fig. 18: Acceptance for the most complicated ϕ decay being considered in this experiment. The acceptance is convoluted with the bremsstrahlung spectrum and assumes 4 GeV electrons. Details are given in the text.

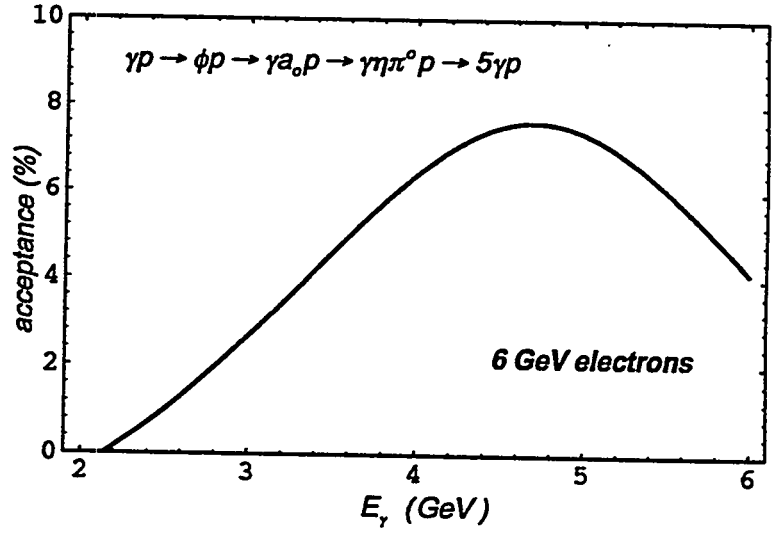


Fig. 19: Acceptance for the most complicated ϕ decay being considered in this experiment. The acceptance is convoluted with the bremsstrahlung spectrum and assumes 6 GeV electrons. Details are given in the text.

and have a minimum energy of *150 MeV*. There is evidence, from our studies in E852, that we will be able to relax these requirement somewhat, thus increasing the acceptance. Table 1 shows the expected yields for a 30-day run with *4 GeV* photons. *If instead, a 6 GeV photon beam is used, the overall yields are doubled.*

Table of Expected Yields

Assumptions: 1-in Be target, $\sigma_\phi = 0.5$ *μb* for *4 GeV* photons at 5×10^7 *tagged photons/sec*
Yield: *2.5 million φ's/day* *For acceptance estimates the minimum photon energy is 150 MeV*

Decay Mode $\phi \rightarrow$	*BR(%)*	*BR in all photons* 10^{-4}	*Number of photons*	*Acceptance (%)*	*Acceptance times BR* 10^{-4}	*Yield of Events in 30 Days*
$\pi^\circ\gamma$	0.13	13	3	35	4.5	38,000
$\eta\gamma$	1.3	52	3	35	18.2	150,000
$\eta'\gamma$ ✓	0.04	0.09	3	30	0.03	250
$\omega\gamma$ ✓	5	43	4	20	8.6	75,000
$\omega\pi^\circ$ ✓✓	0.001	0.09	5	10	0.01	75
$a_o\gamma \rightarrow \eta\pi^\circ\gamma$ ✓	0.10	10	5	7	1	5,300
$f_o\gamma \rightarrow \pi^\circ\pi^\circ\gamma$ ✓	0.20	20	5	10	2	15,000

✓ *the measured limit is used* ✓✓ *no limit has been measured, a prediction is used*

For the $\eta'\gamma$ *mode the prediction is about 15 % of the current measured limit*

The following BR are used: $\eta \rightarrow 2\gamma$ *(39 %);* $\eta' \rightarrow 2\gamma$ *(2.2 %);* $\omega \rightarrow \pi^\circ\gamma \rightarrow 3\gamma$ *(8.5 %)*

Table 1: *Expected yields for a 30-day run assuming 4 GeV electrons.*
If 6 GeV electrons are used, the yields are doubled.

3.10 Electromagnetic Backgrounds.

In a tagged photon beam electromagnetic backgrounds are always a serious concern. The electromagnetic backgrounds for this experiment come from at least two sources. A 2 *cm* Be target presents about *6%* of a radiation length so about *6%* of the incident beam can be expected to interact. The major process at high energy is pair production. All pairs are produced at small angles and would exit the downstream end of the target inside of the downstream vacuum pipe. The produced pairs have a 6% chance on average of re-scattering in the target. This gives rise to a *0.4%* background. In general only one of the particles in the pair will scatter and so the event would be below trigger threshold. This background scales as the square of the target thickness so the signal to noise could be optimized at the expense of a loss in event rate. The presence of re-scattered pairs makes it essential that the vacuum pipe be extended downstream of the target to at least the end of the detector.

The second source of background comes from the large number of photons with energies well below those of interest for ϕ production. Photons with energies below the tagger threshold are still present in the beam and pass through the target. While they will never produce triggerable energy depositions they do contribute to the radiation exposure of the detector and the general noise.

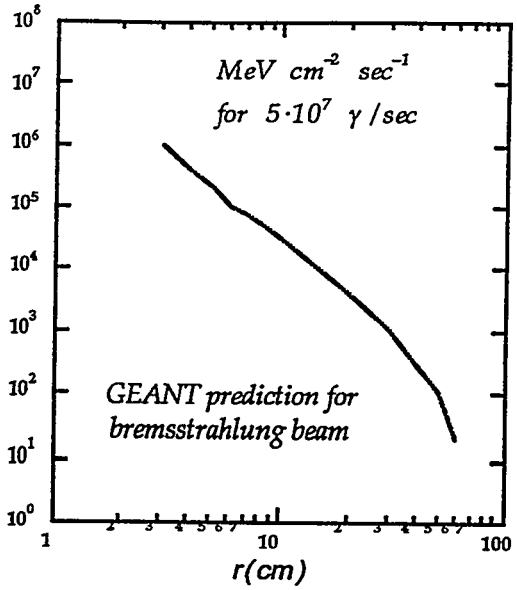


Fig. 20: *Flux of energy at the LGD face as a function of distance from the center of the LGD. This is a GEANT estimate of the electromagnetic background.*

GEANT was used to simulate electromagnetic processes with an incident photon spectrum given by the Bethe-Heitler formula. A tagged photon rate between 2 *GeV* and 4 *GeV* of $5 \cdot 10^7$ */sec* was assumed, which means a total photon rate for photons from *10 MeV* to 4 *GeV* of $6 \cdot 10^8$ */sec* The energy deposited per area per second as a function of radius from the center of the LGD is shown in Fig. 20. The width of the ADC gate is *250 ns.* The results are that for blocks at *6 cm* radius (i.e. the innermost layer) we expect an average of *2.4 MeV* per block per ADC gate, from beam-induced background. The average *hit* energy that produces this is *10-15 MeV.* Thus the average of *2.4 MeV* means (Poisson-distributed) that many blocks have nothing, but about 20 % have a *10-15 MeV* photon. Since a real shower is spread over several blocks, one must add up over (typically) 9 blocks to get the photon energy. Thus there is a pedestal to the ADC signals of order *25 MeV.* This is negligible compared to the resolution of the lead-glass. The same calculation at *20 cm* radius (near the middle of the detector) gives an order-of-magnitude lower average energy, i.e. completely negligible.

3.11 The Collaboration

The collaboration which will cary out the measurements of the rare radiative decays of the ϕ described in this Section includes:

H. Crannell, J. O'Brien and D. Sober *(Catholic University of America, Washington, DC 20064),* M. Kossov, B. Niczyporuk and E. Smith *(Continuous Beam Accelerator Facility, Newport News, VA 23606),* B. Brabson, R. Crittenden, A. Dzierba, J. Gunter, R. Lindenbusch, D. Rust, P. Smith, E. Scott, T. Sulanke and S. Teige *(Indiana University, Bloomington, IN 47405),* J. Bishop, N. Cason, J. Kolata, J. LoSecco, A. Sanjari and W. Shephard *(University of Notre Dame, Notre Dame, IN 46556),* G. Adams, J. Napolitano and M. Witkowski *(Rensselaer Polytechnic Institute, Troy, NY 12180),* B. Bonner, G. Mutchler and S. Ahmad *(Bonner Nuclear Physics Lab at Rice University, Houston, TX 77251),* G. Gilfoyle, P. Rubin and M. Vineyard *(University of Richmond, Richmond, VA 23173), E. Frlez and D. Pocanic (University of Virginia, Charlottesville, VA 22901), and D. Armstrong (College of William and Mary, Williamsburg, VA 23187).* The Spokesman is A. Dzierba and the Co-Spokesman is J. Napolitano.

4. Flying Phi Factory at CEBAF

4.1 Introduction

The point of the experiment described in Section 3 is that there are definite advantages to boosting the ϕ to study its rare radiative decays. One does not have to deal with the delicate radiated photon as in the case of a ϕ produced at rest at e^+e^- *ϕ factories*. In this particular study, not only does photoproduction provide a complementary measurement of these processes with very different systematics, but it may also be a superior method.

At a *ϕ factory*, such as the one being built at Frascati [13,16] the design luminosity $L = 10^{32}\ cm^{-2}\ sec^{-1}$, coupled with an $e^+e^- \rightarrow \phi$ cross section of $4\ \mu b$ yields an expected rate of $400\ \phi's/sec$. In photoproduction, with a incident photon rate of $5 \cdot 10^8\ \gamma/sec$, a 30-cm long LH_2 target and a $\sigma_\phi = 0.5\ \mu b$, the rate of $\phi's$ is $300\ \phi's/sec$. In an e^+e^- collider the ϕ is produced with little background and is tagged by virtue of having the collision take place with $E_{positron} = E_{electron} = m_\phi/2$. In photoprodution the situation is not as clean. Many hadronic processes can take place. However one may be able to exploit the fact that the hadronic production at the ϕ mass is still dominated by the resonance. Indeed, a double-tagging may be employed by considering the dependence of the recoil proton angle *vs* momentum for the recoil proton as shown in Fig. 21. The plot shows the recoil proton for $\gamma p \rightarrow \phi p$ as well as for $\gamma p \rightarrow \rho^o p$ at *6 GeV* incident photons. The same production mechanism (i.e. Eq. 8) is assumed and the natural widths of the ρ and ϕ are included. It should not be difficult to use the combined measurement of the recoil proton momentum and angle, along with event-by-event photon information to kinematically identify the process $\gamma p \rightarrow \phi p$ as part of a first-level trigger.

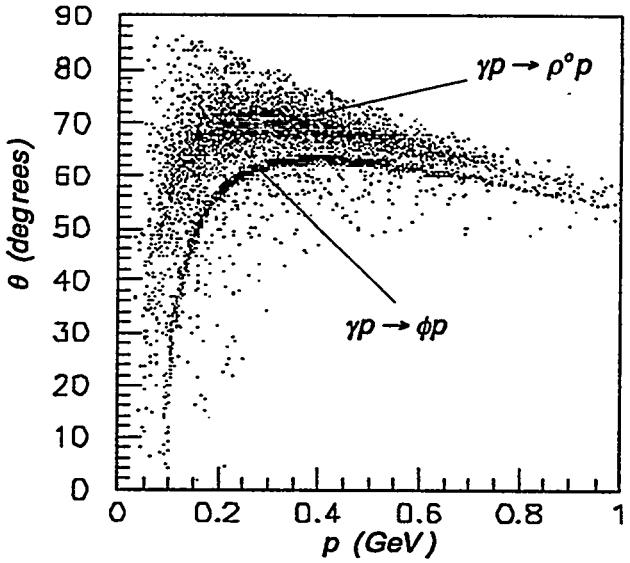


Fig. 21: *Recoil proton kinematics for 6 GeV incident photons*

The goals of the *ϕ factory* include CP and CPT studies. It is tempting to ask whether these studies could also be carried out in a complementary fashion in photoproduction at CEBAF.

---

[16] There are two excellent compedia of theoretical and experimental issues surrounding the physics at the *DAΦNE φ Factory: Proceedings of the Workshop on Physics and Detectors for DAΦNE* , ed. G. Pancheri, (1991) and *The DAΦNE Physics Handbook*, ed. L. Maiani, G. Pancheri and N. Paver, Two Volumes (1992). Both are published by Servizio Documentazione dei Laboratori Nazionali di Frascati.

Can the boost be exploited as in the case of the rare radiative decays ? Can one deal with the different background processes present in photoproduction ? Is it possible that a background can, in fact, be exploited ?

There is one aspect in which the boosted ϕ should definitely help. Referring to Section 3.4 above, the radiated photon in the insidious (for CP studies) decay: $\phi \rightarrow (K_S^o K_S^o \text{ or } K_L^o K_L^o)\gamma$, carries, at most, *24 MeV* of energy. For incident photon energies of *10 GeV*, this *24 MeV* photon is boosted to *480 MeV* and should be easily detectable if indeed this decay is problematic.

In the remainder of this Section several considerations for doing the physics of a stationary ϕ *factory* with a *flying* ϕ *factory* will be examined. It is important to state that these studies are very preliminary but so far the idea is one which probably warrants more studies. In March, 1994 a two-day *Flying* ϕ *Factory Workshop* was held in Bloomington, IN attended by about 50 physicists from Carnegie Mellon, Catholic U., CEBAF, Indiana U and the IUCF, U. of Notre Dame, Novosibirsk, Pittsburgh, Renssalaer Polytechnic, U. of Richmond, Serpukhov, Turin, U. of Virginia and the College of William and Mary. The Workshop uncovered a number of experimental questions and an interesting theoretical possibility to exploit s-wave backgrounds present in photoproduction.



Fig. 22: *A Logo*

Finally, in this age of media sound bites, a catchy name and logo are *de rigueur*. So putting first things first, we present our logo for the *Flying* ϕ *Factory (or the Fleeing Fee Factory,* depending on how you were instructed to pronounce the name of that Greek letter in your classical education) in Fig. 22.

4.2 CP and CPT Studies

In addition to [13] and the article appearing in [16], there have been a number of other articles written on CP, CPT and quantum mechanics tests at a ϕ factory. These include papers by I. Dunietz, J. Hauser and J. L. Rosner [17], C. D. Buchanan *et al* [18], D. Cline [19], P. Huet and M. Peskin [20] and V. A. Kostelecky and R. Potting [21].

---

[17] I. Dunietz, J. Hauser and J. L. Rosner, Phys Rev D35 (1987) 2166.

[18] C. D. Buchanan *et al*, Phys Rev D45 (1992) 4088.

[19] D. Cline, Comments Nucl Part Phys 20 (1992) 241.

[20] P. Huet and M. Peskin, SLAC-PUB-6454 (1994).

[21] V. A. Kostelecky and R. Potting, Nucl Phys B359 (1991) 545 and V. A. Kostelecky and R. Potting, Indiana University (Bloomington) Preprint 265 (1994) and references therein (1994).

The relevant ratio for CP studies is:

$$\frac{|\eta_{oo}|^2}{|\eta_{+-}|^2} = \frac{\Gamma(K_L \to \pi^o\pi^o)/\Gamma(K_L \to \pi^+\pi^-)}{\Gamma(K_S \to \pi^o\pi^o)/\Gamma(K_S \to \pi^+\pi^-)} \cong 1 - 6\,Re\left(\frac{\varepsilon'}{\varepsilon}\right) \qquad \textit{Eq. 10}$$

It is expected that at DAΦNE, ε/ε' will be measured with a precision of 10^{-4} in 1 to 3 years of running [13]. Of course, this ratio will also be measured by the KTeV experiment at Fermilab. Contributions which CEBAF could make in this area will probably come too late. However it is instructive to look at the problems in measuring this quantity. We assume that the decays involving π^o represent more of a challenge than those involving the charged π. Tagging a K_L by requiring that the decay distance exceed say $5 \cdot \beta\gamma c\tau_S$, where τ_s is the K_S lifetime, means we want to measure the proper time, τ, with a precision given by $\delta\tau/\tau_S < 1$. Our Monte Carlo studies, using photon showers from our LGD prototype data, indicate that $\delta\tau/\tau_S \approx 0.7$ for 2 *GeV* $K's$ with $1/p$ falloff.

These Monte Carlo studies also indicate that for a reasonable size detector our acceptance for seeing and analyzing all the photons from the CP-violating $K_S^o \to 2\pi^o$ + $K_L^o \to 2\pi^o$ to be of order 5 %. The transverse size of the detector is more or less fixed with a radius of 2 *m*. The target-to-detector distance depends on the incident energy. It appears that this distance scales linearly with incident photon energy and equal to *6 m* at *6 GeV* and *10 m* at *10 GeV* for a nearly constant acceptance.

The real advantage in studying $\phi \to K_L^oK_S^o$ is that the decay products are correlated. This can be used for CPT tests. In 1991, Kostelecky and Potting pointed out [21] that CPT can be spontaneously broken in a string theory at levels detectable in the $K\overline{K}$ system. The CPT violating parameter, δ (analogous to the CP violating parameter, ε) might be as large as 10^{-4}. To measure δ with sufficient precision in ϕ decays involving K_{l3} decays requires a number of $\phi's$ given by:

$$N_\phi = \frac{500}{\delta^2} \qquad \textit{Eq. 11}$$

This is statistically accessible at a ϕ *factory*.

4.3 s-Wave Background: A Boon or Bust ?

Consider the diagram of Fig. 23a showing ϕ followed by the decay $\phi \to K_L^oK_S^o$. The diagram of Fig. 23b shows direct s-wave $K_S^oK_S^o$ production. Based on measurements made by the authors of [22], we expect that the background under the ϕ in photoproduction to be of order 10^{-3} of the signal, or of the same order as CP violation. The s-wave background in $e^+e^- \to 2\gamma \to K_s^oK_s^o$ is negligibly small, about $4 \cdot 10^{-6}$ of the ϕ signal. Of course another way to produce the s-wave

$K_S^\circ K_S^\circ$ is through the radiative decay of the ϕ which will be present in both photoproduction and e^+e^- and distinguishable in the former but probably not the latter. At first glance, however, the s-wave production of $K^\circ\overline{K}^\circ$ in photoproduction could be a serious problem. However, N. Isgur and V. A. Kostelecky [23] are looking into the possibility of using s-wave/p-wave interference to enhance CP and CPT violating effects by interference of the amplitudes responsible for the latter with the amplitude for s-wave production. This work is in progress. It is interesting to note that the terms involving the interference of CP and CPT violating amplitudes with the s-wave could in fact be studied in some detail since in photoproduction the s-wave amplitude and the p-wave amplitude have some important differences: (1) the p-wave is fairly constant with energy while the s-wave falls off as $1/E_\gamma$; (2) the p-wave is amplitude is strongest in the very forward direction while the s-wave has a kinematic zero in the very forward directions; and (3) the decay angular distribution for the two is different.

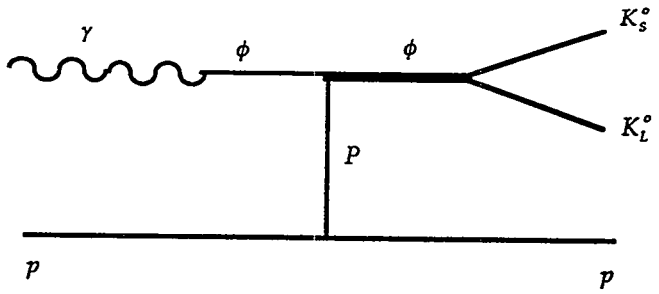


Fig. 23a: *p-wave production of $K_L^\circ K_S^\circ$*

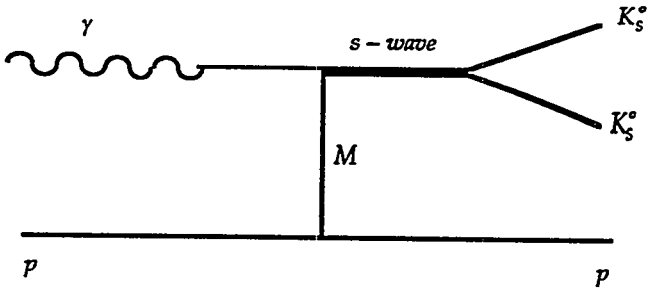


Fig. 23b: *s-wave production of $K_S^\circ K_S^\circ$*

---

[22] D. C. Fries *et al*, Nucl. Phys B143 (1978) 408.

[23] N. Isgur and V. A. Kostelecky, private communiation.

4.4 Photon Beams

The experiment described in Section 3 will use the tagged photon beam in Hall B. The photon tagger magnet optics is described in a note by D. Sober [24]. Tagged photon beams have advantages in being able to achieve high energies but the electromagneic background accompanying the beam can create problems for detectors (see the comment in Section 2.4)

An attractive alternative is to create a photon beam by Compton backscattering of laser beam from an electron beam. Much of what appears in this Section comes from conversations with B. Norum [25].

If a photon from a laser of energy E_ℓ is scattered off of an electron of energy E_e through an angle θ with respect to the incident beam electron direction the energy of the scattered photon E_γ is given by:

$$E_\gamma = \frac{E_\ell(E_e + p_e)}{E_e + E_\ell - (p_e - E_\ell)\cos\theta} \qquad Eq.\ 12$$

where p_e is the momentum of the beam electron.

The plot of maximum electron energy ($\theta = 0$) as a function of laser energy is shown in Fig. 24 for various energies of the electron beam. The dependence of the backscattered photon energy on laboratory angle is shown in Fig. 25. According to B. Norum, photon fluxes of 10^8 /sec are

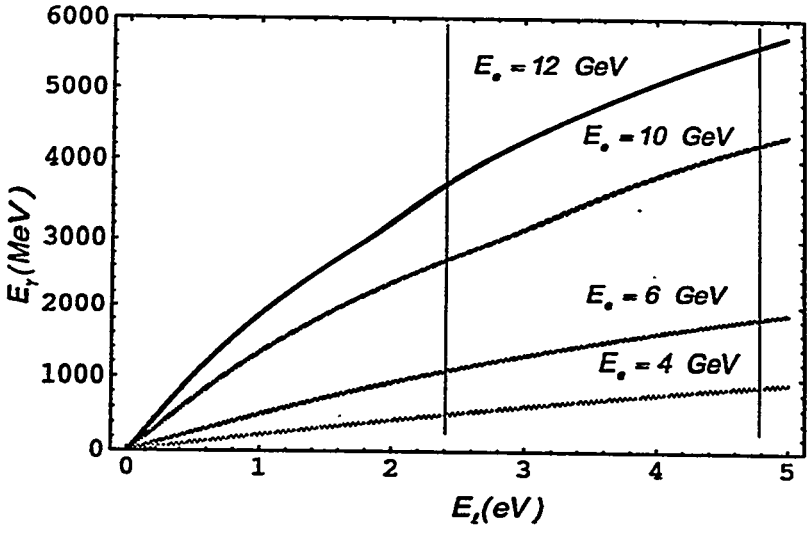


Fig. 24: *Backscattered photon energy (max) as a function of laser energy for various values of the beam energy. The first line corresponds to the 2.4 eV green line in an Ar-ion laser and the second line to a frequency doubled 2.4 eV line.*

[24] D. I. Sober, A Guide to the Optics of the Tagged Photon Magnet, CLAS Note 91-012

[25] Private conversations with B. Norum and B. E. Norum and T. P. Welch, An Intense Polarized Photon Source at CEBAF Hall B, Letter of Intent to the CEBAF PAC, 1993.

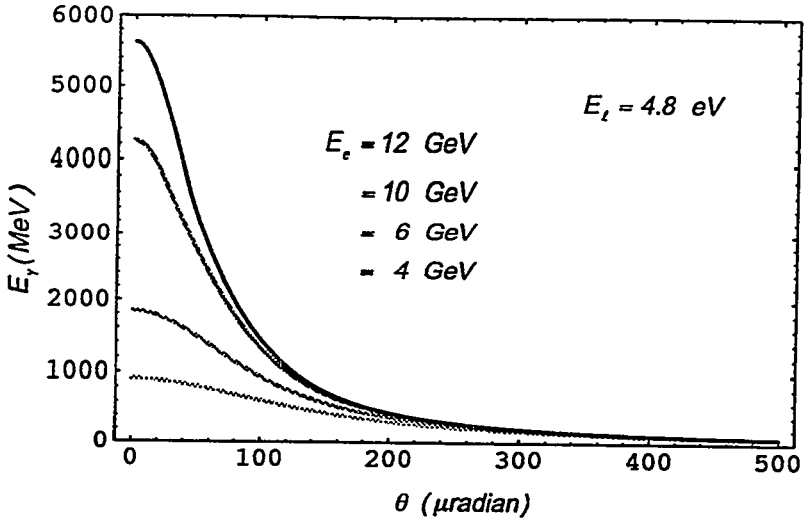


Fig. 25: *Backscattered photon energy as a function of angle with respect to the beam direction, assuming a frequency doubled laser line of 4.8 eV.*

available at the highest energies (refer to Fig. 24) if: (1) electron currents are of the order of *3 μA;* (2) the laser power is *10 W* at *256 nm* (coherent doubling of *512 nm*); (3) high quality mirrors can be developed at *256 nm;* and (4) multiple (2-3) lasers can be used. There are many advantages including (1) 100 % tagging efficiency; (2) all the photons available are in the energy region of interest; (3) there is little background; and (4) the tagger is simpler. It may also be possible to exploit the polarization of the photon beam. A disadvantage is that such a beam requires better shielding of the beam dump to handle the higher currents.

5. Conclusions

Photoproduction of mesons at CEBAF offers the possibility of making real contributions to meson spectroscopy by searching for new states or states which need confirmation. Production of states with incident photons in particular explores the spin 1 and $s\bar{s}$ sectors. The latter is especially important in understanding which states to assign to conventional $q\bar{q}$ nonets and which states may be extraneous and therefore are candidates for non-$q\bar{q}$ states. *The energy upgrade is important.* With incident photon energies between *10 and 12 GeV,* states can be produced with good acceptance. Although charged and neutral detection is desirable, at least for initial studies in a tagged photon beam, a neutral detector can access many states.

There is still a lot to be learned about the light vector mesons (ρ, ω, ϕ) and in this area CEBAF can make important contributions because of the high rates. Rare radiative decays of the ϕ can be studied with initial CEBAF electron energies. Rare radiative decays of the ρ and ω can also be explored. The boosted ϕ is an important factor. However beyond the initial studies improvements can be made by adding charged particle detection. This is especially true for the $\phi \to \eta'\gamma$ decay. An all-neutral experiment can only probe $\eta' \to 2\gamma$, which has a small branching ratio (2 %) and $\eta' \to \eta\pi^\circ\pi^\circ$ which will be difficult for the first stage experiment because of

acceptance. Charged particle detection and momentum analysis may mean that it is important to use a backscattered laser beam.

The backscattered laser beam is an exciting possibility and here the energy upgrade is essential, coupled with progress in lasers and mirrors. This may be the key to doing clean experiments with photons at CEBAF.

Much work needs to be done yet to determine whether or not photoproduction of the ϕ can be used at CEBAF to complement the CP and CPT studies planned for e^+e^- colliders but so far the idea is worth pursuing. More Monte Carlo work is needed on pattern recognition and regeneration effects. The virtue of the boost in accurately pinning down the K decays and thereby helping in K_L^o identification may also be important. The exploitation of s-wave/p-wave interference may prove very important. Other possible experiments using this correlated source of $K^o\overline{K}^o$ should be explored. For example, one could use a K_L^o trigger to look for rare decays of the K_S^o.

Acknowledgements

I want to thank my experimentalist colleagues at Indiana for many fruitful discussions and their generosity with ideas especially Ray Crittenden and Scott Teige. Brian Kern did much of the Monte Carlo work in exploring the flying ϕ factory idea. The beautiful results obtained to date with the E852 LGD are due to the cleverness and hard work of Ben Brabson, Ray Crittenden, Jeff Gunter, Rob Lindenbusch, Matt McKerley, Dave Rust, Paul Smith, Eric Scott, Thom Sulanke, Scott Teige and Zach Ziliak. I have also had many conversations with and have received a lot of encouragement from Alan Kostelcky. John LoSecco worked hard in understanding the acceptance issues for the rare radiative ϕ decay experiment and was generous in sharing his results. My thanks to Blaine Norum for information about backscattered laser beams. I also thank all those who attended the Workshop in Bloomington in early March, especially Eugene Solodov and Julia Thompson. I appreciate the kind invitation to speak at the Energy Upgrade Workshop. Ted Barnes, Jim Napolitano and Paul Stoler did a great job in organizing the meeting. Finally, it is always a pleasure to talk physics with Nathan Isgur.

ISSUES IN LIGHT MESON SPECTROSCOPY: THE CASE FOR MESON SPECTROSCOPY AT CEBAF

Stephen Godfrey
Ottawa-Carleton Institute for Physics
Department of Physics, Carleton University, Ottawa CANADA K1S 5B6

ABSTRACT

I review some outstanding issues in meson spectroscopy. The most important qualitative issue is whether hadrons with explicit gluonic degrees of freedom exist. To answer this question requires a much better understanding of conventional $q\bar{q}$ mesons. I therefore begin by examining the status of conventional meson spectroscopy and how the situation can be improved. The expected properties of gluonic excitations are discussed with particular emphasis on hybrids to give guidance to experimental searches. Multiquark systems are commented upon as they are likely to be important in the mass region under study and will have to be understood better. In the final section I discuss the opportunities that CEBAF can offer for the study of meson spectroscopy.

1. Introduction

It is twenty years since the birth of Quantum Chromodynamics [1], the theory of the strong interactions, and it is not yet clear what the physical states of the theory are. This is an extraordinary statement that we still cannot answer such a basic and fundamental question. Although there is growing evidence for the existence of hadrons with no valence quark content or with an excited glue degree of freedom, we still do not really know if such states exist. An analogy in QED might be not knowing whether positronium existed or not. Clearly we cannot say that we understand QCD until these questions are answered. We have a powerful tool to better understand QCD through the the interplay of theory and experiment. A better understanding of QCD, a non-Abelian gauge theory, will also lead to a better understanding of other non-Abelian gauge theories such as the standard model of the electroweak interaction.

Since it is possible that it may be further decades before we have a thorough theoretical understanding of QCD in the low Q^2 confinement region, we must rely heavily on the insights we can gain from experiment and QCD based models. To a large extent our understanding of hadron structure is based on the constituent quark model in which mesons are made of a quark and antiquark and baryons are made of three quarks [2,3]. However, an important consequence of QCD is the expectation that *exotic* hadrons beyond the naive quark model should also exist; *hybrids, glueballs*, and $q\bar{q}q\bar{q}$ states. Perhaps the discovery of such *exotica* will help us understand *Soft QCD*. The problem is that although there are several exotic meson candidates, no exotic has

been unambiguously identified. What has happened to them? Answering this question has become the major preoccupation of hadron spectroscopists. In this contribution I review the expected properties of *conventional* and *exotic* mesons and how these states might be studied at CEBAF.

As an operational definition I will refer to states predicted by the constituent quark model as *conventional* hadrons and those lying outside the quark model as *exotic* hadrons. I emphasize, however, that there is nothing fundamental about the quark model and the physical states of the theory should be based on the gauge invariant operators one can construct in QCD and will in general include gluonic excitations [4]. Nevertheless, states predicted by the quark model are the only ones that have been unambiguously identified. Finding new types of hadronic matter — the *hybrids* which have constituent quarks and an excited glue degree of freedom and *glueballs* which have no valence quark content what-so-ever [5] is the most important qualitative question in hadron spectroscopy. A serious impediment to the discovery of such states is the sad shape of hadron spectroscopy. In particular, none of the light meson spectra is well mapped out for either orbital or radial excitations. There are also numerous puzzles in light meson spectroscopy, for example, the scalar meson puzzle, the nature of the $f_1(1420)$ and the $f_0(1720)$, and the g_T mesons. The first priority is to sort out light meson spectroscopy so that we have a template against which to compare exotic candidates.

Despite the shape of conventional meson spectroscopy it is the discovery of gluonic excitations in the hadron spectrum which is the most important issue in hadron spectroscopy as it will signify a qualitative difference with the quark model. The primary purpose of the next generation of hadron experiments should be to discover glueballs, hybrids, and other exotic hadrons. There are numerous models describing such states with important qualitative differences so that the discovery of exotics is important to distinguish between the different models and make progress in understanding *soft* QCD.

2. Conventional Mesons

The Quark Model is 30 years old! It is a useful tool for understanding hadron spectroscopy but we still don't understand why it works. To make progress we need to fill in some of the missing states so that we can either verify the model, find out where it needs to be refined, or possibly show it is wrong. In our quest for *exotic* hadrons we should not forget that *conventional* $q\bar{q}$ mesons can also tell us much about the nature of confinement. For example, the linear Regge trajectories of orbitally excited mesons is a consequence of the linear confining potential [6] and the splittings of orbitally excited multiplets reflects the Lorentz structure of the confining potential [7]. The better we understand hadrons, the more we can test the quark model and ultimately, better understand QCD.

2.1. Quark Model vs Experiment

In the constituent quark model conventional mesons are bound states of a spin $\frac{1}{2}$ quark and a spin $\frac{1}{2}$ antiquark bound by a phenomenological potential which reflects the properties of QCD. The quark and antiquark spins combine to give total spin $\vec{S} = \vec{S}_q + \vec{S}_{\bar{q}} = 0,\ 1$ which is coupled to the orbital angular momentum L to give states

Table 1. The quantum numbers of the conventional $q\bar{q}$ mesons.

		J^{PC}	I=1	I=0 $(n\bar{n})$	I=0 $s\bar{s}$	Strange
L=0	S=0	0^{-+}	π	η	η'	K
	S=1	1^{--}	ρ	ω	ϕ	K^*
L=1	S=0	1^{+-}	b_1	h	h'	K_1
	S=1	0^{++}	a_0	f_0	f_0'	K_0^*
		1^{++}	a_1	f_1	f_1'	K_1
		2^{++}	a_s	f_2	f_2'	K_2^*
L=2	S=0	2^{-+}	π_2	η_2	η_2'	K_2
	S=1	1^{--}	ρ_1	ω_1	ϕ_1	K_1^*
		2^{--}	ρ_2	ω_2	ϕ_2	K_2
		3^{--}	ρ_3	ω_3	ϕ_3	K_3^*
.	.	.	.	.	.	.
.	.	.	.	.	.	.
.	.	.	.	.	.	.

of total angular momentum $\vec{J} = \vec{L} + \vec{S}$ resulting in $J = L,\ L-1,\ L,\ L+1$. This leads to meson parity and charge conjugation given by

$$P = (-1)^{L+1} \text{ and } C = (-1)^{L+S} \tag{1}$$

resulting in the meson states of Table 1.

A meson with $J^{PC} = 1^{-+}$ would be forbidden in the constituent quark model and since quarks have charge either $+2/3$ or $-1/3$ a doubly charged meson, m^{++}, is also forbidden as a *conventional* meson state.

Since we cannot at this point calculate hadron properties from first principles we must rely on QCD motivated models to help interpret experimental resonances. Although there are many models in the literature the constitutent quark model has the greatest success in describing hadron properties. In these models mesons are described by a Schrödinger equation

$$H = T + V_{q\bar{q}} \tag{2}$$

where $V_{q\bar{q}}$ is the effective quark-antiquark potential which consists of a spin-independent confining potential and spin-dependent terms. The confining potential is typically of the form:

$$H^{conf} = -\frac{4}{3}\frac{\alpha_s(r)}{r} + br \tag{3}$$

where the first term comes from one-gluon-exchange and the second term is the linear confining potential. The Coulomb piece dominates at short distance becoming more and more important with increasing quark mass while the linear piece dominates at large distance, becoming more important for the light quark mesons. This is illustrated in Fig. 1 where the rms radii of various mesons are indicated on a plot of a QCD motivated

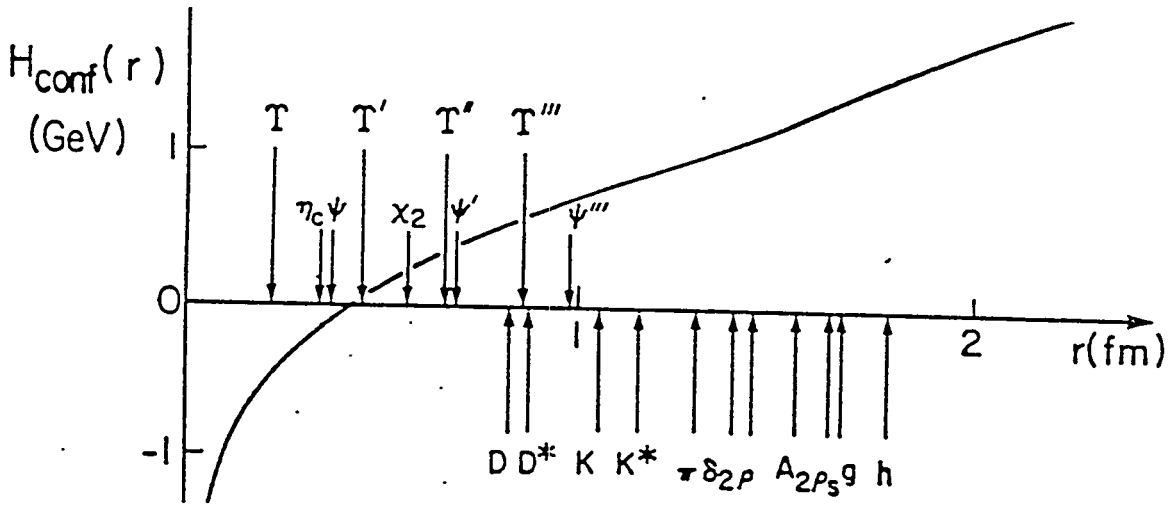


Fig. 1. The $q\bar{q}$ potential.

potential. One sees that mesons composed of the heavy b quarks are relatively small and sit in the Coulombic region of the potential, while the lighter mesons sit in the linear region of the potential. Thus, the study of mesons constructed out of light quarks act as a probe of confinement.

The phenomenological spin dependent Hamiltonian is of the form:

$$H_{spin} = H_{ij}^{hyp} + H_{ij}^{s.o.(cm)} + H_{ij}^{s.o.(tp)} \tag{4}$$

where

$$H_{ij}^{hyp} = \frac{4}{3}\frac{\alpha_s(r)}{m_i m_j}\left\{\frac{8\pi}{3}\vec{S}_i\cdot\vec{S}_j\,\delta^3(\vec{r}_{ij}) + \frac{1}{r_{ij}^3}\left[\frac{3\vec{S}_i\cdot\vec{r}_{ij}\vec{S}_j\cdot\vec{r}_{ij}}{r_{ij}^2} - \vec{S}_i\cdot\vec{S}_j\right]\right\} \tag{5}$$

is the colour hyperfine interaction,

$$H_{ij}^{s.o.(cm)} = \frac{4}{3}\frac{\alpha_s(r)}{r_{ij}^3}\left(\frac{1}{m_i}+\frac{1}{m_j}\right)\left(\frac{\vec{S}_i}{m_i}+\frac{\vec{S}_j}{m_j}\right)\cdot\vec{L} \tag{6}$$

is the spin-orbit colour magnetic piece arising from the one-gluon exchange and

$$H_{ij}^{s.o.(tp)} = -\frac{1}{2r_{ij}}\frac{\partial V(r)}{\partial r_{ij}}\left(\frac{\vec{S}_i}{m_i^2}+\frac{\vec{S}_j}{m_j^2}\right)\cdot\vec{L} \tag{7}$$

is the spin-orbit Thomas precession term where $V(r)$ is the interquark potential. In these formulae $\alpha_s(r)$ is the running coupling constant of QCD.

The colour hyperfine interaction is responsible for ${}^3S_1 - {}^1S_0$ splitting in $\rho-\pi$, K^*-K, and $J/\Psi-\eta_c$. The spin-orbit and tensor piece of the hyperfine interaction

break the degeneracy of the orbitally excited multiplets. The spin-orbit interaction has two contributions, $H_{ij}^{s.o.(cm)}$ and $H_{ij}^{s.o.(tp)}$. Since the hyperfine term is relatively short distance, it becomes less important for higher orbital excitations. Multiplet splittings then become a measure of the spin-orbit splittings, with contributions of opposite sign coming from the short range Lorentz vector one-gluon-exchange and the long range Lorentz scalar linear confinement potential. The ordering of states within a multiplet of given orbital angular momentum gives information on the relative importance of the two pieces. For example, for the L=1 strange meson multiplet, the quark model predicts $M(^3P_2) > M(^3P_1) > M(^3P_0)$. i.e. the $J = L + 1$ member of the multiplet is more massive than the $J = L - 1$ member. In contrast, for the $L = 4$ multiplet, the quark model predicts $M(^3G_3) > M(^3G_4) > M(^3G_5)$ so now the ordering is inverted with the $J = L - 1$ member more massive than the $J = L + 1$. The reason for this is that higher L mesons have larger radii so the linear part of the potential is more important than the short distance Coulomb piece. Although the details of this inversion are model dependent, the inversion is a general property of QCD motivated potential models. Thus the multiplet splittings act as a probe of the confinement potential so that the study of excited light quark system, such as ones with high orbital angular momentum, provides information on non-perturbative QCD.

In what follows, for purposes of illustration, I will compare experimental data to the results of the particular model with which I am most familiar and which constitutes a comprehensive calculation of meson properties [8,9]. Let us start with the strange meson spectrum which is shown if Fig. 2. The spectrum is as rich as any in atomic physics with a beautiful regularity and numerous transitions, either electromagnetic transitions or strong transitions via π or ρ emission. There is good agreement for the masses of the leading orbital excitations which supports the picture of a linear confinement potential. The $^3S_1 - ^1S_0$ splitting is much smaller than the splitting between the ^3P_J centre of gravity and the $^1P_1$ state which is consistent with the expected properties of short distance one-gluon-exchange and a Lorentz scalar confining potential. A Lorentz vector confining potential would lead to comparable splittings for $^3S_1 - ^1S_0$ and $^3P_J - ^1P_1$. The information decreases as we go to the higher orbitally excited multiplets and for radial excitations. A similar pattern is obtained for the $s\bar{s}$ mesons except that they are even more sparsely mapped out than the strange mesons.

The status of of light meson spectroscopy is summarized in Fig. 3. Starting with the P-wave multiplets, which is the multiplet most filled, we find that even it is not well understood. The scalar mesons (0^{++}) are in a state of confusion due to the possible interpretation of the $a_o(980)$ and $f_0(980)$ as $q\bar{q}q\bar{q}$ states[10-12]. In the 1^{++} sector the $f_1(1420)$ has long been considered to be the $^3P_1$ $s\bar{s}$ meson. Recently the LASS group discovered another state [13] which appears a more likely candidate, the $f_1(1530)$. Finally, the $^1P_1$ $s\bar{s}$ state (h_1') is yet to be confirmed. Turning to the higher mass multiplets, there is good agreement for the masses of the leading orbital excitations between the quark model and experiment supporting the picture of linear confinement. In general, however, the radially excited and orbitally excited mesons are even less understood than the P-waves. In particular, for the $s\bar{s}$ states there is very little known above the $L = 1$ multiplet. Some of my assignments (or lack of assignments) in Fig. 3 are subject to debate but this lack of a consensus underlines the fact that far too little

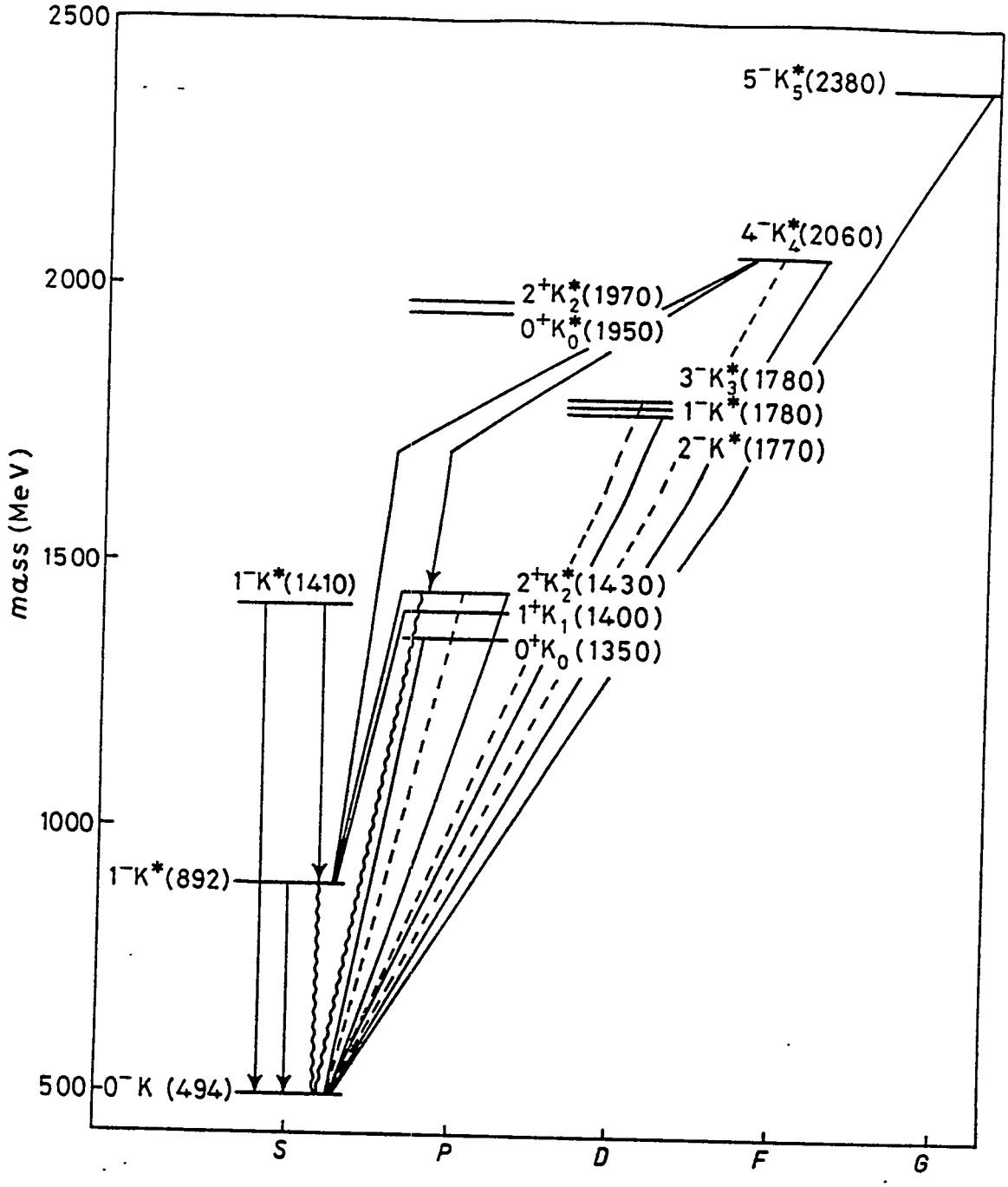


Fig. 2. The level diagram for strange mesons. The wavy lines represent γ emission, the solid lines represent π emission and the dashed lines ρ emission.

is known about light meson spectroscopy. Without completing at least some of these multiplets we can hardly say we understand the meson spectrum.

2.2. Some Puzzles in Mesons

In addition to the obvious searches for the missing mesons there are numerous puzzles in meson spectroscopy which may be hints of new types of hadronic matter. I will only mention some of them here and refer the interested reader to other contributions and to the literature for a more detailed account [14-16].

The $\eta(1440)$ (formerly the $\iota(1440)$) is seen in the gluon rich J/ψ radiative decay the ι and is therefore a prime candidate for a glueball [5]. It is now believed to be three separate states; two 0^{-+} and a 1^{++} [15]. Two isoscalar radially excited pseudoscalars (2^1S_0) are expected to lie in this mass region so until we obtain a more complete understanding of the 2^1S_0 nonet the issue will remain cloudy. Another problem adding to the general confusion involves the misidentification of the $E(1420)$.

The $f_0(1750)$ (formerly the $\theta(1750)$) is also seen in J/ψ radiative decay to $K\bar{K}$ making it another glueball candidate [5]. Although a number of 2^{++} states, both radially excited P-waves and orbitally excited F-waves are expected, none seem to fit the θ. Further evidence for its exotic character is the fact that it was not seen in $K\bar{K}$ by the LASS group. Dooley, Swanson and Barnes speculate that the θ is a linear combination of loosely bound $K^*\bar{K}^*$ and $\omega\phi$ pairs [17].

The $f_1(1420)$ (formerly the E(1420)) has for a long time thought to be the 1^3P_1 $J^{PC} = 1^{++}$ $s\bar{s}$ meson. Recently the LASS group established the existence of another axial vector meson at about 1530 MeV which appears to be a much stronger candidate for this state [13]. If this is the case what is the E(1420)? and does this puzzle have anything to do with the the $\iota(1440)$ puzzle? Both states lie just above $K^*\bar{K}$ threshold and perhaps we are again seeing some manifestation of multiquark physics.

There are numerous puzzles besides the ones just mentioned. For instance what is the explanation of the g_T 2^{++} tensor mesons seen at Brookhaven in $\pi p \to K\bar{K}$ [18]? Are they glueballs or are they conventional mesons or do they have a totally different explanation? Above, I mentioned that the 0^{++} $\delta(980)$ and $S^*(980)$ mesons are thought to be $K\bar{K}$ molecules. If this is indeed the case where are the $^3P_0$ $q\bar{q}$ states? Recently, candidates for the $^3P_0$ $q\bar{q}$ states have been observed but they have yet to be confirmed.

There are clearly many puzzles remaining in meson spectroscopy which require both detailed experimental and theoretical study.

2.3. Hunting Missing States

Given our unsatisfactory knowledge of light meson spectroscopy how do we find the missing states and solve some of the puzzles? One can see from Fig. 3 that as we go to higher mass the number of states multiply rapidly so that in general we will have to find the missing states in a large background of other states. It is therefore highly unlikely that we will have any success in unravelling the spectroscopy by bump hunting. Rather, we will need high statistics experiments to perform partial wave analysis to filter by J^{PC} quantum numbers. To assist us in this process a guide to the expected properties will be useful and we refer to quark model predictions for the expected masses and decay modes [8,9]. This can give us insight into why some states are missing and

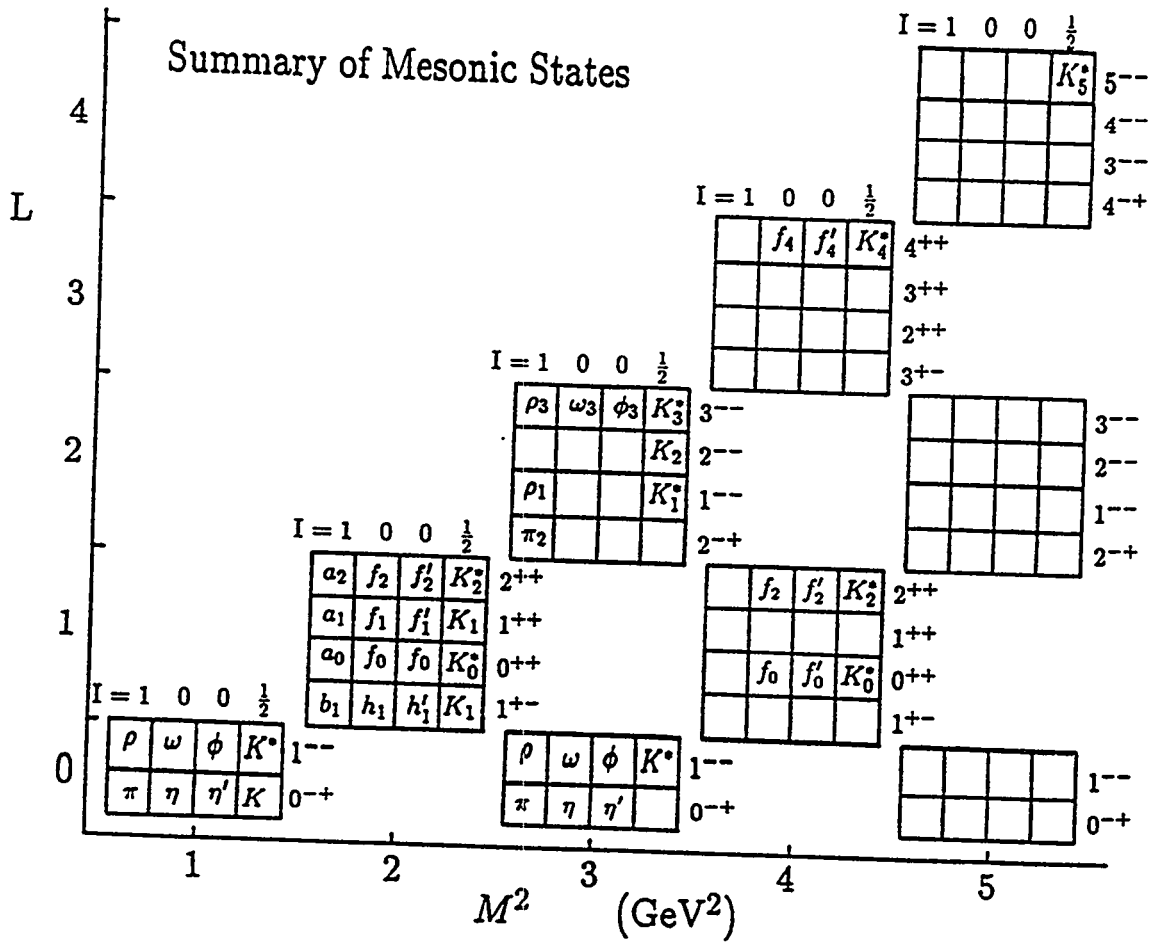


Fig. 3. Summary of mesonic states with light quarks.

how to look for them. As an example of what such a search would entail we examine some missing states whose quark model predictions are listed in Tables 2 and 3.

Starting with the $\eta_2(1^1D_2)$ we expect it to be almost degenerate in mass with its non-strange isoscalar partner, the π_2 (formerly the $A_3(1680)$). From Table 2 we see that it is expected to be rather broad and it decays predominantly through the a_2 isobar which in turn decays to $\rho\pi$. The final state is expected to have 4π's making it rather complicated to reconstruct the original η_2 resonance. The $\rho_2(1^3D_2)$ will also decay dominantly to a 4π final state. The ω_2 decays to the simpler $\rho\pi$ final state with a moderate width but since it has a similar mass as the $\pi_2(1680)$ which also decays to $\rho\pi$ it is possible that it is masked by the π_2. The $s\bar{s}$ states, the $\eta_2'(1^1D_2)$ and the $\phi_2(1^3D_2)$, are both relatively narrow and one would expect that they would have been observed. In fact the LASS group has recently reported seeing them in $K\bar{K}\pi$. The likely reason that they have been so difficult to find is that they are produced rather weakly. The strange mesons, the $K_2(1^1D_2)$ and the $K_2(1^3D_2)$ lie at around 1800 MeV. They decay to some relatively simple channels and are predicted to have a moderate width. It is possible that they have been sited as the $L(1770)$'s. The final state in the table is the broad 1^{--} ω_1. Structure has been seen in this mass region but the experimental situation is likely confused due to the nearby broad 2^3S_1 1^{--} state which is expected to lie at around 1450 MeV and overlaps and interferes with the 1^3D_1 state.

One can perform a similar analysis of other multiplets. In Table 3 I give the expected properties of some orbitally and radially excited mesons. As listed, most of these states appear to be relatively narrow with dominant branching ratios to simple final states. There are candidates for several of these states. For example, an f_2 is observed with mass 1810 MeV, width $\sim$ 200 MeV (with large uncertainties) and with $BR(f_2 \to \pi\pi) \sim 20\%$. Although the observed mass is consistent with the quark model predictions, the predicted width is at least a factor of two small. This discrepancy might be due to additional decay modes not considered in the analysis, which only includes two body modes, or it may reflect the sensitivity of the decay widths to the details of the meson wavefunction where a slight shift in the node of the $2P$ wavefunction or possibly mixing with nearby states, can have a large effect on the decay width. Similarly, the observed mass of the $K_2^*(1980)$ agrees with the quark model prediction and the decay properties are not inconsistent with the quark model ($\Gamma^{theory} \simeq 150$ MeV vs $\Gamma^{expt} \simeq 240$ MeV). Therefore, the predictions of Table 3 should be taken as a rough guide to the expected properties of radially excited P-wave mesons and until they are more fully tested against experiment they should not be taken too literally. In addition, there is a need for further theoretical work, to try to understand more complicated decay modes, and model dependent effects on the meson properties.

2.4. Future Directions

From the preceeding sections we conclude that we need a far better understanding of meson spectroscopy before we can say that we understand it and before we can exclude conventional interpretations of an exotic candidate with conventional quantum numbers. The first step is to find some of the missing states. It will be important to fill in both the orbitally excited multiplets and the radially excited multiplets. These missing states will lie in a large background of other states. To find them, results from the LASS spectrometer group show us that we will need unprecedented statistics along

Table 2. Quark Model predictions for the propeties of the missing L=2 mesons. The masses and widths are given in MeV. The masses come from Ref. 8 and the widths from Ref. 9.

Meson State	Property	Prediction
$\eta_2(1^1D_2)$	Mass	1680
	width	~ 400
	$BR(\eta_2 \to a_2\pi)$	$\sim 70\%$
	$BR(\eta_2 \to \rho\rho)$	$\sim 10\%$
	$BR(\eta_2 \to K^*\bar{K} + c.c.)$	$\sim 10\%$
$\eta_2' (1^1D_2)$	Mass	1890
	width	~ 150
	$BR(\eta_2' \to K^*\bar{K} + c.c.)$	$\sim 100\%$
$K_2 (1^1D_2)$	Mass	1780
	width	~ 300
	$BR(K_2 \to K^* f(1280))$	$\sim 30\%$
	$BR(K_2 \to \rho K)$	$\sim 20\%$
$\omega_1 (1^3D_1)$	Mass	1660
	width	~ 600
	$BR(\omega_1 \to B\pi)$	~ 70 %
	$BR(\omega_1 \to \rho\pi)$	$\sim 15\%$
$K_2 (1^3D_2)$	Mass	1810
	width	~ 300
	$BR(K_2 \to K^*(1420)\pi)$	~ 50 %
	$BR(K_2 \to K^*\pi)$	~ 30 %
$\rho_2 (1^3D_2)$	Mass	1700
	width	~ 500
	$BR(\rho_2 \to [a_2\pi]_S)$	$\sim 55\%$
	$BR(\rho_2 \to \omega\pi)$	$\sim 12\%$
	$BR(\rho_2 \to \rho\rho)$	$\sim 12\%$
$\omega_2 (1^3D_2)$	Mass	1700
	width	~ 250
	$BR(\omega_2 \to \rho\pi)$	~ 60 %
	$BR(\omega_2 \to K^*\bar{K})$	~ 20 %
$\phi_2 (1^3D_2)$	Mass	1910
	width	~ 250
	$BR(\phi_2 \to K^*\bar{K} + c.c.)$	$\sim 55\%$
	$BR(\phi_2 \to \phi\eta)$	$\sim 25\%$

Table 3. Quark Model predictions for the properties of some of the N=2 P-wave mesons. The masses and widths are given in MeV. The masses come from ref. 8 and the widths from ref. 9.

Meson State	Property	Prediction
$a_2(2^3P_2)$	Mass	1820
	width	~ 140
	$BR(a_2 \to \rho\pi)$	$\sim 70\%$
	$BR(a_2 \to \eta\pi)$	$\sim 10\%$
	$BR(a_2 \to K\bar{K})$	$\sim 10\%$
	$BR(a_2 \to \eta'\pi)$	$\sim 10\%$
	$BR(a_2 \to K^*\bar{K})$	$\sim 10\%$
$a_2(1^3F_2)$	Mass	2050
$f_2\ (2^3P_2)$	Mass	1820
	width	~ 90
	$BR(f_2 \to \pi\pi)$	$\sim 50\%$
	$BR(f_2 \to K\bar{K})$	$\sim 20\%$
	$BR(f_2 \to K^*\bar{K})$	$\sim 15\%$
$f_2\ (1^3F_2)$	Mass	2050
$f_2'\ (2^3P_2)$	Mass	2040
	width	~ 110
	$BR(f_2' \to K\bar{K})$	$\sim 35\%$
	$BR(f_2' \to \eta\eta)$	$\sim 10\%$
	$BR(f_2' \to \eta'\eta)$	$\sim 10\%$
	$BR(f_2' \to K^*\bar{K})$	$\sim 43\%$
$f_2'\ (1^3F_2)$	Mass	2240
$K_2^*\ (2^3P_2)$	Mass	1940
	width	~ 150
	$BR(K_2^* \to K\pi)$	$\sim 20\%$
	$BR(K_2^* \to K^*\pi)$	$\sim 20\%$
	$BR(K_2^* \to \rho K)$	$\sim 20\%$
	$BR(K_2^* \to K^*\pi)$	$\sim 20\%$
$K_2^*\ (1^3F_2)$	Mass	2150

with a partial wave analysis to filter the J^{PC} quantum numbers.

We will also need to develop new experimental and theoretical techniques to study broad resonances. From the experimental side it is clear that it will not be easy to identify a broad resonance in a background of other broad resonances and in the presence of new production thresholds. From the theoretical side most quark model calculations have treated mesons in the valence quark limit without considering the influence of coupling to production and decay channels. We are at the point in our understanding that these effects can no longer be ignored as they can make significant changes to the observed hadron masses and decay properties. These effects are starting to be examined by Barnes, Swanson, and Weinstein [19,20] . In addition, we can no longer ignore final state interactions. Some progress has been made on this problem by Barnes and Swanson [21]. It will be necessary to understand how to obtain observed cross sections starting with the underlying spectrum when decay channel coupling is taken into account along with final state interactions of the decay products.

3. Gluonic Excitations [5]

The complication in QCD which makes it so difficult to solve is the presence of boson-boson interactions required by gauge invariance which in perturbation theory gives rise to rather complicated three and four-boson couplings. Although it is difficult to extract physical properties from the QCD Lagrangian it is these gluon self couplings which lead to the belief that gluons play a dual role in QCD; as mediators of the strong force as in the conventional $q\bar{q}$ mesons and qqq baryons, and as constituents in glueballs and hybrids. The problem at present is that it is not even clear what the correct degrees of freedom are for soft QCD so that the predictions of the different models must be viewed with caution. Nevertheless, the discovery of glueballs or hybrids would be an important advance in our understanding QCD in the "soft" region.

In searching for glueballs and hybrids there are two ways of distinguishing them from conventional states:

1. To look for an excess of observed states over that predicted by the quark model. For this method to succeed we need a very good understanding of conventional mesons so that we can rule out a conventional interpretation of a newly found state. The previous section has shown the difficulties of this approach given our incomplete knowledge of conventional mesons and the general confusion in the 1.5 to 2.5 GeV mass region.

2. Search for exotic quantum numbers which would signal states that cannot be conventional quark model states.

Both approaches require a knowledge of expected glueball and hybrid properties which we will examine in what follows.

We begin by sketching out two models of soft QCD whose results we will use in what follows. The qualitative differences of these models stresses our ignorance of the low Q^2 regime of QCD.

3.1. *The Bag Model [22-26]*

In the bag model [26] hadrons are viewed as a region of space enclosing a fixed number of quarks and gluons with the model made Lorentz invariant by the addition of a surface pressure term, B_0, to the Lagrangian density. Inside the bag the quark fields, ψ, obey the free Dirac equation along with the boundary conditions that; 1) there is no colour current through the bag surface (S), and 2) pressure balance determines the bag surface.

$$\begin{aligned} (\not{p} - m)\psi = 0 \quad & \text{inside S} \\ \psi = 0 \quad & \text{outside S} \end{aligned} \tag{8}$$

The lowest energy solutions have quarks in $1S_{1/2}$, $1P_{1/2}$, $1P_{3/2}$ eigenmodes. Gluons in the Bag obey the free Helmholtz equation subject to the same boundary conditions.

$$\begin{aligned} (\nabla^2 + \omega^2)\vec{A}^a = 0 \quad & \text{inside S} \\ \vec{A}^a = 0 \quad & \text{outside S} \end{aligned} \tag{9}$$

The solutions are the transverse electric (TE) and transverse magnetic (TM) cavity resonator modes with $J^{PC} = 1^{+-}$ and $J^{PC} = 1^{--}$ respectively. In the zeroth order bag model, the mass of a hadron is simply the sum of the quark and gluon constituent energies and the energy of the bag itself. To go beyond the zeroth order bag model involves including contributions from gluon exchange [22,23].

3.2. *The Flux Tube Model*

The flux tube model of hadrons [27,28] is based on the strong coupling limit of QCD [29] with its parameters fixed from the familiar meson and baryon sectors. The significant difference between the flux tube approach and the bag model approach is that the eigenstates of the strong coupling limit of (lattice) QCD consist of, not quarks and gluons as in the bag model, but quarks on lattice sites connected by arbitrary paths of flux links or in the absence of quarks, of arbitrary closed loops of flux (glueloops). It is assumed that the flux tube picture survives departures from the strong coupling limit or in other words, that the flux tubes do indeed form a reasonable set of basis states, and that the adiabatic treatment of the flux tubes in the presence of quark motion is reasonable.

In this picture the string states define adiabatic quark potentials analogous to the nuclear potentials in molecular physics where adiabatic surfaces are defined for the nuclear motion based on the faster moving electronic potentials. We should then expect a tower of quark states built on each string adiabatic surface. This is illustrated pictorially in Fig. 4. In the flux tube model conventional hadrons correspond to gluonic fields in the ground states.

3.3. *Pure Glue States*

Both the bag model and flux tube model expect that hadrons will exist with no valence quark content at all. The predictions for glueball masses vary considerably from calculation to calculation. I use the flux tube model predictions as a guide because of their agreement with lattice calculations [29,30]. These are shown in Fig. 5. The flux

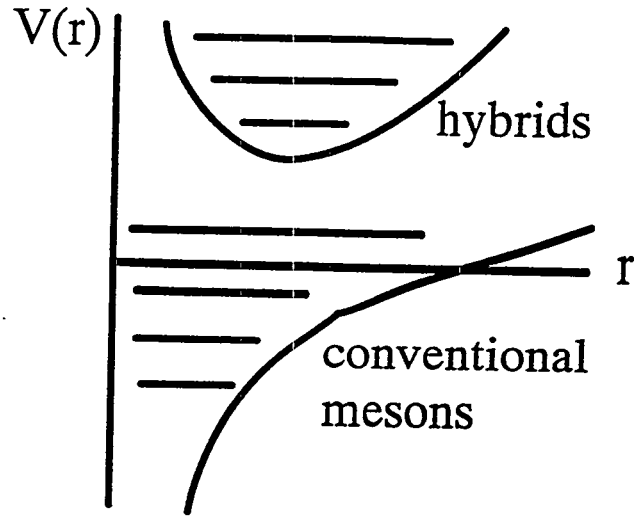


Fig. 4. The adiabatic quark potentials of the flux tube model.

tube model predicts that the lowest glueloop (glueball) is a 0^{++} at 1.5 GeV with all other states above 2 GeV and the lowest J^{PC} exotic at around 2.5 GeV. For comparison, the bag model predictions are considerably lower with $M_{0^{++},2^{++}} = 1$ GeV, $M_{0^{++},2^{++}} = 1.6$ GeV, and $M_{0^{-+},2^{-+}} = 1.3$ GeV. Because of the uncertainty in the scalar meson sector it seems likely that it would be very difficult to distinguish a scalar meson from the poorly understood conventional mesons*. More generally, it will be difficult to unambiguously determine that any state with conventional quantum numbers is a glueball due to the dense background of conventional mesons. The best bet will then be to find glueballs with exotic quantum numbers. Unfortunately these states are all expected to have mass greater than 2.5 GeV and so will be difficult to find. In addition, from the CEBAF point of view, glueballs are not expected to couple strongly to either photons or vector mesons so are likely to be difficult to produce at CEBAF. Glueballs therefore do not seem to be the best place to start our search for gluonic hadrons.

3.4. Hybrid Mesons

From our previous discussion it appears that the most fruitful method to search for hybrids is to search for states with quantum numbers inconsistent with quark model predictions.

The first step in this approach is to enumerate the hybrid J^{PC} quantum numbers. To do this in a model independent manner obeying gauge invariance we form gauge invariant operators [32,33] from a colour octet $q\bar{q}$ operator and a gluon field strength.

$$O = (\bar{\psi}\Gamma\frac{\lambda_a}{2}\psi) \otimes (\vec{E}^a \text{ or } \vec{B}^a) \tag{10}$$

*Although the excess of scalar mesons beyond the quark model predictions is seen as evidence for glueballs in this sector

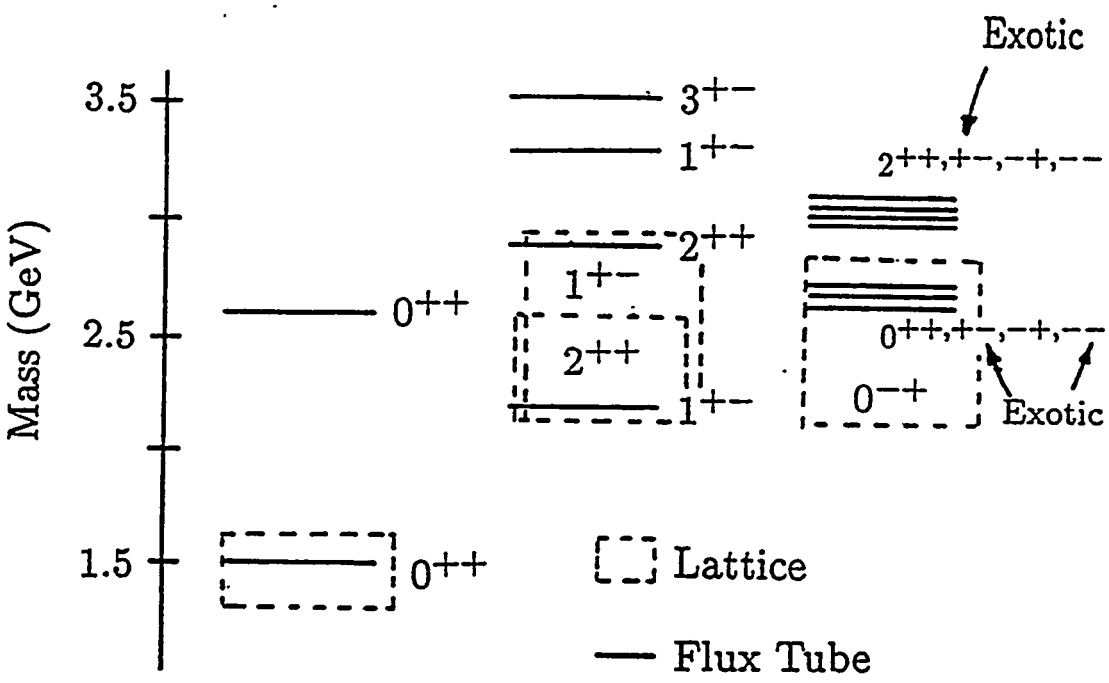


Fig. 5. The low lying glueball mass spectrum. The flux tube results come from ref. 27 and the lattice results from ref. 31.

The resulting composite operator, known as an interpolating field, is equally applicable to all approaches, from the Bag-model to the flux tube model in addition to more rigorous lattice gauge theory calculations. For example the interpolating field for the 1^{-+} state is given by $(\bar{\psi}\vec{\gamma}\psi)\times\vec{B}$ and for the 2^{+-} by $(\bar{\psi}\vec{\gamma}\gamma_5\psi)\otimes\vec{B}$. The quantum numbers of the low lying hybrids are given by:

$$\begin{array}{cccc} 2^{++} & 2^{-+} & \underline{2^{+-}} & 2^{--} \\ 1^{++} & \underline{1^{-+}} & 1^{+-} & 1^{--} \\ 0^{++} & 0^{-+} & \underline{0^{+-}} & \underline{0^{--}} \end{array}$$

Higher J operators can also be constructed but presumably they are higher in mass and more difficult to produce. The underlined $q\bar{q}g$ states have exotic quantum numbers not present in the constituent quark model. If these exotic states are sufficiently low in mass and do not have exceedingly large widths they could provide the *smoking gun* evidence for hybrids which we are seeking: Their discovery would unambiguously signal hadron spectroscopy beyond the quark model.

3.4.1. Hybrid Masses

Bag Model Predictions: To make hybrids we combine a colour octet gluon with a $q\bar{q}$ pair in a colour octet to obtain a colour singlet:

$$(q\bar{q})_8 \times g_8 = (q\bar{q}g)_1 + \ldots.$$

The lowest $q\bar{q}g$ hybrid meson multiplets are constructed from a colour octet $q\bar{q}$ with $J^{PC} = 0^{-+}$ or 1^{--}, each in the $J^{PC} = (1/2)^+$ mode, and a gluon in the lightest TE mode with $J^{PC} = 1^{+-}$ resulting in the following lowest lying hybrids;

$$2^{-+},\ 1^{-+},\ 1^{--},\ 0^{-+}.$$

The SU(3) flavour quantum numbers of a hybrid are those of the component $q\bar{q}$ pair so that hybrid mesons span the familiar SU(3) flavour nonets. However, the I=0 and I=1 states are not degenerate because in the isoscalar hybrids, the relative ease of internal annihilation of the $q\bar{q}$ pair which is already in a colour octet, shifts the mass.

Some representative results of bag model calculations of the hybrid spectrum which include spin-dependent forces due to gluon exchange [22-24] are shown in Fig. 6 along with constituent quark model predictions for conventional mesons. Different calculations are in reasonable agreement for the splittings but differ on the multiplet mass. The 0^{-+}, 2^{-+}, and 1^{--} hybrid nonets are near in mass to $q\bar{q}$ states with the same quantum numbers which can result in considerable mixing. This can only confuse the situation when determining if a state is a hybrid or conventional meson. Thus, the discovery of such states would be difficult to be convincing because they are also candidates for conventional states.

Flux Tube Model Predictions: There are two types of hybrids in this model, vibrational hybrids which correspond to excitations of the quantum string into higher

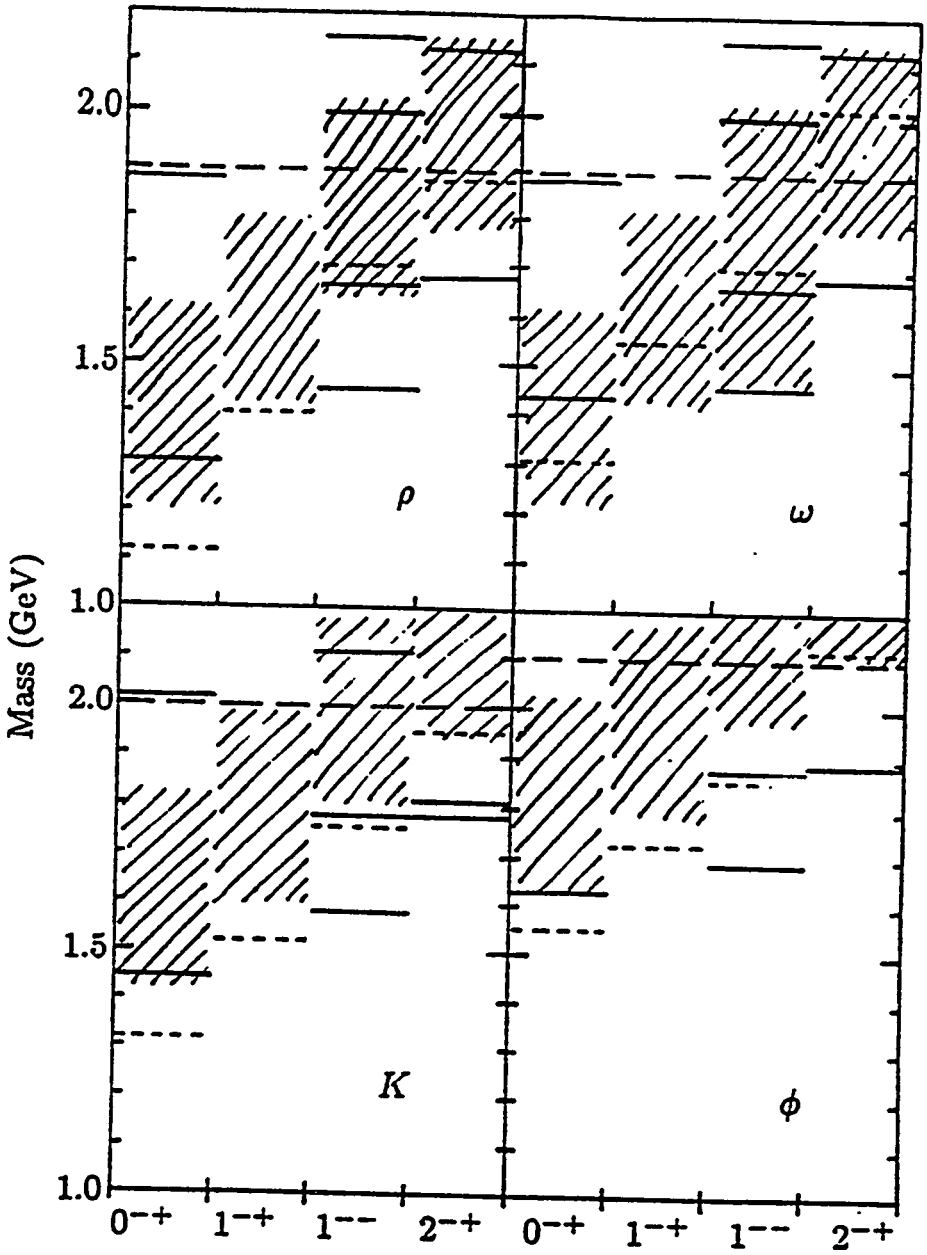


Fig. 6. Hybrid mass predictions. The short dashed lines are the bag model predictions of Barnes Close and deViron, ref. 22. The shaded region are the bag model predictions of Chanowitz and Sharpe for a range of values of the quark and gluon self energies, ref. 23. The long dashed lines are the flux tube model predictons of Isgur and Paton, ref 27. The solid lines are the conventional $q\bar{q}$ predictions of the relativized quark model, ref. 8.

string normal modes, and topological hybrids which have more complicated string topologies and correspond to higher energy adiabatic surfaces. The latter are expected to be much higher in energy so we will not discuss them further.

The adiabatic potentials are characterized by mode occupation numbers with a polarization index and a string mode index. The first excited state is doubly degenerate with phonons of tranverse vibration with $\sigma = \pm 1$ angular momentum about the $q\bar{q}$ axis. When combined with spin we get the 8 nearly degenerate nonets of hybrid mesons:

$$J^{PC} = 0^{\pm\mp} \quad 1^{\pm\mp} \quad 2^{\pm\mp} \quad 1^{\pm\pm}$$

with masses approximately 1.9 ± 0.1 GeV for hybrids with no strange quark content. Among these states are three J^{PC} exotic nonets with nine neutral members having $J^{PC} = 2^{+-}$, 1^{-+}, and 0^{+-}. These results should be contrasted to the bag model where there is no such degeneracy because the TM mode is much higher in mass than the TE mode. These results are compared to bag model results in Fig. 6.

3.4.2. Hybrid Decays

In the previous section we came to the conclusion that the most promising approach for finding hybrids is to look for ones with exotic quantum numbers. Even so, there are numerous states to consider so, for the sake of brevity, we take the $\hat{\rho}$ and $\hat{\phi}$ 1^{-+} exotics as examples. Possible decays are given by:

$$\begin{aligned}
\hat{\rho} &\rightarrow [\underline{\pi\eta}, \underline{\pi\eta'}, \pi\rho, K^*\bar{K}, \eta\rho, \ldots]_P \\
&\rightarrow [\pi b_1, \pi f_1, \eta a_1, K K_1 \ldots]_S \\
\hat{\phi} &\rightarrow [\underline{\eta\eta'}, k\bar{K}(1400), K^*\bar{K}, \ldots]_P \\
&\rightarrow [\bar{K} Q_2]_S \\
&\rightarrow [\bar{K} Q_1]_D
\end{aligned} \tag{11}$$

The underlined decays to two distinct pseudoscalars in a relative P-wave is a unique signature of the 1^{-+} state.

Given this long list of decays we turn to the various models for guidance to which modes are likely to be dominant. One would naively expect S-wave mesons in the $\pi\eta$ or $\pi\rho$ channels to be dominant due to the large available phase space. However, a common feature of the various models is the selection rule that the gluonic excitation cannot usually transfer its angular momentum to the final state meson pairs as relative angular momentum but must instead appear as internal orbital angular momentum of the $q\bar{q}$ pairs.† This eliminates $\pi\eta$, $\pi\rho$, $\pi\eta'$, $\eta\rho$, $\eta\eta'$, and $K^*\bar{K}$. The selection rule suppresses the decay channels which would likely be large and may make hybrids stable enough to appear as conventional resonances while at the same time explaining why hybrids with exotic J^{PC} have yet to be seen; they do not couple strongly to simple final states.

In particular, in the Bag model the dominant decays occur when the valence gluon forms a colour octet $J^{PC} = 1^{+-}$ $q\bar{q}$ pair in which either q or $\bar{q}$ is in a P-wave

†I note however, that this selection rule does not appear to be absolute.

mode. The bag then contains two $q\bar{q}$ colour octets which after rearrangement fall apart into $q\bar{q}$ singlets, one in an S-wave ground state with $J^{PC} = 0^{-+}, 1^{--}$ and the other in an L=1 $J^{PC} = (0,1,2)^{++}, 1^{+-}$, i.e. $J^{PC} = 1^{-+} \rightarrow \pi f_1$ or ηa_1.

The flux tube model also predicts that the low lying hybrids will decay preferentially to final states with one ground state S-wave and one excited P-wave meson; $b_1(1235)\pi$, $a_2(1320)\pi$, $K_2^*(1420)\bar{K}$, $\pi(1300)\pi, \ldots$, rather than two ground state mesons like $\pi\pi$, $\rho\pi$, $K\bar{K}$. The reason for this is that the relative coordinates of the two final state mesons are parallel to the initial meson axis and so cannot absorb the unit of string angular momentum about the initial meson axis. Hence the string angular momentum is absorbed as an internal meson orbital angular momentum and the selection rule is broken for final states with different spatial wavefunctions [34]. The flux tube model expects stronger coupling to final states with one S-wave and one P-wave final state meson.

The flux tube model predictions are listed in Table 4. The flux tube model predicts that the $\hat{a}_2$, $\hat{a}_0$, and $\hat{f}'_0$ are probably too broad to appear as resonances. The $\hat{\omega}_1$ decays mainly to $[a_1\pi]_S$ and $[\pi(1300)\pi]_P$ with $\Gamma \sim 100$ MeV which would make it difficult to reconstruct the original hybrid given the broad widths of the final state mesons. Similar problems also make the $\hat{\phi}_1$ difficult to find. According to the flux tube model the best bets for finding hybrids are: $\hat{\rho}_1$, $\hat{f}_2$, $\hat{f}_0$, and $\hat{f}'_2$.

What we conclude from all this is that the favoured final states all contain broad P-wave mesons. To reconstruct the original resonance an isobar analysis will be essential and to do this we will again need unprecedented statistics to pull a signal from the background.

4. Multiquark States

Multiquarks are discussed in detail in the contribution of Weinstein [20]. Here I comment briefly on some points relevant to meson spectroscopy. Upon considering $qq\bar{q}\bar{q}$ systems we find that the colour couplings are not unique as they are in mesons and baryons and whether or not multiquark states exist is a dynamical question. It is possible that multiquark states exist as bound states [35] but it is also possible that $qq\bar{q}\bar{q}$ configurations lead to meson-meson potentials [12]. Both must be taken into account when attempting to unravel the meson spectrum.

A study of the J^{PC} sector of the $qq\bar{q}\bar{q}$ system found that weakly bound $K\bar{K}$ "molecules" exist in the isospin zero and one sectors in analogy to the deuteron. It was suggested that these two bound states be identified with the $f_0(975)$ and $a_0(980)$ (the S^* and δ). The meson-meson potentials which come from this picture, when used with a coupled channel Schrodinger equation, reproduce the observed phase shifts for the δ and S^* in $\pi\pi$ scattering [12]. The $K\bar{K}$ molecules are the exception however, as the model predicts that in general the $qq\bar{q}\bar{q}$ ground states are two unbound mesons.

There is evidence that meson-meson potentials must be considered in other processes as well. In the reaction $\gamma\gamma \rightarrow \pi^+\pi^-$ the meson-meson potentials are needed along with $q\bar{q}$ resonances to reproduce the $\gamma\gamma \rightarrow \pi^+\pi^-$ cross section data [36]. Enhancements in the production of low invariant mass $\pi\pi$ pairs have been observed in a number of processes; $\eta' \rightarrow \eta\pi\pi$, $\psi' \rightarrow J/\psi\pi\pi$, $\Upsilon(nS) \rightarrow \Upsilon(mS)\pi\pi$, and $\psi \rightarrow \omega\pi\pi$. Similar enhancements have also been seen in some $K\pi$ channels in $\bar{p}p \rightarrow K\bar{K}\pi$. The conclusion

Table 4. The dominant decays of the low-lying exotic hybrid mesons. From ref. 28.

Hybrid State	$[\text{decay mode}]_{\text{L of decay}}$	Partial Width (MeV)
$\hat{a}_2^{+-}(1900)$	$\rightarrow [\pi a_2]_P$	450
	$\rightarrow [\pi a_1]_P$	100
	$\rightarrow [\pi h_1]_P$	150
$\hat{f}_2^{+-}(1900)$	$\rightarrow [\pi b_1]_P$	500
$\hat{f'}_2^{+-}(2100)$	$\rightarrow [K\bar{K}_2^* + c.c.]_P$	250
	$\rightarrow [\bar{K}Q_2 + c.c.]_P$	200
$\hat{\omega}_1^{-+}(1900)$	$\rightarrow [\pi a_1]_{S,D}$	100,70
	$\rightarrow [\pi\pi(1300)]_P$	100
	$\rightarrow [\bar{K}Q_2 + c.c.]_S$	100
$\hat{\rho}_1^{-+}(1900)$	$\rightarrow [\pi b_1]_{S,D}$	100, 30
	$\rightarrow [\pi f_1]_{S,D}$	30, 20
$\hat{\phi}_1^{-+}(2100)$	$\rightarrow [\bar{K}Q_1 + c.c.]_D$	80
	$\rightarrow [\bar{K}Q_2 + c.c.]_S$	250
	$\rightarrow [\bar{K}K(1400) + c.c.]_P$	30
$\hat{a}_0^{+-}(1900)$	$\rightarrow [\pi a_1]_P$	800
	$\rightarrow [\pi h_1]_P$	100
	$\rightarrow [\pi\pi(1300)]_S$	900
$\hat{f}_0^{+-}(1900)$	$\rightarrow [\pi b_1]_P$	250
$\hat{f'}_0^{+-}(2100)$	$\rightarrow [\bar{K}Q_1 + c.c.]_P$	800
	$\rightarrow [\bar{K}Q_2 + c.c.]_P$	50
	$\rightarrow [\bar{K}K(1400) + c.c.]_S$	800

drawn from these examples is that final state interactions arising from meson-meson potentials will play a central role in understanding the 1 to 3 GeV mass region. So far only pseudoscalar mesons in the final state have been considered so the next logical step is to extend the analysis to vector-vector and pseudoscalar-vector channels. Perhaps these multiquark effects are the key to the E/ι and θ puzzles.

5. Meson Spectroscopy at CEBAF

CEBAF offers a number of possibilities for studying meson spectroscopy using high intensity photon beams incident on nuclear targets. Using the CEBAF electron beam high energy photons can be produced by either bremstrahlung through a thin radiator or backscattering a high powered laser from the incident electron beam (a "Compton Collider"). The resulting photon energy will be close to the original beam energy resulting in center of mass energies ranging from $\sim$ 4 GeV for an 8 GeV electron beam to $\sim$ 4.8 GeV for a 12 GeV incident electron beam. The photons can be used to photoproduce meson resonances covering the poorly explored region of 2 to 4 GeV where many conventional and non-conventional mesons are expected to lie. In particular, the lowest lying hybrid mesons which are expected at around 2 GeV.

The basic production mechanism is that, through vector meson dominance, the photon has vector meson components such as the ρ, ω, and ϕ so that the nucleon target is interacting with the vector meson component of the photon. There are numerous ways that the vector meson can then interact with the nucleon target to produce excited final state mesons which differ primarily by the t-channel exchange mechanism. These are illustrated in Fig. 7. Excited states can be produced via diffraction — the exchange of a (colourless) pomeron; inelastic production where the original target nucleon is excited into, say, an N^*; and charge exchange where a charged pion is exchanged in the t-channel so that the target nucleon is excited into, for example, a Δ^{++}. In addition, the photon can interact as a photon through Primakof production where, the photon excites a t-channel π to produce the final state meson. Finally, the photon can interact with a t-channel photon to produce a final state resonance via two photon fusion. Taken together CEBAF offers a wide range of complementary production mechanisms which can help decipher the underlying meson structure.

Because the photons have a relatively large $s\bar{s}$ content they are a good source of strangeonium states. Because the s-quark is intermediate in mass between the heavier c and b quarks where we believe that quark potential models are reasonable approximations to QCD and the lighter u and d quarks where relativistic effects make the naive quark models suspect, strangeonium spectroscopy provides a useful bridge between these two extremes. Thus, CEBAF can add considerably to our knowledge of both the radially excited and orbitally excited strangeonium states which are important for our understanding of soft QCD.

In addition, it has been speculated that photoproduction experiments are a good place to search for hybrids [28]. The basic idea is that the glue in the vector mesons is excited by the t-channel particle exchange to produce a hybrid meson. However, detailed calculations of this production mechanism do not presently exist and are only now being performed [37].

In summary, CEBAF offers some interesting production mechanisms for mesons. With the extremely high intensity of the electron beam, and hence of the photon

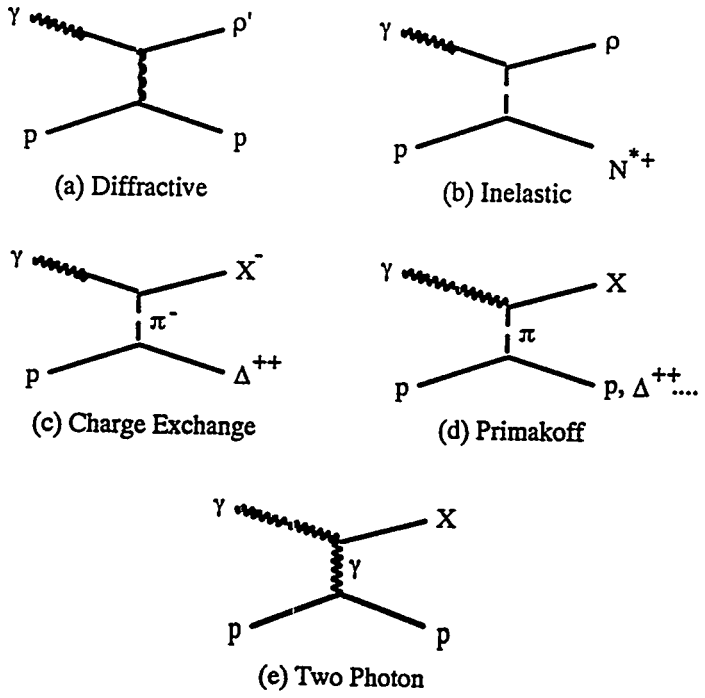


Fig. 7. Meson production mechanisms at CEBAF.

beam it offers the possibility of the very high statistics needed for the next generation of meson spectroscopy experiments. It may turn out that CEBAF will be the long awaited KAON factory.

6. Final Comments

I hope I have demonstrated that meson spectroscopy is an extremely rich subject with fundamental unanswered questions. Our present knowledge of hadron spectroscopy is a very shaky foundation on which to base our understanding of QCD. At present it is not even clear what the relevant degrees of freedom are for describing this regime of QCD. The first step to understanding *soft* QCD is to find the missing conventional $q\bar{q}$ states. Until we understand conventional hadrons better it will be very difficult to make progress in finding evidence for the gluonic degree of freedom in the hadron spectrum which is the outstanding issue.

Although it is conceivable that hybrid states with non-exotic quantum numbers could be identified as being excess states beyond those predicted by the quark model, given the very broad range of predictions for hybrid masses, I very much doubt that this is the most fruitful approach. It is more likely that, to be successful, a hybrid search should focus on the exotic properties of hybrids which would offer unambiguous evidence of new physics. The most uncontroversial such characteristic is that all models agree that one of the lowest hybrids will have exotic J^{PC} quantum numbers 1^{-+} with mass about 1.6 ± 0.3 GeV. The presence of a resonance signal in this channel would be

strong evidence for the discovery of a hybrid so it seems sensible that this be the place to begin any experimental search.

One should appreciate that the study of $q\bar{q}$, hybrids, glueballs, and $qq\bar{q}\bar{q}$ is an indivisable subject since they are all governed by the same theory — QCD, and require the same experiments. To unravel the meson spectrum in the 1 to 3 GeV mass region will take unprecedented statistics. It is important that many hadron properties be studied in many different channels. CEBAF has an important role in meson physics. Because of the high $s\bar{s}$ content of the photon it will be able to produce large numbers of $s\bar{s}$ states significantly improving our incomplete knowledge of this sector. CEBAF also offers the possibility of discovering hybrid mesons which would provide evidence for gluonic excitations in mesons.

ACKNOWLEDGEMENTS

I would like to thank the organizers of the Workshop on CEBAF at Higher Energies for the invitation to participate in a very lively and enjoyable meeting. In particular, I would like to thank Ted Barnes and Jim Napolitano for their kind invitation to speak. I am looking forward to many future meetings on meson physics at CEBAF. This work was supported by the Natural Science and Engineering Research Council of Canada.

References

1. M. Fritzch, M. Gell-Mann, and H. Leutwyler, Phys. Lett. **47B**, 365 (1971); D.J. Gross and F. Wilczek, Phys. Rev. **D8**, 3497 (1973); S. Weinberg, Phys. Rev. Lett. **31**, 494 (1973).
2. G. Zweig, CERN preprint 8419/TH.412; 8182/Th.401 (1964; unpublished); M. Gell-Mann, Phys. Lett. **8**, 214 (1964).
3. For an overview of the current status of the quark model see S. Godfrey, *The Constituent Quark Model: A Status Report* Nuovo Cimento **102A**, 1 (1989).
4. R.L. Jaffe, K. Johnson, and Z. Ryzak, Ann. of Phys. **168**, 344 (1986).
5. For reviews of the subject see for example: S. Godfrey, *Mesons, Hybrids, and Glueballs: The Search for New Forms of Hadronic Matter*, Zeit. Phys. **C46**, S93 (1990); T. Barnes, *The Exotic Atoms of QCD: Glueballs, Hybrids, and Baryonia*, proceedings of the School of Physics of Exotic Atoms, Erice Sicily, 1984; *The Bag Model and Hybrid Mesons*, proceedings of the SIN School of Strong Interactions, Zuoz Switzerland, SIN report (1985); M. Chanowitz, *Meson Spectroscopy Viewed from J/ψ Decay: Gluonic States at BEBC*, Proceedings of the Charm Physics Symposium, eds. M.-H. Ye and T. Huang (Gordon and Breach, New York, 1987); F. Close, *Gluonic Hadrons*, Rep. Prog. Phys. **51**, 833 (1988); S. Godfrey, *An Overview of Hybrid Meson Phenomenology*, proceedings of the BNL Workshop on Glueballs, Hybrids, and Exotic Hadrons, ed. S.-U. Chung, Upton New York, 1988 (AIP, New York, 1989); N. Isgur, *Hadron Spectroscopy: An Overview with Strings Attached, ibid.*
6. S. Godfrey, Phys. Rev. **D31**, 2375 (1985).
7. S. Godfrey, Phys. Lett. **162B**, 367 (1985).
8. See S. Godfrey and N. Isgur, Phys. Rev. **D32**, 189 (1985); **D34**, 899 (1986) and references therein.
9. R. Kokoski and N. Isgur, Phys. Rev. **D35**, 907 (1987).

10. R.L. Jaffe, Phys. Rev. **D15**, 267,281 (1977); **D17**, 1444 (1978).
11. J. Weinstein and N. Isgur, Phys. Rev. Lett. **48**, 659 (1982); Phys. Rev. **D27**, 588 (1983).
12. J. Weinstein and N. Isgur, University of Toronto report, UTPT-89-03 (1989; unpublished).
13. D. Aston *et al.* Phys. Lett. **B201**, 573 (1988).
14. S.U. Chung, these proceedings.
15. S.U. Chung, Z. Phys. **C46**, S111 (1990).
16. A thorough review of meson spectroscopy is given by S.U. Chung and S. Godfrey, in preparation.
17. K. Dooley, E.S. Swanson, and T. Barnes, Phys. Lett. **B275**, 478 (1992).
18. A. Etkin *et al.* Phys. Lett. **B201**, 568 (1988).
19. T. Barnes, E.S. Swanson, and J. Weinstein, ORNL-CCIP-92-06, UTK-92-4, UMS/HEP 92-021 (1992); T. Barnes and E.S. Swanson, Phys. Rev. **D46**, 131 (1992).
20. J. Weinstein, these proceedings.
21. T. Barnes and E.S. Swanson, MIT-CTP-2026, ORNL-CCIP-91-23, UTK-91-08 (1991).
22. T. Barnes, F.E. Close, and F. deViron, Nucl. Phys. **B224**, 241 (1983).
23. M. Chanowitz and S.R. Sharpe, Nucl. Phys. **B222**, 211 (1983).
24. M. Flensberg, C. Peterson, and L. Sköld, Z. Phys. **C22**, 293 (1984).
25. For earlier work see P. Hasenfratz, R.R. Horgan, J. Kuti, and J.M. Richard, Phys. Lett. **95B**, 299 (1980); F. de Viron and J. Weyers, Nucl. Phys. **B195**, 391 (1981).
26. A. Chodos *et al.*, Phys. Rev. **D9**, 3471 (1984); T. de Grand *et al.* Phys. Rev. **D12**, 2060 (1975).
27. N. Isgur and J. Paton, Phys. Lett. **124B**, 247 (1983); Phys. Rev. **D31**, 2910 (1985).
28. N. Isgur, R. Kokoski, and J. Paton, Phys. Rev. Lett. **54**, 869 (1985).
29. See for instance J. Kogut, Rev. Mod. Phys. **51**, 659 (1985); **55**, 775 (1983); M. Creutz, *Quarks, Gluons, and Lattices*, Cambridge University Press (Cambridge, 1983).
30. G. Schierholz, *Status of Lattic Glueball Mass Calculations*, proceedings of the BNL Workshop on Glueballs, Hybrids, and Exotic Hadrons, ed. S.-U. Chung, Upton New York, 1988 (AIP, New York, 1989).
31. C. Michael and M. Teper, Univ. of Oxford preprint (1988).
32. T. Barnes, *The Bag Model and Hybrid Mesons*, proceedings of the SIN School of Strong Interactions, Zuoz Switzerland, SIN report (1985).
33. For a more thorough discussion see R.L. Jaffe, K. Johnson, and Z. Ryzak, ref. 4.
34. The selection rule was first pointed out by the Orsay group in the context of constituent gluon models.
35. R.L. Jaffe, Phys. Rev. **D15**, 267, 281 (1977); **D17**, 1444 (1978).
36. T. Barnes, K. Dooley, and N. Isgur, Phys. Lett. **183B**, 210 (1987).
37. H. Blundell and S. Godfrey, in progress.

Exotic Meson Spectroscopy with CLAS

Gary Adams and Jim Napolitano
Physics Department, Rensselaer Polytechnic Institute
Troy, NY 12180

The identification and study of mesons with explicit gluonic degrees of freedom will provide major constraints on nonperturbative QCD and models thereof. CLAS will provide a unique opportunity for studying these resonances by measuring photoproduction of multi-meson final states.

1. Introduction

In this paper we will define "exotic" mesons to be those which have bound gluons in their constituent wave functions, including those which have quantum numbers that are incompatible with a simple $q\bar{q}$ assignment. Such states are predicted by QCD because gluons carry color quantum numbers. It is this property which adds much of the complexity to QCD and results in an attractive interaction between two gluons, and between gluons and quarks. The states which offer the best chance of detection are hybrid mesons with $q\bar{q}g$ structure, and low mass glueballs, gg. These are predicted to lie in the mass range 1.3 - 2.5 GeV.[1-10]

Experimental work on meson spectroscopy essentially stopped after large pieces of the conventional spectrum had been mapped out, and therefore only a few experiments have been devoted to searching for exotic states. The work of the GAMS [11] and VES [12] collaborations are particularly noteworthy since they report evidence for new states with unusual quantum numbers, $J^{PC}= 1^{-+}$, which are excited in $\pi^-p\rightarrow\pi\eta N$ at 1.235 and 1.318 GeV, respectively. These are transverse-electric hybrid candidates. BNL experiment E818 also has low statistics results which hint at 1^{-+} strength going to $f_1(1285)\pi$, at 1.6-2.2 GeV.[13] Two recent BNL experiments are searching for exotic mesons which decay to neutral channels (E852) and to $\phi\phi$ (E881). Only two papers offer pertinent data from photon induced reactions: Atkinson, et al.[14] see evidence for a new state around 1.9 GeV which decays to $b_1(1235)\pi$ (see below) but were unable to identify quantum numbers, and Condo, et al. [15] have identified a state at 1.77 GeV decaying to $\rho\pi$ which has $J^{PC}= 1^{-+}$, 2^{-+}, or 3^{++}. If 1^{-+} is the proper assignment then this is an exotic meson.

The glueball sector is no better understood than the exotic hybrids. The low lying 0^{++} spectrum is rather crowded, with at least one state between 1.0 and 1.5 GeV likely to be the lowest glueball. Lindenbaum et al. [16] have identified three 2^{++} states which are high enough in energy to decay to $\phi\phi$ by measuring $\pi^-p\rightarrow\phi\phi n$. Since this is an OZI suppressed channel it seems likely that at least some of these are not excited by quark exchange, and are therefore glueball candidates. Also, the low lying glueballs, transverse-magnetic hybrids, and conventional mesons all have "conventional" quantum numbers so one must rely on measured transition strengths to help distinguish the states.

The excitation of exotic mesons remains one of the most fundamental tests of non-

perturbative QCD remaining to be performed. More specifically, the masses and coupling strengths of the exotic mesons will provide needed input into the numerous models of non-perturbative QCD. Very little work has been done on exotic-meson searches with photon beams. For photon energies above a few GeV the hadronic components of the photon propagator become apparent. The Vector Meson Dominance approximation shows that a large part of the beam can be thought of as a beam of low-mass vector mesons ρ,ω, and ϕ. In this sense photons are unique because they carry spin-1 and couple readily to all quark flavors. These features of diffractive photoproduction will be useful in searching for exotic mesons.

2. Transverse-electric Hybrids

The masses and decay channels of the hybrid mesons have been extensively studied in the flux-tube model.[3-5] In this model the vibrational spectrum of an excited gluon flux tube couples to a conventional quark anti-quark state to produce hybrid mesons. Of particular interest is a spectrum of nine low-lying I=0,1 states between 1.9 and 2.2 GeV which have quantum numbers that cannot be formed from a quark-antiquark pair. They arise from coupling transverse-electric (TE) gluons with $J^{PC}= 1^{+-}$ to conventional quark configurations. Due to the small acceptance of CLAS at forward angles, it is advantageous to produce the neutral members, which allows the recoiling proton to be detected at large angles. Table 1 lists some decays with predicted widths less than 300 MeV, and narrow

Table 1: Predicted masses and decays of TE hybrids.

	J^{PC}	Decay	Γ(MeV)	Final State	Acc. X BR(%)
$\hat{\rho}$ (2000)	1^{-+}	$\pi b_1(1235)$	150	$\pi^+\pi^-\pi^+\pi^-(\pi^0)$	.14x.64=9%
$\hat{\omega}$ (1900)	1^{-+}	$KK_1(1400)$	100	$K^\pm \pi^\mp K^\pm \pi^\mp$	.14x.06=1%
$\hat{\phi}$ (2100)	1^{-+}	$KK_1(1400)$	250	$K^\pm \pi^\mp K^\pm \pi^\mp$	.14x.14=2%
$\hat{f}_0$ (2200) [a]	0^{+-}	$\pi b_1(1235)$ $KK_1(1270)$	250-500	$\pi^+\pi^-\pi^+\pi^-(\pi^0)$	.14x.89=12%
$\hat{f}'_2$ (2100)	2^{+-}	$KK_1(1400)$ $KK_2(1430)$	200 250	$K^\pm \pi^\mp K^\pm \pi^\mp$ $K^+K^-\gamma\gamma$	.14x.09=1% .14x.08=1%

a. Mass and widths are very sensitive to the strength of the L • S interaction (see Ref. 5). The quoted branching ratio is for the smaller width.

intermediate states. Of those, only decays leading to less than five detected mesons are listed. This is an important constraint, and one which may explain why hybrids have been so poorly studied. The transverse-electric (TE) hybrids have quark spins coupled to S=1. This has the effect that decays to one light meson, and one heavy meson with J=1 or 2, are

favored, leading to at least three mesons in the final state. In our case an odd number of mesons requires at least one to be neutral, and photons must be detected in the final state. Therefore the final states all have an even number of charged mesons and an even number of photons.

The existence of vector-meson quark configurations in the 1^{-+} hybrids emphasizes an important distinction between photon and meson probes. The photon (or vector meson) beam can excite those states by 1^{+-} gluon exchange (no spin flip) or by b_1 or h_1 exchange. No readily available hadron beam offers such a simple excitation mechanism. This is particularly interesting for the $\hat{\phi}(2100)$ and $\hat{f}'_2(2100)$ because hadron beams are not a ready source of $s\bar{s}$ pairs.

In addition to the decay channels listed in Table 1, one should also measure the $\rho\pi$ channel discussed in the introduction. This is accessible in the $\pi^+\pi^-\gamma\gamma$ final state. The $\eta\pi$ channel is not well suited to a CLAS experiment, since it decays to four photons.

3. Glueballs and Transverse-magnetic Hybrids

The spectrum of exotic hadrons is not limited to those with unusual quantum numbers. In fact there are far more states which cannot be distinguished from conventional mesons by their quantum numbers. If the arguments given above are modified to allow exchange of $J^{PC}= 1^-$ gluons or vector mesons then the transverse-magnetic (TM) hybrids will be excited. All of these states are expected at rather high energy (at about the same mass as the TE states), so not much mixing is expected with the conventional states.[6] Here also photo-excitation can play an important role, since any new spectroscopy will help to identify the full set of low-lying states. However it is possible that something more can be learned by looking at specific final states. Chanowitz and

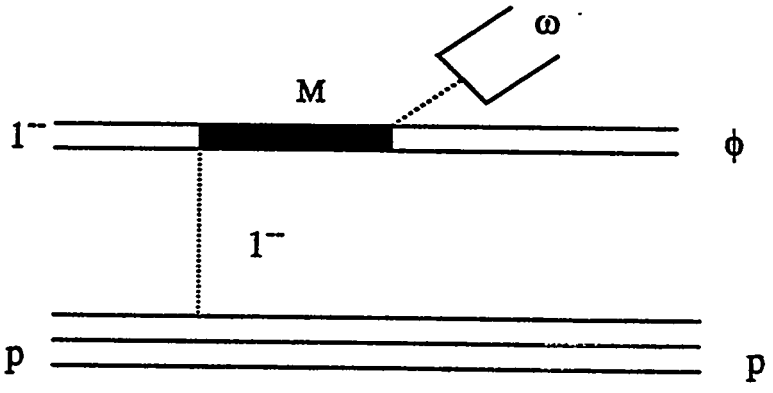


Fig. 1 - Quark diagram for resonant photoproduction of $\omega\phi$ through the vector meson component of the photon beam.

Sharpe[6] argue that TM gluons couple much more strongly to $s\bar{s}$ than to other quark flavors

and therefore TM hybrids (J^{PC}= 1^{+-}, 0^{++}, 1^{++}, 2^{++}) should decay to kaon rich final states.Among these, the ones involving OZI forbidden channels for conventional $q\bar{q}$ decay arethe most selective (e.g., Fig. 1).Thus one is lead to the final states which have one ϕ and one non-strange meson, i.e., $\phi\pi^0$, $\phi\eta$, $\phi\rho$, and $\phi\omega$. Table 2 lists these decays for the low

Table 2: Expected decays of TM hybrids. Branching ratios are for secondary decays only.

J^{PC}	Decay	Final State	Acc. X BR(%)
1^{+-}	$\phi\pi^0$	$K^+K^-\gamma\gamma$	.14x.49=7%
	$\phi\eta$	$K^+K^-\gamma\gamma$	.14x.19=3%
0^{++}, 1^{++}, 2^{++}	$\phi\rho$	$K^+K^-\pi^+\pi^-$	.14x.24=3%
	$\phi\omega$	$K^+K^-\pi^+\pi^-$ (π^0)	.14x.44=6%
	$\phi\phi$ (0^{++}, 2^{++})	$K^+K^-K^+K^-$	.14x.24=3%

lying TM hybrids. Unfortunately the non-resonant background amplitudes for these channels are not completely OZI suppressed, as shown in Fig. 2. Therefore it may be quite difficult to identify the desired resonances.

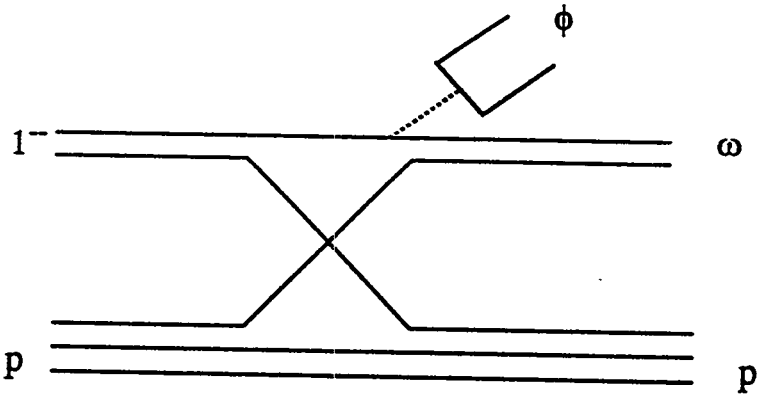


Fig.2 - Quark diagram for nonresonant photoproduction of $\omega\phi$ through the vector meson component of the photon beam.

Similar considerations apply to the glueball states. The latest theoretical calculation predicts the lowest gg states to have J^{PC}= 0^{++} (1.6 GeV), and 2^{++} (2.3 GeV).[8-10] Lindenbaum et al.[16]. have identified three 2^{++} states at 2.01, 2.30, and 2.34 GeV which decay to $\phi\phi$. Since this is an OZI forbidden channel for both non-exotic mesons and nonresonant amplitudes, they conclude that these must be glueballs. No attempt was made to explain the large number of closely spaced glueball candidates, and it see seems likely that at least one of these is an $s\bar{s}$ meson.[17] The $s\bar{s}$ spectrum is poorly understood for

masses above the $\phi_3(1850)$, and the Particle Data Group list at least five 2^{++} states that must be considered candidates. In our case $\phi\phi$ production is not OZI suppressed due to the $s\bar{s}$ component in the beam. Thus one might expect $s\bar{s}$ mesons to be copiously produced with photon beams. Therefore a comparison of the $\omega\phi$ and $\phi\phi$ channels could help to distinguish glueballs from $s\bar{s}$ mesons. This adds the decay channel $\phi\phi \rightarrow K^+K^-K^+K^-$ to the list of desired triggers (see Table 2).

3. Experiment

Due to the diffractive nature of photoproduction experiments, one expects strong forward peaking of the final state mesons. In the example given below we assume an e^{9t} distribution of events, but the actual value of the exponent is not critical for the simulation. CLAS is not an ideal spectrometer for this purpose because it has limited azimuthal acceptance at forward scattering angles. Nevertheless CLAS can serve the purpose of making the initial survey of exotic meson production quite well. It has rather large angular coverage, photon detection, π/K separation up to about 2 GeV/c, and a tagged photon beam. The states in question are expected at masses around 2 GeV, so the beam threshold energy is 4 GeV. Adding some energy to open up phase space raises the desired beam energy to 5 - 6 GeV. Since all of the chosen decays are charge neutral, equal numbers of positive and negative mesons will be detected. Thus one gains in overall acceptance by reducing the magnetic field, to remove the charge bias. The present estimates were made at $B=B_0/5$.

Two of the decays listed in Table 1 have large predicted branching to $b_1\pi$, so this is a logical place to start a simulation. This channel has the advantage that the b_1 (Γ= 155 MeV) decays to narrow $\omega\pi$ mesons. Because of this we assume that it will not be necessary to detect the π^0 from the decay of the ω. This means that the π^0 will be detected by missing mass, and its momentum calculated from four-momentum conservation. The detected particles are $\pi^+\pi^-\pi^+\pi^-p$.

A monte-carlo simulation of this decay branch was made using the code FASTMC, for beam energies from 4.5 to 6.0 GeV. The decay chain discussed above (with proton detection) was simulated for a 1.9 GeV resonance. The final meson momentum spectra were all very similar, indicating that any five-body decay would give about the same results. Fig. 3 compares the generated and detected spectra for the pion resulting from b_1 decay, at a beam energy of 5 GeV. No obvious momentum bias is present.The pions peak at scattering angels around 14°, with a tail extending out to 90°. Recoiling protons peak further out in angle, at 28°, and are limited to momenta from 500 to 800 MeV/c, again with no obvious bias. A reconstructed ω mass resolution of 40 MeV FWHM results. Fig. 4 shows the final measured resolution for the hybrid mass. The peak width of 100 MeV FWHM is sufficient for studying the states listed in Tables 1 and 2, however, it is important to realize that mass resolution can be traded for acceptance by raising the magnetic field in CLAS. This effect has not been studied in detail.

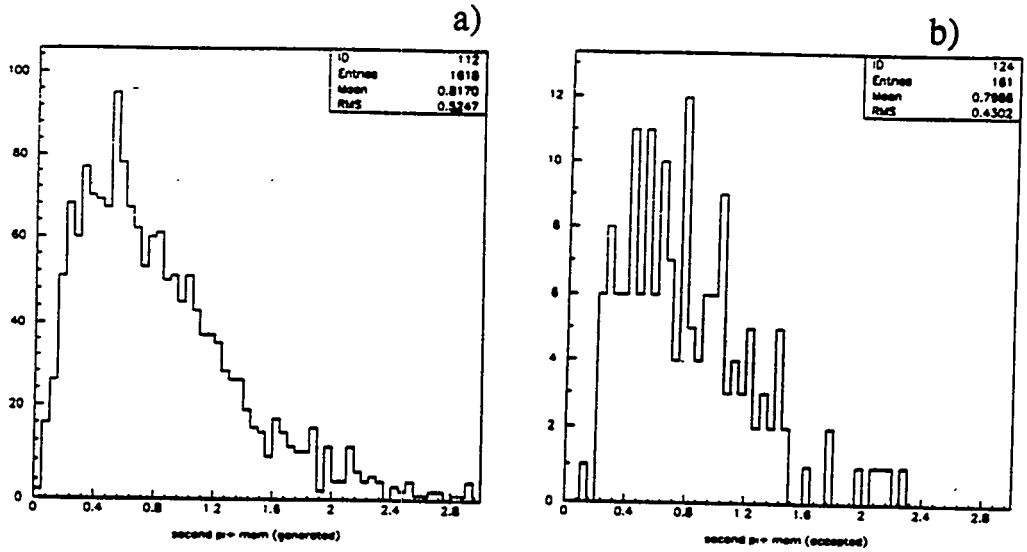


Fig. 3 - Momentum spectra a) generated by the monte-carlo, and b) accepted by CLAS, measured in GeV/c.

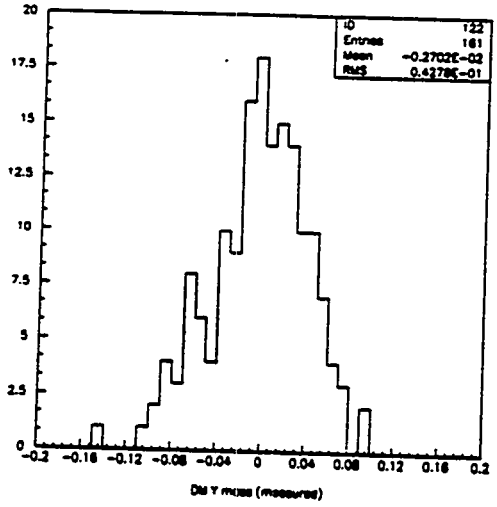


Fig. 4 - Difference between generated and measured hybrid mass, in GeV.

The overall CLAS acceptance was found to be weakly dependent on beam energy, but strongly dependent on target position. Moving the target upstream by one meter from the nominal position increased the acceptance from 5% to 14%, and a total displacement of two meters raised the acceptance to 18%. The middle value was included in Tables 1 and 2, and also used to estimate the acceptance for other triggers. We have assumed that the acceptance for photons in the CLAS shower counter is about the same as the charged

particle acceptance. Since all of the proposed triggers in the tables have four light particles plus one proton, the acceptance for each of these will also be about 14%. The shower counter forms an integral part of triggers such as $\rho\pi^0$. However the performance of the shower counter for these cases has not yet been studied. No corrections have been made for particle decays in flight. Also, the branching ratios listed in the tables are rough estimates which assume all available charge channels after the first decay are equally probable.

A count rate estimate has been made for the $b_1\pi$ channel using the photoproduction data from the CERN Omega collaboration.[14] Those measurements were made with 25-50 GeV photons, and since typical diffractive production cross sections fall slowly with energy, those data will give a reasonable lower limit to aim for. They measured a total integrated cross section of 10 nb/100 MeV in a very poorly determined peak at 1.9 GeV (Fig. 5).

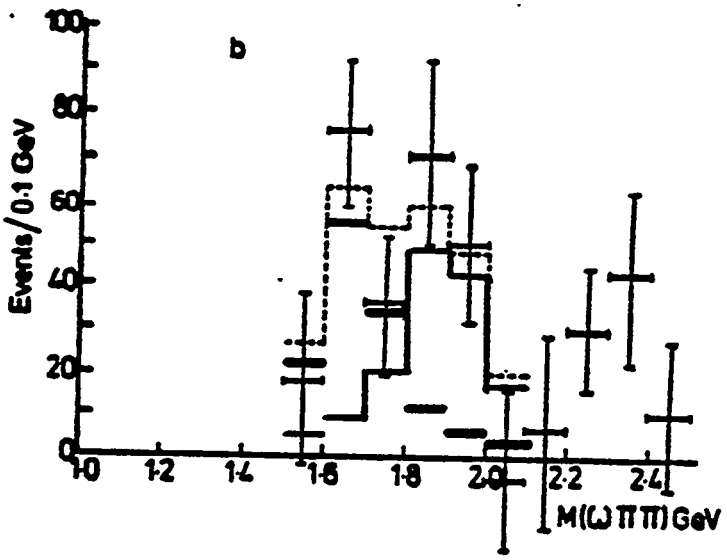


Fig. 5 - The $b_1\pi$ mass spectrum taken with 25-50 GeV photons. The low lying peak is from $\omega(1670)$. Additional strength above background was reported in a peak at about 1.9 GeV (solid line).

Therefore new experiments should be designed to detect resonances at the level of 2 nb. Assuming a 10 cm LH_2 target and a photon flux of 10^8/s, we estimate a total reaction rate of 300/hr. Multiplying by the 14% detection efficiency gives a detected rate of 42/hr.

4. Conclusions

The present estimates show that a credible search can be made for exotic mesons by using the CLAS to measure photoproduction of multi-meson final states. Two trigger types offer the best chance for finding exotic mesons: i) five charged particles and no photons, and ii) three charged particles and two photons. Detected rates are expected to be a few percent of the production rates.

The non-uniform acceptance of CLAS will complicate the necessary partial wave analyses, and special running conditions will limit the amount of beam time that can be

devoted to this subject. In the event that exotic mesons are identified with CLAS, or by some other experiment, it will be desirable to study their photo-excitation mechanisms in some detail. Therefore future work should have a dedicated facility tailored to measurements of diffractive production. Such a facility should have good forward angle coverage and high-resolution photon detection.

This work was supported by the National Science Foundation. The authors wish to acknowledge many stimulating discussions with N. Isgur on this subject.

5. References

1 F.E. Close, Rep. Prog. Phys. 51, 833 (1988).

2 Glueballs, Hybrids and Exotic Hadrons, AIP Conf. Proc. no. 185 (AIP, New York, 1988) ed. Suh-Urk Chung.

3 Nathan Isgur and Richard Kokoski, Phys. Rev. Lett. 54, 869 (1985).

4 Nathan Isgur and Jack Paton, Phys. Rev. D31, 2910 (1985).

5 John Merlin and Jack Paton, Phys. Rev. D35, 1668 (1987).

6 Michael Chanowitz and Stephen Sharpe, Phys. Lett. B132, 413 (1983).

7 T. Barnes, F.E. Close, and F. de Viron, Nucl. Phys. B224, 241 (1983).

8 B.S. Bali, et al., Phys. Lett. B309, 378 (1993).

9 K. Bitar, et al., Phys. Rev. D44, 2090 (1991).

10 C. Michael and M. Teper, Phys. Lett. B206, 299 (1988).

11 D. Alde, Phys. Lett. B205, 397 (1988); M. Boutemeur and M. Poulet, Proc. 3rd Int. Conf. on Hadron Spectroscopy (1989) p. 119.

12 G.M. Beladidze, et al., Phys. Lett. B313, 276 (1993).

13 J.H. Lee, et al., Phys. Lett. B323, 227 (1994).

14 M. Atkinson, et al., Z. Phys. C - Particles and Fields 34, 157 (1987).

15 G.T. Condo, et al., Phys. Rev. D43, 2787 (1991).

16 S.J. Lindebaum, Comm. Nucl. Part. Phys. 13, 285 (1984); S.J. Lindenbaum, AIP Conf. Proc. no. 185 (AIP, New York, 1989) p. 68, ed. Suh Urk Chung; A. Etkin, et al., Phys. Lett. B201, 568 (1988).

17 Stephen Godfrey and Nathan Isgur, Phys. Rev. D32, 189 (1985).

PROBLEMS IN BARYON SPECTROSCOPY*

SIMON CAPSTICK
Supercomputer Computations Research Institute
and
Department of Physics
The Florida State University
Tallahassee, Florida, 32306

ABSTRACT

Current issues and problems in the physics of ground- and excited-state baryons are considered, and are classified into those which should be resolved by CEBAF in its present form, and those which may require CEBAF to undergo an energy upgrade to 8 GeV or more. Recent theoretical developments designed to address these problems are outlined.

1. Introduction

Can whatever is possible at CEBAF at 6 GeV be done better at 8 GeV? For now we ignore experimental issues, such as whether or not is it possible to detect the final-state particles from the reactions. Then higher initial electron energy means that for the electroproduction process

$$e^- + N \rightarrow e^- + X \rightarrow e^- + N + \text{mesons}$$

we can reach states X with larger mass. In this process the states X can be conventional qqq excitations of the nucleon, or possibly a baryon with excited glue (a hybrid). This reaction can also proceed via a two step process where X first decays to, for example, a ground- or excited-state hyperon in association with a kaon.

Higher energy also means more counts at larger Q^2. This will allow us to extend measurements of the form factors for the transitions $N \rightarrow X$ to higher Q^2, possibly allowing a description of the structure of the constituent quark. Whether or not we will be able to map out the transition to the regime of perturbative QCD remains controversial.

The following represents a personal perspective and should in no way be considered an exhaustive list of the issues in, or the contributors to, this field. First, we consider some problems which should be resolved by CEBAF in its present form, and then we describe problems which may also require exploration in a second generation of experiments at higher energy.

*Talk presented at the Workshop "CEBAF at Higher Energies", held at CEBAF, Newport News, Virginia, 14-16 April 1994.

2. Excited-Baryon Physics Issues Resolvable by CEBAF at 6 GeV

2.1. Controversial light states

There are some fundamental issues from the analysis of $N\pi \rightarrow N\pi$ experiments which remain unresolved. As an example, consider the resonance $\Delta\frac{3}{2}^+(1600)P_{33}$, conventionally described in the quark model as a radial excitation of $\Delta(1232)$. This state is poorly established, and is much lighter than quark-model expectations of around 1800 MeV. Its photocouplings are not well-known, but look quite different from those predicted by the quark model. Similarly the Roper resonance $N\frac{1}{2}^+(1440)P_{11}$, with a conventional quark-model description as a radial excitation of the nucleon, is 100 MeV lighter than model expectations. Its nonrelativistic quark model photocouplings [1], although small, do not correspond to the photocouplings extracted from the data, and may have the wrong sign. Relativistic corrections to the transition operator $H_{\rm em}$ and the wavefunctions do not help resolve this discrepancy [2]. This has led to the proposal of hybrid models of the Roper resonance [3]. Since the quark-model description of the mass and photocouplings of the next P_{11} resonance, $N\frac{1}{2}^+(1710)$, appears to be satisfactory, such models have to account for the lack of an extra state in this mass range. There has been some controversy about the number of poles present in the $N\pi$ P_{11} partial wave at this mass; it now appears that there is only one very broad physical pole [4]. A relativistic calculation (described below) of the Roper-resonance electro-excitation amplitudes [5] using crude wavefunctions, shows that the electroexcitation amplitudes for this state are strongly sensitive to relativistic effects. It is clear that experiments at CEBAF with its present maximum energy will provide crucial information for these controversial lower-mass states.

2.2. 'Missing' baryons

There are also light excited states which are predicted to exist by the symmetric constituent quark model which do not appear in the $N\pi$ analyses. Calculations of the $N\pi$ couplings of these states, in both the elementary-meson-emission [1] and [6] $^3P_0$ models, show that these states are expected to decouple from their production channel. It is crucially important that these states be found, as there are asymmetric (quark-diquark) models which ascribe their absence to a reduction in the number of dynamical degrees of freedom in the baryon. These states should be found in experiments at CEBAF which will examine multipion final states [7], where the 'missing'-baryon intermediate state decays by first emitting an excited meson (i.e. to $N\rho$, $N\omega$, $N\eta$, $N\eta'$, etc.), or to a lighter excited baryon (such as $\Delta(1232)$ or the Roper resonance) plus a pion. Calculations [1,8,9] have shown that many of these states should couple strongly to $N\pi\pi$ through the channels $N\rho$ and $\Delta(1232)\pi$.

3. Issues Which May Require CEBAF at 6 and 8 GeV

3.1. Virtual-photon couplings

Little is known experimentally about the virtual-photon couplings of excited baryon states beyond $\Delta(1232)$; previous theoretical estimates of their electromagnetic transition helicity form factors $A_\lambda^N(Q^2)$ have used a nonrelativistic treatment of the relative motion of the recoiling (struck) quark, and of the electromagnetic current matrix elements. This leads to problems at suprisingly small values of Q^2, i.e. when $Q \gg p_q \simeq m_q$, where the latter is of the order of a few hundred MeV. If we picture the photodecay process $B \to N\gamma$ in impulse approximation, where B is heavy, even photocouplings can involve a large recoil momentum of the emitting quark. To have a complete picture of these processes we should, ideally, solve the relativistic three-body bound-state problem; the resulting wavefunctions would then be used in a relativistically invariant calculation of the one-, two-, and three-body electromagnetic currents.

One approach to the calculation of these baryon electromagnetic currents in relativistic impulse approximation (i.e. restricted to one-body currents) is that of relativistic Hamiltonian dynamics [10]. Here [5] we expand the relativistic three-body wavefunctions in some convenient basis, and then perform a relativistic treatment of the internal kinematics of the quarks, the recoil boosts, and the evaluation of the electromagnetic current matrix elements. As a first pass we have calculated using only single (oscillator-) basis states as crude representatives of the wavefunctions, in order to look for sensitivities to relativistic effects, by comparing to a non-relativistic calculation using the same single-basis-state wavefunctions.

Our results confirm the results of other authors [11], that this approach can give good agreement for the nucleon elastic form factors out to suprisingly large Q^2. We have also compared nonrelativistic and relativistic treatments for basis states which can be used to represent $\Delta(1232)$, radial excitations of the nucleon and $\Delta(1232)$, and all of the low-lying P-wave states. The result [5] is that there can be sizeable relativistic effects.

What kind of experiments can be performed at a higher energy CEBAF to help shed light on this crucial physics? Let us assume that the standard-energy CEBAF sorts out the details of the Q^2 dependence of the helicity amplitudes $A_\lambda^N(Q^2)$ for the lighter states. All of these calculations are in terms of, and can be shown to require, electromagnetic form factors for the constituent quarks, $F_{1q}(Q^2)$ and $F_{2q}(Q^2)$. Can these be extracted from experiments to measure the baryon transition form factors at higher Q^2? This will require good models of the electromagnetic transitions of composite baryons, but is potentially very interesting physics. Experiments such as these can test the constituent quark model where it is most stressed; at higher $\sqrt{s}$ (mass) or Q^2, or both.

3.2. Strong decays

The baryon strong-decay calculations described above have a fundamental problem; they use the narrow resonance approximation, in which resonances are treated in isolation and total widths are assumed small in comparison to the masses. In practice excited baryon states often have large widths to many open channels which cause many states to overlap in a given mass range. There exist calculations which go beyond this approximation. [12]

Calculations of the $N\pi$ decay amplitudes of the higher mass nonstrange states [6] (in the $^3P_0$ model, within the narrow resonance approximation) are able to demonstrate some nice patterns which reflect those in the data, where the lightest predicted state [13] in many partial waves (i.e. of a given isospin, spin and parity) couples strongly and corresponds in mass to the observed state. There are also obvious problems which arise; as an example there are several instances of two states nearby in mass in the same partial wave which are predicted to have small $A_{N\pi}$, whereas only one state is seen in the partial-wave analysis, with a larger $A_{N\pi}$. We expect that this is due to decay-channel mixing of the pair of states, which can be expected to drive one state down in mass while giving it a larger coupling. [14]

In order to address these difficulties, we must perform a coupled-channel calculation [12] of the decay amplitudes, where baryon meson loops are allowed to renormalize the masses and wavefunctions of all of the states in question, and also affect the transition amplitudes between the states. This can be thought of as one way to include higher Fock-space components, such as $qqq(q\bar{q})$, into the wavefunctions.

In order for experiments at CEBAF to sort out the physics of these higher mass states, we will require a large number of events between $\sqrt{s} = 2$ and 3 GeV. This will be easier to accomplish if CEBAF is upgraded to 8 GeV. We also will require the information resulting from the partial-wave analyses of experiments at CEBAF at lower energy, and the resulting experience in applying the best analysis techniques.

3.3. Hybrid baryons

Much of the physics detailed above can be used to lay the groundwork for a search for exotic states with baryon quantum numbers, such as states with excited glue. A 'smoking-gun' signal for a hybrid baryon is unlikely; as in the meson sector it is likely to be complicated by mixing, and the quantum numbers of hybrid baryons are not exotic. One way to proceed is to count states in a given mass range, and look for an excess of states over the quark model predictions for conventional qqq excitations in that range. This is likely to be difficult given that we have not yet seen about one third of the nonstrange states predicted by the model below about 2 GeV. A more promising approach is to find a state which *may* be superfluous, *and* has anomalous electromagnetic couplings or strong couplings (or both) [15]. This approach obviously requires that we understand as much as possible about the strong decays and electromagnetic couplings of excited-baryon states.

3.4. Strange-Baryon Physics Without a Kaon Source

Given that we now cannot expect to have a source of kaons available in the near future for direct $\bar{K}N$ production of strange-baryon resonances, the physics of excited strange resonances is best accessed at CEBAF or an upgraded CEBAF. This is through associated production in kaon electro- or photoproduction

$$e^- + N \rightarrow e^- + X \rightarrow e^- + (\Lambda, \Sigma)^* + K,$$

with the ground- or excited-state hyperon subsequently decaying to $\bar{K}N$ or other final states. These experiments are obviously more difficult than direct production. The spectroscopy of excited hyperon states is in much poorer shape than that of the nonstrange states; there are fewer 'N=2 band' states seen, and there is the same decoupling from $\bar{K}N$ which causes predicted states to be missing in the analyses. The latter can be found at CEBAF by using events where the excited hyperon decays to something other than $\bar{K}N$.

There are problems in the theory of these states even at the lightest masses; the $\Lambda\frac{1}{2}^-(1405)$ is predicted to be degenerate with its $J^P = \frac{3}{2}^-$ partner, which is 100 MeV higher than in the analyses of the data. It is generally accepted that this state may be a $\bar{K}N$ bound state, or at least has a large $qqq(\bar{q}q)$ component in its wavefunction. This again points to a need for a coupled-channel analysis of all nearby states, rather than a treatment of this state in isolation. Although some of this physics will be addressed in lower-energy experiments at CEBAF, these experiments do require the extra energy required to make a pair of strange quarks, and we require that the final state particles have enough relative momentum to be seperated in the detector. There may be, therefore, distinct advantages to designing experiments with a higher-energy beam. This is certainly true for the more massive excited states.

4. Conclusions

It is fundamental to understanding QCD that we understand baryons. Lattice gauge theory and similar ab-initio approaches may not ever work, say, for the sixth P_{11} resonance. The constituent quark model has its failings but is calculable and hopefully correctable.

We are currently working on incorporating relativity into the calculation of the spectrum and wavefunctions and the electromagnetic couplings of the resulting states, as well as the incorporation of decay-channel mixings into the calculation of their strong decays. It will require the analysis of a large amount of new data, and the application of many of these theoretical ideas, to extract some potentially exciting new physics from CEBAF. This may include the form factors of the constituent quark, and the exploration of 'molecule'-like $qqq(\bar{q}q)$ states, and states with excited glue. Sorting this out from the background of conventional qqq excitations requires the completion of the current generation of experiments at the lower energy CEBAF, and will be made easier by an upgrade to 8 GeV or more.

5. References

1. R. Koniuk and N. Isgur, Phys. Rev. **D21** 1868, 1980.
2. S. Capstick, Phys. Rev. **D46**, 1965 (1992).
3. Z.-P. Li, Phys. Rev. **D44**, 2841 (1991); Z.-P. Li. V. Burkert, and Z.-J. Li, Phys. Rev. **D46**, 70 (1992).
4. R.E. Cutkosky and S. Wang, Phys. Rev. **D42**, 235 (1990); D.M. Manley and E.M. Saleski, Phys. Rev. **D45**, 4002 (1992).
5. S. Capstick and B.D. Keister, "Baryon Resonance Electroexcitation in a Light-Cone Model", May 1994, to be published in the Proceedings of the *14th International IUPAP Conference on Few Body Problems in Physics* (Williamsburg and Newport News, Virginia); to be submitted to Physical Review D.
6. S. Capstick and W. Roberts, Phys. Rev. **D47**, 1994 (1993).
7. S. Dytman *et al.*, CEBAF proposal 89-039; B. G. Ritchie *et al.*, CEBAF proposal 91-008; V. Burkert *et al.*, CEBAF proposal 91-024; J. Napolitano *et al.*, CEBAF proposal 93-033.
8. R. Koniuk, Nucl. Phys. **B195**, 452 (1982); N. Isgur, in *Proceedings of the CEBAF/SURA 1984 Summer Workshop*, Newport News, Virginia, 1984. edited by F. Gross and R.R. Whitney (CEBAF, Newport News, 1984); Fl. Stancu and P. Stassart, Phys. Rev. **D42**, 1521 (1990); Phys. Rev. **D47**, 2140 (1993).
9. S. Capstick and W. Roberts, Phys. Rev. **D49**, 4570-4586 (1994).
10. B. D. Keister and W. N. Polyzou, Adv. Nucl. Phys. **20**, 225 (1991).
11. P.-L. Chung and F. Coester, Phys. Rev. **D44**, 229 (1991); F. Schlumpf, Phys. Rev. **D48**, 4478 (1993); F. Schlumpf, Mod. Phys. Lett. **A8**, 2135 (1993).
12. Many authors have considered this problem; for a partial list of publications on this topic see Ref. 6.
13. S. Capstick and N. Isgur, Phys. Rev. **D34**, 2809 (1986).
14. Richard E. Cutkosky, private communication.
15. That the Roper resonance meets many of these requirements has not escaped the attention of many authors; for example, see Zhenping Li in Ref. 3.

ELECTROMAGNETIC PRODUCTION OF VERY LIGHT GLUINOS*

Carl E. Carlson and Marc Sher
Physics Department, College of William and Mary, Williamsburg, VA 23187

and

Larry Weinstein
Physics Department, Old Dominion University, Norfolk, VA 23529

ABSTRACT

Current experiments allow the possibility of gluino masses below about 600 MeV if the lifetime of the gluino is longer than 100 picoseconds. If the mass and lifetime are in this window, then electromagnetic production of pairs of gluino-gluon bound states can provide a means to observe them. The cross section is large enough that the window can be fully explored, up to lifetimes exceeding a microsecond, at high luminosity electron accelerators. A discussion of signatures and a table of event rates for various possibilities at CEBAF is given.

1. Introduction

The most popular extension of the standard model is supersymmetry. Supersymmetric models explain the hierarchy of scales between the electroweak, grand unified and Planck scales, automatically incorporate gravity, and may solve several cosmological problems. Most importantly, supersymmetric models explicitly predict the Weinberg angle–the predicted value is $\sin^2\theta_w = 0.2329 \pm 0.0026$, compared with the experimental value of 0.2324 ± 0.0006. For this reason, over a third of all papers written in particle physics in the last year have dealt with supersymmetry.

In supersymmetric models, all particles have associated partners with identical quantum numbers except a difference of 1/2 in spin. Thus, gauge bosons have spin 1/2 partners (called gluinos, winos, zinos and photinos); quarks have spin zero partners (called squarks). The partner of the gluon, the gluino, is a neutral, color octet fermion.

In recent years, an apparent inconsistency between the value of α_s at low energies and that at the mass of the Z has led to a revival of interest in the possibility of very light gluinos.[1] Although the latest data seems to be consistent, within errors, both with and without light gluinos, the possibility that the gluino is extremely light needs to be thoroughly explored.

In 1987, the UA1 Collaboration[2] published a detailed analysis of the experimental searches for gluinos. They found three allowed windows in the gluino-squark mass plane: (i) gluino masses below approximately 600 MeV and squark mass above something like 100 GeV, (ii) a triangular window for gluino masses between 2.5 and 4.0 GeV and squark masses

*Presented by M.S.

between 100 and 400 GeV and (iii) a window for gluino masses between 2.0 and 5.0 GeV and squark masses in the TeV range. These windows are all controversial; looking at the long listings in the Particle Data Group table[3] for gluino masses will show the extent of the controversy. In this proposal, we will focus on the most intriguing window—gluino masses below 1 GeV.

Because of R-parity, gluinos will always be produced in pairs. Once produced, they will either combine with each other into a $\tilde{g}\tilde{g}$ state, a "glueballino," and then annihilate quickly into hadrons, or else they will hadronize with gluons or quarks into a "glueballino" ($g\tilde{g}$) or a "gluino hybrid" or "hybridino" ($\tilde{g}q\overline{q}$) state. In the case of the single gluino hadron, the lightest resulting state will be long-lived, since the gluino will decay into a $q\overline{q}\tilde{\gamma}$ via squark exchange with a lifetime approximately given by[4]

$$\tau \sim 3 \times 10^{-12} \text{ sec.} \left(\frac{1 \text{ GeV}}{\widetilde{M}}\right)^5 \left(\frac{m_{\text{squark}}}{m_W}\right)^4, \tag{1}$$

where $\widetilde{M}$ is the mass of the $g\tilde{g}$ or $\tilde{g}q\overline{q}$ state. For squark masses between 100 and 1000 GeV, this gives lifetimes ranging from ten picoseconds to a hundred nanoseconds.

Present limits on light gluino masses come from searches for $\tilde{g}\tilde{g}$ gluinoballs in radiative heavy vector meson decays (e.g., $\Upsilon \to \gamma +$ gluinoballs). Such processes have the advantage of being completely independent of the gluino lifetime, squark masses, etc. The best bound comes from CUSB,[5] who exclude gluinos with masses between 600 and 2200 MeV coming from radiative Υ decays. The lower bound comes from the low detection efficiency of low multiplicity final states, and is quite uncertain.* The bound has been criticized[6] since the determination of the expected branching ratio[7] is very strongly dependent on the value of the wave function at the origin of the gluino-ball, and is thus quite model-dependent, and because decays into more expectable things such as $\gamma + \eta'$ and $\gamma +$ glueball have also not been seen.

Lifetime limits come from searches for $g\tilde{g}$ glueballinos or a $\tilde{g}q\overline{q}$ states in beam dump experiments. Such experiments have conclusively ruled out[8] gluinos with lifetimes less than $10^{-10} - 10^{-11}$ seconds. If a $\tilde{g}q\overline{q}$ *charged* state has a lifetime greater than $\sim 10^{-10}$ seconds, then it would have been detected[9] in hyperon beam experiments. However, if the mass of the $\tilde{g}q\overline{q}$ state is sufficiently greater than the glueballino then it will decay strongly into the glueballino, and such a bound would not be relevant.† We conclude that there may still be a window for gluino masses less than approximately 1000 MeV and lifetimes between 100 picoseconds and a microsecond if the lightest gluino containing hadron is a $g\tilde{g}$ glueballino. In this note, we will propose an experiment that could close this window—or find the gluino.

In order to detect the decays of a neutral particle whose lifetime could be as long as a microsecond, one needs to produce them with very little kinetic energy (i.e. a relatively low

*The bound refers to half the gluinoball mass. The gluinos could conceivably be somewhat heavier or lighter, or even massless.

†In several models, the $\tilde{g}d\overline{u}$ state will be sufficiently heavy to decay into a glueballino and one or two pions; however, in most of these models, the $\tilde{g}s\overline{u}$ state will not be able to decay strongly into a glueballino and a kaon. In these models, the uncertainties in the masses are sufficiently large that such a decay cannot be excluded; furthermore, the W-mediated decay of the $\tilde{g}s\overline{u}$ into a glueballino and a charged pion will occur with a lifetime of approximately $10^{-10} - 10^{-11}$ seconds, and thus might not be detected in the hyperon beam.

energy machine) and with a very high luminosity. We will consider the photoproduction of light gluinos off a proton target at a high luminosity electron accelerator.

2. Photoproduction of light gluinos

The relevant diagrams are shown in Fig. 1. We will first consider the production rate of light gluinos, and then discuss signatures in the next section. The detailed expression for the matrix element and cross section can be found in a recent Letter.[10] For various incoming photon energies and various particle masses, we obtain the cross-sections shown in Figure 2.

We envision each gluino within a glueballino (a bound state of gluinos with gluons) so that the mass necessarily produced is at least that of the glueballino, and in evaluating our formulas we have interpreted $\tilde{m}$ as the glueballino mass. Regular glueballs are not massless even though the gluon is, and we anticipate that the glueballino will be in the same mass range, namely a mass of about 1.5 GeV for the lightest example (see, e.g., the lattice gauge results reported in Ref. 11). Our cross section is sensitive to this mass, as may be seen from the figures, where we present results for $\tilde{m}$ being both 1.0 and 1.5 GeV. The cross section is in contrast insensitive to changes in the quark mass.

3. Signatures of gluino production at CEBAF

A gluino in the mass and lifetime range we are considering has certain aspects of a long lived particle and other aspects of a short lived particle. The particle is in fact long lived so that there should be a noticeable gap between its production point and decay point. The gluino will decay into a photino plus non-supersymmetric particles and the photino will exit undetected and with its energy undetermined. The ordinary matter from the glueballino decay will therefore have a variable energy and will appear like a strongly unstable particle with a wide width. The apparent width of the decay will of course not have a lorentzian shape, but this may not be apparent if the statistics are limited in a first experiment.

The ordinary matter from glueballino decay will decay strongly into mesons. Because we are looking for very light glueballinos, we will look for very light decay products, i.e.: pions. Thus, the glueballino signature will be detecting two or more pions coming from a vertex away from the target. We can use the CEBAF Large Acceptance Detector (CLAS) to do this. The CLAS has an angular coverage of about 75% forward of $\theta = 45°$, a vertex resolution of a few mm, can measure vertex, three-momentum and identity for charged particles with $p > 200$ MeV/c, and can measure vertices for charged particles with $p > 120$ MeV/c. It can measure energy and identity for neutral particles emitted within 45° of the beam. There are several possible decays to look for: 2, 3 or 4 pion. The two pion decay will have the most background from $(\pi, 2\pi)$ secondary scattering from detector material and from K_L decay. The three pion decay will be $\pi^+\pi^-\pi^\circ$. Since we cannot reconstruct π° trajectories, the event will appear as a two pion event plus a possibly unrelated π°. The four pion decay, $\pi^+\pi^+\pi^-\pi^-$ coming from a common vertex away from the target, will have the clearest signature. If we detect all four pions, then it is completely unambiguous; if we only detect three of the four pions then it is still unambiguous since K_L can only decay into two charged pions and a neutral pion.

There are two general ways to detect gluinos with the CEBAF CLAS, conventional and beam dump. Table 1 shows the various probabilities involved for an 8 GeV electron

beam. The photoproduction cross-section for a 1 GeV glueballino is 10^{-32} cm^2 at 8 GeV. The electroproduction cross-section is smaller by α (or by $\alpha/2\pi$), $\sigma = 10^{-34}$ to 10^{-35} cm^2. The photoproduction measurement uses the tagged photon beam incident on a target in the usual position in the CLAS. The maximum luminosity is approximately $2 \cdot 10^7$ tagged photons per second ($6 < E_\gamma < 8$ GeV) incident on a 4 gram/cm^2 target or about $5 \cdot 10^{31}$/(sec-cm^2). The maximum electroproduction luminosity is 10^{34}/(sec-cm^2). Thus, the production rate for photoproduction will be 10^{-32}cm$^2 \cdot 5 \cdot 10^{31}$ /(sec-cm^2) = 0.5 per second. The identifiable event rate in the detector will be less than the production rate due to several kinematic effects (see Table 1 for numbers):

- The decay probability refers to the probability that the glueballino will decay in a region inside the first CLAS detector. Since the first detector is approximately 1 m from the target, we are sensitive to glueballino decays between 1 cm and 1 m from the target. An 8 GeV/c photon will make a glueballino with $\beta\gamma \approx 2$. 100% of glueballinos with a 1 ns lifetime, 15% of glueballinos with a 10 ns lifetime and 0.15% of glueballinos with a 1000 ns lifetime decay in our detection volume. The numbers can be increased by moving the target back (upstream) one meter.

- The branching ratio for the glueballino remnant to decay to four charged pions is expected to be at least 1%.

- The glueballino will be formed with a large enough momentum (2 to 3 GeV/c) that all of its decay pions should be energetic enough to be detected.

- The solid angle factor is the probability of detecting three out of four charged pions in the 75% forward angle coverage of the CLAS which is 0.7.

The detection rate will be the product of the production rate, the decay probability, the branching ratio to 4π, and the solid angle factor. See Table 1 for the various yields. This experiment would be most sensitive to the shorter lifetime glueballinos. This kind of experiment could run as a parasitic data-sifting experiment without dedicated beamtime.

In order to increase the luminosity, we could do the experiment as a dedicated 'beam dump' experiment, putting the target at the photon tagger (ten meters upstream of the CLAS), using the tagger magnet to dump the electron beam and to bend the positive particles away from the CLAS and looking for glueballino decays in the detector. The aperture of the tagger magnet limits us to glueballinos produced in a forward angle cone of 1°. In this case, the beam dump decay probability depends on the opening angle for glueballino production. We assume an opening angle of 12°. Using the tagger magnet to sweep charged particles away should allow us to increase the luminosity to 10^{37}. Table 1 shows the results. This technique is only slightly superior to the conventional experiments for the shorter lived glueballinos.

Factor \ Experiment:	Photo-production	Electro-production	Beam Dump
Cross-section (cm^2)	10^{-32}	10^{-34}	10^{-34}
Luminosity (cm^{-2}-s^{-1})	$5 \cdot 10^{31}$	10^{34}	10^{37}
Decay Probability ($\tau = 10$ ns)	0.15	0.15	$3 \cdot 10^{-4}$
Decay Probability ($\tau = 100$ ns)	0.02	0.02	$1 \cdot 10^{-4}$
Decay Probability ($\tau = 1000$ ns)	0.002	0.002	$1 \cdot 10^{-4}$
Branching Ratio (4π)	0.01	0.01	0.01
Solid Angle Factor	0.7	0.7	0.7
Yield ($\tau = 10$ ns) (per day)	50	100	200
Yield ($\tau = 100$ ns) (per day)	7	14	60
Yield ($\tau = 1000$ ns) (per day)	0.7	1.4	$2 \cdot 10^{-5}$

Table 1. CLAS gluino experiments with an 8 GeV electron beam

There is a window in glueballino mass of 1.0 to 1.5 GeV. Using the anticipated CEBAF 6 GeV electron beam, we can detect or rule out 1.0 GeV glueballinos (in the shorter lifetime region) with CLAS. Using an upgraded 8 GeV electron beam, we can detect or rule out the existence of 1.0 to 1.2 GeV glueballinos over the entire lifetime range. To detect or rule out the existence of glueballinos with a mass of 1.5 GeV, we would need a 12 GeV electron beam.

References

1. L. Clavelli, Phys. Rev. D **46**, 2112 (1992).
2. UA1 Collaboration, C. Albajar *et al.*, Phys. Lett. B **198**, 261 (1987).
3. Particle Data Group, K. Hikasa *et al.*, Phys. Rev. D **45**, S1 (1992).
4. H. E. Haber and G. L. Kane, Phys. Reports **117**, 75 (1985).
5. CUSB Collaboration, Phys. Lett. B **186**, 233 (1987).
6. L. Clavelli, P.W. Coulter and K. Yuan, Phys. Rev. D **47**, 1973 (1993).
7. W.-Y. Keung and A. Khare, Phys. Rev. D **29**, 2657 (1984); T. Goldman and H. Haber, Physica D **15**, 181 (1985).
8. R.C. Ball *et al.*, Phys. Rev. Lett. **53**, 1314 (1984); F. Bergsma *et al.*, Phys. Lett. **121B**, 429 (1983); G.R. Farrar, Phys. Rev. Lett. **55**, 895 (1985); M. Cooper-Sarkar *et al.*, Phys. Lett. **160B**, 212 (1985).
9. T. Goldman, Phys. Lett **78B**, 110 (1978); G.R. Farrar and P. Fayet, Phys. Lett. **76B**, 442, 575 (1978).
10. C.E. Carlson and M. Sher, Phys. Rev. Lett. **72**, 2686 (1994).
11. C. Michael and M. Teper, Nucl. Phys. B **314**, 347 (1989).

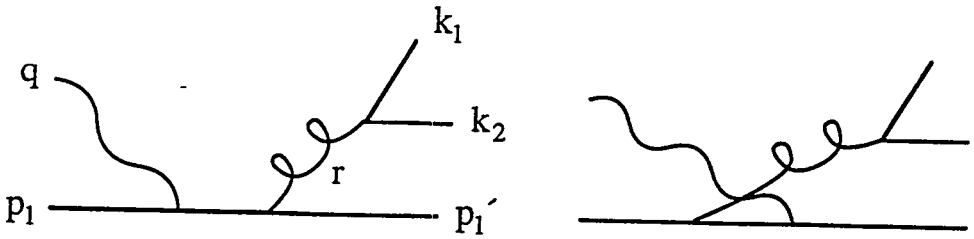


Fig. 1. Feynman diagrams for photoproduction of gluino pairs via photoproduction off a quark. The corkscrew line is a gluon and the lines labeled k_1 and k_2 are the gluinos.

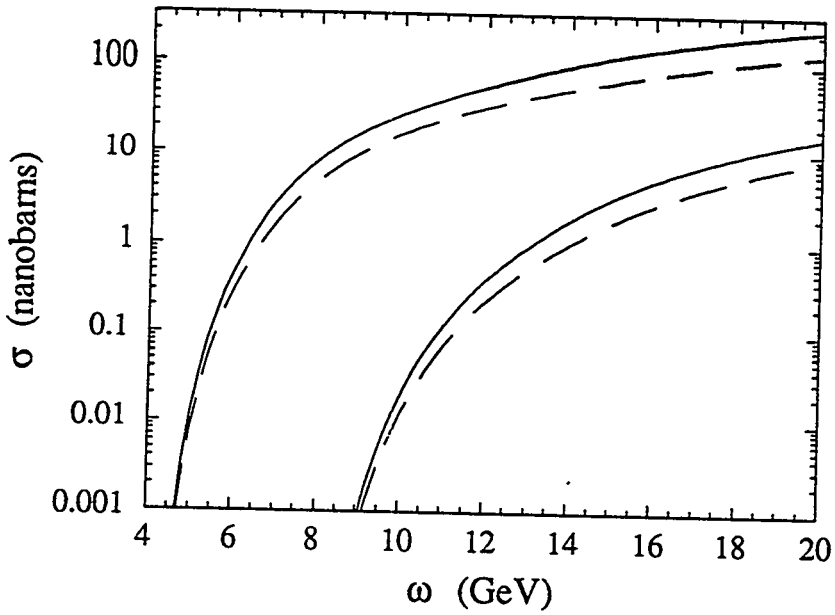


Fig. 2. The total cross section for photoproduction of glueballino pairs. The upper curves are both for glueballino mass (inserted for $\tilde{m}$ in our formulas) of 1.0 GeV and the lower curves have glueballino mass 1.5 GeV. The solid curves are for quark mass m_q of 0.3 GeV and the dashed curves use m_q = 1.0 GeV. The CTEQ1L quark distributions at their benchmark of $Q^2 = 4$ GeV^2 were used for this figure. As seen, the results are sensitive to gluino mass but not to quark mass.

Solenoidal Detectors in Spectroscopy

Dan Coffman
Laboratory of Nuclear Studies, Cornell University
Ithaca, NY 14853

Abstract
This report discusses the operation of solenoidal detectors for charged particle detection. A simple detector is evaluated as a general purpose spectrometer for CEBAF.

Introduction

Solenoidal detectors have long been used in colliding beam experiments. This choice of geometry seems particularly natural at an electron-positron collider where the center-of-mass system is at rest in the laboratory. In such a situation a solenoidal detector affords good resolution with a large and fairly uniform acceptance. This attractive hermiticity, among other considerations, lead to the adoption of solenoidal detectors for both the CERN and FNAL $p\,\overline{p}$ colliders. More recently solenoidal detectors have been employed at CERN and BNL in stopping hadron experiments. The Zeus detector at DESY is a solenoidal detector, albeit of unusual design, even though the kinematics of the collisions at HERA are more similar to those of a fixed target experiment.

A solenoidal detector may be operated quite successfully in a fixed target facility. The LASS detector at SLAC was able to record 115 million triggers when exposed to an 11 GeV K^- beam. This ability to function in a high rate environment is, of course, crucial to any modern detector. The solenoial field offers an additional benefit in a photoproduction experiment: $e^+\,e^-$ pairs from photons converting in the target are not normally scattered into the detector. Each member of the pair typically has only very little momentum transverse to the beam direction and so tends to "curl up" in the magnetic field and pass harmlessly through the apparatus.

The trajectory of a charged particle in a uniform solenoidal field is, as is well known, a helix. The momentum is determined by extracting the five parameters describing this helix. Good momentum resolution dictates a strong magnetic field

of a high degree of uniformity. The strength of the field must, however, be matched carefully to the physics process of interest. If it is too strong, low momentum particles will often be lost. In addition, large acceptance requires a large active volume. For these reasons of strength, uniformity, and volume the spectrometer magnet is often of a superconducting design.

The drift chambers used for tracking must also be carefully designed. Operation of a chamber within a strong solenoidal field is by no means easily accomplished. Also, multiple scattering must scrupulously be minimized, especially in a fixed target application given the long lever arm between chamber planes.

A Model Detector

The model detector is illustrated in figure 1. It consists of a target one meter upstream of a solenoidal charged particle detector and a calorimeter hodoscope. The magnet has a field strength of 1.5 Tesla, a bore radius of 0.8 m, and a length of 1.5 m. Located within the magnet are six planes of drift chambers of 150 μm spatial resolution. The chambers alternate in "x" and "y" views. The calorimeter is an array of lead glass blocks with spatial resolution of 5 mm and energy resolution of $\frac{\sigma}{E} = \left(2 + \frac{5}{\sqrt{E}}\right)\%$. Each detector element has a hole of radius 0.1 m in its center to allow passage of beam particles.

This detector will be used in a model experiment to establish the existence of a vector meson $C(1480)$ previously seen by only one experiment. The reaction to be investigated is $\gamma p \rightarrow C\,p$; $C \rightarrow \phi\,\pi^0$; $\phi \rightarrow K^+K^-$; $\pi^0 \rightarrow \gamma\gamma$. Establishment of the desired state requires only the reconstruction of the ϕ and the π^0. Measuring the properties of the meson may require detecting the recoil proton as well.

The performance of the detector is simulated in a straightforward manner. A beam of real, unpolarized photons is incident on the target. The production cross section is assumed to be of the form

$$\frac{d\sigma}{dt} \propto e^{-8|t|}$$

The various unstable states are decayed until all that remain are the five stable

particles. The photons are propagated to the calorimeter if they pass through the magnet's bore. At the calorimeter, the positions and energies of the photons are smeared according to the assumed resolutions.

The charged particles are propagated through the drift chamber planes. The resolution of their momenta is estimated through a "parameter level" study. This should correctly reproduce the effect of the chambers' spatial resolution. It does not, it should be emphasized, take multiple scattering into account.

The model detector performs quite well. That the target is substantially upstream of the detector allows many of the charged particles to reach the drift chambers in spite of their typically small polar angles as measured with respect to the beam direction. In addition, this long lever arm allows these polar angles to be measured extremely well.

For the detection of the C alone, the acceptance is over 11% when the ϕ and π^0 are required to have reconstructed masses within two standard deviations of their nominal masses. The acceptance is pratically constant over a range of photon energies from three to four GeV. The mass resolution of the C is about 20 MeV/c^2, dominated entirely by the photon energy resolution of the calorimeter. If the proton is required to be detected as well, the acceptance falls to about 5% and is now a fairly strong function of the photon energy, being nil at threshold, peaking at about three GeV, and thereafter falling slowly with photon energy. The mass spectra of the π^0 and the C are shown in figures 2 and 3.

Discussion

The model detector demonstrates that a solenoidal detector could work well in a photoproduction experiment at CEBAF. It is crucial, though, that a realistic study include the effects of multiple scattering in the drift chamber planes. These could be quite substantial. In addition, the energy resolution of the calorimeter is likely to be degraded due to pair conversions. Finally, the acceptance depends strongly on the position of the target. For a given process of interest there is almost certainly an optimal target position.

Conclusions

Solenoidal detectors are commonly used high energy physics laboratories. A simple study demonstrates the feasibility of such a detector in a high rate photoproduction experiment at CEBAF. The relative simplicity of the design, large acceptance, and general flexibility makes this perhaps an attractive option. Such a detector should be subjected to a serious, realistic evaluation in order to optimize the parameters of the design and to estimate carefully the resolution of the system.

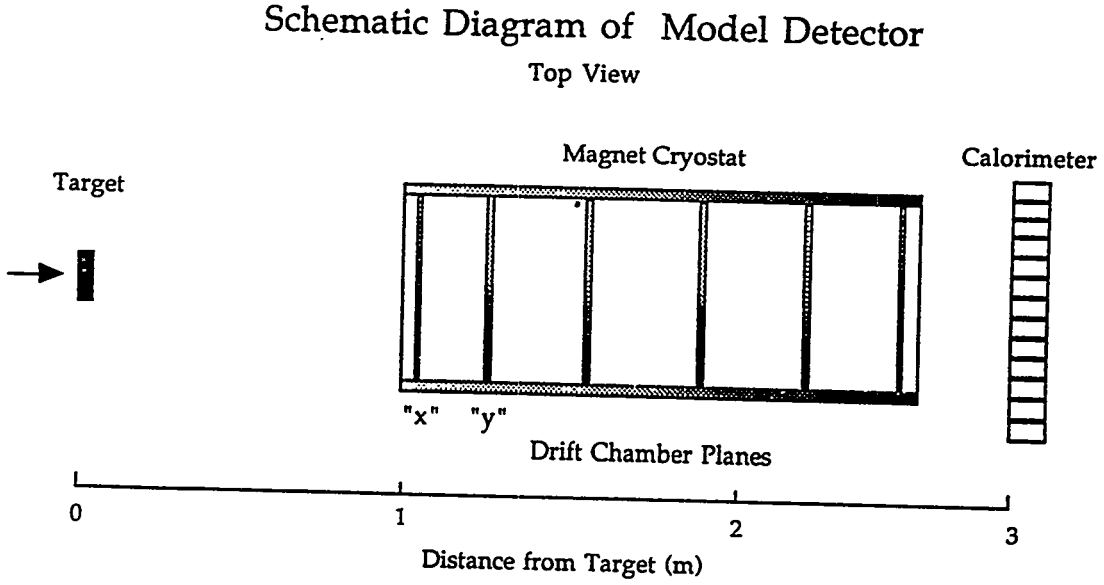
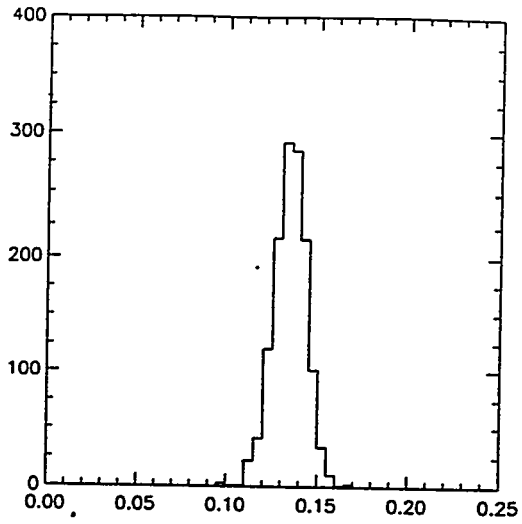
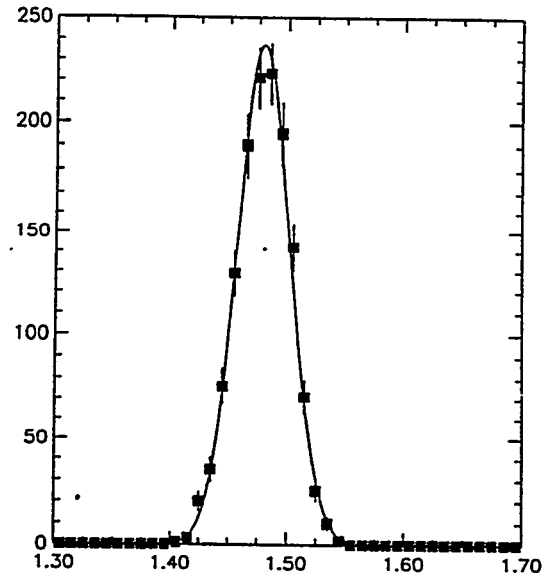


Figure 1: Illustration of Model Detector



Firgure 2: Mass spectrum of π^0 (GeV/c^2)



Firgure 3: Mass spectrum of C (GeV/c^2)

Using Contour Plots in Electroproduction to Examine Regions in ϵ, Q^2, W Space

H. Funsten, College of William and Mary

June 9, 1994

Abstract

In determining incident CEBAF beam energies for CLAS electroproduction experiments that separate the longitudinal and transverse cross section components, contour plots of ϵ defined over a 2 dimensional Q^2, W space can be useful. This note describes an approximate method of constructing such plots.

1 Introduction

In electroproduction reactions large acceptance spectrometers, such as the CEBAF Hall B CLAS spectrometer, can detect a wide kinematic region in outgoing electron energy, E', and angle, θ_e. This permits simultaneous data accumulation over an extended range of the variables characterising the physics of the reaction: ϵ and Q^2, the virtual photon's polarization and invariant mass^2, and W, the invariant mass of the combined virtual photon - target system.

The reaction physics and desired event rate determine regions in the W, Q^2 plane to be used for data analysis. For example, in investigating the Q^2 dependence of N* resonances, a typical W, Q^2 region would be centered at W - M = .5 GeV, Q^2 = 2.3 GeV^2 and have widths ΔW = 0.1 GeV and ΔQ^2= 1 GeV^2 . Such a region is schematically represented by the lower left hand box in Fig. 1.

In many cases it is desirable to approximately determine the extent of ϵ intervals that correspond to specified W, Q^2 regions at a given incident electron beam energy, E. This note describes the use of contour plots to determine these intervals.

2 Surfaces in W, Q^2, ϵ Space

For a given E, the variables W, Q^2, and ϵ are constrained by the kinematics at the electron vertex to form a surface, $\mathcal{S}$(E), in the W, Q^2, ϵ 3 - space. By varying E, a family of such surfaces will be formed. Choosing the positive z axis along ϵ, surfaces belonging to larger E overlie those with smaller E.

Populations of ϵ intervals corresponding to W, Q^2 regions can be estimated by transforming the given W, Q^2 regions to corresponding regions on $\mathcal{S}$(E) and projecting

onto the ϵ axis. The results can be visualized by use of constant ϵ contour plots of $\mathcal{S}$(E) superimposed on boundaries of the given W, Q^2 regions.

3 Calculation of the Surfaces

The kinematic equations for the electron vertex are:

$$W = (M^2 + 2M\nu - Q^2)^{1/2} \tag{1}$$

$$Q^2 = 4EE' \sin^2(\theta_e/2) \tag{2}$$

$$\nu = E - E' \tag{3}$$

$$\epsilon = \left[1 + 2\left(1 + \frac{\nu^2}{Q^2}\right)\tan^2\left(\frac{\theta_e}{2}\right)\right]^{-1} \tag{4}$$

where M is the target nucleon rest mass; $m_e \ll M$, $Q^2 \geq 0$.

$\mathcal{S}$(E) is obtained by eliminating E', ν, and θ_e in 1) - 4). It is helpful to rewrite 1) as:

$$\nu = \omega' + q \tag{5}$$

using the substitutions:

$$\omega' = \frac{W^2 - M^2}{2M}$$
$$q = \frac{Q^2}{2M} \tag{6}$$

It will be shown below that the substitutions 6) additionally result in reducing rounded contours in W, Q^2, ϵ space to approximately flat $\mathcal{S}$(E) contours in ω', q, ϵ space.

2) - 6) yield

$$\frac{q^2}{2} + [\omega' + M\,(1+\xi) + 2E\xi]\,q + \frac{\omega'^2}{2} - 2E^2\xi + 2E\xi\omega' = 0$$
$$\xi = \frac{1}{2}\left(\frac{1}{\epsilon} - 1\right) \tag{7}$$

For a fixed E, 7) yields surface $\mathcal{S}$(E) in the 3 – space of ω', q, ξ(or ϵ). The corresponding $\mathcal{S}$(E) in 3 - space of W, Q^2, ϵ is then obtained by using 6).

The electron beam energy, E, needed for a measurement at a given ω', q, ξ corresponding to W, Q^2, ϵ, is obtained from 7)

$$E = \frac{-B \pm \sqrt{B^2 - 4AC}}{2A}$$
$$A = 2\xi$$
$$B = -2\xi\,(\omega' + q)$$
$$C = -qM\,(1+\xi) - \frac{\omega'^2}{2} - \omega' q - \frac{q^2}{2}. \tag{8}$$

4 ω', q, ϵ Contours

Constant ϵ contours of $\mathcal{S}$(E) are obtained from 7) by giving ϵ values from 0 to 1, (ξ from ∞ to 0). This leads to a quadratic equation for q in terms of ω':

$$aq^2 + bq + c = 0 \tag{9}$$

where:

$$a = \frac{1}{2}$$
$$b = \omega' + M\,(1+\xi) + 2E\xi$$
$$c = \frac{1}{2}\omega'^2 - 2E^2\xi + 2E\xi\omega' \tag{10}$$

On the ω', q plane $\epsilon = 0$, $\xi = \infty$. In 9), the highest order terms in ξ are

$$\xi(qM + 2Eq - 2E^2 + 2E\omega') \tag{11}$$

Hence for $\epsilon = 0$, $\mathcal{S}$(E) intersects the q, ω' plane in the straight line:

$$qM + 2Eq - 2E^2 + 2E\omega' = 0 \tag{12}$$

which intersects the q and ω'axes at

$$\omega'_{int} = E$$
$$q_{int} = \frac{E}{1 + \frac{M}{2E}}. \tag{13}$$

The flatness of $\mathcal{S}$(E) on the ω', q plane is retained above it as can be seen by examining the quadratic discriminant in 9):

$$\sqrt{b^2 - 4ac} = \sqrt{(M\xi')^2 + 4E\hat{E}\xi\hat{\xi} + 2M\hat{\xi}\omega'} \tag{14}$$

where $\hat{E} = E + M$ and $\hat{\xi} = \xi + 1$. At CEBAF energies and $\epsilon \leq 0.8$ the last term in the square root in 14) is $\leq\approx 30\%$ of the sum of the first two. Hence 14) is constant with

ω' to $\approx \pm$ 8% and, for a contour line $0 \leq \epsilon \leq 0.8$, q and ω' are approximately linearly related. As a result, the shape of $\mathcal{S}$(E) is approximately that of a tilted plane, with the ω', q axes intersections (i.e., at $\epsilon = 0$), ω'_{int}, q_{int} given by 13) above. As shown in Fig 2, as $\epsilon \rightarrow 1$ the slope of the plane decreases and $\mathcal{S}$(E) levels off.

The approximate planar behavior of $\mathcal{S}$(E) leads to an evaluation of ϵ valid to within $\pm$ 10% for $\epsilon \leq 0.8$:

$$\epsilon \approx 1.8 \left(1 - \frac{\omega'}{\omega'_{int}} - \frac{q}{q_{int}}\right) \tag{15}$$

[1] Supported by NSF.

Figure Captions

Fig. 1 shows contours of ϵ with W and Q^2. E = 6 GeV. Shown at the lower left is a typical data region, centered at W - M = 0.5 GeV, Q^2 = 2.3 GeV^2 , with widths Δ W = 0.1 GeV and $\Delta Q^2 = 1 GeV^2$.

Fig 2 shows contours of ϵ with ω' and q. E = 6 GeV. In contrast to Fig. 1, the contours are approximately straight lines. The intersection of $\mathcal{S}$(E) with the ω' axis, ω'_{int}, is E. For given values of ω' and q, equation 15) can be used to yield approximate values of ϵ . Shown at the lower left is the same W, Q^2 data region as in Fig. 1.

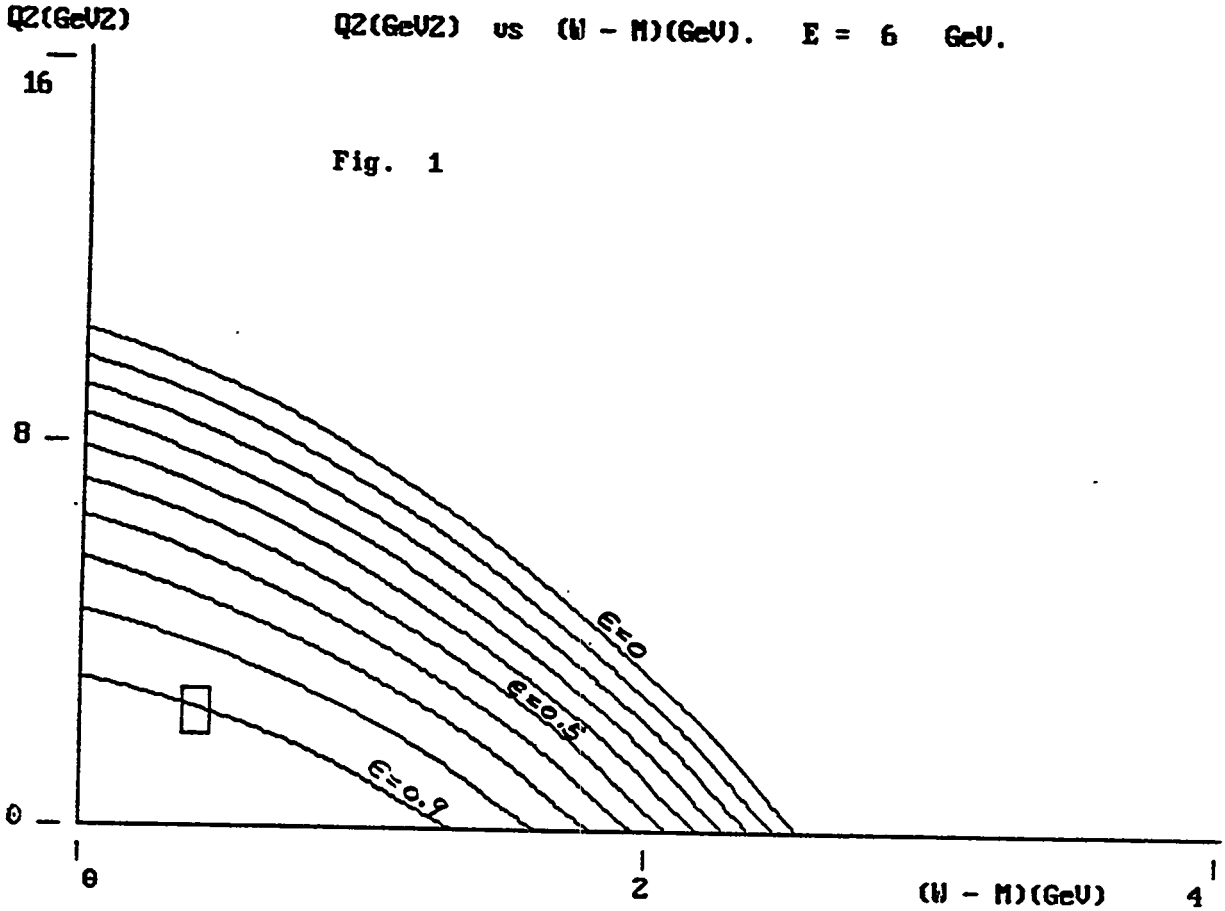
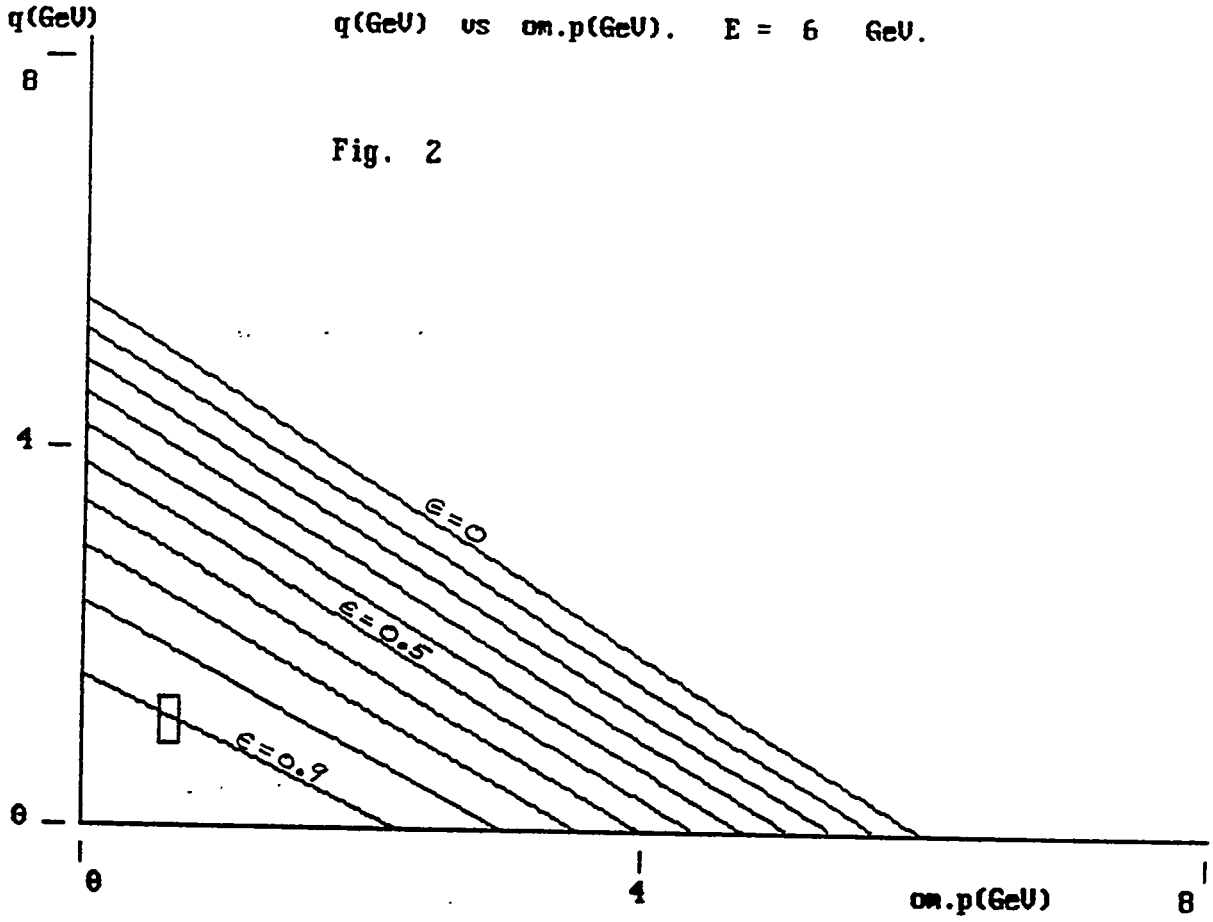


Fig. 1



q(GeV) vs om.p(GeV). E = 6 GeV.

Fig. 2

Spin 0 Decay Angular Distribution for Interfering Mesons in Electroproduction.

H. FUNSTEN, W & M , G. GILFOYLE, U. of R.

1 Introduction

Self analyzing meson electroproduction experiments are currently being planned for the CEBAF CLAS detector. These experiments deduce the spin polarization of outgoing unstable spin s ¿ 0 mesons from their decay angular distribution, $W(\theta, \phi)$. The large angular acceptence of the CLAS detector permits kinematic tracking of a sufficient number of these events to accurately determine electroproduction amplitudes from the deduced polarization.

Maximum polarization information is obtained from $W(\theta, \phi)$ for decay into spin 0 daughters. The helicity of the decaying meson is transferred to the the daughter's relative orbital angular momentum m - projection; none is "absorbed" into daughter helicities. The decaying meson's helicity maximally appears in $W(\theta, \phi)$.

$W(\theta, \phi)$ for spin 0 daughters has been derived for 1) vector meson electroproduction [Schil 70] and 2) general interfering mesons produced by incident pions, [Martin 75]. This paper derives $W(\theta, \phi)$ for electroproduction of two interfering mesons that decay into spin 0 daughters. An application is made to the case of interfering scalar and vector mesons. The derivation is an extension of [Schil 70] using the general decay formalism of [Martin 75]. The expressions can be easily extended to the case of N interfering mesons since interference occurrs pairwise in the observable $W(\theta, \phi)$, a quadratic function of the meson amplitudes.

The derivation uses the virtual photon density matrix of [Schil 70] which is transformed by a meson electroproduction transition operator, T. The resulting density matrix for the interfering mesons is then converted into a corresponding statistical tensor and contracted into the efficiency tensor for spin 0 daughters.

2 Virtual Photon Density Matrix

The virtual photon, density matrix projection scheme of [Schil 70] is used. The density matrix for a (spin 1) virtual photon, $\rho_{\mu,\mu'}(\gamma_V)$ is projected onto 9 ($\alpha = 0, ..., 8$) basis hermitian density matrices Σ^α, (equns. 64, 65) of [Schil 70]):

$$\rho_{\mu,\mu'}(\gamma_V) = \sum_\alpha \Sigma^\alpha_{\mu,\mu'} \Pi^\alpha(\epsilon, \Phi). \qquad (1)$$

The projection components, Π^α, contain the kinematics of the electron

vertex, i.e., ϵ, the polarization of the virtual photon, and Φ, the angle between the electron and hadron scattering planes. Examples of Σ and Π are:

$$\Sigma^2 = \begin{pmatrix} 0 & 0 & -i \\ 0 & 0 & 0 \\ i & 0 & 0 \end{pmatrix}$$

$$\Pi^1(\epsilon, \Phi) = -\epsilon \; cos2\Phi,$$
$$\Pi^2(\epsilon, \Phi). = -\epsilon \; sin2\Phi. \qquad (2)$$

The projection has the advantages of:

1. Each α component is associated with a physical polarization of the virtual photon, e.g., unpolarized transverse ($\alpha = 0$), longitudinal ($\alpha = 4$), longitudinal - transverse ($\alpha = 5, 6$), etc.,
2. Three components ($\alpha = 3, 7, 8$) give the dependence on the electron polarization, P. The polarization is longitudinal since $\mid Q^2 \mid >> m_e^2$.

$$\Pi_3 = P\sqrt{1-\epsilon^2},$$
$$\Pi_7 = P\sqrt{2\epsilon(1-\epsilon)}\cos\Phi,$$
$$\Pi_8 = P\sqrt{2\epsilon(1-\epsilon)}\sin\Phi.$$

3. Each Σ_i has a definite symmetry under negation of helicities.

3 Meson Density Matrix

The density matrix for interfering mesons is $\rho^{\ell_1,\ell_2}_{\lambda_1,\lambda_2}(mesons)$ where ℓ_i is the spin of the outgoing electroproduced meson, λ_i is its helicity, For the case of 2 interfering mesons of spins l_1, l_2 there will be 4 density matrices. Two represent direct terms in $W(\theta, \phi, \Phi)$: $\ell_1 = \ell_2 = l_1$ and $\ell_1 = \ell_2 = l_2$.. The other two represent interference terms in $W(\theta, \phi, \Phi)$: $\ell_1 = l_1, \ell_2 = l_2$ and $\ell_1 = l_2, \ell_2 = l_1$.

4 Meson Electroproduction Operator

The dynamics of $W(\theta, \phi, \Phi)$are contained in the electroproduction operator $\mathbf{T} = T^{\ell_i;1}_{\lambda_i,\mu}$ where μ is the helicity of the incoming (spin 1) virtual photon. For the case of no polarization measurements on the incoming or outgoing nucleon spins the electroproduction operator transforms

the incident virtual photon density matrix into the outgoing interfering mesons density matrix:

$$\rho^{\ell_1,\ell_2}_{\lambda_1,\lambda_2}(mesons) = \frac{1}{2}\sum_{\mu,\mu'}, T^{\ell_1,1}_{\lambda_1,\mu} T^{*\ \ell_2,1}_{\lambda_2,\mu'} \rho_{\mu,\mu'}(\gamma V) \tag{3}$$

As will be shown below, the behavior of $W(\theta,\phi,\Phi)$ depends on the symmetry properties of $\rho^{\ell_1,\ell_2}_{\lambda_1,\lambda_2}(mesons)$ under helicity negation which, by equn 3) depends on corresponding symmetry properties of T and, through $\rho_{\mu,\mu'}(\gamma V)$, upon Σ^α. If T is parity invariant it has symmetry under helicity negation given by the Jacob - Wick relation [Jacob 59]:

$$T^{\ell_i,1}_{\lambda_i,\mu} = \eta(-1)^{\lambda_i-\mu} T^{\ell_i,1}_{-\lambda_i,-\mu} \tag{4}$$

where η is the overall naturality of the incoming photon and outgoing meson i:

$$\eta = \eta_{\gamma V}\eta_i \tag{5}$$

$$\eta_i = parity_i(-1)^{spin_i},\ \ \eta_{\gamma V} = +1 \tag{6}$$

The symmetry properties of Σ^α are listed in [Schil 70], Table 1. For the case of single vector electroproduction and for the direct terms for two interfering mesons, ($l_1 = l_2$ in 3)), the symmetry properties of $\rho^{\ell_1,\ell_2}_{\lambda_1,\lambda_2}(mesons)$ are given by [Schil 70] equn. 79). For the cross terms ($\ell_1 \neq \ell_2$ in 3) [Schil 70] equns 79) should be multiplied by $\eta_1\eta_2$.

The helicity relations also permit having to specify only about half of the $3(2\ell_i+1)$ complex parameters of $T^{\ell_i,1}_{\lambda_i,\mu}$.

5 Decay Distribution

$W(\theta,\phi)$ is obtained by contracting [Ferg 65] the spin statistical tensor of the outgoing two meson system, $\rho_{L,\Lambda}(\ell_1,\ell_2)$with $\epsilon_{L,\Lambda}(\ell_1,\ell_2,\theta,\phi)$, the efficiency spin statistical tensor for detection of the two spin 0 decay daughters at spherical angles θ,ϕ. The decaying meson rest frame is used:

$$W(\theta,\phi) = \Sigma^{\ell_1,\ell_2}_{L,\Lambda}\left[\rho_{L,\Lambda}(\ell_1,\ell_2)\epsilon_{L,\Lambda}(\ell_1,\ell_2,\theta,\phi)\right] \tag{7}$$

where $L = \ell_1 \otimes \ell_2$, $\Lambda = \lambda_1 - \lambda_2$. Use of spin tensors instead of spin density matrices facilitate expression of $W(\theta,\phi)$ in terms of a single rotation operator, shown below.

The statistical tensor for the interfering mesons $\rho_{L,\Lambda}(\ell_1,\ell_2)$ can be written in terms of $\rho^{\ell_1,\ell_2}_{\lambda_1,\lambda_2}(mesons)$using a
$\ell_1 \otimes \ell_2 = L$ Clebsch - Gordon coupling coefficient:

$$\rho_{L,\Lambda}(\ell_1,\ell_2) = \Sigma_{\lambda_1,\lambda_2}(-1)^{\ell_2+\lambda_2}(\ell_1,\lambda_1,\ell_2,-\lambda_2 \mid L,\Lambda)\rho^{\ell_1,\ell_2}_{\lambda_1,\lambda_2}(mesons). \tag{8}$$

$\epsilon_{L,\Lambda}(\ell_1, \ell_2)$ is evaluated [Ferg 65] by noting that in the decaying meson's rest frame the spin ℓ_i meson decays into the two spin 0 daughters in a plane wave state with angular momentum ℓ_i. Choosing the z axis along the decay direction $\lambda_i = 0$ and the amplitude is $\frac{\hat{\ell}_i}{\sqrt{4\pi}}$, $\hat{\ell}_i = \sqrt{2\ell_i + 1}$. For two interfering mesons with spins ℓ_1, ℓ_2, the efficiency matrix for the decay is then:

$$\epsilon_{0,0}^{\ell_1,\ell_2} = \frac{\hat{\ell}_1 \hat{\ell}_2}{4\pi}. \tag{9}$$

The density matrix $\epsilon_{0,0}^{\ell_1,\ell_2}$is coupled into a corresponding statistical tensor:

$$\epsilon_{L,0}(\ell_1, \ell_2) = \epsilon_{0,0}^{\ell_1,\ell_2}(-1)^{\ell_2}(\ell_1, 0, \ell_2, 0) \mid L, 0) \tag{10}$$

Note that the above Clebsch - Gordon coefficient yields:

$$\ell_1 + \ell_2 + L = even \tag{11}$$

Rotation of $\epsilon_{L,0}(\ell_1, \ell_2)$by the Wigner rotation matrix,

$$\mathcal{D}^L_{\Lambda,0}(\theta, \phi) = \frac{\sqrt{4\pi}}{\hat{L}} Y^{*L}_M(\theta, \phi) \tag{12}$$

then expresses $\epsilon_{L,0}(\ell_1, \ell_2, \theta, \phi)$ in terms of an arbitrary axis at spherical angles θ, ϕ relative to the decay direction. That is,

$$\epsilon_{L,0}(\ell_1, \ell_2, \theta, \phi) = \mathcal{D}^L_{\Lambda,0}(\theta, \phi)\epsilon_{L,0}(\ell_1, \ell_2) \tag{13}$$

The axis will be taken to be the outgoing decaying meson's momentum direction in the hadronic cms (helicity system).

6 Final Results

Substitution of 8) - 13) into 7) yields:

$$W(\theta, \phi, \Phi) = \sum_{L,M} \langle Y^L_M \rangle Y^{*L}_M(\theta, \phi) \tag{14}$$

$$\langle Y^L_M \rangle = \sum_{\lambda_1,\lambda_2}^{\ell_1,\ell_2} \frac{\hat{\ell}_1 \hat{\ell}_2}{\hat{L}} (-1)^{\lambda_2} (\ell_1, \lambda_1, \ell_2, -\lambda_2 \mid L, \Lambda)(\ell_1, 0, \ell_2, 0) \mid L, 0)$$
$$\cdot \rho^{\ell_1,\ell_2}_{\lambda_1,\lambda_2}(mesons).$$

where $\rho^{\ell_1,\ell_2}_{\lambda_1,\lambda_2}(mesons)$ is given by 3); $\rho_{\mu,\mu'}(\gamma_V)$ is, in turn, given by 1). The Φ dependence of $W(\theta, \phi, \Phi)$comes from the Φ dependence of Π.

7 Helicity Symmetries

The decay angular distribution multipole moment $\langle Y_M^L \rangle$ has the behavior:

$$\langle Y_M^L \rangle = (-1)^M \langle Y_{-M}^{*L} \rangle \tag{15}$$

from the Hermicity of $\rho_{\lambda_1,\lambda_2}^{\ell_1,\ell_2}(mesons)$and Clebsch - Gordon coefficient symmetry relations. This insures that $W(\theta,\phi)$is real. In addition, the parity conditions 3) - 5) yield

$$\langle Y_M^L \rangle = Real \ / \ Imaginary \tag{16}$$

if:

$$\eta = +1/-1, \quad \alpha = 0,1,4,5 \tag{17}$$

$$\eta = -1/+1, \quad \alpha = 2,3,6,7. \tag{18}$$

Thus by the Φ behavior of Π, (e.g. equation 2)), [Schil 70], Table 1, T symmetries will implicitly appear in not only the θ,ϕ but the Φ variation of $W(\theta,\phi,\Phi)$.

8 Application to Interfering Vector - Scalar Mesons

Experiments that measure $W(\theta,\phi,\Phi)$permit detection of mesons with small electroproduction amplitude by their interference with a larger amplitude neighboring meson. $W(\theta,\phi,\Phi)$was calculated for a $f_0(975)$ scalar meson interfering with a $\rho(770)$ vector meson. The above expressions were coded to give simulated sensitivities to the transverse and longitudinal electroproduction amplitudes and phases of the $f_0(975)$ to relative the $\rho(770)$. As an example :

For approximately 5,000 events in $W(\theta,\phi)$, the relative error (rms) in transverse $f_0(975)$ to transverse $\rho(770)$ amplitude is $\approx$ 5 %; that in cosine of the relative transverse phase angle is $\approx$ 15 %.

9 Coding of Expressions

The expressions for $W(\theta,\phi,\Phi)$, (equations 1), 3) and 14)) are currently being coded in C++ for the general case of $l_1, l_2 \leq 2$. The work is being performed by S. Boyd, J. Finander, and C. Wahlquist.

References

[Ferg 65] A. J. Ferguson, "Angular Correlation Methods in Gamma - Ray Spectroscopy" 1965, Horth - Holland Publishing Co.

[Jacob 59] M. Jacob and G. C. Wick, Annals of Physics, 7 (1959), 404.

[Martin 75] A. D. Martin and C. Michael, Nucl. Phys., B84 (1975) 83

[Schil 70] K. Schilling and G. Wolf, Nucl. Phys. B61 (1973) 381.

NEW RESULTS IN MESON SPECTROSCOPY FROM THE CRYSTAL BARREL EXPERIMENT

Curtis A. Meyer
Carnegie Mellon University, Pittsburgh, PA 15213

The Crystal Barrel Collaboration

ABSTRACT

Recent observations by the Crystal Barrel experiment of two scalar resonances, $f_0(1365)$ and $a_0(1450)$ have allowed us to clarify the members of the scalar nonet. In addition, a third scalar, $f_0(1500)$, appears to be supernumerary, and is a candidate for the scalar glueball expected near 1500 MeV.

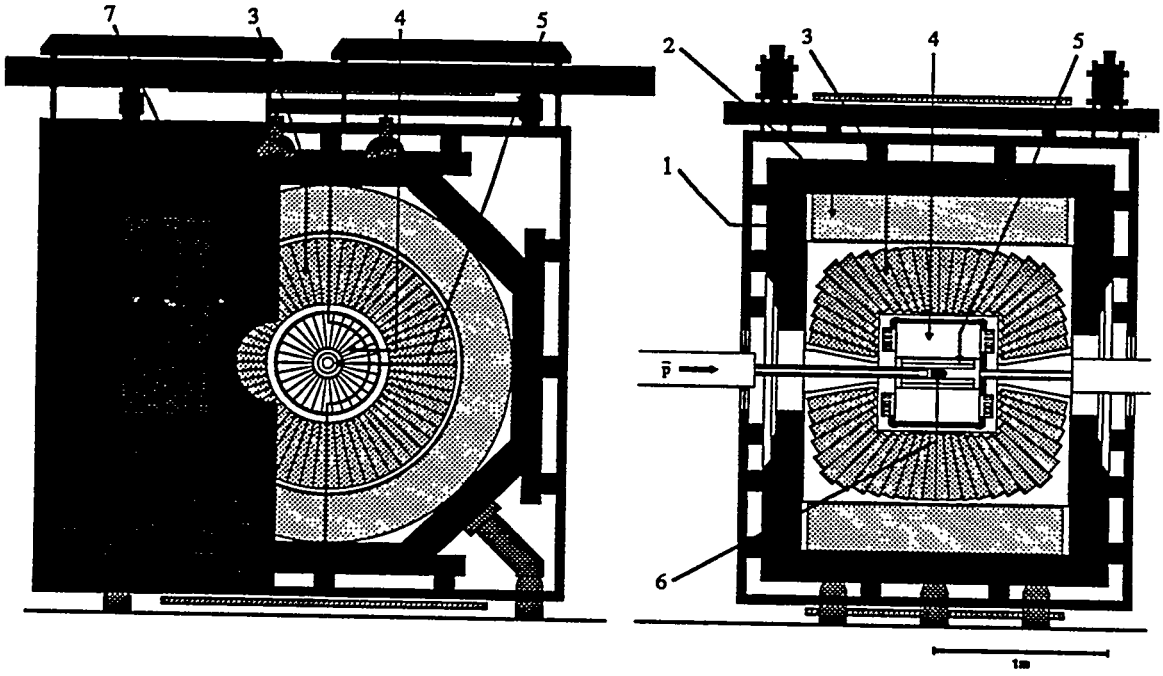


Figure 1: The Crystal Barrel detector. Magnet yoke (1), magnet coils (2), CsI–calorimeter (3), JDC (4), PWC (5), target (6), one half of the endplate (7).

1. The Crystal Barrel Detector

The Crystal Barrel detector at LEAR [1] is a nearly 4π apparatus for both charged particles and photons. The detector is used to study $\bar{p}p$ annihilation at rest and in flight, (up to 1.9GeV/c), and has been very productive in the field of meson spectroscopy. In particular, the scalar nonet, $J^{PC} = 0^{++}$ is now much better understood, and a good candidate for the scalar glueball now exists.

The detector is shown in Fig. 1. The antiprotons enter along the axis of the 1.5 T

solenoidal field, and stop in a liquid hydrogen target. They annihilate, and the resulting $\pi^{\pm}$, $K^{\pm}$ and γ's are tracked outward through the detector. Immediately outside the hydrogen target are two cylindrical multiwire proportional chambers used to either trigger on or veto events with charged particles. Next is a 23 layer cylindrical drift chamber, (JDC). The chamber is divided axially into 30 sectors, with an 8mm wire spacing between adjacent radial layers. The wires are read out at each end to provide a z–measurement through charge division. Outside the JDC is the CsI(Tl) barrel built with 1380 16 radiation length crystals. The crystals are arranged in a center–pointing geometry, and the calorimeter has achieved an energy resolution of 2.5% at 1GeV.

2. New Results

The data discussed in this paper come from two triggers; the all–neutral trigger, (no charged particles in the PWC), and the minimum–bias trigger, (a $\bar{p}$ entering the liquid hydrogen target). The 6γ final state is obtained from $16.8 \cdot 10^6$ all neutral annihilations at rest, while the $\pi^+\pi^-\pi^\circ\pi^\circ\pi^\circ$ data are from $3.8 \cdot 10^6$ minimum–bias events. In the 6γ final state, we reconstruct $\bar{p}p \to \pi^\circ\pi^\circ\pi^\circ$ (712k events), $\bar{p}p \to \pi^\circ\pi^\circ\eta$ (187k events), $\bar{p}p \to \pi^\circ\eta\eta$ (31k events), and $\bar{p}p \to \pi^\circ\eta\eta'$ (130 events), where π°, η and η' are all detected in their 2γ decay modes. These data have been analyzed using two different methods, the K–matrix formalism [2] and the N/D method [3]. Both methods use a coupled channel approach, allowing both $\pi\pi$ or $\eta\eta$ and an unseen $K\bar{K}$ decay.

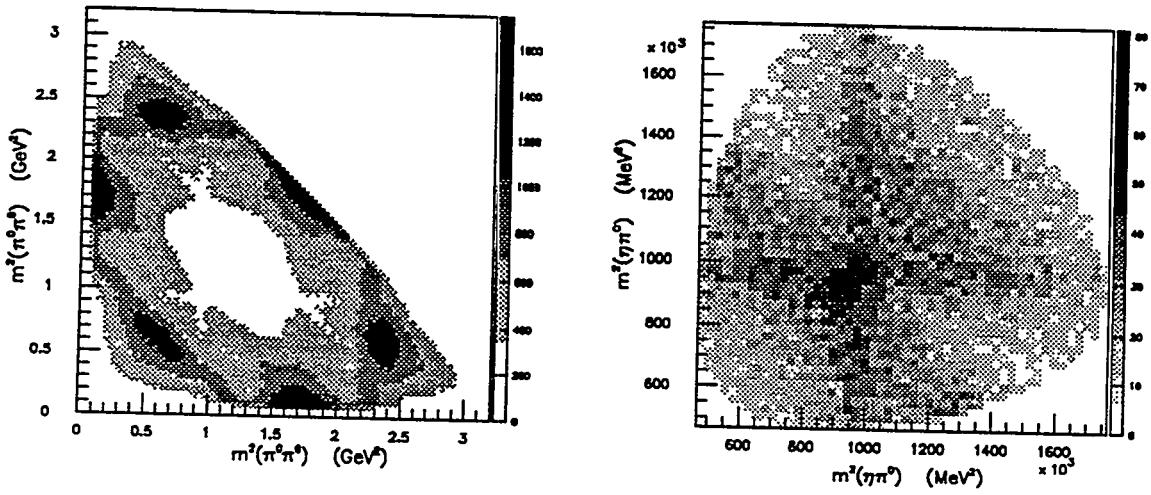


Figure 2: The Dalitz plots for $\bar{p}p \to \pi^\circ\pi^\circ\pi^\circ$ (left) and $\pi^\circ\eta\eta$ (right).

The $\bar{p}p \to \pi^\circ\pi^\circ\pi^\circ$ Dalitz plot (Fig. 2–left) has 3–fold symmetry, meaning that resonances are seen simultaneously as three bands, vertical, horizontal and diagonal. In the vertical, one sees a band near 0.9 GeV^2 corresponding to the $f_0(975)$. The two blobs at the upper and lower edge of the plot near 1.7 GeV^2 corresponds to the $f_2(1270)$, and the vertical band near 2.25 GeV^2 corresponds to a new scalar resonance, the $f_0(1500)$. The blob near 2.4 GeV^2 is caused by reflections from the low–mass $\pi\pi$ system, and a tensor state, ($J^{PC} = 2^{++}$) near 1550 MeV. In addition, the fit to this

Dalitz plot requires a broad, inelastic scalar state at a mass of 1365 MeV, which is probably the $f_0(1400)$.

The $\eta\eta\pi^\circ$ Dalitz plot has a 2–fold symmetry. Resonances in the $\eta\pi^\circ$ system are seen as horizontal and vertical bands, while resonances in the $\eta\eta$ system are seen as diagonal bands. The Dalitz plot , (Fig. 2–right) shows a clear signal for the $a_0(980) \to \eta\pi^\circ$ as the horizontal and vertical crossing bands near $950 \cdot 10^3$ MeV^2. In addition, there are two diagonal bands corresponding to the $f_0(1365) \to \eta\eta$ and the $f_0(1500) \to \eta\eta$. A simultaneous spin–parity analysis [4] of both $\pi^\circ\pi^\circ\pi^\circ$ and $\eta\eta\pi^\circ$ yields the following parameters for the two isoscalar scalar resonances. (Note: we indicate a mass of 1500 for the second f_0 because a second analysis leads to a mass between 1480 and 1520.)

$$f_0(1365) \quad m = 1365^{+20}_{-55} \quad \Gamma = 267 \pm 70$$
$$f_0(1500) \quad m = 1520 \pm 25 \quad \Gamma = 148^{+20}_{-25}$$

The Dalitz plot for $\bar{p}p \to \eta\pi^\circ\pi^\circ$ (Fig. 3–left), exibits a very complicated interference pattern which is evidence for dominance of a single initial state. This is confirmed by a spin–parity analysis [5] of these data coupled to $\pi^\circ\pi^\circ\pi^\circ$ and $\eta\eta\pi^\circ$. The $\eta\pi^\circ\pi^\circ$ final state arises almost entirely from the $^1S_0$ state of the $\bar{p}p$ atom. The analysis explains the data using the following amplitudes. [$\pi\pi$ S–wave] Including the AMP

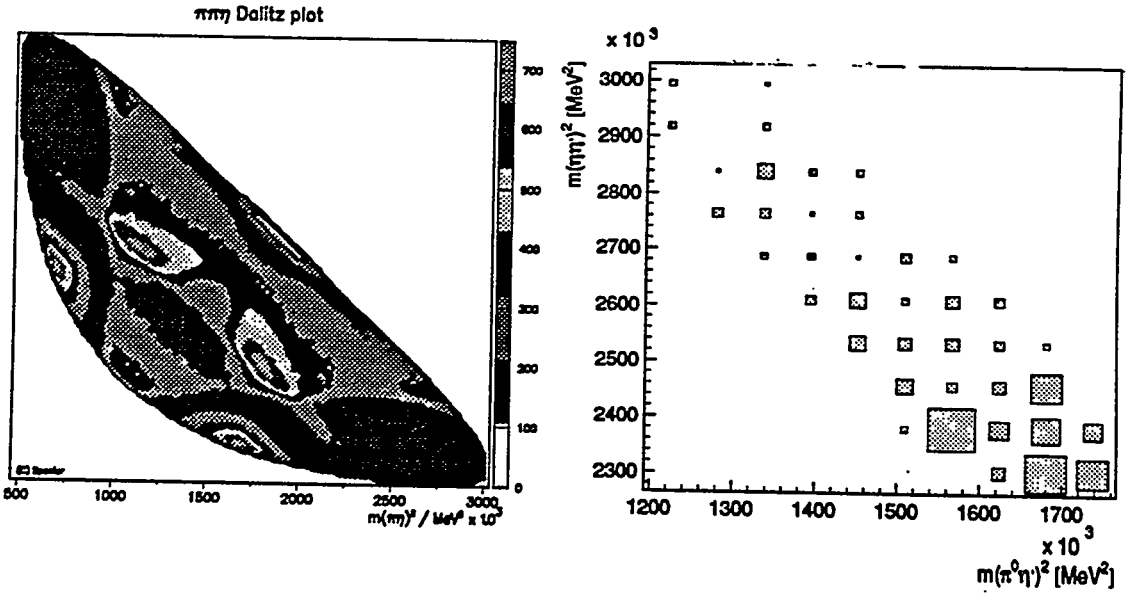


Figure 3: The Dalitz plots for $\bar{p}p \to \pi^\circ\pi^\circ\eta$ (left) and $\eta'\eta\pi^\circ$ (right).

parametrization [6], $f_0(975)$ and $f_0(1365)$ explain 50 to 55% of the data. [$\pi\eta$ S–wave] The $a_0(980)$ explains 13 to 15% of the data. In addition the data demand a second resonance, the $a_0(1450)$ which explains 5% of the data. Ignoring the second resonance causes the χ^2/N_{dof} to increase from 1.2 to 2.5. [$\pi\eta$ P–wave] A broad non–resonant background wave is needed to explain about 1.5 to 4.5% of the data. We exclude a resonance interpretation with the mass and width reported by GAMS for the $\hat{\rho}(1405)$ [7]. [$\eta\pi$ d–wave] The $a_2(1320)$ describes 18 to 28% of the data. In addition, a second a_2

is needed to account for about 2% of the data. However, its mass is at the edge of phase space, and we do not claim that this is a resonance.

The Dalitz plot for $\bar{p}p \to \eta'\eta\pi^\circ$ is shown in Fig. 3–right. Of the 158 events in this plot, 28 are estimated to be from background distributed uniformly over the plot. The enhancement in the lower right corner of the plot is most likely a structure in the $\eta'\eta$ system. A spin parity analysis is currently under way to determine if this is the $f_0(1500) \to \eta'\eta$.

The system $\bar{p}p \to \pi^+\pi^-\pi^\circ\pi^\circ\pi^\circ$ has been examined to search for resonances decaying into $\rho^+\rho^-$ [8]. The mass–mass plot, (Fig. 4–right) shows an enhancement in the $\rho^+\rho^-$ data over the background. The analysis of these data show the presence of a scalar resonance X decaying into $\rho\rho$ and $\sigma\sigma$, where σ is the $\pi\pi$ s–wave as given by the AMP parametrization [6]. We find $m_X = 1374 \pm 38$ MeV and $\Gamma_X = 375 \pm 61$ MeV. Under the assumption that this is isoscalar, it is probably the inelastic $f_0(1365)$ seen above, and we estimate that its 4π:2π decay ratio is approximately 5:1.

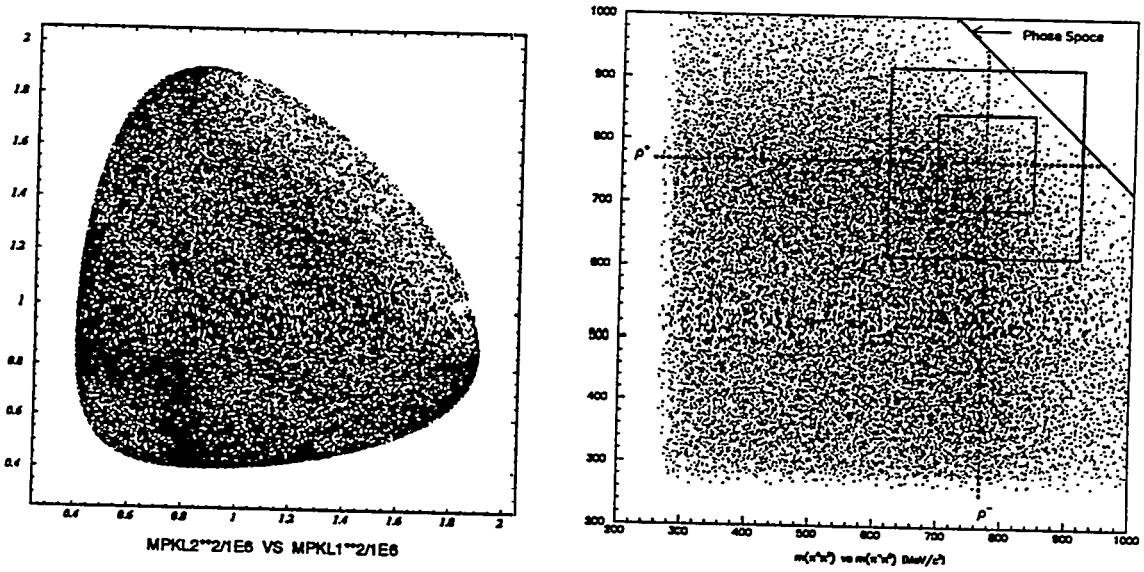


Figure 4: The Dalitz plots for $\bar{p}p \to \pi^\circ K_L K_L$ (left) and the mass–mass plot from $\pi^+\pi^-\pi^\circ\pi^\circ\pi^\circ$.

Finally, the $K\bar{K}\pi^\circ$ final state is very important in classifying mesons. In Fig. 4–left is shown a very preliminary Dalitz plot for the $K_L K_L \pi^\circ$ final state. The $K^*(890)$ can be seen as crossing horizontal and vertical bands near 0.8 GeV^2. In addition, there are hints of three diagonal bands ($K_L K_L$ resonances). A spin parity analysis to determine if any of these bands are 0^{++} is still underway. However, this analysis will be unable to distinguish between isospin 0 and 1.

3. The Scalar Nonet

In Table 1 are shown the ground state $L = 1$ nonets in the quark model as assigned by the Particle Data Group [9]. Normally, the octet and singlet $I = 0$ members of the nonets are mixed. The mixing angle can be computed from the Gell-mann Okubo formula, where Θ_q is from the quadratic formula, and Θ_l is from the linear formula. In the case of an ideally mixed nonet, (complete separation between the $u\bar{u} + d\bar{d}$ and the $s\bar{s}$ components), $\Theta = 35.3°$. In table 1 are given the two mixing angles for the PDG assignments for all except the scalars. Most of these are fairly close to ideally mixed.

$^{2S+1}L_J$ J^{PC}	$I=1$ $u\bar{d}$, $u\bar{u}$, $d\bar{d}$	$I=0$ $u\bar{u}$, $d\bar{d}$,		$I=0$ $s\bar{s}$		$I=1/2$ $\bar{s}u$, $\bar{s}d$	Θ_q (Θ_l)
$^1P_1$ 1^{+-}	$b_1(1235)$ $\Gamma = 155$	$h_1(1170)$, $\Gamma = 360$,		$h_1'(1380)$ $\Gamma = 80$	$K\bar{K}^*$	$K_1(1270)$ $K_1(1400)$	$41°$ $(40°)$
$^3P_0$ 0^{++}	$a_0(980)$ $\Gamma = 57$	$f_0(975)$, $\Gamma = 47$,	20% $K\bar{K}$	$f_0(1400)$ $\Gamma = 400$	93% $\pi\pi$	$K_0^*(1430)$ $\Gamma = 287$	
$^3P_1$ 1^{++}	$a_1(1260)$ $\Gamma = 400$	$f_1(1285)$, $\Gamma = 25$,	$K\bar{K}^*$	$f_1(1510)$ $\Gamma = 35$	10% $K\bar{K}$	$K_1^*(1400)$ $K_1(1270)$	$38°$ $(36°)$
$^3P_2$ 2^{++}	$a_2(1320)$ $\Gamma = 110$	$f_2(1270)$, $\Gamma = 185$,	5% $K\bar{K}$	$f_2'(1525)$ $\Gamma = 85$	71% $K\bar{K}$	$K_2(1430)$ $\Gamma = 105$	$31°$ $(29°)$
New 0^{++} Assignment							
$^3P_0$ 0^{++}	$a_0(1450)$ $\Gamma = 250$	$f_0(1365)$, $\Gamma = 267$,	$\approx$70% 4π	$f_0(1520)$ $\Gamma = 80$	$K\bar{K}$	$K_0^*(1430)$ $\Gamma = 287$	$49°$ $(48°)$

Table 1: The $L = 1$ mesons shown with their widths and some decay fractions.

Looking at the 0^{++} assignment, it is fairly clear that the $a_0(980)$ and the $f_0(975)$ do not fit well into the nonet. Other evidence from both two–photon couplings and J/ψ decays indicate that these states are not simple $q\bar{q}$ systems. Given that these are not members of the scalar nonet, what are the members? The $f_0(1365)$, (probably the $f_0(1400)$), is a good candidate for the lightest $I = 0$ member. In addition the $a_0(1450)$ fits naturally in as the $I = 1$ member. There are now three possible candidates for the $I = 0$ mostly $s\bar{s}$ member. The Crystal Barrel $f_0(1500)$, the LASS $f_0(1520)$ [10] and the GAMS $f_0(1590)$ or G meson [11]. Given that that $f_0(1365)$ and $a_0(1450)$ are very similar in mass, we expect the last member to be mostly $s\bar{s}$, with strong couplings to $K\bar{K}$. The decays of the $f_2'(1525)$ can guide us: $K\bar{K}$ 71%, $\eta\eta$ 28% and $\pi\pi$ 1%. Crystal Barrel observes no strong $K\bar{K}$ signal for the $f_0(1500)$, which probably rules this state out. The LASS state is observed in $K\bar{K}$, while the GAMS state is seen to decay into $\eta'\eta$, $\eta\eta$ and $4\pi°$. If we assume that the LASS state is the missing member, then we will fill out the scalar nonet as in the last column of table 1.

This leaves the $f_0(1500)$ and $f_0(1590)$ as extra scalar states — what are they? Earlier analysis of the $\eta\eta\pi$ by Crystal Barrel found the $f_0(1500)$ at a mass of 1560 MeV [12]. Coupled channel analysis as well as better analysis procedure have shifted the mass down to the 1500 MeV value. While the GAMS state is seen to decay most strongly

to $\eta'\eta$, Crystal Barrel places an upper limit on $\eta\eta$:$\eta'\eta$ of 4:1. It seems unlikely that these are the same states.

Lattice calculations predict that the lowest mass scalar glueball should have a mass around 1500 MeV. In addition, the decay modes for a glueball are expected to be flavor blind. If we assume that the enhancement seen in the $\eta'\eta$ invariant mass is indeed the $f_0(1500)$, then from the Crystal Barrel data, one can extract the following production and decay ratios [13].

$$\begin{aligned} BR(\bar{p}p \to \pi^\circ f_0(1500), f_0(1500) \to \pi\pi) &= (38 \pm 10.0) \cdot 10^{-4} \\ BR(\bar{p}p \to \pi^\circ f_0(1500), f_0(1500) \to \eta\eta) &= (6.3 \pm 2.8) \cdot 10^{-4} \\ BR(\bar{p}p \to \pi^\circ f_0(1500), f_0(1500) \to \eta'\eta) &= (1.5 \pm 0.5) \cdot 10^{-4} \end{aligned}$$

These have been corrected for the 2γ decay modes, and the isospin of the π. In order to identify the $f_0(1500)$ as a scalar glueball, it will be necessary to see its $K\bar{K}$ decay. This is currently under investigation, as evidenced by the K_LK_L data above. In addition, a specials K_SK_S trigger will be brought online at the end of '94. From bubble chamber results for $\bar{p}p \to \pi^\circ K\bar{K}$ [14], one can obtain an upper limit for $f_0(1500) \to K\bar{K}$. This then leads to the following decay pattern:

$$f_0(1500) \to \pi\pi : \eta\eta : \eta'\eta : K\bar{K} = 3 : (0.72 \pm 0.37) : (1.05 \pm 0.44) :< 0.40$$

which is very suggestive of the flavor blind decay of a glueball, but without information of the $K\bar{K}$ decay mode it is very difficult to confirm this. In addition, the preliminary results still await the completion of the ongoing spin–partity analysis, and the planned collection of $K\bar{K}\pi$ data at the end of '94.

4. References

1. E. Aker *et al.*, **Nucl. Instrum. Methods A321**, 69, (1992).
2. S. U. Chung, *et al.*, submitted to **Z. Phys. C**, (1994).
3. D. V. Bugg, *et al.*, submitted to **Phys. Rev. D.**, (1994).
4. V. V. Anisovich, *et al.*, **Phys. Lett. B323**, 233, (1994).
5. C. Amsler, *et al.*, Submitted to **Phys. Lett. B**, (1994).
6. K. L. Au, D. Morgan and M. R. Pennington, **Phys. Rev. D35**, 1633, (1987).
7. M. Boutemeur and M. Poulet, Hadron 89, ed. F. Binon, J. M. Frère, J. P. Peigneux – (Ed. Frontiérs 1989), p.119.
8. C. Amsler, *et al.*, **Phys. Lett. B322**, 431, (1994).
9. K. Hikasa, *et al.*, **Phys. Rev. D45 II**, (1992).
10. D. Aston *et al.*, **Nucl. Phys. B301**, 525, (1988).
11. F. Binon *et al.*, **Nuovo Cimento 78A**, 313, (1983), and **80A**, 303, (1984).
12. C. Amsler *et al.*, **Phys. Lett. B291**, 347, (1992).
13. R. Hackmann, Proceedings of the Recontre de Moriond, (1994).
14. L. Gray *et al.*, **Phys. Rev. D27**, 307, (1983).

PHOTOPRODUCTION OF THE ETA PRIME MESON IN THE EFFECTIVE LAGRANGIAN APPROACH*

Nimai C. Mukhopadhyay**, J. F. Zhang**

Physics Department, Rensselaer Polytechnic Institute

Troy, NY 12180-3590

and

M. Benmerrouche***

Saskatchewan Accelerator Laboratry, University of Saskatchewan

Saskaton, SK S7N 0W0, Canada

July, 1994

ABSTRACT

In the framework of the effective Lagrangian approach, we study the η' photoproduction off protons, of great interest at CEBAF I and II. We calculate the contributions from the leading nucleon Born terms, vector meson exchanges, and estimate the resonance contributions, using the transition amplitudes from the recent quark model estimates by Capstick and Roberts. We discuss implications for the CEBAF experiments.

1 Introduction

In this contribution, we study the photoproduction of the η' meson off nucleon:

$$\gamma + p \rightarrow \eta' + p, \tag{1}$$

using the effective Lagrangian approach(ELA)[1]. Structures of the eta and eta prime mesons are of fundamental interest in QCD[2], as are the couplings of baryon resonances to the meson-nucleon and the photon-nucleon channels. Thus, the photoproduction of eta prime is of great interest at CEBAF[3].

From the quark model point of view the eta and eta prime mesons are very interesting. There are also issues concerning the single-octet mixing angle[4], the mass formula of eta and eta prime[5] and the decays[6] of J/ψ to $\phi\eta'$, $\omega\eta'$ and $\rho\eta'$. Recently, Capstick and Roberts[7] have used the quark model to conclude that the negative parity baryons between 1.9 to 2.2 GeV should dominate the $N\eta'$ channel coupling. However, there is almost no theoretical discussion so far on the analytical structure of eta prime photoproduction amplitude. Also there is very little information about the $\eta' NN$ coupling and the $\eta' NR$ amplitudes, N being the nucleon, and R, the relevant resonances. Very little experimental data exist about the η' photoproduction. The only available data consist of three data points from a 1968 experiment, done at DESY[8], and a few more from the unpublished results of the same experiment, reported by G. Wolf and P. Söding[9]. There is an approved proposal at CEBAF on the η' photoproduction[3].

Having thoroughly studied properties of the eta photoproduction[1, 2], a natural next step for us is to study the rôles of the relevant Born and resonance contributions to the η' photoproductions. We wish to find out which resonances contribute most, along with the relative importance of the vertices involving the $\eta' NN$, the $\eta' NR$ and the role of the relevant form factors in the η' photoproduction.

2 Tree-level Structure of the Amplitude

Previous investigations of the pion and eta photoproduction by using ELA[1, 2] have shown us the usefulness of the ELA. Here we follow the same approach. We consider the tree-level structure of the η' photoproduction amplitude, starting with the s- and the u-channel nucleon Born terms, adding to that t-channel vector mesons (ρ, ω) and the s- and the u-channel resonance excitations.

The form of the ELA of the η' photoproduction is similar to that for the η case. However, paucity of data for the former forces us to adopt a different strategy here. We fix as many parameters as possible, by using the masses and total widths of the known resonances from the compilations of the Particle Data Group (PDG-92). We also use the work of Capstick and Roberts[7] for their predictions for the decay ratio and the helicity amplitudes of the relevant baryons in the framework of the quark shell model. Thus, our work provides for an opportunity to test the quark model predictions

Table 1: Contributions to the real part of the E_{0+} multipole, in units of $10^{-3}/m_{\pi+}$, for the η', η and π^0 photoproduction at their respective thresholds for the pseudoscalar meson-nucleon coupling. In the last column, numbers in the parenthesis are those for the pseudovector pi-N-N coupling.

Contributions	η'	η	π^0
Nucleon Born terms	-0.13	-6.0	-7.9, (-2.5)
Vector mesons	0.89	2.9	0.04
Dominant resonance	6.05	12.1	0.4
other resonances	-0.19	0.3	0.1
Total	6.62	9.2	-7.4, (-2.0)
Experiment	$--$	$--$	-2.0 ± 0.2

experimentally at CEBAF.

3 Our Preliminary Results

The contributions to the real part of the E_{0+} multipole for the η' are compared with those for the η and the π^0 photoproduction at their respective thresholds in Table 1. From this table we can get an idea of the differences of various contributions to this particular amplitude for these three mesons.

In order to reproduce the old experimental data for the η' photoproduction[8], we must use suitable form factors at the meson-hadron vertices.

In Fig. 1 we show the eta prime total photoproduction cross section vs. E_γ(photon energy) compared with exparimental data, discussed above, using the masses and widths of the PDG-92, along with the decay ratios and helicity amplitudes of quark model of Capstick and Roberts. We have adjusted the off-shell parameters of the $N^*(2080)$ resonance and the form factors to reproduce the data.

Our preliminary results, shown above, indicate that the excitation of the $N^*(2080)$ plays the dominant role. This is quite interesting from the spectroscopic point of view.

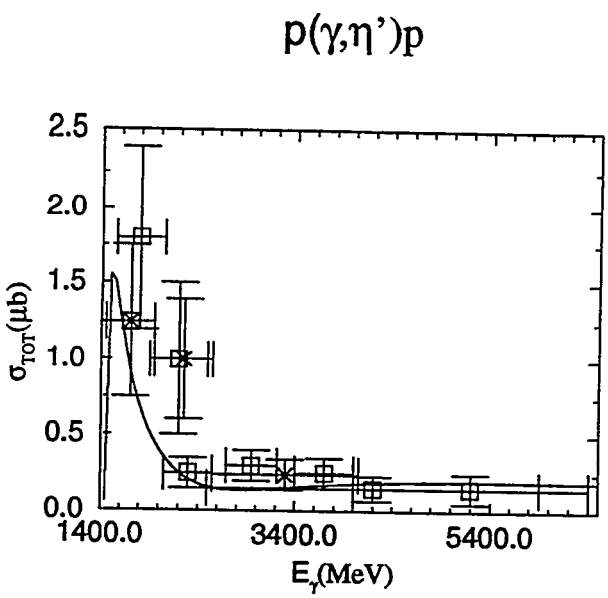


Figure 1: Calculated total eta prime photoproduction cross section compared with the available world supply of experimental data. $g_{\eta'} = 1.9$, where solid line is the calculated result, star is from ref. 8, and square is from ref. 9.

4 Conclusions

At this stage we believe we are seeing a promising aspect of the eta prime photoproduction channel in exploring selective resonances around 2 GeV, a nice prospect both for the CEBAF I and II. This should allow more precise tests of the quark model at this interesting region of $W \approx 2GeV$.

* Presented by N. C. Mukhopadhyay
** Supported by the U. S. Department of Energy
*** Supported by the Natural Science and Engineering Research Council of Canada

References

[1] R.M.Davidson, N. C. Mukhopadhyay and R.S.Wittman, *Phys. Rev.* **D43** (1991) 71, and references therein. N. C. Mukhopadhyay, and R.M.Davidson, *Phys. Rep.*, to be published.

[2] M. Benmerrouche, and N. C. Mukhopadhyay, *Phys. Rev. Lett.* **67** (1991) 1070; M. Benmerrouche, N. C. Mukhopadhyay and J. F. Zhang, submitted to *Phys. Rev.* **D**; J. F. Zhang, N. C. Mukhopadhyay, and M. Benmerrouche, *Bull. Am. Phys. Soc.* **39** (1994) 1092.

[3] B. G. Ritchie *et al.*, *CEBAF proposal* # 91-008; S. Dytman *et al.*, private communication (1994).

[4] F. Iachello, N. C. Mukhopadhyay and L. Zhang, *Phys. Rev.* **D44** (1991) 898.

[5] F. E. Close, *An Introduction to Quarks and Partons*, (Academic Press, New York, 1979).

[6] R. M. Baltrusaitis, *Phys. Rev.* **D32** (1985) 2883; J. Jousset *et al.*, *Phys. Rev.* **D41** (1990) 1389.

[7] S. Capstick, *Phys. Rev.* **D46** (1992) 2864; S. Capstick and W. Roberts,*Phys. Rev.* **D49** (1994) 4570.

[8] R. Erbe *et al.*,*Phys Rev.* **175** (1968) 1669.

[9] G. Wolf and P. Söding, *Electromagnetic Interactions of Hadrons*, **Vol.2**, A. Donnachie and G. Shaw, editors, Plenum (New York,1978).

SENSITIVITY TO PROPERTIES OF THE PHI-MESON IN THE NUCLEON STRUCTURE IN THE CHIRAL SOLITON MODEL*

Nimai C. Mukhopadhyay** and L. Zhang**

Physics Department, Rensselaer Polytechnic Institute

Troy, NY 12180-3590

July, 1994

ABSTRACT

The influence of the ϕ-meson on the nucleon properties in the chiral soliton model is discussed.

1 Introduction

Properties of the ϕ-meson and its photo- and electroproduction are of fundamental interest to CEBAF and its possible future extension. The quark model assigns ϕ an $s\bar{s}$ structure, thus forbidding the radiative decay $\phi \to \pi^0\gamma$. Experimentally it is also found to be suppressed, yielding a branching fraction of 1.3×10^{-3}. However, $\phi \to \rho\pi$ and $\phi \to \pi^+\pi^-\pi^0$ are not suppressed at all. Thus, it is possible to incorporate the widths of these decays into the framework of the chiral soliton model[1], by making use of a specific model for the compliance with the OZI rule. Such a model is, for example, the $\omega - \phi$ mixing model[2]. Consequence of this in the context of a chiral soliton model, which builds on the $\pi\rho\omega a_1(f_1)$ meson effective Lagrangian[1], is the content of this report.

2 Results

We summarize, in Table 1, nucleon observables computed in our chiral soliton model, with and without the ϕ-decay constraints put in, by using the

Table 1: Nucleon observables calculated in our chiral soliton model. Model A has no ϕ-decay constraint, B does. Notations are standard and units are obvious.

	M_H	g_A	$g_{\pi NN}$	μ_V	$< r >_E^{I=0}$	$< r >_M^{I=1}$	r_A	σ
A	1379	0.90	13.30	2.06	0.91	0.92	0.62	43.5
B	1070	0.59	6.74	1.22	0.72	0.76	0.45	23.0
Exp.	939	1.26	13.45	2.35	0.79	0.87	0.63	45
	± 1	± 0.01	± 0.05	± 0.00	± 0.01	± 0.07	0.03	± 10

picture[2]

$$\phi_{physical} = \phi + \varepsilon\omega \tag{1}$$

where

$$\phi = s\bar{s}, \quad \omega = \frac{1}{\sqrt{2}}(u\bar{u} + d\bar{d}), \tag{2}$$

and ε is determined from the flavor SU(3) mass splitting,

$$\varepsilon = 0.060 \pm 0.014. \tag{3}$$

We notice that *the phenomenological outcome, for the soliton properties is worse, for all soliton properties under consideration, except mass of the soliton, when we take into account the ϕ- decay properties*, in Model B. The nucleon properties computed here are the leading order ones in the $(N_c)^{-1}$ expansion, N_c being the number of colors in QCD.

3 Summary and Conclusions

Our attempt to include the ϕ- decay properties in the chiral soliton model makes nucleon properties almost universally worse, if we take the picture of ϕ, discussed above, for the protection of the OZI rule. This is not a failure of the chiral soliton model, but an indication that *the OZI rule, in general, and its influence on the ϕ decays, in particular, are not understood at present*, despite many brave attempts[3]. The Wess-Zumino-Witten sector of the chiral soliton model is sensitive to the way we preserve this rule.

Thus, in the context of nucleon structure, the ϕ-physics here offers a reminder that we are far from solving the problem of strange quark contents in ordinary (supposedly non-strange) hadrons. We need to understand the *phi* properties a great deal better. CEBAF I and II could help in this enterprise.

* Presented by N. C. Mukhopadhyay

** Supported by the U. S. Department of Energy

References

[1] L. Zhang, and N. C. Mukhopadhyay *Mod. Phys. Lett.* **A9** (1994) 935, and *Phys. Rev.* **D**, in press.

[2] P. Jain *et al.*, *Phys. Rev.* **D37** (1988) 3253; U.-G. Meissner *et al.*, *ibid.* **D39** (1989) 1956; **D40** (1989) 362(E).

[3] See, for example, P. Geiger and N. Isgur, *Phys. Rev.* **D47** (1993) 5050.

A TAU-CHARM FACTORY AT CEBAF

KAMAL K. SETH*

Northwestern University, Evanston, IL 60208, USA

ABSTRACT

It is proposed that a Tau Charm Factory represents a natural extension of CEBAF into higher energy domains. The exciting nature of the physics of charm quarks and tau leptons is briefly reviewed and it is suggested that the concept of a linac-ring collider as a Tau Charm Factory at CEBAF should be seriously studied.

1. Introduction

As we all know, we have the holy trinity of the families of fundamental particles. The $(u,d)(e,\nu_e)$ family is the domain of classical nuclear physics and we have been playing with them for a long time. At Bates and CEBAF we study systems which contain these quarks using leptonic and photonic probes. In this domain cross sections are large (mb) but the validity of perturbative QCD (PQCD) is highly questionable because of very large relativistic corrections. The second family is $(c,s)(\mu,\nu_\mu)$. Classical medium energy physics has been working with the three members of this quartet s,μ and ν_μ for a long time, and CEBAF will no doubt continue to be heavily involved with systems of u,d and s quarks. The charm quark has not yet been claimed by medium energy physics. What a pity! Because cross sections are still quite large, $(\mu b \rightarrow nb)$, PQCD predictions work remarkably well, and relativistic complications appear to be manageable. Coming to the last family $(t,b)(\tau,\nu_\tau)$, we note that the Top is so far only in Fermilab's domain, Beauty is chased by many but caught by few, and τ and ν_τ are still looking for a home. My proposal, in a nutshell, is that medium energy physics should lay a claim to the physics of the charm quark, the tau lepton and its partner, the tau neutrino, while our high energy brethren are still chasing the Top and the Higgs! What this means is to build a Tau Charm Factory. And I suggest that CEBAF is a natural place to build it.

2. A Linac-Ring Collider (LRC) at CEBAF

Let us first look at a bit of elementary kinematics. As we know, the

*This research was supported in part by the U.S.Department of Energy.

Table 1: Center of mass energy available for new particle production

Target	$E(e^-)$ (GeV) 4	6	8
Stationary Proton Target			
$\sqrt{s} - m_p$	1.96	2.55	2.96
Positron in a ring (annihilation)			
$\sqrt{s}$ for $E(e^+) = 1$ GeV	4.00	4.90	5.66
2 GeV	5.66	6.93	8.00
4 GeV	8.00	9.80	11.31

center of mass energy $\sqrt{s}$ available for two colliding particles with masses, momenta and total energies (m_1, p_1, E_1) and (m_2, p_2, E_2) is given by:

$$\sqrt{s} = p_1 + p_2 = (m_1^2 + m_2^2 + 2E_1E_2 - 2\vec{p}_1 \cdot \vec{p}_2)^{1/2} \qquad (1)$$

In Table 1 I list the threshold 'reach' for new particle production in two situations, a CEBAF beam of electrons hitting a proton target, and a CEBAF electron beam colliding with a circulating positron beam of energy 1-4 GeV in a ring.

The message of Table 1 is clear. Even with an 8 GeV electron beam hitting a stationary proton target, the physics that CEBAF can address remains restricted to the physics of u, d and s quarks. On the other hand, even with a 1 GeV positron ring we open up an entirely new dimension of physics for CEBAF. It can address

Tau physics	(with CEBAF $E(e^-) \geq 4.0$ GeV)
Charmonium spectroscopy	(with $E(e^-) \geq 4.0$ GeV)
Open-charm physics	(with $E(e^-) \geq 4.2$ GeV)

This is jumping into the middle of new physics, not just nibbling at its edges! The possibility is downright exciting!

Let me therefore develop this scenario a bit further. I am talking of a LINAC-RING COLLIDER (LRC) at CEBAF. I am talking of a 6 GeV e^- beam from the CEBAF LINAC colliding with, for example, a 2 GeV positron beam in a ring, something like what I show schematically in Fig. 1. I am not an accelerator expert, but I believe that the LRC scenario is not a wild one. LRC's have been studied in the past, e.g., by as distinguished an accelerator expert as M. Tigner, as candidates for an asymmetric Beauty Factory. I realize that in these design studies the LINAC was being designed, right from the beginning to work with a ring, and this is not the case at CEBAF. But the Beauty Factory designers were talking about luminosities on the order of $10^{33} - 10^{34} cm^{-2} s^{-1}$. I am prepared, at least for now, to be far

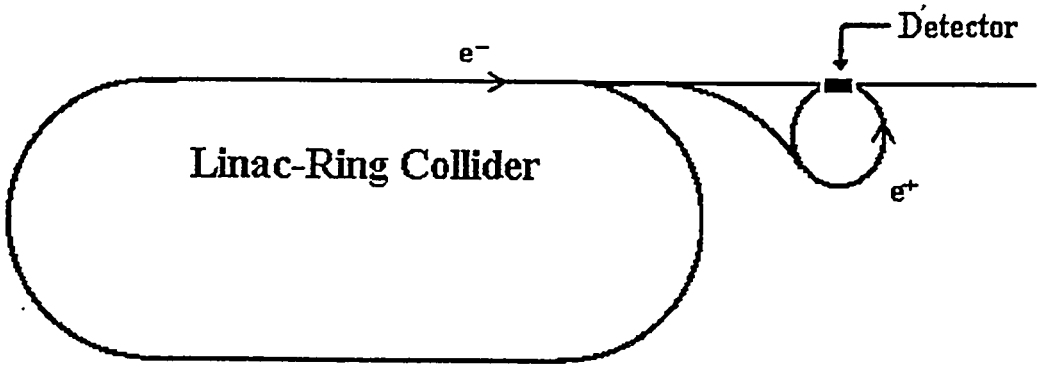


Fig. 1: The Linac-Ring Collider (LRC) at CEBAF.

more modest. I will settle for a luminosity of $3 \times 10^{31} cm^{-2} s^{-1}$. Surely the accelerator experts at CEBAF and elsewhere can rise to this challenge!

So let me assume that they have risen and met the challenge, and given me a LRC with a luminosity of $3 \times 10^{31} cm^{-2} s^{-1}$. What great, wonderful and exciting things can we do?

I do not have space here to develop even a small part of the immense amount of cutting-edge physics that one can do with a facility like this. I refer the reader for detailed discussions to several published reports on the physics of Tau-Charm Factories [1] and to my talk on charmonium at the Few-Body Physics Conference at Williamsburg [2]. Here I present what amounts to just a list of some of the most interesting physics which are possible at the proposed τCF.

Before I go any further, let me mention another imperative of this program. While a 2 GeV positron ring is an affair of <$5 million, in order to exploit the τCF a state-of-the-art detector is needed. Such a 4π detector has excellent charged particle detection, identification and momentum analysis, photon detection with the very best energy and angular resolution, and near 100% hermeticity (see Fig. 2). Such a detector does not come cheap.

3. The Physics of τCF

Let me first list a few special $\sqrt{s}$ points (see Fig. 3):

3096.9(5) MeV:	J/ψ calibration, Yield$(J/\psi) = 6 \times 10^8/year$
3552(3) MeV:	$\tau^+\tau^-$ threshold, Yield$(\tau^+\tau^-) = 0.5 \times 10^5/year$
3686.0(10) MeV:	ψ', highest yield of τ, Yield $(\tau^+\tau^-) = 2 \times 10^5/year$
3770(3) MeV:	ψ'', provides pure $D^0\overline{D}^0$, D^+D^-
4030, 4160 MeV:	ψ''', $\psi^{(4)}$, possibly the best places for $D_s{}^+D_s{}^-$
> 4415 MeV:	Beyond where presently-known charm physics stops

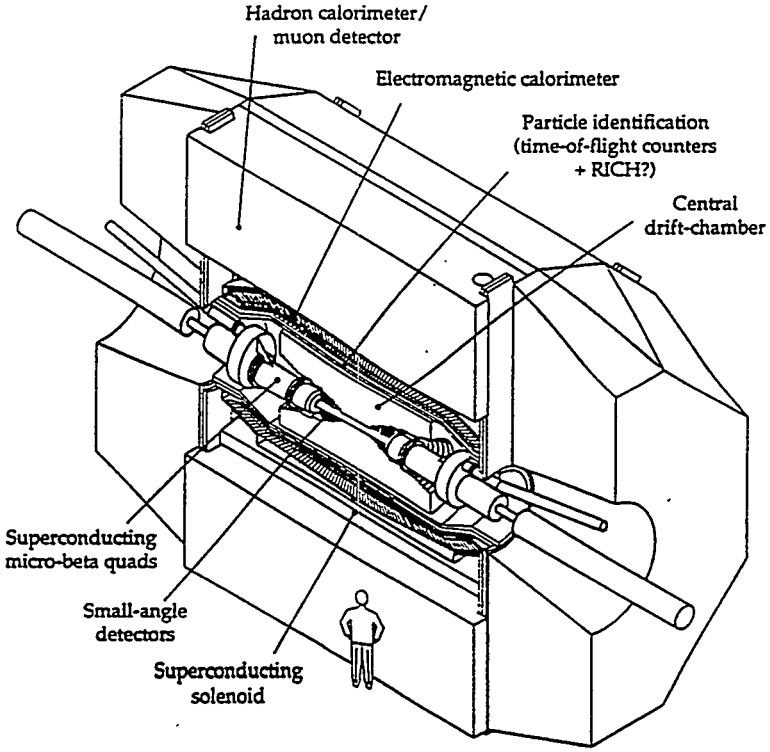


Fig. 2: Artist's rendition of a proposed τCF Detector.

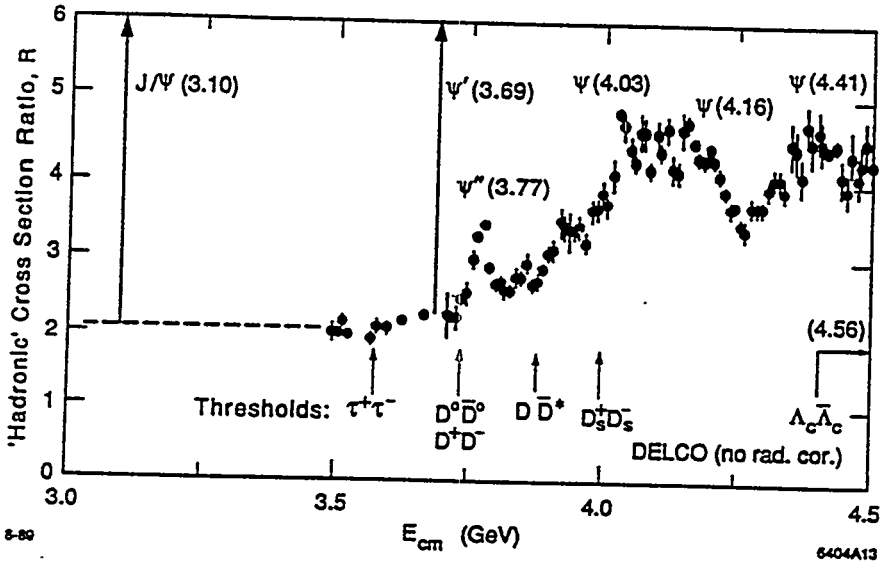


Fig. 3: Ratio of hadronic to leptonic cross sections for e^+e^- annihilation.

3.1. Tau Physics

3.1.1. Tau Mass

Tau was discovered in threshold production, but until recently the best mass determination came from Z^0 decay. A recent measurement at the Beijing BEPC [3] has beautifully illustrated the advantages of threshold measurements, with

$$M(\tau) = 1776.9^{+0.4}_{-0.5} \pm 0.2\text{MeV} \tag{2}$$

At the LRC(τCF), using high-resolution optics, we can expect $\Delta M(\tau) \approx$ 0.1MeV.

3.1.2. ν_τ Mass

If $m(\nu_l) \propto m(l)^2$, as some theoretical conjectures suggest, a 1 MeV sensitivity in $m(\nu_\tau)$ is equivalent to a 0.1 MeV sensitivity in electron neutrino mass. It has been estimated that it is possible to achieve such a sensitivity at τCF.

3.1.3. Branching Ratios for τ Decays

Precision measurements at τCF (0.1% level) can test Standard Model predictions and provide, for example, tests of the universality of lepton charge currents, elucidate the current structure (V-A) of the $\tau\nu_\tau W$ vertex, test possible lepton number violation ($\tau \rightarrow l\gamma$), and CP violation in the lepton sector.

For extensive discussion of τ-physics I refer the reader to a recent review by M. Perl [4].

3.2. Physics of Open Charm

Again, very detailed reviews exist in the literature [5]. Here I just list a few exciting topics.

3.2.1. $D^0\overline{D}^0$ Mixing and CP Violation

In the Standard Model $D^0\overline{D}^0$ mixing is predicted to be small

$$r_D = \frac{BR(D^0 \rightarrow \overline{D}^0 \rightarrow \bar{f})}{BR(D^0 \rightarrow f)} \leq 10^{-5} - 10^{-4}, \tag{3}$$

but in nearly all extensions of the Standard Model enhanced rates are predicted. Present experimental limits are at the 10^{-3} level. At a τCF these can be brought down to the $< 10^{-5}$ level.

CP violation asymmetries of the type

$$A = \frac{D^0\overline{D}^0 \to (l^+X) + f}{D^0\overline{D}^0 \to (l^-X) + f}, \qquad where\, f = K^+K^-(CP\,\text{eigenstate}) \qquad (4)$$

can be measured at a 1% level. As a matter of fact a single event of the type

$$\psi'' \to D^0\overline{D}^0 \to (K^+K^-)(K^-K^+) \qquad (5)$$

would prove CP violation in the u-quark sector.

3.2.2. CKM Matrix Elements

At the moment V_{cs} and V_{cd} are known only at the 10 - 20 % level experimentally. By measuring $D^0 \to K^-e^+\nu_e$ and $D^0 \to \pi^-e^+\nu_e$ to 1%, τCF could determine V_{cs} and V_{cd} at a 1% level.

3.2.3. Pure Leptonic D-decays

In the Standard Model $D^+ \to l^+\nu_l$ and $D_s^+ \to l^+\nu_l$ decays are predicted rigorously. It is important to measure them because they give the weak decay constants f_D, f_{D_S} and V_{cd}/V_{cs}. At the τCF these can be measured at a 1 - 2 % level, a level that exists so far only for π decay,

$$BR(\pi^+ \to \mu^+\nu_\mu)/BR(\pi^+ \to e^+\nu_e). \qquad (6)$$

3.2.4. Rare D-decays

Many rare D-decays can be studied at τCF. For example the lepton flavour-violating decays $D^0 \to e^\pm\mu^\mp$ can be measured at the level of $\sim 10^{-8}$.

3.3. Charmonium Physics

This is a vast subject. Despite twenty years of studies at the conventional e^+e^- colliders, the tough questions of charmonium physics remain unanswered. Some of these have recently been addressed by Fermilab experiment E760 in which charmonium states are directly produced by two- and three-gluon proton-antiproton annihilations. However, a great amount remains, and will remain unaddressed unless a τCF is built somewhere. Let me *list* here some of the interesting problems which are discussed in detail elsewhere. [2]

3.3.1. J/ψ and ψ' Widths

Recently E760 has claimed that the J/ψ total width is about 50% larger than what was believed for the last 20 years. It is important to verify this in an independent experiment. Only a τCF, operating in a high-resolution mode, can achieve the energy resolution required to test this. I remind you that a τCF with a luminosity of 3×10^{31} produces $6 \times 10^8 J/\psi$ per year.

3.3.2. The Vector States above the $D\overline{D}$ threshold

This region was investigated by PLUTO, DASP, DELCO and SLAC, and their results differ considerably. The electron branching ratios for ψ'', ψ''', $\psi^{(4)}$, $\psi^{(5)}$, are suspiciously all quoted to be $\sim 1 \times 10^{-5}$. Their decays into $D\overline{D}$, $D^*\overline{D}$, and $D^*\overline{D}^*$ are only poorly known. The $^3D_2$, $^1D_2$, and the radial excitations of P states have never been observed. The region above the $D\overline{D}$ threshold remains essentially unexplored from the point of view of charmonium spectroscopy.

3.3.3. Two Photon Decays of Triplet P-states (χ_J)

The decays $^3P_{2,0} \rightarrow \gamma\gamma$ are difficult to measure. Photon-photon fusion and $\bar{p}p$ annihilation experiments give very different answers. At a τCF one gets $\sim 1 \times 10^6 \chi_o, \chi_1, \chi_2$, each per month, via $\psi' \rightarrow \chi_J \gamma$. This should make it possible to study $\chi_o \rightarrow 2\gamma$ and $\chi_2 \rightarrow 2\gamma$ with very high precision.

3.3.4. The Singlet States of Charmonium

Except for $\eta_c(1^1S_0)$ state of charmonium, no singlet states were ever identified convincingly in e^+e^- experiments. This is because they are weakly excited (or forbidden) in e^+e^- radiative transitions. Recently E760 has discovered the $h_c(^1P_1)$ state of charmonium but failed to find $\eta_c'(2^1S_0)$. All these can be beautifully studied at a τCF, because of huge projected yields, e.g., $\sim 10^6 \eta_c$ per month by M1 decays of J/ψ. At the τCF even the $^1P_1$ state becomes accessible via $\psi' \rightarrow {}^1P_1\pi^0$, or $\eta_c' \rightarrow {}^1P_1\gamma$.

3.3.5. The Hadron/Lepton Ratio, R

Perhaps the most celebrated and fundamental measurement is

$$R = \frac{\sigma(e^+e^- \rightarrow hadrons)}{\sigma(e^+e^- \rightarrow l^+l^-)} = \sum_{i=1}^{n_f} Q_f^2 \qquad (7)$$

which provides a measure of the sum of the charges of open flavors. It is in the measurement of this ratio that the J/ψ was discovered. Yet it is extremely poorly measured in the region $E_{cm} < 7$GeV. One does not really know how

it rises near the opening of new flavor thresholds. Its measurement must be among the highest priorty projects for a τCF.

4. Summary

Attempts to increase e^- energy at CEBAF must be made, but they are not likely to bring the $\sqrt{s}$ reach of CEBAF to new flavors. This must be done by considering e^+e^- annihilation possibilities. A Linac-Ring Collider at CEBAF offers one such possibility. It opens up the world of tau and charm physics at CEBAF - physics whose fundamental importance is second to none. The possibility must be seriously investigated.

5. References

1. For a detailed discussion of the design and physics of τCF, see *Proc. Tau-Charm Factory Workshop, Stanford (1989)*, ed. L. V. Beers, SLAC-343 (1989); Also, *Proc. Tau-Charm Factory Workshop, Marbella (1993)*, ed. J. Kirkby (World Scientific, Singapore, 1994).
2. Kamal K. Seth, *Proc. XIV Int. Conf. on Few Body Physics, Williambsburg (1994)*, ed. F. Gross, (AIP, New York) (in press).
3. BES Collaboration, *Proc XVI Int. Symp. on Lepton-Photon Interactions, Ithaca (1993)*, ed. P. Drell and D. Rubin (AIP, New York, 1994), p. 530.
4. Martin L. Perl, *Rep. Prog. Phys.*, 55 (1992) 653; see also A. J. Weinstein and R. Stroynowski, *Ann. Rev. Nucl. Part. Sci*, 43 (1993) 457.
5. D. Hitlin, in *Charm Physics*, ed. M-H. Ye and T. Huang, (Gordon Breach, New York, 1987) pp. 219-338; see also I. Bigi, *loc. cit* pp. 339-426; J. P. Cumalat, in *The Fermilab Meeting, DPF '92*, ed. C. H. Albright *et al.* (World Scientific, Singapore, 1993), pp. 197-212.

UM-HEP-94-007
July 15, 1994

Spectroscopy, Scattering, and $K\bar{K}$ Molecules.[1]

John Weinstein

Department of Physics and Astronomy,
University of Mississippi, University, MS 38677.

Abstract

We present a pedagogical description of a new theoretical technique, based on the multichannel Schrödinger equation, for simultaneously applying the quark model to both meson spectroscopy and meson-meson scattering. This is an extension of an earlier analysis which led to the prediction that the $f_0(975)$ and $a_0(980)$ scalar mesons are $K\bar{K}$ molecular states.

The quark model attempts to represent the main features of QCD, the theory describing the interactions of colored constituents of matter. We use it to find effective intermeson potentials which we then insert into a multichannel formulation of the Schrödinger equation. Solving this equation numerically yields predictions for meson masses, widths, and couplings to asymptotic states, as well as the parameters of the S-matrix.

One approach to finding the meson spectrum of the quark model has been to solve the eigenvalue problem numerically

$$H_{q\bar{q}}\,\psi_A(\vec{r}_{q\bar{q}}) = \mathrm{M}_A\,\psi_A(\vec{r}_{q\bar{q}}) \tag{1}$$

where the $q\bar{q}$ Hamiltonian is

$$H_{q\bar{q}} = -\frac{\hbar^2}{2\,\mu_{q\bar{q}}}\frac{\mathrm{d}^2}{\mathrm{d}\vec{r}_{q\bar{q}}{}^2} + m_q + m_{\bar{q}} + V_{q\bar{q}}(r_{q\bar{q}}) \tag{2}$$

and the $q\bar{q}$ potential is, for example,

$$\begin{aligned} V_{q\bar{q}}(r_{q\bar{q}}) = \; & -\left[\tfrac{3}{4}\,b\,r_{q\bar{q}} - \frac{\alpha_c}{r_{q\bar{q}}} + \tfrac{3}{4}\,C\right]\,\vec{F}_q\cdot\vec{F}_{\bar{q}} \\ & -\frac{8\pi}{3}\frac{\alpha_h}{m_q m_{\bar{q}}}\left[\frac{\sigma^3}{\pi^{3/2}}\,\mathrm{e}^{-\sigma^2 r_{q\bar{q}}^2}\right]\vec{S}_q\cdot\vec{S}_{\bar{q}}\;\vec{F}_q\cdot\vec{F}_{\bar{q}} \end{aligned} \tag{3}$$

with $\vec{F}_q = \frac{1}{2}\vec{\lambda}$ and $\vec{F}_{\bar{q}} = -\frac{1}{2}\vec{\lambda}^*$. Solutions yield the meson masses M_A and the wavefunctions $\psi_A(r_{q\bar{q}})$. In this particular formulation the light quark sectors of the Hamiltonian have seven parameters, $m_u = m_d$, m_s, b, α_c, C, α_h, and σ, (though one may have more, depending upon the level of sophistication desired) which are fixed by experimental data. With these parameters fixed predictions of all other meson masses follow.

The eigenenergies M_A can be found by requiring that the wavefunction (obtained by integrating the radial component of eq. (1) outward from $r_{q\bar{q}} = 0$ using finite difference methods) vanish at infinity. As one can see from Figure 1 the eigenenergies may be determined to an arbitrarily high accuracy, although from experience we only expect quark model predictions to be accurate at the level of 10 MeV.

When one solves this eigenvalue problem one is implicitly assuming that the resonance under study has a unique energy and is therefore stable. Most hadrons however, are not stable; usually

[1]Invited contribution to the Workshop on Higher Energies at CEBAF, Newport News, VA, April 14-16, 1994.

they decay hadronically and are very short lived. A resonance with a typical hadronic width of 200 MeV lives approximately as long as light takes to cross it, so the narrow width approximation is very crude except for the proton and those hadrons which decay only weakly or electromagnetically.

This situation is particularly troubling if one's goal is to extract the spectroscopy of wide and interfering hadrons, glueballs, and hybrids from experimental data; the narrow width approximation is an inadequate tool for this job. One would clearly prefer a scheme in which the properties of the resonances are extracted in a manner more analogous to the way that they are actually created and observed; namely as short-lived resonances interfering with other overlapping short-lived resonances, as some effectively stable (two-hadron) initial state makes a transition to some (perhaps different) effectively stable (multi-hadron) final state. Here we will describe a particular scheme for studying two-meson to two-meson transitions mediated by quark exchange effects and s-channel meson resonances.

Note that we consider quark exchange rather than t-channel meson exchange between interacting hadrons. We do this because the range of meson exchange is of order $\hbar/m_{meson}$, which is less than 1 fm for all mesons except the pion. At this range the physical picture of two hadrons, each $\approx$1 fm in diameter, exchanging a meson $\approx$1 fm in diameter is inconsistent; all three wavefunctions overlap significantly. Under these conditions quark exchange processes seem highly probable so we might expect quark exchange effects to be very important, in disagreement with the historically accepted picture of meson exchange. In baryon-baryon scattering, where there are no s-channel $q\bar{q}$ or qqq resonances, meson exchange requires a coupling of the $qqq\,qqq$ state to the higher Fock space component $qqq\,qqq\,q\bar{q}$ (as one can see by drawing the quark line diagrams) and quark exchange is, in fact, a lower order diagram in $\alpha_{\rm strong}$ for BB scattering.

We were originally led to realize the importance of quark exchange in a variational study [1] of the $qq\bar{q}\bar{q}$ ground state wavefunction $\psi^0_{qq\bar{q}\bar{q}}$ in the $J^P = 0^+$ sector. There $\psi^0_{qq\bar{q}\bar{q}}$ represented interacting mesons only when the trial wavefunctions contained symmetry terms reflecting quark exchange and when the Hamiltonian included the contact hyperfine interaction, otherwise $\psi^0_{qq\bar{q}\bar{q}}$ represented essentially non-interacting psuedoscalar meson pairs. We were able to extract meson-meson potentials by using the $qq\bar{q}\bar{q}$ Hamiltonian (based directly on a generalization of $H_{q\bar{q}}$ above) and the variational method to find the ground-state wavefunction $\psi^0_{qq\bar{q}\bar{q}}$ and energy of the fully interacting $qq\bar{q}\bar{q}$ system. We also included in the Hamiltonian a weak color independent quadratic potential

$$V_\epsilon \equiv \sum_{i\neq j} \tfrac{1}{2}\epsilon\, r_{ij}^2. \tag{4}$$

between all constituent pairs ij to prevent repulsive or non-binding meson-meson systems from drifting beyond their interaction range. We then interpreted the wavefunction

$$\psi_{AB}(\vec{r}_{AB}) = \langle \psi_A\, \psi_B |\, \delta(\vec{r}_A - \vec{r}_B + \vec{r}_{AB}) | \psi^0_{qq\bar{q}\bar{q}} \rangle \tag{5}$$

as the amplitude for finding meson A at $\vec{r}_A$ and meson B at $\vec{r}_B$, separated by $\vec{r}_{AB}$, within $\psi^0_{qq\bar{q}\bar{q}}$. Inverting the radial Schrödinger equation for ψ_{AB} allowed us to extract an effective central AB interaction potential $V_{AB-AB}(r_{AB})$:

$$V_{AB-AB}(r_{AB}) = \frac{\hbar^2}{2\,\mu_{AB}} \left[\frac{\mathrm{d}^2}{\mathrm{d}r_{AB}^2}\,\psi_{AB}(r_{AB})\right] \psi^{-1}_{AB}(r_{AB}) + \mathrm{E}_{AB} - 4\,\tfrac{1}{2}\epsilon\, r_{AB}^2 \tag{6}$$

where E_{AB} is the binding energy of the interacting mesons. These Gaussian-like potentials can then be used, either directly or as "equivalent" square well potentials, in a Schrödinger equation to

find, for example, the phase shift for I=3/2 Kπ scattering. As is clear from Figure 2, this extracted phase shift compares favorably to experiment [2].

Based on the successes of this technique, and the results for the S-wave scalar meson sector, Barnes *et al.* [3,4] developed more widely applicable Born approximation techniques for extracting potentials based on one gluon exchange (OGE) followed by quark (or antiquark) exchange, with interactions normally mediated by the contact OGE hyperfine interaction. For the particular case of meson-meson scattering Swanson [4] has shown that the effective intermeson potentials can be modelled accurately by the multi-Gaussian form

$$V_{AB-CD} = \sum a_i \, e^{-\frac{1}{2}(r_{AB}/b_i)^2} \tag{7}$$

where the a_i and b_i depend on the particular reaction $AB \to CD$ and are determined from the OGE matrix elements. Figure 3 compares the I=2 $\pi\pi$ prediction [3] to experimental data [5]. Agreement between these various theoretical approaches is encouraging in those sectors where comparisions are possible.

Another important interaction mechanism (mentioned above) in many meson-meson or baryon-meson channels is the formation of s-channel resonances. In fact, it is just these diagrams which allow us to calculate the masses and widths of short lived meson resonances in the physically relistic manner alluded to above. The creation of a single $q\bar{q}$ resonance R from an initial $q\bar{q}\,q\bar{q}$ state AB is accomplished by $q\bar{q}$ annihilation and, in our cuurent work, this is modelled by a transistion potential

$$V_{AB\cdot R} = g_{AB\cdot R}\,(r_{AB})^{L_{AB}}\, e^{-(r_{AB}/r_0)^2} \tag{8}$$

where $g_{AB\cdot R}$ is a constant, L_{AB} is the angular momentum of the asymptotic state AB, and r_0 is a characterstic range. Energy dependent phase space factors, which are expected to increase the amplitude for the reactions $AB \to R \to AB$ as the AB invariant mass increases, are being incorporated in the model [6].

As a first application of this coupled channel model, consider a 2-channel Schrödinger equation which describes S-wave $K\pi$ scattering with both quark exchange potentials and an s-channel coupling of $K\pi$ to the $K_0^*(1430)$ scalar resonance:

$$\begin{bmatrix} H_{K\pi-K\pi} & V_{K\pi\cdot K_0^*} \\ V_{K\pi\cdot K_0^*} & H_{u\bar{s}} \end{bmatrix} \begin{bmatrix} \psi_{K\pi}(r_{K\pi}) \\ \psi_{K_0^*}(r_{u\bar{s}}) \end{bmatrix} = \mathrm{M}_{K\pi} \begin{bmatrix} \psi_{K\pi}(r_{K\pi}) \\ \psi_{K_0^*}(r_{u\bar{s}}) \end{bmatrix}. \tag{9}$$

In this equation

$$H_{K\pi-K\pi} = -\frac{\hbar^2}{2\mu_{K\pi}} \frac{\mathrm{d}^2}{\mathrm{d}r_{K\pi}^2} + m_K + m_\pi + V_{K\pi-K\pi}, \tag{10}$$

where the quark exchange potential $V_{K\pi-K\pi}$ is given by, for example, eq. (7);

$V_{K\pi\cdot K_0^*}$ is a transition potential coupling the $K\pi$ state to the K_0^*, as in eq. (8);

$H_{u\bar{s}}$ is exactly the quark model Hamiltonian for the K_0^* and is given by equations (2) and (3) above; and

$\mathrm{M}_{K\pi}$ is the $K\pi$ invariant mass, and takes on values $> m_K + m_\pi$.

From eq. (9) we can see clearly how embedding the old $q\bar{q}$ Hamiltonian in a matrix formulation enables us to preserve it's established role while also allowing us to couple the $q\bar{q}$ state to its asymptotic states. In fact, solutions of the eigenvalue equation (1) can be recovered from the scattering equation (9) by allowing the off-diagonal potential to become vanishingly small, as we shall see below.

A standard description of the phase shift for the process $K\pi \to K_0^* \to K\pi$ is the Breit-Wigner given by

$$\delta_{K\pi}^{BW} = \arctan\left(\frac{\frac{1}{2}\Gamma_{K_0^*}}{M_{K_0^*} - M_{K\pi}}\right). \tag{11}$$

Choosing the limit $V_{K\pi-K\pi} = 0$ in eq. (10) means that the only $K\pi$ interaction mechanism in eq. (9) is through $K_0^*(1430)$ s-channel resonance formation and, in Figure 4, we show that the resulting phase shift effectively reproduces the Breit-Wigner result. This establishes an essential and non-trivial correspondence between eq. (9) and eq. (11).

In Figure 5 we see that as $g_{K\pi\cdot K_0^*}$ vanishes the K_0^* becomes increasing narrow, or stable, and we recover the original zero width results of eq. (1) from eq. (9), as required. Now, however, the resonance mass $M_{K_0^*}$ is given by the value of $M_{K\pi}$ as $\delta_{K\pi}$ passes through 90° rather than as the eigenvalue of a discrete eigenvalue equation. When we increase the value of $g_{K\pi\cdot K_0^*}$ however, the resulting phase shift departs radically from the Breit-Wigner form and the K_0^* mass decreases. At some sufficiently large value of $g_{K\pi\cdot K_0^*}$ the coupling of the $K\pi$ asymptotic state to the K_0^* actually binds the $K\pi$ system! We therefore conclude that open channels have dramatic effects on the properties of the s-channels resonances, and suggest that a complete reanalysis of the meson spectroscopy, with new values for the Hamiltonian parameters, is called for [6].

Another interesting feature of the multichannel Schrödinger formulation is that we can also obtain the radial excitations of any particular J^P state simply by increasing the scattering energy (for example, $M_{K\pi}$ above). In Figure 6 we see the first four radial excitations of the $^3P_0$ $K_0^*(1430)$ meson as peaks in a plot of $[\sin(\delta_{K\pi})]^2$ as a function of the $K\pi$ invariant mass, in the 2-channel approximation of $K\pi \to K_0^*(1430) \to K\pi$ without quark exchange effects. (The higher radial states appear narrower because there are no phase space factors in eq. (8), as mentioned above.)

We now consider the 4-channel generalization of eq. (9) applied to the $\{K\pi, K\eta, K\eta', K_0^*(1430)\}$ S-wave scattering system, for which there is excellent data from LASS [7]. In Figure 7 we show the phase shift found by solving the 4-channel Schrödinger equation with both quark exchange and K_0^* resonance effects (using equivalent square well potentials). As one can see, very good agreement with data is obtained. In Figure 8 we show the phase shift which results when only meson-meson couplings to the K_0^* are considered; the agreement with data evidently becomes quite poor. In Figure 9 we show the phase shift resulting when only quark exchange effects are included and we see what might be parameterized as an "effective range polynomial background" in a partial wave analysis, suggesting that quark exchange effects are the physical source of such backgrounds. In this sector it is also clear that the data favors the inclusion of both quark exchange and s-channel resonance contributions.

In Figure 10 we show the $\pi\eta$ phase shift from the 4-channel solution of the $\{\pi\eta, K\bar{K}, \pi\eta', a_0(1320)\}$ scattering system. While $\pi\eta$ elastic phases shifts have never been experimentally extracted the $a_0(980)$ has been seen in both $\pi\eta$ and $K\bar{K}$ final states. In the coupled channel model this resonance is due to exchange effects which bind the $K\bar{K}$ system into a molecular state. This interpretation provides a transparent explanation for the narrow width of the $a_0(980)$ relative to the $q\bar{q}$ quark model prediction of several hundred MeV and the strong coupling to the $K\bar{K}$ channel when that threshold is crossed, as well as many other observations [1,8].

In Figure 11 we show the I=0 $\pi\pi$ phase shift from the 7-channel $\{\pi\pi, K\bar{K}, \eta\eta, \eta\eta', \eta'\eta', f_0(1400), f_0'(1525)\}$ scattering system, with a compilation of experimental data [9]. The narrow $f_0(975)$ resonance near $K\bar{K}$ threshold is interpreted as a $K\bar{K}$ molecular bound state. As one solves the Schrödinger equation at each scattering energy, one obtains the wavefunction for each component

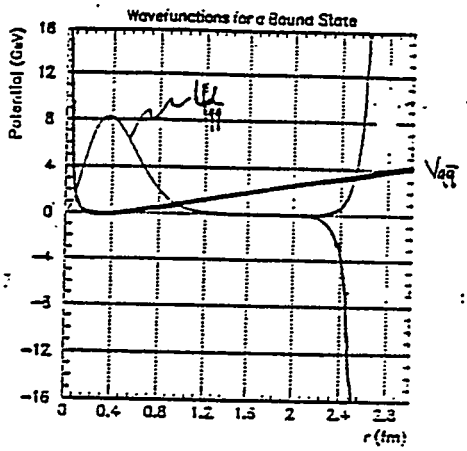


Figure 1: The integrated wavefunction for a particular $V_{q\bar{q}}$ at trial energies M_A =1549.9009 and 1549.9010 MeV. The actual eigenmass lies between these values.

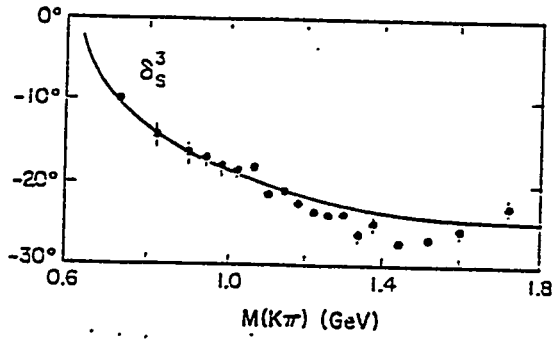


Figure 2: The I=3/2 $K\pi$ phase shifts from the variational extraction and data from [2].

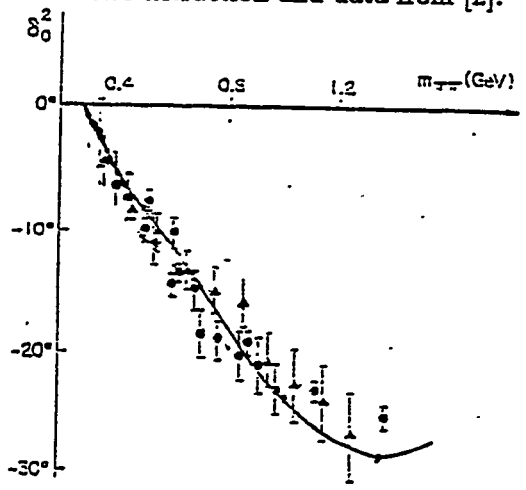


Figure 3: I=2 $\pi\pi$ phase shifts from the Born approximation [3] and data from [5].

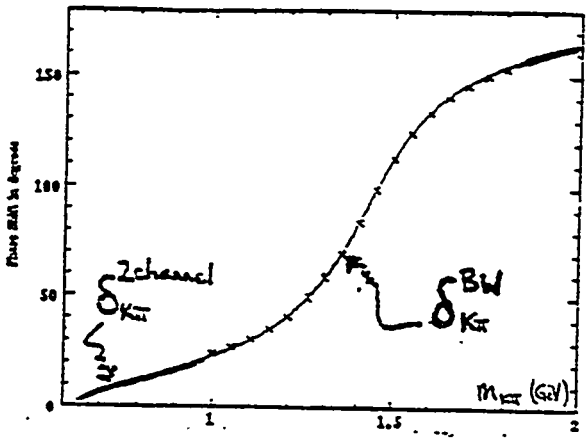


Figure 4: Compare $\delta^{BW}_{K\pi}$ with the result from the 2-channel Schrödinger equation with a vanishing quark exchange potential.

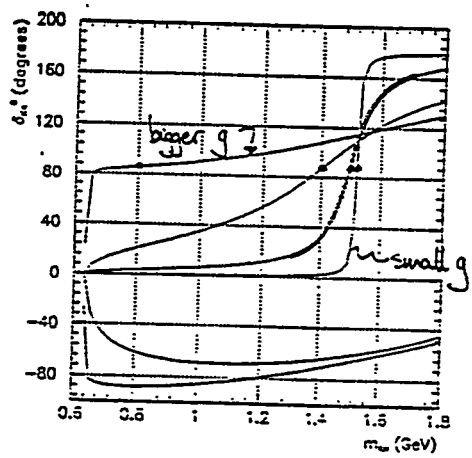


Figure 5: The variation of the $K\pi$ phase shift as $g_{K\pi\text{-}K^*_0}$ changes in strength.

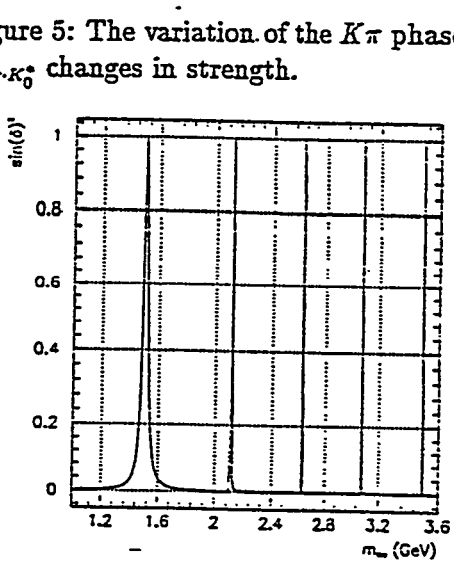


Figure 6: The $K^*_0(1430)$ and it's first four radial excitations as peaks in $[\sin(\delta_{K\pi})]^2$.

of the (vector) wavefunction ψ, and these components are shown in Figure 12 at a $\pi\pi$ invariant mass of 975 MeV. Here we can see the dominance of the $K\bar{K}$ component of the wavefunction near $K\bar{K}$ threshold, with significant contributions also coming from the $\eta\eta$, f_0', and f_0 components. The interpretation of the $f_0(975)$ and $a_0(980)$ as $K\bar{K}$ molecular states has many appealing features which have been discussed elsewhere [1,8]. Of particular relevance to CEBAF is a test of the $K\bar{K}$ molecule picture using in-flight radiative decays of $\phi(1020)$ mesons [10].

In conclusion, we emphasize that the multichannel Schrödinger equation approach treats meson spectroscopy and meson-meson scattering on an equal footing. It reproduces the Breit-Wigner and meson spectroscopy results for s-channel resonances in the narrow width approximation, but also describes the effects of strong resonance couplings to open decay channels and quark exchange effects. The use of quark exchange potentials plus couplings to s-channel resonances in the multichannel Schrödinger equation, as opposed to the traditional model of t-channel meson exchange, leads to impressive agreements with a wide variety of experimental obsevations. The $K\pi$ data show that both quark exchange and s-shannel resonance formation are important. This approach can be applied to all of meson spectroscopy and two-body scattering; it is clearly in its infancy and promises to provide many insights into the spectroscopy and dynamics of hadrons. It may ultimately prove to be an essential analytical tool for resolving the meson spectrum and identifying glueball and hybrid states.

References

[1] J. Weinstein, Phys. Rev. **D47**, 911 (1993). J. Weinstein and N. Isgur, Phys. Rev. **D43**, 95 (1991); Phys. Rev. **D41**, 2236 (1990); Phys. Rev. Lett. 48, 659 (1982); Phys. Rev. **D27**, 588 (1983).

[2] P. Estabrooks *et al.*, Nucl. Phy. **B133**, 490 (1978).

[3] T. Barnes, E.S. Swanson, Phys. Rev. C49, 1166 (1994); T. Barnes, S. Capstick, M.D. Kovarik, E.S. Swanson, Phys. Rev. C48, 539 (1993); T. Barnes, E.S. Swanson, Phys. Rev. **D46**, 131 (1992); T. Barnes, E. Swanson, J. Weinstein, Phys. Rev. **D46**, 4868 (1992).

[4] E.S. Swanson, Ann. Phy. **220**, 73 (1992).

[5] F. Wagner *et al.*, *Proc. XVII Int. Conf. on High Energy Physics*, London, England, 1974; W. Hoogland *et al.*, Nucl. Phy. **B126**, 109, (1977).

[6] J. Weinstein, "A New Approach to Meson Spectroscopy", University of Mississippi preprint, UM-HEP-94-008, in preparation.

[7] D. Aston *et al.*, Nucl. Phy. **B296**, 493 (1988).

[8] For the Δ I=1/2 rule in K decay see N. Isgur, K. Maltman, J. Weinstein, T. Barnes, Phys. Rev. Lett. 64, 161 (1990); for $\gamma\gamma$ couplings see T. Barnes, Phys. Lett. **B165**, 434 (1985); for effects in $\iota \to K\bar{K}\pi$ decays see M. Frank, N. Isgur, P.J. O'Donnell, and J. Weinstein, Phys. Rev. **D32**, 2971, (1985); Phys. Lett. 158B, 442, (1985); for the effects in $J/\psi \to V[PP]_{S-wave}$ see J. Weinstein, Proceedings of the τ-Charm Factory Workshop, Stanford Linear Accelerator Center, Stanford CA, May 1989.

[9] G. Grayer *et al.*, Nucl. Phy. **B75**, 189 (1974); S.D. Protopopescu *et al.*, Phy. Rev. **D7**, 1280 (1973); L. Rosselet *et al.*, Phy. Rev. **D15**, 574 (1977).

[10] See A.R. Dzierba, these proceedings.

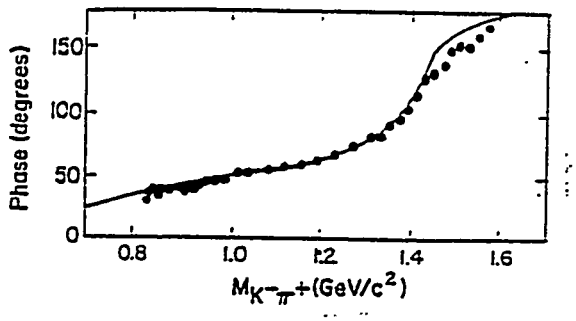


Figure 7: The $K\pi$ phase shift using the 4-channel Schrödinger equation and both quark exchange potentials and couplings to the K_0^* meson. The data is from LASS [7].

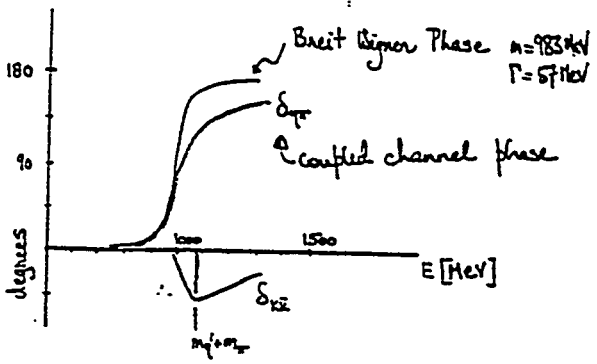


Figure 10: The predicted $\pi\eta$ phase shift compared to a Breit-Wigner having the mass and width of the $a_0(980)$.

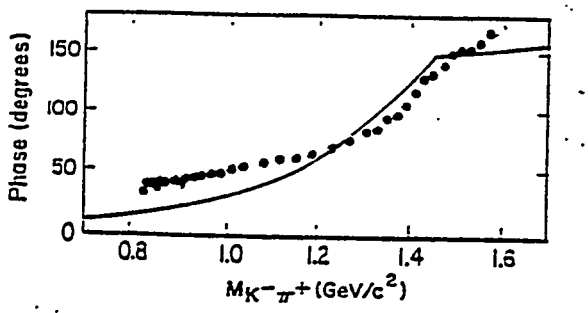


Figure 8: The $K\pi$ phase shift using the 4-channel Schrödinger equation and only couplings to the K_0^* meson. The data is from LASS [7].

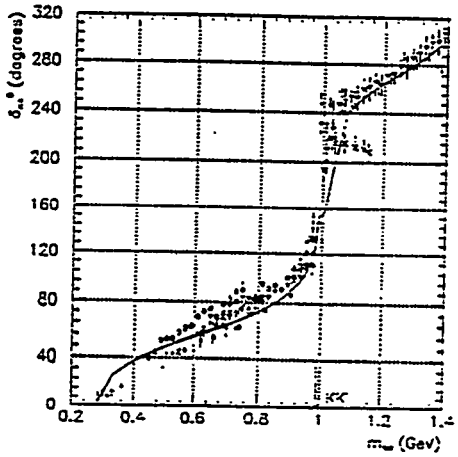


Figure 11: The I=0 $\pi\pi$ elastic phase shift with data from [9].

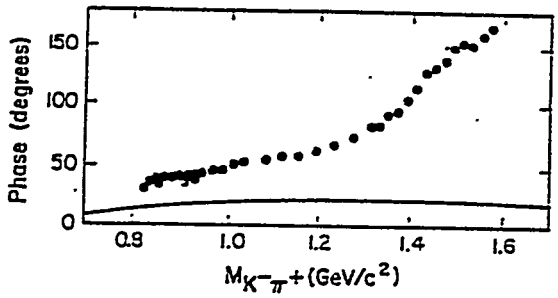


Figure 9: The $K\pi$ phase shift using the 4-channel Schrödinger equation and only quark exchange potentials. The data is from LASS [7].

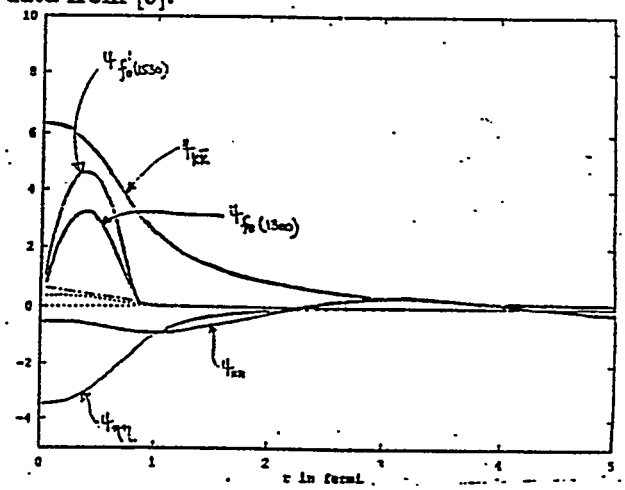


Figure 12: Wavefunctions from the 7-channel solution at the $f_0(975)$ mass.

Working Group on Form Factors and Exclusive Reactions

Organizers: G. Petratos & P. Stoler

Exclusive Reactions at High Q^2 with CEBAF at Higher Energies

PAUL STOLER
Physics Department, Rensselaer Polytechnic Institute
Troy, NY 12180

GERASIMOS G. PETRATOS
Department of Physics and Center for Nuclear Research
Kent State University, Kent, OH 44242

1 Introduction

Our earliest and most successful understanding of meson and baryon structure has been based on a model of constituent quarks moving in a phenomenological mean field which is supposed to represent the effects of complicated, but as yet uncalculated, gluonic interactions. Refinements to such models in terms of residual interactions such as color hyperfine interactions improve agreement with experimental spectroscopy. As momentum transfers increase this type of simple model becomes inadequate and one must search for additional degrees of freedom to account for the observed data. However, since these models are not fundamental, the pursuit to apply it to regions of ever increasing momentum transfer becomes fruitless. The constituent quarks themselves are the manifestations of a complexity of interacting valence quarks, sea quarks and gluons in the non-perturbative domain, and it is in terms of these fundamental entities which we must learn to describe mesons and baryons.

The situation is analogous to that of the nucleus. A great deal of theoretical effort has gone into models involving constituent protons and neutrons, with interactions modeled in terms of meson fields. Thus, many of the low energy properties of nuclear matter are well described in terms of a mean field shell model, with residual perturbative nucleon-nucleon interactions. However, with increasing momentum transfer (resolution) the model becomes more complicated and eventually, as in the case of the baryon, less useful. A more fundamental approach requires the description of nuclear matter in terms of the variables of QCD in the non-perturbative domain. The fact that this may prove to be a very difficult task does not in any way diminish its importance.

The primary problem then at higher momentum transfer Q^2 ($\equiv -q^2$) is the need for the theory of the structure of hadronic matter in the non-perturbative domain. It is instructive to express the wave function of a hadron as a series of states with increasingly greater numbers of quarks and gluons. This is known as a Fock state expansion. Fock states for mesons and baryons can be schematically written

$$|M> = |q\bar{q}> + |q\bar{q}G> + |q\bar{q}q\bar{q}> +... \quad 1.$$

and

$$|B> = |qqq> + |qqqG> + |qqq\bar{q}q> +... \quad 2.$$

The first ('leading') terms in equations 1 and 2 are the valence quark states which have the least complexity and are believed to dominate exclusive reactions at asymptotically large values of momentum transfer. For a nucleus such as a deuteron the expansion would involve two such clusters, plus something else. This something else includes the (rather weak) exchange of gluons and quarks which are responsible for the nuclear binding. Additionally, there may be structures which cannot exist in a single isolated baryon. For example, each cluster in a nucleus may have small component of net color consistent with the overall deuteron being in a color singlet state.

At this time hadronic structure, i.e. the wave functions of hadronic states in terms of the fundamental QCD substructures, remains unsolved. One of the primary motivations of our physics program is to elucidate wherever possible the various components of the hadronic Fock states. It is our point of view that CEBAF at higher energies will provide an important step in this program.

2 The Program of Exclusive Reactions at High Momentum Transfer

Exclusive reactions involving only a few particles in the final state are very powerful in that they involve a minimum number of degrees of freedom, and the greatest simplicity of interpretation.

From an exclusive reaction one can extract the exclusive amplitudes. These amplitudes are the convolution of the hadronic structures with the reaction mechanism. If the reaction mechanism is well understood we have a handle on the structure. A simple example is the measurement of the elastic form factors which are the diagonal amplitudes for the hadronic absorption of virtual photons. If we assume that the reaction occurs through the exchange of a single virtual photon which interacts with the charges and currents of the target nucleon in a precisely understood way, then we immediately extract the electromagnetic structure of the hadron. In this case the key is the control of the reaction mechanism, i.e. the exchange of a single photon. More generally, transition form factors allow us to access the structure of hadronic excited states, which greatly enhances the experimental basis for theoretical comparisons.

At this point we discuss the physics motivations for our proposed program of exclusive reaction experiments. These experiments have been uniquely matched to the proposed properties of CEBAF. The program we propose is a systematic study of the structure of mesons, baryons and nuclei by a

variety of exclusive reactions at momentum transfers not previously possible, which will lead to a clearer understanding the structure of hadronic matter. We stress at the outset that this is part of an evolving program, and in addition, we expect that there will emerge some exciting surprises and diversions, which is often the case when a new type of facility becomes operational.

The subjects of the proposed experiments are divided as follows:

1. Form factors of mesons.
2. Elastic and transition form factors of baryons.
3. Form factors and photodisintegration of deuterium.
4. Meson photo- and electroproduction.

3 Form Factors of Mesons and Baryons

A central part of the program is the measurement of elastic and transition form factors for mesons and baryons over a large range of Q^2. At low Q^2 these form factors cannot yet be described in terms of QCD, since the microscopic reaction mechanisms are non-perturbative, and the structures are very complicated and not yet well understood. In order to make sense of exclusive reactions one needs models which simplify the description of the complicated structure in terms of as few degrees of freedom as possible. This is the realm where first vector meson dominance, and then constituent quark models (CQM) have been applied with varying degrees of success. One of the major programs of the initial stage of CEBAF will be to try to elucidate exclusive reactions and hadronic structure in the lower Q^2 regime in terms of these CQM.

In the opposite kinematic extreme, at very high Q^2, it is generally agreed that the reaction mechanism should be much simpler. That is, the reaction involves only that part of the hadron structure which consists of the valence quarks, i.e. the first terms in equations 1 and 2, with perturbative exchanges of the minimal number of hard gluons. For mesons we have two quarks exchanging one gluon, and for baryons we have three quarks exchanging two gluons. This is shown schematically in Figures 1a and 1b.

In this high Q^2 regime the momentum of the virtual photon flows through the exchanged gluons, so that it is postulated that form factors are describable by perturbative QCD (PQCD), and may be factorized in the following simple form (Br-89, Le-80, Li-92):

$$F(Q^2) = \int_0^1 \int_0^1 dxdy \int dk_\perp^2 \; \Phi_F(y, k_{\perp f})^* \; T_H \; \Phi_I(x, k_{\perp i}) \qquad 3.$$

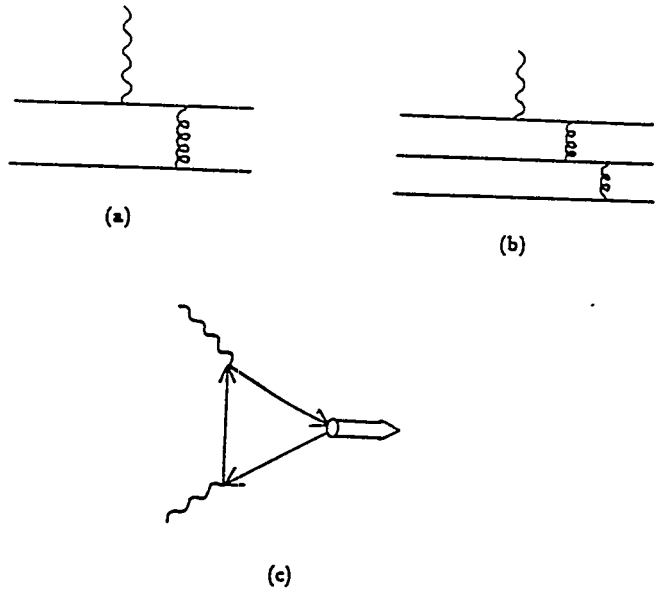


Figure 1: Examples of leading order diagrams contributing to elastic and inelastic transition form factors. a) and b) The perturbative hard scattering amplitude T_H, for mesons and baryons respectively. c)π° production via purely electromagnetic processes.

$\Phi_{I,F}$ are the valence quark distribution functions for the initial and final hadron states respectively. For mesons $x = (x_1 - x_2)$ and $y = (y_1 - y_2)$ denote the relative longitudinal momentum fractions, and $k_{\perp i,f}$ denote the perpendicular momenta of the initial and final meson states respectively. For baryons the analogous quantities are $x_i, y_i, k_{\perp i}$ with $i = 1,2,3$. The distribution functions also evolve slowly with Q^2. Since quark helicity conservation in this case implies hadron helicity conservation, $F(Q^2)$ is a helicity conserving form factor. For example, in elastic e-p scattering $F(Q^2)$ corresponds to the helicity conserving Dirac form factor F_1. The two main ingredients are the hard transition operator T_H, which is purely perturbative and the valence quark distribution amplitudes Φ, which are in general non-perturbative.

To leading order, diagrams such as in Figure 1 result in the following functional forms for the transition amplitude T_H.

For mesons

$$T_H = \frac{\alpha_s(Q^2)}{Q^2} f(x,y),$$

and for baryons

$$T_H = \frac{\alpha_s^2(Q^2)}{Q^4} f(x,y),$$

where $x \equiv x_1, x_2, ..., etc.$ The helicity conserving form factors are then predicted to scale approximately as Q^{-2} and Q^{-4} for mesons and baryons respectively. More generally one has the dimensional counting rule $T_H \propto (Q^2)^{n-1}$, where n is the number of valence quarks. There is also a logarithmic decrease due to the Q^2 dependence of the running coupling constant α_s, but this would presumably be observable only over a large range of Q^2. For exclusive experiments involving multiple hadronic states the PQCD scaling law takes the form $d\sigma/dt = 1/s^{n-2}$.

Strictly speaking, these PQCD techniques can be applied only in the limit $Q^2 \to \infty$. With CEBAF at higher energies we will be somewhere between the two extreme approaches. Where we are in the complexity scale is not known, and certainly not agreed upon by various factions of the theoretical community. One of the important goals of our program is to determine where we are. Does PQCD play a significant role in the energy and momentum range which will be available to CEBAF?

The existing experimental evidence does not contradict the assertion that PQCD plays an important role within the proposed CEBAF energies. Remarkably, many observables already appear to approach the predicted dimensional counting behavior. The most compelling case is the helicity conserving elastic form-factor of the proton, which has been measured up to $Q^2 = 35$ GeV^2/c^2 (Si-93). There is also supportive evidence (St-93) in the case of baryon excitations, as well as pion photoproduction and electroproduction, and deuteron elastic scattering and photodisintegration.

However, there is a great deal of controversy as to whether the "apparent" scaling over limited kinematical intervals is sufficient. It is not our intent here to try to decide these questions. If we take the non-prejudicial point of view that at CEBAF non-perturbative, as well as perturbative processes will contribute to exclusive reactions, we must develop theoretical techniques for dealing with these. Recently, there has been progress (Ra-94) in applying the concept QCD sum rules in the transition region where such soft processes will be important.

3.1 Meson Form Factors

The study of meson form factors have especially high priority for two reasons. Firstly, the intrinsically simpler structure of mesons make them easier to deal with theoretically than baryons. Numerous theoretical papers have appeared, or are in progress, which calculate the pion form factor in the multi-GeV^2/c^2 range of Q^2. There are too many to reference explicitly; however, see contributions in this workshop Ji-94,Mi-94, Sa-94, Ra-94.

Secondly, the approach to PQCD scaling is expected to occur at lower Q^2 for mesons than for baryons, since there is a greater probability for two valence quarks to find themselves close together and to be turned around coherently by the interchange of a single gluon, than for the baryons which

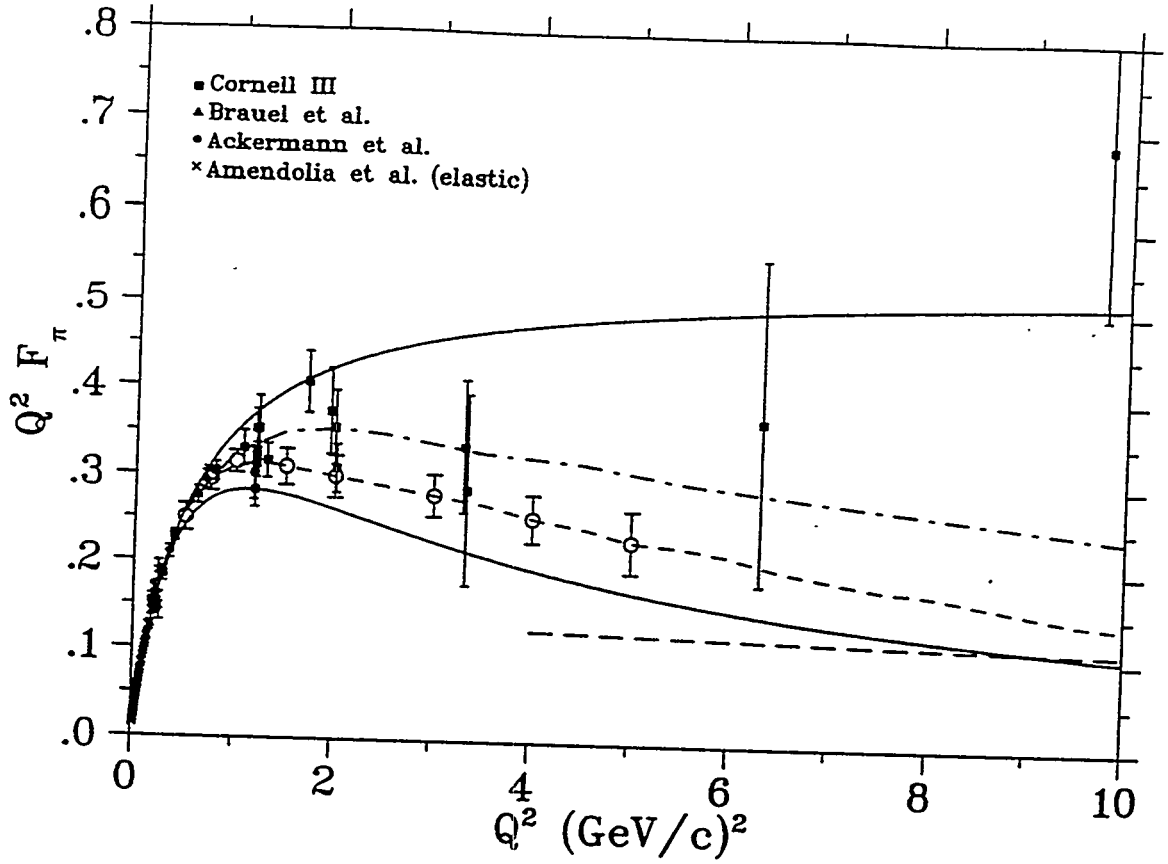


Figure 2: The form factor of the π^+ meson $Q^2F_\pi(Q^2)$ vs Q^2. The experimental points near 6 and 9 GeV^2/c^2 were not the result of an $L-T$ separation but invoked extrapolations from lower Q^2 data and are thus less reliable. The various curves are due to model calculations discussed in Ma-94, from which the figure is obtained.

require at least three valence quarks exchanging two gluons. Thus, if hard processes play a dominant role at CEBAF energies, they are most likely to appear in the pion form factor.

Using QCD sum rules, Chernyak and Zhitnitski were able to obtain a simple form of the pion $q\bar{q}$ valence quark distribution amplitude in terms of an operator product expansion of the non-perturbative quark and gluon condensates. Their distribution amplitude $\Phi^{CZ}(x)$ inserted into equation 3 is often used as a baseline for calculations of the pion form factor. One finds a significant part of the form factor involves gluon exchange momenta which are in the non-PQCD regime (Is-89). On the other hand it has been pointed out (Li-92) that radiative effects in the non-perturbative regime (the so called 'Sudakov' effects) strongly suppress the non-perturbative contributions to the form factors, even at relatively low values of Q^2. Figure 2 shows all we know about the experimental pion form factor, and results of several theoretical calculations.

Reliable data exist for $Q^2 < 3$ GeV^2/c^2, which is not really high enough to test PQCD scaling assumptions nor to resolve the large theoretical discrepancies. An important goal of the exclusive

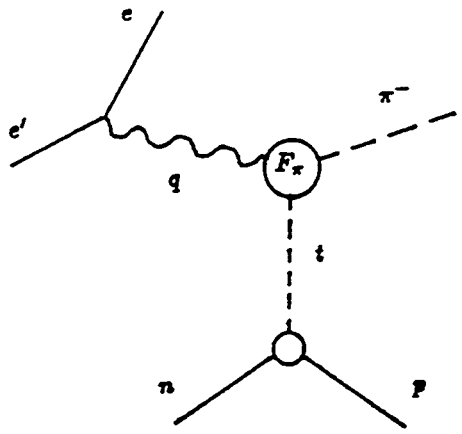


Figure 3: Interpretation of t-channel π^+ production in terms of the pion form factor F_π.

program is to extend the pion form factor out to as high Q^2 possible. With an 8-10 GeV electron beam we can expect to make reliable measurements up to $Q^2 \sim 6$ GeV^2/c^2(Ma-94), as shown by the mock data superimposed on Figure 2.

The pion form factor is obtained by means of t-channel electroproduction (see Figure 3), in which we assume the electron scatters from the virtual pionic current in the nucleon. The relationship between the longitudinal component of the electron scattering cross section and the pion form factor is given by

$$\sigma_L \sim -\frac{t g^2_{\pi NN}(t)}{(t-m_\pi^2)^2} F_\pi^2(Q^2) \qquad \text{as } t \to m_\pi^2$$

where t is the squared momentum transfer to the nucleon, and $g^2_{\pi NN}(t)$ is the πNN coupling. There are important theoretical issues in the interpretation of the data which will need to be investigated in parallel. For example, how do we treat the off shell nature of the struck pion, and how do we extrapolate the data to the physical pole at $t = -m_\pi^2$? The measurement of the kaon form factor is also a possibility. However, in this case the extrapolation to the physical pole at $t = -m_K^2$ is much more serious (Ba-94).

An important collateral measurement will be the $\pi^\circ - \gamma$ transition form factor obtained in the purely electromagnetic production of the π° (Figure 1c). Since this involves only α_e and not α_s, and proceeds through leading order, it can serve as a powerful constraint on distribution amplitudes which are used in PQCD based calculations (Af-94, Ra-94). Curiously, one finds that in a purely PQCD

framework both Φ^{as} and Φ^{CZ} overestimate data on the $\pi^\circ - \gamma$ form factor at lower Q^2. On the other hand the calculation of Li-92 with Φ^{CZ} including Sudakov effects appears to account well for the π^+ form factor in the same Q^2 region. Experimentally, this π° form factor can be accessed via either the Primakoff effect, or virtual Compton scattering. It is found that the latter is more favorable for CEBAF, and it is intended to pursue such measurements. One of the experimental-theoretical issues involving the interpretation is to find kinematic conditions which minimize the competing diffractive contribution.

3.2 Baryon Form Factors

Here we consider together nucleon elastic form factors and transition form factors involving resonant states of nucleons. Since there exist stable on-shell baryon targets, i.e. nucleons, and there are a large variety of final states of spin and isospin, a wealth of experimental information can be accessed. It turns out that due to the limitations of previous generation accelerators very little data exist at high Q^2. CEBAF will make a significant contribution in providing such data.

Scattering cross section, either elastic or resonant, may be written in terms of longitudinal and transverse form-factors G_E and G_T:

$$\frac{d\sigma}{dE'd\Omega_e} = \sigma_{Mott} f_{rec} \left\{ \frac{|G_E|^2 + \tau^* |G_T|^2}{1+\tau^*} + 2\tau^* |G_T|^2 tan^2\theta/2 \right\} R(W)$$

where $\tau^* = (Q^2 + W_R^2 - M_N^2)^2/4M_N^2Q^2$. Note that for elastic scattering $\tau^* \rightarrow \tau = Q^2/4M_N^2$. For elastic scattering ,$R(W) = \delta(W - M_N)$ while for inelastic scattering from a resonance, $R(W)$ has a (Breit-Wigner) resonant shape. These form factors are expressed in terms of a helicity conserving amplitude G_+ and helicity non-conserving amplitudes $G_\circ$ and G_- as follows:

$$G_\circ = G_E, \qquad \frac{1}{2}(|G_+|^2 + |G_-|^2) = \tau^* |G_T|^2.$$

3.3 Elastic Nucleon form factors.

For elastic scattering we have

$$G_+ = \frac{Q}{\sqrt{2}M_N} G_M = \frac{Q}{\sqrt{2}M_N}(F_1 + \kappa F_2)$$

$$G_o = G_E = F_1 - \frac{Q^2}{4M_N^2}\kappa F_2.$$

For both proton and neutron targets there are two helicity conserving and two helicity non-conserving form factors, G_M^P, G_M^N and G_E^P, G_E^N respectively. At low Q^2 (less than a few GeV^2/c^2) all the form factors are consistent with a dipole Q^2 dependence, ie. $1/(1+Q^2/\Lambda^2)^2$. G_M^P is the best known experimentally, followed by G_M^N, and then in order G_E^P and G_E^N. A major program is already planned to measure the latter two up to a Q^2 of a few GeV^2/c^2.

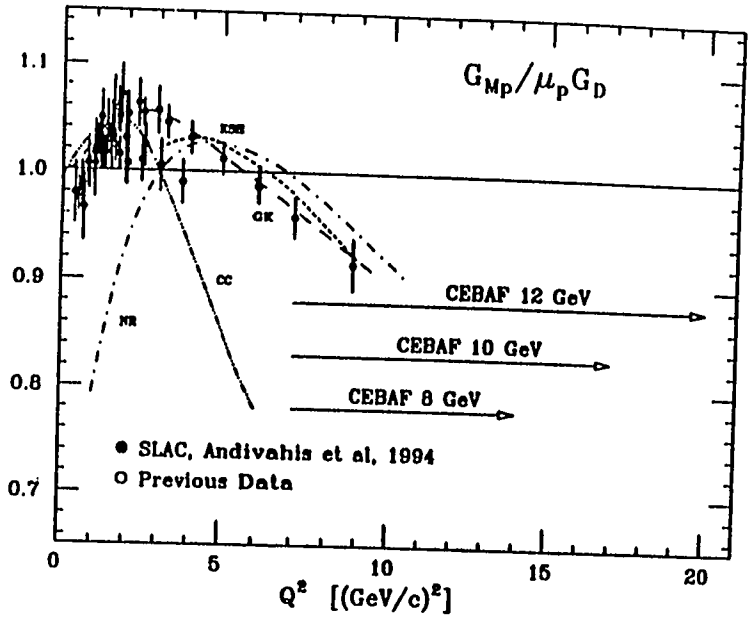
Only G_M^P has been measured at high Q^2 (Si-93). Data exist up to a $Q^2 \sim 30$ GeV^2/c^2, shown in Figure 4a up to about 20 GeV^2/c^2. The Q^2 dependence is in remarkable agreement with a $1/Q^4$ times a logarithmic decrease predicted by PQCD calculations, and PQCD sum rule calculations using e.g. $\Phi^{CZ}(x_i)$ amplitudes have obtained good normalizations as well. However, there are those who argue that this is fortuitous, and the form factor can be fit over the existing data by soft processes as well (Is-88) . Only global tests involving all available form factors can hope to seriously select from opposing points of view. We stress the importance of measuring the helicity non-conserving form factors out to as high Q^2 as possible since they are driven by non-leading processes, and therefore offer important constraints on the relative importance of soft and hard processes with varying Q^2.

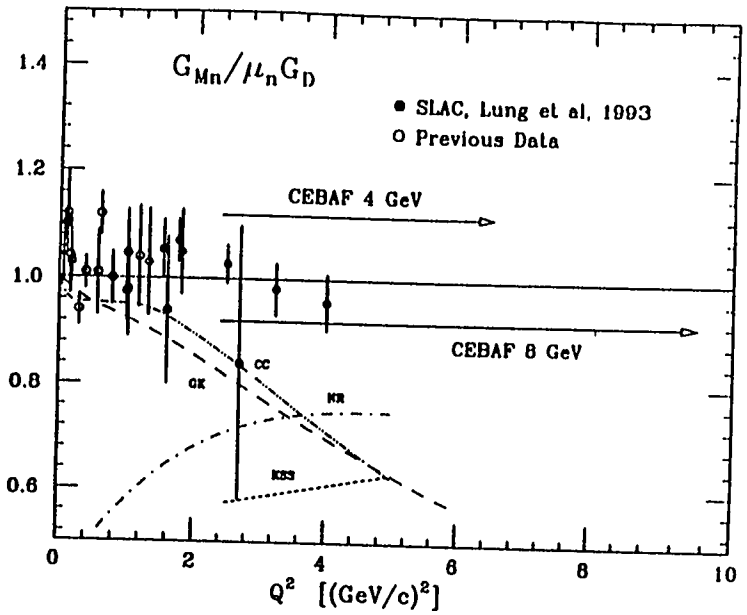
The other three form factors are much less well known. Figure 4 shows what is presently known about them. We see that although several models obtain good agreement with G_M^P, the other form factors are already selective in the lower Q^2 range. For example, the semi-phenomenological hybrid model of Gari and Krümplemann appears to be ruled out by G_E^N. The model of Radyushkin (Ra-94), which is a QCD sum rules approach in which the form factors are dominated by soft processes over the entire measurable range of Q^2, appears to agree with G_M^P in the moderately high region of Q^2, but has difficulty with G_M^P in the highest Q^2 region, and difficulty with G_E^N and G_M^N at moderately low values of Q^2. Clearly, improving the quality of the data and extending them to higher Q^2 is very important, and a major part of our program.

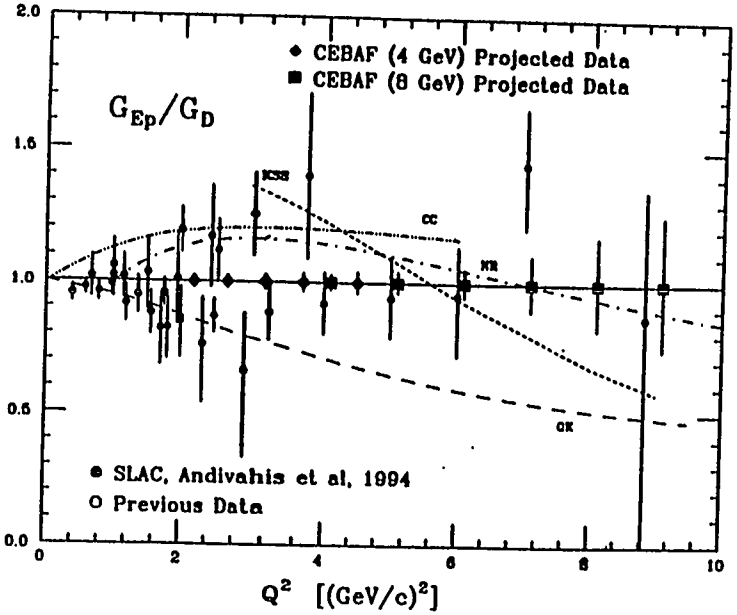
It is generally overlooked that even the data on G_M^P has not really been obtained from a Rosenbluth separation, but was obtained under the assumption (probably very good) that at the kinematics of the experiment the contribution of G_E^P is very small. With CEBAF at 8 GeV an excellent separation can be carried out up to about $Q^2 \sim 14$GeV^2/c^2, and an even higher Q^2 accessed with a 10 or 12 GeV beam (Pe-94).

For G_E^P quality data exists only for low Q^2. This is because a Rosenbluth separation is difficult due to the dominance of G_M^P as Q^2 increases. However, using polarization one is sensitive to the ratio G_E^P/G_M^P, which should allow us to make measurements at Q^2 approaching 10 GeV^2/c^2. (Vo-94).

In the case of the neutron, the experimental difficulties are much increased due to the absence of charge and the necessity of measuring the neutron imbedded in a nucleus such as deuterium or ^{3}He, with their attendant Fermi motions. For G_M^N rather good data exists for Q^2 up to about 4 GeV^2/c^2. We see that the data doesn't really agree well with any of the low Q^2 models. Even with a 4 GeV







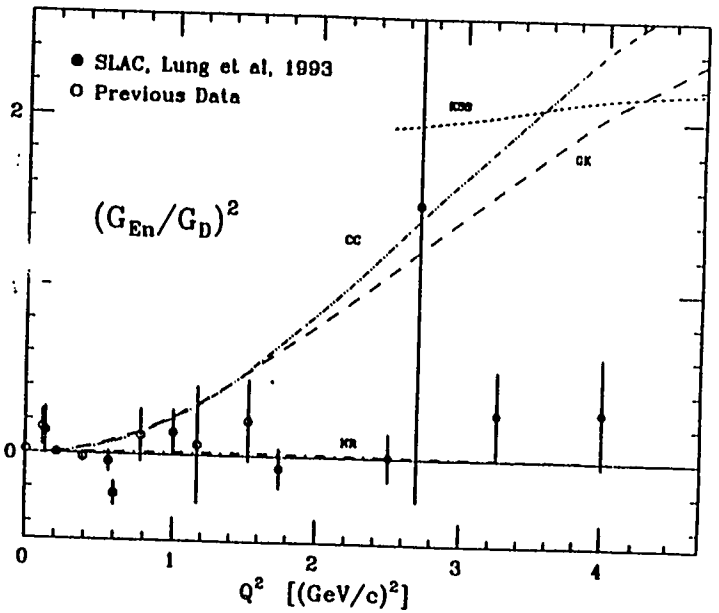


Figure 4: The elastic form factors as a function of Q^2: a)G_M^P and b)G_M^N, where the projected range accessible at E_e = 4,8,10 and 12 GeV are indicated by arrows, c)G_E^P, where the projected CEBAF data is indicated by solid diamonds (E_e = 4 GeV) and solid squares (E_e = 8 GeV), and d)G_E^N.

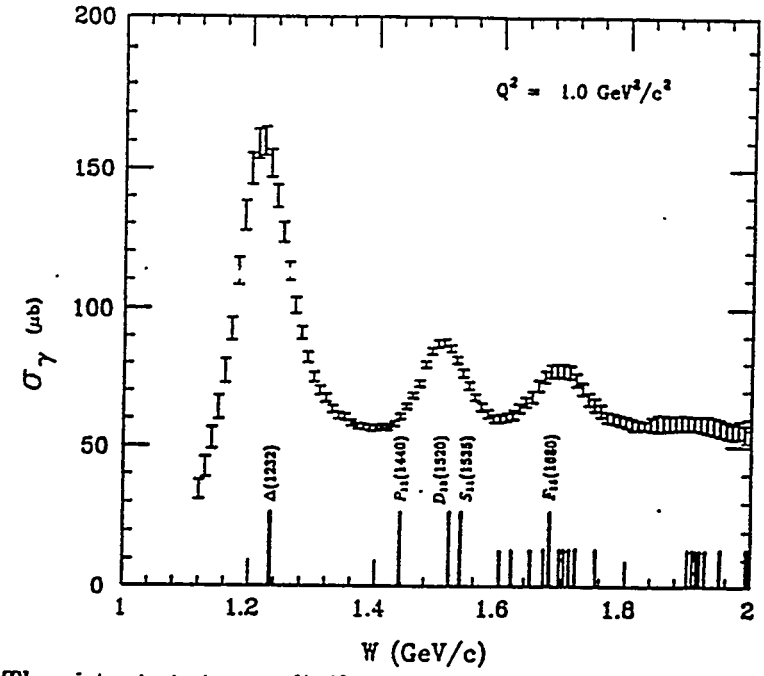


Figure 5: The virtual photon excitation curve for electron scattering at $Q^2 = 1$ GeV^2/c^2.

beam we believe we can make good measurements up to about 7 GeV^2/c^2, and with an 8 GeV beam one can extend the measurement to about 10 GeV^2/c^2 (Br-94).

The situation for G_E^N is currently unsatisfactory at all Q^2. In the higher Q^2 region there is only some limited data up to Q^2= 4 GeV^2/c^2. Currently there are programs for G_E^N measurements at lower values of Q^2 using polarimetry techniques. Extending these measurements to higher Q^2 will be difficult because of the necessity of extracting information about a small falling form factor from deuterium or ^3He polarized targets, however this should be investigated.

3.4 Resonance transition form factors.

Baryon resonance form factors are completely analogous to elastic form factors, and at high Q^2 would also be calculated according to equation 3. Their measurement as a function of Q^2 will constitute an important part of our exclusive program in that they will provide structure information about excited states of the nucleon. To illustrate some of the issues, Figure 5 shows the inclusive electron scattering cross section in the resonance region at $Q^2 = 1$ GeV^2/c^2.

There are about twenty broadly overlapping resonances which can only be separated by performing exclusive experiments in which their decay products are observed. We don't know very much about the structure of these resonance at $Q^2 > 0$. The only existing exclusive data are of moderate quality for the four dominant excitations, the $\Delta(1232), D_{13}(1520)$, $S_{11}(1535)$ and $F_{15}(1680)$, and nothing exists for any resonance at $Q^2 > 3$ GeV^2/c^2. An analysis of existing inclusive data, as shown in Figure 6, indicates the possibility that, except for the $\Delta(1232)$, the transition to scaling behavior may begin

within the Q^2 capabilities of the CEBAF.

The two most attractive cases to study will be the $\Delta(1232)$ and the $S_{11}(1535)$.

The $\Delta(1232)$ is the only resonance which does not have a large overlap with other resonances. Its form factor decreases faster than the other form factors for reasons which are not currently understood. Where it begins to approach a $1/Q^4$ behavior is not yet determined though there has been an extensive analysis of existing inclusive data (Ke-94). An intriguing suggestion (Ca-88) is that the leading order contribution is anomalously small, so that we are seeing the relatively increased effects of non-leading amplitudes, which fall faster with Q^2. For the $\Delta(1232)$ at low Q^2 the multipoles $M_{1+} >> E_{1+}$, in agreement with CQM. This implies that the ratio of helicity non-conserving and helicity conserving amplitudes $G_-/G_+ = \sqrt{3}$. However, in the PQCD limit $G_-/G_+ = 0$ which implies $M_{1+} = E_{1+}$. Thus, the $\Delta(1232)$ may be a favorable case to study the transition from CQM to PQCD.

The $S_{11}(1535)$ is an attractive case in that it is the only major resonance with a strong η decay channel, so that it can be cleanly accessed through the reaction $p(e, e'p)\eta$. Its amplitude is purely helicity conserving G_+ and, as seen in Figure 6 may approach the PQCD predicted scaling behavior at a fairly low Q^2.

A very interesting concept is that of duality between resonance and non-resonance continuum in the W region where they overlap. One observed early on (Bl-70) that the rate of decrease with Q^2 of the resonance cross sections approximately follows the extrapolation of the deep inelastic scaling into the resonance region, suggesting that both types of processes are related by the same underlying physics (Bl-70). Recently this was put on more firm ground and extended to much higher Q^2 (Ca-92). However, all of this is based on analyses of inclusive data which cannot effectively separate non-resonance from resonance contributions. It has been pointed out (Mu-94) that in order to access this very fundamental point one really needs to have a clean separation of resonance and non-resonance data over a large range of Q^2. This can only be accomplished via the measurement of exclusive reactions at a CEBAF.

In summary, with an 8 GeV beam, we will have enough counting rate to measure resonance form factors at $Q^2 > 10$ GeV^2/c^2(St-94)

4 Reactions Involving Few Nucleon Systems

A crucial goal of our program is to extend the underlying physics of baryon structure in terms of quarks and gluons to an understanding of the mechanisms by which baryons bind to form nuclei. This remains the major unsolved mystery of nuclear physics. The best way to approach this problem is to begin with the simplest multi-baryonic systems, in particular the deuteron, and also ^{3}He. As few baryon structures they remain "simple" enough so that the entire reaction mechanism may be treated

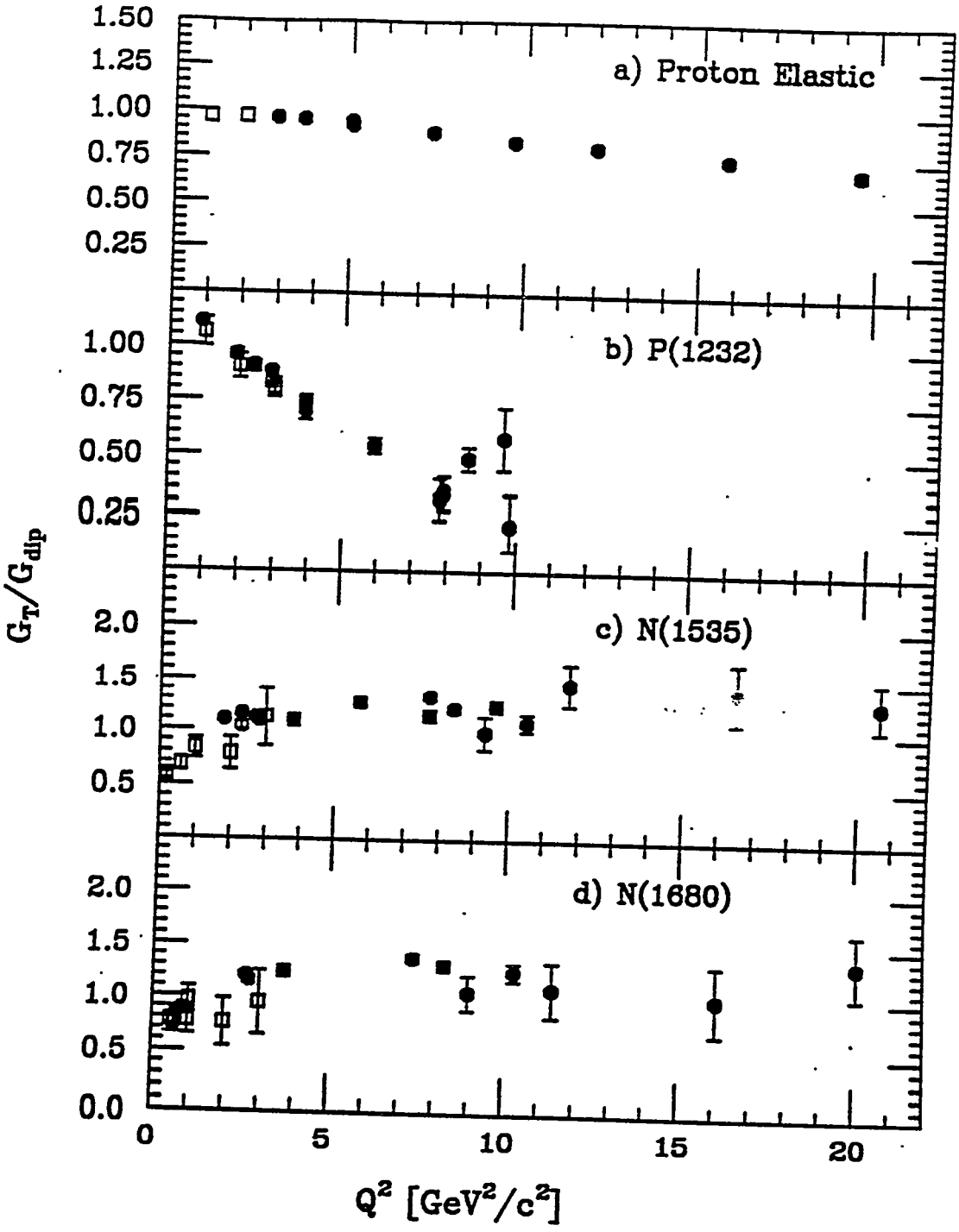


Figure 6: Baryon form factors divided by the dipole shape as a function of Q^2. For proton elastic $G_{dip} = \mu_p(1+Q^2)^{-2}$ The form factors of the peaks in the resonance region corresponding to the excitation energies of the $\Delta(1232)$, $N^*(1535)$ and $N^*(1680)$, and are divided by $G_{dip} = 3(1+Q^2)^{-2}$. (from St-94.)

microscopically. In addition, the binding of the two nucleon system is rather weak so that one may deal with relatively small variants of the constituent baryon basic substructure.

One method of attack, as we advocated for the single baryon, is to measure some very basic experimental quantities over a very large kinematic range and determine the region of transition between traditional non-QCD descriptions and those requiring quarks and gluons. For baryons this involves the measurement of elastic and transition form factors over a large range of Q^2 and trying to observe the region where constituent quark models are no longer adequate.

For nuclei the approach is somewhat analogous. However, here there are three basic viewpoints which need to be sorted out. At low energies the appropriate descriptions treat the nucleons as fundamental objects with form factors, and all strong interactions are treated in terms of meson exchanges. Another approach is to treat the nucleons as composed of constituent quarks and interactions mediated by exchanges of constituent quarks and by ad-hoc potentials. The third approach, which is the most fundamental, is again to treat the systems totally in terms of QCD, that is current quarks and gluons. Again, this only becomes analytically tractable at asymptotically high momentum transfers.

Among the specific reactions which have been proposed for study are:

a. Elastic scattering: $e + d \rightarrow e' + d$, $e + {}^3He \rightarrow e' + {}^3He$

b. Photodisintegration: $\gamma + d \rightarrow p + n$

c. Neutral pion production: $\gamma + d \rightarrow d + \pi^0$

In all cases, for the highest momentum transfers which have been experimentally observed, it is not yet clear which of the three approaches is the most valid, i.e. whether we have evolved to the regime where it is necessary to invoke QCD to explain the results.

For example, consider the case of the deuterium elastic form factors, reaction a. above. In the spirit of PQCD scaling, the dimensional counting rules predict the form factor $[A(Q^2)]^{1/2} \rightarrow (Q^2)^{(n-1)} \rightarrow (Q^2)^5$. Figure 7, from (Pe-94), shows the status of the existing data, which effectively stops at $Q^2 \sim 4$ GeV^2/c^2. The figure shows that dimensional scaling has not yet set in. This is not surprising even for proponents of PQCD, since it is generally recognized that the more complex the system, i.e. the greater the number of valence quarks, the higher Q^2 one must go in order to see effects of hard processes. Also shown in Figure 7 is the projected good quality data which can be obtained up to $Q^2 \sim$ 9 GeV^2/c^2.

Another case is reaction b., the two-body photodisintegration of deuterium. For this reaction the relevant variables are s and t rather than Q^2. The QCD scaling laws predict $d\sigma/dt \propto s^{-11}$. There

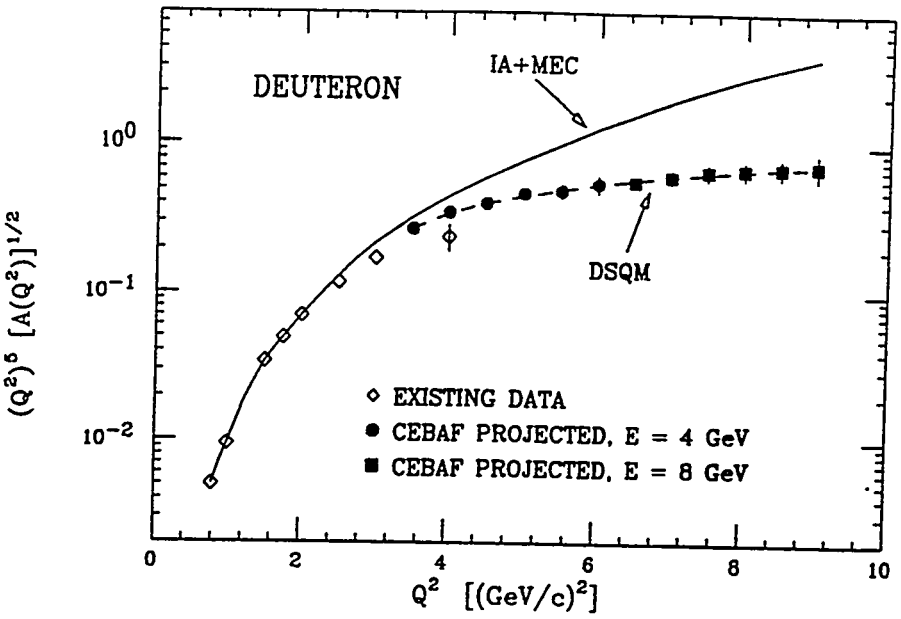


Figure 7: The deuteron elastic form factor $[A(Q^2)]^{1/2}$ vs Q^2. The existing data, shown by open diamonds, is from SLAC. The projected data (Pe-94) is given by full circles and squares.

have been measurements at SLAC out to a maximum photon energy of about 2.75 GeV. The data are shown in Figure 8 for $\theta_{cm} = 90°$.

Again, the apparent approach to the scaling prediction is suggestive, but not conclusive, since there appears to be an angular dependence which needs to be investigated, and once again there is considerable theoretical activity to try to explain as much of the data via baryon and meson exchange models, as well as PQCD based models. This type of data is needed at higher s and also as a function of t. A program of these measurements is planned for CEBAF. With an 8 GeV beam measurements can be extended up to $s \sim 6 - 8$ GeV^2/c^2. Also, polarization data would be important in giving information about the onset of helicity conservation, which is a necessary signature of the onset of PQCD. The possibility of measuring the recoil proton polarization is discussed in Gi-94.

5 Exclusive Meson Production

There are other experiments which will also shed light on the reaction mechanism for exclusive experiments. We note (Gi-94) that single pion production at energies above the resonance region is also predicted to obey dimensional counting rules with s. However there is an absence of data in the crucial region $2.5 < s < 6$ GeV^2/c^2, which CEBAF will be in a uniquely good position to provide. Also, as in the case of deuteron photodisintegration, measurement of the polarization of the recoiling nucleon will give valuable information about the onset of helicity conserving mechanisms.

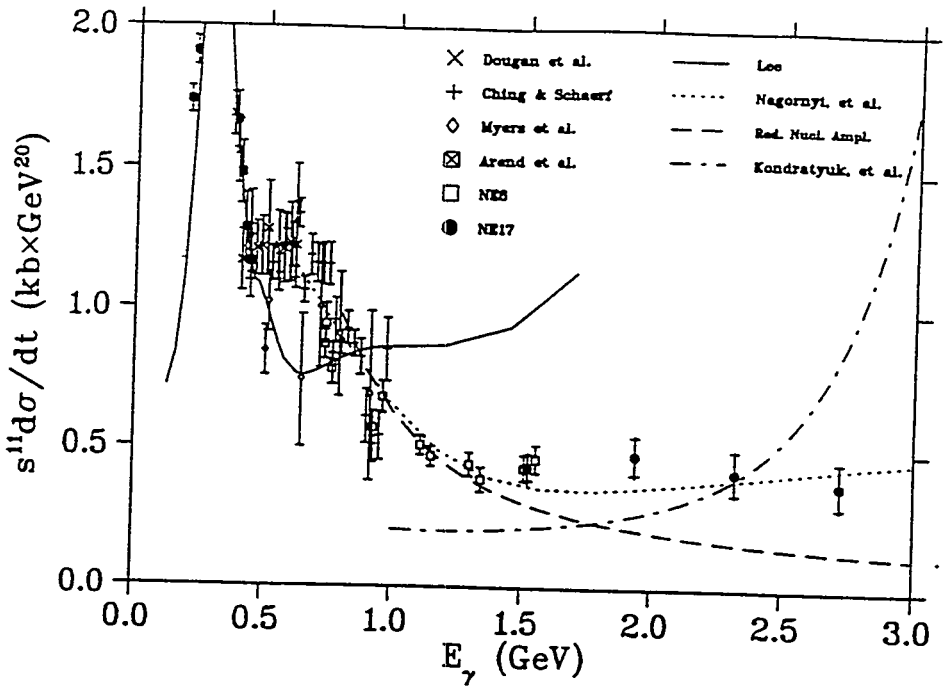


Figure 8: The reaction $d(\gamma,p)n$ as a function of s for $\theta_{cm} = 90°$. Data is from SLAC, and curves correspond to various theoretical calculations (from Po-94).

In fact, it is pointed out in contribution (Ni-94) that it will be necessary to comprehensively measure pion and kaon production at excitations above the resonances to elucidate the leading twist mechanisms involved in the reaction mechanisms. This is really a wide open field which will be ideally matched to CEBAF at higher energies.

6 Conclusion.

Currently there is a big controversy about the mechanisms which are responsible for exclusive reactions at momentum transfers of a few GeV^2/c^2 and beyond. Much of the currently available data appear to follow the PQCD dimensional scaling rules. However, from a theoretical point of view, as discussed in Ra-94, it is difficult to see how PQCD can play a major role at momentum transfers corresponding to existing data. One of the major problems is to reproduce the magnitude of existing form factors using existing PQCD baryon distribution functions. It seems clear that the data point to some fundamentally interesting phenomena, which have not yet been understood. It is also just as certain that we will never resolve these outstanding issues based upon existing data. What we desperately need is to measure additional exclusive amplitudes at higher momentum transfers.

7 References:

(Af-94) A. Afanasev, J. Gomez and N. Nanda, contribution to this workshop.

(Ba-94) K. Baker, contribution to this workshop.
(Br-89) S.J. Brodsky, Lectures at the 27th International School of Subnuclear Physics, Ettore Majorana Center for Scientific Culture, Erice (1989),SLAC-PUB-5116, and references therein.
(Br-94) W. Brooks, contribution to this workshop.
(Ca-92) C.E. Carlson and N.C. Mukhopadhyay, Phys Rev. **D47**, 1737 (1993).
(Ca-88) C.E. Carlson and J.L. Poor, Phys Rev. **D38**, (1988) 2758.
(Ch-84) V.L. Chernyak and A.R. Zhitnitsky, Phys. Rep. **112**, 173 (1984).
(Gi-94) R. Gilman, contribution to this workshop.
(Is-88) N. Isgur and C.H. Llewellyn-Smith, Nucl. Phys. **B317**, 526 (1988).
(Is-89) N. Isgur and C.H. Llewellyn-Smith, Phys. Lett. **B217**, 535 (1989).
(Ji-94) C-R. Ji, A. Pang and A. Sczcepaniak, contribution to this workshop.
(Ke-94) C. Keppel, contribution to this workshop.
(Le-80) G.P. Lepage and S.J. Brodsky, Phys. Rev. **D22**,(1980) 2180.
(Li-92) H-N. Li, SUNY Stony Brook report ITP-SB-92-25.
(Li-92a) H-N. Li and G. Sterman, SUNY-Stony Brook report ITP-SB-92-10
(Ma-94) D. Mack, contribution to this workshop.
(Mi-94) G. Miller, contribution to this workshop.
(Mu-94) N.C. Mukhopadhyay, contribution to this workshop.
(Ni-94) B. Niczyporuk, contribution to this workshop.
(Pe-94) G. Petratos, contribution to this workshop.
(Po-94) D. Potterveld, contribution to this workshop.
(Ra-94) A. Radyushkin, contribution to this workshop.
(Si-93) A. Sill et al., Phys. Rev. D48, 29, (1993).
(St-93) P. Stoler, Physics Reports **226**, (1993) 103.
(St-94) P. Stoler, contribution to this workshop.
(Vo-94) E. Voutier, contribution to this workshop.

EXCLUSIVE PROCESSES: TESTS OF COHERENT QCD PHENOMENA AND NUCLEON SUBSTRUCTURE AT CEBAF

STANLEY J. BRODSKY
Stanford Linear Accelerator Center, Stanford University
Stanford, CA 94309 USA

ABSTRACT

Measurements of exclusive processes such as electroproduction, photoproduction, and Compton scattering are among the most sensitive probes of proton structure and coherent phenomena in quantum chromodynamics. The continuous electron beam at CEBAF, upgraded in laboratory energy to 10–12 GeV, will allow a systematic study of exclusive, semi-inclusive, and inclusive reactions in a kinematic range well-tuned to the study of fundamental nucleon and nuclear substructure. I also discuss the potential at CEBAF for studying novel QCD phenomena at the charm production threshold, including the possible production of nuclear-bound quarkonium.

1. Introduction: Electroproduction at CEBAF

Quantum Chromodynamics has become the central focus of particle and nuclear physics since it potentially can describe all strong interactions in terms of fundamental quark and gluon degrees of freedom. Although there have been many empirical successes of QCD, crucial elements of the theory remain unexplored. For example, the fundamental structure of hadronic wavefunctions, the nature of confinement, and the structure of the QCD vacuum are understood only qualitatively at best. The study of hadronic wavefunctions has now become even more critical in view of the need to understand exclusive and inclusive charm and bottom hadronic from first principles. An important challenge is to devise tests of the theory and hadron structure at the amplitude level which can be made as systematically precise as possible.

A characteristic scale of quantum chromodynamics is the mean transverse momentum of quarks within hadrons: $\langle k_T^2 \rangle^{1/2} \simeq 200 - 300$ MeV. Hadronic processes involving momentum transfer much larger than this scale $Q^2 \gg \langle k_T^2 \rangle^{1/2}$ can be traced to underlying hard scattering process $T_H(Q)$ involving the minimal number of quark and gluons. Because of asymptotic freedom, $T_H(Q)$ can be computed in perturbation theory as an expansion in powers of $\alpha_s(Q^*)$, where $Q^* = \mathcal{O}(Q)$. This observation is the basis of the QCD factorization theorems, in which color confinement and the non-perturbative effects of hadronic binding are isolated in terms of

the hadron structure functions and fragmentation functions in the case of inclusive reactions, and distribution amplitudes $\phi_H(x,Q)$ in the case of exclusive reactions.[1] Processes which involve the hard scattering of more than the minimum numbers of quarks or gluons are "higher-twist"; *i.e.* they are dynamically suppressed by powers of Λ^2/Q^2.

The extended laboratory electron energy range now being contemplated at CEBAF, up to 10-12 GeV, allows one to probe QCD effects in the transition regime between coherent and incoherent quark subprocesses. In the case of inclusive electroproduction at CEBAF, the dominant subprocess at large momentum transfer corresponds to the electron scattering on one of the quark constituents of the target nucleon or nucleus. Thus the deep inelastic cross section $d\sigma(eN \to e'X)$ is to first approximation given by the convolution of the hard scattering $d\sigma(eq \to e'q')$ cross section, multiplied by target structure functions $G_{q/N}(x,Q)$, the probability distributions describing the spin and flavor distributions of quarks in the proton, neutron, or nuclei at light-cone momentum fraction $x = k^+/p^+ = (k^0 + k^3)/(p^0 + p^3)$. On-shell kinematics allows one to identify x with the Bjorken variable $x_{bj} = Q^2/2p \cdot q$. Since the beam is continuous and the number of produced hadrons is not enormous, one can measure the complete final state in electroproduction at CEBAF, and thus follow the evolution of the produced quarks and gluons from the hard subprocess and the remnant quarks and gluons spectators from the target into final state hadronic systems. Since the momentum transfers is moderate, one can also detect the non-factorizing effects of coherence, such as the interference between subprocesses in which the electron scatters on different quarks in the target.

At very high electroproduction energies, for example in electron-proton collisions at HERA, deep inelastic lepton scattering has only minimal sensitivity to the valence parton structure of the proton. From the perspective of the proton rest frame, the high energy virtual photon fluctuates into virtual $q\bar{q}$ system which then scatters on the gluonic field of the target; *i.e.*, physics associated with photon dissociation and central rapidity region processes. Thus physics at HERA focuses more on the structure of the photon rather than resolving nucleon substructure. In contrast, at CEBAF energies, the dominant electroproduction physics is controlled by the quark structure of the target nucleon or nucleus.

Monte-Carlo and string fragmentation programs are often used to simulate the main features of the final state hadronization in electroproduction; However the goal is to acquire a fundamental understanding of hadronization at the amplitude level. Studies at CEBAF have the potential for studying the basic physical processes involved in the processes in which a confined quark or gluon turns into hadronic matter. In the case of nuclear target, one can resolve the effects of the background nuclear field such as quark energy loss transverse momentum smearing and co-mover interactions on the materialization of the final state.

Although the energy range proposed for an upgraded CEBAF is well-tuned to resolving proton structure in QCD, in general one also needs to take into account coherent effects and multiparticle subprocesses. For example, at moderate momentum

transfers, the electron will often interact with more than one target constituent; *e.g.*, $eqq \to e'q'q'$. Since the two quarks can scatter coherently as a bosonic system, they can produce a large longitudinal cross section $R = \sigma_L/\sigma_T$. The two quarks together carry a large fraction of the target momentum, and thus such higher twist contributions can actually dominate the electroproduction cross section at large $x \sim 1$.

Although higher twist terms may complicate the physical interpretation of electroproduction at CEBAF, they are important and interesting topics in their own right. For example, Brandenburg, Khoze, Müller, and I[2] have recently shown that measurements of the $\cos\phi$ and $\cos 2\phi$ azimuthal angular dependence of the lepton in the Drell-Yan process $HN \to \ell\bar{\ell}X$ with $H = \pi, K, \bar{p}$ and p at forward x_F are sensitive to the shape of the projectile's distribution amplitudes. One can analytically cross these predictions to obtain a theory of meson electroproduction including higher twist contributions where the meson interacts directly within the hard subprocess. In the case of meson electroproduction, ϕ is the azimuthal angle between the lepton scattering plane and the meson production plane. Thus measurements at CEBAF of the full azimuthal and polar angular distribution of the lepton system in meson electroproduction and lepton pair hadroproduction should provide an important measure of the structure of hadrons at the amplitude level.

The study of exclusive reactions at CEBAF such as elastic electron-proton scattering, real and virtual Compton scattering, and meson electroproduction, provides a complimentary measure of nucleon structure to the purely inclusive studies.[3] An analogy is an electron microscope, where information from both elastic and inelastic scattering are combined to generate the image of the target. In exclusive reactions in QCD all of the constituents of the scattered hadrons must be rearranged from the initial to final state. Dimensional counting rules[4] show that the leading subprocesses to order Q^{-1} involve the minimum number of incident and final constituents. Furthermore, the valence quarks exchange their hard momenta when their transverse separations are small: $b_\perp^i = \mathcal{O}(Q^{-1})$. Thus large momentum transfer exclusive reactions are controlled by the hadron distribution amplitudes $\phi_H(x_i, Q)$, the valence light-cone Fock wavefunction at small transverse separation. This leads to the remarkable "color transparency"[5] property of QCD, since such small color singlet fluctuations have only minimal initial and final state interactions as they transit through nuclei. In addition, the study of exclusive pion and kaon electroproduction over a large kinelatic range of energy and momentum transfer is necessary in order to reliably determine the spacelike meson form factors. A more detailed discussion will be presented in Section 4.

In the case of electroproduction at CEBAF one can use a nuclear target as a "color filter" to separate large and small structure events. Recently, the E665 group at Fermilab[6] has reported preliminary results on coherent and incoherent ρ leptoproduction in nuclei. At low momentum transfer, the ρ vis strongly absorbed, as in conventional Glauber theory; however, as Q^2 increases beyond a few GeV^2 the reactions tend to occur uniformly throughout the nuclear volume, as predicted by color transparency. Thus diffractive muo-production of ρ mesons occurs in a nuclear

target without final absorption of the ρ in the nucleus. More generally, by using nuclear targets, one can change the hadronic environment and study not only the shadowing and antishadowing of nuclear structure functions, but also the influence of the nuclear field on evolution of the final state hadronic system, including the induced radiation of the outgoing quarks.[7] It will be clearly interesting to trace the color transparency effects seen in vector meson leptoproduction at Fermilab to the lower CEBAF energy range where the formation times are moderate.

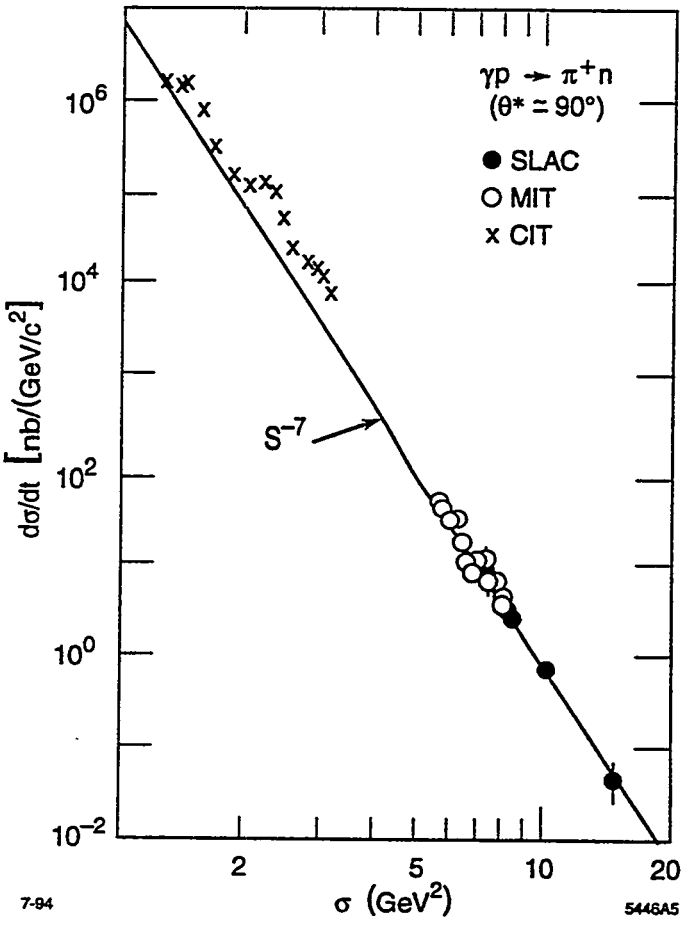


Figure 1. Comparison of photoproduction data with the dimensional counting power-law prediction. The data are summarized in Ref. 8.

A central prediction of perturbative QCD for exclusive electroproduction at large momentum transfer is fixed center-of-mass angle scaling:

$$\frac{d\sigma}{dt}(\gamma^* p \to MB) = \frac{f(t/s, Q^2/s)}{s^N}.$$

The nominal scaling power $N \simeq 7$ follows from dimensional counting: there are 4 incident and 5 outgoing elementary fields. One important test of this scaling is shown in Fig. 1 for pion photoproduction $\gamma p \to \pi^+ n$ at $\theta_{cm} = \pi/2$. The nominal s^{-7} predicted power law behavior is consistent with experiment over the energy range contemplated at CEBAF. This scaling behavior needs to be checked systematically in electroproduction, for example, as a function of virtual photon mass and polarization, and the angular and energy range. The leading power should correspond to helicity amplitudes which conserve the total hadron helicity from the initial and final state, independent of the photon polarization. Hadron helicity conservation is discussed in more detail in Section 4.

In general PQCD dimensional counting has been shown to be good guide to the scaling behavior of general fixed angle two-body scattering reactions.[3] A systematic study of meson-baryon reactions has recently been completed at Brookhaven.[9] The large relative normalization of large angle cross sections such as $K^+p \to K^+p$ compared to $K^-p \to K^-p$ shows that the dominant interaction controlling exclusive processes at large momentum transfer involves the interchange of the valence quarks[10] rather than multiple gluon exchange. Other important tests involve exclusive two-photon reactions such as $\gamma^*\gamma \to M^0$, $\gamma\gamma \to M\overline{M}$, and proton-proton annihilation. The general success of dimensional counting in the fixed angle domain is evidence that leading twist PQCD mechanisms dominate exclusive amplitudes and form factors at momentum transfers $Q^2 \sim 5$ GeV^2.

The structure of hadron wavefunctions in terms of their quark and gluon degrees of freedom at the amplitude level remains one of the most important frontiers in QCD studies. The natural formulation of hadron wavefunctions is the light-cone Fock expansion.[3] As noted above, the basic quantity which characterizes the part of the hadron bound state which enters exclusive hard-scattering subprocesses is the gauge and frame-independent distribution amplitude $\phi(x_i, Q)$ which in turn describes the valence quark structure of the hadrons at impact separation $b^i_\perp = \mathcal{O}(Q^{-1})$ is a function of the light-cone momentum fractions. The work of Sterman *et al.*,[11] has shown in detail how Sudakov suppression of large size configurations of the hadron wavefunctions are suppressed in large momentum transfer exclusive processes, confirming the validity of the PQCD description of these processes and the corresponding predictions of QCD color transparency. The interrelation of the Landshoff triple-gluon contributions to elastic proton-proton scattering to hard scattering PQCD mechanisms such as quark interchange has now been clarified by Sterman and Sotiropoulos.[12]

QCD sum rule methods and lattice gauge theory now supply important theoretical constraints on the form of the distribution amplitudes, although the reliability of these predictions is unknown. There is now much theoretical work exploring other non-perturbative QCD methods such as light-cone Hamiltonian diagonalization. One can also derive constraints on hadron light-cone wavefunctions from their static properties such as the baryon magnetic moments and their axial couplings.

2. The Charm Threshold in Electroproduction

One of the most interesting physics areas which can be studied at CEBAF at electron beam energies above 8 GeV will be the onset of charm electroproduction. The threshold virtual photon energy for the lowest hidden charm system $\gamma^* p \rightarrow \eta_c(2.9788\text{GeV})p(0.9383\text{GeV})$ is $\nu_{th} = q \cdot p/M = 7.707$ GeV $+(Q^2/2M_p)$. The production of open charm $\gamma^* p \rightarrow D^0(1.8645\text{GeV})\Lambda_c(2.2849\text{GeV})$ begins at $\nu_{th} = 8.7057$ GeV $+(Q^2/2M_p)$. In the threshold regime one probes extreme configurations of the proton target quark structure as it strains to produce the new heavy systems. The study of this physics also has implications for the charm structure function at large x_{bj} and the threshold production of heavy systems such as beauty, top, and supersymmetric particles.

Although the charm electroproduction cross section is inevitably suppressed at threshold by phase space, there is reason to believe that the production rate will be substantially enhanced by dynamical effects in non-perturbative QCD. Because of the disparate charmonium and proton size scales, one can classify and compute their two-gluon exchange couplings using the operator product expansion. Luke, Manohar, and Savage[13] have shown that the scalar part of the two-gluon exchange interaction is related to the trace of the energy momentum tensor and thus its coupling to nucleons or nuclei is proportional to the target mass. The two-gluon coupling to the small size charmonium state can be computed using conventional potential models. This analysis leads to the remarkable prediction that there is a strong QCD van der Waal attraction of the quarkonium state to ordinary hadrons at small relative velocity. DeTeramond, Schmidt, and I[14] have argued that the QCD van der Waal effects at low relative velocity could be sufficiently strong as to bind charmonium states to ordinary hadrons or light nuclei. Such nuclear-bound quarkonium states could show up as narrow s—channel resonance in electroproduction: $\gamma^* p \rightarrow (\eta_c p)$, $\gamma^* d \rightarrow (\eta_c d)$, $\gamma^* p \rightarrow (J/\psi p)$, etc. just below the charmonium production threshold. This could be a very interesting experiment CEBAF. However, it should be emphasized that even if the QCD van der Waals force is not sufficient to actually form bound states, one still expects to see strong threshold effects in the production cross section perhaps similar to the enhancements that have been observed for η production at threshold.[15]

Note that even though the rate at threshold may be small, the cross section can be enhanced by using nuclear Fermi-motion to effectively increase the available energy. For example, the anti-deuteron was first observed below the nominal threshold energy in the 1960s at Brookhaven by Ting and Lederman using heavy nuclei as targets. It is also interesting to use the charm threshold to measure the extreme limits of the Fermi momentum spectrum, since its origin involves nuclear short-range interactions.

In the case of open charm, the simplest electroproduction mechanism is quark interchange, as illustrated in Fig. 2. The interchange amplitude can be written in an

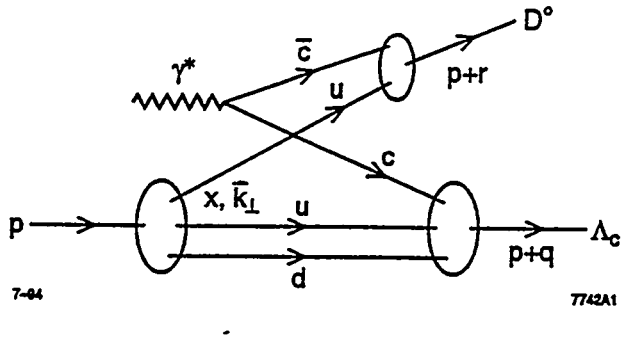


Figure 2. Quark interchange contribution to charm electroproduction.

elegant form as a convolution over valence light-cone wavefunctions:

$$\int \frac{d^2k_\perp dx}{16\pi^3}\psi_D^\dagger(x,k_T{+}xr_\perp)\psi_{\Lambda_c}^\dagger(x,k_T{+}(1{-}x)q_\perp)\Delta\psi_{\gamma^*}(x,k_T{+}xr_\perp{+}(1{-}x)q_\perp)\psi_p(x,k_T),$$

where $q_\perp^2 = -t, r_\perp^2 = -u$ and Δ is the inverse of the light-cone energy denominator. The complete analysis is given in Ref. 10.

There are a number of experiments which indicate that non-perturbative QCD mechanisms are necessary for understanding heavy quark production in the regimes where either the charm system is produced at extreme kinematic configurations such as large x_F or large x_{bj} or at small relative velocity to other quarks:

1. The anomalously high $c(x)$ distribution measured at large x_{bj} by EMC.[16] The CERN measurements disagree with photon-gluon fusion by a factor of 20 to 30 at $Q^2 = 75$ GeV^2 and $x_{bj} = 75$ GeV^2.
2. In the case of J/ψ hadroproduction from pion beams, the CERN experiment NA-3 has reported a strong excess of quarkonium at large x_F with a non-factorizing nuclear dependence. In addition, the Fermilab Chicago-Iowa Princeton group has reported an anomalously sudden change in polarization of the J/ψ at large x_F in $\pi N \to \mu^+\mu^- X$. The dramatic shift to longitudinal polarization is inconsistent with leading order QCD predictions.
3. An interesting unresolved issue is the leading particle effect in charmed hadron production. The quark structure of leading D mesons has been shown to depend strongly on the valence quantum numbers of the beam hadron in direct conflict with the factorization principle at the heart of most perturbative QCD predictions. The mechanisms in which the beam quarks and heavy quarks coalesce is at the heart of hadronization dynamics, and much more critical work will be needed especially in the production of b-quark systems.

4. There are other signals for anomalous charm baryon hadroproduction at large x_F, including the reports of Λ_c production from E-400 at Fermilab using neutron beams and the measurements of WA-62 from CERN which observed charm-strange baryons using hyperon beams. There are also measurements from NA-3 at CERN which show that double J/ψ pairs are hadro-produced only at large x_F.

5. The anomalously strong nuclear dependence of large x_F J/ψ hadroproduction, as reported by NA10 and E789 are in direct contradiction to leading-twist PQCD factorization.

Much of the above physics can be accounted for by the picture of Hoyer, Mueller, Tang and myself,[17] where the hadronization in a high energy collision occurs in the following novel way: the heavy quark system is first formed as a virtual fluctuation as a light-cone Fock state component in the incoming hadron wavefunction; a light spectator quark is then stripped away in the target leaving the $Q\overline{Q}$ system to hadronize into the final heavy hadrons. This type of intrinsic heavy quark picture also explains the excess of charm quarks seen in the EMC measurements of the charm structure function of the nucleon. This new picture of hadron formation opens up a whole new avenue for studying the far-off-shell structure of hadrons. It is thus critical that a new measurement of the charm and beauty structure functions be performed.

Measurements of charm electroproduction near threshold at CEBAF should provide new insights into the collective multi-quark mechanisms needed to understand the charm production anomalies.

3. Virtual Compton Scattering

The Compton scattering process $\gamma p \to \gamma p$ is the fundamental way to "look" at proton structure. Virtual Compton scattering $\gamma^* p \to \gamma p$ is particularly interesting to measure at CEBAF since it can be probed as a function of the photon's transverse or longitudinal polarization, the target polarization, over a large domain of kinematics s, t, u, and photon virtuality $Q^2 = -q^2$.

It should be noted that the cross section for the process $ep \to e'p\gamma$ receives contributions not only from virtual Compton scattering, but also from Bethe-Heitler bremmstrahlung from the scattered electron. The two processes lead to the same final state, and thus they interfere. The Bethe-Heitler process is completely determined from elastic ep scattering and is purely real. Thus one can use the interference between the Compton and bremmstrahlung processes to determine the real part of the Compton amplitude.[18] In the case of deep inelastic Compton scattering $ep \to e\gamma X$, one can use the same interference effect to deduce new structure functions and sum rules proportional to the sum of quark charges cubed.[19]

There are many different physics aspects of virtual Compton scattering depending on the accessed kinematical domain.

1. In the case of low energy virtual Compton scattering with $s = (q+p)^2 \simeq M_N^2$. one can study the s-channel effects of baryon resonances in the Compton amplitude and their relative coupling as a function of photon virtuality.[20]
2. In the Regge limit $s \gg -t$ and fixed Q^2 one can use the Regge pole analysis, as in the paper of Damashek and Gilman.[21] Each Compton helicity amplitude has the form of a sum over $t-$channel Regge exchange contributions: $\mathcal{M} = \Sigma_R s^{\alpha_R(t)} \beta(t, Q^2)$. In Compton scattering one can have contribution from all C-even exchanges: the diffractive Pomeron contributions,the pion and A_2 and f^0 $C = +$ Reggeon trajectories. In addition, QCD predicts a special contribution which cannot occur in hadron-hadron scattering: a $j = 0$ fixed pole, the Kronecker $\delta_{j,0}$ contribution, which can be traced to the presence of quark Z-graphs.
3. An important feature of the Regge theory which is testable in virtual Compton scattering is that the Regge trajectory $\alpha_R(t)$ must be independent of Q^2 at fixed $-t$. Only the residue $\beta(t, Q^2)$ can depend on the photon virtuality. In fact, one expects that all of the normal trajectories have decreased couplings to the virtual; Compton amplitude as Q^2 increases, leaving the $j = 0$ fixed pole as the dominant and surviving contribution to the amplitude. This special contribution to Compton scattering gives an energy independent contribution to the real part of the $\gamma^* p \to \gamma p$ amplitude.[18] The $t-$dependence of the $j = 0$ fixed pole amplitude is expected to be similar to that of the helicity-conserving Dirac form factor of the proton.
4. As the momentum transfer squared to the proton increases $-t$, the Pomeron trajectory is expected to stay at $\alpha_p(-t) \simeq 1$. The non-singlet Regge trajectories are predicted to decrease monotonically to $\alpha_R(-t) \simeq 0$. For a recent discussion and further references see Ref. 22.
5. In the large momentum transfer domain with fixed $\cos\theta_{cm}$ the virtual exclusive Compton amplitude $\gamma^* p \to \gamma p$ can be analysed using perturbative QCD factorization. Detailed QCD predictions have been made by Kronfeld and Nizic, Hyer, and Gunion *et al.*. This will be discussed in detail in Section 5. In addition at CEBAF, one may be able to test these predictions as a function of photon polarization and virtuality.

4. Exclusive Processes and the Structure of Hadrons[23]

The analysis of exclusive hadronic amplitudes such as form factors, electroweak transition matrix elements, and two-body scattering amplitudes has remained among the most challenging computational problems in quantum chromodynamics. The physics of exclusive amplitudes clearly depends on the fundamental relativistic structure of the hadrons as well as the dynamics governing quark and gluon propagation, QCD vacuum structure, Regge behavior, and color confinement. Numerical predictions for exclusive processes involving low momentum transfer are beginning to be obtained from lattice gauge theory and QCD sum rules. However, the most interesting

insights into hadron structure at the amplitude level and the most transparent connections to the underlying QCD physics emerges at high momentum transfer where perturbative analyses for the leading twist contributions to exclusive processes can be combined with non-perturbative hadron wavefunction information.

The least-complicated exclusive amplitudes to analyze from first principles in QCD are the space-like electromagnetic form factors of hadrons. An elastic form factor is the probability amplitude for a hadron to remain intact after absorbing momentum q by its local quark current. If one uses light-cone quantization in the $q^+ = q^0 + q^z = 0$ frame with $\vec{q}_\perp{}^2 = -q^2 = Q^2$, then vacuum fluctuation contributions to the j^+ current can be avoided. Nevertheless, the computation of an elastic form factor requires knowledge of all of the hadron's light-cone Fock state wavefunctions. For example, the helicity-conserving form factor has the form[24]

$$F(Q^2) = \frac{\langle p+q|j^+|p\rangle}{/2p^+}$$

$$= \sum_{n,\lambda_i} \sum_a e_a \int \prod_i \frac{dx_i\, d^2\vec{k}_{\perp i}}{16\pi^3}\, \psi_n^{(\Lambda)*}(x_i, \vec{\ell}_{\perp i}, \lambda_i)\, \psi_n^{(\Lambda)}(x_i, \vec{k}_{\perp i}, \lambda_i).$$

The constituents in the initial state have longitudinal light-cone momentum fractions $x_i = (k^0 + k^z)_i/(p^0 + p^z)$, relative transverse momentum, $\vec{k}_{\perp i}$, and helicities λ_i. Here e_a is the charge of the struck quark, $\Lambda^2 \gg \vec{q}_\perp^{\,2}$, and the transverse momenta in the final state are

$$\vec{\ell}_{\perp i} \equiv \begin{cases} \vec{k}_{\perp i} - x_i\vec{q}_\perp + \vec{q}_\perp & \text{for the struck quark} \\ \vec{k}_{\perp i} - x_i\vec{q}_\perp & \text{for all other partons.} \end{cases}$$

In principle, one can obtain all of the required Fock State wavefunctions by diagonalizing the light-cone QCD Hamiltonian.[25] This has in fact been done for meson and baryon wavefunctions in the case of QCD in one-space and one-time dimensions, but the corresponding task appears to be formidable for QCD(3+1).

Fortunately, because of asymptotic freedom and the point-like behavior of quark and gluon interactions at short distances, the computation of exclusive amplitudes in QCD becomes much simpler at large momentum transfer. The primary ingredient in the analysis is factorization: the non-perturbative dynamics of the bound states can be isolated in terms of process-independent distribution amplitudes, and the dynamics of the momentum transfer to the hadrons can be isolated in terms of perturbatively-calculable hard-scattering quark and gluon subprocesses. Thus general properties of exclusive reactions at large momentum transfer can be derived without explicit knowledge of the non-perturbative structure of the theory.[3]

The most characteristic feature of an exclusive amplitude in QCD is that it falls off slowly with momentum transfer, not as an exponential or a Gaussian, but as an inverse power of $Q = p_T$ which is directly related to the degree of complexity of the scattering hadrons. The nominal power-law fall-off[4] $\mathcal{M} \sim Q^{4-n}$ of an exclusive amplitude at large momentum transfer reflects the elementary scaling of the lowest-order connected quark and gluon tree graphs obtained by replacing each of the external hadrons by its respective collinear quarks. Here n is the total number of initial state and final state lepton, photon, or quark fields entering or leaving the hard scattering subprocess. The empirical success of the dimensional counting rules for the power-law fall-off of form factors and general fixed center-of-mass angle scattering amplitudes gave early and important evidence for the scale-invariance of quark and gluon interactions at short distances.

Thus only the valence-quark Fock components of the hadron wavefunctions contribute to the leading power-law fall-off of an exclusive amplitude. In particular, since the internal momentum transfer at the quark level is required to be large, one can obtain the basic scaling and helicity structure of the hadron amplitude by simply iterating the gluon-exchange term in the effective potential for the light-cone wavefunctions. The result is that exclusive amplitudes at high momentum transfer Q^2 can be written in a factorized form as a convolution of process-independent "distribution amplitudes" $\phi(x_i, Q)$, one for each hadron involved in the amplitude, with a hard-scattering amplitude T_H describing the scattering of the valence quarks from the initial to final state.[26,27]

The distribution amplitude is the fundamental gauge invariant wavefunction which describes the fractional longitudinal momentum distributions of the valence quarks in a hadron integrated over transverse momentum up to the scale Q.[26] For example, the pion's electromagnetic form factor can be written as[26,27,28]

$$F_\pi(Q^2) = \int_0^1 dx \int_0^1 dy\, \phi_\pi^*(y,Q)\, T_H(x,y,Q)\, \phi_\pi(x,Q) \left(1 + \mathcal{O}\left(\frac{1}{Q}\right)\right).$$

Here T_H is the scattering amplitude obtained when pions replaced by collinear $q\bar{q}$ pairs. This factorized form is the prototype for the factorization of general exclusive amplitudes in QCD at high momentum transfer. All of the non-perturbative dynamics is factorized into the distribution amplitudes,[26] $\phi_B(x_i, \lambda_i, Q)$, for the baryons with $x_1 + x_2 + x_3 = 1$, and $\phi_M(x_i, \lambda_i, Q)$, for the mesons with $x_1 + x_2 = 1$ which sum all internal momentum transfers up to the scale Q^2. On the other hand, all momentum transfers higher than Q^2 appear in T_H, which can be computed perturbatively in powers of the QCD running coupling constant $\alpha_s(Q^2)$. The distribution amplitudes are thus the process-independent hadron wavefunctions which interpolate between the QCD bound state and their valence quarks at transverse separation $b_\perp \simeq 1/Q$. The pion's distribution amplitude, for example, is directly related to its valence light-cone

wavefunction:

$$\phi_\pi(x,Q) = \int \frac{d^2\vec{k}_\perp}{16\pi^3}\,\psi^{(Q)}_{q\bar{q}/\pi}(x,\vec{k}_\perp)$$

$$= P^+_\pi \int \frac{dz^-}{4\pi}\, e^{ixP^+_\pi z^-/2} \left\langle 0 \left| \overline{\psi}(0)\,\frac{\gamma^+\gamma_5}{2\sqrt{2n_c}}\,\psi(z) \right| \pi \right\rangle^{(Q)} \Big|_{z^+ = \vec{z}_\perp = 0}$$

The $\vec{k}_\perp$ integration is cut off by the ultraviolet cutoff $\Lambda = Q$ implicit in the wavefunction; thus only valence Fock states with invariant mass squared $\mathcal{M}^2 \leq Q^2$ contribute.

Given the factorized structure of exclusive amplitudes at large momentum transfer, one can read off a number of general features of the PQCD predictions: the dimensional counting rules, hadron helicity conservation, and color transparency.[3] QCD also predicts calculable corrections to the nominal dimensional counting power-law behavior due to the running of the strong coupling constant, higher order corrections to the hard scattering amplitude, Sudakov effects, pinch singularities, as well as the evolution of the hadron distribution amplitudes, $\phi_H(x_i,Q)$.

Evolution equations for the meson and baryon distribution amplitudes can be derived and employed in analogy to the evolution of structure functions.[3,29] If one can calculate the distribution amplitude at an initial scale Q_0 using QCD sum rules or lattice gauge theory,[29] then one can determine $\phi(x_i,Q)$ at higher momentum scales via evolution equations in $\log Q^2$ or equivalently, the operator product expansion.[30] Empirical constraints on the hadron distribution amplitudes can be obtained from the normalization and scaling of form factors at large momentum transfer and the angular dependence of two body scattering amplitudes.

Perhaps the most surprising feature of the QCD predictions for exclusive processes in QCD is "color transparency",[5] which reflects the fact that only the small transverse separation $b_\perp \sim 1/Q$ valence wavefunction can contribute to exclusive amplitude at large momentum transfer. Since these color-singlet states have small color-dipole moments, they will have small initial and final state interactions. In particular if the large momentum transfer occurs as a quasi-elastic process within a nucleus, there will be minimal initial state or final state absorption—in striking contrast to the standard picture of strong absorption predicted in Glauber theory. A careful treatment of color transparency requires consideration of the expansion time and coherence length of the small size configurations.[31]

5. A Detailed Example: Compton Scattering in Perturbative QCD

Exclusive reactions involving two real or virtual photons provide a particularly interesting testing ground for QCD because of the relative simplicity of the couplings of the photons to the underlying quark currents, and the absence of significant initial state interactions—any remnant of vector-meson dominance contributions

is suppressed at large momentum transfer, and the photon enters the amplitude as a direct point-like coupling.

The simplest example of a two-photon exclusive process is the $\gamma^*(q)\gamma \to M^0$ process which is measurable in tagged $e^+e^- \to e^+e^-M^0$ reactions. The photon to neutral meson transition form factor $F_{\gamma\to M^0}(Q^2)$ is predicted to fall as $1/Q^2$—modulo calculable logarithmic corrections from the evolution of the meson distribution amplitude. This QCD prediction reflects the elementary scaling of the quark propagator at high momentum transfer, the same scale-free behavior which leads to Bjorken scaling of the deep inelastic lepton-nucleon cross sections. The existing data from TPC/$\gamma\gamma$ are consistent with the predicted scaling and normalization of the transition form factors for the π^0, η_0, and η'.

The angular distributions for the hadron pair production processes $\gamma\gamma \to H\overline{H}$ are sensitive to the x_i dependence of the hadron distribution amplitudes.[32] Lowest order predictions for meson pair production in two photon collisions using this formalism are given in Refs. 32 and 29; the analysis of the $\gamma\gamma$ to meson pair process has been carried out to next-to-leading order in $\alpha_s(Q^2)$ by Nizic.[33] The Mark II and TPC/$\gamma\gamma$ measurements of $\gamma\gamma \to \pi^+\pi^-$ and $\gamma\gamma \to K^+K^-$ reactions are also consistent with PQCD expectations. A review of this work is given in Ref. 34.

Compton scattering $\gamma p \to \gamma p$ at large momentum transfer and its s-channel crossed reactions $\gamma\gamma \to \bar{p}p$ and $\bar{p}p \to \gamma\gamma$ are classic tests of the perturbative QCD formalism for exclusive reactions. At leading twist, each helicity amplitude has the factorized form,[3]

$$\mathcal{M}^{\lambda\lambda'}_{hh'}(s,t) = \sum_{d,i} \int [dx][dy]\phi_i(x_1,x_2,x_3,\widetilde{Q}) T_i^{(d)}(x,h,\lambda;y,h',\lambda';s,t)\phi_i(y_1,y_2,y_3;\widetilde{Q}) \ .$$

The index i labels the three contributing valence Fock amplitudes at the renormalization scale $\widetilde{Q}$. The index d labels the 378 connected Feynman diagrams which contribute to the eight-point hard scattering amplitude $qqq\gamma \to qqq\gamma$ at the tree level; *i.e.* at order $\alpha\alpha_s^2(\widehat{Q})$. The arguments $\widehat{Q}$ of the QCD running coupling constant can be evaluated amplitude by amplitude using the methods of Ref. 76and 77 as discussed in the Introduction. The evaluation of the hard scattering amplitudes $T_i^{(d)}(x,h,\lambda;y,h',\lambda';s,t)$ has now been done by several groups.[35,36,37,38]

An important simplification of Compton scattering in PQCD is the fact that pinch singularities are readily integrable and do not change the nominal power-law behavior of the basic amplitudes.[37] Physically, the pinch singularities correspond to the existence of potentially on-shell intermediate states in the hard scattering amplitudes. This leads to a non-trivial phase structure of the Compton amplitude. Such phases can in principle be measured by interfering the virtual Compton process in $e^\pm p \to e^\pm p\gamma$ with the purely real Bethe-Heitler bremsstrahlung amplitude.[39] A careful analytic treatment of the integration over the on-shell intermediate states has been given by Kronfeld and Nizic.[37]

The most characteristic feature of the PQCD predictions is the scaling of the differential Compton cross section at fixed t/s or θ_{CM}

$$s^6 \frac{d\sigma}{dt}(\gamma p \to \gamma p) = F\left(\frac{t}{s}\right) .$$

The power s^6 reflects the fact that 8 elementary fields enter or leave the hard scattering subprocess.[4] The scaling of the existing data[40] is remarkably consistent with the PQCD power-law prediction, but measurements at higher energies and momentum transfer are needed to test the predicted logarithmic corrections to this scaling behavior and determine the angular distribution of the scaled cross section over as large a range as possible.

The predictions for the normalization of the Compton cross section and the shape of its angular distribution are sensitive to the shape of the proton distribution amplitude $\phi_p(x_i, Q)$. The forms predicted for the proton distribution amplitude from QCD sum-rule constraints[29] by Chernyak, Oglobin, and Zhitnitskii, and King and Sachrajda, appear to give a reasonable representation of the existing data. A definitive prediction for the normalization of form factors and other exclusive amplitudes in perturbative QCD will require not only a careful analysis of the non-perturbative input for the distribution amplitudes, but also a detailed calculation of the crossed-graph and other irreducible contributions to the hard-scattering QCD kernels.

More recent QCD sum rule analyses of the proton distribution amplitude are given in Ref. 41. These distributions, which predict that approximately 65% of the proton's momentum is carried by the u quark with helicity parallel to the proton's helicity also provide empirically consistent predictions for the normalization of the proton's form factor and the $J/\psi \to p\bar{p}$ decay rate. The crossing behavior from spacelike Compton scattering to the timelike annihilation channels will also provide important tests and constraints on the PQCD formalism and the shape of the proton distribution amplitudes. Predictions for the time-like processes have been made by Farrar *et al.*,[35] Millers and Gunion[36], and Hyer.[38]

The theoretical uncertainties from finite nucleon mass corrections, the magnitude of the QCD running coupling constant, and the normalization of the proton distribution amplitude largely cancel out in the ratio of Compton to elastic differential cross sections

$$R_{\gamma p/e^- p}(s, \theta_{cm}) = \frac{d\sigma(\gamma p \to \gamma p)}{dt} \Big/ \frac{d\sigma(e^- p \to e^- p)}{dt},$$

which is predicted by QCD to be essentially independent of s at large momentum transfer. If this scaling continues to be confirmed, then the center-of-mass angular dependence of $R_{\gamma p/e^- p}(s, \theta_{cm})$ will be one of the best ways to determine the shape of $\phi_p(x_i, Q)$.

6. Lepto-Production of Vector Mesons as a Test of PQCD and Color Transparency

The study of real and virtual photoproduction of vector mesons on protons and nuclei provides an elegant illustration of the emergence of perturbative QCD features in the large momentum transfer domain.[7,42,43]

1. At small momentum transfer and high energy where the coherence length $2\nu/(\mathcal{M}^2+Q^2)$ is large compared to the target size, the incident photon is expected to act as a coherent sum of vector mesons with mass squared $\mathcal{M}^2 \leq \mathcal{O}(Q^2)$. This is the generalized vector meson dominance picture of photon interactions. In addition, s—channel helicity conservation predicts that the vector meson will be dominantly produced with transverse polarization equal to that of the incident photon.
2. At small momentum transfer where photon interactions are dominantly hadron-like, the cross section for vector meson photoproduction on a nucleus should have the same nuclear properties as meson-nucleon scattering. Due to the optical theorem, the forward high energy coherent nuclear amplitude $\gamma^* A \to V^0 A$ must then scale with the nuclear size the same as the total hadron-nucleus cross section; *i.e.* $A^{2/3}$. The t—dependence of the coherent nuclear cross section is of the form $d\sigma/dt \sim \exp^{b_A t}$ where $b_A \propto R_A^2$ and R_A is the nuclear size. Thus the total coherent cross section $\sigma(\gamma^* A \to V^0 A)$ is predicted to scale with nuclear number as $A^{4/3}/R_A^2 \sim A^{2/3}$.
3. The predictions for $\gamma^* A \to V^0 A'$ are in striking contrast to the above results when Q^2 becomes large compared to Λ^2_{QCD}. The virtual quark loop connecting the photon to the vector meson is now highly virtual, and only the point-like piece of the photon and the small transverse size of the valence $q\bar{q}$ light-cone wavefunction of the vector meson enter the exclusive amplitude. Thus at high Q^2 the nuclear absorption in the initial and final state should vanish, and the nuclear amplitude becomes additive: $M(\gamma^* A \to V^0 A') = A^1 M(\gamma^* N \to V^0 N')$. The integrated coherent cross section $\sigma(\gamma^* A \to V^0 A)$ is thus predicted to scale with nuclear number as $A^2/R_A^2 \sim A^{4/3}$. This contrasting nuclear dependence of the virtual photoproduction cross section provides a dramatic test of color transparency. Preliminary results from E665[6] for ρ lepto-production at Fermilab appear to confirm these QCD predictions.
4. Another important prediction of PQCD in the large Q^2 domain is that the vector meson should be produced with zero helicity since it is formed from a quark and antiquark with equal and opposite helicities.[44] The change-over from transverse to longitudinal vector meson polarization with increasing Q^2 also appears to be confirmed by the E665 data.
5. At large photon virtuality Q^2 the photon and vector meson will act as point-like

systems, and thus the $t-$ dependence of the differential cross section $d\sigma/dt(\gamma^* p \to V^0 p')$ should only reflect the finite size of the scattered nucleon. At large t the form factors should reflect the underlying two-gluon exchange structure of the PQCD Pomeron.

6. At large momentum transfer $-t \gg \Lambda^2_{QCD}$, $-u \gg \Lambda^2_{QCD}$, PQCD predicts that the photoproduction cross section has the nominal fixed CM angle scaling: $d\sigma/dt(\gamma p \to V^0 p') \sim f(\theta_{CM})/s^7$. The dominant amplitudes will conserve hadron helicity: $\lambda_{p'} + \lambda_V = \lambda_p$.

7. At larger momentum transfers $-t > R_A^2$, one can study quasi-elastic leptoproduction in the nucleus; $d\sigma/dt(\gamma^* A \to V^0 N' X)$ where X represents a sum over excited nuclear states, but without extra particle production. When $p_T^2 \gg \Lambda^2_{QCD}$, color transparency predicts the absence of initial or final state absorption of the incident photon and the outgoing meson and nucleon. Thus the quasi-elastic cross section should approach additivity in nuclear number at large momentum transfer. As I have emphasized in the Introduction, these illuminating studies and tests of PQCD can be carried out in detail at CEBAF.

7. When Do Leading-Twist Predictions for Exclusive Processes Become Applicable?

The factorized predictions for exclusive amplitudes are evidently rigorous predictions of QCD at large momentum transfer. However, it is important to understand the kinematic domain where the leading twist predictions become valid. The basic scales of QCD are set by the quark masses and the scale Λ_{QCD} which parameterizes the QCD running coupling constant. Thus one normally would expect that the leading power-law predictions should become dominant at momentum transfers exceeding these parameters. In the case of inclusive reactions, Bjorken scaling is already apparent at momentum transfers $Q \sim 1$ GeV or less.

In fact, the data for hadron form factors is consistent with the onset of PQCD scaling at momentum transfers of a few GeV. [45] has shown that the measurements of the transition form factors of the proton to the $N(1535)$ and $N(1680)$ resonances are consistent with the predicted PQCD Q^{-4} scaling to beyond $Q^2 = 20\ GeV^2$. The normalization is also in reasonable agreement with that predicted from QCD sum rule constraints on the nucleon distribution amplitudes, allowing for uncertainties from higher order QCD corrections. In the case of the proton to $\Delta(1232)$ transition, the form factor falls faster that Q^{-4}. This anomalous behavior is, in fact, predicted by QCD sum rule constraints, since unlike the proton, the Δ has a highly symmetric distribution amplitude which results in a small net coupling to the QCD hard scattering amplitude. The observed scaling pattern of the transition form factors gives strong support to the QCD sum rule predictions and PQCD factorization.

Isgur and Llewellyn Smith[46] and Radyushkin[47] have raised the concern that important contributions to exclusive processes could arise from the endpoint regions

$x_i \to 1$; such behavior would imply the breakdown of PQCD factorization. For example, the denominator of the hard scattering amplitudes, *e.g.*, $T_H \propto \alpha_s/[(1-x)(1-y)Q^2]$ for the meson form factor becomes singular in the endpoint integration region at $x \sim 1$ and $y \sim 1$. Such endpoint regions are even further emphasized when one assumes the strongly asymmetric forms for the hadron distribution amplitudes derived from QCD sum rules. However, it is important to note that these endpoint regimes correspond to scattering processes where one quark carries nearly all of the proton's momentum and is at a fixed transverse separation $b_\perp$ from the spectator quarks.

When a quark which is isolated in space receives a large momentum transfer x_iQ, it will normally strongly radiate gluons into the final state due to the displacement of both its initial and final self-field, which is contrary to the requirements of exclusive scattering. For example, in QED the radiation from the initial and final state charged lines is controlled by the coherent sum $\sum_i(\epsilon \cdot p_i/k \cdot p_i)\eta_i q_i$ where q_i and p_i are the charges four-momenta of the charged lines, ϵ and k are polarization and four-momentum of the radiation, and $\eta_i = \pm 1$ for initial and final state particles, respectively. Radiation will occur for any finite momentum transfer scattering as long as the photon's wavelength is less than the size of the initial and final neutral bound states. The probability amplitude that radiation does not occur is given by rapidly falling Sudakov form factor, as first discussed by in Refs. 26 and 48. An elegant and much more complete discussion has now been given by Botts and Li and Sterman.[11] The radiation from the colored lines in QCD have similar coherence properties as in QED:[49] because of the destructive color interference of the radiators, the momentum of the radiated gluon in a QCD hard scattering process only ranges from k of order $1/b_\perp$, where color screening occurs, up to the momentum transfer x_iQ of the scattered quarks. This analysis and unitarity allows one to compute the probability that no radiation occurs during the hard scattering.[11,38] It is given by a rapidly falling exponentiated Sudakov form factor $S = S(x_iQ, b_\perp, \Lambda_{QCD})$; thus at large Q and fixed impact separation, the Sudakov factor strongly suppresses the endpoint contribution. On the other hand, when $b_\perp = \mathcal{O}(x_iQ)^{-1}$, the Sudakov form factor is of order 1, and the radiation leads to logarithmic evolution and contributions of higher order in $\alpha_s(Q^2)$, the corrections already contained in the PQCD predictions.[26,48,50] This is the starting point of the detailed analysis of the suppression of endpoint contributions to meson and baryon form factors and its quantitative effect on the PQCD predictions recently presented by Li and Sterman.[11] This analysis has now also been applied to two-photon reactions and the timelike proton form factor by Hyer.[38]

Thus the leading PQCD contributions to large momentum transfer exclusive reactions derive from wavefunction configurations where the valence quarks are at small transverse separation $b_\perp = \mathcal{O}(1/k_\perp) = \mathcal{O}(1/Q)$, the regime where there is no Sudakov suppression. Furthermore, as noted by Li and Sterman, the hard scattering amplitude loses its singular endpoint structure if one explicitly retains the valence quark transverse momenta in the denominators. For example, in the case of the pion form factor, the hard scattering amplitude is effectively modified to the form

$$T_H \propto \frac{\alpha_s}{(1-x)(1-y)Q^2 + (k_1^\perp + k_2^\perp)^2}.$$

The Sudakov effect thus ensures that the denominators are always protected at large momentum transfers. In their numerical studies, Li and Sterman find that the pion form factor becomes relatively insensitive to soft gluon exchange at momentum transfers beyond 20 Λ_{QCD}. In the case of the proton Dirac form factor, the corresponding analysis by Li[11] is in good agreement with experiment at momentum transfers greater than 3 GeV. Thus the leading twist QCD predictions based on the factorization of long and short distance physics appear to be self-consistent and valid for momentum transfers as low as a few GeV, thus accounting for the empirical success of quark counting rules in exclusive process phenomenology. The Sudakov effect suppression also enhances the QCD "color transparency" phenomena, since only small color singlet wavefunction configurations can scatter at large momentum transfer without radiation.[5]

The extension of the leading order PQCD analysis to higher orders including Sudakov effects is technically very challenging. Thus far, the next-to-leading $\alpha_s(Q^2)$ corrections to the hard scattering amplitudes T_H have been computed for only a few exclusive processes: the meson form factor, the photon-to-meson transition form factors, and $\gamma\gamma$ to meson pairs. There are many outstanding theoretical issues which are being resolved, such as how to extend these calculations to baryon processes, how to set the renormalization scale in α_s,[76,77] how to implement conformal symmetry and its breaking,[30,51] and how to formulate and solve the evolution equations for the hadron distribution amplitudes to next-to-leading order.

An important question for evaluating exclusive amplitudes in the transition region between hard and soft QCD processes is how to analytically separate perturbative contributions from contributions intrinsic to the bound-state wavefunction itself. The physical amplitude of course must be independent of the choice separation scale μ. Recently Ji, Pang, and Szczepaniak have observed that the natural variable to make this separation is the light-cone energy or equivalently the invariant mass of the off-shell partonic system, rather than gluon virtuality of T_H. The PQCD contributions from the invariant mass regime $\mu > 1$ GeV can then account substantially for the empirical pion form factor at $Q^2 > 1$ GeV^2. One also expects significant contributions from PQCD from higher order contributions.

It should be emphasized that the measurements of the pion form factor from electroproduction at large Q^2 are quite uncertain since they requires extrapolation to the pion $t-$ channel pole. CEBAF measurements can thus contribute significantly to this fundamental hadronic measure.

One of the most significant problems in computing the normalization of perturbative QCD predictions for exclusive processes is the uncertainty in setting the renormalization scale μ of the QCD coupling $\alpha_s(\mu)$ in the hard scattering amplitude T_H. A related problem is the question of the corresponding scale to use in evaluating the hadron distribution amplitudes.

Given a renormalization scheme, the QCD Lagrangian $\mathcal{L}_{QCD}$ is a function of the bare parameters $\alpha_s(\mu), m_q(\mu)$, etc. In principle, the values of the bare parameters can be fixed given a set of input measurements. Thus given a finite number of empirical values, all other QCD observables should be computable order by order in perturbation theory. The relation between the input and output observables must be independent of the choice of the renormalization scale μ as well as the choice of intermediate renormalization scheme. This invariance of the predictions for observables under changes of the intermediate renormalization scheme constitutes the generalized renormalization group invariance of Peterman and Stückelberg.[79]

Recently, Hung Jung Lu and I[77] have shown how this problem can be avoided by directly relating observables through commensurate scale relations. The conventional $\overline{MS}$ scheme serves as an intermediary calculational tool, but it can be systematically eliminated when relating observables. For example, the entire radiative corrections to the annihilation cross section is expressed as the effective charge $\alpha_R(Q)$ where $Q = \sqrt{s}$:

$$R(Q) \equiv 3 \sum_f Q_f^2 \left[1 + \frac{\alpha_R(Q)}{\pi}\right].$$

Similarly, we can define the entire radiative correction to the Bjorken sum rule as the effective charge $\alpha_{g_1}(Q)$ where Q is the lepton momentum transfer:

$$\int_0^1 dx \left[g_1^{ep}(x,Q^2) - g_1^{en}(x,Q^2)\right] \equiv \frac{1}{6}\left[\frac{g_A}{g_V}\right]\left[1 - \frac{\alpha_{g_1}(Q)}{\pi}\right].$$

We now use the known expressions to three loops in $\overline{MS}$ scheme and choose the scales Q^* and Q^{**} to re-sum all quark and gluon vacuum polarization corrections into the running couplings.[76] The relative scales insure that each observable pass through the heavy quark thresholds at their commensurate physical scales. The final result is remarkably simple:

$$\frac{\alpha_{g_1}(Q)}{\pi} = \frac{\alpha_R(Q^*)}{\pi} - \left(\frac{\alpha_R(Q^{**})}{\pi}\right)^2 + \left(\frac{\alpha_R(Q^{***})}{\pi}\right)^3 + \cdots$$

The fundamental test of QCD is then to verify empirically that the observables track in both normalization and shape as given by these relations. The coefficients in the series (aside for a factor of C_F, which can be absorbed in the definition of α_s) are actually independent of color and are the same in abelian, non-abelian, and conformal gauge theory. The non-Abelian structure of the theory is reflected in the scales Q^* and Q^{**}. The commensurate scale relations thus provide fundamental tests of QCD which can be made increasingly precise and independent of any scheme or other theoretical convention.

In the case of exclusive processes, the coupling associated with each virtual gluon exchange carrying momentum transfer ℓ_i^μ in the hard-scattering subprocess tree amplitude T_H can be identified with the running coupling $\alpha_V(\ell_i^2)$ appearing in the heavy quark potential.[80] We can determine the numerical values for $\alpha_V(Q^2)$ in many ways: directly from the heavy quarkonium spectrum and heavy quark lattice gauge theory[81] or from the commensurate scale relations which connect the α_V scheme to $\alpha_{\overline{MS}}$, or effective charges such as α_R, α_{g_1}, the Gross-Llewellyn Smith sum rule, etc. at their appropriate commensurate scales. Note that higher order corrections to the hard scattering amplitude from crossed graph kernels contribute even if the theory were conformal invariant; *i.e.* even of the coupling did not run. A related method can be used to choose the separation scale which controls the evolution of the hadron distribution amplitudes. By using this procedure, one should be able to substantially reduce the uncertainty in form factors and other exclusive processes from renormalization scale and scheme ambiguities.

8. Other Applications of Large Momentum Transfer Exclusive QCD.

The factorization techniques used to derive the leading-twist behavior of exclusive amplitudes have general applicability to processes where hadron wavefunctions have to be evaluated at far off-shell configurations. In each of these applications, one can separate the perturbative quark and gluon dynamics from momentum transfer higher than a scale Q from the non-perturbative long-distance physics contained in the distribution amplitudes $\phi(x_i, Q)$. For example at $x \sim 1$ the struck quark in deep inelastic lepton-hadron scattering is kinematically far off shell and space-like. Thus the leading power law fall off in $(1-x)$ is determined by iterating the gluon exchange kernel in the valence Fock state wavefunction. In this way one derives "spectator" counting rules for the nominal power law behavior [e.g. $G_{q/p}(x) \sim (1-x)^3$] and helicity-retention rules at $x \to 1$. The resulting structure functions connect smoothly to the behavior of large momentum transfer elastic and inelastic transition form factors at fixed $\mathcal{M}^2$. In fact, when $(1-x)Q^2$ is fixed, the usual evolution of the structure functions breaks down and there is no increase in the effective power beyond that given by the spectator counting rules. Further discussion may be found in Ref. 52.

Higher-twist corrections to inclusive reactions are of two types: coherent corrections which depend on the multiparticle structure of hadrons, and single particle corrections, such as mass and condensate insertions, which affect single quark or single gluon propagators. Exclusive processes represent the completely coherent limit of dynamical higher twist terms in inclusive reactions. At fixed $(1-x)Q^2$, the multiquark higher twist contributions can be computed using the exclusive factorization analysis, and they contribute at the same order as the leading twist terms.[53,17] Strong higher-twist corrections are in fact observed in the angular and Q^2–dependence of Drell-Yan processes and in deep inelastic lepton scattering at $x \sim 1$.[54]

The factorization techniques used to derive the leading twist contributions to form factors can also be applied to the exclusive decays of heavy hadrons when

large momentum transfers are involved. An interesting example of this analysis is "atomic alchemy",[55] *i.e.* the exclusive decays of muonic atoms to electronic atoms plus neutrinos. In this case, the calculation requires the high momentum tail of the atomic wavefunctions, which in turn can be obtained via the iteration of the relativistic atomic bound-state equations. Again one obtains a factorization theorem for exclusive atomic transitions where the atomic wavefunction at the origin plays the role of the distribution amplitude.

9. Exclusive Nuclear Processes

An ultimate goal of QCD phenomenology is to describe the nuclear force and the structure of nuclei in terms of quark and gluon degrees of freedom.

One of the most elegant areas of application of QCD to nuclear physics is the domain of large momentum transfer exclusive nuclear processes. Rigorous results have been given by Lepage, Ji and myself[56] for the asymptotic properties of the deuteron form factor at large momentum transfer. In the asymptotic $Q^2 \to \infty$ limit the deuteron distribution amplitude, which controls large momentum transfer deuteron reactions, becomes fully symmetric among the five possible color-singlet combinations of the six quarks. One can also study the evolution of the "hidden color" components (orthogonal to the np and $\Delta\Delta$ degrees of freedom) from intermediate to large momentum transfer scales; the results also give constraints on the nature of the nuclear force at short distances in QCD. The existence of hidden color degrees of freedom further illustrates the complexity of nuclear systems in QCD. It is conceivable that six-quark d^* resonances corresponds to these new degrees of freedom may be found by careful searches of the $\gamma^* d \to \gamma d$ and $\gamma^* d \to \pi d$ channels.

The basic scaling law for the helicity-conserving deuteron form factor is $F_d(Q^2) \sim 1/Q^{10}$ which comes from simple quark counting rules, as well as perturbative QCD. One cannot expect this asymptotic prediction to become accurate until very large Q^2 is reached since the momentum transfer has to be shared by at least six constituents. However, one can identify the QCD physics due to the compositeness of the nucleus, with respect to its nucleon degrees of freedom by using the reduced amplitude formalism.[57] For example, consider the deuteron form factor in QCD. By definition this quantity is the probability amplitude for the deuteron to scatter from p to $p+q$ but remain intact. Note that for vanishing nuclear binding energy $\epsilon_d \to 0$, the deuteron can be regarded as two nucleons sharing the deuteron four-momentum (see Fig. 3). The momentum ℓ is limited by the binding and can thus be neglected. To first approximation the proton and neutron share the deuteron's momentum equally. Since the deuteron form factor contains the probability amplitudes for the proton and neutron to scatter from $p/2$ to $p/2+q/2$; it is natural to define the reduced deuteron form factor[57,58,59]

$$f_d(Q^2) \equiv \frac{F_d(Q^2)}{F_{1N}\left(\frac{Q^2}{4}\right) F_{1N}\left(\frac{Q^2}{4}\right)}.$$

The effect of nucleon compositeness is removed from the reduced form factor. QCD then predicts the scaling

$$f_d(Q^2) \sim \frac{1}{Q^2}$$

i.e. the same scaling law as a meson form factor. Diagrammatically, the extra power of $1/Q^2$ comes from the propagator of the struck quark line, the one propagator not contained in the nucleon form factors. Because of hadron helicity conservation, the prediction is for the leading helicity-conserving deuteron form factor ($\lambda = \lambda' = 0$.) As shown in Fig. 4, this scaling is consistent with experiment for $Q = p_T \gtrsim 1$ GeV.

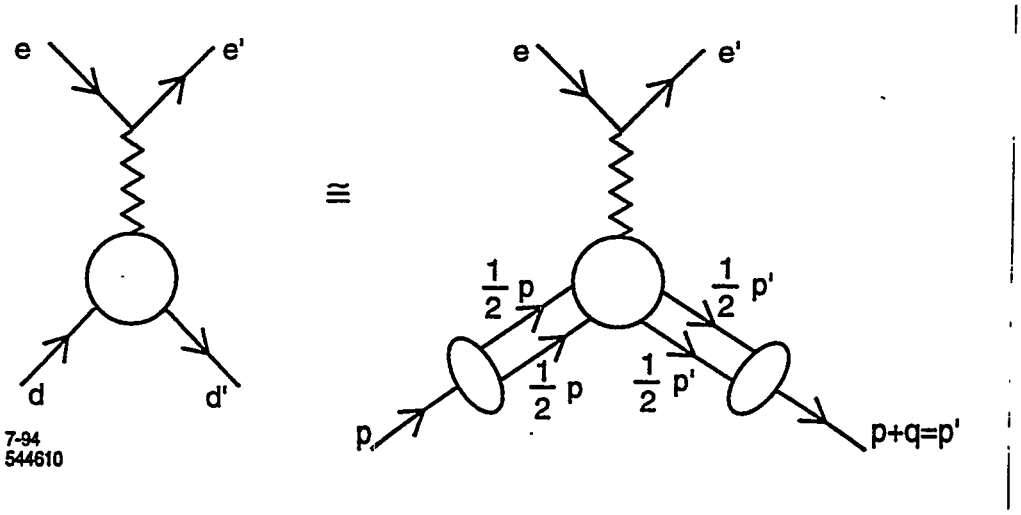


Figure 3. Application of the reduced amplitude formalism to the deuteron form factor at large momentum transfer.

The distinction between the QCD and other treatments of nuclear amplitudes is particularly clear in the reaction $\gamma d \to np$; *i.e.* photo-disintegration of the deuteron at fixed center of mass angle. Using dimensional counting, the leading power-law prediction from QCD is simply $\frac{d\sigma}{dt}(\gamma d \to np) \sim F(\theta_{\rm cm})/s^{11}$. Again we note that the virtual momenta are partitioned among many quarks and gluons, so that finite mass corrections will be significant at low to medium energies. Nevertheless, one can test the basic QCD dynamics in these reactions taking into account much of the finite-mass, higher-twist corrections by using the "reduced amplitude" formalism.[58,59] Thus the photo-disintegration amplitude contains the probability amplitude (*i.e.* nucleon form factors) for the proton and neutron to each remain intact after absorbing momentum transfers $p_p - 1/2p_d$ and $p_n - 1/2p_d$, respectively (see Fig. 5). After the form factors are removed, the remaining "reduced" amplitude should scale as $F(\theta_{\rm cm})/p_T$. The single inverse power of transverse momentum p_T is the slowest conceivable in any theory, but it is the unique power predicted by PQCD.

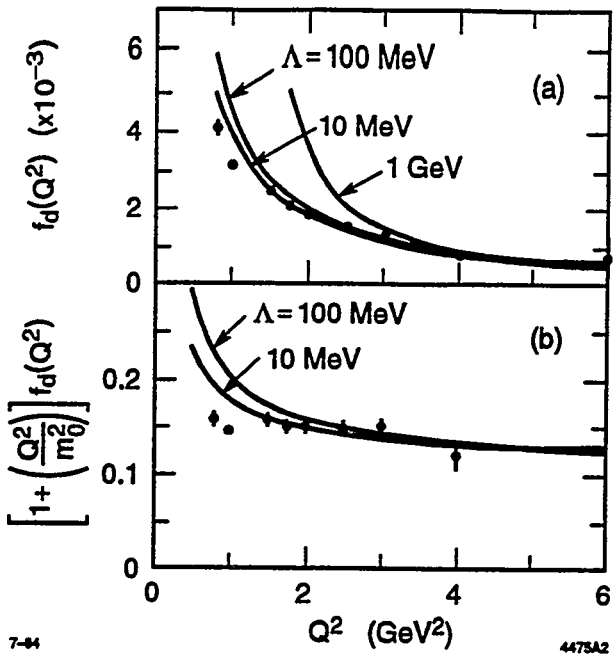


Figure 4. Scaling of the deuteron reduced form factor. The data are summarized in Ref. 58.

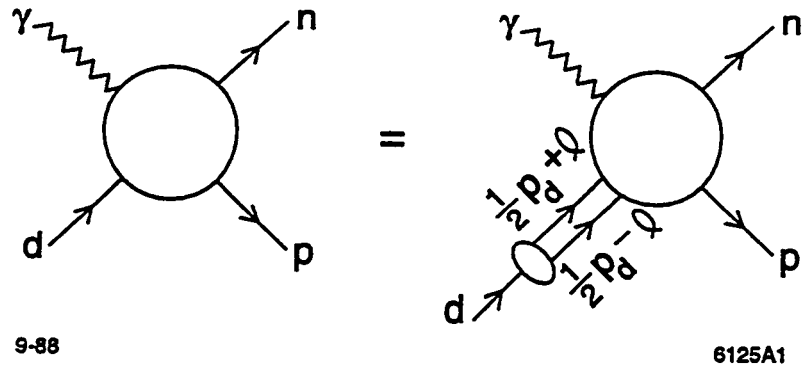


Figure 5. Construction of the reduced nuclear amplitude for two-body inelastic deuteron reactions.[58]

The prediction that $f(\theta_{cm})$ is energy dependent at high-momentum transfer is compared with experiment in Fig. 6. It is particularly striking to see the QCD prediction verified at incident photon lab energies as low as 1 GeV. A comparison with a standard nuclear physics model with exchange currents is also shown for comparison as the solid curve in Fig. 6(a). The fact that this prediction falls less fast than the data suggests that meson and nucleon compositeness are not taken to into account

correctly. An extension of these data to other angles and higher energy would clearly be very valuable.

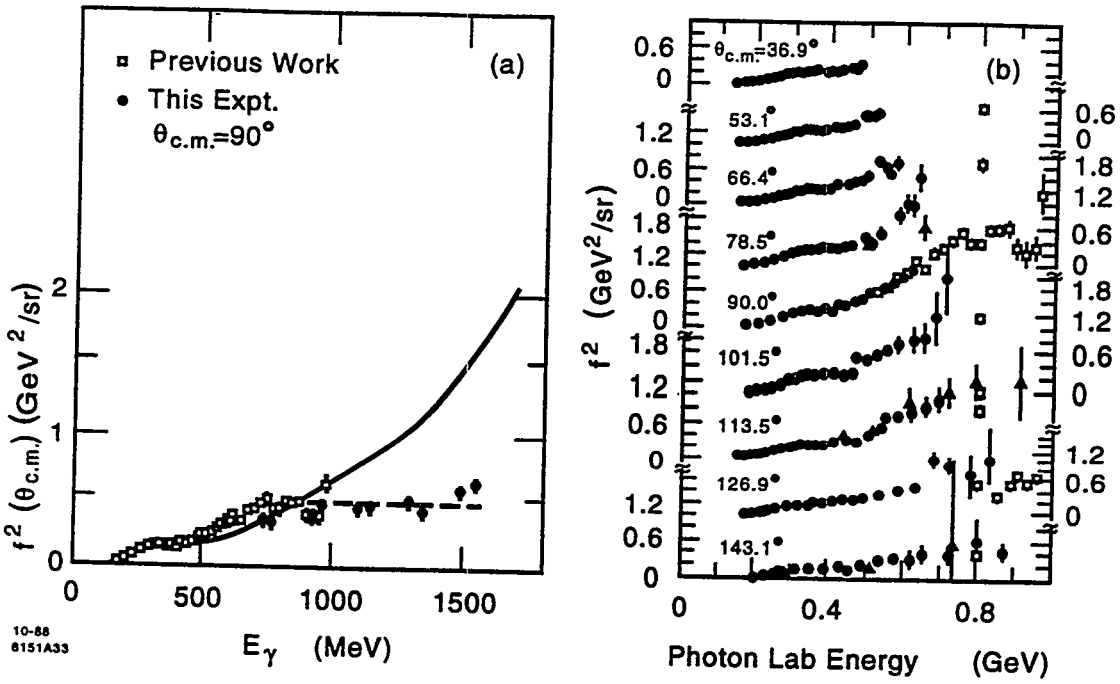


Figure 6. Comparison of deuteron photodisintegration data with the scaling prediction which requires $f^2(\theta_{cm})$ to be at most logarithmically dependent on energy at large momentum transfer. The data in (a) are from the recent experiment of Ref. 60. The nuclear physics prediction shown in (a) is from Ref. 61. The data in (b) are from Ref. 62.

The derivation of the evolution equation for the deuteron and other multi-quark states is given in Refs. 56 and 59. In the case of the deuteron, the evolution equation couples five different color singlet states composed of the six quarks. The leading anomalous dimension for the deuteron distribution amplitude and the helicity-conserving deuteron form factor at asymptotic Q^2 is given in Ref. 56.

There are a number of related tests of QCD and reduced amplitudes which require $\overline{p}$ beams[59] such as $\overline{p}d \to \gamma n$ and $\overline{p}d \to \pi p$ in the fixed $\theta_{\rm cm}$ region. These reactions are particularly interesting tests of QCD in nuclei. Dimensional counting rules predict the asymptotic behavior $\frac{d\sigma}{dt}(\overline{p}d \to \pi p) \sim \frac{1}{(p_T^2)^{12}} f(\theta_{\rm cm})$ since there are 14 initial and final quanta involved. Again one notes that the $\overline{p}d \to \pi p$ amplitude contains a factor representing the probability amplitude (*i.e.* form factor) for the proton to remain intact after absorbing momentum transfer squared $\widehat{t} = (p - 1/2p_d)^2$ and the $\overline{N}N$ time-like form factor at $\widehat{s} = (\overline{p} + 1/2p_d)^2$. Thus $\mathcal{M}_{\overline{p}d \to \pi p} \sim F_{1N}(\widehat{t})\, F_{1N}(\widehat{s})\, \mathcal{M}_r$,

where $\mathcal{M}_r$ has the same QCD scaling properties as quark meson scattering. One thus predicts

$$\frac{\frac{d\sigma}{d\Omega}(\overline{p}d \to \pi p)}{F_{1N}^2(\hat{t})\, F_{1N}^2(\hat{s})} \sim \frac{f(\Omega)}{p_T^2}.$$

The reduced amplitude scaling for $\gamma d \to pn$ at large angles and $p_T \gtrsim 1$ GeV (see Fig. 6). One thus expects similar precocious scaling behavior to hold for $\overline{p}d \to \pi p$ and other $\overline{p}d$ exclusive reduced amplitudes. An analysis by Kondratyuk and Sapozhnikov[63] shows that standard nuclear physics wavefunctions and interactions cannot explain the magnitude of the data for two-body anti-proton annihilation reactions such as $\overline{p}d \to \pi p$.

10. Outstanding Phenomenological Issues in Exclusive Processes.

Although most large momentum transfer exclusive reactions appears to be empirically consistent with perturbative QCD expectations, there are a number of glaring exceptions where theory and experiment diverge. If one accepts that the underlying formalism for the leading twist behavior of exclusive reactions is reliable, then these exceptions provide important insights into new physical mechanisms within QCD.

What accounts for the structure in the spin correlations in pp elastic scattering at large momentum transfer? Measurements[64] of large angle pp elastic scattering at Argonne and Brookhaven show a dramatic spin-spin correlation A_{NN} which reaches ~ 0.6 at $\sqrt{s} \sim 5$ GeV: *i.e.* the spin-analyzed cross section is four times larger if the protons scatter with their spins parallel and normal to the scattering plane compared to antiparallel. The explanation for this phenomena is far from settled. The most popular explanations[65] are based on the interference of Landshoff pinch singularities[66] with the quark interchange amplitude, but there is no understanding why the Landshoff contribution would itself have a large A_{NN}[67] or sufficient normalization[68] to explain this phenomena. Guy de Teramond and I have proposed[69] that the large spin correlations reflects inelastic channels corresponding to the production of charm at threshold. This effect leads to enhancement in the $J = L = S = 1$ $pp \to pp$ partial wave which implies a large value of A_{NN} at the energies sufficient to produce open charm. This explanation would be confirmed by the observation of a sizeable charm production in pp collisions at a rate of order of 1 microbarn. A similar enhancement of A_{NN} is seen at the open strangeness threshold regime. and is consistent with the 1 millibarn cross section observed for the production of strange hadrons just above threshold. The heavy quark explanation has received some support from the work of Luke, Savage, and Manohar,[13] who have shown that the interactions of $c\bar{c}$ systems at low relative velocity with hadrons is enhanced due to the QCD scale anomaly; in fact, the scalar exchange interaction is predicted to be strong enough to bind charmonium to heavy nuclei.[14]

Why does QCD color transparency appear to break down in quasielastic pp scattering. The Brookhaven measurements[70] of the transparency ratio for large angle quasi-elastic pp scattering increases with momentum transfer, as predicted by PQCD, but the ratio then appears to revert to normal absorption at $\sqrt{s} \sim 5$ GeV. This suggests that whatever is causing the structure in A_{NN} at the same energies and angles involves large transverse sizes and is far from perturbative in origin. The charm threshold effect is a candidate for this type of explanation.

The preliminary results for the SLAC color transparency experiment NE-18[71] indicate that color transparency in quasi-elastic ep scattering is not a strong effect up to the accessible momentum transfers. Higher momentum transfers exceeding 5 GeV are needed for a decisive test. A sensitive test of color transparency is provided by measuring the sign of the derivative of the transparency ratio $\frac{d\sigma dQ^2(eA\to e'p(A-1))}{Zd\sigma dQ^2(ep\to e'p)}$. Perturbative QCD predicts a positive slope, whereas conventional Glauber theory predicts a negative derivative in the low Q^2 domain.

Why does the J/ψ decay copiously to $\rho\pi$? According to the principle of hadron helicity conservation[44] in exclusive decays, the J/ψ produced with $J_z = \pm 1$ in e^+e^- annihilation should not decay to vector plus pseudoscalar meson pairs. In fact, this is true for the ψ' and other S-state charmonium states, but in the case of the J/ψ, the $\rho\pi$ and KK^* psuedoscalar-vector meson channels are actually the dominant two-body hadronic decays. A possible explanation is that the J/ψ mixes with a nearby gluonic or hybrid $J = 1$ state $\mathcal{O}$ that favors vector plus pseudoscalar meson pair decay.[72] One can search for the $\mathcal{O}$ by looking for a $\rho\pi$ mass peak near the J/ψ in the decay $\psi' \to \pi\pi\mathcal{O} \to \pi\pi\rho\pi$.

Why do effective Reggeon trajectories flatten to values below $\alpha_R(t) = 0$ at large momentum transfer? A fundamental prediction of perturbative QCD is that the Reggeon trajectories $\alpha_\rho(t)$ and $\alpha_{A_2}(t)$ governing charge exchange reactions at high energies $s \gg -t$ monotonically approach zero at large spacelike momentum transfer.[73] More generally, the leading Reggeon in an exclusive process will reflect the minimal particle number exchange quantum numbers: two gluons in the case of the Pomeron, three gluons in the case of the Odderon, and quark plus anti-quark in the case of meson exchange trajectories. Because of asymptotic freedom the leading trajectory at large momentum transfer is thus simply $j_1 + j_2 - 1$ with corrections of order $\sqrt{\alpha_s}(-t)$. The asymptotic prediction $\lim_{-t\to\infty} \alpha_R(t) = 0$ reflects the fact that a weakly interacting quark-antiquark pair is exchanged in the $t-$channel.[73] Thus one expects that the effective ρ Reggeon should asymptote at $\alpha_\rho(t) \to 0$ at large $-t$. However, measurements of the inclusive processes $\pi^- p \to \pi^0 X$ at $s \simeq 300$ GeV^2 and $8 > -t > 2$GeV^2 indicate that the effective non-singlet ρ trajectory becomes negative at large $-t$.[74] Thorn, Tang and I have recently shown that the hard QCD part of the trajectory is weakly coupled and that its contribution may well be hidden until much higher energy.[75] Quark interchange[10] may thus be the dominant subprocess at presently accessible kinematic ranges. We also show that Reggeon contributions to exclusive and semi-inclusive mesonic exchange hadron reactions can be systematically studied in perturbative QCD.

Why is quark interchange the dominant mechanism for large-angle hadron-hadron scattering? The comprehensive measurements at BNL[9] of the relative normalization and angular dependence of a large set of exclusive hadron scattering channels strongly suggests that the dominant mechanism for scattering hadrons at large momentum transfer is quark interchange.[10] For example, if gluon exchange were the dominant mechanism, then the differential cross sections for $K^+p \to K^+p$ and $K^-p \to K^-p$ at large p_T would be roughly equal in magnitude and angular shape. In fact they have grossly different magnitudes and shapes. The $K^+p \to K^+p$ cross section has the approximate form predicted by the exchange of their common u quark. A possible explanation of this fact is that quark interchange involves the least number of large momentum exchanges within the hadron scattering amplitude.

The short-distance structure of hadrons, hadron dynamics, and hadronization is thus one of the frontier areas of study in testing quantum chromodynamics. Electroproduction at CEBAF will play an essential role in resolving this fundamental area of physics.

Acknowledgements

I wish to thank Carl Carlson and Paul Stoler and the other members of the organizing committee for organizing an outstanding meeting in Elba. I also thank Tom Hyer for helpful conversations. This work was supported by the U.S. Department of Energy under Contract No. DE-AC03-76SF00515.

REFERENCES

[1] See, *e.g.*, the volume *Perturbative Quantum Chromodynamics,* Edited by A.H. Mueller. World Scientific, 1989.

[2] A. Brandenburg, S. J. Brodsky, V. V. Khoze, and D. Müller, SLAC-PUB-6464 (1994), to be published in Phys. Rev. Lett.

[3] For a review of the theory of exclusive processes in QCD and additional references see S. J. Brodsky and G. P. Lepage in *Perturbative Quantum Chromodynamics*, edited by A. Mueller (World Scientific, Singapore, 1989).

[4] S. J. Brodsky and G. R. Farrar, *Phys. Rev.* **D11** (1975) 1309.

[5] S. J. Brodsky and A. H. Mueller, *Phys. Lett.* **206B** (1988) 685, and references therein; G. Bertsch, S. J. Brodsky, A. S. Goldhaber, J.F. Gunion, *Phys. Rev. Lett.* **47** (1981) 297.

[6] E665 Collaboration (G. Y. Fang, *et al.*), FERMILAB-CONF-94-041-E, (1994). Presented at the *23rd International Multiparticle Dynamics Symposium*, 1993, Aspen.

[7] S. J. Brodsky, L. Frankfurt, J. F. Gunion, A. H. Mueller, and M. Strikman, SLAC-PUB-6412, (1994). (To be published in *Phys. Rev. D.*)

[8] R. L. Anderson *et al.*, *Phys. Rev. Lett.* **30** (1973) 627.

[9] A. Carroll, Presented at the *Workshop on Exclusive Processes at High Momentum Transfer*, Elba, Italy, 1993; C. White *et al.*, BNL-49059, (1993); B. R. Baller *et al.*, *Phys. Rev. Lett.* **60** (1988) 1118.

[10] J. F. Gunion, S. J. Brodsky, and R. Blankenbecler, *Phys. Rev.* **D8** (1973) 287.

[11] J. Botts and G. Sterman, *Nucl. Phys.* **B325** (1989) 62; *Phys. Lett.* **B224** (1989) 201; J. Botts, J.-W. Qiu, and G. Sterman, *Nucl. Phys.* **A527** (1991) 577. H. N. Li and G. Sterman, *Nucl. Phys.* **B381** (1992) 129. H. N. Li, Stony Brook preprint ITP-SB-92-25 (1991).

[12] M. G. Sotiropoulos and G. Sterman ITP-SB-93-59 (1993), ITP-SB-93-83 (1994).

[13] M. Luke, A. V. Manohar, M. J. Savage, *Phys. Lett.* **B288** (1992) 355.

[14] S. J. Brodsky, and G. F. de Teramond, and I. A. Schmidt, *Phys. Rev. Lett.* **64** (1990) 1011.

[15] See, *e.g.*, C. Wilkin, *Phys. Rev.* **C47** (1993) 938.

[16] For a review of intrinsic heavy quark phenomena and further references, see S. J. Brodsky, SLAC-PUB-6304, *CCAST Symposium on Particle Physics at the Fermi Scale*, Beijing, China, (1993); and R. Vogt, S. J. Brodsky, and P. Hoyer *Nucl. Phys.* **B383** (1992) 643.

[17] S. J. Brodsky, P. Hoyer, A. H. Mueller, W-K. Tang, *Nucl. Phys.* **B369** (1992) 519.

[18] S. J. Brodsky, F. E. Close, J. F. Gunion, *Phys. Rev.* **D5** (1972) 1384.

[19] S. J. Brodsky, J. F. Gunion, R. Jaffe (SLAC), *Phys. Rev.* **D6** (1972) 2487.

[20] S. J. Brodsky, A. C. Hearn, R. G. Parsons, *Phys. Rev.* **187** (1969) 1899.

[21] M. Damashek, F. J. Gilman, *Phys. Rev.* **D1** (1970) 1319.

[22] S. J. Brodsky, W.-K. Tang, C. B. Thorn, *Phys. Lett.* **B318** (1993) 203.

[23] Part of this section was also presented at the at the *Workshop on Exclusive Processes at High Momentum Transfer*, Elba, Italy, 1993.

[24] S. D. Drell and T. M. Yan, *Phys. Rev. Lett.* **24** (1970) 181.

[25] S. J. Brodsky and H. C. Pauli in *Recent Aspects of Quantum Fields*, H. Mitter and H. Gausterer, Eds.; Lecture Notes in Physics, Vol. 396, Springer-Verlag, Berlin, Heidelberg, (1991), and reference therein.

[26] G. P. Lepage and S. J. Brodsky, *Phys. Rev.* **D22**, 2157 (1980); *Phys. Lett.* **87B** (1979) 359; *Phys. Rev. Lett.* **43** (1979) 545, 1625E.

[27] General QCD analyses of exclusive processes are given in Ref. 26, S. J. Brodsky and G. P. Lepage, SLAC-PUB-2294, presented at the *Workshop on Current Topics in High Energy Physics*, Caltech (Feb. 1979), S. J. Brodsky, in the *Proceedings of the La Jolla Institute Summer Workshop on QCD*, La Jolla (1978), A. V. Efremov and A. V. Radyushkin, *Phys. Lett.* **B94** (1980) 245, V. L. Chernyak, V. G. Serbo, and A. R. Zhitnitskii, *Yad. Fiz.* **31,** (1980) 1069, S. J. Brodsky, Y. Frishman, G. P. Lepage, and C. Sachrajda, *Phys. Lett.* **91B** (1980) 239, and A. Duncan and A. H. Mueller, *Phys. Rev.* **D21** (1980) 1636.

[28] QCD predictions for the pion form factor at asymptotic Q^2 have ben given by V. L. Chernyak, A. R. Zhitnitskii, and V. G. Serbo, *JETP Lett.* **26** (1977) 594, D. R. Jackson, Ph.D. Thesis, Cal Tech (1977), and G. Farrar and D. Jackson, *Phys. Rev. Lett.* **43** (1979) 246; and Ref. 27. See also A. M. Polyakov, *Proceedings of the International Symposium on Lepton and Photon Interactions at High Energies*, Stanford (1975), and G. Parisi, *Phys. Lett.* **84B** (1979) 225. See also S. J. Brodsky and G. P. Lepage, in *High Energy Physics–1980, Proceedings of the XXth International Conference*, Madison, Wisconsin, edited by L. Durand and L. G. Pondrom (AIP, New York, 1981); p. 568. A. V. Efremov and A. V. Radyushkin, Rev. Nuovo Cimento **3**, 1 (1980); and Ref. 27. V. L. Chernyak and A. R. Zhitnitskii, *JETP Lett.* **25** (1977) 11; M. K. Chase, *Nucl. Phys.* **B167** (1980) 125.

[29] V. L. Chernyak and A. R. Zhitnitskii, *Phys. Rept.* **112** (1984) 173; V. L. Chernyak, A. A. Oglobin, and I. R. Zhitnitskii, *Sov. J. Nucl. Phys.* **48** (1988) 536; I. D. King and C. T. Sachrajda, *Nucl. Phys.* **B297** (1987) 785; M. Gari and N. G. Stefanis, *Phys. Rev.* **D35** (1987) 1074; and references therein.

[30] S. J. Brodsky, Y. Frishman, G. P. Lepage and C. Sachrajda, Ref. 27. M. E. Peskin, *Phys. Lett.* **88B** (1979) 128.

[31] See, for example, B. K. Jennings and G.A. Miller DOE-ER-40427-00-N93-11, (1993) and *Phys. Lett.***B236** (1990) 209; G. R. Farrar, H. Liu, L. L. Frankfurt, and M. I. Strikman, *Phys. Rev. Lett.* **61** (1988) 686; N. N. Nikolaev and B. G. Zakharov, *Z. Phys.* **C49** (1991) 607; L. L. Frankfurt, M. I. Strikman, and M. B. Zhalov, preprint (1993); J. P. Ralston and B. Pire, *Phys. Rev. Lett.* **61** (1988) 1823, and in the *Proceedings of the 1989 24th Rencontre de Moriond* (1989).

[32] S. J. Brodsky and G. P. Lepage, *Phys. Rev.* **D24** (1981) 1808.

[33] B. Nizic, *Fizika* **18** (1986) 113.

[34] For a review of exclusive two-photon processes, see S. J. Brodsky, *Proceedings of the Tau-Charm Workshop*, Stanford, CA (1989).

[35] G. R. Farrar, *et al. Nucl. Phys.* **B311** (1989) 585.

[36] D. Millers and J. F. Gunion, *Phys. Rev.* **D34** (1986) 2657.

[37] A. N. Kronfeld and B. Nizic, *Phys. Rev.* **D44** (1991) 3445; B. Nizic, *Phys. Rev.* **D35**(1987) 80.

[38] T. Hyer, *Phys. Rev.* **D47** (1993) 3875.

[39] S. J. Brodsky, F. E. Close, J. F. Gunion, *Phys. Rev.* **D6** (1972) 177.

[40] M. A. Shupe, *et al.*, *Phys. Rev.* **D19** (1979) 1921.

[41] M. Bergmann and N. G. Stefanis, Bochum preprints RUB-TPH-36/93, RUB-TPH-46/93, and RUB-TPH-47/93.

[42] S. J. Brodsky, in the *Proceedings of the Topical Conference on Electronuclear Physics with Internal Targets*, Stanford, (1989).

[43] B. Z. Kopeliovich, J. Nemchick, N. N. Nikolaev, B. G. Zakharov, *Phys. Lett.* **B309** (1993) 179.

[44] G. P. Lepage and S. J. Brodsky, *Phys. Rev.* **D24** (1981) 2848.

[45] P. Stoler, *Phys. Rev.* **D44** (1991) 73, *Phys. Rev. Lett.* **66** (1991) 1003.

[46] N. Isgur and C. H. Llewellyn Smith, *Phys. Rev. Lett.* **52** (1984) 1080; *Phys. Lett* **B217** (1989) 535.

[47] A. V. Radyushkin, *Nucl. Phys.* **A532** (1991) 141.

[48] A. Duncan, and A. H. Mueller, *Phys. Lett.* **90B** (1980) 159.

[49] S. J. Brodsky and J. F. Gunion, *Phys. Rev. Lett.* **37** (1976) 402.

[50] A. Szczepaniak and L. Mankiewicz, *Phys. Lett.* **B266** (1991) 153.

[51] D. Müller, SLAC-PUB (1993).

[52] S. J. Brodsky, I. A. Schmidt, *Phys. Lett.* **B234** (1990) 144, and references therein; S. J. Brodsky, in the *Proceedings of the International Symposium on High-Energy Spin Physics,* Nagoya, Japan, (1992).

[53] S. J. Brodsky, E. L. Berger, G. Peter Lepage, *Proceedings of the Drell-Yan Workshop*, Fermilab (1982); E. L. Berger and S. J. Brodsky, *Phys. Rev. Lett.* **42** (1979) 940. For a recent analysis and additional references see S. S. Agaev, *Z. Phys.* **C57** (1993) 403.

[54] See, *e.g.*, J. S. Conway *et al.*, *Phys. Rev.* **D39** (1989) 92.

[55] C. Greub, D. Wyler, S. J. Brodsky, and C. T. Munger, SLAC-PUB-6487, (1994).

[56] S.J. Brodsky, C.-R. Ji and G.P. Lepage, *Phys. Rev. Lett.* **51** (1983) 83.

[57] S. J. Brodsky, B. T. Chertok, *Phys. Rev.* **D14** (1976) 3003.

[58] S. J. Brodsky and J. R. Hiller, *Phys. Rev.* **C28** (1983) 475.

[59] C. R. Ji and S. J. Brodsky, *Phys. Rev.* **D34** (1986) 1460; **D33** (1986) 1951, 1406, 2653. For a review of multi-quark evolution, see S. J. Brodsky, C.-R. Ji, SLAC-PUB-3747, (1985).

[60] J. Napolitano *et al.*, ANL preprint PHY–5265–ME–88 (1988).

[61] T. S.-H. Lee, ANL preprint (1988).

[62] H. Myers *et al.*, *Phys. Rev.* **121** (1961) 630; R. Ching and C. Schaerf, *Phys. Rev.* **141** (1966) 1320; P. Dougan *et al.*, *Z. Phys. A* **276** (1976) 55.

[63] L.A. Kondratyuk and M. G. Sapozhnikov, Dubna preprint E4-88-808.

[64] For a summary of the spin correlation data see A. D. Krisch, *Nucl. Phys. B (Proc. Suppl.)* **25B** (1992) 285.

[65] See, for example, J. P. Ralston and B. Pire, *Phys. Rev. Lett.* **49** (1982) 1605; C. E. Carlson, M. Chachkhunashvili, F. Myhrer, *Phys. Rev.* **D46** (1992) 2891; G. P. Ramsey, D. Sivers, *Phys. Rev.* **D47** (1992) 93; and references therein.

[66] P. V. Landshoff, *Phys. Rev* **D10** (1974) 1024.

[67] S. J. Brodsky, C. E. Carlson, H. J. Lipkin, *Phys. Rev.* **D20** (1979) 2278.

[68] Presented at the INT - Fermilab Workshop on *Perspectives of High Energy Strong Interaction Physics at Hadron Facilities* (1993).

[69] S. J. Brodsky and G. F. de Teramond, *Phys. Rev. Lett.* **60** (1988) 1924.

[70] See S. Heppelmann, *Nucl. Phys. B, Proc. Suppl.* **12** (1990) 159, and references therein.

[71] A. Lung, Presented at the *Workshop on Exclusive Processes at High Momentum Transfer*, Elba, Italy, 1993.

[72] S. J. Brodsky, G. Peter Lepage, S. F.Tuan, *Phys. Rev. Lett.* **59** (1987) 621, and references therein.

[73] R. Kirshner and L. N. Lipatov, *Sov. Phys. JETP* **56** (1982) 266; *Nucl. Phys.* **B213** (1983) 122.

[74] R. Blankenbecler, S. J. Brodsky, J. F. Gunion, and R. Savit, *Phys. Rev.* **D8** (1973) 4117.

[75] S. J. Brodsky, W-K. Tang, and C. B. Thorn, SLAC-PUB-6227 (1993).

[76] S. J. Brodsky, G. P. Lepage, and P. B. Mackenzie, *Phys. Rev.* **D28** (1983) 228.

[77] S. J. Brodsky, H. J. Lu, SLAC-PUB-6481, (1994).

[78] C.-R. Ji, A. Pang, and A. Szczepaniak, North Carolina State University preprint (1994).

[79] E. C. G. Stückelberg and A. Peterman, *Helv. Phys. Acta* **26** (1953) 499. A. Peterman, *Phys. Rept.* **53C** (1979) 157.

[80] A similar method is discussed in B. Nizic, *Phys. Rev.* **D35** (1987) 93.

[81] G. P. Lepage, P. B. Mackenzie, *Phys. Rev.* **D48** (1993) 2250.

FORM FACTORS OF THE TRANSITIONS $\gamma^*\pi^0 \to \gamma$ AND $\gamma^*\eta \to \gamma$

Andrei Afanasev[1]
Continuous Electron Beam Accelerator Facility
12000 Jefferson Ave., Newport News, VA 23606

ABSTRACT

We discuss possibilities to study $\gamma^*\pi^0 \to \gamma$ and $\gamma^*\eta \to \gamma$ transition form factors at CEBAF energies. We show that for 4 GeV electron beam, these form factors can be measured at CEBAF for the 4–momentum transfers $Q^2 \leq 2.5$ (GeV/c)^2 using virtual Compton scattering on the proton and nuclear target in the kinematic regime of low momentum transfers to the target. These measurements can be extended to $Q^2 \leq 4.0$ (GeV/c)^2 using the electron beam with the energy 6 GeV.

1. Introduction and Physics Motivation

The Q^2 dependence of the form factor of the $\gamma^*M \to \gamma$ transition ($F_{\gamma^*\gamma M}$) where M is a pseudoscalar meson (e.g., π^0, η, or η') is an important tool to test perturbative QCD in exclusive reactions; the transition $\gamma^*\pi^0 \to \gamma$ is especially remarkable because, when combined with charged pion form factor measurements, it provides a way to determine the QCD running coupling constant $\alpha_s(Q^2)$ [1]. On the quark level, this transition is described in terms of the quark triangle diagram (Fig.1). For the case of pion, it corresponds to the Adler–Bell–Jackiw [2] axial anomaly extended to the region where one of the photons is virtual.

In the time–like region ($Q^2 < 0$), these form factors were measured in the decays $\pi^0 \to e^+e^-\gamma$ (see Refs.[3] and [4] for a review). For the space–like momentum transfers ($Q^2 > 0$), $F_{\gamma^*\gamma M}$ was measured at PETRA in the processes $e^-e^+ \to e^-e^+M$. [5] The form factors were studied theoretically in different approaches based on both perturbative QCD [1] and QCD sum rules, [6,7] and effective theories like the linear σ model and Nambu-Jona-Lasinio model. [8]

Although meson production in e^+e^- collisions is the cleanest way to study the form factors $F_{\gamma^*\gamma M}$, this technique suffers large statistical and systematic uncertainties (Fig.2). It is also possible to address this issue at the electron accelerator such as CEBAF where electrons are scattered on a fixed nuclear target. In this case, there are two different ways to access the transitions.

i) Primakoff effect [9] (Fig.3a) in which the incoming photon interacts with the Coulomb field of the nucleus producing π^0 in the final state. This process is dominant if the target recoil momentum is very low. In a recent publication, [10] this process was considered theoretically with the conclusion that only very low values of Q^2 can be covered this way if the kinematics is chosen so that a standard mechanism of π^0

[1]Permanent address: *Kharkov Institute of Physics and Technology, Kharkov 310108, Ukraine*

electroproduction is suppressed. There is yet another reason that limits the sensitivity of this method to the $\gamma^*\gamma \to \pi^0$ transitions, *viz.*, ρ^0– and ω–exchanges in the (same) t–channel (Fig.3b). In principle, one can get rid of these exchanges choosing low $|t|$ values. A simple estimate shows that the inequality $|t| < 2 \cdot 10^{-4}$ (GeV/c)^2 should be satisfied for the Primakoff mechanism to take over ρ^0– and ω–exchanges. For 4 (6) GeV electron beam, it corresponds to $Q^2 < 0.1$ (0.15) (GeV/c)^2 for the π^0 production; these low values of $|t|$ are kinematically forbidden for η and heavier meson production. It means that at CEBAF energies, the Primakoff mechanism provides a possibility only to measure the slope of $F_{\gamma^*\gamma\pi^0}(Q^2)$ at low Q^2.

ii) A study of $\gamma^*M \to \gamma$ transitions on mesons emitted by a proton and/or nuclear target (Fig.4a). In fact, it is a virtual Compton scattering, $\gamma^*A \to \gamma A$, in the region of low recoil momentum of the target. Its advantage over the Primakoff mechanism is that it permits to cover the Q^2 range up to 2.5 (3.5) (GeV/c)^2 for 4 (6) GeV electron beam. Here we would like to focus on this reaction in more detail and discuss kinematics, theoretical issues and possible experimental solutions.

2. Kinematics

The notation for the 4–momenta of the particles involved in the reaction $eA \to eA\gamma$ is shown in Fig.4a. This is a t–channel diagram for the virtual Compton scattering (Fig.4b). The competing mechanism, Bethe–Heitler (Fig.4c), is known to be strongly peaked along the momenta of initial and final electrons. For definiteness, let us consider scattering on the proton keeping in mind possible extension to other nuclear targets.

To have the t–channel contribution to the virtual Compton amplitude enhanced compared to other channels, we need to minimize the values of t. We can write

$$\begin{aligned} -t \;\equiv\; -k^2 &= -2M^2 + \frac{1}{2s}(s+M^2+Q^2)(s+M^2) \\ &\quad -\frac{\cos\alpha}{2s}[\lambda(s,-Q^2,M^2)\lambda(s,0,M^2)]^{1/2} \end{aligned} \tag{1}$$

$$Q^2 \;\equiv\; -q^2 = 2EE'(1-\cos\theta) \tag{2}$$

$$s \;\equiv\; (q+p_1)^2 = -Q^2 + (E-E')2M + M^2 \tag{3}$$

where M is the mass of the proton, $E(E')$ is the initial (final) electron energy, θ is the electron scattering angle in the lab, α is the proton scattering angle in c.m.s. and $\lambda(x,y,z) \equiv x^2+y^2+z^2-2xy-2xz-2yz$. For the given E and θ, the final electron energy is limited by

$$E'_{max} = \frac{EM}{E(1-\cos\theta)+M}$$

Apparently, the lowest $|t|$ values are reached when α=0. The corresponding plot of t_{min} against Q^2 is shown in Fig.5 for E=4 GeV as a function of electron scattering angles. It can be seen from Fig.5 that at $|t|_{min}$=0.15 (GeV/c)^2 (which corresponds to the recoil proton momentum about 400 MeV/c). Varying the electron scattering

angles from 25° to 90°, we explore the Q^2 region 1.5 to 2.5 (GeV/c)^2, while the invariant mass $\sqrt{s}$ changes from 1.9 to 2.4 GeV. The 6 GeV electron beam that will be available at the second step at CEBAF will make it possible to extend the measurements of $F_{\gamma^*\gamma M}$ up to $Q^2 \leq 4.0$ (GeV/c)^2.

3. Theoretical and Experimental Issues

The electromagnetic vertex of $\gamma^* M \rightarrow \gamma$ transition is described by the structure $\epsilon_{\alpha\beta\gamma\delta}\epsilon_\alpha\epsilon'_\beta q_\gamma q'_\delta \cdot F_{\gamma^*\gamma M}$, where $\epsilon(\epsilon')$ corresponds to the polarization 4–vector of initial (final) photon. To maximize the t–channel contribution through the propagator factor $1/(t-m_\pi^2)$, one has to choose forward angles of photon scattering. If both the photons were real in this case ($q = q'$), the antisymmetric electromagnetic vertex would turn to zero. However, for the virtual Compton scattering, the electromagnetic vertex gives a factor $(q \cdot q')$ which is nonzero and large. This simple argument demonstrates an advantage of using virtual photons in studying pseudoscalar meson couplings. In the general case of non-forward photon scattering, the pseudoscalar meson poles give nonzero contributions to all four structure functions of the reaction $p(e, e'p)\gamma$.

If we choose a proton as a target, it is possible to have both π^0 and η, η' exchanges in the t–channel. One would like to separate these contributions. To do this, we can a) use the mass differences between these particles and b) take advantage of the fact that their isospins are different. On the first way, we can choose t to be low enough so that η–exchange is suppressed. Indeed, taking $|t| = m_\pi^2 \approx 0.02$ (GeV/c)^2, we estimate the η contribution to be suppressed by a factor of 15, while at $|t| = 0.15$ (GeV/c)^2 this factor is reduced to about 5. So, π^0 and η contributions can be separated measuring $|t|$ dependence of the cross section at fixed Q^2. The other way is to choose an isoscalar target (e.g., ^{4}He). In this case, π^0 exchange will be forbidden and we will observe pure isoscalar exchanges. We plan to make use of both these methods.

In the Regge limit $s >> -t$ and fixed Q^2 one can use the Regge pole analysis to treat the amplitude of virtual Compton scattering. The diffractive mechanisms become important then which can be described by a Pomeron exchange. It means that for large s and small t, we could study the $\gamma^* P \rightarrow \gamma$ vertex, where P stands for a Pomeron. Contributions of other Reggeon trajectories should be considered also. However, we need higher electron beam energies for the Regge parametrization to be valid. This question needs further study.

We plan to study the Q^2 dependence of the form factors $F_{\gamma^*\gamma M}$ at CEBAF Hall A using the standard Hall A experimental equipment. [11] The liquid hydrogen target will be exposed to the 4 GeV electron beam at luminosity $3 \cdot 10^{38}$ cm^{-2} s^{-1}. The scattered electron and the recoil proton will be detected in coincidence by two HRS. The reaction of interest is kinematically separated from the Bethe–Heitler mechanism. Possible background from electroproduction of neutral pions will be eliminated by the missing mass technique taking advantage of high momentum resolution of Hall A spectrometers. There might be complications due to multiple scattering of the recoil proton since its momenta are relatively low (400–500 MeV/c). The other way to approach low t is detection of the final photon (having 2–3 GeV energies) instead

of the proton. It will require an additional shower counter to be installed. These and other issues of the experimental procedure will be studied in detail. The next step is doing the measurements on the isoscalar nuclear target, such as ^{4}He. The measurement can be extended to higher Q^2 when the 6 GeV electron beam becomes available at CEBAF.

4. Acknowledgements

I would like to acknowledge useful discussions with S. Brodsky, L. Frankfurt, J. Goity, N. Isgur, and A. Radyushkin. My special thanks are to the CEBAF Hall A Group for their support and encouragement.

5. References

1. S. Brodsky, P. Lepage, *Phys. Rev.* **D24**, 1808 (1981);
2. S. Adler, *Phys. Rev.* **177**, 2426 (1969); J. Bell, R.Jackiw, *Nuovo Cimento* **60A**, 47 (1969).
3. *Review of Particle Properties* (1992).
4. L. G. Landsberg, *Phys. Rep.* **128**, 301 (1985).
5. H.-J. Behrend *et al.* (CELLO Collab.),*Z. Phys.***49**, 401 (1991).
6. A. S. Gorskii, *Sov. J. Nucl. Phys.* **46**, 537 (1987).
7. A. Radyushkin, *private communication.*
8. H. Ito, W. W. Buck, F. Gross, *Phys. Lett.* **B287**, 23 (1992).
9. H. Primakoff,*Phys. Rev.* **81**, 899 (1957).
10. E. Hadjimichael, S. Fallieros,*Phys. Rev.* **C39**, 1438 (1989)
11. CEBAF Letter of Intent #LOI-94/005. Co-Spokesmen: A. Afanasev, J. Gomez, and S. Nanda.

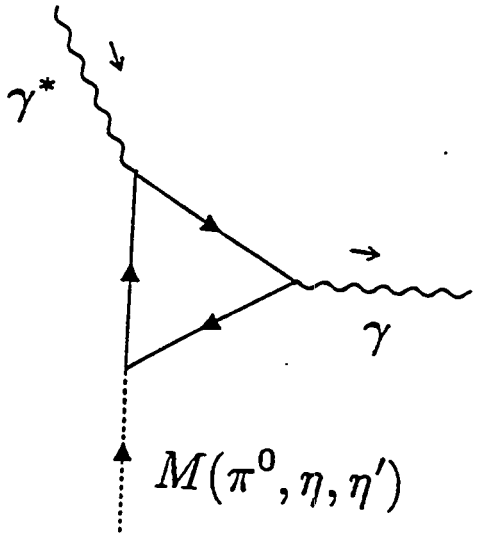


Fig. 1 The quark triangle diagram describing the $\gamma^* M \to \gamma$ transition.

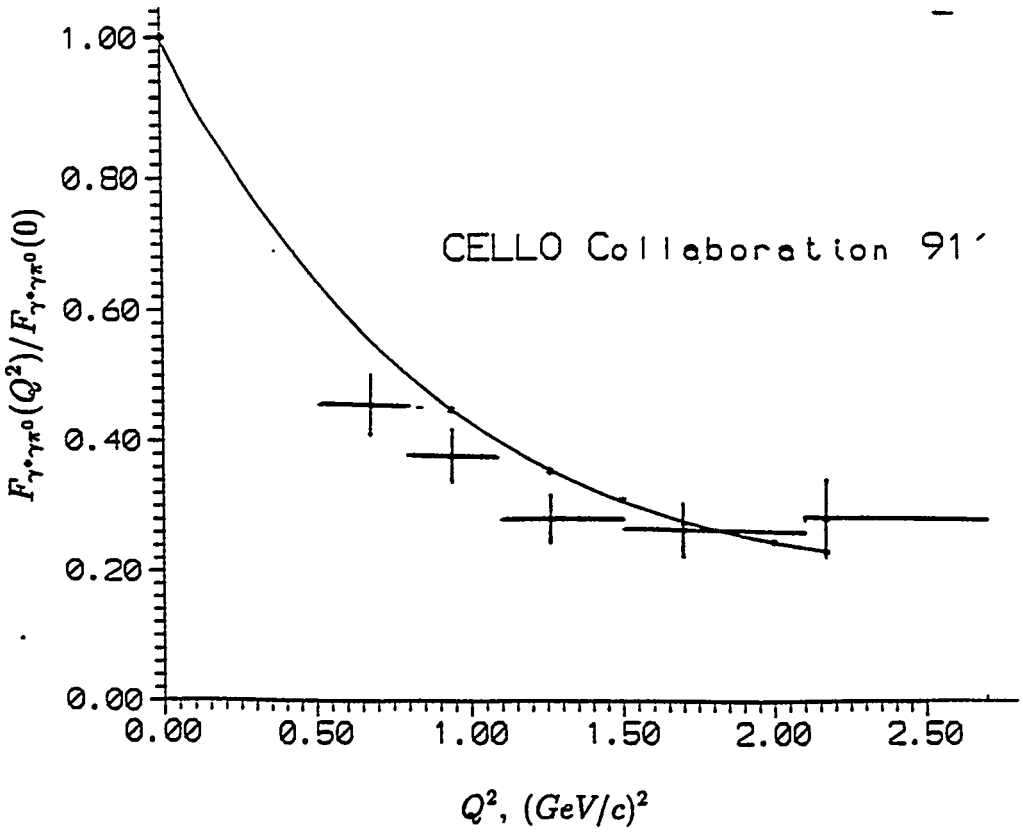


Fig. 2 Experimental data for $F_{\gamma^*\gamma\pi^0}$ form factor from Ref.[5]; the curve is the QCD sum rules calculation from Ref.[7].

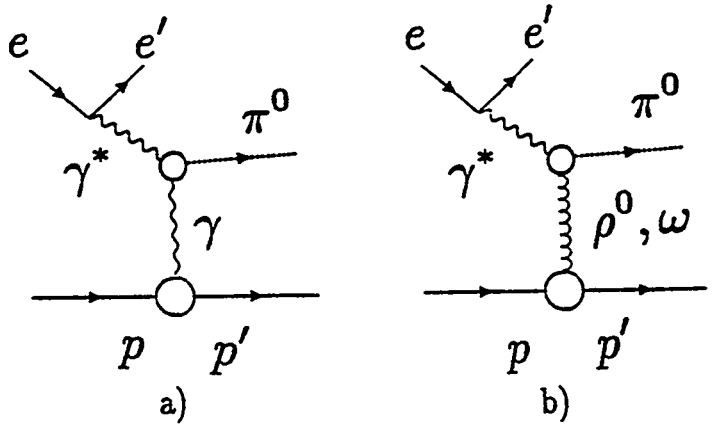


Fig. 3 a) Primakoff mechanism for the neutral pion production; b) Vector meson exchanges in the t–channel

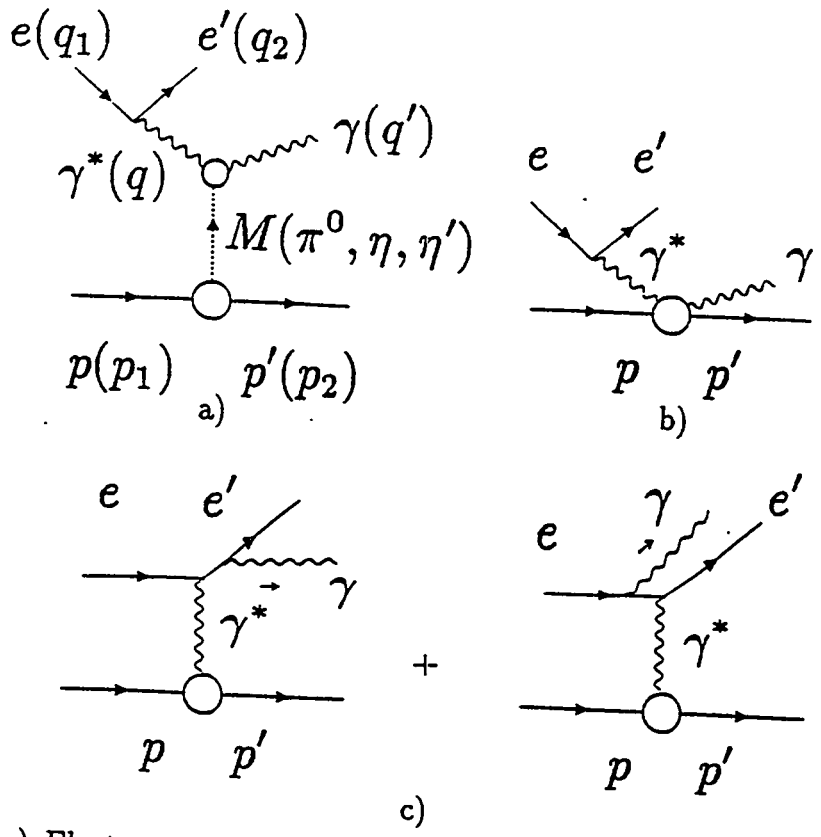


Fig. 4 a) Electromagnetic interaction of the neutral pseudoscalar meson emitted by the nuclear target; b) Virtual Compton scattering amplitude; c) Bethe–Heitler amplitude.

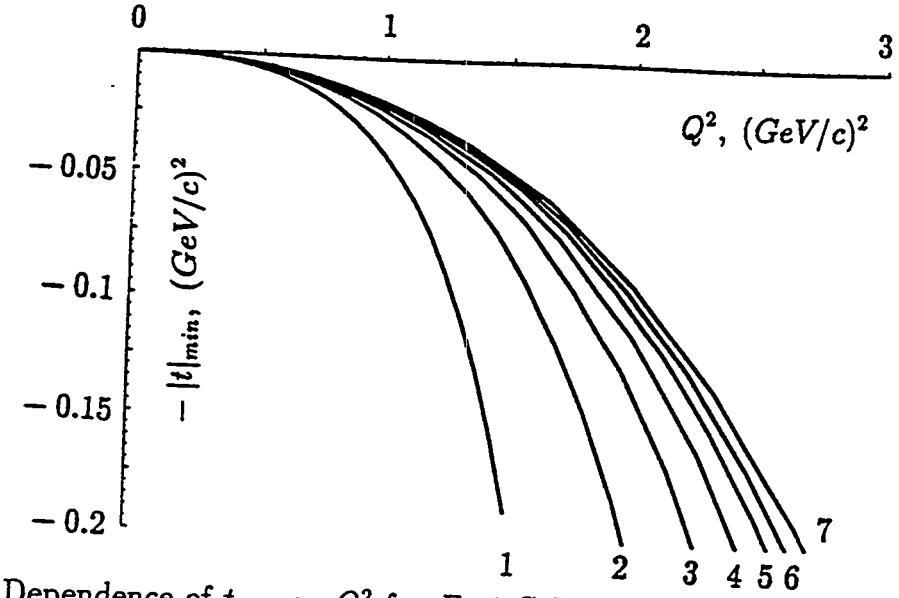


Fig. 5 Dependence of t_{min} on Q^2 for E=4 GeV as a function of electron scattering angles (proton target). The curves 1-7 correspond to the electron scattering angles 25, 35, 45, 55, 65, 75, and 90 deg.

CEBAF at Higher Energies and the Kaon Electromagnetic Form Factor

O.K. Baker, Hampton University and CEBAF

ABSTRACT

The electromagnetic production of strangeness, the physics of exciting systems having strangeness degrees of freedom (production of hadrons with one or more strange constituent quarks) using electromagnetic probes (real or virtual photons), is one of the frontier areas of research which will be investigated at the Continuous Electron Beam Accelerator Facility (CEBAF) when it becomes operational. CEBAF is expected to have an important impact upon this field of research using its specialized set of detection instruments and high quality electron beam. This paper focusses upon one aspect of the associated production of strangeness - the determination of the kaon electromagnetic form factor at high squared momentum transfers.

Single kaon electroproduction could be used to determine the kaon form factor[1-4] for spacelike values of the photon mass squared ($q^2 < 0$) where

$$q^2 = -Q^2 = (p' - p)^2 = (p'_0 - p_0)^2 - (|\mathbf{p}'| - |\mathbf{p}|)^2 \quad (1)$$

$$= -4EE'\sin^2(\theta/2). \quad (2)$$

Here E(E') is the incident (scattered) electron energy, p(p') is the electron's momentum, and θ is the scattering angle. The analysis of the data to extract the form factor requires use of the Chew-Low extrapolation procedure to be explained below. The procedure assumes that the kaon pole, in this case, dominates the virtual photoproduction cross section for small t (close to t_{min}). Here t is the momentum transfer variable $-(\gamma_v - p_K)^2$, the difference between the virtual photon's and electroproduced kaon's four momentum. If the pole in the denominator is multiplied out of the experimental cross sections, the resulting data should lie on a smooth curve which can be extrapolated to the pole position in t. This gives the residue of the pole. If the coupling constants involved are known beforehand, then the kaon form factor can, in principle, be determined[5-16].

Presented in fig. (1) is the present knowledge of the kaon form factor. The data[2] was obtained by scattering high energy kaons from atomic electrons and is confined to $Q^2 \leq 0.07(\text{Gev/c})^2$. As can be seen, only a limited region in Q^2 can be accessed in this manner. The two dased curves in the figure are from a parametrization of the form factor in the vector meson dominance model (VMD) of virtual photon scattering using rho and phi masses as indicated. This is explained in reference 1 which is the source of the figure. The VMD model of this scattering assumes that the virtual photon converts into a vector meson before interacting with the target nucleon. The full curve in the figure is from a QCD inspired model. Also indicated in fig. (1) is the region of Q^2 to be accessed by this

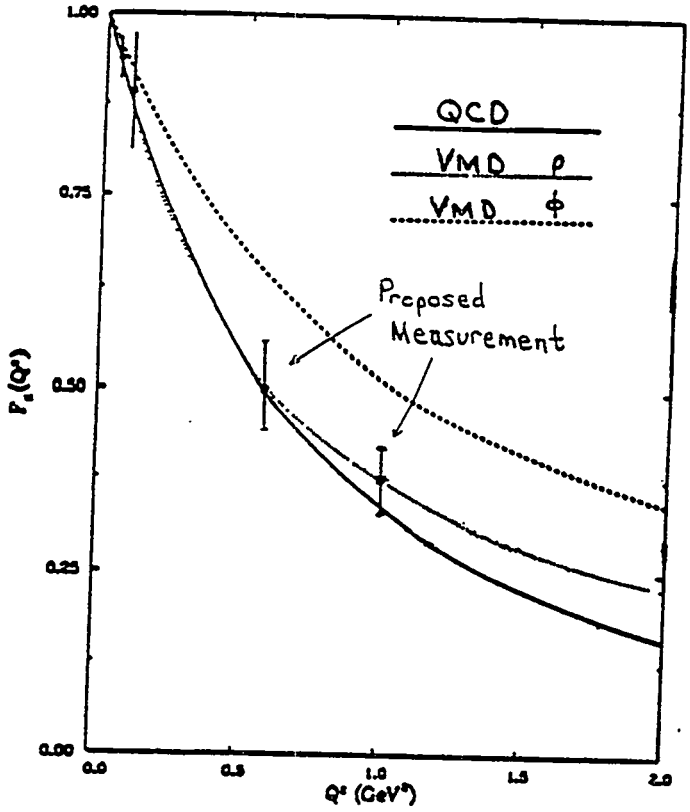


Figure 1. The kaon form factor plotted versus the momentum transfer squared. The present data extends only up to about 0.05 GeV^2/c^2. The three curves are explained in the text. This figure is taken from reference 1. Higher CEBAF beam energies would enable new data to be gathered at higher and lower Q^2.

experiment. It is proposed that the data be gathered with sufficient precision to distinguish between the various models shown. This may indicate a QCD signature in nuclear physics.

From the formulas given in the appendix of Devenish et. al., the residue of the kaon pole in the differential cross section can be calculated.

At the kaon pole, one has

$$(t-\mu^2)^2 d\sigma|_{t=\mu^2} = N(\mu^2)F_K^2(Q^2) \tag{3}$$

where

$$N(t) = (-t)8c(ge)^2(q^2\sin^2\theta(\frac{1+\epsilon\cos 2\phi}{2}) + \epsilon\frac{(|p|E_K - p_o q\cos\theta)^2}{|p|^2}) \tag{4}$$

and F_K is the kaon form factor. c depends on the normalization of the data and is given, for example, in the appendix of reference 7. g is the kaon-hyperon-nucleon coupling constant, ϕ is the azimuthal angle between the electron and hadron scattering planes, ϵ is the virtual photon polarization parameter, E_K is the kaon energy, and μ is the meson mass.

Each data point at fixed W and Q^2 will be multiplied by $(t-\mu^2)^2/N(\mu^2)$, and then the resulting points will be fit with a straight line.

An experimental program to determine, separately, the 4 terms of the cross section due to virtual photoproduction of kaons with particular emphasis on the longitudinal (σ_L) and transverse (σ_U) cross sections is ideally suited for Hall C using the High Momentum

Spectrometer (HMS) to detect the scattered electron and the Short Orbit Spectrometer (SOS) to detect, in coincidence with the HMS, the electroproduced kaon before its decay in flight[17-18]. An overview of Hall C in this mode is shown in fig. 2.

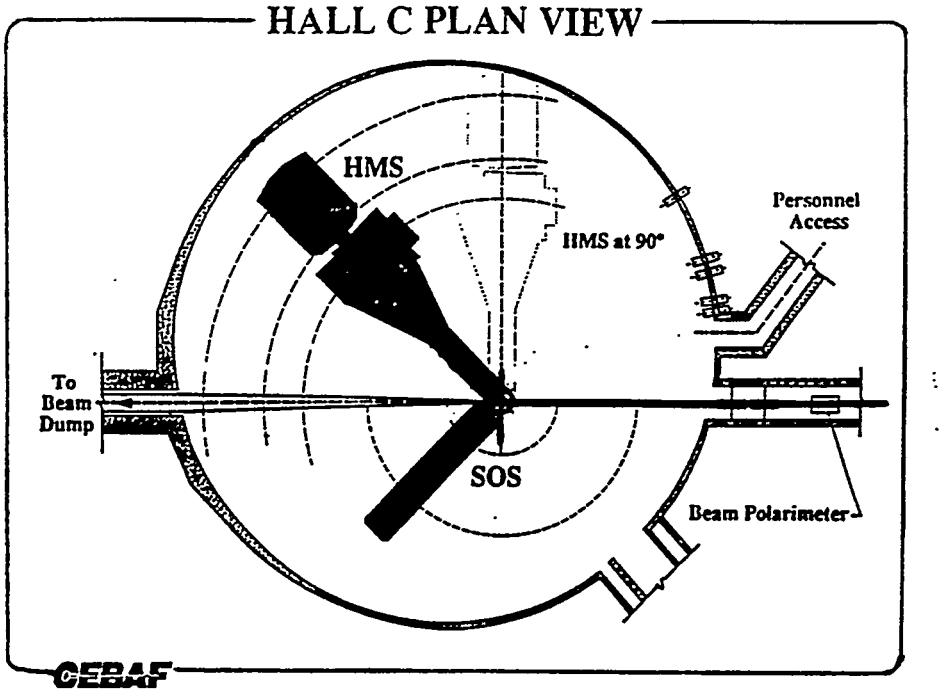


Figure 2. The Hall C setup using the HMS and SOS detectors.

So far there has been only a crude attempt[19] to separate σ_U and σ_L. This longitudinal/transverse separation will be possible with the CEBAF beam and the spectrometers in Hall C. The longitudinal cross section, σ_L is proportional to the kaon form factor. Separation of the longitudinal contribution to the cross section and therefore the determination of the kaon form factor will depend upon their relative magnitudes. (It would be more difficult to separate a very small contribution from a relatively very large contribution). Each of the terms has a small momentum transfer squared (Q^2) and angular (θ_K) dependence. These two separate contributions have not been measured accurately in the momentum transfer region of interest here. The large uncertainty in the data which exists presently don't allow too stringent a prediction to be made on their relative contributions. Nevertheless, the trend of the data of reference 19 indicates that in the region of $Q^2 \leq 4$ GeV^2/c^2, the unpolarized transverse contribution and that of the longitudinal polarized term are comparable.

Along the virtual photon direction (which is where the SOS spectrometer central axis will be positioned), the interference terms can be averaged to zero. This is due to the finite acceptance of the SOS. It will be possible, therefore, to perform the required Rosenbluth separation and single out the term due to longitudinally polarized photons in a straightforward way. This is achieved by varying the virtual photon polarization, ϵ, and simultaneously averaging over all ϕ. It is proposed to do this at Q^2 up to 2 GeV^2/c^2 with

existing CEBAF energies. Representative kinematical parameters for the separation are shown in Table I. In general, all values of ϵ between and including the ones shown in the Table are attainable.

This measurement requires that the transverse and longitudinal cross sections defined above be separated (with the interference terms averaging to zero) while keeping t and W constant (over some finite range) for each Q^2 setting. A higher incident electron beam energy would allow data to be taken for lower Q^2 points where connection to existing data is possible. Higher Q^2 data also become possible with higher CEBAF energies where more model sensitivity is present from theoretical calculations.

TABLE I
Representative Kinematic Parameters for Separation of σ_L and σ_U

Q^2	E_e	E'_e	θ_e	θ_γ	ν	W	x	ϵ
0.25	1.97	0.72	24.21	12.69	1.25	1.72	0.11	0.60
0.25	2.23	0.98	19.51	14.03	1.25	1.72	0.11	0.70
0.25	3.56	2.31	10.01	17.34	1.25	1.72	0.11	0.90
0.50	2.19	0.70	33.56	13.22	1.50	1.79	0.18	0.50
0.50	2.72	1.22	22.33	16.28	1.50	1.79	0.18	0.70
0.50	3.24	1.74	17.15	17.99	1.50	1.79	0.18	0.80
1.00	2.62	0.87	38.66	15.65	1.75	1.78	0.31	0.50
1.00	3.27	1.52	25.87	19.26	1.75	1.78	0.31	0.70
1.00	5.27	3.52	13.34	23.75	1.75	1.78	0.31	0.90
1.50	2.68	0.78	50.27	15.32	1.90	1.72	0.42	0.40
1.50	3.21	1.31	34.74	19.29	1.90	1.72	0.42	0.60
1.50	5.88	3.98	14.55	26.38	1.90	1.72	0.42	0.90
2.00	2.98	0.88	51.63	15.88	2.10	1.68	0.51	0.40
2.00	3.58	1.48	35.75	19.20	2.10	1.68	0.51	0.60
2.00	4.85	2.75	22.34	24.37	2.10	1.68	0.51	0.90

Energy in GeV; Momentum in GeV/c; Angles in Degrees

Since extraction of the kaon form factor requires a separation of longitudinal and transverse cross sections as well as a study of the t-dependence of the data, the Table shows how a higher CEBAF energy would lead to better data. The extrapolation in ϵ would be over a larger range and t_{min} would be smaller so that smaller systematic uncertainties are expected.

Future programs could possibly include a study of these separate contributions to kaon electroproduction on heavy nuclei[20-21]. Differences between these separate terms for bare protons and those embedded in a nuclear medium may then be observed.

To summarize, the use of CEBAF at higher energies (up to 6 GeV) using the spectrometers which currently exist in Hall C - the HMS for electron detection and the SOS

for kaon detection (and possibly the converse of this at the higher energies) impacts three areas in the determination of the kaon electromagnetic form factor:

1. Data can be collected for lower Q^2 (≈ 0.2 (GeV/c)^2)
2. Data can be collected at higher Q^2 (≈ 3.0 (GeV/c)^2)
3. Improved systematic errors on existing proposed Q^2 range ($0.5 \leq Q^2 \leq 2.0$ (GeV/c)^2)

This work is supported by the Department of Energy award DE-FG05-91ER40620.

References

1. C. Ji and R. Cotanch, Phys. Rev. D 41, 2319 (1990).
2. S. R. Amendolia et. al., Phys. Lett. B 178, 435 (1986).
3. F. Felicetti and Y. Srivastava, Phys. Lett. 107B, 227 (1981).
4. M. Lutz and W. Weise, Nucl. Phys. A518, 156 (1990).
5. E. Amaldi et. al., **Pion Electroproduction**, Springer-Verlag Publishing Co., N. Y. (1979).
6. C. W. Akerlof et. al., Phys. Rev. D16, 147 (1966).
7. R. C. E. Devenish and D. H. Lyth, Phys. Rev. D5, 47 (1972).
8. F. Gutbrod and G. Kramer, Nucl. Phys. B49, 461 (1972).
9. C. N. Brown et. al., Phys. Rev. D 8, 91 (1973).
10. R. H. Dalitz and D. R. Yennie, Phys. Rev. 105, 1598 (1957).
11. W. Frazer, Phys. Rev. 115, 1763 (1959).
12. C. W. Akerlof et. al., Phys. Rev. 163, 1482 (1967).
13. L. Hand, Phys. Rev. 129, 1834 (1963).
14. F. A. Berends and G. B. West, Phys. Rev. 188, 2538 (1969).
15. F. A. Berends, Phys. Rev D1, 2590 (1970).
16. C. J. Bebek et. al., Phys. Rev. D 17, 1693 (1978).
17. CEBAF Conceptual Design Report, (1990).
18. C. Yan et. al., HMS Users Manual, CEBAF (1991).
19. C. J. Bebek et. al., Phys. Rev. D 15, 3082 (1977).
20. S. R. Cotanch and S. S. Hsiao, Nucl. Phys. A 450, 4192 (1986).
21. T. W. Donnelly, CEBAF Summer Workshop (1984).

PROSPECTS FOR MEASURING G_{M_N} IN CLAS WITH HIGHER CEBAF BEAM ENERGIES

W. BROOKS
CEBAF
Newport News, VA 23601, USA

ABSTRACT

The possibility exists for extending a planned measurement of the neutron magnetic form factor to higher values of momentum transfer. The theoretical interest and the experimental method are described. Problems associated with higher Q^2 measurements are discussed. It is concluded that measurements of moderate precision may be possible up to a Q^2 of 8-9.5 GeV^2, more than doubling the range of the data currently available.

1. Introduction

The structure of the proton and neutron at small distance scales is one of the most fundamental issues in high energy nuclear physics. Electron elastic scattering provides the most direct measurement of the electromagnetic charge and current distributions in the nucleon ground state. These may be expressed by the Sachs form factors $G_E(Q^2)$ and $G_M(Q^2)$.

In general the proton form factors are better known than those of the neutron. The proton magnetic form factor has been measured with high accuracy[1] up to Q^2=9 GeV^2. Although the proton electric form factor data at higher Q^2 are currently less accurate than those for the magnetic form factor, improved measurements are planned at CEBAF[2]. For the neutron $G_E(Q^2)$ is quite small for values of Q^2 in the few GeV^2 range, and the scattering is dominated by $G_M(Q^2)$. Historically the data from different measurements of the neutron magnetic form factor have been somewhat inconsistent; the dominant errors are typically systematic. A survey of common experimental approaches has been published[3]. There have been several recent precision determinations of $G_{M_n}(Q^2)$ for Q^2 <1 GeV^2 using exclusive measurements[4]. The only existing high-quality data at higher Q^2 are the NE11 inclusive data from SLAC[5], which extend to Q^2=4 GeV^2. Most of the recent data at higher Q^2 is plotted in Fig. 1; the uncertainties shown are systematic errors.

Theoretical calculations have been performed in a variety of frameworks to describe nucleon form factor data. Models based on vector meson dominance were historically the first moderately successful approaches. Quark dimensional scaling and PQCD have been used to predict the high Q^2 behavior. Constituent quark model calculations now exist within a variety of formalisms which describe the form factor data with varying degrees of success. At least one QCD lattice calculation in the quenched approximation has been performed[6]; in the next few years one may hope that more

precise lattice QCD calculations will become available which will have calculational uncertainties comparable to the accuracy of the experimental data.

In addition to the lattice calculation, a second category of QCD calculations have been performed[7]. In this method, QCD sum rules based on quark-hadron duality are used to calculate the soft nonperturbative contribution to the nucleon form factors. Only the contribution from the lowest order scattering diagram was included. The prediction reproduces the proton data fairly well at Q^2 >5 GeV^2; it is expected that the calculation will converge to the data at sufficiently high Q. In the neutron data a trend toward convergence between the calculation and the data is seen, but the data does not extend to sufficiently high Q^2 to test this interesting calculation in the lower portion of the transition region between the confinement regime and PQCD.

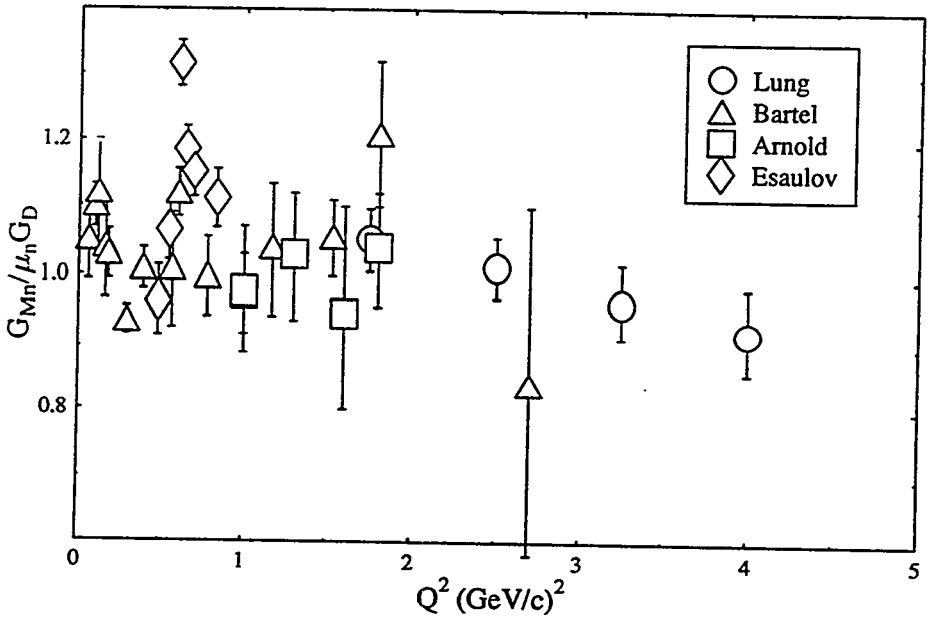


Fig. 1. Existing G_{M_n} data at higher momentum transfer.

2. Experimental Method

Recently a CEBAF proposal was approved to measure $G_{M_n}(Q^2)$ using the CLAS in Hall B[8]. This is a precision measurement which spans the entire range in Q^2 of 0.3 to 5 GeV^2. Due to the large acceptance of the spectrometer the data is acquired over a broad range in scattering angle and momenta simultaneously, and so a continuous coverage in Q^2 is achieved with only two beam energy settings. At E_{beam}=2.4 GeV with outbending electrons, coincidence measurements down to Q^2=0.3 GeV^2 are possible. With a beam energy of 4.0 GeV and the opposite field polarity, measurements up to Q^2=5 GeV^2 are feasible with a few hundred hours of running. Under these conditions the limitation in accuracy at higher Q^2 is due to statistical errors, not systematic errors, and the detector acceptance does not extend beyond this kinematic

point.

The approach taken here is designed to minimize systematic errors due both to experimental problems and theoretical issues. The method consists of comparing the ratio of the e-n differential cross section to the e-p differential cross section for quasielastic kinematics using a deuterium target. The neutron magnetic form factor is then extracted using the much better known proton form factors. The higher momentum neutrons will be detected with high efficiency with the CLAS electromagnetic shower calorimeter (see Fig. 2). Lower momentum neutrons may be identified in the time-of-flight scintillators. While the neutron detection efficiency is much lower for these scintillators, the rate of low-momentum neutrons is much higher and the efficiency is nearly independent of neutron momentum in the range of interest.

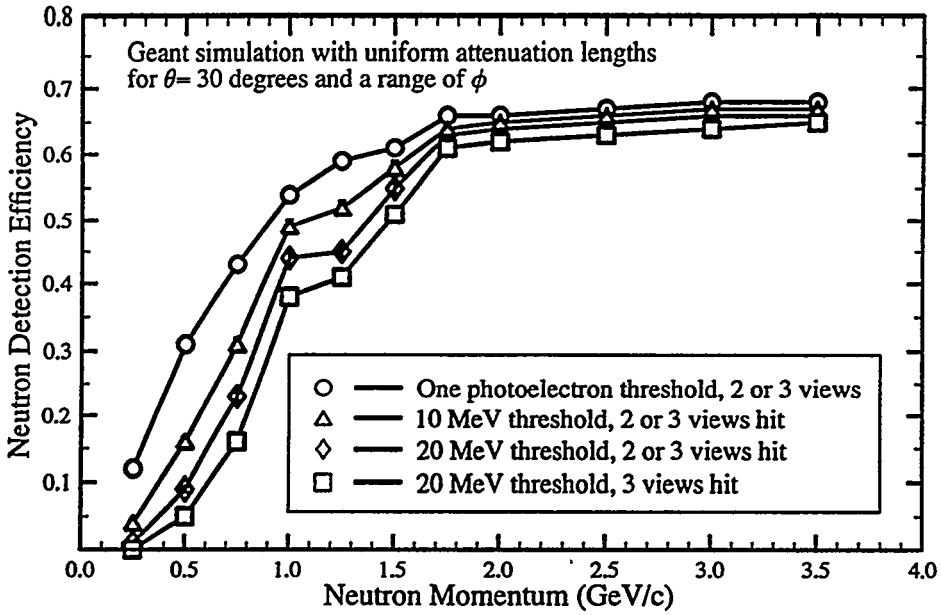


Fig. 2. Neutron detection efficiency in the electromagnetic shower calorimeter.

The strategy of measuring the quasielastic ratio in deuterium has been used previously at lower energies[3,4]. It has the experimental advantage that the luminosity does not enter into the measurement, and the theoretical advantage that final state interactions, meson exchange currents, isobar configurations, and relativistic effects on this ratio are small especially at larger momentum transfer[8,9]. In addition, a number of radiative processes are the same for both proton and neutron, reducing sensitivity to radiative correction errors particularly at higher Q^2.

The typical dominant error in this method is the measurement of the neutron detection efficiency. This problem is dealt with in the CLAS by exploiting its high efficiency for identifying multiparticle final states. Two targets are used simultaneously. Events originating from different targets are identified via ray tracing; a vertex resolution along the beam axis of better than 3 mm is expected, allowing the two targets to be quite close together. In this scheme, one target is deuterium for the

quasi-elastic data and the other is a hydrogen target. The neutron detection efficiency is monitored continuously via the reaction $ep \rightarrow en\pi^+$ from the latter target. The neutron is tagged via the electron-pion coincidence; in addition, the scattering angle of the neutron is identified with an accuracy of up to a tenth of a degree, and the neutron momentum is determined. Since this is a high rate reaction the statistical error incurred is minimal, and sensitivity to such systematic errors as time dependence and rate dependence of phototube gains is completely eliminated since the calibration data and quasielastic data are taken simultaneously. The largest residual systematic error in determining the neutron detection efficiency is due to the calibration target being at a slightly different position from the deuterium target; this effect is minimized by choosing a target length and separation distance which is negligible compared to the 5 meter distance between either target and the electromagnetic calorimeter.

3. Implications of Higher Beam Energy

3.1. Acceptance and Statistics

The primary advantage which would be obtained from higher incident beam energy is that the Q^2 acceptance limit of the spectrometer increases significantly. This may be parameterized in a simple way by the ratio of beam energy to the practical spectrometer Q^2 acceptance limit. This function is plotted in Fig. 3. It may be seen for example that the Q^2 acceptance limit of the spectrometer is expected to exceed 9 GeV^2 for a beam energy of 8 GeV for quasielastic scattering from deuterium.

With no cuts the statistical error on G_{M_n} for a few hundred hours of running at 8 GeV is still only about 7% at a Q^2 of 9.5 GeV^2 for 4% Q^2 bins, improving at lower Q^2. It is however necessary to consider certain of the systematic errors which grow with beam energy in order to gain an overall picture of the quality of the measurement.

3.2. Sources of Experimental Uncertainty

The two largest systematic uncertainties at high Q^2 are the suppression of the inelastic background and the uncertainty in G_{M_p}. The latter error enters in a ratio of 1:1 for the higher values of Q^2. The quoted systematic errors on the recent SLAC measurements of G_{M_p} are at the level of a few percent.

Suppression of the inelastic background is likely to be the largest systematic error at higher Q^2. Several factors contribute to this effect; although the neutron angular resolution improves slightly at higher momentum, the momentum resolution of the electron and proton worsens, decreasing the capacity to resolve quasielastic events from inelastic events. The quasielastic cross section drops rapidly with increasing momentum transfer while the nonresonant inelastic background does not, so that the intrinsic signal-to-noise ratio becomes less favorable. Because the method relies on a ratio of neutron events to proton events, it is critical to ensure that the cuts on the proton and neutron are made in an identical way and on simple spectra which are straightforward to interpret. Four cuts on the data will be employed. First, fiducial cuts will be made on the electron angle to eliminate edge effects in the detectors.

Second, a cut on the angle between the nucleon and the virtual photon will strongly select quasielastic kinematics over resonance production kinematics. Third, a single arm missing mass cut will reduce inelastic reactions somewhat further. Finally, a "multiparticle cut" will identify and discard events which have more than one hadron in the final state, further reducing the inelastic background which is predominantly single pion production. This cut makes good use of the high acceptance of CLAS for multiparticle final states.

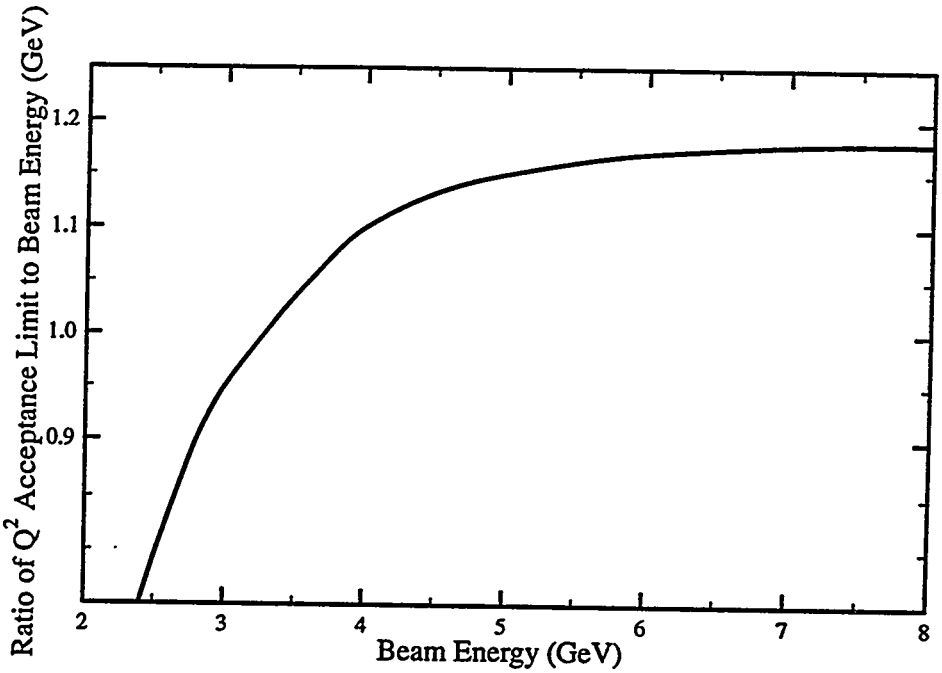


Fig. 3. Ratio of Q^2 acceptance limit to beam energy in CLAS.

Fig. 4 shows the expected single arm missing mass spectrum with the other three cuts applied for a beam energy of 4 GeV and $Q^2 = 4$ GeV^2. It is seen that the signal-to-background ratio is kept to a manageable level at least for these kinematics. This simulation may be tested with measured data in several ways. For higher momentum transfer it is likely that the systematic errors due to this effect may be kept below the 5-7% level; further study through detailed simulation is required to determine these uncertainties accurately.

4. Summary

It is likely that the currently planned precision measurement of G_{M_n} in the range Q^2=0.3-5.0 GeV^2 may be extended to a moderate precision measurement at higher momentum transfer if higher beam energies become available. The leading systematic errors would be suppression of inelastic background, uncertainty in G_{M_p}, and the neutron detection efficiency. The acceptance limit for a beam energy of 8 GeV is Q^2=9.5 GeV^2, and at this energy a statistical error of 7-8% could be attained in a few hundred hours of running at a luminosity of $10\text{x}10^{33}$ s^{-1}cm^{-2}. The existence

of data at these momentum transfers would more than double the current range of data available and would provide a test of constituent quark models and QCD-based calculations in the higher-energy domain of the confinement regime.

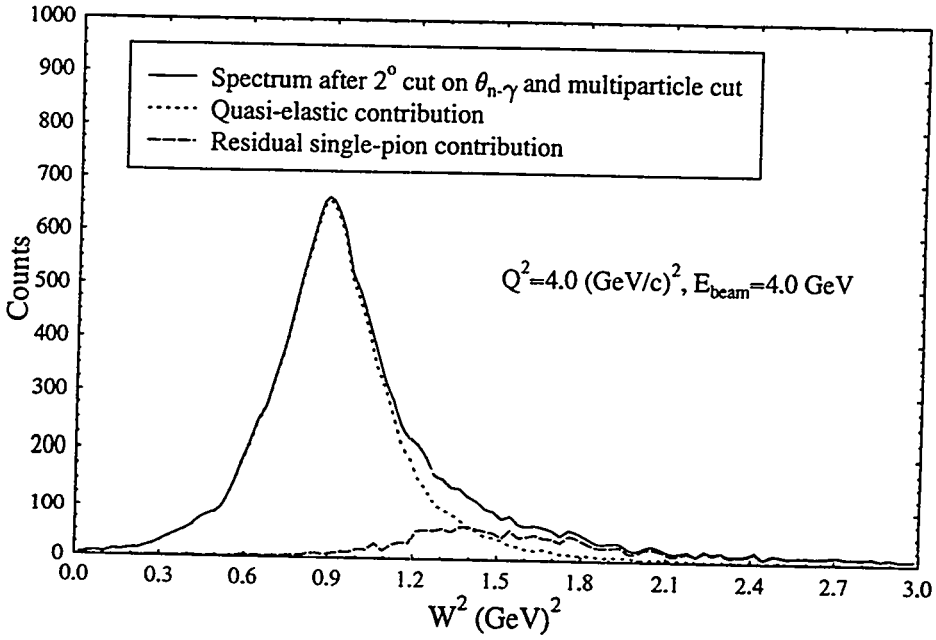


Fig. 4. Effect of cuts on single arm missing mass spectrum (see text).

5. Acknowledgements

The author would like to thank M. Vineyard of the University of Richmond (co-spokesperson of CEBAF proposal PR-94-017) for providing simulation results, and B. A. Mecking for many useful discussions and simulation results.

6. References

1. P. E. Bosted *et al.*, *Phys. Rev. Lett.* **68** (1992) 3841.
2. C. F. Perdrisat (spokesperson) CEBAF E-93-027.
3. I. Sick, Proc. of Sixth Amsterdam Mini-Conference (1989) p. 193.
4. F. C. P. Joosse, Ph. D. thesis, Utrecht (1993); J. Jourdan and F. Klein, Proc. of Few Body XIV Conf. (1994).
5. A. Lung *et al.*, *Phys. Rev. Lett.* **70** (1993) 718.
6. W. Wilcox, T. Draper, and K. F. Liu, *Phys. Rev* **D46** (1992) 1109.
7. V. A. Nesterenko and A. V. Radyushkin, *Phys. Lett.* **128B**, (1983) 439.
8. W. K. Brooks and M. F. Vineyard (spokespersons) CEBAF E-94-017.
9. H. Arenhoevel, private communication.

THE CHARGE FORM FACTOR OF PSEUDOSCALAR MESONS IN A RELATIVISTIC CONSTITUENT QUARK MODEL*

F. CARDARELLI, E. PACE
Department of Physics, University of Rome "Tor Vergata" and INFN Sezione Tor Vergata, Via della Ricerca Scientifica, I-00133 Roma, Italy

I.L. GRACH, I.M. NARODETSKII
Institute of Theoretical and Experimental Physics Moscow 117259, Russia

G. SALMÈ, S. SIMULA
Istituto Nazionale di Fisica Nucleare, Sezione Sanità Viale Regina Elena 299, I-00161 Roma, Italy

ABSTRACT

The charge form factor of pseudoscalar mesons has been investigated in the light-cone formalism, up to Q^2 relevant to CEBAF energies. The consequences of adopting the meson wave functions generated through the Godfrey-Isgur $q\bar{q}$ potential, which reproduces the mass spectra, are discussed.

1. Light-cone formalism

The charge form factor of pseudoscalar (S-wave) mesons, as well as the axial-vector weak decay constant, are analyzed using the wave function obtained within the relativized constituent quark model of ref. [1], which properly describes meson (and baryon) mass spectra in terms of an effective $q\bar{q}$ interaction composed by a one-gluon-exchange term and a linear confining potential. The relativistic effects on electroweak properties have been taken into account by adopting the light-cone formalism[2-4], which is the natural framework for constructing a relativistic quark model featuring the dominance of the $q\bar{q}$ component of mesons[5]. Within such a scheme the high momentum components, generated in the meson wave function by the one-gluon-exchange term, sharply affect both the charge form factor and the weak decay constant, and an agreement with existing experimental data can be achieved by introducing an effective axial-vector coupling constant and a charge form factor for the constituent quark[4].

The light-cone wave functions are eigenfunctions of the mass operator

$$M = M_0 + V = \sqrt{m_q{}^2 + k^2} + \sqrt{m_{\bar{q}}^2 + k^2} \; + \; V \tag{1}$$

*Presented by G. Salmè

where V is a Poincaré invariant interaction term, m_q ($m_{\bar{q}}$) the constituent quark (antiquark) mass and $k^2 = k_\perp^2 + k_n^2$. The longitudinal momentum k_n is defined as

$$k_n = (\xi - \frac{1}{2})M_0 + \frac{m_{\bar{q}}^2 - m_q^2}{2M_0} \tag{2}$$

and the intrinsic light-cone variables $\vec{k}_\perp$ and ξ are

$$\xi = p_q^+/P^+ = 1 - p_{\bar{q}}^+/P^+ \qquad \vec{k}_\perp = \vec{p}_{q\perp} - \xi\vec{P}_\perp = -\vec{p}_{\bar{q}\perp} + (1-\xi)\vec{P}_\perp \tag{3}$$

In Eq. (3) $\vec{P} \equiv (P^+, \vec{P}_\perp) = \vec{p}_q + \vec{p}_{\bar{q}}$ is the total light-cone momentum of the meson and $\vec{p}_q(\vec{p}_{\bar{q}})$ the corresponding one of the quark (antiquark).

Following the Brodsky-Huang-Lepage prescription [6], the meson radial wave function $w(k^2)$ (see Eq. (7) of ref. [4]) is identified with the equal-time radial wave function in the meson rest-frame. This wave function has been obtained by introducing in the mass operator of Eq.(1), after a Melosh rotation, the effective $q\bar{q}$ Hamiltonian proposed by Godfrey and Isgur (GI)[1] for the description of meson mass spectra, viz.

$$\left[\sqrt{m_q^2 + k^2} + \sqrt{m_{\bar{q}}^2 + k^2} + V_{q\bar{q}}\right]\ w(k^2)|00\rangle\ =\ M_{q\bar{q}}\ w(k^2)|00\rangle \tag{4}$$

where $M_{q\bar{q}}$ is the meson mass, $|00\rangle = \sum_{\nu\bar{\nu}}\langle\frac{1}{2}\nu\frac{1}{2}\bar{\nu}|00\rangle\chi_\nu\chi_{\bar{\nu}}$ is the equal-time spin factor and $V_{q\bar{q}}$ is the effective $q\bar{q}$ potential, which in the GI scheme is composed by a one-gluon-exchange term (dominant at short separations) and a flavour-independent linear-confining term (dominant at large separations). In order to analyze the effects of different terms of the GI $q\bar{q}$ interaction, two other choices of $w(k^2)$ will be considered; the first one is the solution of eq. (4) obtained after switching off the one-gluon-exchange part of the GI $V_{q\bar{q}}$, whereas the second choice is given by the solution of eq. (4) where only the spin-independent part of the one-gluon-exchange interaction is retained. The three different forms of $w(k^2)$, denoted hereafter by $w_{(GI)}$, $w_{(conf)}$ and $w_{(si)}$, are compared in Fig. 1 for the pion: it can be seen that $w_{(GI)}$ is characterized by high momentum components ($k > 0.5\ GeV/c$), which are totally absent in $w_{(conf)}$, whereas the effects of the spin-spin part of the one-gluon-exchange interaction strongly modifies the wave function at $k > 1\ GeV/c$. It is worth noting that the mass eigenvalues corresponding to $w_{(conf)}$ and $w_{(si)}$ sharply differ from the one corresponding to $w_{(GI)}$, e.g. for the pion the eigenvalue becomes $1.24\ GeV$ for $w_{(conf)}$, $.655\ GeV$ for $w_{(si)}$ and $.149\ GeV$ for $w_{(GI)}$, respectively.

2. Numerical calculation

Before calculating the charge form factor, we have computed the axial-vector weak decay constant of pseudoscalar mesons, f_A^{PS}, (which yields information on the wave function at the origin) in the light-cone approach of ref. [3] and introducing an axial-vector coupling constant of the constituent quark, $g_A^q(0)$ [4]. The results

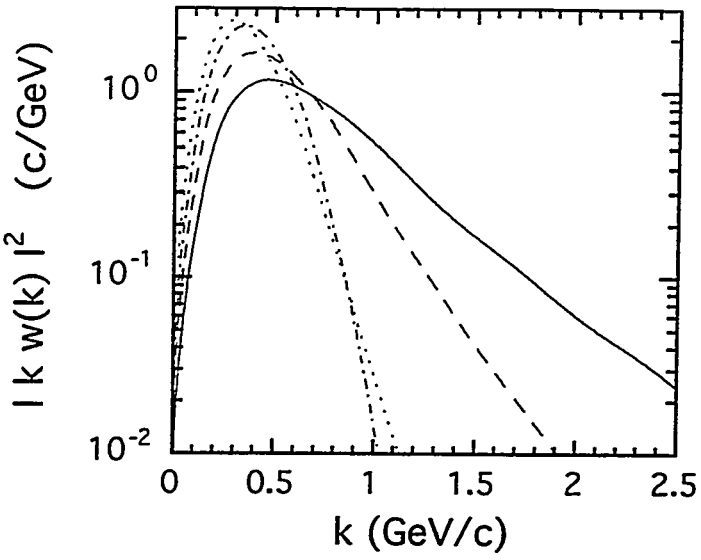


Fig. 1. The function $|k \cdot w(k^2)|^2$ for the pion versus the internal momentum k. Dot-dashed line: gaussian-like wave function of ref. [3]. Dotted line: $w_{(conf)}$ obtained using only the confinement part of the $q\bar{q}$ interaction of ref. [1]. Dashed line: $w_{(si)}$ obtained neglecting the spin-spin part of the $q\bar{q}$ interaction of ref. [1]. Solid line: $w_{(GI)}$ obtained using the full $q\bar{q}$ interaction of ref. [1]. After ref. [4].

are reported in Table 1, where it can be seen that, in presence of hard constituent quarks, a reasonable agreement both with the experimental data and the lattice QCD calculations can be obtained for all the considered pseudoscalar mesons by choosing $g_A^q(0) \neq 1$ and flavour independent (in Table 1 the value $g_A^q(0) = 0.726$ has been chosen in order to reproduce the central value of the experimental data for f_A^π).

Table 1. Axial - vector weak decay constant f_A^{PS} for various pseudoscalar mesons and different values of the axial - vector weak coupling constant $g_A^q(0)$ of the constituent quark. Experimental data and lattice QCD calculations are also shown. After ref.[4].

	conf	*GI*	*GI*		
meson	$g_A^q = 1$	$g_A^q = 1$	$g_A^q = 0.726$	*lattice QCD*	*exp. data*
π	91.2	127.3	92.4		92.4±0.2. [7]
K	108.6	159.9	116.1	107±7 [8]	113.4±1.1 [7]
D	124.4	215.3	156.3	156±9 [9] 147±8 [10] 154±7 [8]	<219 [7]
D_s	142.1	252.8	183.5	163±7 [10] 170±7 [8]	
B	101.3	184.1	133.6	141±16 [9] 132±9 [10]	
B_s	116.8	220.6	160.1	146±7 [10]	

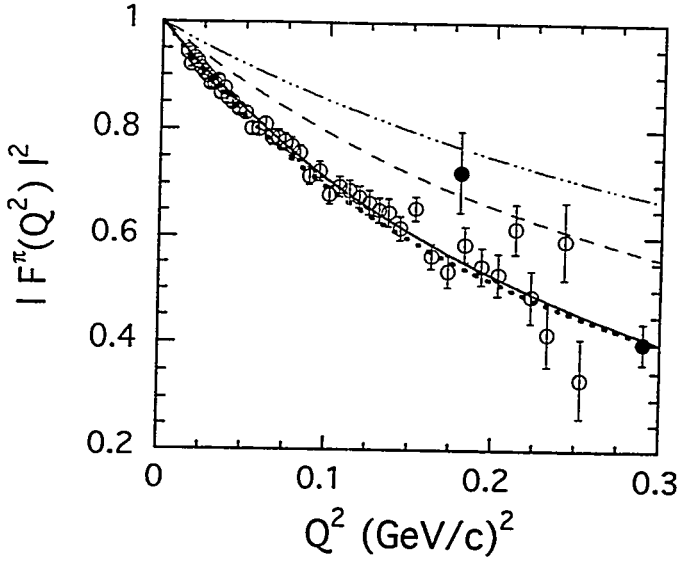


Fig. 2. The square of the charge form factor of the pion at low values of the four-momentum transfer. The dotted, dashed and dot-dashed lines are obtained using the wave functions $w_{(conf)}$, $w_{(si)}$ and $w_{(GI)}$, respectively, and adopting $F^q = 1$. The solid line is obtained using $w_{(GI)}$ and the monopole form for F^q with $< r^2 >_q$=(0.48 fm)^2, see text. Experimental data are from refs. [12a] (open dots) and [12b] (full dots). After ref. [4]

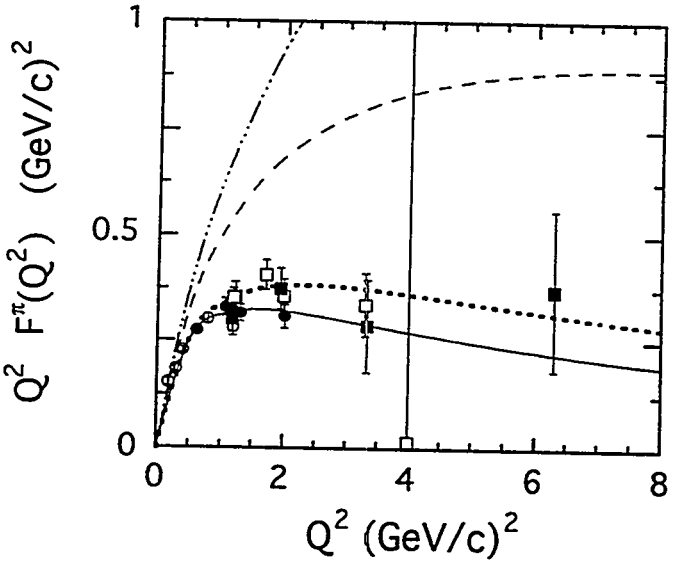


Fig. 3. The charge form factor of the pion versus Q^2. The dotted, dashed and dot-dashed lines are obtained using the wave functions $w_{(conf)}$, $w_{(si)}$ and $w_{(GI)}$, respectively, and adopting $F^q = 1$. The solid line is obtained using $w_{(GI)}$ and the monopole form for F^q with $< r^2 >_q$=(0.48 fm)^2, see text. Experimental data are from refs. [12a] (open dots), [12b] (full dots), [12c] (open squares) and [12d] (full squares). After ref. [4]

It should be pointed out that our results for the ratios $f_A^{D_s}/f_A^D$ and $f_A^{B_s}/f_A^B$ are 1.17 and 1.20, respectively, in good agreement with the corresponding predictions 1.21 ± 0.06 and 1.22 ± 0.02 obtained from QCD sum rules[11].

Let us now investigate the sensitivity of the charge form factor to soft and hard constituent quarks. Following refs. [2-3] and introducing a charge form factor of the constituent quark $F^q(Q^2)$, one gets

$$F^{PS}(Q^2) = e_q F^q(Q^2) H(Q^2, m_q, m_{\bar{q}}) + e_{\bar{q}} F^{\bar{q}}(Q^2) H(Q^2, m_{\bar{q}}, m_q) \qquad (5)$$

where e_q is the charge of the constituent quark and $H(Q^2, m_1, m_2)$ is given by Eq.(15) of ref.[4]. The results for F^π, obtained by using the wave functions $w_{(GI)}$, $w_{(conf)}$ and $w_{(si)}$ and $F^q = 1$ (as for the current quarks) are compared in Fig. 2 at low Q^2 and in Fig.3 in the whole range of the existing experimental data[12]. It can be seen that the pion form factor is strongly affected by hard constituent quarks both at low and high Q^2 and that the theoretical predictions based on soft constituent quarks only ($w_{(conf)}$) compare favourably with the experimental data for values of Q^2 up to several $(GeV/c)^2$, in agreement with the results of refs. [2,3]. From Fig. 2 it is also clear that the pion charge radius $< r^2 >_\pi \equiv -6(dF^\pi/dQ^2)_{Q^2=0}$ is strongly underestimated when the full GI $q\bar{q}$ potential is considered. Let us introduce a simple monopole form factor for the constituent quark, $F^u = F^d = 1/(1+Q^2 < r^2 >_q /6)$, and fix $< r^2 >_u = < r^2 >_d = (0.48\ fm)^2$ in order to reproduce the experimental value ($< r^2 >_\pi^{exp} = (0.660 \pm 0.024\ fm)^2$ [12e]) of the pion charge radius. It can be clearly seen from Figs. 2-3 that a single phenomenological form factor of the constituent quark is able to bring theoretical predictions, based on the full GI $q\bar{q}$ interaction, in agreement with the experimental data for values of Q^2 up to several $(GeV/c)^2$.

For the kaon charge form factor we have assumed a flavour independent form factor of the constituent quark, i.e. $F^u = F^d = F^s$, and we have adopted the monopole form with $< r^2 >_q = (0.48\ fm)^2$ (i.e., the same charge radius for the constituent quark used for the pion). When the full GI $q\bar{q}$ interaction is considered, one gets a K^+ charge form factor and a K^0 charge radius essentially in agreement with existing experimental data[4]. In Fig.4 the charge form factor of the kaon obtained by using $w_{(GI)}$ and the monopole form factor of the constituent quark is presented. It should be pointed out that experimental data of the same quality as those of the pion (for low and intermediate values of Q^2), are necessary in order to reliably check different theoretical predictions.

The extension of our calculations to the electroweak properties of the nucleon and, for the meson sector, the comparison of theoretical predictions with precise experimental data in a wide range of Q^2 for charge as well as transition form factors (as planned at CEBAF) should allow to check in more detail the hypotheses underlying our investigation.

3. References

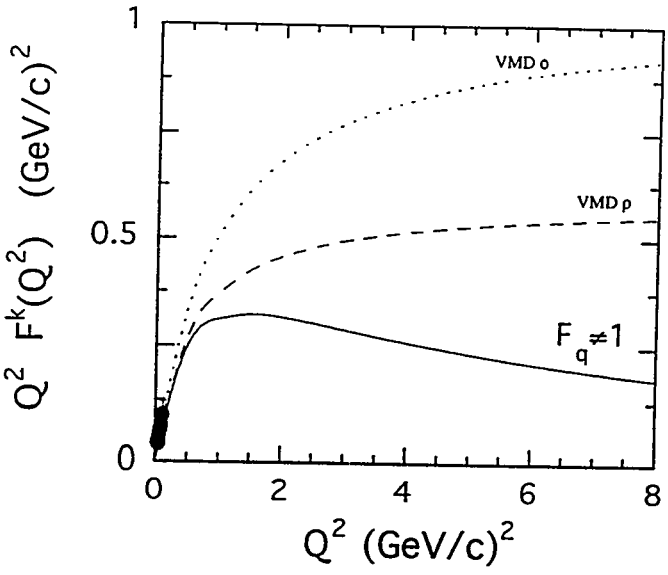


Fig. 4. The charge form factor of the kaon versus Q^2. The solid line is obtained using $w_{(GI)}$ and the monopole form for F^q with $< r^2 >_q =$ (0.48 fm)^2, see text. Experimental data are from ref. [13]. Curves corresponding to a simple Vector Dominance Model are also shown:dotted line:ϕ-meson,dashed line:ρ-meson. (cfr. ref.[14]).

1. S. Godfrey and N. Isgur: Phys. Rev. **D32** (1985) 185; S. Capstik and N. Isgur: Phys. Rev. **D39** (1986) 2809.
2. P.L. Chung, F. Coester and W.N. Polyzou: Phys. Lett. **B205** (1988) 545.
3. W. Jaus : Phys. Rev. **D41** (1990) 3394; W. Jaus and D. Wyler : Phys. Rev. **D41** (1990) 3405; W. Jaus : Phys. Rev. **D44** (1991) 2851.
4. F. Cardarelli et al.:Phys. Lett. B, in press and references quoted therein.
5. L.L. Frankfurt and M.I. Strikman: Phys. Rep. **76** (1981) 215.
6. S.J. Brodsky, T. Huang and G.P. Lepage: in Particles and Fields, edited by A.Z. Capri and A.N. Kamal (Plenum, New York, 1983), p.143.
7. Particle Data Group, K. Hikasa et al.: Phys. Rev. **D45** (1992) VII.1.
8. A. Abada et al.: Nucl. Phys. **B376** (1992) 172.
9. UKQCD Collaboration: Nucl. Phys. **B30** (Proc. Suppl.) (1993) 461.
10. C. Bernard et al.: Nucl. Phys. **B30** (Proc. Suppl.) (1993) 465.
11. C.A. Dominguez and N. Paver : Phys. Lett. **B318** (1993) 629.
12. a) C.N. Brown et al.: Phys. Rev. **D8** (1973) 92; b) C.J. Bebek et al.: Phys. Rev. **D9** (1974) 1229; c) C.J. Bebek et al.: Phys. Rev. **D13** (1976) 25; d) C.J. Bebek et al.: Phys. Rev. **D17** (1978) 1693; e) S.R. Amendolia et al.: Phys. Lett. **146B** (1984) 116.
13. a) S.R. Amendolia et al.: Nucl. Phys. **B277** (1986) 168; b) S.R. Amendolia et al.: Phys. Lett. **146B** (1984) 116; c) S.R.Amendolia et al.: Phys. Lett. **178B** (1986) 435; d) E.B. Dally et al.: Phys. Rev. Lett. **45** (1980) 232.
14. C.R. Ji and S.R. Cotanch: Phys. Rev. **D37** (1990) 2319.

THE BLOOM-GILMAN DUALITY AND LEADING LOGARITHMS*

Carl E. Carlson[a] and Nimai C. Mukhopadhyay[b]

[a] *Physics Department, College of William and Mary*

Williamsburg, Virginia 23187

[b] *Physics Department, Rensselaer Polytechnic Institute*

Troy, NY 12180-3590

July, 1994

ABSTRACT

The existing inclusive electroproduction data base allows us a look at the issue of the relative behaviors of background and resonance excitations, a part of the Bloom-Gilman duality. These data lack accuracy at high Q^2, but establish PQCD scaling in the resonance region and even allow us a glimpse at the leading logarithmic corrections due to the gluon radiation and its possible quenching at large W and x. These should inspire better quality experimental tests at facilities like CEBAF II.

1 Introduction

Now that CEBAF is here, it is quite appropriate to ponder over the question, *what if* CEBAF had an electron beam of 8 GeV energy and higher. Before such a prospect becomes a realistic proposal, this workshop seeks to identify interesting physics issues that need *critically* such a higher energy facility. Purpose of this paper is to point out one such high-Q^2 physics problem that could be helped at such a facility: investigation of the leading log effects from QCD in the resonance electroweak form factors[1]. One of most fundamental issues in hadron physics is the possibility of reaching the perturbative domain of quantum chromodynamics(PQCD): in such a domain, the PQCD rules the behavor of the electroweak structure function[2]. There is still considerable debate on the domain of validity of the PQCD.

2 The PQCD Rules for Helicity Amplitudes for Electroexciting a Resonance

For the helicity amplitudes $G_{\pm,0}$, defined in the Breit frame, for the electroproduction of a resonance, the PQCD rules tell us[2]

$$G_i = \frac{g_i}{Q^n} \tag{1}$$

where for $i = +, 0$ and $-$ respectively, $n = 3$, 4 and 5, where Q^2 is the invariant mass squared and g_i's are constants *modulo* $logQ^2$, dependent on the distribution amplitude of the relevant hadrons. In the amplitudes by Chernyak and Zhitniksky, there is an accidental cancellation, making g_+ really small[3]. Checking such a prediction is a fundamental enterprise in the resonance physics. Stoler's analysis[4] leads support to this particular prospect for the Delta(1232), though it has been recently called into question by Davidson and Mukhopadhyay[5] in a different approach, indicating intrinsic model dependence in this sort of analysis.

Another interesting point in the PQCD rule has been pointed out by the present authors[6]. The above rules have bacically assumed three quarks as the leading Fock components for the baryons. In the case of hybrids, which contain valence gluons, the transverse electroproduction is small, compared to "normal" baryons. but the longitudinal one is not, and it scales like that for the normal baryons. Similarly, characteristic high momentum transfer signatures of PQCD can tell whether hadrons such as the $\Lambda(1405)$, $f_0(575)$ and $a_0(980)$ have normal three-quark (baryon), quark-antiquark(mesons) leading Fock configurations.

3 The Bloom-Gilman Duality

First noted by Bloom and Gilman[7], more than two decades ago, this duality contains two parts:

(a) Resonances excited in the e-p scattering fall at roughly same rate as the background underneath them with increasing $q^2 = -Q^2$.

(b) The smooth scaling limit seen at high Q^2 and W for the structure function $\nu W_2(\omega')$, where $\omega' = 1 + W^2/Q^2$, is an accurate average for bumps seen at lower Q^2 and W, but at same ω'.

It is the second observation that connects the above behavior with the classical definition of duality, originally proposed by Dolan, Horn and Schmid[8].

The BG duality can be explained by the PQCD rules, as was shown by DeRújula, Georgi and Politzer[9] and the present authors[2]. DeRújula *et al.* showed that the corrections to the lower moments of the structure function due to final state interactions (or higher twist effects) are small, while the corrections to higher moments are large. Thus, the average value of the structure function cannot be very different from its values at high Q^2. The present authors extended this concept to the longitudinal structure function as well.

The BG duality has a strong significance for testing of the PQCD rules in the resonance region: Due to the first part of the duality, there is no need to separate the background and resonance, as has been done by Stoler[4] and other authors[10]. to test the PQCD rule. The structure function *as a whole* can be checked for scaling.

Carlson and Mukhopadhyay[1] have examined the dual relationship between the resonance and the scaling curves for the inelastic structure function in the Q^2 range of 1 to 17 $(GeV/c)^2$ and found *no exception* to this rule. Thus, W_2, averaged over sutable range of the Bjoken x (or the equivalent Nachtmann ξ) yields the smooth curve seen at higher values of Q^2 at the same value,x, but all resonance regions. *Looked this way, even the Delta(1232), earlier suspected of "misbehaving", appears quite "normal" or "unexceptional".*

We have done the above analysis by dividing the resonance regions into three zones, $1.12 \leq W \leq 1.38$ the domain of the Delta(1232); $1.38 \leq W \leq 1.62$, the region containing $N^*(1520)$ and $N^*(1535)$; $1.61 \leq W \leq 1.80 GeV$, with resonance bumps around 1.7 GeV. The analysis computes the integrals

$$I_i = \int_{\Delta x_i} dx F_2(x, Q^2), \tag{2}$$

and

$$S_i = \int_{\Delta x_i} dx F_2^{scaling}(x), \tag{3}$$

where Δx_i is the region of x corresponding to the above W intervals. We have then computed the ratios $R_i = I_i/S_i$. We have used the *constancy* of each R_i as the test for the BG duality. We have also used the Nachtmann variable $\xi = 2x/(1+\sqrt{1+Q^2/\nu^2})$, better for the inclusion of the target mass

effect and we have tested various scaling functions[11]. Our conclusion: *The BG duality works nicely above Q^2 of the order of four GeV^2, in all three resonance regions!*

4 Leading Logs: Are Gluon Radiations Damped at High x?

We have recently studied[1] leading log corrections to the inelastic scattering structure function at high Bjorken x. We first investigate these corrections on the parton distribution function. Starting woth the Altarelli-Parisi equation having unsuppressed gluon radiation, we find

$$q(x,t) = N_0(1-x)^{4+4C_F(\ell n \ell n Q^2/\beta_1}, \tag{4}$$

where q(x, t) is the quark distribution function of a given flavor , starting with the form

$$q(x,t_0) = N_0(1-x)^b, \tag{5}$$

where b is a constant, t_0 corresponds to some Q_0^2; symbols here have the usual meaning:

$$t = \ell n(Q^2/\Lambda^2), \tag{6}$$

$$\beta_1 = 11 - (\frac{2}{3}n_f) \tag{7}$$

n_f, the number of fermion flavors,

$$\ell n \ell n Q^2 = \ell n(\frac{\ell n(Q^2/\Lambda^2)}{\ell n(Q_0^2/\Lambda^2)}) \equiv T(Q). \tag{8}$$

We find, for $Q_0^2 = 4\ GeV^2$ and $Q^2 \approx 20 GeV^2$, F_2 changes by about 0.57 due to the logarithmic corrections in the Delta region. Similar conclusions are reached for other resonances.

Moral: *Logs are important!*

5 The Bloom-Gilman Duality, Leading Logs and Higher Twists

Our observations can be summarized as follows:

(1) The inclusion of logarithmic effects helps to make the BG duality idea work *better.*

(2). For distribution amplitudes due to Chernyak and Zhitnitsky and King and Sachrajda, just to mention two we have examined, the BG duality is logarithmically violated.

(3). At $W > 2GeV$ and high x ($x > 0.70$), the *uncorrected* $(1-x)^3$ form fits the data better, in agreement with an argument due to Brodsky *et al.*[12] that the logarithms are *healed* in the region where$(1-x)Q^2$ is small.

Points (1) and (3) will not contradict each other if we introduce a W-dependent higher twist correction such that we have

$$F_2 \propto (1-x)^{3+\frac{16}{3}T(Q)/\beta_1}(1+C_2\frac{m_N^2}{W^2}). \tag{9}$$

¿From the available data, we get

$$C_2 = 1.7. \tag{10}$$

6 Concluding Remarks

The existing inclusive electroproduction data in the resonance region, poor though they are, still give valuable insights into the Bloom-Gilman duality and the effects of the gluonic radiation via logarithms. Log corrections seem to be important in the resonance region, but at high x and $W > 2GeV$, a plain $(1-x)^3$ fits the data. This requires a hypothesis of evolution healing or the presence of higher twist effects. Measuring structure function over a range of x at fixed values of W and Q^2 respectively would deepen our insight into these mechanisms.

That brings us to CEBAF II. Amen to that!

7 Acknowledgement

We are grateful for our research support from the NSF(CEC) and the U. S. Department of Energy (NCM). We thank S. Brodsky and P. Stoler for many helpful discussions.

* Invited talk at the 1994 CEBAF workshop, presented by N. C. Mukhopadhyay.

References

[1] C. E. Carlson and N. C. Mukhopadhyay,*Preprint RPI-94-N90* (WM-94-106), (May 1994), to be published.

[2] C. E.Carlson and N. C. Mukhopadhyay, *Phys. Rev.* **D41** (1990) 2343 and refs. therein.

[3] V. L. Chernyak and I. R. Zhitnitsky, *Nucl. Phys.* **B246** (1984) 52; *Phys. Rep.* **112** (1984) 173.

[4] P. Stoler, *Phys. Rep.* **226** (1993) 103 and refs. therein.

[5] R. M. Davidson and N.C. Mukhopadhyay, *Preprint* RPI-94-N93, (June 1994), to be published.

[6] C. E. Carlson and N. C. Mukhopadhyay, *Phys. Rev. Lett.* **67** (1991) 3745.

[7] E. D. Bloom and F. J. Gilman, *Phys.Rev. Lett.* **25** (1970) 1140.

[8] R. Dolan, D. Horn and C. Schmid, *Phys. Rev.* **166** (1968) 1768.

[9] A. De Rújula, H. Georgi and H. D. Politzer, *Ann. Phys.* (N. Y.) **103** (1977) 315.

[10] C. Koeppel, *Ph. D Thesis* (American Univ., 1994), unpublished.

[11] C. E. Carlson and N. C. Mukhopadhyay, *Phys. Rev.* **D47** (1993) R1737.

[12] S. J. Brodsky, private communication, (1994). S. J. Brodsky, T. Huang and G. P. Lepage, *Particle and Fields* **2**, ed. A. Z. Capri and A. N. Kamal (Plennm, New York, 1982).

DEATH TO PERTURBATIVE QCD IN EXCLUSIVE PROCESSES ?

Robert Eckardt, Jörg Hansper, and Manfred F. Gari
Ruhr-Universität Bochum, Institut für Theoretische Physik, Agr. Mittelenergiephysik
D-44780 Bochum, Germany, e-mail: QCD-MEP@gari.MEP.Ruhr-Uni-Bochum.de

ABSTRACT

We discuss the question of whether perturbative QCD is applicable in calculations of exclusive processes at available momentum transfers. We show that the currently used method of determining hadronic quark distribution amplitudes from QCD sum rules yields wave functions which are *completely* undetermined because the polynomial expansion diverges. Because of the indeterminacy of the wave functions no statement can be made at present as to whether perturbative QCD is valid.
We emphasize the necessity of a *rigorous* discussion of the subject and the importance of experimental data in the range of interest.

1. The application of perturbative QCD

The question of applicability of perturbative QCD at currently available momentum transfers has been discussed controversially in the last years. It is beyond doubt that a pure perturbative treatment of exclusive reactions is without success. Instead, one assumes in the framework of the hard-scattering formalism[1,2] that perturbative (hard) and nonperturbative (soft) contributions factorize. It is believed that the wave function covers the nonperturbative description. A form factor can than be expressed as

$$F(Q^2) = \int [dy, dx] \;\; \hat{\phi}^*(y, \tilde{Q}_y^2)\; T_H(y, x; Q^2)\; \hat{\phi}(x, \tilde{Q}_x^2)\;, \tag{1}$$

where $\tilde{Q}_x := \min_i\{x_i\}\, Q$. This corresponds to diagrams like those shown in Fig. 1.

The quark distribution amplitude, which is defined from the wave function by the projection operation

$$\phi(x, \mu^2) := \int_{\vec{k}_\perp^2 < \mu^2} [d^2 k_{\perp i}]\; \psi(x_i, \vec{k}_{\perp i})\;, \tag{2}$$

contains the nonperturbative information of the bound state and is independent from the reaction under investigation.

The hard-scattering amplitude T_H contains the perturbative contributions of the process, i.e. the contributions from hard gluon exchanges which lead to product terms of the form $\alpha_S(k_i^2)/k_i^2$. These factors originate from the gluon propagators and the dynamical coupling α_S that depends on the four-momentum k_i of the exchanged gluon.

However, in the way the formalism is applied conventionally[5-10], the full dynamical dependence of α_S on the internal gluon momenta k is not taken into account but only in an effective way, e.g. $\alpha_S = \alpha_S(Q^2)$ or $\alpha_S = \alpha_S(\bar{k}^2)$, where $\bar{k}^2$ is the *average*

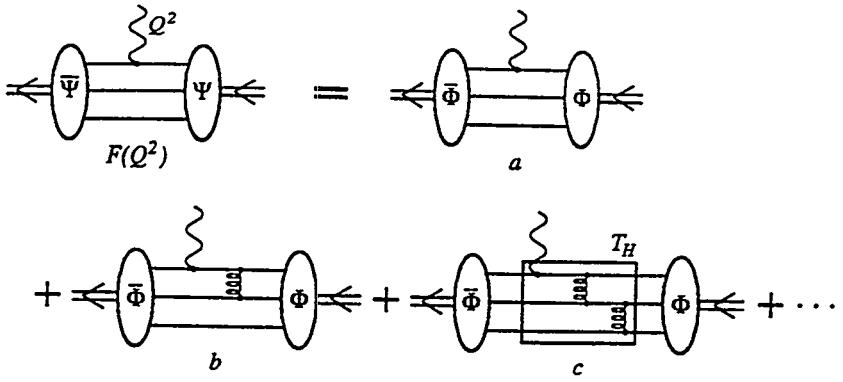


Fig. 1. The (baryonic) form factor F expressed in terms of distribution amplitudes $\phi := \hat{P}\psi$ and hard gluon exchanges. Depending on the choice of the projection operator $\hat{P}$, diagrams *a* and *b* may also give important contributions. However, when $\hat{P}$ is taken in the form of Eq. (2)[2] those diagrams vanish because of non-collinearity. To avoid the non-perturbative end-point contributions in longitudinal momentum-fraction space, one can take into account the effect of perpendicular momenta. This has been done by including an effective gluon mass[3] $\frac{\alpha_S(k^2)}{k^2} \to \frac{\alpha_S(xyQ^2+m_g^2)}{xyQ^2+m_g^2}$, or by explicitly integrating over $k_\perp$ and summing soft gluon contributions up into an exponential factor in the distribution amplitude[4].

virtuality of the exchanged gluon. For instance, the authors of Ref. 10 use for the averaged gluon coupling within a nucleon $\bar{\alpha}_S := \alpha_S(\bar{k}_i^2) = \sqrt{\alpha_S(0.427\,Q^2)\;\alpha_S(0.178\,Q^2)}$. Furthermore, transverse momenta are completely neglected and the evolution of the nucleon distribution amplitude is not taken into account either.

Using these approximations, the form factor for example for the nucleon becomes $F(Q^2) = I[\phi_N] \cdot \bar{\alpha}_S^2/Q^4$, where $I[\phi_N]$ is a functional of the wave function $\phi_N(x)$. In particular, $I[\phi_N]$ is simply a *constant* factor if one and the same wave function is considered for different Q^2 so that the whole Q^2-dependence of the form factor is given solely by $\bar{\alpha}_S^2/Q^4$. Corresponding plots of the nucleon Dirac form factor and the N-Δ transition form factor are sketched in Fig. 2 in comparison to experimental data.

2. The indeterminacy of the distribution amplitudes

All approximations have in common that they presume the knowledge of the quark distribution amplitude ϕ. The expansion coefficients of the distribution amplitude are usually determined from the function's moments, which can be calculated from QCD sum rule techniques. Observables, like form factors and decay widths, depend more or less strongly on the precise form of this distribution amplitude. However, we have shown in recent works[13] that the widely used ansatz of expanding the wave function into a set of orthogonal polynomials leads to a *completely undetermined* distribution amplitude. This can be seen very drastically from the pion quark distribution amplitude in Fig. 3. The *extreme sensitivity* of the expansion coefficients to *small changes* in the moments leads to a *non-converging* polynomial expansion as it is exempli-

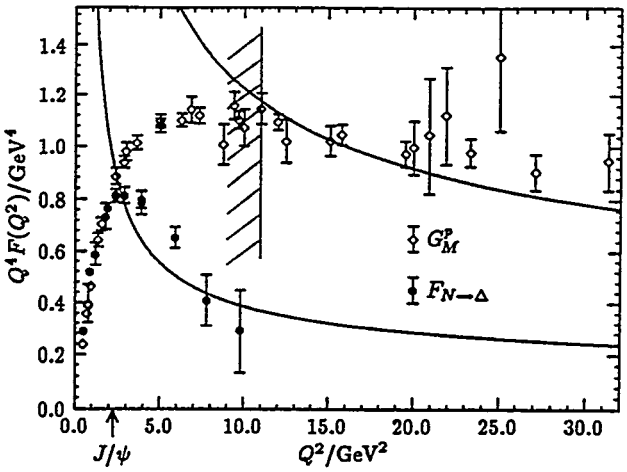


Fig. 2. The elastic proton form factor and the N-Δ transition form factor in comparison with the respective experimental data[11,12]. The form factor calculations were performed with the amplitudes of Ref. 10 and the use of effective gluon virtualities, which gives the logarithmic decay. From the proton form factor one can conclude that perturbative QCD is applicable down to $\approx 10\,\mathrm{GeV}^2$ as indicated by the hatched area. For the N-Δ form factor data exist only up to $\approx 10\,\mathrm{GeV}^2$ and thus perturbative QCD is believed to be valid down to $\approx 4\,\mathrm{GeV}^2$, in spite of the fact that proton form factor cannot be described down there. For reference, also the mass squared of the J/ψ is shown, which indicates the relevant scale for the calculation of the $J/\psi \to p\bar{p}$ decay width. Since it is believed that perturbative QCD is also applicable for the J/ψ-decay with the same nucleon distribution amplitudes as in the case of the nucleon form factor, it should have become clear that a more rigorous approach is badly needed.

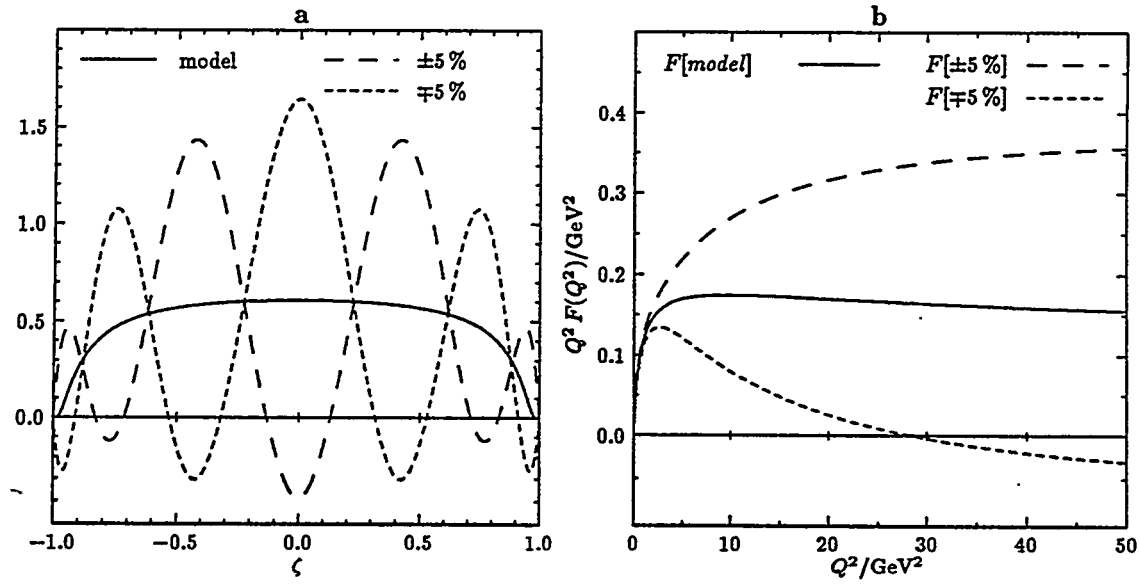


Fig. 3. *a*: The test-model pion wave function and its approximations as constructed from the model's moments with imposed deviations of $\pm 5\,\%$ and $\mp 5\,\%$. The error bars in the moments obtained from QCD sum rules may range up to $\approx 30\,\%$ [5,14,15]. *b*: The form factors of the model and its 5 % approximations, calculated in the hard-scattering scheme. The form factor was not calculated using the approximation $F(Q^2) \sim \bar{\alpha}_S/Q^2 \cdot I^2$, but using the Q^2-evolution of the wave function and the coupling constant depending on the gluon virtuality, which allows a sign change.

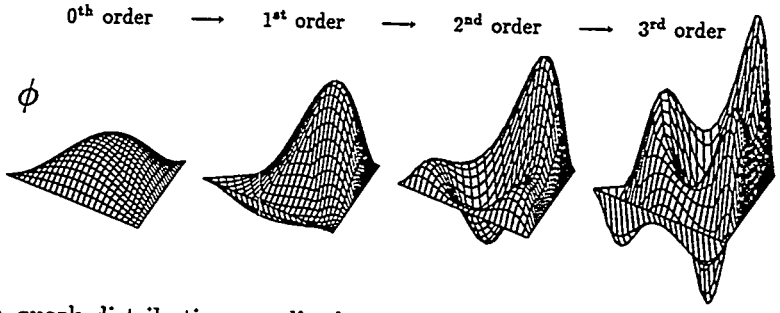


Fig. 4. Nucleon quark distribution amplitudes with increasing order of expansion. They were calculated from the moments of their respective order. This shows that there is no convergence in the expansion. Instead of refining the approximation, higher polynomials produce more and more artificial oscillations which results in "neurotic" wave functions.

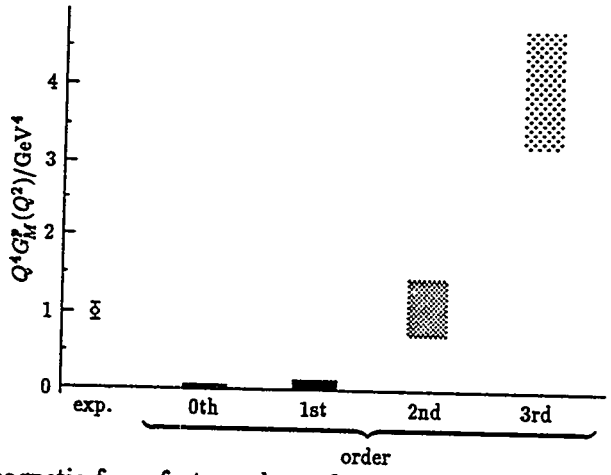


Fig. 5. Typical proton magnetic form factor values of quark distribution amplitudes of different order compared to an experimental value, all at 20 GeV^2. Although second order functions seem to reproduce experiment, this order is not singled out by physically meaningful arguments. Instead, one has no criterion to remove the artificial (wrong) oscillations from a "neurotic" wave function in order to obtain a physical one.

fied for the nucleon in Fig. 4. The moments thus play only the role of theoretical constraints to the wave function which are necessary but *not* sufficient conditions.

In particular, calculations of physical observables such as form factors or exclusive decays by means of such "neurotic" functions – as we call functions, showing this artificial behaviour – cannot be expected to give physically meaningful results that are based on QCD, cf. Fig. 5. Additional constraints like a small ratio $|F_1^n/F_1^p|$, e.g. as in Ref. 10, cannot help to make "neurotic" wave functions physical, because this would presuppose that such functions are sufficiently close to the correct one which is not the case. Furthermore, we see how dangerous it is to use experimental information independent of QCD when trying to construct improved wave functions: In Ref. 10, a ratio $R = |F_1^n/F_1^p| < 0.1$ was assumed whereas a new analysis of experimental data shows that $R \approx 0.5$ [16]. Precise measurements, especially for the neutron, are desirable to resolve this contradiction.

Although higher orders exhibit large oscillations, it cannot be expected that the "leading" order can sufficiently describe the behaviour of the distribution amplitude in the end-point regions. In particular, if the "true" wave function is strongly concentrated in the end-point regions, a polynomial expansion may need to include a very large number of polynomials before convergence can be seen, e.g. up to 10^{th} order! This means that, in general, contributions of higher order polynomials are very important and cannot be neglected. In particular, these higher-order polynomials can have significant effects in the calculations of exclusive processes like hadronic form factors.

The consequence is that all calculations performed by means of such distribution amplitudes, like form factors in the hard-scattering formalism, decay widhts, Sudakov effects etc., have lost their physical basis, because well-grounded QCD wave functions are not yet available! Obviously, strong further constraints from QCD (and *not* from experiment) are needed in order to cure the difficulties. It seems that the task of calculating QCD wave functions is still at its very beginning.

We summarize the essential points:

- Concerning the applicability of PQCD in exclusive processes, a *rigorous* discussion of the subject seems to be the outstanding problem.
- It is formally incorrect to determine e.g. a second order polynomial from third or higher order moments[10] because of the order-by-order correspondence between moments and expansion coefficients.
- Even for small changes in the "true" moments of only a few percent, the (uniquely) reconstructed model polynomial shows large artificial oscillations. This causes very large distortions of the shape of the "exact" function, i.e. a completely "neurotic" behaviour of the model polynomial.
- Due to the uncertainties in the moments, the expansion does not converge!
- It has been known for a long time that there is a freedom in constructing polynomial models for the distribution amplitude, but it was not realized that the uncertainties in QCD sum-rule moments lead to a *complete* indeterminacy of the wave functions!
- Since polynomial models *constructed* from QCD sum rules have to be considered as unphysical, it is not possible to amalgamate a physical model out of such functions!
- It is impossible to improve "neurotic" wave functions by imposing additional constraints, e.g. from experiment, because these functions are *completely* unphysical! Obviously, this cannot be cured by additional auxiliary conditions.
- The "true" nucleon distribution amplitude may contain a very large number of polynomials, e.g. up to 10^{th} order. Nevertheless, the second order parts of such expansions are similar to each other and to existing second order models of the nucleon.
- In addition to QCD sum-rule moments, further strong constraints from QCD are needed in order to determine reliable models for QCD wave functions of hadronic states.

At present, there is no possibility to test predictions of perturbative QCD in exclusive processes because no reliable wave functions are available!

A way out of these difficulties has already been pointed out by Nesterenko and Radyushkin[17], who calculated electro-magnetic form factors of the pion and the nucleon *directly* from QCD sum rules, without having recourse to wave functions.

More data, i.e. more precise and at higher Q^2, are needed for the pion form factor and the nucleon form factors to clearify the situation from the experimental side and are of vital interest to check the predictions of existing and future QCD calculations. All these experiments are planned at CEBAF, which will be ideally suited for those precise measurements.

3. Acknowledgements

We are grateful to V.L. Chernyak and J.A. Eden for useful discussions. This work was supported by the Deutsche Forschungsgemeinschaft (Ga 13-153-2) and by the "Ruth und Gert Massenberg-Stiftung". We thank G.E. Brown for inspiration in dealing with deadly titles.

4. References

1. V.L. Chernyak and A.R. Zhitnitskiĭ, JETP Lett. **25**(1977)510.
2. G.P. Lepage and S.J. Brodsky, Phys. Rev. **D22**(1980)2157.
3. J. Hansper, R. Eckardt and M.F. Gari, Z. Phys. **A341**(1992)339, Z. Phys. **A343**(1992)443.
4. J. Botts and G. Sterman, Nucl. Phys. **B325**(1989)62, H.-N. Li and G. Sterman, Nucl. Phys. **B381**(1992)129.
5. V.L. Chernyak and I.R. Zhitnitsky, Phys. Rep. **112**(1984)173.
6. V.L. Chernyak, A.A. Ogloblin and A.R. Zhitnitsky, Z. Phys. **C42**(1989)569.
7. I.D. King and C.T. Sachrajda, Nucl. Phys. **B279**(1987)785.
8. M.F. Gari and N.G. Stefanis, Phys. Rev. **D35**(1987)1074.
9. N.G. Stefanis, Phys. Rev. **D40**(1989)2305.
10. N.G. Stefanis and M. Bergmann, Phys. Rev. **D47**(1993)R3685, Phys. Rev. **D48** (1993)R2290.
11. R.G. Arnold et al., Phys. Rev. Lett. **57**(1986)174.
12. P. Stoler, Phys. Rev. Lett. **66**(1991)1003, Phys. Rev. **D44**(1991)73.
13. R. Eckardt, J. Hansper and M.F. Gari, to be published in Phys. Rev. **D** and Phys. Lett. **B**.
14. M.A. Shifman, A.I. Vainshtain and V.I. Zakharov, Nucl. Phys. **B147**(1979) 385, Nucl. Phys. **B147**(1979)448, Nucl. Phys. **B147**(1979)519.
15. S. Narison, Phys. Lett. **198B**(1987)104, Phys. Lett. **224B**(1989)184.
16. M.F. Gari and W. Krümpelmann, to be published.
17. V.A. Nesterenko and A.V. Radyushkin, Phys. Lett. **115B**(1982)410, Phys. Lett. **128B**(1983)439.

Measurement of $p(\gamma, \vec{p})\pi^0$ at Higher Energies

R. GILMAN
Department of Physics & Astronomy, Rutgers University, P. O. Box 849
Piscataway, NJ 08855-0849, USA
and
Continuous Electron Beam Accelerator Facility, 12000 Jefferson Ave.
Newport News, VA 23606, USA

ROY J. HOLT
Department of Physics, University of Illinois,
Urbana, Il 61801, USA
and
Physics Division, Argonne National Laboratory
Argonne, IL 60439 USA

and

PAUL RUTT
Department of Physics and Astronomy, University of Georgia,
Athens, GA 30602, USA
and
Department of Physics & Astronomy, Rutgers University, P. O. Box 849
Piscataway, NJ 08855-0849 USA

ABSTRACT

The applicability of QCD inspired reaction models vs. nuclear reaction models for exclusive reactions at high beam energy is a topic of current interest. Polarization measurements provide a sensitive test of the reaction dynamics, but no polarization measurements exist for photoreactions in the scaling regime, where pQCD might be applicable. With higher energy beam at CEBAF, it will become possible to extend the range of measurements in pion photoproduction well into the scaling regime and to better determine the underlying reaction mechanism. A set of measurements for existing equipment at CEBAF with 6–8 GeV beam is described, as well as desirable equipment modifications for improving these measurements at the higher energies.

1. Introduction

Quantum Chromo–Dynamics (QCD) provides the framework from which one begins to understand high energy reactions. While absolute cross sections for exclusive reactions are difficult to predict, cross sections are expected to follow constituent counting rules,[1] which specify the s dependence at constant center of mass angle. Measured cross sections typically exhibit such scaling starting at beam energies of a few GeV.[2]

As an alternative approach, one can attempt to understand reactions in the framework of strong interaction, meson–baryon dynamics. This approach is generally accepted at lower energies, where evaluation of QCD is difficult. It generally provides a good description of scattering observables.

Recent extensions[3] of the meson–baryon picture to higher energies indicate that one can obtain, at least approximately and under some extreme assumptions, the same scaling of cross sections as predicted from the quark/gluon picture. It is clearly desirable to try to distinguish between these two pictures of the reaction dynamics. Given the difficulty of making precise measurements of rapidly decreasing cross sections over a wide energy range, it is desirable to investigate polarization observables.

Helicity conservation, expected at high energies if the data is indeed scaling, requires induced polarizations to be zero. Hadron helicity conservation arises from the helicity conservation expected in photon interactions with individual quarks. To the extent that the individual quark mass is much smaller than the photon energy, quark helicity is conserved in high energy processes. Also, in a reaction which occurs at short distances, the small transverse momentum of quarks in a hadron will lead to a small or negligible amount of angular momentum in the direction of the hadron's motion. Thus, quark helicity conservation leads to hadron helicity conservation. Higher–order, non–helicity–conserving processes do occur in QCD, but these processes decrease faster as a function of s, and constraints on their contributions can be made based on measured cross sections. In contrast, reaction theories based on strong interaction meson–baryon dynamics generally require nonzero polarizations, due to interference of resonance and Born amplitudes, and final state interactions. Thus, it is of great interest to examine both cross sections and spin observables for exclusive reactions in the few GeV energy regime to better determine whether one may more simply understand scattering in terms of quark/gluon or meson/baryon degrees of freedom.

Helicity conservation is now known to not hold in either pp elastic scattering at high energies,[4] or in hyperon production in inelastic pp and pA collisions.[5] However, hadron – hadron reactions are relatively complicated. For example, in pp elastic scattering five complex helicity amplitudes exist, and it is believed[6] that quark interchange dominates gluon exchange in the scattering mechanism. Multiple long range gluon exchanges have approximately the same s dependence as the asymptotic amplitude, and the allowed orbital angular momentum in this process can lead to a violation of hadron helicity conservation.

Here we propose to measure the photoreaction $H(\gamma,p)\pi^0$ at CEBAF, in an energy region where the constituent counting rules appear to work. This is a simple reaction from a theoretical viewpoint, because it involves only a few constituents and just two helicity amplitudes. Some of the complications of hadron–hadron reactions discussed above are no longer present. Experimentally, it requires neither a neutron target nor a neutron detector. In the following sections, we will describe existing data, present a set of possible measurements for CEBAF with existing equipment and a 6 GeV beam energy, and discuss what equipment modifications would be desirable, in particular for the higher energy portion of the program.

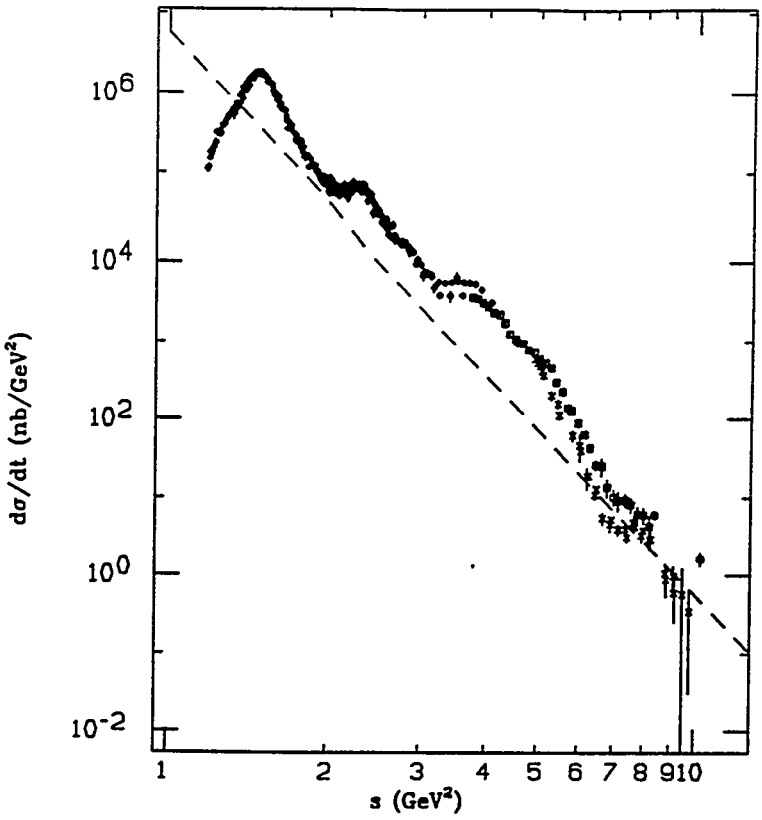


Figure 1: Energy dependence of $H(\gamma,\vec{p})\pi^0$ at 90°_{cm}.

2. Existing measurements of $H(\gamma,\vec{p})\pi^0$

The approximate onset of scaling behavior in pion photoproduction reactions[2] is at a photon energy of $\sim$ 3 GeV, corresponding to s = 6.4 GeV^2, for an angle of 90°_{cm}. At constant center of mass angle, the cross section, $d\sigma/dt$, falls as $\sim s^{-7}$. This behavior can be seen with the data and s^{-7} curve in Figure 1, although the two data sets shown do have different normalization. While firm predictions do not exist for the angular distribution shape, such shapes in the scaling regime generally exhibit strong forward and backward peaking.

Helicity conservation requires that the recoil proton polarization and the polarized target asymmetry be zero in the scaling regime. The polarized photon asymmetry, Σ, is also interesting since it is required by symmetry to be zero at 0°_{cm} and 180°_{cm}, but is expected[7] to be unity at 90°_{cm}. Existing data at lower energies, for E_γ up to 1.2 GeV plus the few data points at higher energies, diasagree with the scaling predictions. Some polarization data are shown in Figure 2.

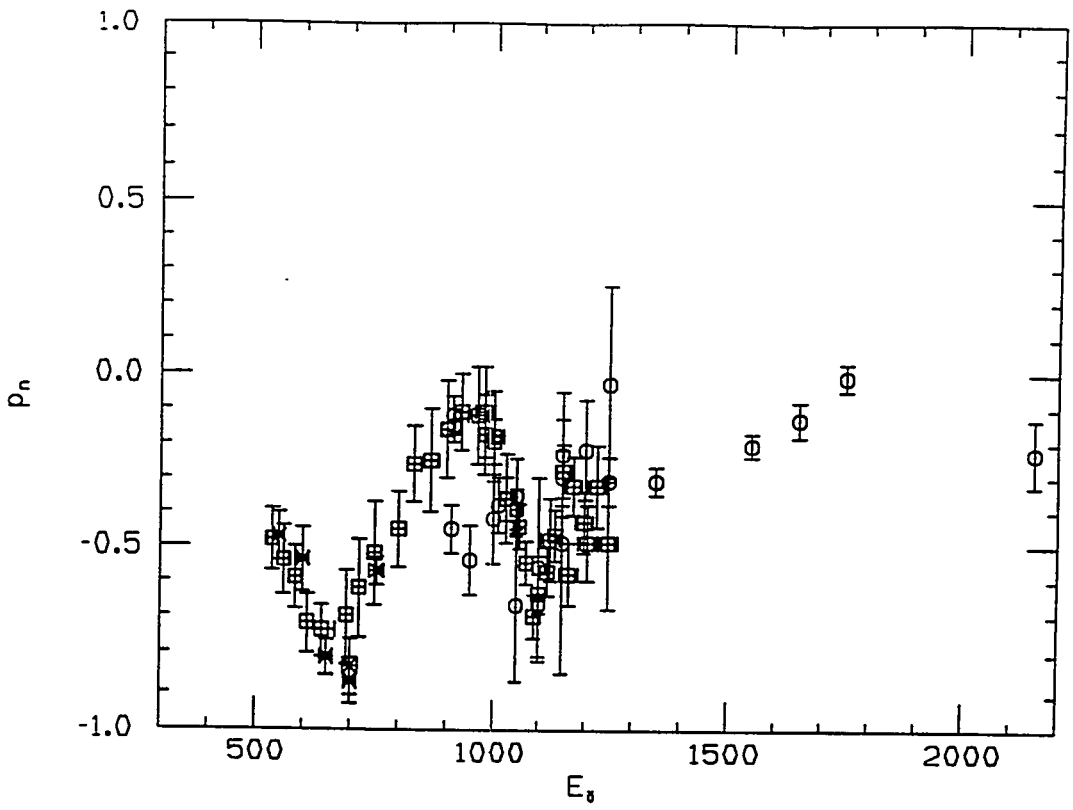


Figure 2: Recoil proton polarization data[9] for $H(\gamma,\vec{p})\pi^0$ at 90°_{cm}.

3. Possible Measurements of $H(\gamma,\vec{p})\pi^0$

For experiments in Halls A and C, pion photoproduction would be measured with the addition of a Bremsstrahlung radiator to the beamline, and with both electron and photon beams passing through the target. Measurements would require the subtraction of radiator–out yields from the radiator–in yields, to remove electroproduction contributions. We also assume here that target vertex resolution is sufficient so that empty target subtractions are not needed. Electron elastic scattering also produces recoil protons that are comparable in yield and slightly higher in energy than those from the reaction of interest, $H(\gamma,\vec{p})\pi^0$, and must be subtracted. In both cases, corrections are needed to account for the change in the energy distribution of the electron beam as it passes through the radiator. Near 90°_{cm}, the kinematic correlation $d\theta_e/d\theta_p$ is nearly unity for ep elastic scattering, and it is benefical to use a second spectrometer arm as a veto.

Illustrative count rates for $H(\gamma,\vec{p})\pi^0$ are shown in Table I. For energies up to 6 GeV, rates are at least 1 Hz, and cross sections may be measured in several hours, including radiator out subtractions. While much of this work can be performed with the 4 GeV/c HRS spectrometers in Hall A, the data at forward angles and high energies require the ~7 GeV/c HMS spectrometer in Hall C.

Table 1 Kinematics and rate estimates for the $H(\gamma,\vec{p})\pi^0$ reaction. The time needed determines the polarization at the target to 0.05 (statistical).

E_γ GeV	θ_{lab} deg	p_p GeV/c	$d\sigma/d\Omega$ nb/sr	I_e μA	$H(\gamma,p)\pi^0$ rate Hz	ep rate Hz	time hours	$\theta_{precess}$ deg
$\theta_{cm} =$	45°							
1	19.5	1.132	44300	0.5	3230	155	1	126
2	17.0	2.067	3430	5.0	1230	130	1	195
3	15.1	2.956	610	20.0	590	110	1*	266
4	13.7	3.829	170	20.0	120	36	2	338
5	12.6	4.696	61	20.0	34	15	8	411
6	11.8	5.558	26	20.0	12	7.2	25	484
7	11.1	6.418	13	20.0	5.2	4.0	20	557
8	10.5	7.277	6.6	20.0	2.4	2.4	1*	630
$\theta_{cm} =$	90°							
1	40.4	0.826	6940	1.0	1010	745	1	107
2	36.3	1.440	465	10.0	335	670	1	148
3	33.0	1.996	76	20.0	72	280	2	189
4	30.5	2.530	20	20.0	14	90	18	232
5	28.4	3.053	6.7	20.0	3.8	36	1*	274
6	26.7	3.569	2.8	20.0	1.4	17	136	317
7	25.3	4.082	1.3	20.0	0.6	9.2	180	360
8	24.1	4.592	0.7	20.0	0.2	5.2	14*	402

* Several points require long times due primarily to spin precession effects. For these points, time required for 10000 counts is given.

As can be seen from the kinematics presented, $H(\gamma,p)\pi^0$ can be most easily measured with existing equipment at angles from about $45°_{cm}$ to $90°_{cm}$. The minimum scattering angle allowed in the lab constrains the forward angle. The background rate from ep elastic scattering increases relative to the $H(\gamma,p)\pi^0$ rate with angle and energy, and reaches a factor of over 10 near 6.0 GeV and $90°_{cm}$.

Time estimates for recoil proton polarization are also given in Table 1. For these measurements, spin precession as the proton passes through the 45° bend of the HRS spectrometer is a concern for some kinematic points. The proton polarization at the target is normal to the reaction plane. This spin is rotated into both longitudinal and normal components at the polarimeter, which measures only the transverse and normal components. If the spin precession is within about 11.5° of 90° or 270°, the normal component of the spin is reduced by a factor of five or more. It becomes difficult to measure not only because of systematic uncertainties in the polarimeter of typically $\pm$ 0.02 $\rightarrow$ 0.03, but also because of the large spin correction factor, which necessitates much greater statistics needed to reduce the uncertainty of the spin at the target. This occurs for the 3 GeV point at $45°_{cm}$, for example. Otherwise, polarization

measurements require of order a few hours to a day over much of the kinematic range shown.

Reduction of the e^-p scattering background is the major issue for these measurements. In particular for the 90°_{cm} points, this background can be effectively reduced by using a second spectrometer arm as a coincident electron detector to veto the ep events. Since the electron and proton have similar momenta in the lab, this technique is most effective with the matched spectrometer pair in Hall A. For forward-angle protons, the electron is at lower momenta and covers a wider angular range, and the HMS and SOS spectrometers in Hall C would provide better matching for ep rejection.

To examine the coincidence vetoing of the ep elastic events, we have run Monte Carlo calculations for the $\gamma p \rightarrow p\pi^0$ and the $ep \rightarrow ep$ reactions. Multiple scattering and energy loss of the electrons in the radiator and target, and of the outgoing protons in the target, were included in these calculations. The spectrometers were assumed to be the Hall A HRS pair. A momentum resolution of 10^{-3} (σ) and an angular resolution of 1 mr (σ) were used for the proton spectrometer. The measured proton energy and angle were then used to calculate the incident photon energy, assuming the reaction was $\gamma p \rightarrow p\pi^0$.

A histogram of the recalculated incident photon energy is shown in Figure 3, for $E_\gamma = 4$ GeV and $\theta_{cm} = 45°$. The solid curve represents the total proton yield in the spectrometer. The dashed line is the contribution from pion photoproduction. The dot-dashed line shows the e^-p background, with the dotted line indicating the part of the background that would be rejected by the use of the second HRS spectrometer as a veto arm. It can be seen that many of the electrons are in the elastic peak, and can be removed from consideration by a simple energy cut. The coincident veto is more effective for 90°_{cm}. In the region to be analyzed, the remaining background constitutes about 10% of the signal, and can be determined and subtracted with radiator out comparisons.

4. New Equipment

From the discussion above, several obvious improvements are possible based on these measurements. One major difficulty is that the electron beam passes through the target and gives rise to ep elastic scattering events. With respect to the polarization, spin precession reduces the asymmetry, increasing the time needed significantly.

Removal of the electron beam requires either a local beam dump or a chicane. One possible solution is development of a chicane that steers the beam around the target. This would make radiator in/out subtractions unnecessary, leading to cleaner experiments. A chicane has already been suggested for one experiment in Hall A.[8]

Since the polarization at the target is purely normal for these measurements, another solution is to have a spectrometer with two dipole magnets with reverse bends, so that the net bend angle is close to 0°. Then the polarization in the focal plane would remain large for all kinematics. However, this would be undesirable for studies of $(\vec{e}, e'\vec{p})$, for which there can be a longitudinal spin component.

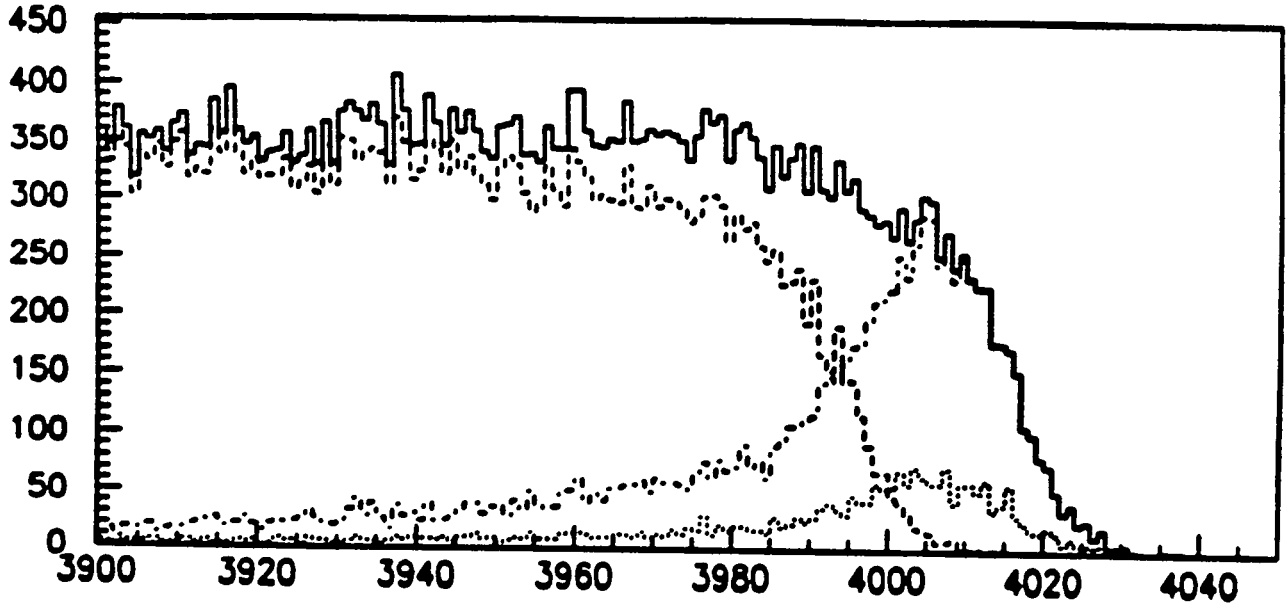


Figure 3: Monte Carlo calculation of recalculated spectrum, counts vs. incident photon energy in MeV. Curves are described in the text.

Spin precession is given by

$$\chi = [(g-2)/2]\gamma\Omega = 1.793\gamma\Omega, \quad (1)$$

where γ=E/m is the usual relativistic factor, and Ω is the bend angle of the spectrometer. Thus, as an alternative, the bend angle should be adjusted so that spin precession is near 180° or 360° for the highest energy protons one wishes to detect. This is possibly a better solution than a near 0° bend angle, as count rates decrease with increasing beam energy, but as the spin rotates away from the normal direction more counts are necessary. This would allow determination of longitudinal spin components for other momenta. To optimize for the 6–GeV, 90°_{cm} protons, with momentum 3.6 GeV/c and $\gamma = 3.9$, we require

$$180^{\circ} \approx 1.793 \times 3.9 \times \Omega, \quad (2)$$

or $\Omega \approx 26^{\circ}$. This is essentially the same as the 25° bend angle of the Hall C HMS spectrometer. Thus, the simplest approach to developing a new spectrometer for these measurements at higher beam energies is to examine modifications needed for the HMS spectrometer to include a focal plane polarimeter and to improve proton particle identification at momenta of 4 – 5 GeV/c. The larger angle measurements would of course require the chicane or a higher momentum second arm in Hall C, for rejection of the e^-p scattering background.

It is clear that these experiments become more difficult as incident energy is increased past 6 GeV up to 8 GeV, and require equipment improvements. Above

6 GeV, polarization measurements require at least one day, and the e^-p background is large. The most cost effective way to continue this program past 6 GeV is probably to install a chicane in Hall C and a proton polarimeter in the HMS spectrometer. With the chicane installed, a higher momentum veto arm is not needed. For these higher momenta, it is also necessary to optimize and calibrate the polarimeter analyzer material.

5. Summary

Photoreactions are inherently simpler processes than hadron – hadron scattering, due to a decrease in the possible number of leading–order processes and of helicity amplitudes. Thus, studies of helicity conservation at beam energies of several GeV, and the applicability of quark/gluon vs. meson/baryon reaction models, are interesting to explore in these reactions. Measurements of $p(\gamma,\vec{p})\pi^0$ are quite feasible at CEBAF, with typical running times of hours with modest beam currents, and for kinematics in the scaling regime. Such measurements are largely feasible with existing equipment, although cleaner measurements and access to higher energies would result from modest improvements.

6. Acknowledgements

We wish to thank T.-S. H. Lee for providing calculations prior to their publication. This work was in part supported by the U.S. Department of Energy, Nuclear Physics Division, under contracts No. W-31-109-ENG-38 (Argonne) and No. DE-FG05-93ER40791 (Georgia), and by the National Science Foundation under Grant PHY-91-22961 (Rutgers).

7. References

[1] V. A. Matveev, R. M. Muradyan, A. N. Tavkhelidze, *Lett. Nuovo Cimento* **7**, 719 (1973); S. J. Brodsky and G. Farrar, *Phys. Rev. Lett.* **31**, 1153 (1973).
[2] R. L. Anderson, *et al.* , *Phys. Rev. D* **14**, 679 (1976); S. J. Brodsky and G. P. Lepage, *Nucl. Phys.* **A 353** 247c (1981).
[3] For the case of deuteron photodisintegration, see Y. Kang, P. Erbs, W. Pfeil, H. Rollnik, *Abstracts of the Particle and Nuclear Intersections Conference*, MIT, Cambridge MA, I-40 (1990); W. Pfeil, private communication; T.-S. H. Lee, *Argonne National Laboratory report PHY-5253-TH-88*; T.-S. H. Lee, *Proceedings of the International Conference on Medium and High Energy Nuclear Physics*, May 23-27, 1988, Taipai, Taiwan, World Scientific (1988) pg. 563; and S. I. Nagornyĭ, Yu. A. Kasatkin, and I. K. Kirichenko, *Sov. J. Nucl. Phys.* **55**, 189 (1992). For pion photoproduction, T.-S. H. Lee, private communication.
[4] See D. G. Crabb *et al.*, *Phys. Rev. Lett.* **65**, 3241 (1990), and references therein.
[5] Lee G. Pondrom, *Phys. Rep.* **122**, 57 (1985); B. Lundberg *et al.*, *Phys. Rev. D* **40**, 3557 (1989).

[6] An experimental demonstration of this is reported in C. White *et al.*, *Phys. Rev. D* 49, 58 (1994). An early theoretical article on this point is Glennys R. Farrar, Steven Gottlieb, Dennis Sivers, and Gerald H. Thomas, *Phys. Rev. D* **20**, 202 (1979).
[7] D. Sivers, private communication.
[8] V. B. Ganenko *et al.*, CEBAF proposal 93-004, Deuteron Photodisintegration by Linear Polarized Photons.
[9] Crosses are from D. E Lundquist, R. L. Anderson, J. V. Allaby, and D. M. Ritson *Phys. Rev.* **168**, 1527 (1968). Squares are from N. V. Goncharov *et al.*, *Zh. Eksp. Teor. Fiz.* **64**, 401 (1973), also available as *Sov. Phys. JETP* **37**, 205 (1974); A. I. Derebchinskii *et al.*, *Zh. Eksp. Teor. Fiz.* **66**, 68 (1974), also available as *Sov. Phys. JETP* **39**, 30 (1975); A. I. Derebchinskii *et al.*, *Zh. Eksp. Teor. Fiz.* **70**, 423 (1976), also available as *Sov. Phys. JETP* **43**, 218 (1976); and A. S. Bratashevskij *et al.*, *Yad. Fiz.* **41**, 1515 (1985), also available as *Sov. J. Nuc. Phys.* **41**, 960 (1985). Circles have been taken from D. Menze, W. Pfeil, and R. Wilcke, *Compilation of Pion Photoproduction Data*, Bonn, 1977.

Pion Form Factor

Chueng-Ryong Ji, Alex Pang and Adam Szczepaniak
Department of Physics, North Carolina State University
Raleigh, NC 27695, USA

ABSTRACT

It is pointed out that the correct criterion to define the legal PQCD contribution to the exclusive processes in the lightcone perturbative expansion should be based on the large off-shellness of the lightcone energy in the intermediate states. In the lightcone perturbative QCD calculation of the pion form factor, we find that the legal PQCD contribution defined by the lightcone energy cut saturates in the smaller Q^2 region compare to that defined by the gluon four-momentum square cut. This is due to the contribution by the highly off-energy-shell gluons in the end point regions of the phase space, indicating that the gluon four-momentum-square cut may have cut too much to define the legal PQCD.

1. Introduction

It has long been debated whether the PQCD is applicable to exclusive processes at the currently available experimental energy regime [1,2,3,4,5]. With the current trend of upgrading the electron beam energy at CEBAF as evidenced in this workshop, this issue becomes more essential to be further clarified. The explicit criticism on the PQCD applicability can be found in the form factors of the pion ($F_\pi(Q^2)$) and the proton ($F_1^P(Q^2), F_2^P(Q^2)$). For the main critique, the "legal" PQCD contribution was defined by the exchanged gluon four momentum square, k_g^2, which should be larger than a typical hadron scale, $\mu^2 < 1GeV^2$. If $\mu^2 \sim 1GeV^2$, the "legal" PQCD contribution was too small to compare with the currently available experimental data at $Q^2 < 10GeV^2$.

However, there is not yet a consensus on which value of μ^2 should be taken to define the "legal" PQCD. Furthermore, the ambiguity of the scale $\tilde{Q}^2$ for the argument of the QCD running coupling constant $\alpha_s(\tilde{Q}^2)$ and the renormalization scheme dependence in the PQCD expansion add more uncertainty to the criticism on PQCD. These issues are quite delicate because the hard scattering amplitude in the leading order PQCD are very sensitive to the values of μ^2 and $\tilde{Q}^2$.

On the other hand, we note that the factorization of the covariant hard scattering amplitude from the non-perturbative quark distribution amplitude is originated from the lightcone quantization method of the QCD Fock state expansion [1]. In the lightcone quantization method, the only criteria of the perturbative expansion is the off-shellness of the lightcone energy in the intermediate states.

This method should be contrasted to the covariant Feynman method based on the off-shellness of the masses of the virtual particles. Thus, in the lightcone

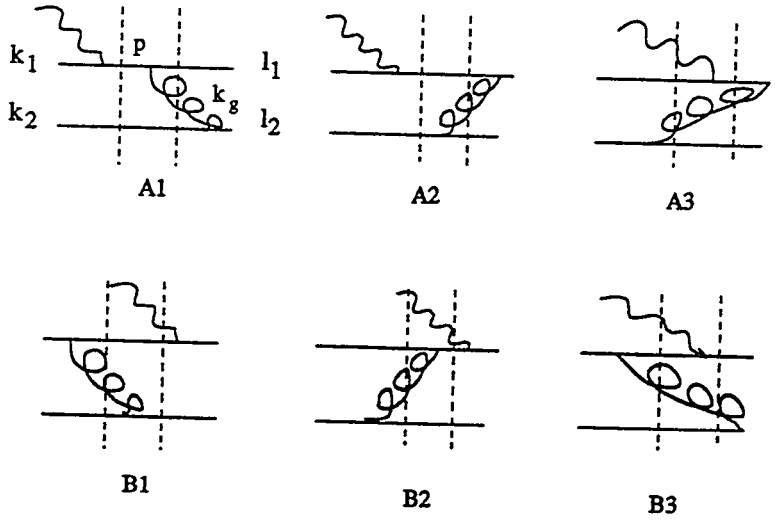


Figure 1: Leading order lightcone time ordered diagrams for the pion form factor, where $k_1 = (x_1, k_\perp), k_2 = (x_2, -k_\perp), l_1 = (y_1, y_1 q_\perp + l_\perp)$ and $l_2 = (y_2, y_2 q_\perp - l_\perp)$ in $(+, \perp)$ components with the "-" component being determined by on-mass-shell conditions. In each diagram, the instantaneous diagrams for the intermediate quark and gluon are implicitly included by using the technique shown in Ref. [1].

quantization point of view, the lightcone energy of the exchanged gluon, $k_g^- = \frac{k_g^2 + \vec{k}_{g\perp}^2}{k_g^+}$, rather than the mass of the virtual gluon, k_g^2, *per se* should be the criteria to determine whether or not the contribution ought to be taken as the "legal" PQCD [6].

In this talk, we investigate this point in the explicit example of the pion form factor calculation using the lightcone perturbation theory. While the present discussion focusses on the pion form factor, the point addressed here is applicable to any other exclusive processes.

2. Pion form factor

The PQCD calculation of the pion form factor in the leading order can be given by

$$F_\pi(Q^2) = \int dx dy d^2\vec{k}_\perp d^2\vec{l}_\perp \psi(x, \vec{k}_\perp) T(x, y, \vec{k}_\perp, \vec{l}_\perp, \vec{q}_\perp) \psi(y, \vec{l}_\perp), \qquad (1)$$

where $\psi(x, \vec{k}_\perp)$ is the lightcone wavefunction of the two-body Fock state and $T(x, y, \vec{k}_\perp, \vec{l}_\perp, \vec{q}_\perp)$ is obtained by the two-body irreducible diagrams. In order to show that the sum of the lightcone time-ordered diagrams is equivalent to the covariant Feynman diagrams, the reducible one gluon exchange diagrams which can be obtained by the lightcone two-body bound state equation of $\psi(x, \vec{k}_\perp)$ are also needed in the leading order calculation [8]. Thus, in the leading order of the lightcone PQCD, the six lightcone time ordered diagrams shown in Fig. 1 should be calculated

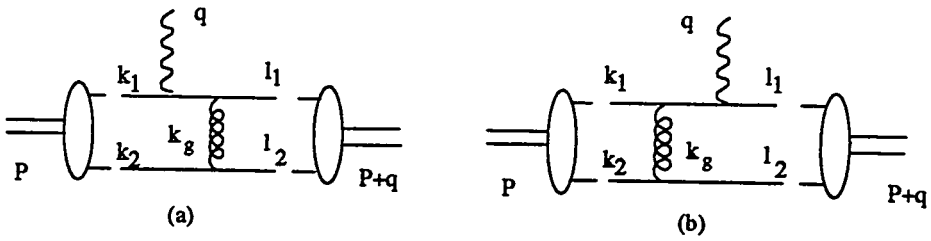


Figure 2: PQCD factorization of the Pion form factor. Leading order covariant Feynman diagrams for the hard scattering amplitude are shown.

in order to establish the equivalence to the convariant hard scattering amplitude. Then, the results are also gauge invariant. In each diagram, the instantaneous diagrams for the intermediate quark and gluon are included using the technique shown in Ref. [1].

The main structure of the each diagram is given by $A_i = \frac{N_i}{D_{1i}D_{2i}}$, where N_i is the numerator expressing the spinor and γ-matrix algebra of the lightcone perturbation theory and D_{1i} and D_{2i} are the energy denominators designated by the dashed line in Fig. 1. Even though the detailed expressions of all D_{1i} and D_{2i} are dependent on i, the general features are same. For example, for A_1, we obtain

$$D_1 = -\frac{1}{x_1 x_2}\left\{(x_2\vec{q_\perp} + \vec{k_\perp})^2 + m^2 - x_1 x_2 M_\pi^2\right\}, \tag{2}$$

$$D_2 = \left(M_\pi^2 - \frac{m^2}{y_1} - \frac{m^2}{x_2}\right) - \frac{1}{y_1 x_2 (y_2 - x_2)}\left\{y_1 y_2 \left(x_2\vec{q_\perp} + \vec{k_\perp} - \frac{x_2}{y_2}\vec{l_\perp}\right)^2 \right. \tag{3}$$

$$\left. + \frac{x_2}{y_2}(y_2 - x_2)\vec{l_\perp^2}\right\}. \tag{4}$$

As one can see, by applying the condition $M_\pi < 2m$ of the bound state pion, D_1 and D_2 do not develop any singularity and they are positive in the entire phase space. Notice that $x > y$ for $i = 1$ to make $\frac{m^2}{y} + \frac{m^2}{1-x} - M_\pi^2 > \frac{m^2}{x(1-x)} - M_\pi^2 > 0$.

We verified that the same properties hold for all energy denominators D_{1i} and D_{2i}. The calculation of N_i needs a care if one considers lightcone gauge A^+=0. In the lightcone gauge, the gluon propagator leads to

$$d_{\mu\nu}(k_g) = -g_{\mu\nu} + \frac{k_g^\nu \eta^\mu + k_g^\mu \eta^\nu}{k_g \cdot \eta}, \tag{5}$$

where $\eta^\nu = (1,0,0,1)$ is a particular line of the lightcone hypersurface. In the leading PQCD of the lowest twist, the terms proportional to $\frac{1}{k_g^+}$ do not contribute and the results are independent from the gauge choice. The results of calculating the six diagrams are equivalent to the covariant calculation of the two Feynman diagrams shown in Fig. 2. If one includes the intrinsic transverse momenta $\vec{k_\perp}, \vec{l_\perp}$ and the mass m of the quarks, the lightcone gauge part proportional to $\frac{1}{k_g^+}$ leads to

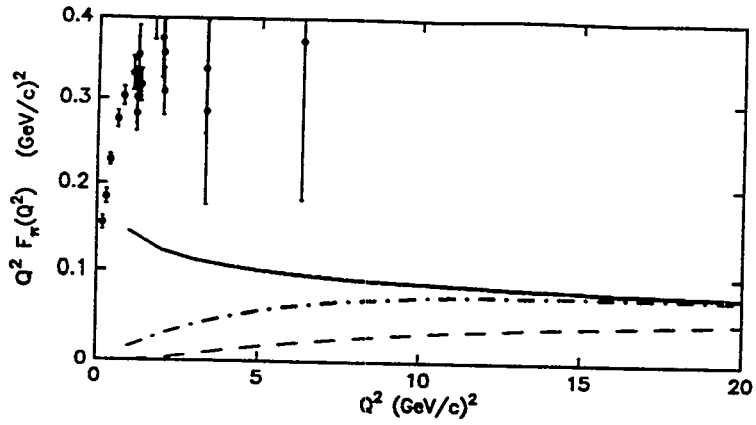


Figure 3: Leading twist PQCD results with $\beta = 0.32\ GeV$

the singularity even though the Feynman gauge part $g_{\mu\nu}$ gives the regular amplitude. This is due to the gauge invariant structure of the amplitudes. The covariant derivative $D_\mu = \partial_\mu + igA_\mu$ makes both the intrinsic transverse momenta $\vec{k}_\perp, \vec{l}_\perp$ and the transverse gauge degree of freedom $g\vec{A}_\perp$ be the same order indicating the need of the higher Fock-state contributions to insure the gauge invariance.

However, we can show that the $\frac{1}{k_g^+}$ terms of $A_1 + B_2 + B_3$ and $B_1 + A_2 + A_3$ are proportional to the lightcone energy differences given by $\Delta_x = M_\pi^2 - \frac{m^2+k_\perp^2}{x(1-x)}$ and $\Delta_y = M_\pi^2 - \frac{m^2+l_\perp^2}{y(1-y)}$. Since our main argument is based on the considerations of the energy denominators, the small changes of the numerator and the choice of the wavefunctions, etc. do not alter our conclusions. To show explicitly how much of the PQCD contribution can come from the end point region, we calculate the form factor in the limit of $\Delta_x = \Delta_y = 0$. For the numerical calculation, we used the lightcone wavefunction suggested by Dziembowski [9] which has the gaussian parameter β. Note that the quark distribution amplitudes obtained by $\beta = 0.32\ GeV$ and $\beta = 0.46\ GeV$ yield those very similar to the asymptotic quark distribution amplitude and the double-hump-shape quark distribution amplitude obtained by Chernyak and Zhitnitsky [10], respectively. However, we should stress that our main point based on the energy denominators is independent from the choice of the wavefunctions. In Figs. 3-5, we compared the three results; solid curve (without any cut), dashed curve ($|k_g^2| > 1\ GeV^2$) and dash-dot curve ($|D_1|$ and $|D_2| > 1\ GeV$). Figs. 3 and 4 are the results without including the masses and the intrinsic transverse momenta of quarks, while Fig. 5 includes the higher-twist effects. In any case, the curves with the lightcone energy cut saturate to the curve without any cut in smaller Q^2 region compare to the curves with the four momentum square cut. As shown in Fig. 5, the recovery to "legal" PQCD was even faster by including the masses and the intrinsic transverse momenta of quarks. The large difference between the dashed and the dash-dot curves comes from the region of $x \sim y < 1 - \frac{\mu}{Q}$. While this region is certainly near to the end points of the quark distribution amplitudes, the gluon in this region are highly off-energy-shell. Thus, from the lightcone quantization point of view, this region should be included in the legal PQCD. Furthermore, we observe that if $|k_g^2| > \mu^2$, then $k_g^0 \sim |k_g^z| > \frac{\mu|q\bar{1}|}{P_z}$

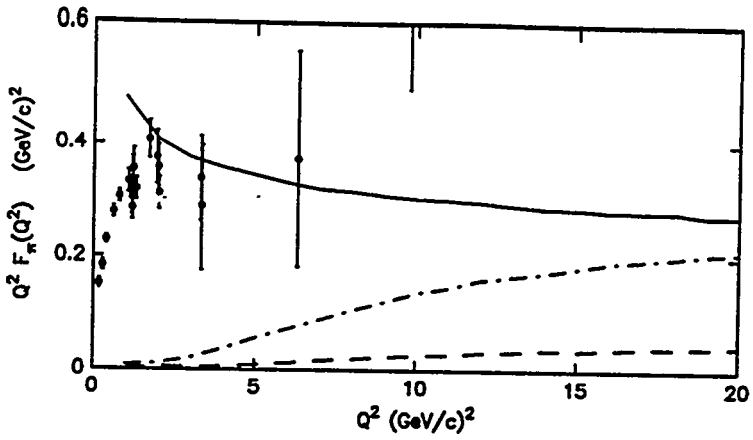


Figure 4: Leading twist PQCD results with $\beta = 0.46\ GeV$

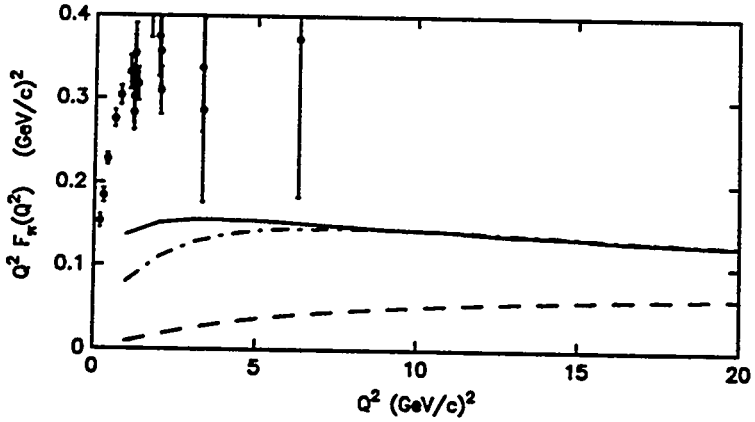


Figure 5: PQCD results including the higher twist effects with $\beta = 0.32\ GeV$

using the covariant calculation (i.e. $k_g = l_2 - k_2$). Thus, it is not clear whether the k_g^2-cut takes into account all the hard gluons which have the momenta bigger than the order of μ. However, we found that the lightcone energy cuts defined by $D_1, D_2 > \mu$ assure the hard gluons to have $k_g^0 \sim |k_g^z| > \mu$.

3. Conclusion

In conclusion, we point out that the gluon four-momentum square cut may have cut too much to define the "legal" PQCD. In order to make sure the $k_g^0 \sim |k_g^z| > \mu$, we considered the lightcone perturbation theory and use the lightcone energy cut to define the legal PQCD. In the end point regions, $x, y > 1 - \frac{\mu}{Q}$, we find the region $x \sim y$, where the gluons are highly off-energy-shell.

4. Acknowledgements

This work is supported by Department of Energy under contract No. DE-FG05-90ER40589 and DE-FG05-88ER40461. AP thank SURA/CEBAF for a graduate fellowship support. We thank S. J. Brodsky, C. Carlson, N. Isgur, A. H. Mueller and A. V. Radyushkin for useful discussions.

5. References

1. S. J. Brodsky and G. P. Lepage, *Phys. Rev. Lett.* **53** (1979) 545; *Phys. Lett.* **B87** (1979) 359; G. P. Lepage and S. J. Brodsky, *Phys. Rev.* **D22** (1980) 2157.
2. N. Isgur and C.H. Llewellyn Smith, *Phys. Rev. Lett.* **52** (1984) 1080; *Phys. Lett.* **B217** (1989) 535; *Nucl. Phys.* bf B317 (1989) 526.
3. A.V. Radyushkin,*Nucl. Phys.* **A523**, (1991) 141c.
4. C.-R. Ji and A. F. Sill and R. M. Lombard-Nelson, *Phys. Rev.* **D36** (1987) 165; C.-R. Ji and F. Amiri, *Phys. Rev.* **D42** (1990) 3764.
5. H. Li and G. Sterman, *Nucl. Phys.* **B325** (1992) 129.
6. A. Szczepaniak and L. Mankiewicz, *Phys. Lett.* **B266** (1991) 153.
7. S. J. Brodsky, G. P. Lepage and P. M. Mackenzie, *Phys. Rev.* **D22** (1983) 228.
8. S. J. Brodsky, C.-R. Ji and M. Sawicki, *Phys. Rev.* **D32** (1985) 1530.
9. Z. Dziembowski, *Phys. Rev.* **D37** (1988) 778.
10. V. L. Chernyak and A.R. Zitnitsky, *Phys. Rep.* **112** (1984) 173.

NUCLEON RESONANCE ELECTROPRODUCTION AT HIGH MOMENTUM TRANSFERS: RESULTS FROM SLAC AND SUGGESTIONS FOR CEBAF

Cynthia Keppel
Virginia Union University
Richmond, VA 23220

Abstract

Nucleon resonance electroproduction results from SLAC Experiment E140X are presented. A CEBAF facility with doubled energy would enable similar high momentum transfer measurements to be made with greater accuracy. Of particular interest are the Delta $P_{33}(1232)$ resonance form factor and $R = \sigma_L/\sigma_T$, the ratio of the longitudinal and transverse components of the cross section. A suggestion is made to study these quantities in conjunction with Bloom-Gilman duality.

THE E140X COLLABORATION

L. Andivahis[1], P. Anthony[3], R. Arnold[1], A. Banerjee[6], A. Bodek[7], P. Bosted[1], J. Button-Schafer[5], S. Dasu[9], P. deBarbaro[7], F. Dietrich[3], J. Dunne[1], R. Ent[4], M. Frodyma[10], R. Gearhart[9], J. Gomez[2], K. Griffioen[6], R. Hicks[5], C. Hyde-Wright[10], C. Keppel[1], S. Kuhn[8], A. Lung[1], N. Makins[4], R. Milner[4], G. Peterson[5], G. Petratos[9], M. Riordan[9] S. Rock[1], S. Rokni[9], M. Spengos[1], L. Stuart[3], Z. Szalata[1], L.H. Tao[1] K. Van Bibber[3], R. Walker[7], K. Wang[5], J. White[1]

1. The American University, Washington, DC 20016
2. CEBAF, Newport News, VA 23606
3. LLNL, Livermore, CA 94550
4. Massachusetts Institute of Technology, Cambridge, MA 02139
5. University of Massachusetts, Amherst, MA 01003
6. University of Pennsylvania, Philadelphia, PA 19104
7. University of Rochester, Rochester, NY 14627
8. Stanford University, Stanford, CA 94309
9. SLAC, Stanford, CA 94305
10. University of Washington, Seattle, WA 98195

INTRODUCTION

SLAC Experiment E140X measured inclusive resonance electroproduction cross sections for electrons with incident energies between 2 GeV and 9.75 GeV scattered from both hydrogen and deuterium targets. Scattered electrons were detected in both the 8 GeV and 1.6 GeV spectrometers in SLAC End Station A. Effort was made in this work to

extend the available range in scattering angle of high momentum transfer (Q^2) resonance electroproduction data. Previous to E140X, 20° was the maximum angle available with reasonable (< 5%) statistics at high Q^2. The spectrometer angle settings for experiment E140X ranged from 14° to 61°. The cross sections were used in conjunction with previous SLAC data to perform Rosenbluth type separations and to measure $R = \sigma_L/\sigma_T$, the ratio of the longitudinal and transverse components of the cross section. The E140X measurements are the only measurements of R available above $Q^2 = 1.5$ (GeV/c)^2 for the resonance region. A global fit to all available SLAC resonance region data has been developed in conjunction with the E140X analysis. The Delta $P_{33}(1232)$ resonance form factor was extracted from the global analysis and a comparison to the perturbative QCD (pQCD) Q^{-4} prediction is made. Similar resonance electroproduction measurements could be obtained from a high energy CEBAF facility which would complement the SLAC results and help to solve existing ambiguities.

$$\mathrm{R} = \sigma_L/\sigma_T$$

The small values of the ratio R measured in deep inelastic lepton proton scattering are typically interpreted to be a consequence of the spin-$\frac{1}{2}$ property of the charged partons involved in the fundamental, quasi-free lepton parton scattering process. In a resonant state probed at moderate momentum transfer the partons are not free, and the above arguments are not necessarily applicable. Large values of R could in principle be possible in the resonance region due to hard gluon exchanges between the quarks.

The assumption of a negligible longitudinal component to the resonance region cross section is testable using a Rosenbluth type method to separate σ_L and σ_T only with the availability of both small and large angle data. The E140X large angle data allows the employment of a separation method to make measurements of $R = \sigma_L/\sigma_T$. Previous to this work, all measurements of R in the resonance region were obtained at relatively low momentum transfers ($Q^2 < 1.5$ (GeV/c)^2) [1, 2, 3]. The E140X results represent the first high Q^2 (up to $Q^2 = 6$ (GeV/c)^2) measurements of R in the resonance region.

The bulk of the R measurements presented will be from a combination of the new E140X large angle data and older SLAC small angle data. This combination provided the angular range necessary for adequate linear fitting and the development of a complete picture of σ_L in the resonance region. For this work, some reananalysis of the older small angle data was necessary. Most noteably, new improved radiative corrections were applied which altered the existing cross section measurements as much as 6%.

The figures below are of R plotted versus momentum transfer squared, Q^2, and missing mass squared, W^2, respectively. These points comprise the new results from this work on hydrogen and are the only existing measurements of this ratio above $Q^2 = 1.5$ (GeV/c)^2 in the resonance region. An error weighted average of the results for all Q^2, W^2 yields $R = .06 \pm .02$.

The error bars are fairly large on this measurement and the data points scatter below and above R equal to zero. The results hint that R is small throughout the region and that the ratio shows no obvious large Q^2 dependence. However, more precise data is certainly needed to make any conclusions.

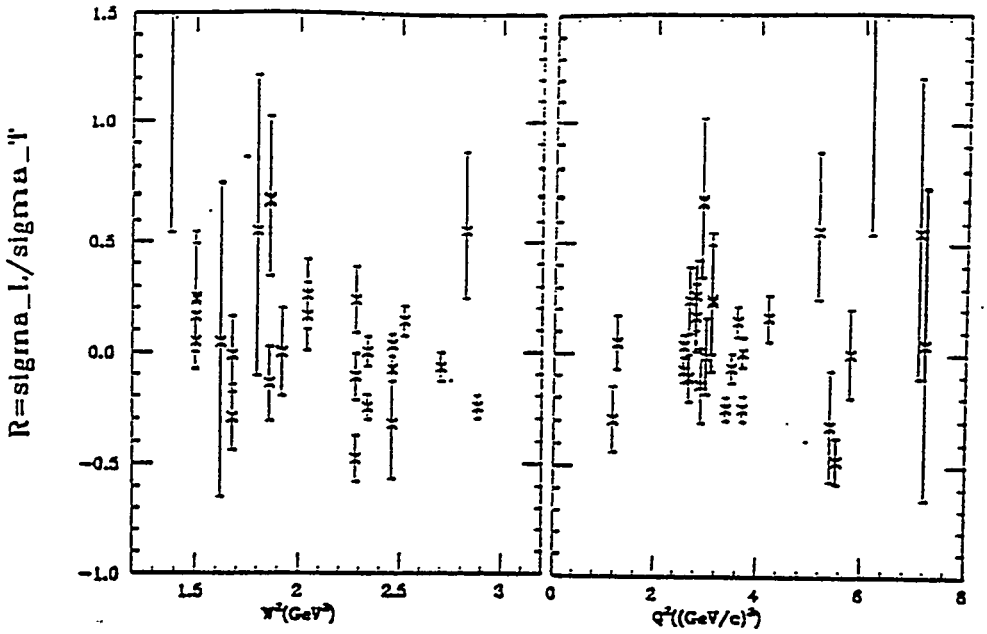


Figure 1: The quantity $R = \sigma_L/\sigma_T$ plotted versus the square of the missing mass W^2 in GeV^2 (left) and of the four momentum transfer Q^2 in $(GeV/c)^2$ (right).

A complete interpretation of R in resonance electroproduction is difficult given the present experimental situation. In deep inelastic scattering, any longitudinal contribution to the cross section is associated with finite transverse momenta or with higher order QCD terms, both helicity-nonconserving terms. The interpretation of the longitudinal component of resonance cross sections is not straightforward even if the reaction at high Q^2 is viewed as a quasi-free lepton parton scattering process. Data from a higher energy CEBAF would be an excellent facility for separated measurements to be made which would help to increase our understanding of the longitudinal component.

BLOOM-GILMAN DUALITY

Over 20 years ago Bloom and Gilman observed the behavior of elastic scattering and of the electroproduction of nucleon resonances to be closely related to the behavior of deep inelastic electron-nucleon scattering[4, 5]. This observation is termed Bloom-Gilman duality. Precisely, the prominent resonances (and the background) in inclusive electroproduction seem to follow in magnitude the deep inelastic structure function $F2$ at corresponding values of the scaling variable $\omega\prime$ where

$$\omega\prime = 1 + \frac{W^2}{Q^2}. \tag{1}$$

Bloom and Gilman assumed a constant small value for the ratio R for the resonances, consistent with that observed in deep inelastic scattering. Although the proton and higher mass resonance form factors obey the leading order pQCD Q^{-4} prediction, the Delta $P_{33}(1232)$ is an anomaly and decreases significantly faster (at least for $Q^2 < 2$ $(GeV/c)^2$). To preserve Bloom-Gilman duality it has been suggested that R is quite large for the Δ, i.e. that the cross section has a significant longitudinal component, allowing the observed scaling behavior of νW_2 for the Δ to be similar to the other resonances and to the proton[6]. Precision high momentum transfer measurements of R are necessary to test this notion and, generally, to aid in the understanding of Bloom-Gilman duality.

The existence of Bloom-Gilman duality opens very interesting questions. The relationship between resonance electroproduction and the scaling behavior observed in deep inelastic scattering points to a common origin for both phenomena. A common fundamental quark description for both properites of electroproduction may become possible by studying Bloom- Gilman duality with new resonance electroproduction data and better measurements of R from an enhanced energy CEBAF.

GLOBAL FIT AND Δ RESONANCE FORM FACTOR EXTRACTION

The reanalysis of existing SLAC data used to obtain σ_L/σ_T separations was concurrent with the development of a global fit to all SLAC nucleon resonance electroproduction data. An excellent global fit to existing SLAC deep inelastic data was developed for SLAC experiment E140 by Whitlow et al[7]. A reliable global fit covering both the deep inelastic and resonance regions for all SLAC kinematics is both necessary for accurate radiative correction calculations for electron scattering experiments and desirable for rate and background calculations and for testing electron nucleon scattering models. A global fit to all SLAC inelastic data (a global resonance region fit linked to the Whitlow global deep inelastic fit) has been developed. The global fit yields an overall χ^2 per 53 degrees of freedom equal to 1.71.

Using the global fit results for the resonant and non-resonant cross section components, values for the Δ resonance form factor were extracted for all existing SLAC data. The results are shown below plotted as a function of Q^2. Errors include statistical and systematic errors, as well as estimated model errors for the nonresonant contribution. The form factors are plotted normalized to the dipole form factor $F_D = \mu_p G_D$. G_D is the dipole shape given by:

$$(1+\frac{Q^2}{0.71})^{-2}. \tag{2}$$

The proton anomalous magnetic moment $\mu_p = 2.79$ nm.

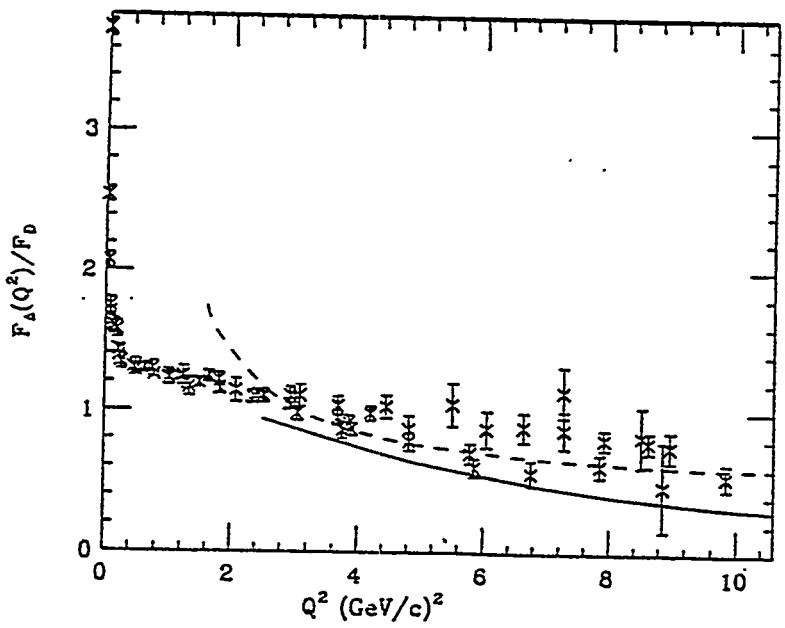


Figure 2: The Delta $P_{33}(1232)$ resonance form factor normalized to the dipole form factor and plotted as a function of Q^2. The solid line curve is the diquark model fit of Kroll et al. The dashed curve is the model prediction of Stefanis and Bergmann.

The diquark model fit of Kroll et al[8] (solid line curve) and the model prediction of Stefanis and Bergman[9] (dashed line curve) are also plotted. The result from Stefanis and Bergmann uses various nucleon distribution amplitudes[10, 11] combined with various $\Delta(1232)$ distribution amplitudes[12, 13]. The most promising features of the original models were retained, resulting in a new "heterotic" model which agrees fairly well with the data.

The Kroll curve falls below the data. This model was tuned to agree with the Stoler analysis[14, 15, 16] which indicates a faster decrease in the ratio F_Δ/F_D with Q^2 than is seen in this work. The rapid decrease of the $\Delta(1232)$ form factor is modelled with a diquark representation that inherently takes into account nonperturbative effects due to strong two-quark correlations. The nucleons are pictured composed of a single quark and a spatially extended diquark. This model predicts a non-negligible longitudinal contribution to the resonance region cross section which is not consistent with the R results from this analysis as discussed above.

The E140X results hint that a pQCD description of F_Δ may be valid in a kinematic range accessible with precision high momentum transfer measurements from a high energy CEBAF facility. A fundamental challenge in physics today is to describe the structure of hadrons in terms of their elementary quark and gluon constituents. The study of electromagnetic transitions to resonant excited states is an important area for testing models of baryon structure. The new SLAC results confirm previous observations that F_Δ decreases more rapidly than Q^{-4} and therefore more rapidly than the elastic and higher mass resonance form factors. The new results, however, decrease less quickly than previous results[15, 16] and indicate the possible onset of leading order behavior around $Q^2 = 2$ (GeV/c)^2. Observation of the predicted leading order pQCD behavior of F_Δ, possible at a high energy CEBAF, could indicate at which momentum transfer pQCD is a valid description of electromagnetic resonance transitions and baryon structure.

CONCLUSIONS

Resonance region cross sections have been measured at SLAC for both hydrogen and deuterium from $Q^2 = 1.0$ to 9.75 (GeV/c)^2. This Q^2 range overlaps significantly with previous SLAC resonance region data, but represents a dramatic increase in scattering angle range. The new cross sections have been measured from 14° to 61° with a typical statistical accuracy of $< 5\%$.

The large angular range of the new data made it possible to perform Rosenbluth separations across the entire resonance region ($1 < W^2 < 4$ GeV^2) up to $Q^2 = 7.2$ (GeV/c)^2. These are the only measurements of $R = \sigma_L/\sigma_T$ available greater than $Q^2 = 1.5$ (GeV/c)^2 for the resonance region. A more precise and complete data set could be obtained from a high energy CEBAF facility. R was found to be small within large errors for the entire (W^2, Q^2) range measured.

A global fit to all SLAC resonance region data has been developed. This fit smoothly links with a global fit to SLAC deep inelastic scattering. The fit is reliable over the ranges $1.15 < W^2 < 4.0$ GeV^2 and $0.5 < Q^2 < 10.0$ (GeV/c)^2. This fit will be useful both for radiative correction calculations and for rate predictions for CEBAF experiments at higher energies.

Improved measurements of the ratio R, considered in conjunction with a reliable global model of deep inelastic scattering and with precision resonance electroproduction data, could be used to investigate Bloom-Gilman duality. In this duality may lie evidence for a common origin of both resonance electroproduction and deep inelastic scattering.

The $\Delta(1232)$ form factor has been extracted from the global fit and found to fall faster than the Q^{-4} prediction from leading order pQCD. It was not found to fall as fast as previous results indicated. The model dependence of this result could be improved with higher precision large momentum transfer data obtained from an energy doubled CEBAF.

REFERENCES

1. F.W. Brasse et al., Nucl. Phys. B110:413, 1976
2. Drees et al., Z. Phy. C7:11, 1981
3. Alder et al., Nucl. Phys. B48, 1972
4. E.D. Bloom and F.J. Gilman, Phys. Rev. D4:2901, 1970
5. E.D. Bloom and F.J. Gilman, Phys. Rev. Lett. 25:1140, 1970
6. C.E. Carlson and N.C. Mukhopadhyay, Phys. Rev. D47:1737, 1993
7. L.W. Whitlow et al., Phys. Lett. B250:193, 1990
8. P. Kroll, M. Schurmann, W. Schweiger, Z. Phys. A342:429, 1992
9. N. Stefanis and M. Bergmann, Phys. Lett. B325:183, 1993
10. V.Chernyak, A.Ogloblin, and I.Zhitnitsky, Z. Phys. C42:569, 1989
11. M. Gari and N.G. Stefanis, Phys. Rev. D35:1074, 1987
12. C.E.Carlson, Phys. Rev. D34:2704, 1986
13. G.R. Farrar and D.R. Jackson, Phys. Rev. Lett. 35:21, 1975
14. P. Stoler, Phys. Reports, 226:103, 1993
15. P. Stoler, Phys. Rev. Lett. 66:1003, 1991
16. P. Stoler, Phys. Rev. D44:73, 1991

MEASUREMENT OF THE PION FORM FACTOR AT HIGHER ENERGIES*

David J. Mack
Physics Division, CEBAF
12000 Jefferson Avenue
Newport News, Virginia, 23606 U.S.A.

ABSTRACT

One of the strongest arguments for increasing the nominal CEBAF beam energy to equal or exceed 6 GeV is that one would be able to make quality high Q^2 measurements of the charged pion form factor.

1. Introduction

The charged pion form factor, F_π , is used to conveniently summarize information about the (non-pointlike) distribution of charge in the pion. A measurement of F_π at 'large' Q^2 (ie, > 1) is interesting because it tests QCD inspired models of the pion in a region where the perturbative contributions are thought to be significant. Fortunately for the accuracy of these models, the pion wave function is relatively simple when compared to that of the nucleon, and is also normalized in the asymptotic limit by the pion decay constant. The reason the PQCD diagram contribution is thought to be significant in the $Q^2 > 1$ region is that, because the pion consists of only two quarks, only a single hard gluon must be exchanged (as opposed to two hard gluons in the case of a nucleon which consists of three quarks).

The most direct means of measuring F_π is to scatter pions from atomic electrons. At very low Q^2, such experiments have shown[1] that F_π is given to a good approximation by the vector meson dominance prediction

$$F_\pi = \frac{1}{1 + Q^2/M_\rho^2}. \tag{1}$$

However, even with 300 GeV pion beams, the maximum Q^2 measured with this technique is only .28 $(GeV/c)^2$.

At $Q^2 \gg 1$ $(GeV/c)^2$, the PQCD prediction for F_π is[2]

$$F_\pi = \frac{-2f_\pi^2}{b\, ln(Q^2)} \frac{1}{Q^2} \tag{2}$$

*Some of this material was reported at the 1993 Elba Workshop on High Momentum Transfer Reactions.

where F_π is the pion decay constant. If QCD is the correct theory of the strong interactions, then the character of F_π must change considerably between these two extremes of Q^2. But how is one to explore this interesting transition region?

Following an early suggestion by Frazer[3], F_π can be determined at higher Q^2 by pion electroproduction. In this case the target is the cloud of virtual pions surrounding the proton, with the likelihood of finding a pion of a given momentum proportional to $g_{\pi NN}(t)$. For sufficiently small values of $-t$, the longitudinal response σ_L is dominated by the contribution from the pion pole

$$\sigma_L \propto \frac{-tg^2(t)}{(t-m_\pi^2)^2} F_\pi^2(Q^2) \tag{3}$$

With properly chosen kinematics the longitudinal response can be much larger than the transverse response. In practice, one does not use this simple expression but rather the best available model of pion electroproduction treating F_π as a free parameter.

2. Opportunities at Higher Energy

The CEA-CSA electroproduction data[4] are shown in Figure 1. There are inconsistencies near $Q^2 = 1$ $(GeV/c)^2$ which need to be cleaned up. Above Q^2 = 1-2 $(GeV/c)^2$, the data have very large statistical errors. Systematic errors were large since for some of the data points no backward angle data exist, and for others the forward and backward angle measurements were from different experiments. From top to bottom in the same figure the curves are the extrapolated monopole form factor[1], an estimate of soft contributions[5], a Bethe-Salpeter model[6], and the asymptotic QCD prediction[2]. Clearly the existing data above $Q^2 = 2$ $(GeV/c)^2$ have little power to differentiate between any of these models.

The proposal submitted by our collaboration[7] to the CEBAF Program Advisory Committee is in two phases. Phase I covers the Q^2 range of .5-1.5 $(GeV/c)^2$, and is well suited to an accelerator with maximum energy of 4 GeV. We will make L-T separations in a single experiment with the same apparatus. Although improved measurements are most badly needed at higher Q^2, the various models begin to diverge above $Q^2 = 1$ $(GeV/c)^2$, so precise measurements at $Q^2 = 1$ and 1.5 $(GeV/c)^2$ will be useful. We also plan to do a better search of physics backgrounds than has been achieved previously. Phase I of our proposal is approved, and if all goes well will take place in 1996, after the first series of shakedown experiments.

Phase II covers the Q^2 range of 2-5 $(GeV/c)^2$. In this region existing data are of poor quality, so the interest in an improved series of measurements is high. While the 6 GeV beam called for in the proposal would be adequate for a measurement at Q^2 = 2 $(GeV/c)^2$, the distance from the pole increases rapidly with Q^2 and $-t_{min}$ would reach .72 $(GeV/c)^2$ at $Q^2 = 5$ $(GeV/c)^2$. This value of $-t_{min}$, on the order of the squared nucleon mass, is very far from the pion pole. Although no systematic studies of non-pole backgrounds are available (which is why we plan to perform them), such backgrounds could be large at this value of $-t_{min}$.[8] The only way to reduce the

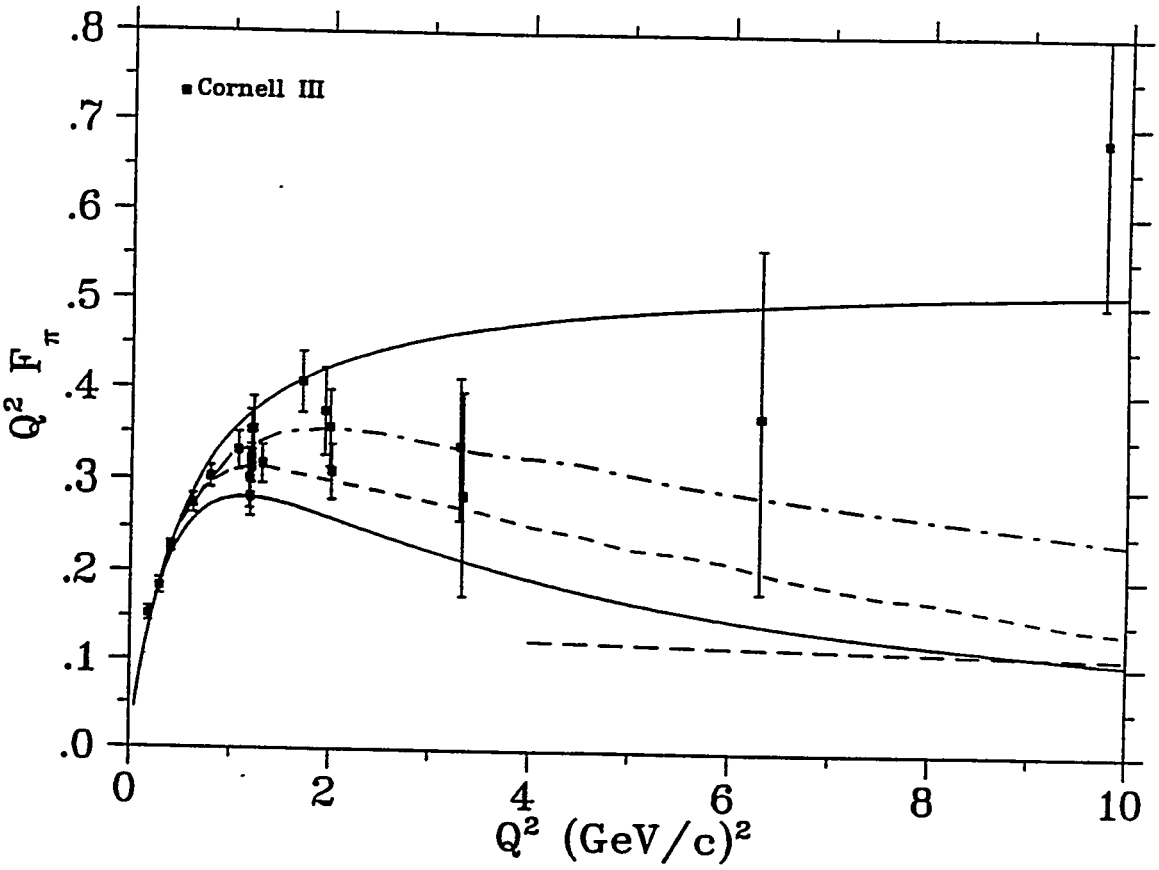


Figure 1: Existing data for Q^2F_π from electroproduction at large Q^2.

distance to the pion pole, while keeping Q^2 fixed, is to increase the invariant mass of the virtual photon-nucleon system, W. This requires higher beam energy.

To investigate possible improvements which could be obtained by performing CEBAF F_π measurements at higher energy, Table 1 was constructed assuming beam energies of 4, 6, 8, and 10 GeV. Only two Q^2 values were examined, 2.5 and 5.0 $(GeV/c)^2$. Two important figures of merit for the experiment are $\Delta\epsilon$ (the longitudinal polarization lever arm) and $-t_{min}$ (the distance to the pion pole). In an ideal experiment $\Delta\epsilon$ would be as large as 1, and $-t_{min}$ would be as small as zero. There is some degree of trade-off between these two figures of merit, but generally I have strived for a minimum $\Delta\epsilon$ of about .3 and let $-t_{min}$ fall where it may.

Options A and C assume the existing 4 GeV/c x 4 GeV/c and 1.7 GeV/c x 7 GeV/c spectrometer pairs in Halls A and C, respectively. Option D assumes a new 6 GeV/c x 6 GeV/c pair, and C* assumes a new 10 GeV/c spectrometer in coincidence with the Hall C High Momentum Spectrometer. With the existing apparatus in endstations A or C, a measurement at $Q^2 = 2.5$ $(GeV/c)^2$ is barely possible with a

Table 1: Figures of merit at $Q^2 = 2.5$ and 5.0 $(GeV/c)^2$ for F_π measurements at CEBAF assuming beam energies of 4, 6, 8, and 10 GeV. See text for explanation.

Q^2	FOM's	4 GeV C A D C*	6 GeV C A D C*	8 GeV C A D C*	10 GeV C A D C*
2.5	$\Delta\epsilon$	.11	.31 .30 " "	.31 .44 .31 "	.31 .44 .41 "
	$-t_{min}$	.27	.27 .18 " "	.27 .18 .12 "	.27 .18 .12 "
5.0	$\Delta\epsilon$	no soln.	.15	.15 .42 .30 "	.15 .45 .31 "
	$-t_{min}$		.72	.72 .72 .50 "	.72 .72 .36 "

4 GeV beam due to the small $\Delta\epsilon$ lever arm. Improved apparatus would not help since the measurement would be limited by beam energy. At 6 GeV, a good quality measurement at $Q^2 = 2.5$ $(GeV/c)^2$ becomes possible, especially in endstation A where both electron and hadron arms have maximum central momenta of 4 GeV. The Hall D and C* options would not permit better figures of merit than the Hall A option; the measurement would be again limited by beam energy. Higher beam energies would improve the figures of merit further at $Q^2 = 2.5$ $(GeV/c)^2$, but since a good measurement appears possible with 6 GeV beam this alone would not justify increasing the CEBAF beam energy further.

It is worth pointing out that at about 6 GeV, endstation C would become obsolete for most coincidence studies since there would be very little kinematic flexibility given the maximum central momentum of the Short Orbit Spectrometer of 1.7 GeV/c. Carlini[9] has proposed a 10 GeV/c, semi-fixed angle, resistive spectrometer. Increasing the beam energy to 8 GeV would make better measurements possible at $Q^2 = 2.5$ $(GeV/c)^2$ assuming one had the new endstation C* spectrometer.

According to Table 1 , the justification for beam energies above 6 GeV comes from the $Q^2 = 5.0$ $(GeV/c)^2$ measurement. Unfortunately, $-t_{min}$ increases rapidly with Q^2 at fixed beam energy. Even with a 10 GeV beam and option D or C* equipment, the figures of merit allow only a fair measurement: $-t_{min} = .36$ $(GeV/c)^2$. Although this would be very useful data, it appears that one would require a 12-16 GeV beam energy to make good quality measurements of F_π at $Q^2 = 5$ $(GeV/c)^2$. Again, a new spectrometer would be needed.

3. Summary

An increase in the CEBAF beam energy to 6 GeV would be very welcome. One could make a much improved F_π measurement at $Q^2 = 2$ $(GeV/c)^2$ while limping

along with the existing endstation hardware. With a beam energy of at least 10 GeV and a new spectrometer, one could make reasonable measurements at $Q^2 = 5$ $(GeV/c)^2$. Good measurments would require higher beam energy, probably 12-16 GeV.

4. Acknowledgements

I would like to thank Paul Stoler for strongly supporting the CEBAF energy upgrade and helping to make this workshop possible.

5. References

1. S.R. Amendolia *et al.*, Phys. Lett. **146B**, 116 (1984), and Nucl. Phys. **B277**, 168 (1986).
2. G.R. Farrar and D.R. Jackson, Phys. Rev. Lett. **43**, 246 (1979).
3. W.R. Frazer, Phys. Rev. **115**, 1763 (1959).
4. C.J. Bebek *et al.*, Phys. Rev. Lett. **37**, 1326 (1976); Phys. Rev. D **17**, 1693 (1978).
5. N. Isgur and C.H. Llewellyn Smith, Phys. Rev. Lett. **52**, 1080 (1984).
6. O.C. Jacob and L.S. Kisslinger, Phys. Lett. B **243**, 323 (1990).
7. D.J. Mack *et al.*, CEBAF proposal PR-093-021.
8. C.E. Carlson and J. Milana, Phys. Rev. Lett. **65**, 1717 (1990).
9. R. Carlini, private communication.

Electroproduction of Pseudoscalar Mesons Above the Resonance Region

Bogdan B. Niczyporuk
Continuous Electron Beam Accelerator Facility
Newport News, VA 23606. USA

*Presented at the "Workshop on CEBAF at Higher Energies"
CEBAF, Newport News, April 14-16, 1994

ABSTRACT

In this paper, we have revisited twenty year old data considering the progress achieved in related fields. To make further progress in our understanding of strong interactions, we need much better quality of exclusive electroproduction data. A measurement of the differential cross section $\sigma(t, W, Q^2)$ for the reactions $e^- + p \rightarrow e^- + \pi^+(K^+) + n(\Lambda^o)$ at a beam energy of $\geq 4\ GeV$ is proposed. Data will be collected simultaneously for both reactions using the CLAS detector at CEBAF in the following kinematical region: $Q^2 > 1\ GeV^2$ and $W > 2\ GeV$. One of the most interesting aspects of electroproduction is that it can be used to measure photoproduction amplitudes as functions of the photon mass squared Q^2 and momentum transfer t. Emphasis is given to measuring the differential cross sections for $t \sim m^2_{\pi,K}$. Above the resonance region ($W > 2\ GeV$), the cross section is dominated by the amplitudes for scalar photons. Measured angular distributions of produced mesons will be used to estimate the contribution of various amplitudes to the cross sections. High statistics and good quality data collected simultaneously using a large acceptance detector will improve our understanding of nucleon structure as well as the hadronic properties of the photon.

1 Introduction

Strong interactions of quarks are governed by quantum chromodynamics (QCD) with SU(3) symmetry where the gauge boson is the gluon. QCD provides a theoretical framework for formulating the structure of hadrons, in particular that of the proton, in terms of quarks and gluons. This structure is revealed when the proton is probed by a virtual photon.

The photon is a gauge particle mediating electromagnetic interactions. Its point-like nature is built into the Standard Model. The electromagnetic behavior of the photon can be calculated more accurately than one can measure experimentally. But besides mediating electromagnetism, the photon can occasionally fluctuate (dissociate) into quark pairs which take part in strong interactions. This aspect of the photon is far from understood. The hadronic side of the photon is a rich field, both theoretically and experimentally, and is being studied using a range of reactions at all major accelerators and storage rings [1, 2].

The first indication of photon structure was probably e^+e^- pair creation in an electromagnetic field. In hadronic interactions, the photon was first regarded as structureless (apart from radiative corrections due to its e^+e^- pair content). As photon energies increased to the multi-GeV range, the photon was found to have an internal structure of its own. Photon-hadron interactions can be understood if the physical photon is viewed as a superposition of a bare photon and an accompanying small hadronic component that feels conventional hadronic interactions, but has the same quantum numbers as the photon (VMD model). To understand this, consider electron-nucleon scattering. This process is mediated by a virtual photon and is characterized by two variables. These variables may be taken as the photon energy, $\nu = E - E'$, and the squared 4-momentum transfer, $Q^2 = (p_e - p_{e'})^2$, between the incident and scattered electron, which measures the virtuality of the photon. The uncertainty principle states that the probability of a photon interacting hadronically increases with the photon energy ν (large coherence length $l_c \sim 2\nu/(Q^2 + m_V^2)$), but decreases with Q^2 (small transverse size of quark configurations $r_{q\bar{q}}^2 \sim (Q^2 + m_V^2)^{-1}$). The photon-quark coupling found in electron-nucleon scattering also allows a simple interpretation of electron-positron annihilation into hadrons at high energies: the virtual photon created in the annihilation splits into a quark-antiquark pair which in turn produces the observed hadrons. The hadronic states (vec-

tor mesons plus continuum) seen at electron-positron colliders are precisely those into which a virtual photon can fluctuate. The total cross section is proportional to the fractional charge squared of all quarks that can be produced at given total energy $\sqrt{s}$ ($s = -Q^2 \equiv q^2$). The spectral function $R(q^2) = \sigma(e^+e^- \to q\bar{q})/(e^+e^- \to \mu^+\mu^-)$ for $q^2 < 1\ GeV^2$ is dominated by production of vector mesons (ρ,ω and φ). For $q^2 > 1\ GeV^2$, the spectrum extends into the $q\bar{q}$ continuum and heavy vector mesons. The transition of the virtual photon into hadronic systems is also observed in e^+e^- collisions leading to a two-photon interaction. In the latter case, one of the photons with very small virtuality interacts with the other one with high virtuality. The interaction can be thought of as a DIS of one photon on the other, similar to the probing of a nucleon by a highly virtual photon [3].

According to our present knowledge, the nucleon consists of three "valence" quarks and many binding particles that keep the quarks together, the gluons. Gluons transform quite often (but only for a fleeting moment) into pairs of quarks and antiquarks. Therefore, the proton contains, besides the three valence quarks, a "sea" of gluons and quark pairs frequently called "partons". At very high energies, the inelastic electron-proton cross section was found to be surprisingly large (rather than falling off with Q^2 as expected in VMD). Thus, electron-nucleon scattering at very high energies, when the photon again becomes a point-like object (very small $r_{q\bar{q}}$), should be the sum of (virtual) photon-parton scatterings; the dimensionless scaling variable $x = Q^2/2m_p\nu$ is the momentum fraction of the nucleon carried by the struck parton. The closer the proton is scrutinized, the more quarks and gluons should be seen. The distribution of events over these two parameters (x and Q^2) provides a measure of the parton density inside a proton. The increase of the structure function $F_2(x, Q^2)$ at very small values of x has been recently observed at HERA [4, 5].

As we mentioned above, a large fraction of the real (or low Q^2) photoabsorption cross section occurs via vector meson dominance (diffractive mechanism). Aside from diffractive processes, the hadrons produced by the intermediate vector mesons have mostly small longitudinal momentum fractions, just as in hadron-nucleon scattering. By triggering on fast hadrons and/or by forcing a charge exchange mechanism (such as charged meson electroproduction), we can essentially eliminate the diffractive component (VMD). The virtual or real photon interacts with a nucleon by first transforming into a $q\bar{q}$ pair (continuum or intermediate hadronic state) at distance

l_c, which then propagates and interacts strongly with the partons inside the nucleon. The model we have in mind here [6] is similar to Bethe-Heitler pair production by the virtual photon in the Coulomb field of a target nucleon. The intermediate $q\bar{q}$ state, into which the virtual photon fluctuates, scatters most strongly in an asymmetric configuration [7, 8], where one of the quarks carries only a small fraction of the photon energy. That is, one should observe an enhancement of the cross section at small momentum transfers t to the recoil nucleon. At high momentum transfers t (the c.m. scattering angle of produced mesons is $\sim 90^o$ for a symmetric configuration), the cross sections for electroproduction of π^+ and K^+ should be approximately equal.

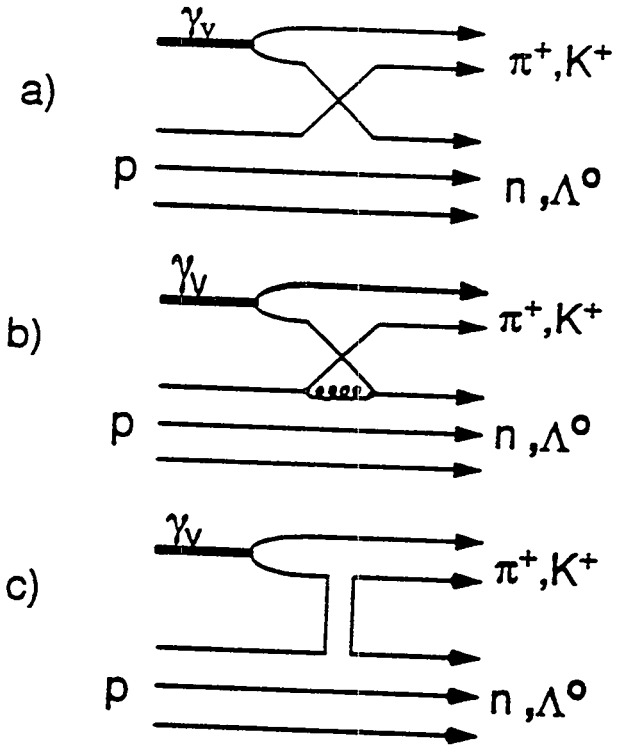


Fig. 1. The quark exchange mechanisms for electroproduction of mesons.

At very low t, the effect of valence quarks in a proton should be overshadowed by the copious presence of low-momentum $q\bar{q}$ pairs that make up the

sea (non-perturbative contributions). Additionally, electroproduction of K^+ mesons will be suppressed due to the heavier strange quark mass (threshold effects). The quark exchange mechanisms for the electroproduction of charged mesons are schematically pictured by graphs shown in Fig. 1. As can be seen, the photon interacts much like a conventional hadron with the proton (via QCD dynamics between partonic constituents).

In summary, we should no longer regard the photon-nucleon coupling (similar to pion-nucleon coupling) as a fundamental constant but as an "epiphenomenon" that reflects the structure of photons and nucleons. The form factors determined experimentally only parametrize our ignorance of their detailed internal structure.

It is commonly thought that the non-valence components in a proton are a consequence of the very high Q^2 limit (and use of the infinite momentum frame) and that at low Q^2 the proton is basically just the three valence quarks. We will argue in this paper that the sea quarks are numerous even in the proton rest frame and that their effects should also be seen at lower energies. Additionally, the study of exclusive reactions in electron-proton interactions at energies from 4 to 16 GeV has a few advantages: i) relatively high cross sections yield good statistical accuracy, and ii) low multiplicity simplifies the data analysis since we are not dealing with jets.

2 Experimental Data

2.1 Photoproduction Data

Except that the photoproduction cross sections are typically smaller by a factor of around 200, the general features (s dependence, t dependence, etc.) of photoproduction reactions are similar to those of the corresponding hadronic reactions. It is therefore natural to try to understand them in the same theoretical framework that is applied to hadronic processes. For example, a comparison [9] of 5 GeV $\gamma p \to \pi^+ n$ data multiplied by a scale factor (equal to the ratio of πp to γp total cross sections) and the corresponding $\pi^- p \to \pi N$ data shows similar qualitative features: i) there exist forward and backward peaks separated by a central region, and ii) the cross sections in the central region are approximately symmetric about 90° in the center of mass. These general similarities imply that the π^- first dissociates in the

field of a proton into quark pairs ($\bar{u}d$) and then takes part in strong interactions like the photon (via quark exchange mechanisms). In Fig. 2, we show

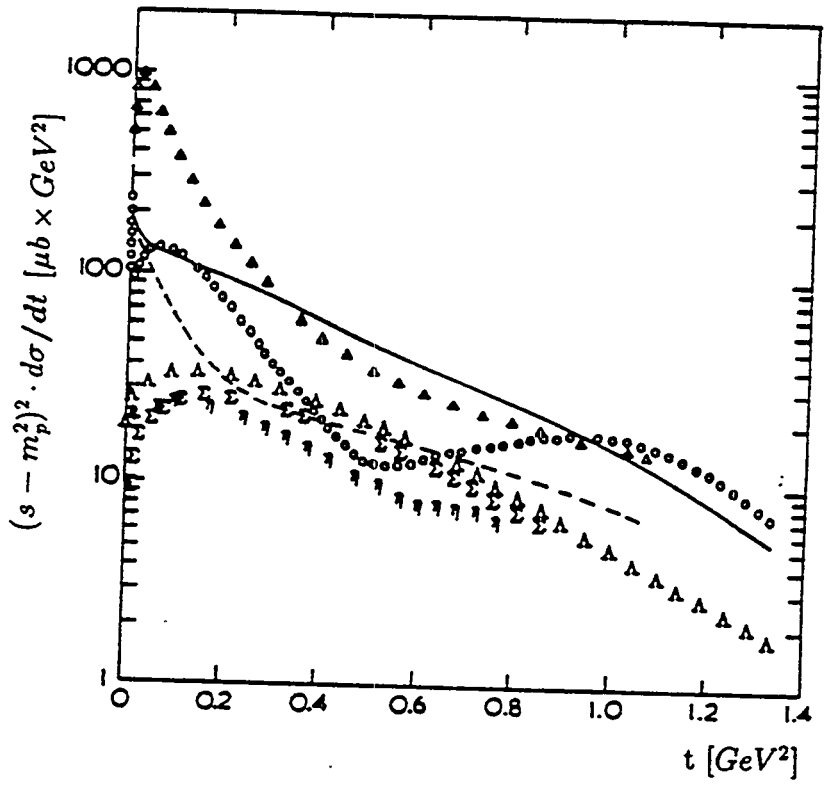


Fig. 2. Forward pseudoscalar photoproduction cross sections $(s-m_p^2)^2 \cdot d\sigma/dt$ plotted against t for various reactions: solid line, $\gamma p \to \pi^+ n$; dashed line, $\gamma n \to \pi^- p$; (o) $\gamma p \to \pi^o p$; (Δ) $\gamma p \to \pi^- \Delta^{++}$; ($\eta$) $\gamma p \to \eta^o p$; (Λ) $\gamma p \to K^+ \Lambda^o$; ($\Sigma$) $\gamma p \to K^+ \Sigma^o$.

forward pseudoscalar photoproduction cross sections $(s-m_p^2)^2 \cdot d\sigma/dt$ plotted against t for various reactions [10], where s is the center-of-mass energy squared: $s = m_p^2 + 2m_p E_\gamma$. The cross sections (see Fig. 2) differ by two

orders of magnitude near $t = 0$ and have very different angular distributions. These differences can be ascribed to the fact that these reactions may have different t-channel exchanges. For $t > 0.7\ GeV^2$, the differences between the various reactions disappear, all showing universal $E_\gamma^{-2}e^{-3t}$ behavior. This falloff in t is slower than is typical for hadronic reactions ($\sim e^{-8t}$). The most notable features of the angular distributions are the pronounced structures for very small $t < m_\pi^2$ observed in $\gamma p \to \pi^+ n$ [11], $\gamma p \to \pi^- \Delta^{++}$ [12], and $\gamma n \to \pi^- p$, the reactions in which π exchange is allowed. For example, the $\gamma p \to \pi^- \Delta^{++}$ cross section falls off at very small t, in contrast to the sharp forward peak seen in $\gamma p \to \pi^+ n$ cross sections.

The inverse reaction of $\gamma p \to \pi^+ n$ is $\pi^+ n \to \rho^o p$. Unfortunately, good quality data exist [13] only for the reaction $\pi^- p \to \rho^o n$ at 17.2 GeV. The differential cross section as a function of t shows the behavior expected for one-pion exchange (spin flip amplitude) which should vanish at $t = 0$. The most interesting observation for the $\pi^- p \to \rho^o n$ reaction is the presence of strong polarization effects [14], i.e. a large left-right polarized target asymmetry (presence of amplitudes without nucleon spin flip as a $J^{PC} = 1^{++}$ exchange) in the low t region. A sizable asymmetry was also observed [16] in π^+ photoproduction from a polarized target at 5 and 16 GeV. A typical value of the asymmetry is about -0.5 in both experiments. This is very surprising since according to general belief this region should be dominated by one-pion exchange and should therefore show little or no polarization effects.

The photoproduction of strange particles via $\gamma p \to K^+ \Lambda^o$ is similar to the photoproduction of π^+ mesons via $\gamma p \to \pi^+ n$. In particular, the central region cross sections are similar in magnitude for both reactions [9]. This suggests that in the central region the real photon fluctuates into $d\bar{d}$ or $s\bar{s}$ quark pairs with equal probability, as is observed in e^+e^- annihilations (where $\Delta R_d = \Delta R_s$). We also see that the ratio of the cross sections decreases systematically as we go to smaller values of momentum transfer t. The cross sections for the reaction $\gamma p \to K^+ \Lambda^o$ have been measured [17] at t values from 0.005 to 2 GeV^2 and at photon energies 5, 8, 11 and 16 GeV (see Fig. 2). For $t > 0.2\ GeV^2$, the $K^+\Lambda^o$ cross sections are about one third of the $\pi^+ n$ photoproduction cross sections, having nearly the same energy and momentum transfer dependences. However, the $K^+\Lambda^o$ cross sections fall off at very small t, in contrast to the sharp forward spike seen in the $\pi^+ n$ cross sections. This aspect is far from understood, and reflects the internal structure of the nucleon and as well as that of the photon.

2.2 Electroproduction Data

The existing data on the electroproduction of charged pions [18, 19, 20, 21, 22] and charged kaons [23, 24] for $W > 2\ GeV$ are sparse and poor in quality. The experimental aparatus used in these experiments consisted of two focusing magnetic spectrometers, which covered narrow intervals of Δt and ΔQ^2, and had small solid angles $\Delta\Omega$. The main motivation for these experiments was to determine the longitudinal-transverse interference term and/or to extract the pion (kaon) electromagnetic form factor (using a dispersion-theory model) at higher Q^2 that are inaccessible in pion-electron [25, 26, 27] and kaon-electron [28] scattering experiments.

The procedure of extracting a virtual photon cross section $d\sigma_{\gamma_v p}/dtd\phi$ from the observed electroproduction cross section is based on a one-photon approximation. Here the electrons are regarded as providing a beam of virtual photons of known polarization ϵ, mass squared Q^2, and energy ν. Electroproduction reactions can be described in terms of form factors that are generalizations of the form factors observed in elastic electron-proton scattering, or in terms of cross sections that are extensions of the photoproduction cross sections. The most general form of the differential cross section σ for the reactions

$$e^- + p \rightarrow e^- + \pi^+(K^+) + n(\Lambda^o) \tag{1}$$

can be written in terms of four structure functions (unpolarized beam and target) [29]:

$$\sigma(W, Q^2, t, \phi) \;=\; \sigma_T + \epsilon\sigma_L + \epsilon\sigma_{TT}cos2\phi + \sqrt{\epsilon(\epsilon+1)/2}\cdot\sigma_{LT}cos\phi \tag{2}$$

where σ_T, σ_L, σ_{TT}, and σ_{LT} are functions of the variables: Q^2, W (hadronic mass squared $W^2 = 2m_p\nu - Q^2 + m_p^2$), and $t \equiv (p_{\gamma_v} - p_{\pi,K})^2 - t_{min}$ (or θ^*, the angle between the virtual photon and meson in the hadronic center of mass W). The dependence on the azimuthal angle ϕ (angle of the meson relative to the electron scattering plane: $\phi \equiv \phi^*$) is shown explicitly in Eq. (2). The parameter ϵ is the polarization of the virtual photon. The term σ_T represents the cross section for transverse photons, σ_L represents the cross section for longitudinal photons, σ_{TT} is the interference between the transverse amplitudes, and σ_{LT} is the interference between the transverse and longitudinal amplitudes. The terms σ_{TT} and σ_{LT} approach zero as $t \rightarrow 0$, and the terms

σ_L and σ_{LT} vanish as $Q^2 \to 0$. In eq. (2), the structure functions σ_T and σ_{TT} (as in photoproduction) can be further decomposed into two parts: $\sigma_\perp$ corresponds to incident photons polarized perpendicular to the hadronic plane, and $\sigma_\parallel$ corresponds to photons polarized parallel to the hadronic plane. This yields: $\sigma_T = (\sigma_\parallel + \sigma_\perp)/2$, $\sigma_{TT} = (\sigma_\parallel - \sigma_\perp)/2$, and $\sigma_{LT} \sim Re(A_L \cdot A_\parallel)$. The sharp forward peak observed in π^+ photoproduction (see solid line in Fig. 2) is due to the rapid variation of $\sigma_\parallel$ with t, as is confirmed by polarized beam asymmetry data.

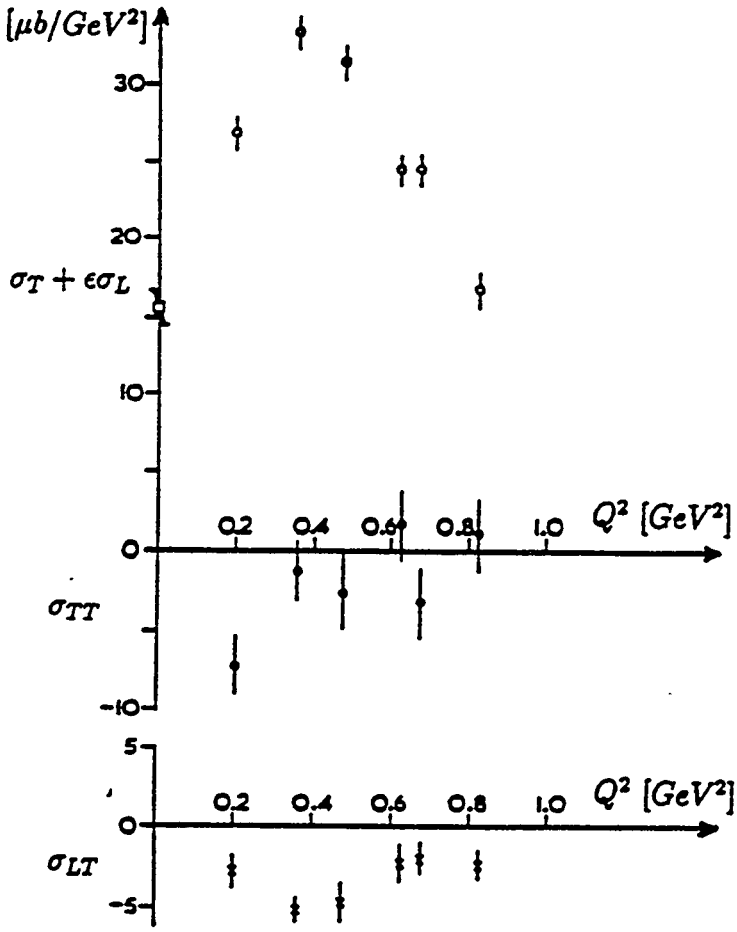


Fig. 3. Q^2 dependences of the $\gamma_v p \to \pi^+ n$ differential cross section components for $W = 2.2\ GeV$ and $t = 0.01\ GeV^2$ [18]: (o) $\sigma_T + \epsilon\sigma_L$, (•) σ_{TT}, (×) σ_{LT}, and (□) photoproduction cross section at $Q^2 = 0$.

In Fig. 3, we plot the Q^2 dependences of the $\gamma_v p \to \pi^+ n$ differential cross section components for $W = 2.2\ GeV$ and $t = 0.01\ GeV^2$ [18]: (o) $\sigma_T + \epsilon\sigma_L$, (•) σ_{TT}, and (×) σ_{LT}. The photoproduction cross section (□) at $Q^2 = 0$ is also shown. These results, together with CEA data [19] at $W = 2.15\ GeV$, clearly show that the reaction is dominated by $\sigma_T + \epsilon\sigma_L$. The rapid increase with Q^2 is apparently caused by the longitudinal cross section σ_L, which vanishes at $Q^2 = 0$ and exceeds the transverse component σ_T by a factor of 3 at $Q^2 = 0.26\ GeV^2$. Low statistics Cornell data [22] for $Q^2 > 1.0\ GeV^2$ also indicate that as Q^2 increases the longitudinal term becomes the dominant part of the cross section for $t < m_\pi^2$. It is worth mentioning that, in the small t region, the observed t dependence of σ_L is approximately e^{-15t} [18]. This falloff is much faster than in photoproduction data for $t > m_\pi^2$ ($\sigma_T \sim e^{-3t}$).

We conclude that the field of electroproduction is still in its infancy. The general features of electroproduction reactions are in reasonable qualitative agreement with photoproduction data, taking into account their apparent Q^2 dependence. To make further progress in our understanding of strong interactions, we need much better quality of exclusive electroproduction data. In addition, a reasonable amount of polarization data will help us to unravel amplitudes and assumptions about the nature of the exchanges. Analysis of the angular distributions of produced mesons may give us information about the quantum numbers of exchanged objects [14, 15]. Determination of the pion (kaon) form factor from electroproduction data (extraction of $\sigma_{||}$ and σ_L) is justified only if we have a model which describes all aspects of the data.

We propose to measure the differential cross section $\sigma(t, W, Q^2)$ for the reactions $e^- + p \to e^- + \pi^+(K^+) + n(\Lambda^o)$ at a beam energy of $\geq 4\ GeV$ using the CLAS detector at CEBAF. Data will be collected simultaneously for both reactions in the following kinematical region: $Q^2 > 1\ GeV^2$ and $W > 2\ GeV$. One of the most interesting aspects of electroproduction is that it can be used to measure photoproduction amplitudes as functions of the photon mass squared Q^2 and momentum transfer t. Emphasis is given to measuring the differential cross sections for momentum transfers $t \sim m_{\pi,K}^2$. High statistics and good quality data collected simultaneously using a large acceptance detector will improve our understanding of nucleon structure as well as the hadronic properties of the photon.

3 Simulation

We have used the SDA Package [30] to simulate the $ep \rightarrow e\pi^+(K^+)n(\Lambda^o)$ reactions and to reconstruct the events accepted in the CLAS detector. In order to estimate rates we have used the following form of differential cross sections [31]:

$$\frac{d^2\sigma}{dQ^2dW} = \frac{\alpha}{\pi}\frac{W\sqrt{(W^2+Q^2-m_p^2)^2+4m_p^2Q^2}}{(s-m_p^2)^2Q^2}\frac{1}{1-\epsilon}\frac{d\sigma_{\gamma_v p}(W,Q^2,\theta^*,\phi^*)}{d\Omega_{\pi,K}} \quad (3)$$

where s is the center-of-mass energy squared: $s = m_p^2 + 2m_pE_{beam}$.

In eq. (3) we multiplied the measured cross section $d\sigma_{\gamma_v p}(W,Q^2,\theta^*,\phi^*)/d\Omega_\pi$ at $Q^2 = 0.4\ GeV^2$ and $W = 2.15\ GeV$ [19] by the ratio of form factors $F_\pi^2(0.4)/F_\pi^2(Q^2)$ using a simple pole form. In Table 1, as an example, we show the expected rates of π^+ mesons produced (N_{prod}/hr) and reconstructed

Table 1: Expected rates of produced (N_{prod}/hr) and reconstructed (N_{obs}/hr) π^+ mesons using the CLAS detector at a luminosity of $10^{34}cm^{-2}s^{-1}$ for $\Delta W = (2.0-2.2)\ GeV$ and $\Delta\Omega_\pi = 2\pi\int sin\theta_\pi^* d\theta_\pi^* = 0.377sr$ ($\theta_\pi^* < 20^o$).

	N_{prod}/hr	N_{obs}/hr	σ_{MM} [GeV]	σ_t [GeV^2]
ΔQ^2: 1.0 - 1.5 GeV^2 $E_{beam} = 4.0\ GeV$	2278	798	0.0040	0.0030
ΔQ^2: 1.5 - 2.0 GeV^2 $E_{beam} = 4.5\ GeV$	846	406	0.0044	0.0036
ΔQ^2: 2.0 - 2.5 GeV^2 $E_{beam} = 5.0\ GeV$	397	217	0.0045	0.0042
ΔQ^2: 2.5 - 3.0 GeV^2 $E_{beam} = 5.5\ GeV$	210	124	0.0048	0.0050

(N_{obs}/hr) with a one hour run of the CLAS detector at a luminosity $L = 10^{34}cm^{-2}s^{-1}$ for $\Delta W = 2.0-2.2\ GeV$ and $\Delta\Omega_\pi = 2\pi\int sin\theta_\pi^* d\theta_\pi^* = 0.377sr$

($\theta^*_\pi < 20°$). The corresponding rates for K^+ electroproduction are expected to be about 5 - 10 times smaller. The average missing mass σ_{MM} and 4-momentum transfer σ_t resolutions (assuming we measure the final electrons and mesons with a full magnetic field in the CLAS detector) [32] are also shown in Table 1. It is also worthwhile to mention that for the kinematic variables described in Table 1 (where $\theta^*_\pi < 20°$), the reconstructed mesons have laboratory scattering angles $\theta_{\pi,K}$ ranging from 8° to 25°.

For $2.0 < W < 2.2$, $\theta^*_\pi < 20°$, and any bin of ΔQ^2 in the range $1.0 < Q^2 < 3.0$, the acceptance $A_{cc}(\theta^*_\pi, \phi^*_\pi)$ is about (35 - 60)% with no holes in the $(\theta^*_\pi, \phi^*_\pi)$-plane. That will allow us to use the measured angular distributions of produced mesons to estimate the contribution of various amplitudes to the cross sections.

Conclusion

In this paper, we have revisited twenty year old data considering the progress achieved in related fields. To make further progress in our understanding of strong interactions, we need much better quality of exclusive electroproduction data. We have shown that using the present equipment under construction at CEBAF with a beam energy of $< 6\ GeV$, we will obtain good quality electroproduction data that will improve our understanding of nucleon structure as well as the hadronic properties of the photon. In order to access higher W and Q^2 at higher beam energies, we need to design a new large acceptance forward detector.

Acknowledgements

I would like to thank Bernhard Mecking for his useful comments, and Mike Niczyporuk for proof reading several drafts of this paper.

References

[1] T.H. Bauer *et al.*, Rev. of Mod. Phys. **v.50** (1978)261.

[2] H. Abramowicz *et al.*, Int. J. of Mod. Phys. **A8** (1993)1005.

[3] D. Willams *et al.*, Phys. Rev. **D38** (1988)1365.

[4] I. Abt *et al.*, Nucl. Phys. **B407** (1993)515.

[5] H. Abramowicz *et al.*, DESY 93-158

[6] J.D. Bjorken, J.B. Kogut and D.E. Soper, Phys. Rev. **D3** (1971)1382.

[7] S.J. Brodsky and P. Hoyer, Phys. Lett. **B298** (1993)165.

[8] V.D. Duca and S.J. Brodsky, Phys. Rev. **D46** (1992)931.

[9] R.L. Anderson, D.B. Gustavson *et al.*, Phys. Rev. **D14** (1976)679.

[10] J.K. Storrow, p. 263 in "Electromagnetic Interactions of Hadrons", **v.1**, Plenum Press, 1978.

[11] A.M. Boyarski, F. Bulos *et al.*, Phys. Rev. Lett. **20** (1968)300.

[12] A.M. Boyarski, R. Diebold *et al.*, Phys. Rev. Lett. **22** (1969)148.

[13] G. Grayer, B. Hyams *et al.*, Nucl. Phys. **B75** (1974)189.

[14] H. Becker, G. Blanar *et al.*, Nucl. Phys. **B151** (1979)46.

[15] B.B. Niczyporuk, CEBAF-PR-89-040 (1989).

[16] C.C. Morehouse, M. Borghini *et al.*, Phys. Rev. Lett. **25** (1970)835.

[17] A.M. Boyarski, F. Bulos *et al.*, Phys. Rev. Lett. **22** (1969)1131.

[18] C. Driver, K. Heinloth *et al.*, Phys. Lett. **35B** (1971)pp.77-82.

[19] C.N. Brown, C.R. Canizares *et al.*, Phys. Rev. **D8** (1973)92.

[20] C.J. Bebek, C.N Brown *et al.*, Phys. Rev. **D9** (1974)1229.

[21] C.J. Bebek, A. Browman *et al.*, Phys. Rev. Lett. **37** (1976)1326.

[22] C.J. Bebek, C.N Brown *et al.*, Phys. Rev. **D17** (1978)1693.

[23] C.J. Bebek, C.N Brown *et al.*, Phys. Rev. **D15** (1976)594.

[24] T. Azemoon, I. Dammann *et al.*, Nucl. Phys. **B95** (1975)77.

[25] G.T. Adylov, F.K. Aliev *et al.*, Phys. Lett. **B51** (1974)402.

[26] E.B. Dally, D.J. Drickey *et al.*, Phys. Rev. Lett. **39** (1977)1176.

[27] S.R. Amendolia, M. Arik *et al.*, Nucl. Phys. **B277** (1986)168.

[28] S.R. Amendolia, G. Batignani *et al.*, Phys. Lett. **B178** (1986)435.

[29] A. Bartl and W. Majerotto, Nucl. Phys. **B62** (1973)267.

[30] B.B. Niczyporuk, SDA Package (unpublished).

[31] R.G. Roberts, "The Structure of the Proton", Cambridge University Press, 1990.

[32] B.B. Niczyporuk, CEBAF-PR-91-004 (1991).

ELASTIC FORM FACTORS AT HIGHER CEBAF ENERGIES

GERASSIMOS G. PETRATOS
Department of Physics and Center for Nuclear Research
Kent State University, Kent, Ohio, 44242

ABSTRACT

The prospects for elastic scattering from few body systems with higher beam energies at CEBAF is presented. The deuteron and ^{3}He elastic structure functions $A(Q^2)$ can be measured at sufficiently high momentum transfers to study the transition between the conventional meson-nucleon and the constituent quark-gluon descriptions. Possible improvements in the proton magnetic form factor data are also presented.

An upgrade of CEBAF to higher energies will offer unique opportunities in advancing our understanding of nucleon and nuclear structure. Large momentum transfer measurements of the elastic form factors of nucleons and few body systems, in particular, should provide decisive tests of predictions of constituent quark models and quantum chromodynamics.

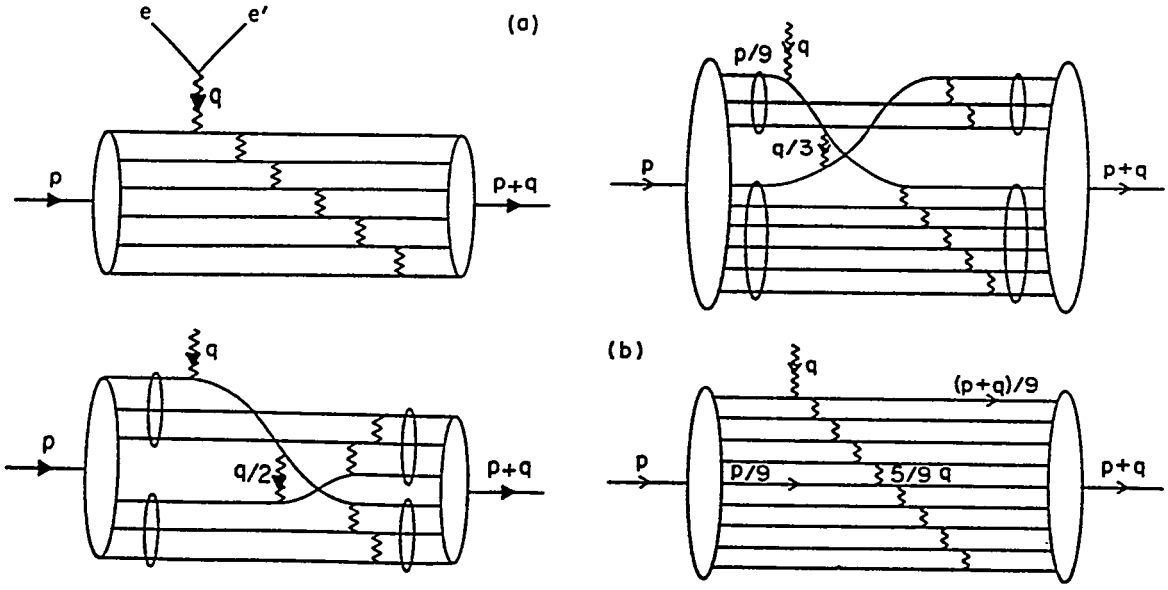


Fig. 1: Elastic electron scattering from deuterium and ^{3}He in the dimensional scaling quark model.

The starting point of the conventional theoretical approach of elastic scattering from the few body systems [1] is the impulse approximation (IA). The deuteron and helium form factors are then convolutions of the nuclear wave function with the form factors of the constituent nucleons. It has long been recognized and overwhelmingly supported by data that the few body form factors are sensitive to the presence of meson exchange currents (MEC) that augment the IA picture.

At large momentum transfers, the few body form factors are expected to be described in terms of quark and gluons constituents within the framework of di-

mensional scaling quark model (DSQM) and perturbative quantum chromodynamics (PQCD) [2]. In this case, their Q^2 evolution depends on compositeness of the nucleus as well as on the dynamics of the forces that rearrange the constituents during the elastic scattering process. The two basic diagrams for this process are shown in Fig. 1 for deuterium (a) and ^{3}He (b). The underlying dynamical mechanism is the hard rescattering of the constituent quarks. The Q^2 dependence of the process is then predicted by simply counting the number of gluon propagators, which implies that the elastic structure functions $A(Q^2)$ of deuterium and helium should fall like $\sqrt{A(Q^2)} \sim (Q^2)^{n-1}$, where $n = 6(9)$ for deuterium (^{3}He). The quark interchange diagrams of Fig. 1 can be regarded as the prototype for MEC: at lower Q^2, where coherent exchanges of gluon interactions can bind the quark lines to form virtual meson states, the quark approach merges with the conventional MEC approach.

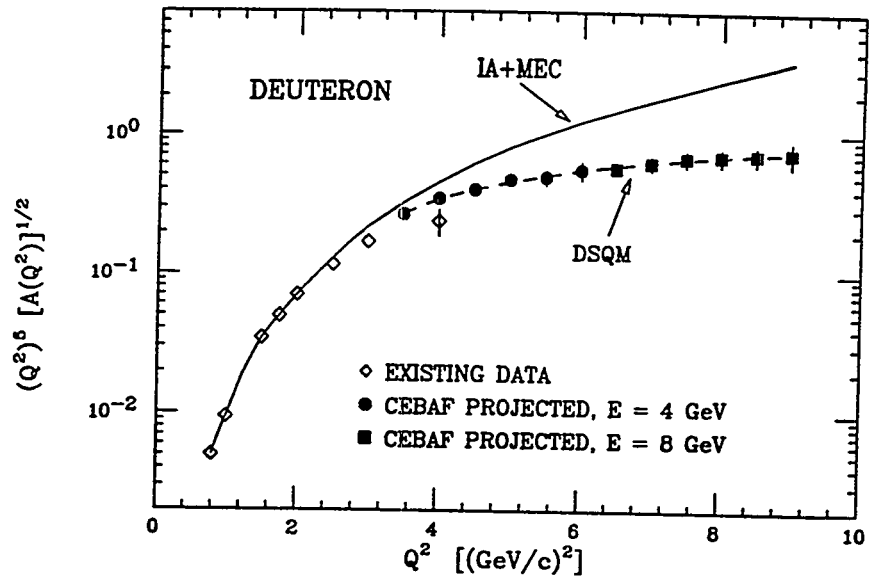


Fig. 2: Existing and possible CEBAF data for the deuteron $A(Q^2)$ with an 8 GeV beam.

The existing data on the deuteron $A(Q^2)$ strongly suggest an approach to the DSQM limit as can be seen in Fig. 2. At the same time the data are described well by the conventional relativistic IA with inclusion of MEC [1]. It is evident that new measurements at larger Q^2, where the DSQM and IA+MEC predictions are drastically different, as shown in Fig. 2, are needed in order to test for their validity.

A higher CEBAF beam energy in excess of 8 GeV is essential for these measurements. Low counting rates will require use of a long deuterium target. The resulting degradation in resolution will require detection of the recoiling deuterons in coincidence with the scattered electrons. A possible experimental scenario would be to use the hadron HRS and a higher momentum (up to 6 GeV/c) upgraded electron HRS Hall-A spectrometers. Assuming a 4 msr electron solid angle [3], a 15 cm long liquid deuterium target and 200 μA beam intensity, $A(Q^2)$ can be measured up to about 10 (GeV/c)^2, as shown in Fig. 2, in about one month of beam time. The quality of the projected data will be sufficient for a test of the theoretical predictions.

The existing data on the ^{3}He $A(Q^2)$, shown in Fig. 3, are in agreement with the meson-nucleon (IA+MEC) calculations at low Q^2 but are fairly inconclusive at the largest momentum transfers. They are consistent with a change in slope, indicative of an onset of scaling, but, at the same time, cannot exclude the presence of a second diffraction minimum as predicted by the conventional theory. As in the case of deuterium, more measurements at higher Q^2 would be crucial in testing the scaling prediction and any possible breakdown of the meson-nucleon framework.

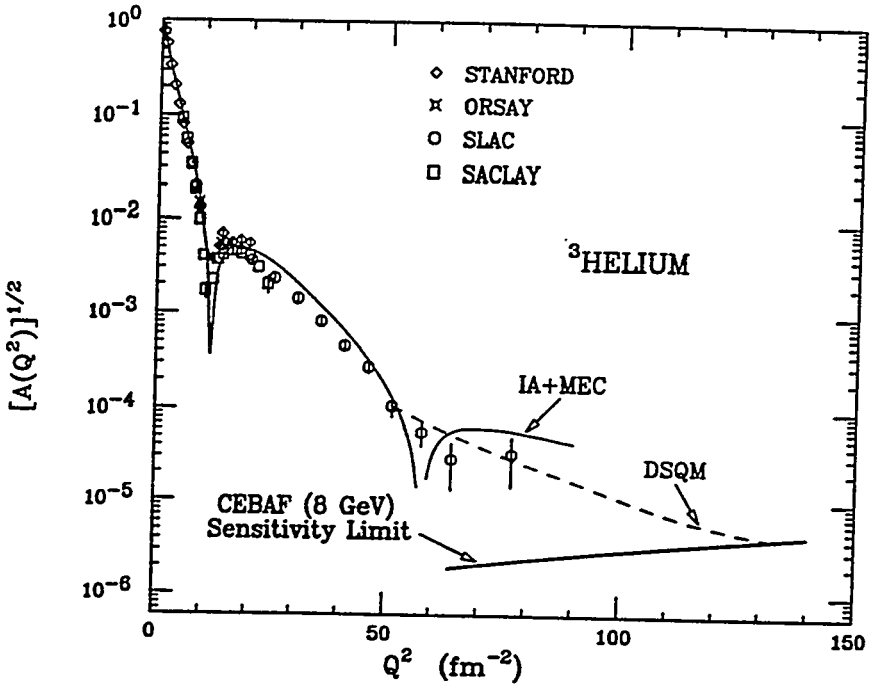


Fig. 3: Existing data for the ^{3}He $A(Q^2)$ and the CEBAF sensitivity limit with an 8 GeV beam.

A future energy upgrade of CEBAF to 8 GeV will allow for new measurements that could double the Q^2 range of the existing data with a ten-fold better sensitivity. The sensitivity is defined as the lowest $[A(Q^2)]^{1/2}$ value that can be measured with ±25% statistical error in a week of beam time and is shown in Fig. 3. The new measurements assume use of the ^{3}He high power cryotarget of Hall-A under construction and an upgraded version of the electron HRS Hall-A spectrometer to 7 GeV/c. Assuming an expected 4 msr spectrometer solid angle, the new measurements would require about one month of beam time.

Higher CEBAF energies will be also instrumental in extending or improving measurements of the nucleon form factors to higher momentum transfers. The case of the neutron form factors is examined in Ref. 4. The case of the proton electric form factor, G_E^p, is examined in Ref. 5. For the magnetic form factor of the proton, G_M^p, the existing data can be significantly improved.

Fig. 4 shows the existing G_M^p data [6], scaled by the dipole formula $G_D = (1 + Q^2/0.71)^{-2}$, from Rosenbluth separations, and from single cross section measurements assuming a model for G_E^p. The open squares assume that the approximate form factor scaling $G_E^p = G_M^p/\mu$ with μ being the proton magnetic moment, measured up to $Q^2 = 7$ (GeV/c)^2, continues at higher Q^2. The open circles assume a possible deviation

from form factor scaling with increasing Q^2. Such a deviation could affect in a sizable way the extracted value of G_M^p, as shown in Fig. 4.

The higher luminosities of CEBAF will allow for precise measurements in short running times even at backward angles where cross section are small. At these angles, G_E^p makes a little contribution to the cross sections, so use of the existing forward angle data will suffice for an extraction of G_M^p without making any assumption for G_E^p. Fig. 4 shows projected data from such an extraction by performing elastic scattering measurements from hydrogen with incident energies up to 12 GeV at scattering angles around 90°. Using an existing large solid angle spectrometer, such as the HRS (Hall-A) or HMS (Hall-C), and a high power cryotarget, the total beam time for these measurements would amount to just a few days.

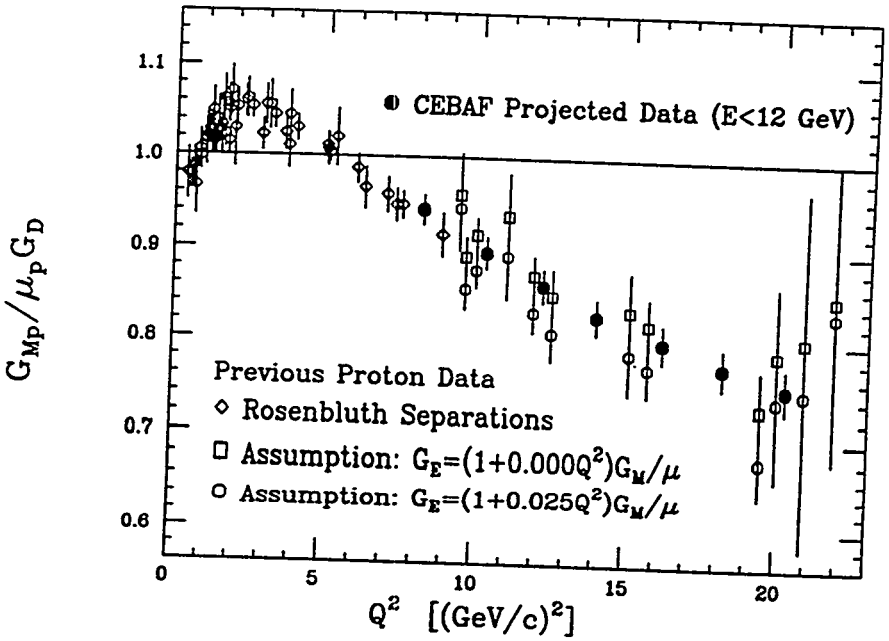


Fig. 4: Existing and possible CEBAF data for the proton magnetic form factor with a 12 GeV beam.

In summary, higher CEBAF energies could extend our knowledge of elastic form factors to higher momentum transfers with measurements requiring reasonable beam times and modest spectrometer upgrades. The new measurements will study the transition from the phenomenological meson-nucleon to the constituent quark-gluon description of the few-body nuclear systems and provide improved data for our understanding of the nucleons within the framework of PQCD.

1. R. Schiavilla, V. Pandharipande and D. Riska, *Phys. Rev.* **C41** (1990) 309; E. Hummel and J. Tjon, *Phys. Rev.* **C42** (1990) 423; and references therein;
2. S. Brodsky and B. Chertok, *Phys. Rev.* **D14** (1976) 3003; S. Brodsky, C.-R. Ji and P. Lepage, *Phys. Rev. Lett.* **51** (1983) 83.
3. J. LeRose and S. Nanda, private communication.
4. W. Brooks, contribution to this Workshop.
5. E. Voutier, contribution to this Workshop.
6. L. Andivahis *et al.*, *SLAC-PUB-6462 (1994)*; A. Sill *et al.*, *Phys. Rev.* **D48** (1993) 29; and references therein.

he submitted manuscript has been authored
r a contractor of the U. S. Government
nder contract No. W-31-109-ENG-38.
ccordingly, the U. S. Government retains a
onexclusive, royalty-free license to publish
reproduce the published form of this
ntribution, or allow others to do so, for
. S. Government purposes.

DEUTERON PHOTO-DISINTEGRATION AT HIGH ENERGIES

DAVID H. POTTERVELD
Physics Division, Argonne National Laboratory
Argonne, Il. 60439, USA

and

ROY J. HOLT
Physics Division, Argonne National Laboratory
Argonne, Il. 60439, USA

Dept. of Physics, University of Illinois
Urbana, IL 61801, USA

ABSTRACT

Current proposals at CEBAF include the measurement of cross sections and polarization observables of exclusive photonuclear reactions such as deuteron photodisintegration and pion photo-production from nucleons. At issue is the applicability of traditional meson-exchange models versus quark models of these reactions at photon energies of several GeV. Beam energies above 4 GeV at CEBAF could make possible the measurement of these reactions over a kinematic range sufficiently broad to distinguish between the models. Estimates of counting rates for a Hall-C experiment to measure the $\gamma d \rightarrow pn$ cross section are presented.

1. Introduction

One of the current issues in nuclear physics is whether quark degrees of freedom become apparent in high energy nuclear reactions. Evidence for such degrees of freedom would be the onset of asymptotic scaling[1,2] in the cross section, and the conservation of hadron helicity[3]. To date, studies have focused on photo-reactions in the few-body systems, where stringent tests of our understanding of short-range nuclear dynamics should be possible[4]. However, almost no polarization data for high energy photonuclear reactions exist, since the emphasis has been on cross section measurements.

Asymptotic scaling predicts that the differential cross section $d\sigma/dt$ obeys the constituent counting rule[5], in which $d\sigma/dt$ scales with energy as $1/s^{n-2}$, where s is the square of the center-of-mass energy and n is the total number of point-like constituents involved in both the initial and final states of the reaction. Asymptotic scaling has been observed in high-energy nucleon-nucleon scattering[6], pion photoproduction from protons[5], and the electromagnetic form factors of the pion, proton and neutron[7], but little data exist for photo-reactions involving nuclei. Recently, cross sections were measured at SLAC for the $\gamma d \rightarrow pn$ reaction[8] for photon energies from

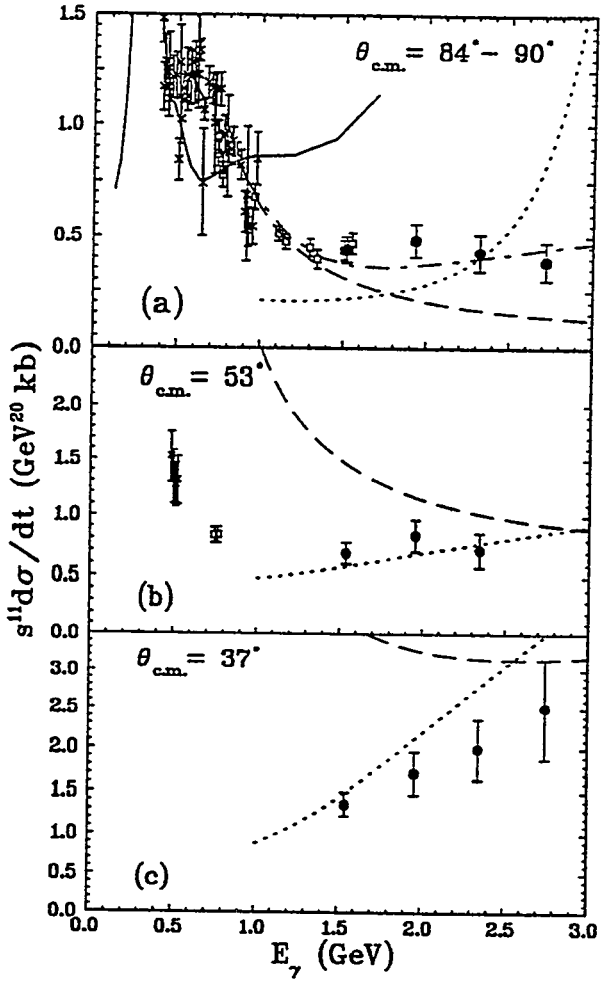


Figure 1: $s^{11}d\sigma/dt$ vs. s, for: (a) $\theta_{cm} = 90°$, (b) $\theta_{cm} = 53°$, (c) $\theta_{cm} = 37°$. Results from SLAC experiment NE17 are plotted as black circles, and earlier data[9,10] are plotted as crosses and open squares. The curves are discussed in the text.

1.5 – 2.8 GeV and center-of-mass scattering angles from 37° – 90°. The counting rule predicts that the cross section will have the form:

$$\frac{d\sigma}{dt} = \frac{h(\theta_{cm})}{s^{11}}, \tag{1}$$

where $h(\theta_{cm})$ can only be determined through more detailed modeling of the dynamics. The data shown in figure 1 seem to agree with this prediction at $\theta_{cm} = 90°$ and 53°, but disagree at 37°.

In general, it is expected that asymptotic scaling requires large values for all the Mandelstam variables s, t, and u. The 37° data correspond to momentum transfers of less that 1 GeV^2 to the outgoing neutron, and this may be too low to be in the scaling regime. The data at all angles are consistent with a threshold in the observance of

scaling around momentum transfers of 1 GeV^2. In this case, scaling at $\theta_{cm} = 37°$ would have an onset at photon energies of around 3 GeV.

Besides the constituent counting rule, the reduced nuclear amplitude analysis[11] (RNA) may apply to deuteron photo-disintegration. This analysis, based on perturbative QCD (PQCD), successfully describes elastic $e - d$ scattering[12] at small s where the counting rule breaks down. The RNA analysis factors out the proton and neutron form factors to describe the reaction in terms of a simpler, 'reduced' reaction involving point-like objects. When applied to deuteron photo-disintegration, one has:

$$\frac{d\sigma}{d\Omega_{\rm cm}} = \frac{1}{[s(s-m_d{}^2)]^{1/2}} F_p^2(t_p) F_n^2(t_n) \frac{1}{p_T^2} f^2(\theta_{cm}), \qquad (2)$$

where the $F_N(t)$ are the nucleon form factors, $t_i = (p_i - p_d/2)^2$ is the momentum transfer to the nucleon, p_T is the transverse momentum in the center-of-mass, and $f(\theta_{cm})$ is the 'reduced nuclear amplitude.' This formulation is expected to work better than constituent counting at small s since soft components are removed by dividing out the nucleon form factors.

The dashed curves in figure 1 represent the RNA prediction for the energy dependence of the cross section. The reduced amplitude $f(\theta_{cm})$ is difficult to calculate[11]; a value was chosen for $\theta_{cm} = 90°$ that agrees with a data point at $E_\gamma = 800$ MeV. This curve falls below the data at higher energies, and does not reach an asymptotic limit. For purposes of comparison, we have plotted the RNA curve for $\theta = 53°$ and $37°$, using the same value of f. These curves show a more rapid decrease in the cross section with photon energy than is consistent with the data, and additionally lie above the data in the energy range studied. This conflicts with the forward and backward peaking expected of the reduced nuclear amplitude[11].

The solid curve in figure 1(a) represents the meson-exchange-based calculation of Lee *et al.*[13] The calculation agrees well with data below 500 MeV, but disagrees with the data above $E_\gamma = 1$ GeV in both energy and angular dependence. (At the forward angles the calculation is off scale.) Y. Kang, *et al.*[14] have calculated the cross section for $\theta_{cm} = 90°$ and $E_\gamma < 1.5$ GeV using a meson-exchange model with a larger number of resonances to achieve better agreement with the data over this energy range. The large number of nucleon resonances makes the extension of these models to higher energies problematic.

The agreement at 90° with the counting rule may not be conclusive evidence of the onset of PQCD. The energy dependence is also consistent with the asymptotic amplitude calculations of Nagornyĭ *et al.*[15], (shown in figure 1 as a dot-dashed curve), which are based only on meson and baryon degrees of freedom. Kondratyuk *et al.*[16] have applied a quark-gluon string model and Regge phenomenology to obtain scaling-like behavior over a limited range of s, (shown in figure 1 as a dotted curve), although there is strong disagreement with the highest energy data.

2. CEBAF Experiments

Further insight into this matter can be achieved at CEBAF through measurements

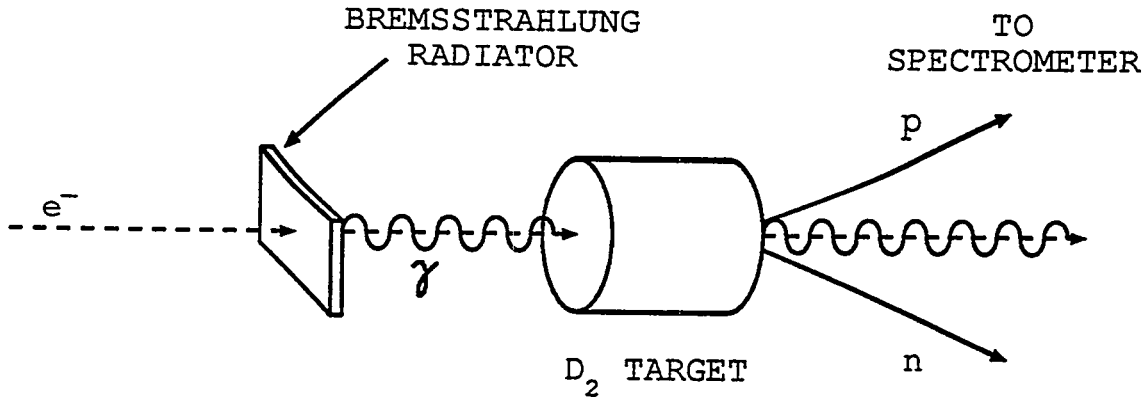


Figure 2: Experimental method for measuring the $\gamma d \rightarrow pn$ cross section.

of these cross sections at higher energies and with better statistics than were possible at SLAC. The experimental technique is substantially the same. A bremsstrahlung photon beam is created by passing the CEBAF electron beam through a removable copper radiator immediately upstream of a cryogenic deuterium target, as shown in figure 2. Protons from the $\gamma d \rightarrow pn$ reactions are detected in one of the hall-C spectrometers. The photon's energy and center-of-mass scattering angle can be calculated from the proton's energy and angle, assuming the proton originated in the $\gamma d \rightarrow pn$ reaction. Only protons corresponding to photons near the bremsstrahlung endpoint are accepted, to exclude events in which a pion was created. Background from the aluminum target walls is eliminated by subtracting events from an identical target cell filled with hydrogen. Electro-disintegration background from the electron beam passing through the target is eliminated by subtracting measurements with the radiator removed from measurements with it inserted. Absolute cross sections are obtained from the scattering rate using the bremsstrahlung yield calculated by numerically integrating the thick-target equations of Matthews and Owens[17].

Estimates for the running time of an experiment in hall-C can be extrapolated from the experience of NE17. In the following, we use a cross section model with s^{-11} energy dependence, and calculate the time needed for a cross section measurement with 10% statistical accuracy. The calculation assumes a 15 cm long target, a 6% radiation lengths thick Cu radiator, and a 6.5 msr solid angle for the HMS spectrometer. The beam current is limited to 30 μA by the allowable radiation level in hall-C. Two hours are allowed for changing beam energies, and a 50% efficiency is assumed for running the experiment. Table 1 lists the kinematic settings and time required for measurements for $\theta_{cm} = 37°$, 53°, and 90°, and photon energies from 2 – 6 GeV in 1 GeV steps. The total time is the sum of the data acquisition time plus the time for energy change, all divided by the efficiency.

Table 1: Running time estimates for $\gamma d \rightarrow pn$ cross section measurement.

E_{beam} (GeV)	θ_{cm} (deg)	θ_{lab} (deg)	P_{spec} (GeV)	Beam time (min)	Total time (hr)
2.0	37	19.9	2.41	1.3	
	53	29.2	2.24	1.5	
	90	53.9	1.70	5.0	4.3
3.0	37	17.5	3.35	26	
	53	25.8	3.09	31	
	90	48.2	2.26	107	10
4.0	37	15.8	4.27	165	
	53	23.4	3.92	191	
	90	44.1	2.81	710	40
5.0	37	14.5	5.19	1044	
	53	21.5	4.74	1219	
	90	40.9	3.34	4962	245
6.0	37	13.6	6.11	5148	
	53	20.1	5.57	6183	
	90	38.3	3.87	24045	1183

3. Conclusions

The time estimates show that measurements to 6 GeV at all three angles would be possible with the existing hall-C equipment, but would require a very long time to complete. However, the forward angle measurements take substantially less time because the cross section is larger—for example, the total time for the 6 GeV, 37° point is only 176 hours if the cross section has an s^{-11} dependence, and only 23.6 hours if the cross section continues the s^{-9} dependence observed in the SLAC data[8]. Experiment 89-012 is approved to make cross-section measurements to 4 GeV at these angles. It thus appears feasible to extend these measurements to 5 GeV at all angles, and 6 GeV at $\theta_{cm} = 37°$, using a higher energy beam at CEBAF. Such measurements should extend well into the scaling regime at all angles, and provide a sensitive test of our understanding of short-range forces and quark degrees of freedom in few-body systems.

4. Acknowlegements

This work was supported by the U.S. Department of Energy, Nuclear Physics Division, under Contract No. W-31-109-ENG-38.

5. References

1. V. A. Matveev, R. M. Muradyan, A. N. Tavkhelidze, *Lett. Nuovo Cimento* **7** (1973) 719.
2. S. Brodsky and G. Farrar, *Phys. Rev. Lett.* **31** (1973) 1153.
3. S. J. Brodsky and G. P. Lepage, *Nucl. Phys.* **A353** (1981) 247c.
4. R. J. Holt, *Phys. Rev.* **C41** (1990) 2400.
5. R. L. Anderson *et al.*, *Phys. Rev.* **D14** (1976) 679.
6. J. Ralston and B. Pire, *Phys. Rev. Lett.* **49** (1982) 1605.
7. S. Rock *et al.*, *Phys. Rev. Lett.* **49** (1982) 1139.
8. E. Belz, Ph.D. thesis, California Institute of Technology (1994).
9. R. Ching and C. Schaerf, *Phys. Rev.* **141** (1966) 1320, P. Dougan *et al.*, *Z. Phys.* **A276** (1976) 55, J. Arends *et al.*, *Nucl. Phys.* **A412** (1984) 509.
10. S. J. Freedman *et al.*, *Phys. Rev.* **C48** (1993) 1864.
11. S. J. Brodsky and J. R. Hiller, *Phys. Rev.* **C28** (1983) 475.
12. S. J. Brodsky and B. T. Chertok, *Phys. Rev.* **D14** (1976) 3003.
13. T.-S. H. Lee, Argonne National Laboratory report PHY-5253-TH-88; T.-S. H. Lee, in *Proceedings of the International Conference on Medium and High Energy Nuclear Physics, May 23-27, 1988, Taipei, Taiwan* (World Scientific, 1988) 563.
14. Y. Kang, P. Erbs, W. Pfeil, H. Rollnik, *Abstracts of the Particle and Nuclear Intersections Conference, MIT* (Cambridge MA, 1990) I-40; W. Pfeil, private communication.
15. S. I. Nagornyĭ, Yu. A. Kasatkin, and I. K. Kirichenko, *Sov. J. Nucl. Phys.* **55** (1992) 189.
16. L. A. Kondratyuk *et al.*, *Phys. Rev.* **C48** (1993) 2491.
17. J. L. Matthews and R. O. Owens, Nucl. Instr. and Meth. **111**, 157 (1973).

NONPERTURBATIVE QCD AND ELASTIC PROCESSES AT CEBAF ENERGIES

A.V.RADYUSHKIN*
Physics Department, Old Dominion University
Norfolk, VA 23529, USA
and
Continuous Electron Beam Accelerator Facility
Newport News, VA 23606, USA

ABSTRACT

We outline how one can approach nonperturbative aspects of the QCD dynamics studying elastic processes at energies accessible at upgraded CEBAF. Our point is that, in the absence of a complete theory of the nonperturbative effects, a possible way out is based on a systematic use of the QCD factorization procedure which separates theoretically understood ("known") short-distance effects and nonperturbative ("unknown") long-distance ones. The latter include hadronic distribution amplitudes, soft components of hadronic form factors *etc.* Incorporating the QCD sum rule version of the QCD factorization approach, one can relate these nonperturbative functions to more fundamental obects, vacuum condensates, which accumulate information about the nonperturbative structure of the QCD vacuum. The emerging QCD sum rule picture of hadronic form factors is characterized by a dominant role of essentially nonperturbative effects in the few GeV region, with perturbative mechanisms starting to show up for momentum transfers Q^2 closer to 10 GeV^2 and higher. Thus, increasing CEBAF energy provides a unique opportunity for a precision study of interplay between the perturbative and nonperturbative phenomena in the QCD description of elastic processes.

1. Hierarchical structure of NpQCD description of elastic processes

"What can we learn about nonperturbative QCD from studying elastic processes at CEBAF energies?" In some sense, *all* we will learn from studying elastic processes at any energy will involve nonperturbative aspects of QCD because the very nature of initial and final state hadrons is essentially nonperturbative. In the few GeV energy range, the nonperturbative effects are especially important and, in fact, play a crucial role. However, it is also true that to learn something about nonperturbative QCD one should formulate first a theoretical framework adequately describing the nonperturbative aspects of quantum chromodynamics. The problem is that the nonperturbative QCD (NpQCD) is not a completed theory yet, and there is no formalism which allows one to calculate nonperturbative effects from the first principles of QCD. Still, because of asymptotic freedom, there are regions of momentum space where QCD is under theoretical control, and these regions can be

*Also at *Laboratory of Theoretical Physics, Joint Institute for Nuclear Research, 141980 Dubna, Russian Federation*

used as a starting point for a step by step penetration into the nonperturbative regions of QCD. This step by step strategy is based on a generic idea that one should make first a full use of what is known, isolate the structures which are unknown, parameterize them in some way and then study the parameterizing functions as separate objects. In fact, this is exactly the procedure developed to study strong interaction physics long before the invention of QCD.

1.1. Form factors

Consider, *e.g.*, a typical CEBAF experiment on electron-proton elastic scattering. The electron properties are known from QED, so one can readily write down the matrix elements for interaction between the electron and electromagnetic field. However, a similar matrix element $\langle P'|J^\mu|P\rangle$ for the proton is not immediately known because the strong interaction physics is involved which cannot be directly approached in a straightforward perturbative framework. Introducing elastic form factors $G_E^p(Q^2), G_M^p(Q^2)$, we accumulate unknown information about the strong interactions (and, hence, about NpQCD) in these two functions. In fact, many models were proposed to calculate $G_E^p(Q^2), G_M^p(Q^2)$ and other hadronic form factors. However, most of these models have a very remote (if any) connection with the basic principles of QCD and QCD Lagrangian. As a result, experimental success or failure of such models usually tells us very little about the nonperturbative aspects of QCD. In other words, to get an informative answer from experiment about NpQCD, the question must be cast in a "QCD language" based on concepts which have a clear and direct relation to the QCD Lagrangian.

1.2. Wave functions

Introducing hadronic form factors, we incorporated only a part of what we know now, namely, the theory of electromagnetic interactions. However, as emphasized above, QCD is not a total *terra incognita*: its short-distance behaviour can be calculated using perturbation theory. In particular, one can use perturbative QCD to calculate the Q^2-dependence of hadronic form factors[1,2,3] at large momentum transfer Q (most probably, very large). According to the factorization theorem[4,5,6], $G^p(Q^2)$ is given by a convolution of the hard scattering amplitude $T(\{x\},\{x'\};Q^2)$ and proton distribution amplitudes (sometimes also called wave functions) $\varphi(x_1,x_2,x_3)$ specifying the probability amplitude to find the proton composed of its three valence quarks carrying the fractions x_1, x_2, and x_3 of its large longitudinal momentum P (of course, $x_1+x_2+x_3=1$). Formallly, the distribution amplitude $\varphi(x_1,x_2,x_3)$ can be defined as a function whose moments are given by proton-to-vacuum matrix elements of some local composite operators

$$\int_0^1 \varphi(x_1,x_2,x_3) x_1^{N_1} x_2^{N_2} x_3^{N_3} \delta(1-\sum_1^3 x_i)\, dx_1 dx_2 dx_3 \sim \langle 0|(D^{N_1}u)(D^{N_2}u)(D^{N_3}d)|P\rangle. \qquad (1)$$

The hard scattering amplitude $T(\{x\},\{x'\};Q^2)$ is calculable from perturbative QCD and, in this sense, is known. On the other hand, the distribution amplitudes $\varphi(x_1,x_2,x_3)$ or matrix elements $\langle 0|O_{\{N\}}|P\rangle$ are unknown functions/parameters describing nonperturbative properties of the nucleons in QCD. These functions are more universal than form factors: the same distribution amplitude can be used to calculate different types of hard elastic amplitudes in perturbative QCD.

1.3. Condensates

As emphasized above, matrix elements $\langle 0|O_{\{N\}}|P\rangle$ are not known in pQCD. However, one can again incorporate asymptotic freedom in the form of the operator product expansion to calculate the large-p^2 behaviour of the correlator

$$\Pi_{\{N\}}(p^2) = i\int \langle 0|T(\mathcal{O}_{\{N\}}(x)\mathcal{O}_{\{0\}}(0)|P\rangle e^{ipx}d^4x \tag{2}$$

of the relevant composite operators.

The operator product expansion represents a two-point correlator as a sum of terms, each of which is a product of perturbatively calculable coefficient function and a vacuum-to-vacuum matrix elements of local operators - condensates[7]. These matrix elements describe/parameterize nonperturbative properties of the QCD vacuum. In some cases, it is convenient to introduce nonlocal condensates[8,9], *e.g.* $\langle 0|\bar{q}(0)q(z)|0\rangle$, which generate the local condensates $\langle 0|\bar{q}(0)q(0)|0\rangle \equiv \langle\bar{q}q\rangle$, $\langle\bar{q}D^2q\rangle$, *etc.* after Taylor expansion in z.

Incorporating the fact that the two-point correlator can be written *via* a dispersion relation as an integral over the hadronic spectrum, one can get a QCD sum rule[10,6]

$$\langle 0|O_{\{N\}}|P\rangle\langle P|O_{\{0\}}|0\rangle e^{-m_p^2/M^2} + \frac{1}{\pi M^2}\int_{threshold}^{\infty}\rho_N(s)e^{-s/M^2} = \Pi^{pert}_{\{N\}}(M^2) + f_q(M^2)\langle\bar{q}q\rangle + f_G(M^2)\langle GG\rangle + \dots\,, \tag{3}$$

in which the proton-to-vacuum matrix element $\langle 0|O_{\{N\}}|P\rangle$ is related to condensates, *i.e.*, to a set of universal numbers (or functions, if one uses the nonlocal condensates) specifying the properties of the nonperturbative QCD vacuum. Knowing these functions, one can calculate $\langle 0|O_{\{N\}}|P\rangle$ from the QCD sum rule, and *vice versa*, knowing matrix elements like $\langle 0|O_{\{N\}}|P\rangle$, one can get information about vacuum condensates. The condensates are more universal than distribution amplitudes: the same set of condensates appears in QCD sum rules for different form factors, distribution amplitudes, decay constants, *etc.*

1.4. Λ_{QCD}

In principle, all the condensates $\langle\bar{q}q\rangle$, $\langle GG\rangle$, *etc.* are determined by the magnitude of the fundamental QCD parameter Λ_{QCD}, *e.g.*, $\langle\bar{q}q\rangle = -a\Lambda^3_{QCD}$, $\langle GG\rangle = b\Lambda^4_{QCD}$, *etc.* However, at present stage of NpQCD, the coefficients a, b, *etc.* are not known. When (and if) the NpQCD will become a complete theory, then Λ_{QCD} will become the only unknown parameter to be extracted from experiment.

1.5. Hierarchy in NpQCD description

To summarize, the nonperturbative aspects of QCD can be described/parameterized by a hierarchy of functions having more and more fundamental nature:

1. Form factors - hadron to hadron matrix elements of various currents, *e.g.*, $\langle P'|J^\mu|P\rangle$.

2. Distribution amplitudes (wave functions) - hadron to vacuum matrix elements of local (for moments) or nonlocal (for distribution amlitudes) composite operators constructed from quark and gluonic fields, *e.g.*, $\langle 0|O_{\{N\}}|P\rangle$.

3. Condensates - vacuum to vacuum matrix elements of local or nonlocal composite operators, *e.g.*, $\langle\bar{q}q\rangle$, $\langle\bar{G}G\rangle$, $\langle\bar{q}(0)q(z)\rangle$, *etc.*

4. Λ_{QCD} - fundamental scale governing all other mass, momentum, distance *etc.* scales in QCD.

2. The simplest form factor: $F_{\gamma\gamma^*\pi^0}(Q^2)$

2.1. Preliminaries

The distribution amplitudes $\varphi_H(\{x_i\})$ are universal functions describing a hadron H in various hard elastic processes. Studying the latter experimentally, one can hope to fix a set of distribution amplitudes which will be in agreement with all the data. Adhering to our strategy of a step by step expansion from simpler situations to more complicated ones, let us consider the simplest case when the hadron has only two constituents. For the pion, the simplest and directly measurable $\langle 0|\mathcal{O}|P\rangle$-type object is the matrix element of the axial current

$$\langle 0|\bar{d}\gamma_5\gamma^\mu u|P\rangle = if_\pi P^\mu. \tag{4}$$

It appears in the amplitude for the $\pi \to \mu\nu$ decay, which involves one known weak interaction vertex and one unknown $\bar{q}q\pi$ vertex parameterized by a single constant f_π. Experimentally, $f_\pi \approx 133\,MeV$. By definition, this constant also fixes the integral normalization of the pion distribution amplitude

$$\int_0^1 \varphi_\pi(x)\,dx = f_\pi\ . \tag{5}$$

Next in complexity are the amplitudes involving three vertices. The problem is simpler when the extra vertex has a known structure, *i.e.*, when it corresponds to an EM or weak current. An example of such an amplitude is the form factor $F_{\gamma\gamma^*\pi^0}(q_1, q_2)$ describing the coupling of the neutral pion to two photons with momenta q_1 and q_2. To apply perturbative QCD, one should be sure that virtuality of at least one of the photons is large. Experimentally, it is difficult to arrange two highly virtual photons, so a reasonable compromise is the situation when one of the photons is real $q_1^2 = 0$ or slightly virtual $-q_1^2 << m_\rho^2$ and another one has a large virtuality $q_2^2 \equiv -Q^2 \gtrsim m_\rho^2$.

The cleanest experimental realization for this form factor is on a e^+e^--machine, *i.e.*, one should study the process $e^+e^- \to e^+e^-\pi^0$ implying the lowest order QED subprocess $e^+e^- \to e^+e^-\gamma\gamma^*$ and subsequent fusion of $\gamma\gamma^*$ into π^0. In this case, the origin of the photons is most clean theoretically, so one directly measures $F_{\gamma\gamma^*\pi^0}(Q^2)$.

For a fixed-target machine like CEBAF, one can imagine two possibilities for the subprocess:
a) $\gamma\gamma^* \to \pi^0$, with an almost real Primakoff photon coming from the hadronic target, or
b) $\gamma^*\pi^0 \to \gamma$, now with a pion extracted from the target and a real photon detected in the final state.
To detect the second subprocess, one should exclude the pomeron exchange. This is a very difficult task though polarization measurements can make this more feasible. With the second subprocess,

one would also face the standard set of problems related to extrapolation to the pion pole. Feasibility of the $F_{\gamma\gamma^*\pi^0}(Q^2)$ experiments at CEBAF is under study[12].

2.2. Theory

In perturbative QCD, the $\gamma\gamma^* \to \pi^0$ form factor is described by a simple diagram similar to the handbag diagram for deep inelastic scattering. It gives[5]:

$$F^{pQCD}_{\gamma\gamma^*\pi^0}(Q^2) = \frac{4\pi}{3Q^2}\int_0^1 \frac{\varphi_\pi(x)}{x}dx + O(1/Q^4), \tag{6}$$

where the unknown nonperturbative information is accumulated by the integral

$$I = \int_0^1 \frac{\varphi_\pi(x)}{x}dx\ . \tag{7}$$

A few remarks are in order here.

1. The pQCD expansion starts with the term of zeroth order in the QCD coupling constant α_s, *i.e.*, the asymptotically leading term has no suppression.This situation is identical to that in deep inelastic scattering. Hence, we have all the reasons to expect that the pQCD description in this case must work at Q^2 as low as $1\,GeV^2$.
2. The value of $F_{\gamma\gamma^*\pi^0}(Q^2)$ at $Q^2 = 0$ reduces to the amplitude for the two-photon decay $\pi^0 \to \gamma\gamma$, and the latter is fixed by the ABJ-anomaly[11].

Thus, despite the fact that the process $\pi^0 \to \gamma\gamma$ for real photons does not involve any large momentum transfer, this amplitude is calculable

$$F^{pQCD}_{\gamma\gamma^*\pi^0}(0) = \frac{1}{\pi f_\pi}, \tag{8}$$

though the result involves another nonperturbative parameter - the pion decay constant f_π. However, its value is well known experimentally: $f_\pi \simeq 133\,MeV$. On the large-Q^2 side, assuming the so-called asymptotic form[1,4,3] for the pion distribution amplitude

$$\varphi^{as}_\pi(x) = 6f_\pi x(1-x)\,, \tag{9}$$

one obtains an absolute prediction for the asymptotic behaviour[5]

$$F^{as}_{\gamma\gamma^*\pi^0}(Q^2) = \frac{4\pi f_\pi}{Q^2} + O(1/Q^4). \tag{10}$$

Brodsky and Lepage[13] proposed an interpolation formula

$$F_{\gamma\gamma^*\pi^0}(Q^2) = \frac{1}{\pi f_\pi\left(1+\frac{Q^2}{4\pi^2 f_\pi^2}\right)} \tag{11}$$

which reproduces both the $Q^2 = 0$ value and the high-Q^2 asymptotics.

The BL-interpolation formula has a monopole form $F_{\gamma\gamma^*\pi^0}(Q^2) \sim 1/(1+Q^2/s_0)$ with the scale $s_0 = 4\pi^2 f_\pi^2 \approx 0.7\,GeV^2$ being numerically very close to the ρ-meson mass squared: $m_\rho^2 \approx 0.6\,GeV^2$.

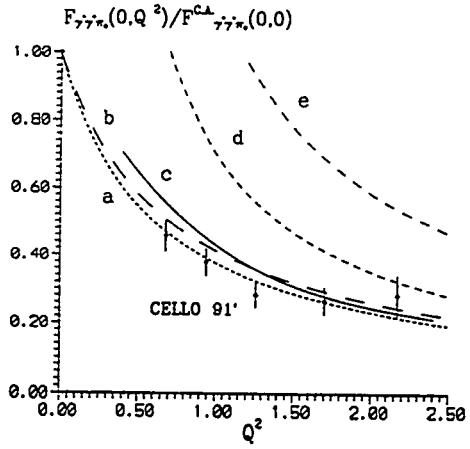


Figure 1: Comparison of experimental data with theoretical predictions for $F_{\gamma\gamma^*\pi^0}(Q^2)$. *a*) VMD, *b*) BL-interpolation & QCD local duality, *c*) Finite-M^2 QCD sum rules, *d*) Leading-twist pQCD with asymptotic distribution amplitude, *e*) Leading-twist pQCD with CZ distribution amplitude.

So, the BL-interpolation suggests a form similar to that based on the VMD expectation $F_{\gamma\gamma^*\pi^0}(Q^2) \sim 1/(1+Q^2/m_\rho^2)$. In fact, as it will be explained later, the combination $s_0 = 4\pi^2 f_\pi^2$ plays an important role in the QCD sum rule analysis of the axial current channel: s_0 gives the pion duality interval or the effective threshold for higher states in this channel, and the BL-interpolation formula exactly coincides with the result based on the so-called local duality prescription[14].

Comparison with existing experimental data[15], shown in Fig.1, shows a good agreement with the BL-interpolation formula and local duality. It should be emphasized here that these approaches assume/require the asymptotic form for the pion distribution amplitude. On the other hand, the curve based on the unmodified lowest-twist pQCD prediction with asymptotic wave function (eq.(10)) goes marginally higher than the data. The situation is even worse if one takes the Chernyak-Zhitnitsky form

$$\varphi_\pi^{CZ}(x) = 30 f_\pi x(1-x)(1-2x)^2 \tag{12}$$

which increases the I-integral by the factor $5/3 \approx 1.67$. A simple monopole-type interpolation to the CZ asymptotics is also excluded. Thus, the $F_{\gamma\gamma^*\pi^0}(Q^2)$ is rather sensitive to the form of the pion distribution amplitude $\varphi_\pi(x)$. In fact, if one agrees that there are no reasons why the interpolated pQCD prediction for this process should not work with, say, 10 or 20 % accuracy for Q^2 between 1 and 2 GeV^2, then one should also agree that existing data exclude the CZ form for the distribution amplitude. On the other hand, the data are absolutely consistent with predictions based on the asymptotic form of $\varphi_\pi(x)$. The data also agree with the VMD-curve and the results of a more detailed ("finite-M^2") QCD sum rule analysis[14].

For further applications, it is also very important to note that the BL-interpolation formula implies a suppression of the hard quark propagator in the region of small virtualities

$$\int_0^1 \frac{\varphi(x)}{xQ^2} dx \to \frac{3 f_\pi}{Q^2 + s_0}. \tag{13}$$

A possible interpretation is that in the regions where the quark virtuality xQ^2 is small, one should take into account effects due to the transverse momentum: $xQ^2 \to (xQ^2 + k_\perp^2)$. Then s_0 may be treated as an average value of the combination $k_\perp^2/x$. This value is not small: $s_0 \approx 0.7\,GeV^2$, and one should expect sizable predasymptotic effects for $Q^2 \simeq 1\,GeV^2$. On the other hand, one should expect that the higher $1/Q^2$-corrections do not strongly affect the pQCD result above $Q^2 \gtrsim 2 - 3\,GeV^2$.

2.3. Lessons

Thus, the analysis of $F_{\gamma\gamma^*\pi^0}(Q^2)$, which is the simplest form factor from both the pQCD and NpQCD (QCD sum rule) points of view, shows that

- The experimentally measured magnitude of this form factor agrees well with the prediction assuming the asymptotic form of the pion distribution amplitude.
- Extrapolating the pQCD prediction $F_{\gamma\gamma^*\pi^0}(Q^2) = 4\pi f_\pi I/Q^2$ into the region of moderate and small Q^2, one should substitute I by a smaller value $I(Q^2) \simeq I/(1 + s_0/Q^2)$ with s_0 being a "typical hadronic scale" $\approx m_\rho^2$.

3. Pion electromagnetic form factor

Now we can make the next step and consider a more complicated case when only one vertex of a 3-point function is known and two are unknown. So, let us discuss the pion electromagnetic form factor $F_{\gamma^*\pi\pi}(Q^2)$ and compare its physics to that of $F_{\gamma\gamma^*\pi^0}(Q^2)$.

The perturbative QCD prediction[1,2,3] is that, at (asymptotically) high Q^2, the pion EM form factor is dominated by a hard gluon exchange

$$F_\pi^{pQCD}(Q^2) = \frac{8}{9}\pi\alpha_s\frac{I^2}{Q^2} + O(1/Q^4) \tag{14}$$

where I is the same integral of the pion distribution amplitude we encountered studying $F_{\gamma\gamma^*\pi}(Q^2)$.

It is instructive to rewrite the pQCD formula as

$$F_\pi^{pQCD}(Q^2) = \frac{4\pi^2 f_\pi^2}{Q^2}\left(\frac{\alpha_s}{\pi}\right)\frac{2}{9}\left(\frac{I^2}{f_\pi^2}\right) = \frac{2}{9}\left(\frac{I^2}{f_\pi^2}\right)\frac{s_0}{Q^2}\left(\frac{\alpha_s}{\pi}\right). \tag{15}$$

For the asymptotic wave function, one has $I/f_\pi = 3$ and $F_\pi^{pQCD,as}(Q^2) = \frac{2s_0}{Q^2}(\alpha_s/\pi)$, or, numerically, $Q^2 F_\pi^{pQCD,as} \to (\alpha_s/\pi)(1.4\,GeV^2)$. "Experimentally", (α_s/π) is close to 1/10. So, this is the high-Q^2 prediction. On the other hand, the pion form factor has an absolute normalization at $Q^2 = 0$: $F_\pi(0) = 1$. To extrapolate the one-gluon-exchange (OGE) term to low Q^2 values, one can try to use the prescription $I \to I/(1 + s_0/Q^2)$ discussed above. In this case, the OGE formula extrapolates into zero at $Q^2 = 0$, indicating that the low-Q^2 behaviour might have nothing to do with the OGE. One can try another extrapolation prescription $I^2 \to I^2/(1+2s_0/Q^2)$ which coincides with the original one in the first $1/Q^2$-correction at large Q^2, but gives an overall monopole formula $F_\pi^{OGE}(Q^2) \sim 1/(Q^2 + 2s_0)$. Then $F_\pi^{OGE}(0) = (I/3f_\pi)^2(\alpha_s/\pi)$. Thus, with the asymptotic wave function $(I/3f_\pi = 1)$, favored by the $F_{\gamma\gamma^*\pi^0}(Q^2)$ data, this extrapolation gives a nonzero, but small $(\alpha_s/\pi) \sim 1/10$ part of the total pion form factor value $F_\pi(0) = 1$. This also suggests that the low-Q^2 behaviour of the pion form factor is dominated by contributions different from the OGE.

One can try also to arrange a brute force interpolation $F_\pi(Q^2) = 1/(1+Q^2/M^2)$ between the $Q^2 = 0$ value and the asymptotic pQCD prediction. Then one should take $M^2 = 2s_0(\alpha_s/\pi)$ which is $0.14\,GeV^2$ for the "standard" value $(\alpha_s/\pi) \approx 0.1$. To make M^2 closer to m_ρ^2, one should take $\alpha_s \sim 1.5$ which seems too large. In any case, pQCD is not applicable if $\alpha_s \gtrsim 1$. If one takes Chernyak-Zhitnitsky wave function, then $I/f_\pi = 5$, and the interpolation parameter M^2 is equal to $\frac{50}{9}\alpha_s/\pi$, and $\alpha_s \simeq 0.5$ puts M^2 close to the desired value around $0.6\,GeV^2$. However, as discussed earlier, the CZ distribution amplitude is ruled out by the data on the $F_{\gamma\gamma^*\pi}(Q^2)$ form factor.

An alternative explanation, suggested by our original interpolation attempt (and by QCD sum rules, as we will see later) is that "1" (*i.e.*, $F_\pi(0)$) does not interpolate into the one-gluon-exchange term, simply because "1" does not and cannot contain the (α_s/π) factor. The very presence of the (α_s/π) factor means that the one-gluon-exchange diagram is a higher-order correction to a diagram which has the zeroth order in α_s. Such a diagram exists and it corresponds to the so-called soft contribution. It describes the situation when the active quark is only slightly virtual both before and after scattering. It is this diagram which provides the pion form factor normalization to unity at zero momentum transfer. The soft contribution F_π^{soft} is totally nonperturbative, it definetely dominates the form factor at low Q^2, and though one may question the range of Q^2 in which this dominance persists, there is no question that the soft contribution plays a very important role at CEBAF energies[16].

4. QCD sum rules: a key(hole) to NpQCD physics

Ideally, one should be able to calculate the NpQCD functions $F_\pi^{soft}(Q^2)$, $F_{\gamma\gamma^*\pi}(Q^2)$, $\varphi_\pi(x)$, $G_N(Q^2)$, $\varphi_N(x_1,x_2,x_3)$, *etc.* from a theory. However, bad news is that there is no such theory yet. Of course, there are some good news coming from the progress of lattice QCD, chiral perturbation theory, QCD sum rules and other approaches going beyond the standard pQCD boundaries. Among these approaches, the QCD sum rule method[7] has the widest range of applications and many impressive results. An attractive feature of the method is that it is based exactly on the idea to use the well-understood properties of QCD in the asymptotic freedom region to probe its nonperturbative dynamics.

4.1. Basics

One of the fundamental ideas of the QCD sum rule approach is that the applicability of pQCD is limited *not* by an uncontrollable increase of $\alpha_s(k^2)$ at small momenta k. Rather, the predictive power of pQCD is limited by nonperturbative effects which appear at momentum transfers for which α_s is still small. Consider, *e.g.*, the one-gluon-exchange diagram discussed above. If momentum k flowing through the gluon line is, say, only $500\,MeV$, one cannot rely on pQCD not because $\alpha_s(500\,MeV)$ is too large (in fact, it is still reasonably small), but because one cannot trust the pQCD formula $D(k) \sim 1/k^2$ for the gluon propagator. Just like the $F_{\gamma\gamma^*\pi}(Q^2)$ form factor has no $1/Q^2$ singularity at small Q^2, the "real-life" gluon propagator will not blow up in small-k^2 region. In other words, the "exact" gluon propagator $D(k)$ (which is a T-product of two gluonic fields averaged over the "physical" vacuum) differs from its perturbative counterpart obtained by averaging the T-product over the perturbative vacuum, and the difference is concentrated in the small-momentum region. At large momenta, the difference vanishes and one can rely on pQCD.

Within the QCD sum rule approach, the objects parameterizing the difference between "real" ("exact", "physical", *etc.*) and perturbative vacua of QCD play a crucial role. Examples include quark condensate $\langle\bar{q}q\rangle$, gluon condensate $\langle GG\rangle$, mixed condensate $\langle\bar{q}(\sigma G)q\rangle$, *etc.*

Another basic concept is the quark-hadron duality. A good example is provided by the e^+e^--annihilation into hadrons. In the low-energy region, $\sigma^{tot}(s, e^+e^- \to hadrons)$, the total cross section contains pronounced resonances and has no similarity to the smooth curve given by a perturbative QCD calculation of $\sigma^{tot}(s, e^+e^- \to q\bar{q})$. However, despite the fact that locally in energy the difference between the theoretical perturbative calculation and experimental nonperturbative result is drastic, if one integrates both cross sections over a large enough energy range $(0, S)$, the results will be very close:

$$\int_0^S \sigma^{tot}(s, e^+e^- \to q\bar{q})\, ds \approx \int_0^S \sigma^{tot}(s, e^+e^- \to hadrons)\, ds\,. \tag{16}$$

In fact, the version of quark-hadron duality incorporated within the QCD sum rule approach is more sophisticated. A typical QCD sum rule has the form

$$\int_0^\infty \rho^{hadron}(s)e^{-s/M^2}\, ds = \int_0^\infty \rho^{quark}(s)e^{-s/M^2}\, ds + a\frac{\langle GG\rangle}{M^2} + b\frac{\langle\bar{q}q\rangle^2}{M^2} + \ldots. \tag{17}$$

Thus, the difference between the idealistic perturbative quark spectrum and the "real-life" hadronic one is measured with an adjustable weight function e^{-s/M^2} (M is usually referred to as the "Borel parameter"), and the result is expressed in terms of quark, gluon, *etc.* condensates $\langle\bar{q}q\rangle, \langle GG\rangle, \ldots$.

Of course, having just a few first condensates, it is possible to reconstruct only the gross features of the physical spectrum. The usual approximation is to represent the physical spectrum by a "first resonance plus continuum" model, with the "continuum" coinciding with the perturbative prediction and starting at some effective threshold $s = s_0$. The value of s_0 and parameters f_R, m_R specifying the first resonance contribution are extracted from the sum rule

$$f_R^2 e^{-m_R^2/M^2} = \int_0^{s_0} \rho^{quark}(s)e^{-s/M^2}\, ds + a\frac{\langle GG\rangle}{M^2} + b\frac{\langle\bar{q}q\rangle^2}{M^2} + \ldots. \tag{18}$$

by requiring the best agreement between its left- and right-hand sides.

4.2. Local duality

Now, if one formally takes $M = \infty$, one obtains the local duality relation

$$f_R^2 = \int_0^{s_0} \rho^{quark}(s)\, ds \tag{19}$$

which states that one can get the lowest resonance contribution by just integrating the perturbative density over the appropriate duality interval s_0 (the bonus of the finite-M^2 QCD sum rules with condensates is that it allows one to calculate s_0 from the condensate values rather than input it as a free parameter).

In the axial-current channel, one has an infinitely narrow pion peak $\rho_\pi = \pi f_\pi^2 \delta(s - m_\pi^2)$, a rather wide peak at $s \approx 1.6\, GeV^2$ corresponding to A_1 and then "continuum" at higher energies. The simplest model is to treat A_1 also as a part of the continuum. For the continuum, the lowest-order perturbative QCD calculation gives an energy independent result $\rho^{pert} = 1/4\pi$. Incorporating the local duality, we get the relation between the pion decay constant and the pion duality interval:

$$s_0 = 4\pi^2 f_\pi^2\,. \tag{20}$$

For the pion distribution amplitude, the local duality prescription gives

$$\varphi_\pi^{LD}(x) = \frac{3s_0}{2\pi^2 f_\pi} x(1-x)\,, \tag{21}$$

which coincides with the asymptotic wave function if one takes $s_0 = 4\pi^2 f_\pi^2$.

As we have seen earlier, the combination $4\pi^2 f_\pi^2$ naturally appears in the Brodsky-Lepage interpolation formula. In fact, the local duality prescription

$$\int_0^{s_0} \rho^{quark}(s)\,ds = \int_0^{s_0} \rho^{hadron}(s)\,ds \tag{22}$$

applied to the relevant spectral density gives the expression[14]

$$F_{\gamma\gamma^*\pi^0}^{(LD)}(Q^2) = \left(\frac{1}{\pi f_\pi}\right) \frac{1}{1+Q^2/s_0} \tag{23}$$

which coincides with the BL formula if $s_0 = 4\pi^2 f_\pi^2$, *i.e.* if the pion duality interval for the 3-point function is equal to that extracted from the basic 2-point function.

Local duality can also be used to get an estimate for the soft contribution to the pion form factor[17]:

$$F_\pi^{soft(LD)}(Q^2) = 1 - \frac{1+\frac{6s_0}{Q^2}}{\left(1+\frac{4s_0}{Q^2}\right)^{3/2}}. \tag{24}$$

For large Q^2, this soft contribution behaves like $6s_0^2/Q^4$, which is one power of s_0/Q^2 down compared to the one-gluon-exchange term.

To get the local duality estimate for the one-gluon-exchange (OGE) contribution, one should perform a two-loop calculation for a three-point function, which is rather involved. However, the $Q^2 = 0$ value can be easily extracted from existing result for the two-point function: $F_\pi^{OGE(LD)}(Q^2=0) = \alpha_s/\pi$. The high-$Q^2$ local duality result coincides with that obtained in pQCD with the asymptotic wave function $F_\pi^{OGE(LD)}(Q^2)|_{Q^2\to\infty} = F_\pi^{pQCD,as}(Q^2) = \frac{2s_0}{Q^2}(\frac{\alpha_s}{\pi})$, and the simplest interpolation is

$$F_\pi^{OGE(LD)}(Q^2) = \left(\frac{\alpha_s}{\pi}\right) \frac{1}{1+Q^2/2s_0} \tag{25}$$

Combining the $O(1)$ (soft) and the $O(\alpha_s)$ ("hard") terms produces the total local duality estimate for the pion form factor

$$F_\pi^{(LD)}(Q^2) = \frac{F_\pi^{soft(LD)}(Q^2) + F_\pi^{OGE(LD)}(Q^2)}{1+\frac{\alpha_s}{\pi}}. \tag{26}$$

The resulting curve is in good agreement with existing data (see Fig.2).

Local duality can be also applied to the nucleon form factors[18]. For the proton magnetic form factor the result is[19]

$$G_M^p(Q^2) = \frac{8}{3}\sqrt{T^2-1}\left\{(4T^2-1)(T^2-1) + (4T^2-3)T\sqrt{T^2-1}\right\}^{-1}, \tag{27}$$

where $T = 1 + Q^2/2s_0$ and the duality interval s_0 for the nucleon[20] is $2.3\,GeV^2$. The agreement with experimental data shown in Fig.2 is also good. The theoretical curve starts to systematically deviate from the data only in the region $Q^2 \gtrsim 15\,GeV^2$.

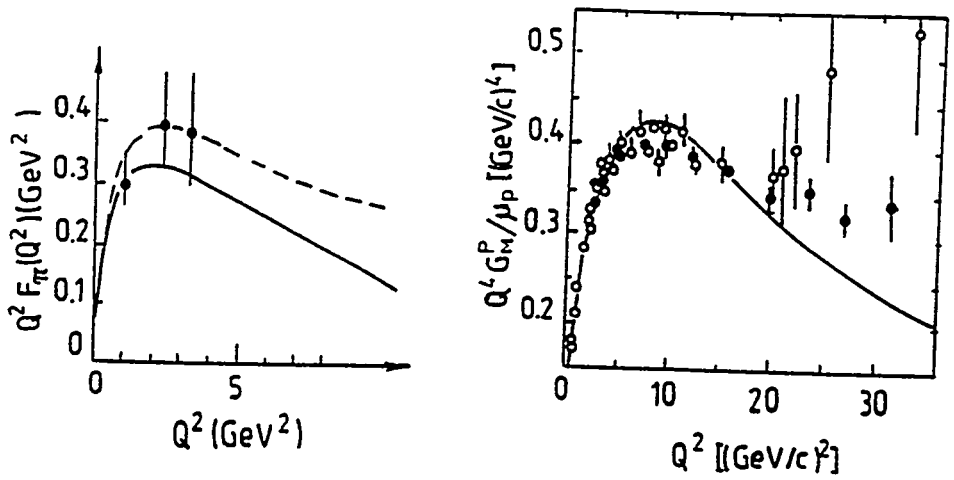


Figure 2: Comparison of local duality predictions with experimental data for pion form factor (left) and proton magnetic form factor (right).

It should be noted, that though local duality works very well in many cases, it has a less fundamental status compared to the original QCD sum rules involving condensates and finite values of the Borel parameter M^2. In fact, only a thorough study of the Borel sum rules can tell whether the duality interval s_0 is really the same in different situations, in particular, if it depends on Q^2 or not in the form factor calculations. Absence of such a dependence is not obvious, because the coefficients characterizing the magnitude of the condensate corrections in a form factor sum rule, usually depend on Q^2. Such a dependence is especially important at large and small Q^2.

4.3. Low Q^2

At small Q^2, the perturbatively calculated coefficient functions contain singularities $\ln(Q^2)$, $1/Q^2$, *etc.* Just like in all cases considered earlier, these singularities simply signalize that one cannot extrapolate the perturbative result into the nonperturbative region. More formally, these singularities are generated by long-distance propagation in the channel related to small momentum Q. As a result, one obtains a new type of NpQCD objects - two-point correlators $\Pi(Q^2)$ taken at low values of Q^2. To evaluate them, one can use again the same old tactics: take the correlator $\Pi(Q^2)$ in the asymptotic freedom region of large Q^2 where one can rely on the operator product expansion (with condensates *etc.*), construct the model hadronic spectrum and then, using this spectrum, calculate $\Pi(Q^2)$ in small-Q^2 region. As a result, one would get $1/(Q^2+m_\rho^2)$ instead of $1/Q^2$, and there will be no singularities for $Q^2=0$, just as expected. In this way, QCD sum rules were used to calculate the low-Q^2 behaviour of pion[21], kaon[22], proton and neutron[23] form factors.

4.4. High Q^2 and nonlocal condensates

At high Q^2, some of the coefficients in front of higher condensates contain factors like Q^2, Q^4, *etc.* and one should resum OPE in some way. It was demonstrated[24] that the Q^2 growth results from the Taylor expansion of the original nonlocal condensates over the local ones. To get rid of this problem, it was suggested[9] to avoid the Taylor expansion and work directly with nonlocal

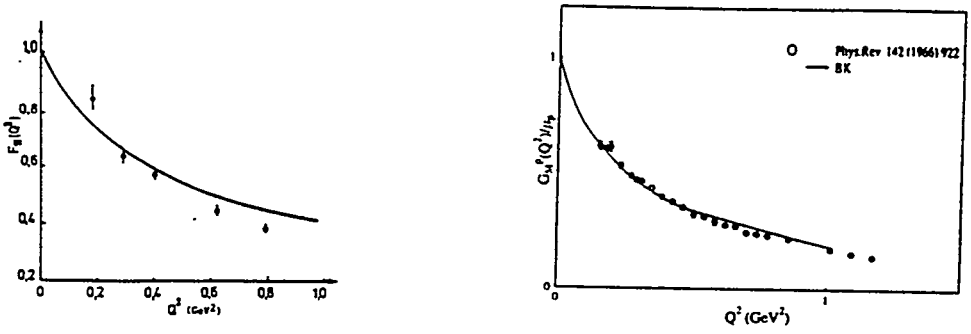


Figure 3: Comparison of QCD sum rule calculations in the low-Q^2 kinematics with experimental data for the pion form factor (left) and proton magnetic form factor (right).

condensates. It is convenient to parameterize the nonlocal condensate $\langle\bar{q}(0)q(z)\rangle$ as

$$\langle\bar{q}(0)q(z)\rangle = \langle\bar{q}q\rangle \int_0^\infty e^{\nu z^2/4} f(\nu)\, d\nu\,. \tag{28}$$

The ν^N-moment of the function $f(\nu)$ is given by matrix element $\langle\bar{q}(D^2)^N q\rangle$, and for this reason one can interpret $f(\nu)$ as the distribution function of vacuum quarks in virtuality.

In particular, for the lowest two moments one has

$$\int_0^\infty f(\nu)\, d\nu = 1\,, \quad \int_0^\infty \nu f(\nu)\, d\nu = \frac{1}{2}\frac{\langle\bar{q}(D^2)q\rangle}{\langle\bar{q}q\rangle} \equiv \frac{\lambda_q^2}{2}, \tag{29}$$

with λ_q^2 having the meaning of the average virtuality of vacuum quarks. Some earlier QCD sum rule studies [20] give the estimate $\lambda_q^2 = 0.4\,GeV^2$. Constructing models of nonlocal condensates, one should satisfy also some other constraints. For instance, if one assumes that the vacuum matrix element $\langle\bar{q}(D^2)^{N_0}q\rangle$ exists, then $f(\nu)$ should vanish faster than $1/\nu^{N_0+1}$ as $s \to \infty$. The opposite, small-ν limit of $f(\nu)$ is governed by the large-$|z|$ properties of the function $Q(z^2)$, *i.e.*, by its behaviour at large space separations or at large values of the imaginary time variable $\tau = iz_0$. The latter case can be easily assessed using the QCD sum rule for the heavy-light meson spectrum in the heavy quark effective theory (HQET). In the HQET, the heavy quark has a trivial propagator $S_Q(z) \sim \delta^3(z)\theta(z_0)$ and, hence, the time dependence of the correlator of two heavy-light currents is determined by the light quark propagator[25]. At large imaginary time τ, the correlator is dominated by the lowest state contribution $\sim e^{-\tau\bar{\Lambda}}$ where $\bar{\Lambda} = (M_Q - m_Q)|_{m_Q\to\infty}$ is the lowest energy level of the mesons in HQET. This means that $Q(z^2) \sim e^{-|z|\bar{\Lambda}}$ for large Euclidean z and $f(\nu) \sim e^{-\bar{\Lambda}^2/\nu}$ in the small-ν region[26]. Numerically, $\bar{\Lambda}$ is around 0.45 GeV. As a result, $f(\nu)$ is a function peaked around $\nu \approx \lambda_q^2/2 \sim 0.2\,GeV^2$. Choosing a different value of the average virtuality λ_q^2 changes the peak location. Calculating $F_\pi^{soft}(Q^2)$ within the QCD sum rules approach and using simple models for the nonlocal condensates, we obtained the curves showing a rather strong dependence on the parameters characterizing the nonlocal condensates[24]. This, in principle, gives a possibility of extracting these parameters from the data. The qualitative observation is that the bigger the average virtuality parameters λ_q^2, λ_G^2, the smaller the soft contribution.

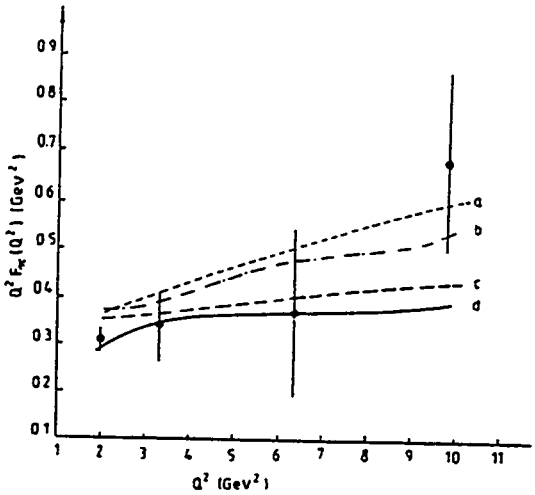


Figure 4: Dependence of $Q^2F_\pi(Q^2)$ on Q^2 for various virtuality parameters of the quark and gluon condensates *a*) $\lambda_q^2 = 0.6\,GeV^2, \lambda_g^2 = 0.3\,GeV^2$; *b*) $\lambda_q^2 = 0.6\,GeV^2, \lambda_g^2 = 0.5\,GeV^2$; *c*) $\lambda_q^2 = 0.8\,GeV^2, \lambda_g^2 = 0.3\,GeV^2$; *d*) $\lambda_q^2 = 0.8\,GeV^2, \lambda_g^2 = 0.5\,GeV^2$.

The nonlocal condensates were also used[9] in QCD sum rules for the pion distribution amplitude $\varphi_\pi(x)$. The trend observed in these studies is that when the average virtuality parameter λ_q^2 increases, the resulting distribution amplitude becomes narrower, changing from the Chernyak-Zhitnitsky form for $\lambda_q^2 = 0$ to the asymptotic form for $\lambda_q^2 \sim 1\,GeV^2$.

From above observations, one can expect that there may be a correlation between the form of the pion distribution amplitude and the size of the soft contribution to the pion form factor, namely, that broad distribution amplitudes, *e.g.*, those of the CZ type imply a large soft contribution, while the narrow ones are accompanied by smaller soft terms. In fact, this correlation really takes place because the QCD sum rules for the moments of the pion distribution amplitude and those for the pion form factor have a very similar structure[19,27].

4.5. Light-cone sum rules

Recently, another way of extending the applicability range of the QCD sum rules to higher Q^2 was proposed[28]. It is based on the analysis of the hadron-to-vacuum matrix elements for the correlator of two currents, *e.g.*, for the pion form factor one should consider

$$T_{\mu\nu}(p_1,p_2) = \int \langle 0|T\{J_\mu(0)j_\nu^5(x)\}|\pi(p_1)\rangle e^{ip_2x}d^4x \tag{30}$$

and apply, at large $Q^2 \equiv -(p_1-p_2)^2$, the operator product expansion

$$T\{J(0)j^5(x)\} \sim \sum_n C_n(x^2)\mathcal{O}_n\ . \tag{31}$$

In this approach, one of the pions (which is in the bracket $|\pi(p_1)\rangle$) appears explicitly and is treated like in pQCD, *i.e.*, decsribed by matrix elements $\langle 0|\mathcal{O}_n|\pi(p)\rangle$ or distribution amplitudes, while another (generated by the current $j_\nu^5(x)$) is extracted from the correlator using the QCD sum rule technique.

As a result, one can explicitly study sensitivity of the soft term to the choice of the pion distribution amplitude. Again, assuming the CZ amplitude, one gets a very large soft term (see

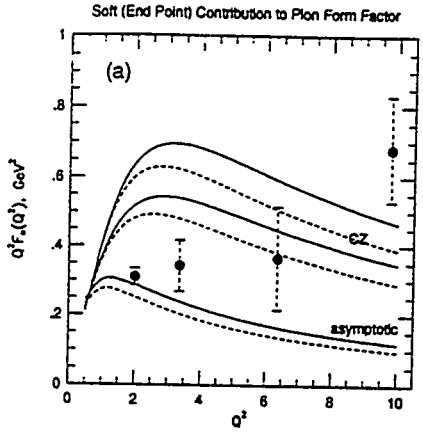


Figure 5: Combination $Q^2F_\pi(Q^2)$ calculated within the light-cone sum rule approach for different choices of the pion distribution amplitude.

Fig.5). One should also remember, that using the CZ form, one obtains a large OGE contribution as well. Hence, in the CZ-case, adding the soft and OGE terms marginally overshoots the data. On the other hand, using the asymptotic form, one obtains a curve comfortably close to experiment.

The light-cone QCD sum rules were also applied to the $\gamma^*\pi \to A_1$ transition form factor[29]. Future applications of the light-cone sum rules should include baryon form factors $G^{e,p}_{E,M}(Q^2)$, transition form factors for $\gamma N \to \Delta, \gamma N \to N^*$, *etc.* transitions, all measurable at CEBAF. The kaon form factor can be calculated both in the light-cone sum rule approach and with standard 3-point sum rules. The results for $F_K(Q^2)$ are sensitive both to the strange-quark mass m_s and to the difference between the strange-quark condensate $\langle\bar{s}s\rangle$ and the "ordinary" $\langle\bar{u}u\rangle$. It should be mentioned, that the results of the QCD sum rule calculations of the kaon form factor in the low-Q^2 region[22] are in good agreement with existing data.

5. Conclusions

Our goal here was to describe a modern picture of the nonperturbative QCD physics behind the elastic electron-hadron scattering processes at CEBAF energies. This picture, formulated directly in terms of quark and gluon fields, is based on a systematic use of the QCD factorization of the short-distance (perturbative) and long-distance (nonperturbative) effects within the framework of the QCD sum rule method. This method relates the nonperturbative dynamics of individual hadrons to nontrivial properties of the QCD vacuum, thus providing a unified description of nonperturbative effects in QCD. The QCD sum rule analysis shows that elastic processes at CEBAF energies are dominated by nonperturbative effects, with possible signatures of the perturbative QCD dynamics in $10\,GeV$ energy region. On several examples, we demonstrated sensitivity of the QCD sum rules predictions for elastic processes to parameters and/or functions describing/parameterizing the nonperturbative aspects of the QCD dynamics. This opens a possibility of experimental determination of these parameters. Such a determination, however, would require both a high precision of CEBAF experimental data and a wider range of energies and momenta involved in these experiments. The increase of CEBAF energy is especially crucial for a detailed study of the interplay between the nonperturbative and perturbative QCD effects in elastic processes.

6. Acknowledgement

I am grateful to R. Ruskov for collaboration on $F_{\gamma\gamma^*\pi}$ form factor. This work was supported by the US Department of Energy under contract DE-AC05-84ER40150.

1. A.V.Radyushkin, JINR preprint P2-10717, Dubna (1977);
   A.V.Efremov and A.V.Radyushkin, *Phys.Lett.* **94B** (1980) 245.
2. V.L.Chernyak, A.R.Zhitnitsky and V.G.Serbo, *JETP Letters* **26** (1977) 594
3. S.J.Brodsky and G.P.Lepage, *Phys.Lett.* **87B** (1979) 359.
4. A.V.Efremov and A.V.Radyushkin, JINR preprint E2-11983, Dubna (October 1978), published in *Theor. Math. Phys.* **42** (1980) 97.
5. G.P.Lepage and S.J.Brodsky, *Phys.Rev.* **D22** (1980) 2157.
6. V.L.Chernyak and A.R.Zhitnitsky, *Phys.Reports* **112** (1984) 173.
7. M.A.Shifman, A.I.Vainshtein and V.I.Zakharov, *Nucl.Phys.* **B147** (1979) 385,448.
8. E.V.Shuryak, *Nucl.Phys.***B203** (1982) 116.
9. S.V.Mikhailov and A.V.Radyushkin, *Phys.Rev.* **D45** (1992) 1754.
10. V.L.Chernyak and A.R.Zhitnitsky, *Nucl.Phys.* **B201** (1982) 492; **B214** (1983) 547(E).
11. S.L.Adler,*Phys.Rev.***177** (1969) 2426; J.S.Bell and R.Jackiw, *Nuovo Cim.***A60** (1967) 47.
12. A.Afanasiev, in progress.
13. S.J. Brodsky and G.P.Lepage, SLAC preprint SLAC-PUB-2587, Stanford (1980).
14. A.V. Radyushkin and R. Ruskov, in preparation.
15. CELLO Collaboration, H.-J.Behrend et al., *Z. Phys.* **C 49** (1991) 401.
16. N. Isgur and C.H. Llewellyn Smith, *Phys.Rev.Lett.* **52** (1984) 1080;
    Nucl.Phys. **B317** (1989) 526.
17. V.A Nesterenko and A.V. Radyushkin, *Phys.Lett.* **115B** (1982) 410.
18. V.A Nesterenko and A.V. Radyushkin, *Phys.Lett.* **128B** (1983) 439.
19. A.V. Radyushkin, *Nucl.Phys.* **A527** (1991) 153c.
20. V.M.Belyaev and B.L.Ioffe, *ZhETF* **83** (1982) 876.
21. V.A Nesterenko and A.V. Radyushkin, *JETP Lett.* **39** (1984) 707.
22. V.A.Beilin, V.A Nesterenko and A.V. Radyushkin, *Int.J.Mod. Phys.* **A3** (1988) 1183 .
23. V.M.Belyaev and Ya.I. Kogan *Int.J.Mod. Phys.* **A8** (1993) 153.
24. A.P.Bakulev and A.V.Radyushkin, *Phys.Lett.* **B271** (1991) 223.
25. A.V.Radyushkin, *Phys.Lett.* **B271** (1991) 218.
26. A.V.Radyushkin, preprint CEBAF-TH-94-13, Newport News (1994).
27. A.V.Radyushkin, In "Baryons-92", ed. by M.Gai, World Scientific (1993) 366.
28. V.M.Braun and I. Halperin, *Phys.Lett.* **B328** (1994) 457.
29. V.M.Belyaev, preprint CEBAF-TH-94-09, Newport News (1994).

Excited Baryon Form-Factors at High Momentum Transfer at CEBAF at Higher Energies

P. Stoler

Physics Deptartment, Rensselaer Polytechnic Institute, Troy NY 12180

Abstract: The possibilities of measuring the properties of excited nucleons at high Q^2 by means of exclusive single meson production at CEBAF with an electron energy of 8 GeV is considered. The motivation is to access short range phenomena in baryon structure, and to investigate the transition from the low Q^2 non-perturbative QCD regime, where constituent quark models are valid, to higher Q^2 where it is believed perturbative QCD plays an increasingly important role. It is found that high quality baryon decay angular distributions can be obtained for the most prominent states up to $Q^2 \sim 12\ GeV^2/c^2$ using a set of moderate resolution, large solid angle magnetic spectrometers.

1 Physics Background:

One of the fundamental problems in physics concerns the non-perturbative structure of baryons and their excitations in terms of elementary quark and gluon constituents. A central issue concerns which models are valid for describing these excitations in different domains of Q^2. At low Q^2 ($< 1\ GeV^2/c^2$), the structure is very complex and as yet unsolved. The constituent quark model (CQM) appears to be a fruitful basis. However, CQM are not fundamental. QCD is so complicated at the hadron scale (low Q^2), that currently it is fruitless to attempt a description in terms of models based on fundamental QCD current quarks and forces. Even lattice approaches are not likely to be attractive in the near future since they attempt to solve the problem by brute force, which is not condusive to yielding physical insight into the problem. One can consider instead of beginning to approaching the problem from the very high Q^2 perspective. Here, perturbative QCD ($PQCD$) descriptions of the transition amplitude should be valid, the involved hadronic structure relatively simple, comprising only the minimum number of (*valence*) quarks. The distribution function of these *valence* quarks are determined by their non-perturbative interaction with the complicated QCD vacuum, and this gives us a handle on treating the non-perturbative QCD ($NPQCD$) structure of a hadron.

Even though there is broad agreement that PQCD techniques are valid for $Q^2 \rightarrow \infty$ there is a great deal of controversy about where in Q^2 is the transition from $NPQCD$ to $PQCD$ descriptions. Recent calculations invoking color radiative (Sudakov) corrections suggest that hard $PQCD$ processes may control hadron form-factors at Q^2 in a range accessable to CEBAF (Li-92,92a). Other calculations (Zh-94) suggest soft NPQCD processes dominate in that range of Q^2. may still

During the past several years, elastic scattering form-factor measurements on protons (Ar-86, Ar-93) have provided the only data on this subject. To test theories in a systematic way and further

constrain wave functions, it will be necessary to measure the evolution of meson and baryon resonance transition form factors at high Q^2.

There are two important aspects which define the problem. On one hand there is the hierarchy of the Q^2 dependence of the transition amplitudes, which are related to the hierarchy of complexities of the participating states. In the $PQCD$ limit, there are well defined Q^2 counting rules. The satisfaction of these counting rules would be an indication of the approach to the domain where $PQCD$ calculation techniques would be valid.

On the other hand, within the framework of $PQCD$ calculations, the valence quark distribution function, which contains the information about the non-perturbative structure, manifests itself in the magnitudes of the the exclusive cross sections. Other valuable information is also contained in logarithmic Q^2 dependences controlled by both the transition amplitude and the quark distribution function.

The physics in the case of baryon resonance transitions has been reviewed in some detail in St-93. A short summary of the issues is presented here.

Form factors at high Q^2 can be factorized utilizing quark helicity conservation (Br-89, Le-80, Li-92):

$$F(Q^2) = \int_0^1 \int_0^1 dxdy\ \Phi_f(y, k_\perp^f)^*\ T_H\ \Phi_i(x, k_\perp^i), \tag{1}$$

where $x = (x_1, x_2, x_3)$ and $y = (y_1, y_2, y_3)$ denote the longitudinal momentum fractions of the initial and final baryon state, and $k_\perp^i$ and $k_\perp^f$ the transverse momentum components. The two main ingredients are the hard transition operator T_H, which is purely perturbative and the three-quark distribution amplitudes Φ, which reflect the non-perturbative interaction of the quarks with the QCD vacuum.

transition operator T_H to leading order in $PQCD$ is determined by processes in which three quarks absorb the virtual photon and remain intact by means of the exchange of two hard gluons. This leads to the functional form

$$T_H = \frac{\alpha_s^2(Q^2)}{Q^4} f(x, y, Q^2). \tag{2}$$

which dominates the Q^2 dependence of the form factor which is then predicted to scale as Q^{-4}, modulated by logarithmic decreases due to the Q^2 dependence of the running coupling constant α_s, and the evolution of the distribution amplitude.

The **three quark distribution amplitudes** $\Phi(x)$ determine the form factor normalizations and signs.

The factor $1/Q^4$ in eq. 2 comes from the momenta of the exchanged gluons $k^2 = f(x, y)Q^2$. Therefore, part of the integral in eq. 1 involves regions of small k^2 where $PQCD$ is not valid. How much of the form factor comes from this non-perturbative region at accessible values of Q^2 is a very controversial issue. A crucial issue is whether the Sudakov suppression of non-perturbative contributions allow one to apply the $PQCD$ techniques at assessible Q^2.

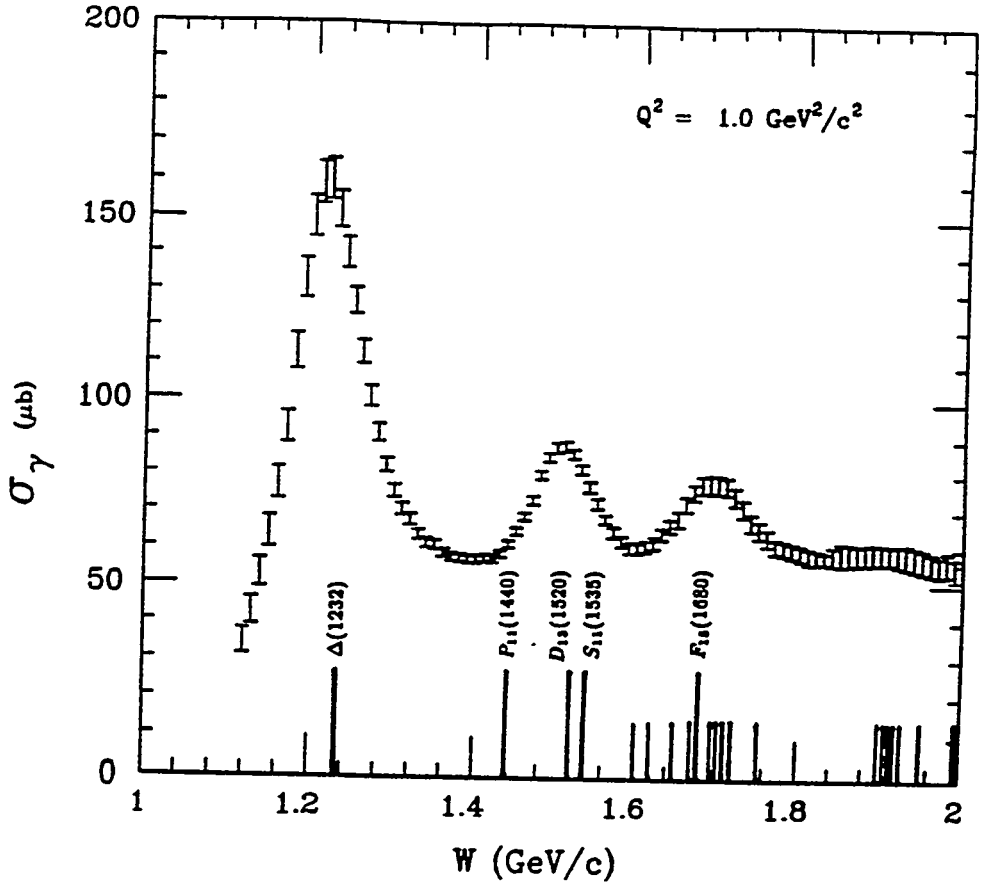


Figure 1: The virtual photon excitation curve for electron scattering at $Q^2 = 1\ GeV^2/c^2$.

The elastic proton helicity conserving form factor is one of the few pieces of data available to challenge theory. Clearly, exclusive data on the individual resonances should be of great value in assessing conflicting theoretical approaches. The most significant feature of the inclusive electron scattering cross section in the resonance region, shown in Figure 1, is the existence of three broad maxima: the first, second and third resonance regions. In this interval there are about 20 known non-strange resonances. The first maximum is due to the $P_{33}(1232)$ or $\Delta(1232)$ resonance. The second resonance region at high Q^2 is mainly due to the $S_{11}(1535)$, with a strong contribution from the $D_{13}(1520)$. In the third resonance region, the strongest excitation at low Q^2 is the $F_{15}(1680)$ state. The relative strength of the other states is not well determined, especially at increasing Q^2.

The current experimental situation for the resonances is that there exist no exclusive data of any kind for Q^2 above 3 GeV^2/c^2. Existing single-arm inclusive electron scattering data have been evaluated (St-93), and equivalent transition form-factors as a function of Q^2 extracted for the three dominant peaks near W = 1232, 1535 and 1680 MeV, by fitting Breit-Wigner resonances together with phenomenological backgrounds to existing inclusive data. The results are shown in Figure 2 Included in Figure 2 is the proton elastic form factor (Ar-86).

In fact the elastic form factor G_M does appear to approach the Q^{-4} behavior above $Q^2 \sim 5\ GeV^2/c^2$ out to the highest measured Q^2 ($\sim 35\ GeV^2/c^2$) (Ar-86). The second and third resonance transition

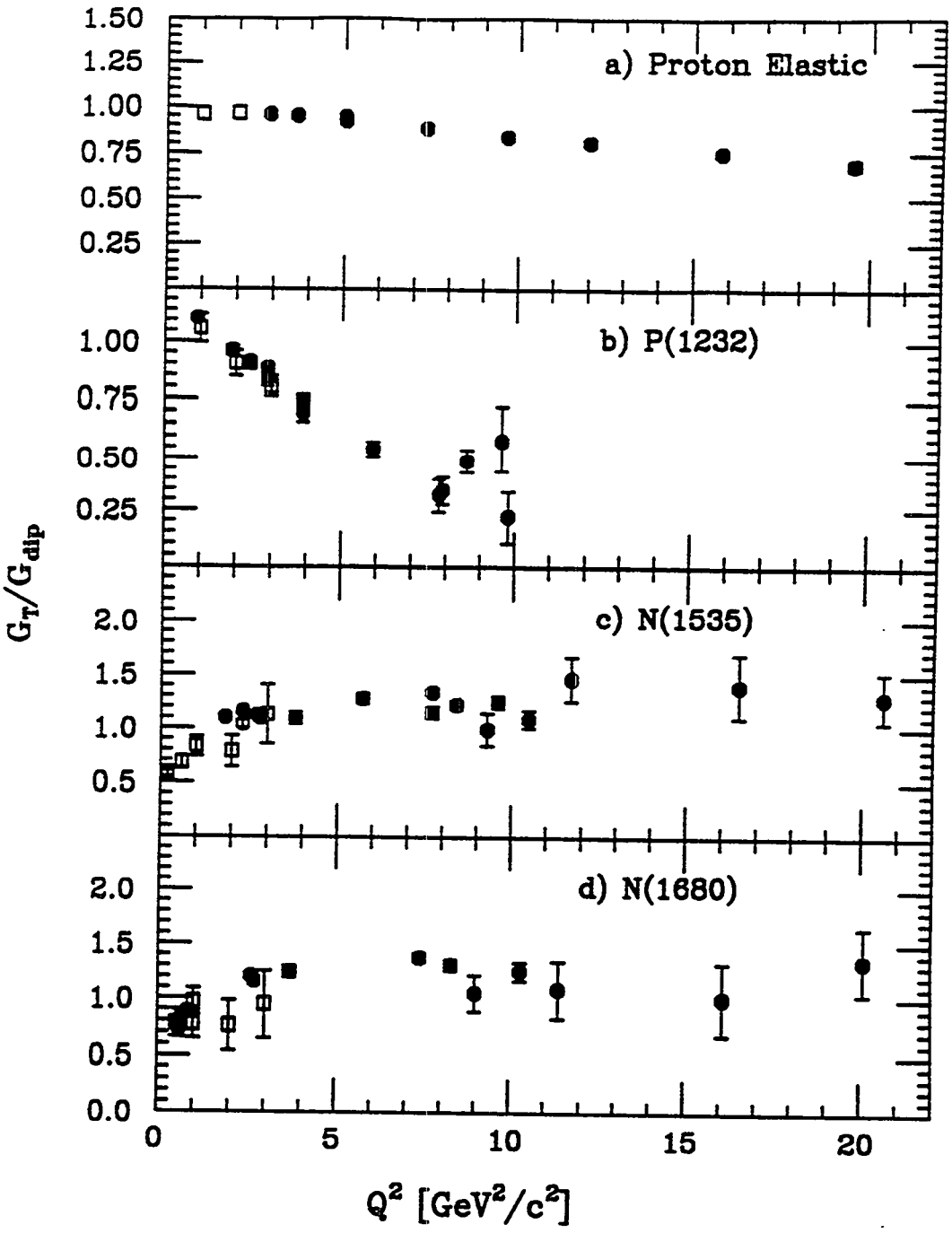


Figure 2: (a) The transverse form-factor $Q^4G_M(Q^2)$ versus Q^2 for elastic scattering from the proton. The data are from Ar-86. (b - d) Analogous form-factors $Q^4G_T(Q^2)$ versus Q^2 from St-93 for transitions to the first, second and third resonances respectively. The notation is from St-93. It was assumed the longitudinal componant equal zero The first resonance (b) is the $\Delta(1232)$. The second resonance (c) at lower Q^2 ($\sim 3\ GeV^2/c^2$) is mostly due to the $S_{11}(1535)$, with a significant contribution from the $D_{13}(1520)$. The third resonance at low Q^2 is dominated by the $F_{15}(1680)$.

form factors also appear to approach the predicted Q^{-4} behavior, within quite large statistical errors.

The $\Delta(1232)$ form-factor decreases faster than the other form-factors for both low and high Q^2 for reasons which are not currently understood. An intriguing suggestion (Ca-88) is that the leading order contribution is anomalously small, so that we are seeing the relatively increased effects of non-leading amplitudes, which fall faster with Q^2. For the $\Delta(1232)$ at low Q^2 the mutipoles $M_{1+} >> E_{1+}$, in agreement with CQM. However, in the $PQCD$ limit $M_{1+} = E_{1+}$. Thus, the $\Delta(1232)$ may be a favorable case to study the transition from CQM to $PQCD$.

2 Experimental Program

Much of the region in Q^2 shown in Figure 2 can be accessed at CEBAF with a beam energy 8 to 10 GeV. For example, the table below shows the global inclusive statistics obtainable in a 30 day run with a beam energy of 8 GeV within kinematic intervals $\Delta W = 0.1 GeV$ $\Delta W = 0.1 GeV$ and $\Delta Q^2/Q^2 = 0.2$.

Q^2	$\Delta(1232)$	$S_{11}(1535)$	$F_{15}(1688)$
4	2×10^7	3×10^7	3×10^7
5	4×10^6	1×10^7	1×10^7
6	1×10^6	7×10^6	5×10^6
7	5×10^5	4×10^6	3×10^6
8	2×10^5	2×10^6	2×10^6
9	1×10^5	1×10^6	1×10^6
10	7×10^4	6×10^5	4×10^5
11	5×10^4	4×10^5	3×10^5
12	3×10^4	3×10^5	2×10^5

To separate individual resonances and their contributing electromagnetic multipoles requires angular distribution measurement of exclusive reactions such as $(e, e'\pi)$ and $(e, e'\eta)$. In addition to isolating resonances and separating their multipoles, exclusive angular distributions will yield a great deal of reduction of the non-resonant background through the selection of decay channel and decay angle kinematic space. For single meson production, detection of either the outgoing nucleon or meson in coincidence with the scattered electron makes the experiment kinematically complete. An important advantage in high Q^2 reactions is that the hadronic reaction products are boosted into a narrow cone relative to the momentum transfer, so that large cm angular acceptances in θ and ϕ can be obtained with relatively modest acceptance spectrometers, although the boost also means that high momenta need to be detected. In order to ascertain the spectrometer requirments the table below shows the

electron energy, and maximum proton and pion momenta and angles relative to the $\vec{q}$ vector for the reaction $e + P \rightarrow \Delta(1232) \rightarrow N + \pi$, with an 8 GeV beam for different values of Q^2.

Q^2 (GeV^2/c^2)	θ_q (deg)	E_2 (GeV)	P_{p-max} (GeV)	θ_{p-max} (deg)	$P_{\pi-max}$ (GeV)	$\theta_{\pi-max}$ (deg)
4	31.1	5.5	3.1	5.4	1.3	41.2
5	27.7	5.0	3.7	4.6	1.5	34.0
6	21.8	4.5	4.2	3.6	1.8	29.1
7	19.2	3.9	4.7	3.2	2.0	25.5
8	16.7	3.4	5.3	2.9	2.2	22.8
9	14.2	2.9	5.8	2.7	2.4	20.6
10	11.6	2.3	6.3	2.5	2.6	18.8
11	8.8	1.8	6.8	2.3	2.8	17.3
12	5.2	1.3	7.4	2.1	3.1	16.0

It is found that the HMS spectrometer in Hall C together a new moderate resolution non-focusing spectrometer with solid angle about 50 msr and maximum momentum about 8 GeV^2/c^2 would be quite adequate to carry out the above program. Such a spectrometer was previously proposed for Hall C (Bu-87,St-88)

References:

(Ar-86) R.G. Arnold et al., Phys. Rev. Lett., 57, (1986) 174.

(Bu-87) V. Burkert, Research program at CEBAF (III), SURA, (1987) 414.

(Br-89) S.J. Brodsky, Lectures at the 27th International School of Subnuclear Physics, Ettore Majorana Center for Scientific Culture, Erice (1989),SLAC-PUB-5116, and references therein.

(Le-80) G.P. Lepage and S.J. Brodsky, Phys. Rev. D22,(1980) 2180.

(Li-92) H-N. Li, SUNY Stony Brook report ITP-SB-92-25.

(Li-92a) H-N. Li and G. Sterman, SUNY-Stony Brook report ITP-SB-92-10,

(St-88) P. Stoler, Proposal for NFS to CEBAF PAC (1988).

(St-93) P. Stoler, Physics Reports,226, (1993) 103.

(Zh-94) A. Zhitnitski, Southern Methodist Univ. Rept. SMU-HEP-94-01.

HELICITY NON-CONSERVING FORM FACTOR OF THE PROTON

E. Voutier, C. Furget, S. Kox and J.S. Réal
Institut des Sciences Nucléaires de Grenoble
IN2P3-CNRS/Université Joseph Fourier
53 Avenue des Martyrs, F-38026 Grenoble cedex, France

ABSTRACT

The study of the hadron structure in the high Q^2 range contributes to the understanding of the mechanisms responsible for the confinement of quarks and gluons. Among the numerous experimental candidates sensitive to these mechanisms, the helicity non-conserving form factor of the proton is a privilegied observable since it is controlled by non-perturbative effects. We investigate here the feasibility of high Q^2 measurements of this form factor by means of the recoil polarization method in the context of the CEBAF 8 GeV facility. For that purpose, we discuss the development of a high energy proton polarimeter, based on the $H(\vec{p},pp)$ elastic scattering, to be placed at the focal plane of a new hadron spectrometer. It is shown that this experimental method significantly improves the knowledge of the helicity non-conserving form factor of the proton up to 10 GeV^2/c^2.

1. Introduction

One of the most exciting challenge of microscopic physics is the understanding of the structure of the hadronic matter in the domain of non-perturbative QCD [1]. This amounts to unravel the mechanisms which produce the confinement of quarks and gluons. The study of hard exclusive processes [2] is expected to adress this issue because above some value of the transferred momentum the reaction amplitude factorizes in a soft non-perturbative part and a hard part which is calculable from perturbative QCD (pQCD).

The present knowledge of these processes, issued from hadronic and/or electromagnetic experiments, is not exhaustive enough and even accurate to select between the different scenarios which intend to describe the confinement. Particularly, the question about the transferred momentum required to enter the perturbative regim of QCD remains, since it relies on the poorly known non-perturbative mechanisms of QCD. The understanding of the confinement is then requiring accurate measurements of experimental observables selective from these processes. The conservation of the hadron helicity during a reaction occuring onto massless quarks is among the fundamental tenets of pQCD. An observable sensitive to helicity non-conservation is therefore implicitly sensitive to the non-perturbative mechanisms of QCD.

Elastic and inelastic electron scattering are the best candidates to reveal the

hadron structure through the interaction of the virtual photon with its quark constituents. The elementary H(e,e'p) elastic scattering is described by the Dirac (F_1) and Pauli (F_2) form factors which contain the information about the internal structure of the proton. While F_1 is helicity conserving, F_2 is helicity non-conserving and therefore pQCD cannot predict its magnitude but only the fact that Q^2F_2/F_1 behaves asymptotically like a constant [3]. Consequently, precise measurements of F_2 in the high Q^2 range should help to understand the non-perturbative mechanisms of QCD and test the scaling prediction supposed to be specific of pQCD.
The separation of the two proton form factors has been reliably performed [4] up to only 6 GeV^2/c^2. Because the cross section is dominated by the reaction transverse amplitude, accurate measurements of F_2 for higher Q^2 can only be achieved via polarization observables [5]. Particularly, the polarization of the recoil protons issued from the elastic scattering of longitudinaly polarized electrons, is sensitive to the interference term between the longitudinal and transverse amplitudes [6]. Hereafter we review the motivations and investigate the feasibility of such an experiment up to 10 GeV^2/c^2 in the context of the 8 GeV energy upgrade of CEBAF.

2. Physics Case

The theoretical understanding of the nucleon form factors at large momentum transfers is based on the factorization between large and short distance physics [3,7-9]. The main result of this approach is that any observable of an exclusive reaction can be written as a convolution of a Distribution Amplitude (DA) with an elementary amplitude T_H representing the scattering of the quarks in a collinear approximation. In the factorization scheme, the helicity conserving form factor of the nucleon reads as [8]

$$F_1(Q^2) = \int_0^1 [dx_i] \int_0^1 [dx_i'] \; \varphi^\dagger(x_i, Q) T_H(x_i, x_i', Q) \varphi(x_i', Q) \qquad (1)$$

where $[dx_i^{(\prime)}] = dx_1^{(\prime)} dx_2^{(\prime)} dx_3^{(\prime)} \; \delta(1-x_1^{(\prime)}-x_2^{(\prime)}-x_3^{(\prime)})$ are the longitudinal momentum fractions carried by the quarks in the initial and final states. T_H consists of all possible tree diagrams contributing to $\gamma^*3q \rightarrow 3q$ (Fig. 1) and is calculated from pQCD. To leading order, the resulting hard scattering amplitude has the form

$$T_H(x_i, x_i', Q) = \frac{\alpha_s^2(Q^2)}{Q^4} \; f(x_i, x_i') \quad . \qquad (2)$$

The DA $\varphi(x_i^{(\prime)}, Q)$ is the average over the transverse momentum of the 3q valence Fock state wave function

$$\varphi(x_i^{(\prime)}, Q) \propto \int_0^Q d^2k_\perp \; \psi(x_i^{(\prime)}, k_\perp) \quad . \qquad (3)$$

The DA is an effective wave function which contains the non-perturbative part of the process and corresponds to the probability amplitude for finding the 3q valence Fock

state in the nucleon with the quarks collinear up to a scale Q.

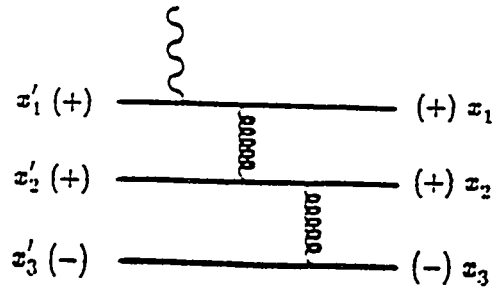


Fig. 1. Typical leading order Feynman diagram contributing to the perturbative hard scattering amplitude. The + and − symbols denote the helicities of the quarks.

This so called Hard Scattering Picture (HSP) for exclusive reactions exhibits two important properties which are independent of an explicit calculation of the hard scattering amplitude and of the choice of the DA's. These are the hadron helicity conservation [10] and the dimensional counting rules [7].

Since T_H involves the coupling of the quarks with a photon or a gluon, i.e. a vector particle, it is chirality conserving. For light flavors, the quark mass can be neglected and therefore chirality equals helicity which implies that T_H is diagonal in helicity space. This in turn implies that the hadron helicity is conserved up to corrections of order m/Q or higher [10]. Moreover this important result is valid to any order of perturbation theory, constituting thus a severe test of the whole factorization scheme. Another consequence of this conservation rule is that any single spin asymmetry should be zero. This statement opposises to high energy nucleon-nucleon scattering experiments [11] where non-zero polarization observables are measured, leading to the violation of helicity conservation up to a 25% level. The confirmation of this violation in electromagnetic processes would imply that either the reaction is not dominated by short transverse distances or that the hard scattering amplitude contains genuine non-perturbative terms such as, for example, quark-quark correlations [12]. Then, the understanding of helicity non-conservation provides information about the non-perturbative mechanisms of QCD.

From dimensional counting rules, it is predicted that the helicity conserving form factor behaves asymptotically like $1/Q^4$. QCD modifies this scaling law by logarithmic factors which originates from the Q dependence of the running coupling constant $\alpha_s(Q^2)$ and of the DA (see Eq. (1) to (3)), but this would presumably be seen only over a large range of Q^2. The F_1 scaling is well satisfied by existing data [13], even at surprisingly low Q^2. The explanation of the apparent relevance of pQCD at low Q^2 is still a lively controversy which is dealing with both the appropriate choice of the DA and the relevant description of the reaction mechanisms. While it is argued that the coupling to higher Fock components through color radiative corrections [14] (Sudakov effect) legitimates the use of pQCD at rather low Q^2, it is claimed that the leading order expansion for the hard scattering amplitude is illegitimate in that Q^2 range due to significant higher twist contributions issued from non-perturbative effects [15]. On the other hand, while total symmetric DA supported by lattice gauge calculations

fails to reproduce F_1 experimental data [16,17], QCD sum rules calculations [18,19] are in fair agreement with experiments but lead to a very asymmetric DA which favors non-perturbative contributions to the reaction process [20-22]. This discussion only reflects the lack of an accurate experimental data set for a large variety of elementary phenomena. In particular, precise measurements of unambiguous non-perturbative observables are needed to get the lower limit of pQCD validity and understand the precocious scaling.

Considering the H(e,e'p) elastic scattering, which corresponds to the simplest reaction between an electromagnetic probe and the hadronic matter, the interaction process is described by the proton electromagnetic current

$$< p+q|J_\mu(0)|p > = \bar{u}(p+q)\left[F_1(Q^2)\gamma_\mu + i\kappa F_2(Q^2)\frac{\sigma_{\mu\nu}q^\nu}{2M}\right]u(p) \qquad (4)$$

where q is the quadrimomentum of the virtual photon with $Q^2 = -q^2$, κ is the anomalous magnetic momentum of the proton and M its mass. The Pauli form factor is a basic experimental observable for testing the helicity conservation rule because the operator which multiplies F_2 in Eq. (4) is chirality non-conserving. Furthermore, due to helicity conservation, the pure HSP cannot predict the magnitude of the helicity non-conserving form factor. Nevertheless, given a simple quark constituent model for the nucleon structure, F_2 is found to behave asymptotically like $1/Q^6$ or equivalently, Q^2F_2/F_1 is almost constant [3] at large Q^2. It is not known how large Q^2 should be, but it is worthwhile to note that in the Q^2 range of interest, non-perturbative models such as the diquark ansatz [12] not only predict a different Q^2 dependence but also a sizeable value for F_2 which should confirm helicity non-conservation (Fig. 2).

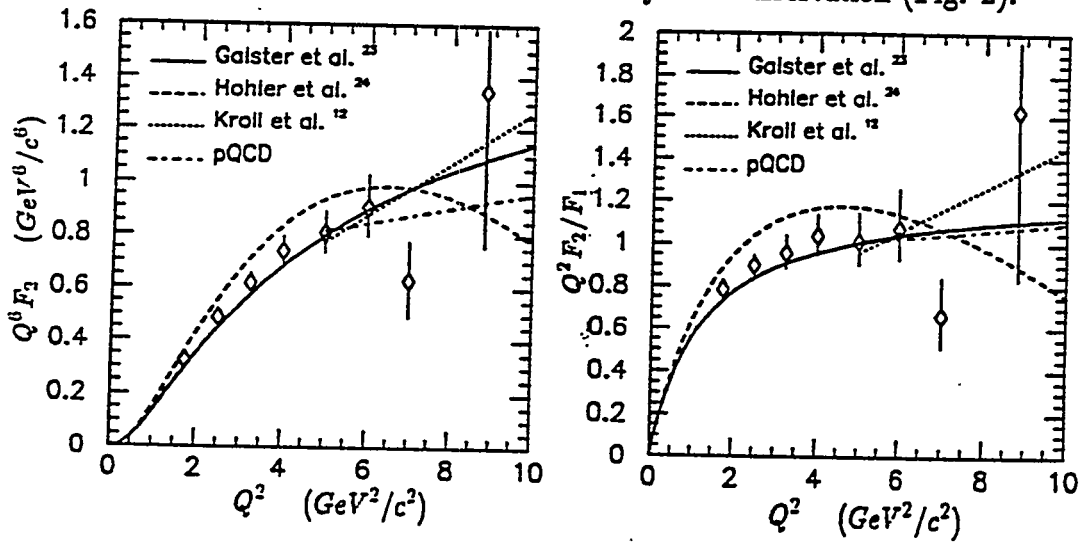


Fig. 2. Q^2 dependence of the helicity non-conserving form factor (a) and of the form factors ratio (b) of the proton as extracted from recent SLAC data [4] together with some model predictions. Note that for the pQCD prediction, only the Q^2 evolution is relevant and not the absolute value as explained in the text.

The present knowledge of F_2 (Fig. 2) does not allow to conclude satisfactorily on both helicity and scaling predictions at large Q^2. The maximum reliable Q^2 is too small to

confirm the apparent consistency with scaling exhibited by experimental data above 3 GeV^2/c^2 and the experimental accuracy is not sufficient to expect a clean selection between the models describing F_2, i.e. to expect to understand univocally helicity non-conservation. In particular, it is clear that above 6 GeV^2/c^2 huge systematic errors dominate this experiment based on a Rosenbluth separation [25]. New generation of experiments must therefore improve the accuracy of experimental data and extend the measurements to higher Q^2. The current design of CEBAF will produce high quality data [26] up to 6 GeV^2/c^2 and we show in the following that the 8 GeV upgrade of CEBAF energy would allow to obtain an accurate data set up to 10 GeV^2/c^2. This would lead to a better understanding of the non-perturbative mechanisms of QCD.

3. Recoil Polarization Method

It is now well known that a reliable Rosenbluth separation of the proton form factors in the high Q^2 range is not possible because of the dominant contribution of the transverse amplitude to the cross section [1]. Since the sixties, it has been stressed that the scattering of polarized electron beams represents a powerful method for electromagnetic form factor measurements [27,28]. Indeed, in addition to the dominant transverse amplitude, the cross section contains an interference term between the longitudinal and transverse amplitudes which acts as an amplifier of the small longitudinal amplitude. Once measuring an asymmetry when using a polarized proton target, or the polarization of the recoil proton if using a polarimeter [6], experimental values for the F_2/F_1 ratio can be deduced with much smaller systematic uncertainties than for the Rosenbluth separation.

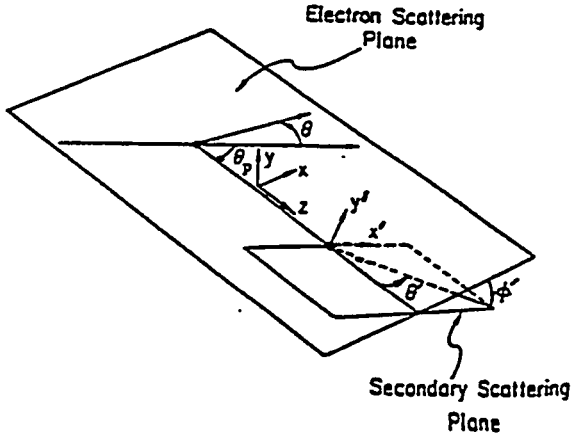


Fig. 3. Definition of the primary and secondary scattering planes.

The cross section for elastic scattering of longitudinally polarized electrons from unpolarized protons including the recoil proton scattering from a secondary target, can be expressed in the one photon exchange approximation as [6]

$$\frac{d^2\sigma^h}{d\Omega_e d\Omega_p} = \frac{d^2\sigma^0}{d\Omega_e d\Omega_p}\,(1 + h\,\mathrm{P}\cdot\mathrm{A}) \qquad (5)$$

where h is the beam helicity ($h = \pm p_b$, the beam polarization) and $A \equiv A_{y'}(\theta')$ is the vector analyzing power of the second scattering depending upon the polar angle θ' of the recoil particle (for our purpose). The polarization P of the recoil proton consists of a sideways and a longitudinal components

$$P_x = -\frac{2\sqrt{\tau(\tau+1)}\,\tan\frac{\theta}{2}}{G_E^2+\tau G_M^2(1+2(1+\tau)\tan^2\frac{\theta}{2})}\,G_E G_M \tag{6}$$

$$P_z = \frac{2\sqrt{\tau(\tau+1)}\,\tan\frac{\theta}{2}}{G_E^2+\tau G_M^2(1+2(1+\tau)\tan^2\frac{\theta}{2})}\,\sqrt{\tau\left(1+2(1+\tau)\tan^2\frac{\theta}{2}\right)}\,G_M^2 \tag{7}$$

with $\tau = Q^2/4M^2$. The helicity conserving and non-conserving form factors of the proton are related to the electric (G_E) and magnetic (G_M) form factors according to

$$F_1 = (G_E+\tau G_M)/(1+\tau) \tag{8}$$

$$F_2 = (G_M - G_E)/\kappa(1+\tau)\ . \tag{9}$$

Assuming that the polarimeter is placed at the focal plane of a spectrometer which deviates upwards charged particles, the precession angle of the proton spin through the spectrometer is given by

$$\chi = \kappa\gamma\Omega_B \tag{10}$$

where $\gamma = E_p/M$ is the Lorentz factor and Ω_B is the bend angle of the spectrometer. Then, the spin dependent part of the cross section reads as

$$\mathrm{P}\cdot\mathrm{A} = P_x A_{y'}(\theta')\sin\phi' + P_z \sin\chi A_{y'}(\theta')\cos\phi'\ . \tag{11}$$

From the Fourier analysis of the point-to-point asymmetry corresponding to two opposite beam polarizations

$$A_s(\theta',\phi') = \frac{\sigma^+ - \sigma^-}{\sigma^+ + \sigma^-} = a(\theta')\sin\phi' + b(\theta')\cos\phi' \tag{12}$$

one gets the amplitudes

$$a(\theta') = p_b\ P_x A_{y'}(\theta') \tag{13}$$

$$b(\theta') = p_b\ P_z \sin\chi A_{y'}(\theta')\ . \tag{14}$$

The ratio of the electromagnetic form factors is then obtained from the ratio of the Fourier amplitudes, as

$$r = \frac{F_2}{F_1} = \frac{1}{\kappa}\,\frac{1-\tau_G}{\tau+\tau_G} \tag{15}$$

with

$$r_G = \frac{G_E}{G_M} = -\frac{a}{b}\sqrt{\tau\left(1+2(1+\tau)\tan^2\frac{\theta}{2}\right)}\sin\chi \qquad (16)$$

which has the nice feature of being independent of both the analyzing power of the second scattering and the polarization of the beam, resulting in a self-calibrated device. The absolute uncertainty of a and b is, in the case of small asymmetries

$$\delta a = \delta b = \sqrt{\frac{2}{\varepsilon N_0}} \qquad (17)$$

where ε is the polarimeter efficiency and $N_0 = N^+ + N^-$ is the total number of incoming protons. The relative uncertainty on the ratio of the electromagnetic form factors is then given by

$$\left(\frac{\delta r}{r}\right)^2 = \left[\frac{r_G^2}{(1-r_G)^2} + \frac{r_G^2}{(\tau+r_G)^2}\right]\left(\frac{\delta r_G}{r_G}\right)^2 \qquad (18)$$

with

$$\left(\frac{\delta r_G}{r_G}\right)^2 = \frac{2}{\varepsilon\overline{A_y^2}N_0}\frac{1}{p_b^2}\left[\frac{1}{P_x^2} + \frac{1}{P_z^2\sin^2\chi}\right] + \left(\frac{\delta\sin\chi}{\sin\chi}\right)^2 \qquad (19)$$

where $\varepsilon\overline{A_y^2}$ is the so called factor of merit (FoM) of the polarimeter. The Eq. (19) yields the guidance lines for the optimization of the experimental set-up: the hadron spectrometer must allow high quality determination of non-zero precession angles and the polarimeter FoM must be as large as possible in order to reduce the uncertainty on the final experimental result and/or the running time of the experiment.

4. Experimental Set-up

The H($\vec{e}$,e'$\vec{p}$) experiment requires the detection of the electron in coincidence with the proton, which polarization is further measured by a polarimeter. In the context of the 8 GeV upgrade of CEBAF energy, the experiment colud be performed with the present High Resolution Electron Spectrometer (HRES) of Hall A but necessitates a new hadron arm because the allowed maximum momentum of the hadron spectrometer forbids the investigation of the high Q^2 region.

4.1. Hadron Spectrometer

The self-calibrated technique previously detailed, involves the precession of the longitudinal component of the proton polarization. Therefore, this technique is not valid if the precession angle approaches zero as expressed by Eq. (19). Indeed, Eq. (19) shows that χ should be close to $\pi/2$ in order to minimize the effects of the precession angle on the statistical uncertainties on the ratio of the form factors.

The resulting constraints are better expressed in terms of the bend angle of the spectrometer which must satisfy

$$\begin{cases} \Omega_B \neq & \frac{2k\pi}{2} & \frac{1}{\kappa(1+2\tau)} & k=0,1,2... \\ \Omega_B = & \frac{(2k'+1)\pi}{2} & \frac{1}{\kappa(1+2\tau)} & k'=0,1,2... \end{cases} \tag{20}$$

whatever the beam energy is. Furthermore, for sake of simplicity, the spectrometer should be designed to accomodate the precession effects with a constant bend angle in the whole Q^2 range of interest. In the 6-10 GeV^2/c^2, the combination of this requirement and of the constraints of Eq. (20) yield the solutions $\Omega_B \approx 9.5°$ or $\Omega_B \approx 26.5°$.

In addition to the bend angle constraint, Eq. (19) exhibits also the sensitivity to the accuracy on the precession angle measurement which is related to the precision on the proton location and incident angle at the focal plane of the spectrometer. Based on the current design of Hall A spectrometers and assuming the control of the bend angle according to Eq. (20), a 1% accuracy for the relative uncertainty on $\sin\chi$ seems realistic and anyway should be one of the goal for a new hadron arm design.

Angular and/or energy mismatch between the electron and hadron arms can affect the experiment leading to large running time. Assuming that the hadron spectrometer is working at variable recoil angles as a function of Q^2, the strongest constraint for the matching of the acceptances is obtained for the lowest Q^2 point together with the highest allowed beam energy. The resulting required hadron spectrometer acceptances are then

$$\begin{cases} \Delta\theta_p &= \pm\ 25 & \text{mrd} \\ \Delta\phi_p &= \pm\ 65 & \text{mrd} \\ \frac{\Delta P_p}{P_p} &= \pm\ 5 & \% \end{cases} \tag{21}$$

quite similar to the design characteristics of Hall A spectrometers. In addition, the protons emerging from the spectrometer have to travel along the whole length of the polarimeter target. The calculation of such an effect requires the complete knowledge of the transport coefficients of the proton beam through the spectrometer. However, a first order estimate leads to a focusing spectrometer with unit linear magnification factors, in agreement with a 10-15 cm diameter for the polarimeter target.

4.2. High Energy Proton Polarimeter

Even though the self-calibrated technique allows to determine the ratio of the electromagnetic form factors independently of the efficiency and the analyzing power of the polarimeter, the uncertainty on this ratio depends strongly upon these two quantities through the factor of merit of the polarimeter. A viable polarimeter requires then a nuclear reaction with a large cross section (efficiency) and a large sensitivity to the polarization (analyzing power) of the incoming particle in the angular range where the differential cross section is maximum.

For high energy protons, the rapidly increasing number of reaction channels and the forward peaked cross section favor the use of low Z analyzer. It is not expected

that a polarimeter based on an inclusive reaction would have a significant overall analyzing power since the analyzing power of the many channels do not have necessarily the same sign. A viable high energy proton polarimeter should therefore be based on an exclusive reaction. An appropriate reaction, already used at Argonne for the measurement of the beam polarization [29], is the H($\vec{p}$,pp) elastic scattering which exhibits significant cross sections and analyzing power in the energy range of interest (Fig. 4).

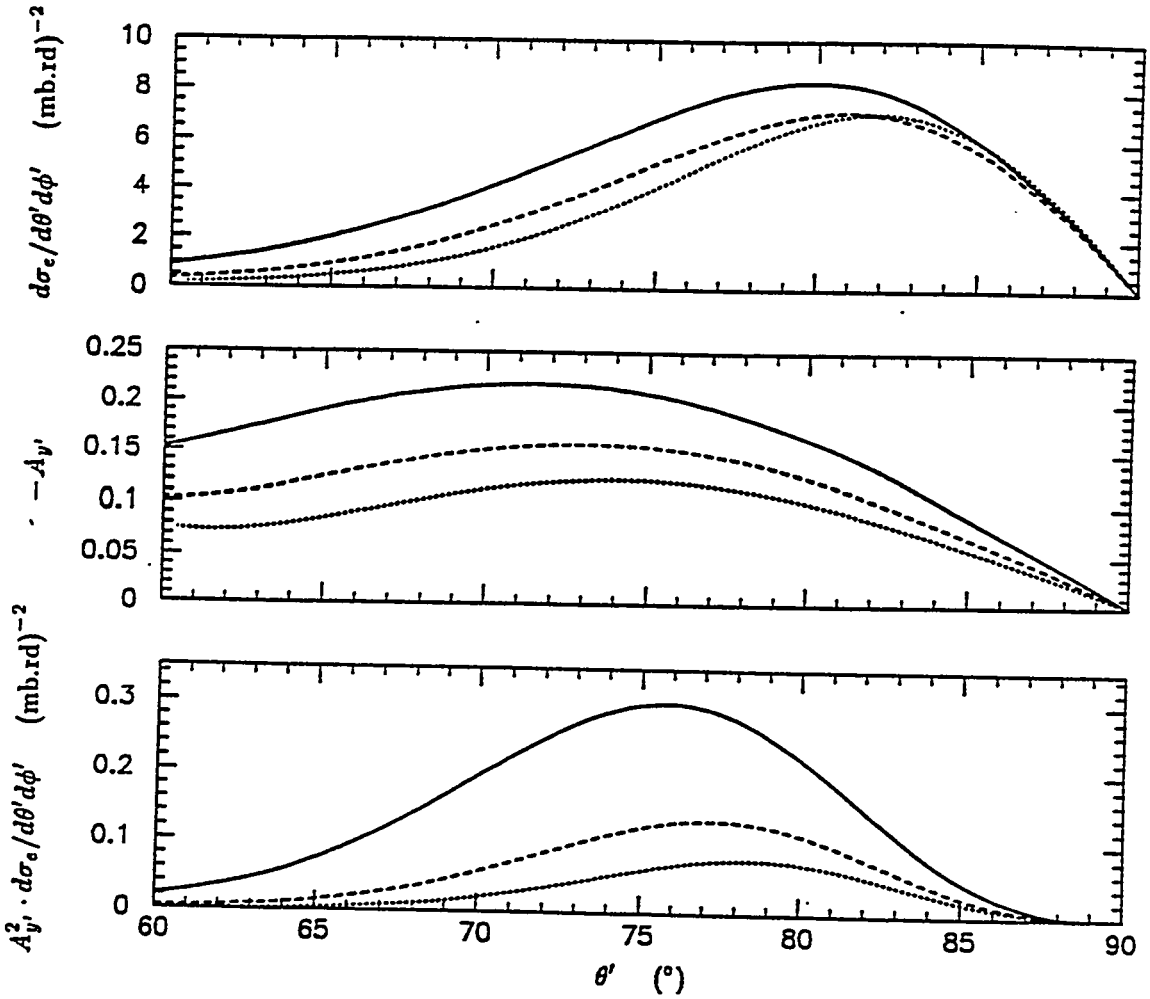


Fig. 4. Differential cross sections [30], analyzing power [29] and local factors of merit for the proton elastic scattering off a liquid hydrogren target, as a function of the recoil proton angle. Curves are shown for a 3 GeV (full line), a 4.5 GeV (dashed line) and a 6 GeV (dotted line) proton kinetic energy.

In the design of a polarimeter, one is primarily concerned by the definition of an efficient solid angle for the detection of the reaction products, which optimization is obtained via the maximization of the *FoM*. Considering a cylindrical detection device, based on a cylindrical liquid hydrogen converter of length L_c, and a proton beam along the converter axis, the efficiency and factor of merit of the polarimeter may be expressed as [31]

$$\varepsilon = \rho_H \int_0^{L_c} dz' \exp\left[-\mu_H z'\right] \int_{\theta'_{min}}^{\theta'_{max}} d\theta' \int_0^{2\pi} d\phi' \; \varepsilon'(z', \theta', \phi') \frac{d\sigma_e}{d\theta' d\phi'} \tag{22}$$

$$FoM = \rho_H \int_0^{L_c} dz' \exp\left[-\mu_H z'\right] \int_{\theta'_{min}}^{\theta'_{max}} d\theta' \int_0^{2\pi} d\phi' \; \varepsilon'(z', \theta', \phi') A_{y'}^2(\theta') \frac{d\sigma_e}{d\theta' d\phi'} \tag{23}$$

where ρ_H is the target atom density, $\mu_H = \rho_H \sigma_t$ the proton total absorption coefficient with σ_t the total p+H cross section and $\varepsilon'(z', \theta', \phi')$ the detection efficiency of the reaction products. The 2π angular coverage for ϕ' is dictated by the self-calibrated method. The rapid decrease of the H(p,pp) differential cross section results in a small θ' efficient range: the angular range corresponding to $2MT' < 0.8$ GeV^2 (T' is the kinetic energy of the recoil proton) yields 80% of the maximum FoM value. Nevertheless, the polarimeter target leads to solid angle reductions which originate from the proton energy loss and its multiple scattering in the converter. While energy loss effects are controlled by the converter diameter, multiple scattering effects essentially constrain its length since the combination of the variations of the proton path length and kinetic energy as a function of the angle results in further significant effects only for small angle protons. Moreover, these two effects are linked by the kinematical constraints of the elastic scattering such that an energy loss cut corresponds to a multiple scattering cut i.e. the optimized converter length depends on the optimized converter diameter. Considering a 10-15 cm converter diameter, the corresponding length is 1.5 m resulting in a threshold proton energy of about 40 MeV and an angular distribution width of about 0.1° which implies the detection of the recoil protons in the angular range $60° \leq \theta' \leq 80°$.

Table 1. Efficiencies and factors of merit.

Q^2 (GeV^2/c^2)	T_p (GeV)	ε %	FoM ($\times 10^{-3}$)
6	3.2	5.0	1.83
7	3.7	4.4	1.27
8	4.3	3.9	0.91
9	4.8	3.7	0.70
10	5.3	3.5	0.55

Table 1 gives the expected efficiencies and factors of merit of the polarimeter in the energy range of interest. These values have been obtained according to the Eq. (22) and (23) using existing experimental data for the analyzing power [29] and the cross sections [30]. These efficiencies also assume $\varepsilon'(z', \theta', \phi') = 1$ which implies that all protons exiting the converter in the angular range of interest are detected and that the elastic process is separated from background events. Since one deals with the detection of charged particles, the first hypothesis seems realistic. The assumption relies then on the ability of the polarimeter to obtain a large signal to noise ratio.
The proposed high energy proton polarimeter (Fig. 5) consists of three different elements: a liquid hydrogen converter, the tracking devices and the identification device.

The reconstruction of the trajectory of the incident proton into the target is obtained after the spectrometer by 2 planar MultiWire Proportional Chambers (MWPCs). The angles of the scattered and recoil protons are measured respectively with 2 planar MWPCs downstream the converter and 2 cylindrical MWPCs surrounding it. The knowledge of the scattering plane and of the incoming proton energy is sufficient for the identification of the elastic process via a missing energy spectrum assuming that the detected charged particles are protons. However, in the energy range of interest the 1π production channels have cross sections of the same order of magnitude than the elastic scattering and generate therefore a significant background. This could result in a complete dilution of the polarization signal but this problem can be solved by identifying the recoil proton and by measuring its energy via the range telescope surrounding the cylindrical MWPCs. The resulting improvement of the signal to noise ratio should ensure the reliability of the calculated FoM.

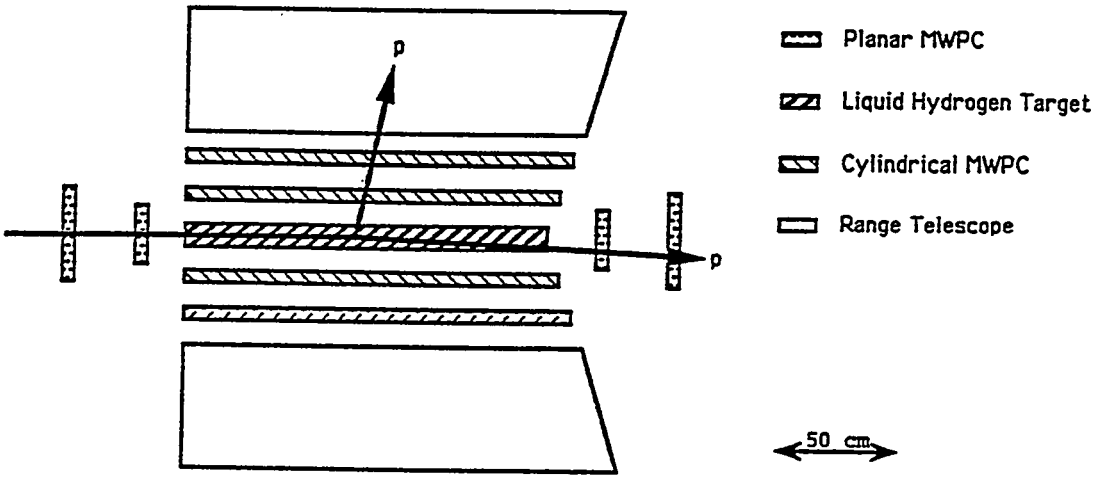


Fig. 5. Schematic view of the high energy proton polarimeter.

5. Counting Rate and Time

This study propose to measure r_G in the 6-10 GeV^2/c^2 Q^2 range by steps of 1 GeV^2/c^2. The choice of the beam energies and electron angles (Tab. 2) is constrained by the 8 GeV maximum beam energy and the 4 GeV/c maximum momentum of the HRES of Hall A. The choice of the Q^2 stepping is linked to the Q^2 binning of the experiment. The selection of the kinematics setting is guided by the minimization of the data taking time for a given statistical error on a and b.
The counting rates and data taking times (Tab. 3) are based on a 100 μA beam intensity, a 0.6 beam polarization and a 10 cm useful length for the primary liquid hydrogen target. They further assume the dipole parametrization [23] for the electromagnetic form factors of the proton. Since the polarimeter is expected to allow the detection of all protons emerging from the spectrometer, the only solid angle reduction originates from the momentum acceptance of the HRES. The decrease of the

number of requested incoming protons (N_0) corresponds to a realistic data taking time requirement for a reasonable relative uncertainty on F_2.
The statistical uncertainties on the various electromagnetic form factors of the proton (Tab. 4) relies in part on the previous G_M SLAC data [4]. Despite the small polarimeter FoM for the highest energies, the quality of the data set for the F_2/F_1 ratio and the helicity non-conserving form factor is shown to be still relevant, especially if taking into consideration that the self-calibrated method leads to small systematical uncertainties.

Table 2. Kinematics of the experiment.

Q^2 $(GeV^2/c)^2$	E (GeV)	θ (°)	E' (GeV)	θ_p (°)	P_p (GeV/c)
6	7.2	26.4	4.0	26.2	4.0
7	7.7	27.7	4.0	23.8	4.6
8	8.0	30.0	3.7	21.4	5.1
9	8.0	34.5	3.2	18.7	5.7
10	8.0	40.0	2.7	16.1	6.2

Table 3. Counting rate and data taking time.

Q^2 $(GeV^2/c)^2$	ΔQ^2 $(GeV^2/c)^2$	σ_{ep} ($\times 10^{-2}$ nb/sr)	R (Hz)	N_0 ($\times 10^6$)	t (h)
6	±0.37	1.68	29.3	51.4	488
7	±0.37	0.71	12.4	19.1	430
8	±0.35	0.29	5.0	9.3	511
9	±0.30	0.11	1.9	5.6	806
10	±0.25	0.04	0.8	3.8	1400

Table 4. Form factor uncertainties.

Q^2 $(GeV^2/c)^2$	$\delta\tau/\tau$ (%)	$\delta G_M/G_M$ (%)	$\delta G_E/G_E$ (%)	$\delta F_1/F_1$ (%)	$\delta F_2/F_2$ (%)
6	3.5	1.2	5.4	1.5	3.2
7	6.5	1.7	10.5	2.3	6.0
8	10.5	2.3	17.6	3.3	10.0
9	15.1	2.8	25.6	4.2	14.5
10	21.4	5.0	35.9	6.4	20.4

6. Conclusions

The importance of helicity non-conserving processes in the understanding of the non-perturbative mechanisms of QCD has motivated this investigation of the feasibility of precise measurements of F_2 in the high Q^2 range. In the context of the 8 GeV upgrade of CEBAF energy, this study shows that such measurements can be

performed in the 6-10 GeV^2/c^2 Q^2 range within an overall running time of 150 days, providing the development of a new hadron spectrometer and of a high energy proton polarimeter based on the exclusive $H(\vec{p},pp)$ elastic scattering.
The main technical issue adressed by this experiment is the development of a long cylindrical liquid hydrogen target. The present design of the polarimeter is based on a 10-15 cm target diameter and 1.5 m target length resulting in a 11-26 liters liquid hydrogen volume. Such a large volume target is already adressed by the phase II of the HARP project [32] involving a more complex geometry. We can then realistically expect that the main part of the technology needed for a long cylindrical converter will be available in a nearby future.
In addition, the experiment can benefit of significant improvements. The successful development of modern polarized electron sources gives strong hopes for the future availability of high beam polarization: the running time would be reduced by a factor 2 if the beam polarization reaches 0.8. Furthermore, experimental data [30] indicates that other channels of the $\vec{p}$+p reaction are sensitive to the proton polarization. In particular, the analyzing power of the Δ^{++} production channel reaches -0.4 in the energy range of interest [33]. From a crude estimate, we could double the FoM of the polarimeter if we manage to identify simultaneously the elastic scattering and the Δ^{++} production channels. Such a goal may necessitate a significant upgrade of the proposed polarimeter with a forward detection device but would in turn decrease the beam time request by a factor 2 and give access to higher Q^2 measurements.

References

1. *The ELFE Project an Electron Laboratory for Europe*, ed. J. Arvieux and E. De Sanctis, Conference Proceedings 44 (Italian Physical Society, Bologna, 1993).
2. *Perturbative Quantum Chromodynamics*, ed. A.H. Mueller, Advanced Series on Directions in High Energy Physics 5 (World Scientific, Singapore, 1989).
3. S.J. Brodsky and G.R. Farrar, *Phys. Rev.* **D11** (1975) 1309.
4. P.E. Bosted et al., *Phys. Rev. Lett.* **68** (1992) 3841.
5. E. Voutier et al., Working Session to work out experimental proposals for the European Electron Accelerator, Clermont-Ferrand, May 25th - July 4th 1992.
6. R.G. Arnold, C.E. Coester and F. Gross, *Phys. Rev.* **C23** (1981) 363.
7. S.J. Brodsky and G.R. Farrar, *Phys. Rev. Lett.* **31** (1973) 1153.
8. G.P. Lepage and S.J. Brodsky, *Phys. Rev. Lett.* **43** (1979) 545.
9. G.P. Lepage and S.J. Brodsky, *Phys. Rev.* **D22** (1980) 2157.
10. S.J. Brodsky and G.P. Lepage, *Phys. Rev.* **D24** (1981) 2848.
11. C. Bourrely, E. Leader and J. Soffer, *Phys. Rep.* **59** (1980) 95.
12. P. Kroll, M. Schürmann and W. Schweiger, *Zeit. für Phys.* **A338** (1991) 339.
13. R.G. Arnold et al., *Phys. Rev. Lett.* **57** (1986) 174.
14. H-N. Li and G. Sterman, *Nucl. Phys.* **B381** (1992) 129.
15. N. Isgur and C.H. Llewellyn Smith, *Phys. Lett.* **B217** (1989) 535; *Nucl. Phys.* **B317** (1989) 526.

16. A.S. Kronfeld and D.M. Photiadis, *Phys. Rev.* **D31** (1985) 2939.
17. S. Gottlieb and A.S. Kronfeld, *Phys. Rev. Lett.* **55** (1985) 2531.
18. V.A. Nesterenko and A.V. Radyushkin, *Phys. Lett.* **B115** (1982) 410; *Phys. Lett.* **B128** (1983) 439.
19. A.V. Radyushkin, *Acta Phys. Pol.* **B15** (1984) 403.
20. V.A. Nesterenko and A.V. Radyushkin, *Sov. J. Nucl. Phys.* **39** (1984) 811.
21. N. Isgur and C.H. Llewellyn Smith, *Phys. Rev. Lett.* **52** (1984) 1080.
22. A.V. Radyushkin, *Nucl. Phys.* **A532** (1991) 141c.
23. S. Galster et al., *Nucl. Phys.* **B32** (1971) 221.
24. G. Höhler et al., *Nucl. Phys.* **B114** (1976) 505.
25. M.N. Rosenbluth, *Phys. Rev.* **79** (1950) 615.
26. C.F. Perdrisat et al., *CEBAF proposal* **PR-89-014** (1989).
27. J.H. Scofield, *Phys. Rev.* **113** (1959) 1599; *Phys. Rev.* **141** (1966) 1352.
28. N. Dombey, *Rev. Mod. Phys.* **41** (1969) 236.
29. H. Spinka et al., *Nucl. Inst. and Meth.* **211** (1983) 239.
30. J. Bystricky and F. Lehar, *Phys. Data* **11-1** Part I and II (1978); *Phys. Data* **11-2** and **11-3** (1981).
31. M.E. Brandan and E. Voutier, *HARP Internal Report* (Grenoble, 1991).
32. Z. Papandreou, *HARP Conceptual Design Report* (Utrecht, 1992).
33. A. Wicklund, *AIP Conf. Proc.* **35**, ed. M. Marshak (1976) 198.

Working Group on Inclusive and Semi-Inclusive Processes

Organizers: B. Frois & P. Mulders

INCLUSIVE AND SEMI-INCLUSIVE DEEP INELASTIC SCATTERING AT CEBAF AT HIGHER ENERGIES

B. FROIS
Service de Physique Nucléaire, Centre d'Etudes de Saclay
F-91191 Gif sur Yvette CEDEX, France

and

P.J. MULDERS
National Institute for Nuclear Physics and High Energy Physics
(NIKHEF-K), P.O. Box 41882, NL-1009 DB Amsterdam, the Netherlands

ABSTRACT

We summarize the discussion on the possibilities of doing inclusive and semi-inclusive deep inelastic scattering experiments at CEBAF with beam energy of the order of 10 GeV.

This summary is based on talks by A. Mueller and A. Schaefer and contributions of N. Bianchi, X. Ji, J.-M. Laget, P. Markowitz, W. Melnitchouk, Z.-E. Meziani, J. Milana, P. Mulders, S. Simula, P. Souder and M. Strikman. These contributions can be found elsewhere in this report.

Electron scattering from a composite target is due to an electroweak interaction, well-described by the exchange of a virtual boson, either a photon or Z^0. The exchanged particle carries a momentum q and probes the distribution of electroweak charges in the target which are carried by the (elementary) constituents, the quarks. Assuming that the momentum of the target is P, the invariant variables are the momentum transfer Q^2 and the energy transfer ν

$$Q^2 = -q^2 \overset{TRF}{=} 4E_e E'_e \sin^2(\theta_e/2), \tag{1}$$

$$\nu = \frac{P \cdot q}{M} \overset{TRF}{=} E_e - E'_e. \tag{2}$$

The momentum transfer is a spacelike vector. In the laboratory frame or target-rest-frame (TRF) these are simply determined by measuring the momentum of the incident and scattered electrons.

Deep inelastic scattering assumes that the electron resolves the quark structure of the nucleon. This requires a sufficiently high momentum transfer to be able to understand the reaction mechanism in terms of perturbative QCD process. A momentum transfer $Q > 1$ to 2 GeV is considered as the typical lower boundary for deep inelastic scattering. Transforming this into a spatial resolution, $\lambda \approx 1/Q$ gives $\lambda = 0.1$ - 0.2 fm. The deep inelastic scattering corresponds to an incoherent sum over scattering off the individual quarks weighted by the squared charges. Besides the momentum

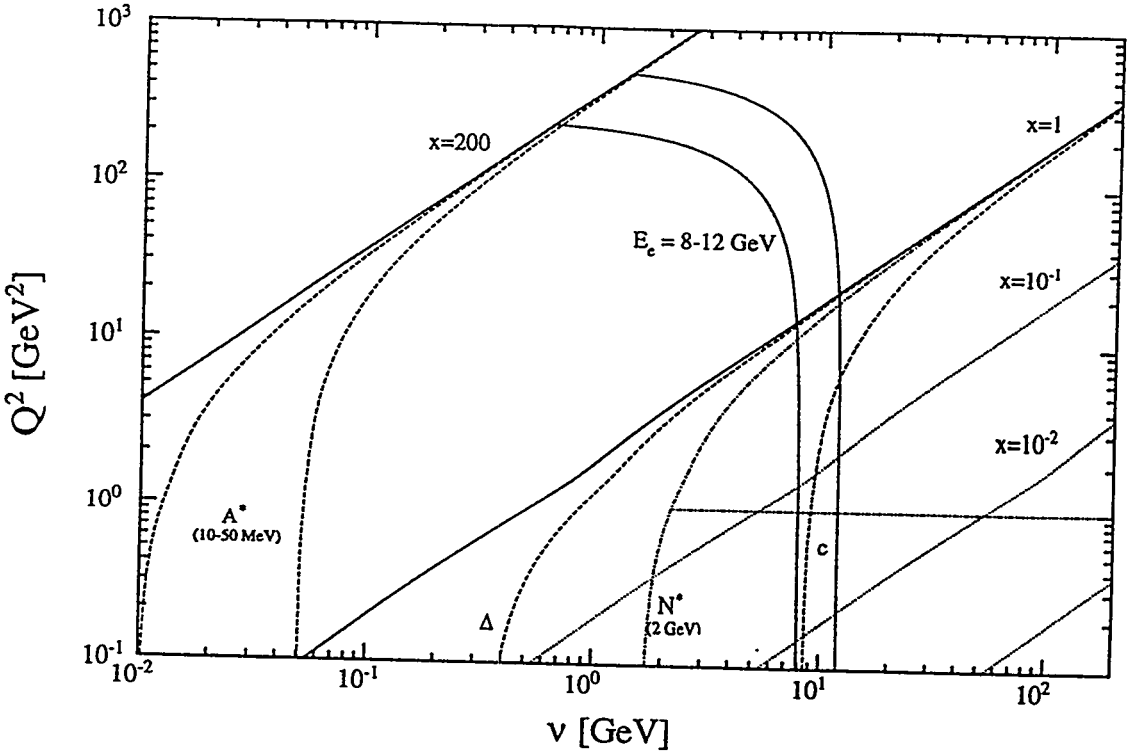


Figure 1: *The kinematic $Q^2 - \nu$ region accessible with a beam energy of 8 - 12 GeV (left of indicated lines). Shown are lines of constant x and constant W.*

transfer, one requires that the invariant mass W of the hadronic system is above the region of discrete baryon resonances, $W \geq 2$ GeV. The invariant mass W is given by

$$W^2 = (P+q)^2 = M^2 + 2M\nu - Q^2 = M^2 + \frac{1-x}{x}Q^2, \tag{3}$$

where x is the Bjorken scaling variable $x = Q^2/2P\cdot q$. The variable x can be interpreted as the fraction of the lightcone momentum of the struck quark compared to that of the nucleon,

$$x = \frac{p^+}{P+} \quad . \tag{4}$$

Note that p is the quark momentum and $p^+ = (p^0 + p^3)/\sqrt{2}$. The two constraints ($Q > 1$ GeV and $W \geq 2$ GeV) restricts the experimental explorations at CEBAF to $1 \leq Q^2 \leq 10$ GeV^2 and $0.1 \leq x \leq 1$ for deep inelastic scattering on a nucleon. Fig. 1 shows the specific domain accessible at CEBAF. Shown are furthermore lines of constant x for $x = 10^{-2}$, 10^{-1}, 1 (elastic scattering off a nucleon), 200 (elastic scattering off a heavy nucleus with $A = 200$), constant $W = M_\Delta$ (dashed, labeled Δ), 2 GeV (dashed, labeled N^*) and W corresponding to the threshold for J/ψ production (dashed, labeled c). The *region of deep inelastic scattering* is bounded by $W = 2$ GeV and the horizontal dot-dashed line corresponding with $Q^2 = 1$ GeV^2. The region between the (dashed) lines for $W = M_\Delta$ and $W = 2$ GeV is the *resonance region.* The right edge of the figure corresponds to $\nu = 200$ GeV, which is about the maximum energy transfer in the CERN muon experiments. The measurement of the valence quark structure of hadrons and the correlations between quarks and gluons by

deep inelastic studies have been extensively discussed in the review of Sloan, Smadja and Voss [1], in the Pegasys proposal [2] and the ELFE proposal [3].

1. The nucleon spin structure

In the study of valence quarks, which carry a sizable fraction of the momentum of the nucleon, an illustrative example of the possibilities at CEBAF is the determination of the precise shape of the polarized structure functions g_1^p and g_1^n at large x-values. Present available data on the neutron spin structure function at high Bjorken variable x stop at a value of 0.5. The precise shape and the threshold behavior for $x \to 1$ does not affect the sum rule but it *is* important for comparison with model calculations of the quark distributions.

In order to test the prediction $A_1 \to 1$ as $x \to 1$, precision data at $x > 0.5$ are necessary. Furthermore, the slope with which the asymmetry reaches unity becomes sensitive to the details of nucleon substructure. Severals constituent quark models, although constrained by the limit at $x = 1$, produce an asymmetry A_1 which behaves differently in the large x region.

From the experimental point of view, measurements of A_1 at high energy are not feasible, because high x implies high E' (usually more than 10 GeV) where the resolution of the high energy spectrometers does not allow a precise measurement of the slope since data are averaged over a wide x range. The low count rate conspires to make the measurement extremely difficult.

Therefore, it has been proposed to use the combination of unique possibilities of a high resolution 8 GeV incident electron beam and the Hall A spectrometers at large scattering angles. This implies a large recoil energy and therefore small E', typically below 4 GeV. The high momentum resolution of Hall A spectrometers allows one to take fine steps in the x region between 0.2 and 0.7, keeping W^2 greater than 4 GeV^2 to insure that the scattering process is in the deep inelastic region. The depolarization factor for a given x is closer to one at large angle, putting CEBAF at an advantage for the measurement using large angle since $A_1 = A_{1\|}/D$. Two identical spectrometers with 10% momentum acceptance allow one to double the solid angle from 7.5 to 15 msr. When combined with a 40 cm long high pressure polarized ^{3}He target and a 15 μA electron beam, this setup offers a superb luminosity of $10^{36}/\mathrm{cm}^2/s$.

The proposal discussed by Meziani at this workshop showed that in 1000 hours of beam time one can achieve a precise measurement of the neutron spin structure function at high x.

2. Parity violation

It was proposed that a parity violation experiment in the deep inelastic region would be of special interest for $x = 0.5, y = 0.5$, where $y \equiv \nu/E_e$. Such a measurement would allow a precise test of the product of the hadron-axial and electron-vector electroweak couplings. This particular point will be less sensitive to structure functions, while measurements for lower x and y values are expected to provide information

about structure functions.

3. Nonleading structure functions

The ratio of longitudinal and transverse cross sections $R(x, Q^2)$ (at relatively small Q^2) is nonzero from a combination of perturbative QCD corrections, which are sensitive to the gluon distribution, higher twist corrections such as target mass corrections, and finally nonperturbative effects. Besides the study of R for a nucleon target, the study of R_A in a nucleus is of interest.

Another topic which we mention is the study of higher twist structure functions. These are of interest because they are a manifestation of correlations between quarks or between quarks and gluons. These correlations vanish as powers of $1/Q$ compared to leading twist and are therefore more prominent at relatively small values of Q^2 (although one must be in the deep inelastic region!). In inclusive unpolarized electron scattering the first higher twist contribution is $\mathcal{O}(1/Q^2)$. At $\mathcal{O}(1/Q)$ higher twist contribution can be measured by using polarized beams and/or the detection of produced hadrons. As compared to the leading contribution, the higher twist contributions turn out to be stronger at larger x-values, as shown in NMC experiments at CERN.

4. Semi-inclusive experiments

A region where deep inelastic experiments are less restricted by energy considerations is the region of $x \geq 1$, accessible in scattering off nuclei. Here the beam luminosity is much more important, as the cross sections are small. After all, one is looking, for example, at one out of six valence quarks which carries a large fraction (more than 1/2) of the momentum of two nucleons, or one is looking at a quark belonging to a high-momentum nucleon in the nucleus. The distinction between these two mechanisms can be made as in the second process one can try to detect another high-momentum nucleon or nuclear rest-system moving in the backward direction. These type of experiments (tagged structure functions) requiring high luminosity and special detector set-ups are well suited for an upgraded CEBAF.

The case of tagged structure functions is an example of a semi-inclusive process in which one (or more) particles are detected in coincidence with the scattered electron. For semi-inclusive processes one distinguishes different production mechanisms such as *target fragmentation* and *current fragmentation*. The latter case, in which one is interested mainly in the particles produced in the forward direction, can at sufficiently high energies be described as a product of quark distribution functions $f_{H\to q}(x)$ and quark fragmentation functions $D_{q\to h}(z)$. Here $z = P \cdot P_h / P \cdot q$, which in the target rest-frame is $z = E_h/\nu$, i.e. the fraction of the energy of the photon or the struck quark taken by the produced hadron. The fragmentation can be used to tag specific quark flavors or their spins, e.g. an s-quark will favor production of K^- (or $\overline{K}^0$) while an $\bar{s}$-quark will favor production of K^+ (or K^0), leading to asymmetries in

hadroproduction of specific particles (that must then be identified). In order for factorization to be valid and to have a sufficiently clear separation of the target and current fragmentation region, an energy of 10 GeV is too low [1].

5. Conclusions

The region which is most important for CEBAF is the transition between the (inclusive) deep inelastic scattering region and the region of exclusive processes, such as the excitation of baryon resonances leading to a specific final state. In exclusive processes the momentum transfer in the t-channel becomes a relevant variable that determines if one can use perturbative QCD methods to describe the process. In this case the object of study is not the quark probabilities in the target, but rather the (lightcone) quark wave functions, which depend on the lightcone momentum fractions $x_i = p_i^+/P^+$ and the perpendicular quark momenta. Focussing on elastic processes or exclusive or semi-inclusive production of vector mesons (ρ, ϕ or J/ψ), one can investigate different components of the wave functions or specific reaction mechanisms.

In summary, it appears that an energy upgrade to about 10 GeV gives a relatively limited access to the region of inclusive deep inelastic scattering and even less to the region where semi-inclusive deep inelastic processes factorize. However, this workshop has shown that such an upgrade of CEBAF beam energy would allow one to address a number of fundamental questions related to the valence quark structure of hadrons. The answers could clarify some puzzles related to the approach to scaling even at modest Q^2-values. For this a broad coverage of the resonance region reaching into the deep inelastic scattering region is important. It is here where the challenge is to connect effective hadronic theories or successful quark models to the underlying theory of quantum chromodynamics.

This work is in part (P.J.M.) supported by the foundation for Fundamental Research of Matter (FOM) and the National Organization for Scientific Research (NWO).

1. T. Sloan, G. Smadja and R. Voss, Phys. Rep. **162** (1988) 46.
2. *PEGASYS proposal* (blue book), IY-112 (1988);
3. *The ELFE project, an electron laboratory for Europe*, Proceedings of the conference on Physics with a 15-30 GeV High Intensity Continuous Beam Electron Accelerator, Mainz, 7-9 October 1992, edited by J. Arvieux and E. De Sanctis, published by the Italian Physical Society, Bologna, Italy.

CU-TP-629

INTERACTIONS OF QUARKS AND GLUONS WITH NUCLEI AT INTERMEDIATE ENERGIES

A.H. MUELLER*
Department of Physics, Columbia University
538 West 120th Street, New York, New York 10027

ABSTRACT

Some processes involving the interaction of medium energy quarks and gluons with nuclear matter are described. Possible mechanisms for the A-dependence of the energy loss of leading protons produced in proton-nucleus collisions are given, and an experiment which may help to distinguish these mechanisms is described. A possible color transparency experiment at CEBAF is described. Experiments to measure energy loss of quarks in nuclear matter and the formation time of hadrons are discussed along with the possibilities of measuring $\sigma_{J/\psi}$ and $\sigma_{\psi'}$ at CEBAF.

1. Introduction

From a particle physics point of view interactions of leptons and hadrons with nuclei can be very instructive because the nucleus can sometimes act as a detector which maps out the evolution of quarks and gluons coming from either the incident hadron or from an outgoing final state hadron. In this context it can be advantageous in some circumstances that the incident particle not have too high an energy. In what follows I shall indicate some reactions where intermediate energy particle interactions with nuclei may offer insights in strong interaction physics which are not available in the corresponding reactions on nucleons.

2. Inelastic Collisions and Absorption

In inelastic proton-proton collisions at intermediate to high energies the most energetic outgoing proton, the leading proton, typically carries about one-half of the incident energy. In proton-nucleus collisions the leading proton carries off even much less energy. Some time ago, Busza and Goldhaber[1] noted that the energy of the leading proton was consistent with

$$p_{leading} \approx (\frac{1}{2})^{\bar{\nu}} p_{inc} \qquad (1)$$

This work is supported in part by the Department of Energy Contract Under Grant DE-FG02-94ER40819

where p_{inc} is the energy of the incident proton and $\bar{\nu}$ is the average number of collisions that the incident proton suffers as it passes through the nucleus.

On the other hand, QCD leads one to believe that the energy loss of a high energy quark passing through nuclear matter is[2,3]

$$\frac{dE}{dx} = -c\ GeV/fm \tag{2}$$

with c on the order of 1. Thus, the higher the energy of the quark the smaller the fractional energy loss it suffers in passing through nuclear matter. High energy gluons should behave similarly with perhaps a constant, c', somewat larger than c in (2). How, then, can a proton lose so much energy in passing through nuclear matter when its constituents lose relatively little energy?

There appear to be three different sources of energy loss when a proton passes through nuclear matter.

(i) The constituent quark wavefunction may be shattered as the proton passes through a nucleus. As the incident proton reaches the front face of the nucleus we may imagine it to be made of three constituent quarks which have transverse momenta on the order of $k_\perp \approx 300 MeV$. As the three quarks pass through the nucleus they interact with the nucleons in the nucleus in a more or less independent manner. Each quark loses little energy in passing through the nucleus and picks up a transverse momentum $\Delta k_\perp$ with

$$(\Delta k_\perp)^2 \approx \bar{\nu}_q < k_{\perp 0}^2 > . \tag{3}$$

$\bar{\nu}_q$ is the number of interactions the quark has with nucleons in the nucleus and $k_{\perp 0}$ is the average transverse momentum of the quark-nucleon interaction. $k_{\perp 0}$ is likely on the order of a few hundred MeV. Thus, when the three quarks emerge from the nucleus their relative transverse momenta are larger than when they entered. How much larger depends on the size of the nucleus. Thus, the three quarks no longer fit comfortably in the proton's wavefunction, and the leading proton may only include one or two of the quarks from the incident proton. Here, clearly, is a mechanism for a significant energy loss.

(ii) The quarks impinging on the nucleus as part of the proton are constituent quarks. They have structure, probably mostly consisting of gluons. As an incident constituent quark passes through the nucleus interactions with nucleons in the nucleus may separate much of the gluonic cloud from the bare quark core. From deep inelastic scattering experiments it is known that the gluons of a constituent quark carry about half the constituent quark's momentum with the other half residing in the bare quark core. Thus, the quarks going into the leading proton may be much barer than those of the incident proton and this is a second source of a considerable energy loss. If, however, the constituent quark is very compact, say of radius 1/5 fm or less then interactions with the nucleus are not likely to be effective in stripping the cloud of gluons from the core.

(iii) Interactions of a quark in the nucleus may stimulate high momentum gluon radiation occurring after the quark has left the nucleus but before the leading proton

has formed. This, again, could be a significant source of energy loss for the leading proton.

Can one distinguish these possible sources of energy loss? Perhaps. Let me describe an experiment which may shed some light on this question. Consider the reactions

$$\gamma + Proton \rightarrow \phi + \text{anything} \tag{4a}$$

$$\gamma + Nucleus \rightarrow \phi + \text{anything} \tag{4b}$$

for both real and virtual photons where the ϕ is the leading (highest momentum) particle in the reaction. A ϕ is chosen rather than a ρ or ω simply because ϕ's are easy to identify in the final state. The same reactions would also be interesting for leading ρ's and ω's. For incident real photons I would guess that the energy loss of the leading ϕ depends on A in very similar manner to that discussed for leading protons in a proton induced reaction. However, for virtual photons, say with $Q^2 \geq 4 - 5GeV^2$ mechanism (ii) is no longer available for energy loss since photons of such a virtuality couple to bare quarks not constituent quarks. Thus, if stripping the gluonic cloud from constituent quarks is the main source of energy loss in proton-nucleus interactions one would expect a dramatic difference in the energy distribution of ϕ's produced in reaction (4b) between real and virtual photons. On the other hand, if constituent quarks are very compact one would expect little difference in energy loss of leading ϕ's for real and virtual γ's.

3. Color Transparency and Double Scattering

Color transparency experiments are probably best done at higher energy than will be available at CEBAF. Nevertheless, an interesting suggestion[5] has recently been made for searching for color transparency effects by measuring double scatterings at intermediate Q^2. Before turning to that suggestion let me briefly review the idea of color transparency.

In elastic electron-proton scattering at large momentum transfer, Q, a quark in the proton absorbs a high momentum virtual photon, of virtuality Q^2, and then quickly shares that momentum with the other quarks in the proton so that the whole system can recoil coherently as a physical proton. In order that the struck quark be able to share a large momentum with the other two quarks in the proton it is necessasry that these two quarks be found almost exactly along the line of motion of the struck quark, in the laboratory system of the proton. As the struck quark passes by the two "spectator" quarks it picks them up, in turn, and the three quarks begin their journey in a point-like configuration, of size $|\Delta\vec{x}| \sim 1/Q$, which later expands to the normal size of a physical proton.

Now consider the quasi-elastic reaction $\gamma(q) + A \rightarrow P' + (A-1)*$ where P' is the momentum of the ejected proton and (A-1)* is a nucleus in some (possibly) excited state. According to our previous discussion the ejected proton begins moving through the nucleus A in a point-like configuration which then should have a small

cross section with nucleons in the nucleus. This is the idea of color transparency. It is necesssary, however, that the ejected proton have a large momentum otherwise the point-like configuration will rapidly expand to a normal proton's size and begin to strongly interact in the nucleus. In quasi-elastic scattering the outgoing proton's momentum is determinedly Q^2, and it is difficult to go to large enough Q^2 so that the resulting Lorentz time dilatation factor be sufficient to insure a point-like configuration passes through a nucleus.

At SLAC in NE18, with $Q^2 \leq 7GeV^2$, the color transparency signal is weak. This is likely due to an insufficient Lorentz factor. There has been a significant effect seen in diffractive ρ production at Fermilab at comparable Q^2, but with a much larger Lorentz factor.

It has recently been sugested[5] that a good way to search for color transparency at intermediate values of Q^2 is to look for double scattering events in a small nucleus. Small nuclei, like helium, are needed in order that a large Lorentz factor not be necessary. One looks for an ejected proton and a recoiling proton coming from final state interaction with the ejected proton. If point-like configurations interact weakly then one should find a suppressed cross section for the final state interaction. Thus, the reaction proceeds in two stages. $\gamma(Q) + P_1 \rightarrow P_1''$ followed by $P_1'' + P_2 P_1' + P_2'$. P_1 and P_2 are protons in a small nucleus. P_1'' is the point-like configuration produced after the virtual photon is absorbed. One measures a highly energetic proton P_1' and a slower recoil proton P_2'. The signal for color transparency is a reduced cross section for $P_1'' + P_2 \rightarrow P_1' + P_2'$. Preliminary studies[5] show that there is likely a reasonable signal at CEBAF.

4. Quark Jets in Nuclear Matter

There are at least two separate types of studies that could be done at CEBAF, especially a CEBAF having 10 GeV electrons. The first concerns the energy loss of a bare quark traversing nuclear matter, while the second deals with the formation time of hadrons in a quark jet.

Consider a deep inelastic scattering event in a nucleus, A. Look at the highest momentum particle produced, the leading particle. Call z the momentum fraction of the virtual photon's momentum that the leading particle carries. If the nucleus A is not too large the leading particle will be formed outside the nucleus as a fragment of the struck quark. If one now varies the nuclear size, A, for a fixed incident virtual photon momentum, q, the spectrum, in z, will vary. On expects the spectrum to soften as A increases due to additional energy loss of the struck quark in larger nuclei. This is a difficult experiment to do at Fermilab where the change in the z spectrum is expected to be very small due to the high energy of the struck quark. It is likely that the z-spectrum of the leading particle will be reasonably strongly modified at CEBAF energies.

In order to determine the time of formation of hadrons in a quark, jet again measures the spectrum of the leading particle. Now, for fixed A, begin at large values of the photon momentum, q, and take measurements as q is lowered. One would expect a fairly sharp cutoff on the upper part of the z-spectrum when q is

lowered to the point that the leading particle begins to be formed in the nuclear medium. the medium should strongly inhibit particle formation. In this way, it may be possible to determine the time of formation of a hadron in a quark jet. Of course, the fact that the quark can be struck by the virtual photon anywhere in the nucleus, and thus that the struck quark does not travel a fixed length before exiting the nucleus, means that one will need to make numerical studies in order to extract the physics of the formtion time of hadrons.

5. J/ψ AND ψ' Cross Sections

Consider the reaction $\gamma(q)+P \rightarrow J/\psi+P'$ where P is a proton in a nucleus, A. The threshold for J/ψ production is $q \approx 8.2$ GeV and at such an incident momentum the J/ψ is formed in a distance smaller than a fermi. Define A_{eff} by

$$\frac{A_{eff}}{A} = \frac{\sigma_{\gamma+A\rightarrow J/\psi+\cdots}}{\sigma_{\gamma+P\rightarrow J/\psi+\cdots}} \tag{5}$$

for measured cross sections. Of course corrections for fermi motion in the nucleus will need to be made in order to refer the nucleon and nuclear cross sections to the same momentum. Theoretically, A_{eff} should be given by

$$A_{eff} = \int_0^R 2\pi b db \int_{-\sqrt{R^2-b^2}}^{\sqrt{R^2-b^2}} n(\underline{b},z) dz e^{-\sigma_{J/\psi}\int_z^{\sqrt{R^2-b^2}} dz' n(\underline{b},z')} \tag{6}$$

where n is the number density of nucleons in the nucleus. Comparing data giving (5) with (6) determines $\sigma_{J/\psi}$ the J/ψ-nucleon cross section. Although $\sigma_{J/\psi}$ has been previously determined at SLAC[6] it would be nice to have another measurement at the somewhat lower CEBAF energies.

When the incident photon energy reaches about 10.8 GeV ψ' production begins, $\gamma(q)+P \rightarrow \psi'+P'$. One expects $\sigma_{\psi'} \approx 4\sigma_{J/\psi}$ because the radius of the ψ' is about twice that of the J/ψ. However, the measurement of $\sigma_{\psi'}$ is subtle because ψ' can be produced in a two-step process $\gamma+P_1 \rightarrow \psi+P_1'$ followed by $\psi+P_2 \rightarrow \psi'+P_2'$ due to a scattering of a ψ off another nucleon in the nucleus. Indeed, this two-step process will likely dominate the ψ' production cross section. As Strikman[7] has pointed out one can eliminate the two-step process by looking only at those ψ' particles with very small transverse momentum. A ψ' which is directly produced at threshold will have very small transverse momentum. At ψ' produced in a two-step process should have $k_\perp'$ on the order of hundreds of MeV. It is important to do a real calculation, including fermi motion effects to see if one really can eliminate the two-step process. If so, a measurement of the ψ' cross section with nucleons might be possible, and would be very interesting, at an upgraded CEBAF.

References

1. W. Busza and A.S. Goldhaber, Phys.Lett.**139B** (235) 1984.
2. M. Gyulassy and X. Wang, Nucl. Phys. (to be published).

3. S.J. Brodsky and P.Hoyer, Phys. Lett.**B298** (1993) 165.
4. This is similar to a mechanism recently discussed by C. Benesh, J. Qiu and J. Vary, ISU-NP-93-15, for J/ψ suppression.
5. K. Egiyan, L. Frankfurt,W. Greenberg, G. Miller, M.. Sargsyan and M. Strikman, Nucl. Phys. A (to be published).
6. J.G. Branson et al., Phys. Rev.Lett. **38** (1977) 1334.
7. M. Strikman, in talk given at CEBAF retreat, May 1993.

MEASURING SPIN-DEPENDENT STRUCTURE FUNCTIONS AT CEBAF

ANDREAS SCHÄFER
Institut für Theoretische Physik, Universität Frankfurt a.M.
D-60054 Frankfurt, Germany

ABSTRACT

We analyse whether CEBAF with a 10 GeV beam could contribute significantly to the understanding of spin-dependent deep-inelastic scattering as well as semi-inclusive reactions. The main advantage of CEBAF is the much better attainable statistics, its great disadvantage its comparably low energy, which limits the accessible x-range to about 0.15 to 0.7. Within these constraints CEBAF could provide
1.) high precision data which would be very valuable to understand the Q^2 dependence of the spin-dependent structure functions $g_1(x)$ and $g_2(x)$ and
2.) the by far most precise determination of the third moments of $g_1(x)$ and $g_2(x)$ the latter of which we argue to be related to a fundamental property of the nucleon.

1. Introduction

The analysis of spin-dependent deep-inelastic scattering is presently one of the most active fields in hadron physics. In addition to the data on deep inelastic scattering [1,2,3] there is also a wealth of data available on spin-effects in semi-inclusive reactions like e.g. pion production[4]. Presently it looks as if theory would slowly succeed in finding close connections between these phenomena such that an even wider field of activities in hadron spin physics can be anticipated for the future. It is generally realized that these experiments offer the opportunity to study fundamental properties of QCD unaccessible by other means. This situation is illustrated by the fact that nearly all the major high-energy laboratories are either already active in this field or plan to do so in the near future. The question we have to focus on is therefore: Suppose that CEBAF could start polarized experiments e.g by the year 1998 with a 10 GeV beam, could it obtain any result which is of fundamental interest and not attainable at any other laboratory?

The perhaps most important aspect of this question is the kinematical one. In deep inelastic scattering (DIS) one sums over all final hadronic states, such that the probability for the reaction can only depend on the outgoing electron momentum. Due to the cylindrical symmetry of the process the cross section depends thus only on the final electron energy E' and the scattering angle θ, see Fig.1. These two observables are usually reexpressed in terms of the two Lorentz-invariants $Q^2 = 4EE'\sin^2\theta$ and $\nu = M(E - E')$ where E is the initial electron energy in the nucleon rest system. The ratio of these quantities is the Bjorken scaling variable $x = Q^2/2\nu$ which can be identified in the naive parton model as the energy fraction carried by the struck quark in the Breit frame, i.e. in a frame where both the electron and the nucleon move fast towards one another. Now, our aim is to test QCD in a situation which

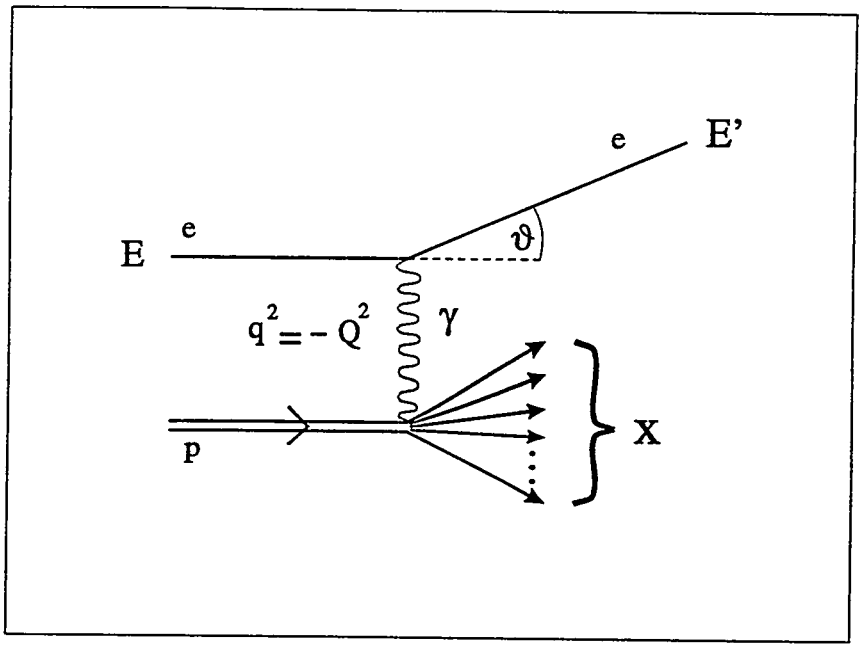


Fig. 1. Schematic view of deep inelastic scattering

can be described by theory. This requires a sufficently large value of Q^2, at least $Q^2 \geq 1\text{GeV}^2$. (Let us not that this is a necessary requirement also for the higher twist effects to be discussed later.) Also one has to avoid the kinematic region in which individual resonances play a dominant role, as one cannot treat these reliably within the framework of QCD. From experience one knows that this requires at least to impose that the nucleon is excited by more than 1 GeV, i.e. the final state mass $W^2 = (P_N + q)^2 = M_N^2 + 2\nu - Q^2 \geq 4$ GeV^2. Finally, in order to keep the corrections under control also the fractional energy loss $y = (E - E')/E$ cannot be too large, usually one requires $y \leq 0.85$. These various requirements are combined in Fig.2 for the envisaged CEBAF energy of 10 GeV. The kinematic area which can at all be used for the study of structure functions is the triangle in the center. Actually this area will still be reduced somewhat further by the acceptance limits of the spectrometer. From this figure it is obvious that only the x-region between 0.15 and 0.7 would be accessible at CEBAF. The question is thus whether the structure functions in this region are of any special interest. We shall argue that they are indeed. To do so we shall proceed in three steps. In section 2 we shall review the definition of $g_1(x)$ and $g_2(x)$ as well as the status of the Bjorken and Ellis-Jaffe sum rules especially the question of Q^2-dependence. In section 3 we shall review the main ideas of operator product expansion and the classification according to twist. In section 4 we argue that the twist three part of the third moment of $g_2(x)$ has a particularly clear and intuitive interpretation which makes it very worthwhile to measure this quantity at CEBAF.

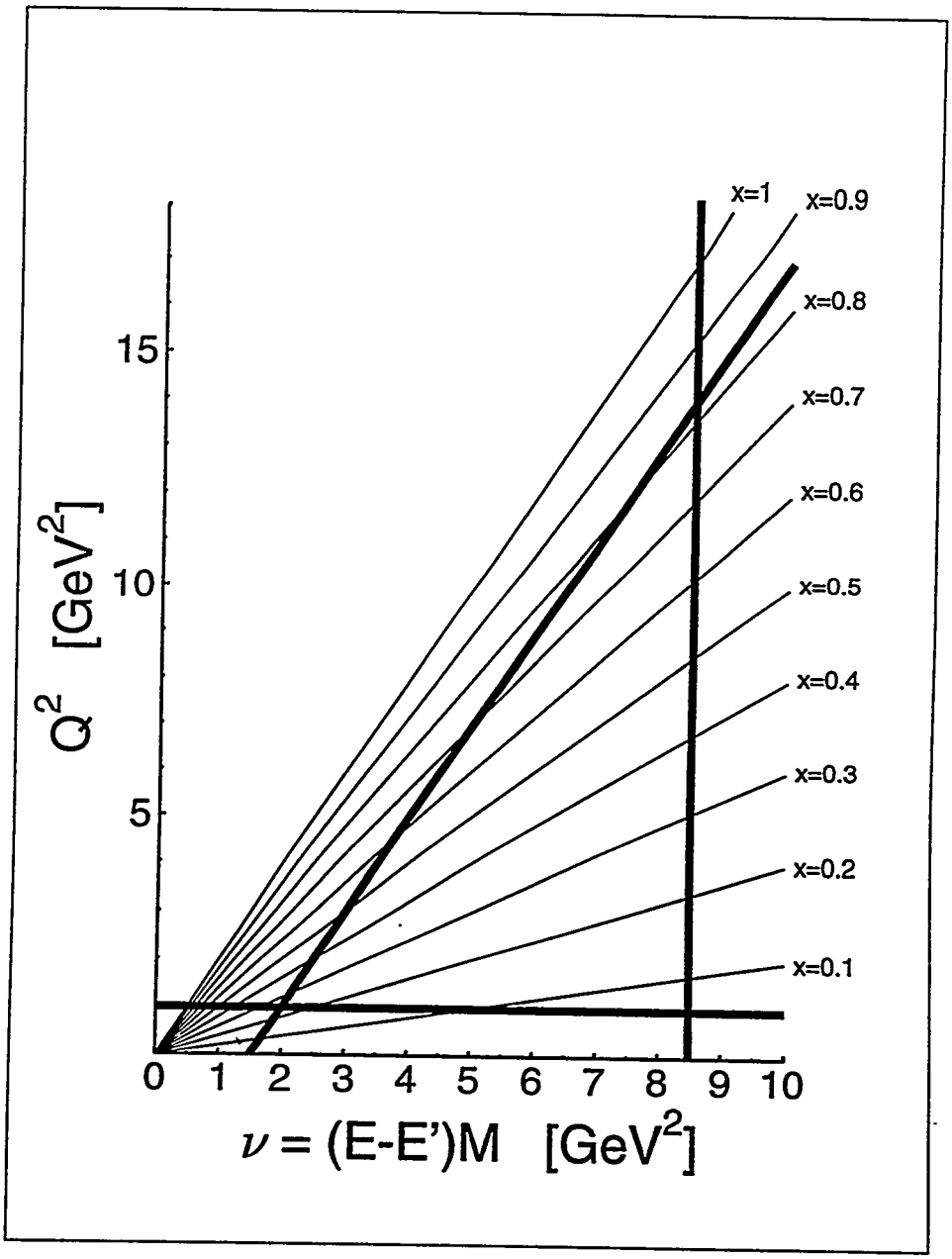


Fig. 2. Kinematic range for a CEBAF experiment at 10 GeV. The light lines correspond to fixed Bjorken x. The three cuts are on fractional energy loss ($y \leq 0.85$), virtuality ($Q^2 \geq 1$ GeV^2) and the total energy of the final hadronic state ($W \geq 2$GeV. Only the central triangle is accecible for experiments. Outside of the central triangle theory is not under control, i.e. the higher order corrections are large and not calculable. This implies also that these corrections, while probably still calculable, are large close to the boundaries, especially close to Q^2=1 GeV^2.

2. The polarized structure functions and their sum rules

The differential cross-section for polarized deep inelastic scattering is usually written in the form

$$\frac{\mathrm{d}^2\sigma}{\mathrm{d}E'\mathrm{d}\Omega} = \frac{E'\alpha^2}{EQ^2} L_{\mu\nu} W^{\mu\nu} \tag{1}$$

$$L_{\mu\nu} = 2(p_\mu p'_\nu + p_\nu p'_\mu - g_{\mu\nu} p \cdot p' + m^2 g_{\mu\nu}) - 2\mathrm{i}\epsilon_{\mu\nu\alpha\beta} q^\alpha s^\beta m \tag{2}$$

$$\begin{aligned} W_{\mu\nu} &= -\left(g_{\mu\nu} - \tfrac{q_\mu q_\nu}{q^2}\right) \tfrac{1}{M} F_1(x,Q^2) + \tfrac{1}{P\cdot q M^2}\left(P_\mu - \tfrac{q\cdot P}{q^2} q_\mu\right)\left(P_\nu - \tfrac{q\cdot P}{q^2} q_\nu\right) F_2(x,Q^2) \\ &+ \tfrac{\mathrm{i}}{P\cdot q}\epsilon_{\mu\nu\alpha\beta} q^\alpha S^\beta g_1(x,Q^2) + \tfrac{\mathrm{i}}{(P\cdot q)^2}\epsilon_{\mu\nu\alpha\beta} q^\alpha (P\cdot q S^\beta - S\cdot q P^\beta) g_2(x,Q^2) \end{aligned} \tag{3}$$

Here M is the nucleon mass, m the lepton mass, P_μ the nucleon momentum p_μ and p'_μ the initial and final lepton momentum, s_μ the electron spin, S_μ the nucleon spin, and q_μ, $q^2 = -Q^2$ the transfered photon momentum. Eq.(3) is the most general Lorentz-structure which conserves the charge current. The spin vectors of e.g. the lepton for transverse polarization take the form $s_\mu = (0,0,1,0)$ and (0,1,0,0) and for longitudinal polarization $s_\mu = \pm(p,0,0,E)/m$.
From Eq.(2) it is obvious that spin effects are supressed by a factors m unless the lepton spin vector provides a factor $1/m$. Therefore on has to use longitudinally polarized leptons. For the nucleon the situation is different. By comparing Eqs.(3) and (2) it is clear that g_1 parametrizes a contribution which arises already for point-like Dirac particles. Therefore it has a simple interpretation in the parton model, namely

$$g_1(x,Q^2) = \frac{1}{2}\sum_i Q_i^2 (q_i^\uparrow(x,Q^2) - q_i^\downarrow(x,Q^2)) \qquad , \qquad i = \mathrm{u}, \bar{\mathrm{u}}, \mathrm{d}, \bar{\mathrm{d}}, \ldots \tag{4}$$

where $q_i^\downarrow(x,Q^2)$ is the probability to hit a quark of flavour i which carries the momentum fraction x and which is polarized along the direction of the nucleon spin, if the latter is probed with a photon of virtuality Q^2. In contrast g_2 has no analogon in Eq.(2) and therefore no simple partonic interpretation. In the absence of interaction it is zero and thus it is most sensitive to the QCD interaction. In the following we shall make this statement more precise. We shall show how to interpret the information contained in g_2 and we shall argue that CEBAF at 10 GeV might be the best place to extract it.
A large literature exists on g_2, we just cite a few relevant papers [5,6,7].

While experiments actually measure $g_1^p(x,Q^2)$ and $g_1^n(x,Q^2)$ in some limited range of x and Q^2, theory can only make clear statements about the odd moments of the structure functions. (We use the convention that the n-th moment has the weight x^{n-1}. Unluckily the definitions used in the literature are not unique.) In view of the statistical accuracy attainable even in optimistically planned experiments this reduces

to just eight numbers

$$\begin{aligned} \int_0^1 g_1^p(x,Q^2)\mathrm{d}x \quad &, \quad \int_0^1 g_1^n(x,Q^2)\mathrm{d}x \\ \int_0^1 x^2 g_1^p(x,Q^2)\mathrm{d}x \quad &, \quad \int_0^1 x^2 g_1^n(x,Q^2)\mathrm{d}x \\ \int_0^1 g_2^p(x,Q^2)\mathrm{d}x \quad &, \quad \int_0^1 g_2^n(x,Q^2)\mathrm{d}x \\ \int_0^1 x^2 g_2^p(x,Q^2)\mathrm{d}x \quad &, \quad \int_0^1 x^2 g_2^n(x,Q^2)\mathrm{d}x \end{aligned} \tag{5}$$

QCD makes firm predictions about the first moments only. The difference of the first two integrals is given by the Bjorken sum rule, which reads with all Q^2 dependent corrections calculated so far

$$\begin{aligned} \int_0^1 (g_1^p(x,Q^2) - g_1^n(x,Q^2))\mathrm{d}x = \frac{g_A}{6g_V}\left[1 - \frac{\alpha}{\pi} - 3.6\left(\frac{\alpha}{\pi}\right)^2 - 20.2\left(\frac{\alpha}{\pi}\right)^3 + ...\right] \\ + \frac{M^2}{9Q^2}(a_2^p + 4d_2^p + 4f_2^p - a_2^n - 4d_2^n - 4f_2^n) + O(M^4/Q^4) \end{aligned} \tag{6}$$

This equation shows two types of corrections, the radiative ones, which come as powers of α/π and the higher twist corrections which are parametrized by a_2, d_2, and f_2. We shall focuss on the latter. The derivation of this result can be found in the paper by Larin and Vermaseren[10] for the radiative corrections and for example in Ehrnsperger et al.[11] or Ji and Unrau[12]. The numerical value of d_2^p and d_2^n was calculated by Balitsky, Braun and Kolesnichenko[13] with the QCD sum rule method. Equ.(6) was used by a number of people to obtain fits to the CERN and SLAC data for g_1^p and g_1^n[14,15,16]. The Bjorken sum rule is a rock-solid prediction of QCD and hardly anybody seriously doubts its correctness. The problem with it is, however, that the Q^2 corrections are sizeable. At present data from CERN and SLAC is available. While the former has a limited statistics the latter is taken down to very small Q^2 of order 1 GeV^2, such that the effects of Q^2 are presently not really under control. Thus the present data are compatible with the Bjorken sum rule, but do not yet constitute a precise test. Such a test will require better data on the Q^2 dependence of the spin structure functions. Thus CEBAF which could provide very precise data on the Q^2 dependence of g_1 and g_2 for $x \geq 0.15$ would also help indirectly to test Bjorken sum rule.

Let us comment at this point on the fundamental difference in Q^2 evolution between polarized and unpolarized deep inelastic scattering. In the unpolarized case the Q^2 dependence is dominated by a factor of the form

$$\left[\ln\left(\frac{Q^2}{Q_0^2}\right)\right]^{-d_i/b} \quad , \quad b = \frac{11 - \frac{2}{3}N_f}{16\pi^2} \tag{7}$$

where d_i is the anomalous dimension of the moment of interest. For the moments of polarized structure functions the anomalous-dimensions are zero. Therefore the Q^2-dependence is much milder and one can hope to treat it reliably down to values of Q^2 as small as 1 GeV^2. This difference has a simple physical origin. If Q^2 is increased more and more quark-antiquark pairs from the sea are resolved and it is the large number of additional quarks which dominates the change in the unpolarized structure functions. These quarks are generated through the coupling to gluons which are vector particles. As the vector coupling γ_μ is helicity conserving they are predominantly unpolarized, at least for not too small values of x. The anomalous dimensions are actually calculated for vanishing quark mass, such that generated sea-quarks are completely unpolarized. Consequently these quarks do not contribute to the polarized structure functions and the only effect of QCD-evolution is that the polarized distributions get softer, because some energy is transferred to the generated quarks. This fact is also contained in the polarized form of the Gribov-Lipatov-Altarelli-Parisi equations. These look in fact very similar to the unpolarized ones except for a slight change in the splitting functions. The splitting function $P_{qG}(z)$ which give the probability that a polarized respectively unpolarized gluon of momentum fraction x splits up in a quark of momentum fraction zx and an antiquark of momentum fraction $(1-z)x$ for the unpolarized case is simply

$$P_{qG}(z) = \frac{1}{2}[z^2 + (1-z)^2] \tag{8}$$

and for the polarized one

$$\Delta P_{qG}(z) = \frac{1}{2}[z^2 - (1-z)^2] \tag{9}$$

The total change in quark number is therefore for the unpolarized case proportional to

$$\int_0^1 \mathrm{d}z P_{qG}(z) = \frac{1}{3} \neq 0 \tag{10}$$

but

$$\int_0^1 \mathrm{d}z \Delta P_{qG}(z) = 0 \tag{11}$$

for the polarized case. Thus the corresponding anomalous dimension is non-zero for the former and zero for the latter.

QCD allows also to make a rather firm statement that the first moments of g_2 should vanish. This statement is called Burkhardt-Cottingham sum rule. The arguments are somewhat technical and not absolutely stringent but still this sum rule has an very high probability to be correct[5,6,7]. There is a recent claim that it should be already violated by perturbative corrections[8], which, however, is extremely hard to believe as the theoretical arguments for the Burkhardt-Cottingham sum rule seem to leave only a loophole for very special genuinely non-perturbative effects. (A recent paper actually claims that the calculation by Mertig and van Neerven was erroneous[9]).

Thus there is only one independent first moment left, which is usually chosen to be that of g_1^p. For it there exists also a prediction which, however, is only partially based on QCD. This prediction, the Ellis-Jaffe sum rule, is based on the assumption that the total spin carried by strange and anti-strange quarks is negligible. In addition it uses flavour SU(3) symmetry including the strange sector which is not of undisputable reliability. The present-day form of this sum rule reads

$$\int_0^1 g_1^p(x,Q^2)\mathrm{d}x = \frac{g_A}{18g_V}\frac{9(F/D)-1}{(F/D)+1}\left[1-\frac{\alpha}{\pi}+...\right] + \frac{M^2}{9M^2}(a_2^p+4d_2^p+4f_2^p)+O(m^4/Q^4) \tag{12}$$

where $F/D = 0.58$ with a hotly debated error. As the Ellis-Jaffe sum rule is not a real QCD prediction it should be rather interpreted as a measure of the strange quark polarization. If its experimental value differs from Eq.(13) this indicates a non-negligible polarization of the strange sea. The present experimental situation is not settled because due to our lack of understanding of the Q^2 dependence it is unclear how the SLAC and CERN data should be compared. One should probably interpret the CERN data as suggestion of a discrepancy with statistical and theoretical uncertainties as well as the complementary data from SLAC combining to an overall uncertainty of the size of the discrepancy. In other words I think that the experimental situation is still inconclusive.

Let us turn next to the third moments. This is the natural domain for polarized CEBAF physics. Due to the weight x^2 the third moments are practically saturated by the contributions for $0.15 \leq x \leq 0.7$. Thus the unrivaled luminosity predicted for a CEBAF spin-experiment should lead to a very precise determination of the third moments.

$$\int_0^1 x^2 g_1^p(x,Q^2)\mathrm{d}x = \frac{1}{2}a_2 + O(M^2/Q^2) \tag{13}$$

gives information about the momentum distribution of the polarized quarks. Its value will determine how the spin is split up between the valence quarks and the sea quarks. If valence quarks carry a large fraction of the spin, as naively expected, it will be large. If instead a large fraction of the spin is carried by the gluons or the sea-quarks than it will be significantly smaller. Thus the third moments of g_1^p and g_1^n are very interesting in their own right. In addition a_2 enters the Bjorken and Ellis-Jaffe sum rule, such that its knowledge is needed to test these sum rules accurately.

While the interpretation of the third moment of g_1 is intuitively clear this is not the case for the third moment of g_2. In the following I shall present our interpretation of it. I shall argue that it is in fact one of the most interesting quantities and that its knowledge would have far reaching implications for the interpretation of other spin-effects in hadron physics. Also let me repeat that CEBAF might be the best place to measure it accurately enough. From the operator product expansion (OPE)

one learns that

$$\int_0^1 x^2 g_2^p(x,Q^2)\mathrm{d}x = -\frac{1}{3}a_2^p + \frac{1}{3}d_2^p + O(M^2/Q^2) \tag{14}$$

where a_2 is determined by the third moment of g_1. Thus the new information is contained in d_2 which is a twist-three contribution. The unique feature of Eq.(14) is that this contribution is not suppressed by a factor of M/Q with respect to the twist 2 contribution a_2. Thus polarized deep-inelastic scattering might determine it with rather high accuracy. To explain the significance of d_2 let us review the basic ideas of OPE. This will also clarify how the equations discussed in this section are derived.

3. Operator product expansion and the definition of twist

In this section the basic concepts of OPE will be reviewed and the correlators defining d_2 and f_2 shall be presented. For simplicity we start with the unpolaized case, for which the hadronic scattering tensor can be written

$$\begin{aligned} W_{\mu\nu} &= \frac{1}{2\pi}\int \mathrm{d}^4x \mathrm{e}^{\mathrm{i}q\cdot x}\frac{1}{2}\sum_{\mathrm{pol}}\langle N|J_\mu(x)J_\nu(x)|N\rangle \\ &= \frac{1}{2\pi}\int \mathrm{d}^4x \mathrm{e}^{\mathrm{i}q\cdot x}\frac{1}{2}\sum_{\mathrm{pol}}\langle N|[J_\mu(x),J_\nu(x)]|N\rangle \end{aligned} \tag{15}$$

The term subtracted in the second line is equal to zero due to energy conservation because the nucleon is the lightest spin-1/2 baryon. (It would contribute for $E_X = E_N - q^0$ while the first contributes for $E_X = E_N + q^0$.) Next one inserts the quark currents for J_μ and uses

$$\begin{aligned} [J_\mu(x),J_\nu(x)] &= [\bar\psi(x)\gamma_\mu\psi(x),\bar\psi(0)\gamma_\nu\psi(0)] \\ &= \bar\psi(x)\gamma_\mu\psi(x),\bar\psi(0)\gamma_\nu\psi(0) - \bar\psi(0)\gamma_\nu\psi(0),\bar\psi(x)\gamma_\mu\psi(x) \\ &= \bar\psi(x)\gamma_\mu S(x)\gamma_\nu\psi(0) - \bar\psi(0)\gamma_\nu S(-x)\gamma_\mu\psi(x) \end{aligned} \tag{16}$$

The crucial point is now that for large negative photon virtuality $q^2 = -Q^2$ only contributions with small x_μ are relevant. Therefore

$$S(x) = \gamma_\mu\partial^\mu\frac{\mathrm{sgn}(x_0)}{2\pi}\delta(x^2) \tag{17}$$

is a universal divergent function and all the information on the hadron from which one scatters is contained in the second factor, which is called correlator.

$$\begin{aligned} \langle N|J_\mu(x)J_\nu(x)|N\rangle = \partial^\lambda\frac{\mathrm{sgn}(x_0)}{2\pi}\delta(x^2) \\ \langle N|\bar\psi(x)\gamma_\mu\gamma_\lambda\gamma_\nu\psi(0) - \bar\psi(0)\gamma_\nu\gamma_\lambda\gamma_\mu\psi(x)|N\rangle \end{aligned} \tag{18}$$

The matrix elements of the correlators will in our case be characterized by a_0, a_2, d_2 and f_2. The next step is a Taylor expansion of the correlators in x_μ. This gives e.g. for the first one

$$\sum \frac{1}{n!} x^{\mu_1} x^{\mu_2} ... x^{\mu_n} \langle N|\bar{\psi}(0) D_{\mu_1} D_{\mu_2} ... D_{\mu_n} \gamma_\mu \gamma_\lambda \gamma_\nu \psi(0)|N\rangle \tag{19}$$

with the gauge invariant differentiations D_μ. The three γ matrices are now substituted by

$$\gamma_\mu \gamma_\lambda \gamma_\nu = g_{\mu\lambda}\gamma_\nu + g_{\nu\lambda}\gamma_\mu - g_{\mu\nu}\gamma_\lambda + i\epsilon_{\mu\lambda\nu\sigma}\gamma^\sigma\gamma_5 \tag{20}$$

such that for unpolarized scattering we have vector-currents and for polarized scattering (remember that this is the antisymmetric part, see Eqs.(2) and (3)) we have axialvector-currents. Thus the correlators are Lorentz-tensors of rank n+1. One can now write down all the various ways in which such a tensor can be constructed from P_μ and $G_{\mu\nu}$ (and S_μ for the polarized case. As x_μ is replaced by q_μ under Fourier-transformation it is then easy to decide which terms are dominant. One finds e.g.

$$\frac{q^{\mu_1} q^{\mu_2} ... q^{\mu_n} P_{\mu_1} P_{\mu_2} ... P_{\mu_n}}{q^{\mu_1} q^{\mu_2} ... q^{\mu_n} M^2 g_{\mu_1\mu_2} ... P_{\mu_n}} = \frac{(P\cdot q)^2}{M^2 Q^2} \gg 1 \tag{21}$$

Thus the leading term is the completely symmetric one and for every trace one gets a supression by Q^2. These terms can be classified by the spin to which the spin-1 vectors P_μ are coupled. The completely symmetric term corresponds to the maximal spin $n+1$ while every trace reduces it by two. Also the total number of derivatives can be expressed by the dimension of the correlator. As the quark fields themselves have energy-dimension 3/2 the total energy-dimension is $3+n$. One defines now

$$\text{twist} = \text{dimension} - \text{spin} = 3 + n - \text{spin} \tag{22}$$

Obviously the twist is 2 for the dominant term, 4 for one trace, 6 for two traces etc. and the higher twists are suppressed by a factor $1/Q^{\text{twist}-2}$. The twist-expansion is therefore a systematic expansion in inverse powers of Q^2. In this expansion each term is uniquely determined by its symmetry property. In our case d_2 is that contribution which involves three indices and the corresponding correlator must be antisymmetric in two of them. Because of $[D_\mu, D_\nu] = gG_{\mu\nu}$ the resulting expression turns out to be

$$\langle PS|\bar{\psi}(\gamma^\alpha g\tilde{G}^{\beta\sigma} + \gamma^\beta g\tilde{G}^{\alpha\sigma})\psi|PS\rangle - \text{traces} = \tag{23}$$
$$2d_2\left[\frac{1}{3}(2P^\alpha P^\beta S^\sigma - P^\alpha S^\beta P^\sigma - S^\alpha P^\beta P^\sigma) - \frac{M^2}{9}(2g^{\alpha\beta}S^\sigma - g^{\sigma\beta}S^\alpha - g^{\alpha\sigma}S^\beta)\right]$$

$$\langle PS|\bar{\psi}\gamma_\alpha g\tilde{G}^{\beta\alpha}\psi|PS\rangle = 2f_2 M^2 S^\beta \tag{24}$$

where the epsilon tensor was absorbed in the dual field strengths.

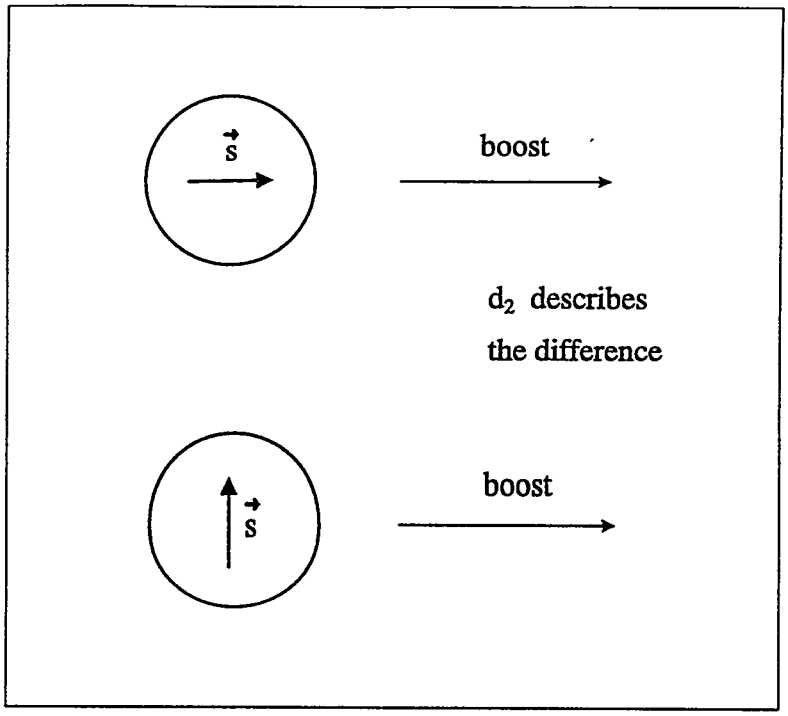


Fig. 3. An illustration of the physical meaning of g_2

4. The far reaching importance of d_2

Eq.(24) looks still rather involved, but it has a very simple meaning. First of all by analysing Eq.(1) to (3) one finds that g_2 describes the difference in the internal structure of nucleons boosted in the direction of its spin or perpendicular to it, see Fig.3. If there where no interaction these would be the same and $g_2(x) \equiv 0$, as e.g. in the naive parton model. For an interacting field theory the boost changes the particles content of the boosted state. (The boost operator is obtained from the Lagrangian and therefore contains creation and annihilation operators.) In fact g_2 gives only for transverse polarization a large contribution. For such a situation let us look at the dominant contribution which is proportional to $P^+P^+S^1$. Here $P^+ = P^0 + P^3$ is a lightcone coordinate. The correlator on the left-hand side of Eq.(24) reads then

$$\langle PS|\bar{\psi}\gamma^+ g\tilde{G}^{+1}\psi|PS\rangle = \langle PS|\bar{\psi}\gamma^0 g\tilde{G}^{01}\psi|PS\rangle + ... \qquad (25)$$

Thus one contribution to d_2 would be the QCD-analogon to a colour-magnetic field parallel to the spin direction of the nucleon. As both the spin and the colour-magnetic field are axialvectors one would them naturally expect to be connected, as is the case for the usual magnetic field coupling to the nucleon magnetic moments. For QCD the situation is, however, slightly more involved as the nucleon state is completely anti-symmetric with respect to colour. Thus the probability to observe a field of any colour is equal and they compensate one-another. In other words: The colour-magnetic field

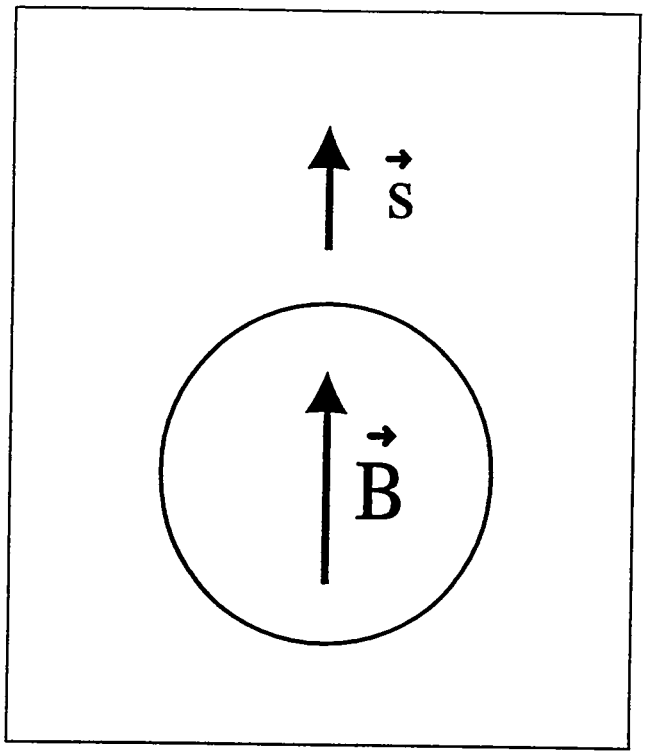


Fig. 4. An illustration of the physical meaning of d_2

is no singlet and therefore its expectation value must vanish. The structure $\psi^\dagger B^1 \psi$, however, is a colour-singlet and therefore it is most natural that it appears, describing the collective gluon fields inside of the nucleon, correlated with the spin direction.

If this interpretation were correct one would expect d_2 to play a role in many different spin effects and this is indeed the case. To demonstrate this point let us shortly discuss a completely different process, namely the single spin asymmetry of photons produced in the collision of an unpolarized proton with a transversely polarized proton, see Fig. 5. As was analysed by Qiu and Sterman [17,19] the leading contribution should come from the interference of the two graphs in Fig. 6. The interference term involves the product of the two graphs in Fig.6. Then for the upper nucleon one gets one factor which is the nucleon correlator of two quark fields and one gluon-field. Any angular asymmetry must be due to the antisymmetric part of the interference matrix element. The antisymmetrisation provides the ϵ-tensor which changes the gluonic field strength into the dual field strength. Qiu and Sterman showed the final result to be proportional to

$$\langle PS|\bar{\psi}(0)\gamma^+ g \int \tilde{G}^{+1}(y^-)\mathrm{d}y^-\psi(0)|PS\rangle = f\langle PS|\bar{\psi}(0)\gamma^+ g\tilde{G}^{+1}(0)\psi(0)|PS\rangle = f\ d_2 \tag{26}$$

where we introduced a constant of proportionality f which depends on how fast the correlation decays with y^-. Usually one assumes for such correlations a Gaussian like

$\exp((y^-)^2/L^2)$ with a correlation length of order 0.2-0.3 fm, which would result in $f = \sqrt{\pi}L$. While the precise value of f is clearly model dependent, Eq.26 illustrates that d_2 is a fundamental quantity for hadron-spin-effects.
Let us note that one can analyse gluon-gluon fusion along the same lines. Then the quark line has to be substituted by another gluon line and the resulting correlator will be a three gluon correlator. That such a term should exist is relatively clear as on can couple three gluons to a colour singlet[?]. This side remark is just ment to illustrate the fact that all the hard hadronic spin effects can be related to just a few characteristic correlators.
One should note, however, that there there do also exist large spin effects which are due to a correlation of spin direction and transverse momentum for quarks being profuced during string breaking. Such effects are not described by simple correlators, as the process involved is not hard but genuinely non-perturbative, and they are generally poorly understood. Even electromagnetic probes like photon production are influenced by these effects, mainly through the decay of asymmetrically produced π^0's. It is, however, possible to seperate the two processes by suitably choosing kinematical constraints.

The great sensitivity of d_2 on the real nature of the QCD interaction is further illustrated by the fact that the two existing predictions derived within the MIT-bag model respectively with QCD sum rules differ drastically in their predictions. QCD sum rules predict $|d_2^n/d_2^p| > 1$ and $d_2^p < 0$ while the bag model without additional features predicts $d_2^n \equiv 0$ and $d_2^p > 0$. Thus, whatever d_2 might turn out to be, it will show that at least one of these models does not describe the spin-sector correctly. As the calculation of structure functions from the bag model requires several assumption which are hard to justify we felt it more worthwhile to try to check and improve the QCD sum rule result.

5. QCD sum rule results for d_2

We do not want to give a self-contained review of QCD sum rules. Such a review was given e.g. by Reinders , Rubinstein and Yazaki[20]. Instead we want to discuss some points which are crucial for d_2.
QCD sum rules are based on the principle of duality. If it is possible to define a region in which both the purely hadronic description as well as a description by a modified form of perturbative QCD converge, then one can extract hadronic properties from the QCD calculation. The modification of perturbative QCD lies in the fact that one introduces condensates to parametrize the genuine non-perturbative effects. Without going into any detail let us just describe in which steps a typical sum rule calculation proceeds. The conceptually easiest case are QCD sum rule calculations for some hadronic mass:
1.) To start one has to construct a quark current with the correct quantum numbers (spin, isospin, parity etc.). For the nucleon the standard choice is the so called Ioffe

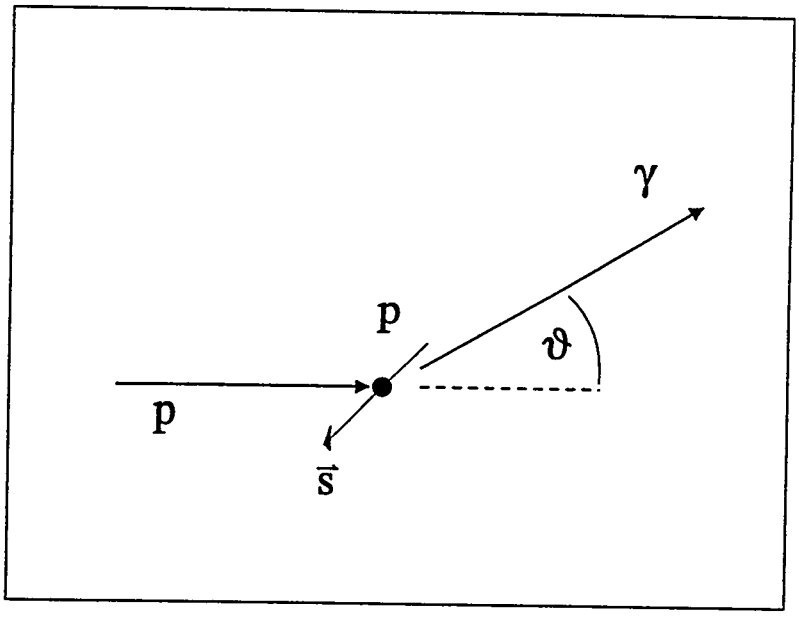


Fig. 5. Single transverse spin asymmetry in direct photon production for proton on proton.

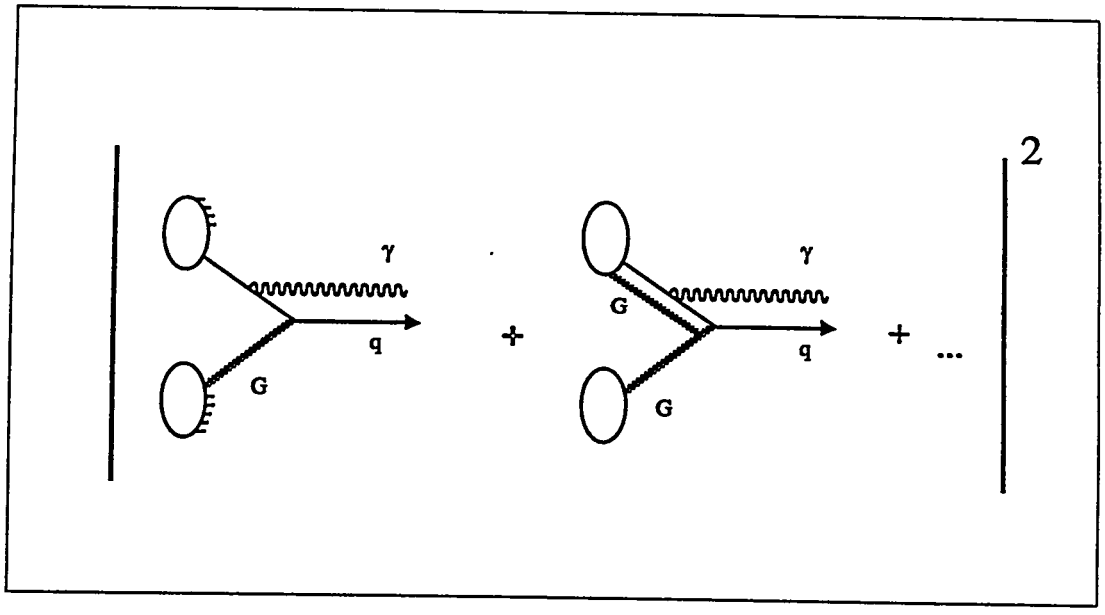


Fig. 6. The two interfering graphs dominantly contributing to the single spin asymmetry

current

$$\eta_N(x) = \epsilon_{abc}\left(u^{at}(x)\gamma_0\gamma_2\gamma_\mu u^b(x)\right)\gamma_5\gamma^\mu d^c(x) \tag{27}$$

which was also used by Balitsky, Braun and Kolesnichenko in their calculation for d_2.
2.) Next, one has to calculate the correlator of interest. If one is interested in a prediction for some hadronic mass this is simply the quadratic current correlator

$$\int \mathrm{d}^4x \mathrm{e}^{\mathrm{i}P\cdot x}\langle 0|T\{\bar{\eta}_N(x)\eta_N(0)\}|0\rangle \tag{28}$$

where P_μ will correspond to the nucleon momentum. For the case of d_2 the situation is conceptually much more difficult. Here the corresponding correlator is

$$\sum_q \int \mathrm{d}^4x\mathrm{d}^4y \mathrm{e}^{\mathrm{i}P\cdot x+\mathrm{i}q\cdot y}\langle 0|T\{\eta_N(x)\ \left[\bar{q}(y)(\gamma^\alpha g\tilde{G}^{\beta\sigma}(y)+\gamma^\beta g\tilde{G}^{\alpha\sigma}(y))q(y)-\text{traces}\right]\eta_N(0)|0\rangle \tag{29}$$

where q runs over all quark flavours. We shall comment on the problems encountered for these so called three-point functions below.
3.) One calculates the correlators using the usual perturbative Feynman-rules of QCD plus the fact that the fields can couple to any of the following condensates instead of propagating freely: $\langle\bar{q}q\rangle$, $\langle\bar{q}\sigma_{\mu\nu}G^{\mu\nu}q\rangle$, $\langle\tilde{G}_{\mu\nu}G^{\mu\nu}\rangle$, etc.. The values of these parameters are determined by a combined fit of all successfully performed sum rule calculations to the corresponding experimental data. Dozens of physical quantities have been calculated so far, specifying the relevant four or five condensates to high accuracy. As an example we show in Fig. 7 the graph which dominates the result of Balitsky, Braun and Koleshnichenko for d_2. The condensate in this case is $\langle\bar{q}q\rangle\langle\bar{q}\sigma_{\mu\nu}G^{\mu\nu}q\rangle$. Other examples can be seen in Fig. 9.

The result of this calculation on the quark level corresponds to a superposition of many different matrix elements between all possible states with the quantum numbers of the nucleon. Therefore a procedure is needed to extract the one matrix element diagonal in the lowest-lying state.
4.) This is achieved by the Borel-transformation

$$\int_0^{s_0} \mathrm{d}s\mathrm{e}^{-s/M^2}\mathrm{Im}(...)\Big|_{s=P^2} \tag{30}$$

where the ellipses stand for the correlator in question. s_0 is the continuum threshold for the combination of quantum numbers one is interested in and is thus, at least in principle an experimentally known quantity. M^2 is a free parameter. It can be used to check the quality of the obtained sum rule. For a good sum rule the result should be insensitive to M^2 if this varies e.g. between 1 and 2 GeV^2. If it is very dependent on M^2 than the result is unreliable. It is rather obvious how the Borel transformation works. The exponential factor suppresses all contributions with a large invariant mass $s = P^2$. This explains also why it is only possible to obtain the properties of the lowest-lying state for any given set of quantum numbers. For a three-point function

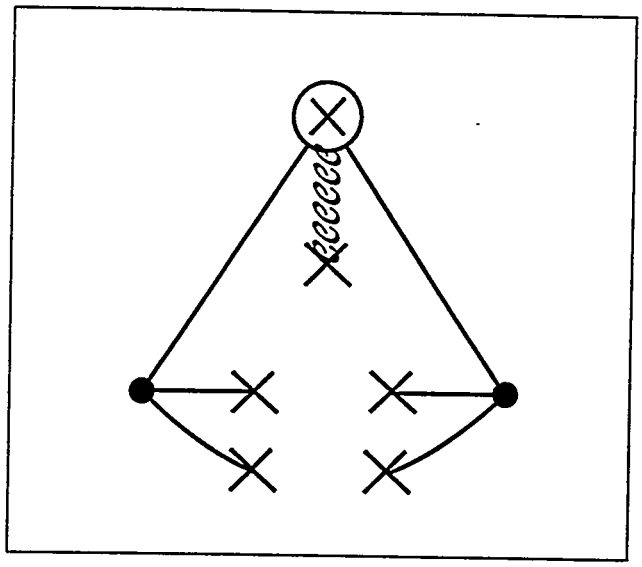


Fig. 7. A perturbative graph of great importance for the calculation of d_2

one has to perform a double Borel-transform, one with respect to $s = P^2$ and one with respect to $s' = (P+q)^2$ to ensure that both the incoming and the outgoing state are the physical nucleon.

While this program sounds rather straightforward there are two subtleties involved. First while one can show explicitely that for large Q^2 the relevant x_μ are small, i.e. one has a short-range correlator between $\bar{\eta}_N(x)$ and $\eta_N(0)$ such that perturbative QCD applies this is not true for y_μ. Therefore one has also to calculate the so called bilocal power corrections (BPC), which describe the large y_μ limit. One should then see that the ultraviolet divergences of the BPC cancel the infrared divergences of the perturbative calculation, demonstrating that the two regions are treated consistently. While this is a problem of great technical complexity it usually turns out to be numerically irrelevant. Quite often the BPC are therefore simply neglected, which is usually o.k., but which is not justified in principle. For d_2 a number of BPC were calculated and they in fact turned out to be small.
The second problem is more bothersome: To make calculations tractable one has to use a relavitely simple current like Eq.(27). This current has, however, additional symmetries, just due to the fact that it is so simple. In this case the two up quarks enter in a very symmetric way. The Borel transformation projects out the right mass eigenstates but does not change this symmetry. This leads to a problem if the symmetry properties of the current are not a symmetry properties of the real physical hadron. In the case of d_2 the following happens. For the Ioffe current the most important graph is that shown in Fig. 7, where the top-most quark line can be either a u or a d. It now happens that the contributions from the two u quarks cancel. The dominant contribution therefore is strongly isospin asymmetric leading to a strong isospin

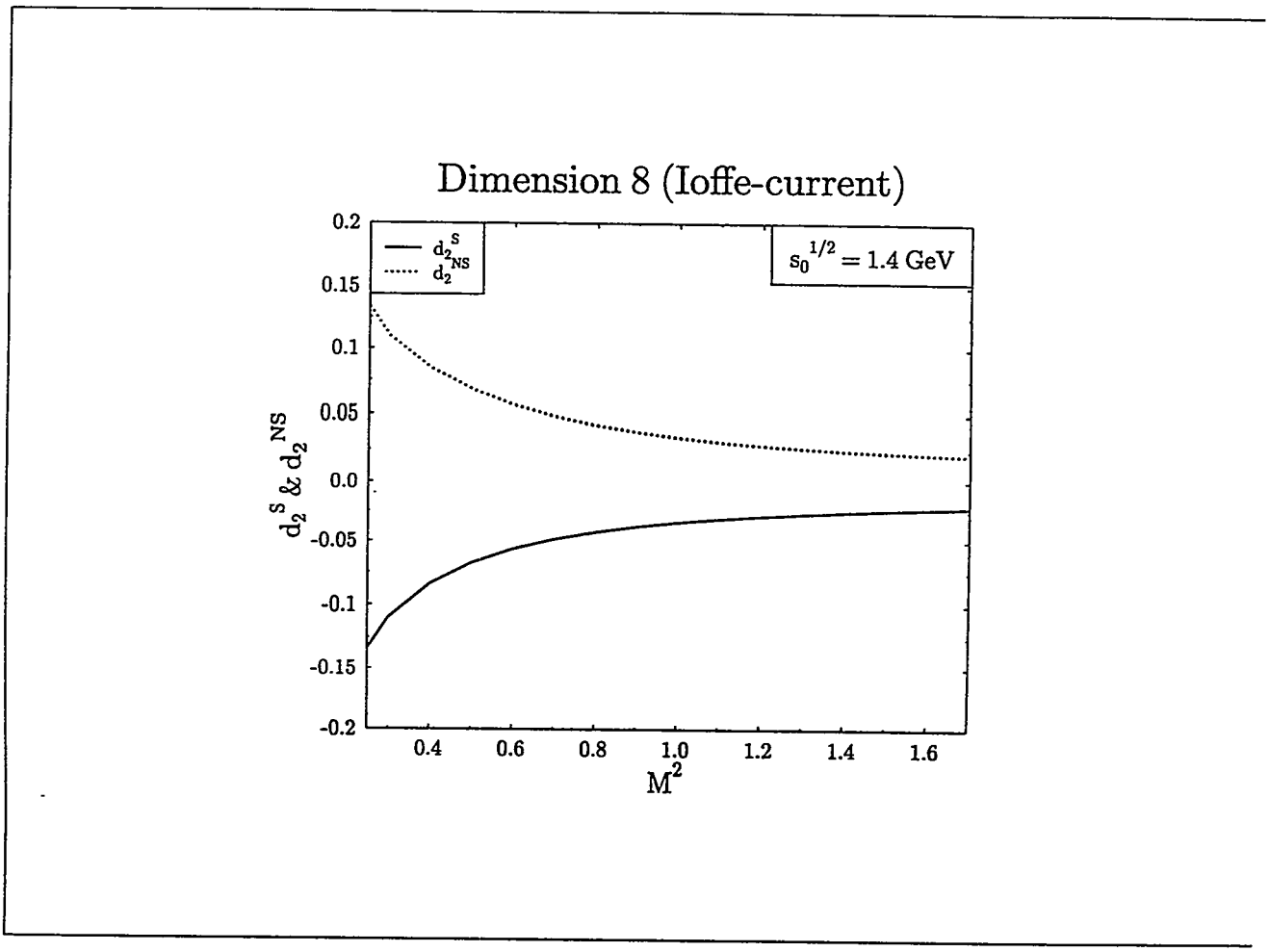


Fig. 8. The results for d_2 using the Ioffe current, without bilocal power corrections.

asymmetry in the predicted d_2. Without BPC corrections and the small corrections from the other graphs d_2^p would be zero. Due to these corrections one gets $d_2^n/d_2^p \approx 4$. This is also shown in Fig. (8) in which the singlet and non-singlet contribution

$$d_2^S = \frac{1}{2}(d_2^p + d_2^n) \qquad , \qquad d_2^{NS} = \frac{1}{2}(d_2^p - d_2^n) \tag{31}$$

are plotted.

The question is now whether this asymmetry is real or an artefact from the specific, simple form of the Ioffe current. Let us remind that according to our interpretation such an asymmetry would have far reaching consequences as it would imply e.g. a strong asymmetry in single-spin photon production. To answer this question we have repeated the calculation of d_2 with a more complex current

$$\eta'_N(x) = \frac{2}{3}\epsilon_{abc}\left(u^{at}(x)\gamma_0\gamma_2\gamma_\mu u^b(x)\right)\gamma_5\gamma^\mu\sigma_{\alpha\beta}[gG^{\alpha\beta}d]^c(x) \tag{32}$$

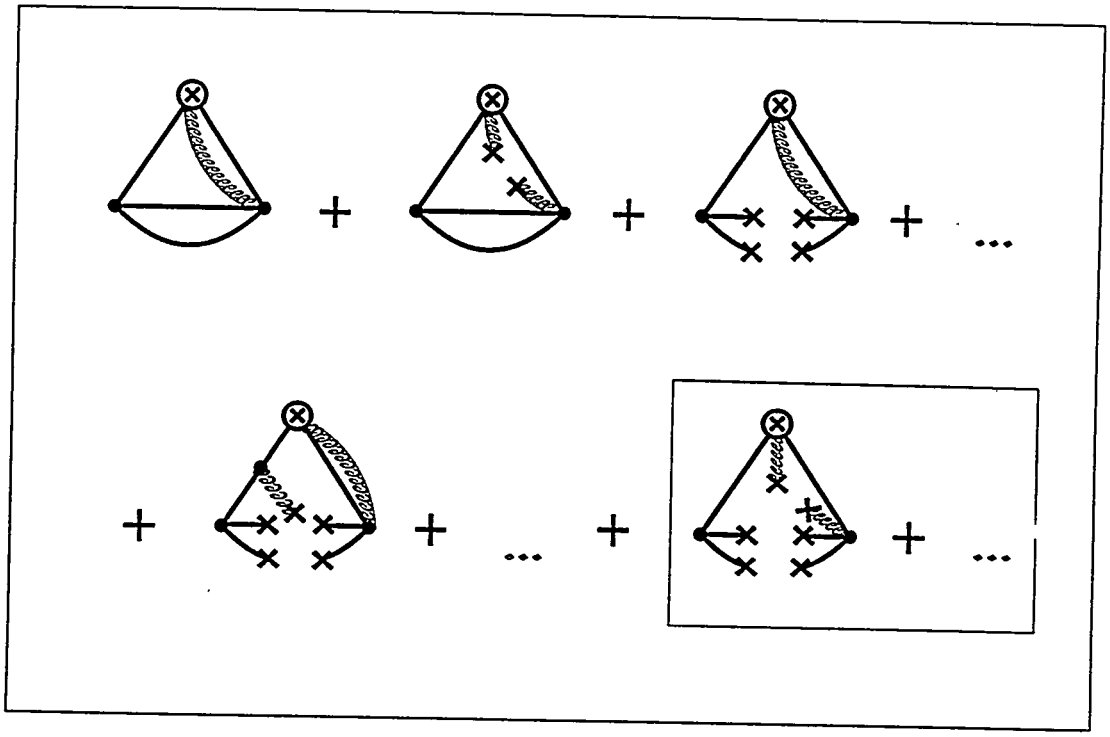


Fig. 9. The perturbative graphs contributing to our calculation of d_2. The last set of graphs are by far the most important ones for the final result.

$$-\frac{2}{3}\epsilon_{abc}\left(u^{at}(x)\gamma_0\gamma_2\gamma_\mu u^b(x)\right)\gamma_5\gamma^\mu\sigma_{\alpha\beta}[gG^{\alpha\beta}d]^c(x)$$

This current does not have the above mentioned symmetry. Consequently the QCD calculation is not dominated by just one graph, but by six different ones coupling to either $\langle\bar{q}q\rangle^2\langle\tilde{G}_{\mu\nu}G^{\mu\nu}\rangle$ or $\langle\bar{q}\sigma_{\mu\nu}G^{\mu\nu}q\rangle^2$, see Fig. 9. Surprisingly the result shows still the same strong asymmetry, see Fig. 10.

Thus it seems that the proton-neutron asymmetry is really a firm prediction of QCD sum rules such that measuring d_2 would be a crucial test of this method.

6. Conclusions

We have argued that a measurement of d_2 is of fundamental importance for the understanding of hadronic spin-effects. We have also argued that the kinematical range of CEBAF while being rather restricted in general should allow to measure d_2 as well as a_2. It was explained by Dr. Z.E. Meziani in the parallel sessions that the luminosity for measuring spin-dependent structure functions at CEBAF is far superior to any other place. The number given is $10^{37}\text{cm}^{-2}\text{s}^{-1}$ for a He^3 target. With this luminosity CEBAF might be the only place to measure d_2 with good accuracy. Because of the marginal kinematic situation (see Fig.2) such a measurement would, however, require a 10 GeV beam. 8 GeV would leave too little parameter space to

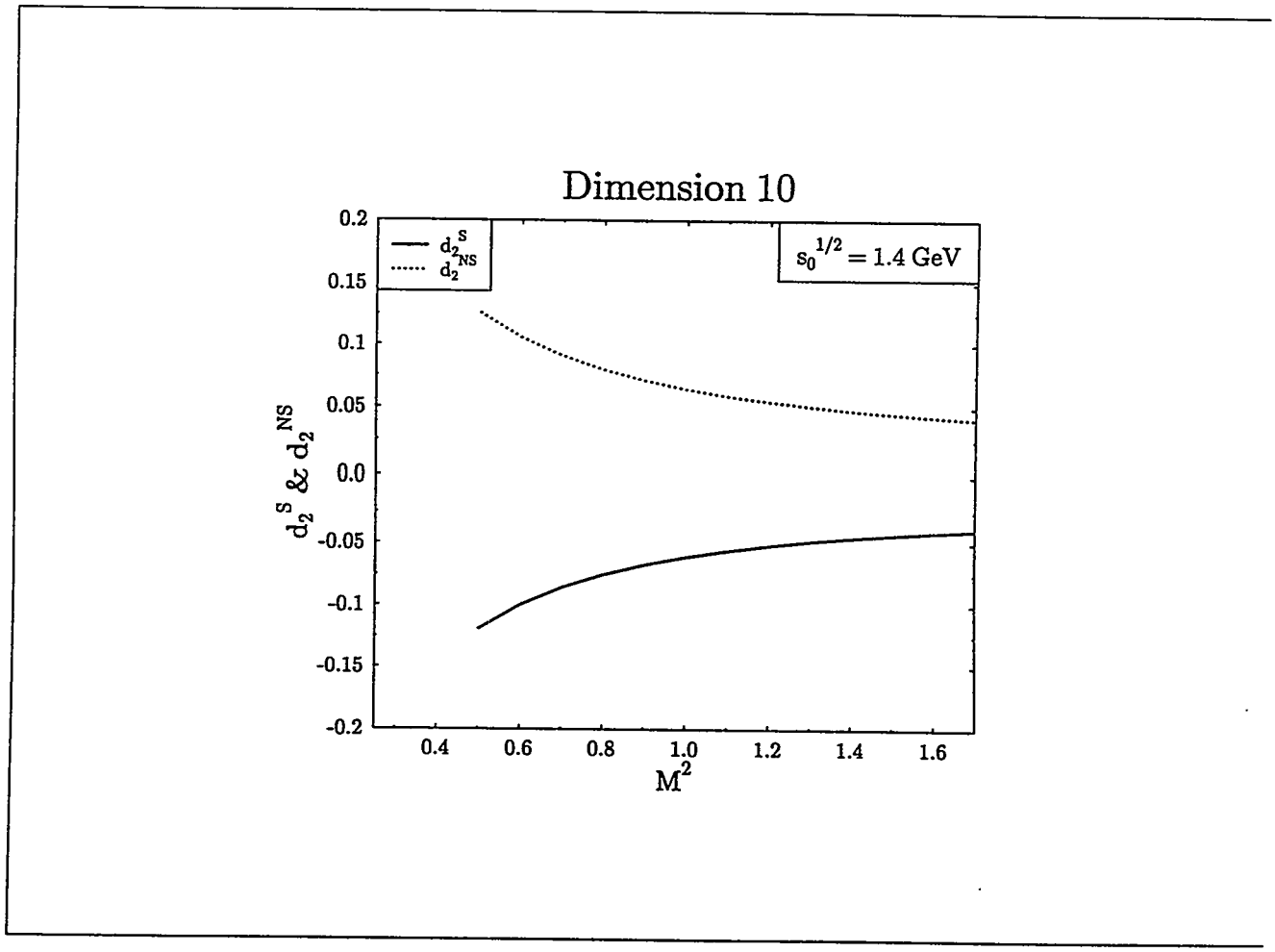


Fig. 10. The results for d_2 using our 3 quark + gluon current, without bilocal power corrections.

control the Q^2 dependence of $g_2(x, Q^2)$.
We have argued that d_2 has the simple physical meaning of a collective gluon field inside of the nucleon, one component of which being the colour magnetic field along the spin direction. We have further argued that d_2 is extremely sensitive on the precise form of the interaction. QCD sum rules and the bag model differ drastically in their prediction, such that a measurement would show that at least one of these models (if not both) does not describe the spin structure of the nucleon correctly. If the asymmetry predicted by QCD sum rules were real this should imply a number of isospin-asymmetric spin effects. Thus the measurement of d_2 would provide the basic piece of information for the interpretation of a wide class of effects.
Finally the precise measurement of d_2 and a_2 allowes to fix the higher-twist corrections to the Bjorken sum rule and determining with high precision the Q^2 dependence of g_1 and g_2 in the x-range of CEBAF would certainly help a lot to understand it also at smaller x values.
Altogether we conclude that measuring $g_1(x, Q^2)$ and $g_2(x, Q^2)$ in the range $0.15 \leq x \leq 0.7$ at CEBAF with a 10 GeV beam would be a very interesting program. Depending on the achievable luminosity it might be superior to any measurement achievable at other accelerators.

7. Acknowledgments

The results presented in this contribution came out from the work of our Frankfurt-Warsaw-Heidelberg collaboration, and I want to thank all its members: B. Ehrnsperger, P. Gornicki, S. Güllenstern, O. Martin, M. Meyer-Hermann, A. Saalfeld, E. Stein and most notably L. Mankiewicz.

8. References

1. EMC, J. Ashman et al., Phys. Lett. **B206** (1988) 364, Nucl. Phys. **B328** (1989) 1
2. SMC, B. Adeva et al., Phys. Lett. **B302** (1993) 533
3. E142 Collaboration, M.J. Alguard et al., Phys. Rev. Lett. **71** (1993) 959
4. FNAL E581/704 Collaboration, D.L. Adams et al., Phys. Lett. **B261** (1991) 201, Phys. Lett. **B264** (1991) 462
5. R.L. Jaffe and X. Ji, Phys. Rev. **D43** (1991) 724
   R.L. Jaffe, Comm. Nucl. Part. Phys. **19** (1990) 239
   X. Ji and Ch. Chou, Phys. Rev. **D42** (1990) 3637
6. A. Ali, V.M. Braun, and G. Hiller, Phys. Lett. **B266** (1991) 117
7. L. Mankiewicz and A. Schäfer, Phys. Lett. **B265** (1991) 167, Phys. Lett. **B274** (1992) 199
8. R. Mertig and W.L. van Neerven, Z. Phys. **C60** (1993) 489
9. G. Altarelli, B. Lampe, P. Nason, and G. Ridolfi, preprint CERN-TH.7254/94
10. S.A. Larin and J.A.M. Vermaseren, Phys. Lett. **B259** (1991) 345

11. B. Ehrnsperger, L. Mankiewicz, and A. Schäfer, Phys. Lett. **B323** (1994) 439
12. X. Ji and P. Unrau, preprint MIT-CTP-2232
13. I.I. Balitsky, V.M. Braun, and A.V. Kolesnichenko, Phys. Lett. **B242** (1990) 245; Erratum: Phys. Lett. **B318** (1993) 648
14. J. Ellis and M. Karliner, preprint CERN-TH-6898/93, TAUP-2052-93
15. F.E. Close and R.G. Roberts, Phys. Lett. **B316** (1993) 165
16. G. Altarelli, P. Nason, and G. Ridolfi, Phys. Lett. **B320** (1994) 152
17. J. Qiu and G. Sterman, Phys. Rev. Lett. **67** (1991) 2264, Nucl. Phys. **B378** (1992) 52
18. A. Schäfer, L. Mankiewicz, P. Gornicki, and S. Güllenstern, Phys. Rev. **D47** (1993) R1
    B. Ehrnsperger, A. Schäfer, W. Greiner, and L. Mankiewicz, Phys. Lett. **B321** (1994) 121
19. X. Ji privat communication
20. L.J. Reinders, H. Rubinstein, and S. Yazaki, Phys. Rep. **127** (1985) 1

A Detailed Study of Nucleon Structure Function in Nuclei in the Valence Quark Region.

N. Bianchi
INFN-Laboratori Nazionali di Frascati, ITALY

Introduction

The so called "EMC effect" discovered during the 1980's[1], has caused a big controversy in the community of nuclear and high energy physicists; during the last ten years, five experiments have been performed in different laboratories and several hundreds of papers about the possible interpretation of the modification of the nucleon structure function inside nuclei have been published. However, from the experimental point of view, the main goal of four experiments (EMC[1], BCDMS[2], NMC[3], FNAL E665[4]) has been to emphasize the region of low x_b, where shadowing effects appear. In the region of valence quarks and nuclear effects ($x_b > 0.1-0.2$) the most reliable data presently available are from the SLAC E139[5] experiment performed in 1983 with only 80 hours of beam time. New precise data in the valence quark region are necessary to measure separate structure functions $F_2(x_b, Q^2)$ and $R^{lt}(x_b, Q^2) = \sigma_l/\sigma_t$, and to investigate the real A-dependence of the ratio between bound and free nucleon structure functions which is not completly defined by the SLAC data. Moreover, from the nuclear physics point of view, a measurement on some unexplored nuclei, like ^{3}He and ^{48}Ca, would be of great interest.

The intermediate scaling region ($0.1 < x_b < 0.7$) would be accessible at CEBAF if the machine energy will reach 6-8 GeV, as suggested by all the tests performed on the RF cavities. This physics program has been already presented in two letter of intents[6].

Proton and Neutron structure functions

A measurement of the proton and neutron structure functions ($F_2^p(x_b)$ and $F_2^n(x_b)$) gives direct information about the momentum distributions of valence and sea quarks inside the nucleon. The hypothesis of similiar sea-quark distributions in proton and neutron is supported by experimental data in the low x_b region ($x_b < 0.01$), where the ratio F_2^n/F_2^p goes to 1; so there is no evidence for the shadowing in the deuteron as suggested by real photon experiments.

At high values of x_b ($x_b > 0.7$) the ratio goes approximately to the value $(\frac{q_{down}}{q_{up}})^2 = 0.25$ obtained in a simple quark model considering the contribution of the double valence quarks only; nevertheless in this region both statistic and systematic error bars are big and the Fermi correction of the deuteron structure function becomes important.

In the intermediate valence quark region ($0.1 < x_b < 0.7$) there is a 10-20% discrepancy among data that can be only partially explained by Q^2 scaling violation. Next to leading order calculation in QCD, including target mass effects, predicts a $[lnQ^2]$ be-

haviour, with a slope between 0 and -0.01 in the intermediate x_b range, while the slope for each data set is systematically bigger (-0.015 for the SLAC data[7]; -0.019 for the combined SLAC and NMC data[9]; -0.02 for the combined SLAC and BCDMS data[7]). For this reason, a precise measure of this ratio at a given Q^2 is of fundamental importance for the measurement of structure functions in non isoscalar nuclei.

Moreover, the integral of the difference of structure functions, $\int_0^1 (F_2^p - F_2^n) dx_b/x_b$, has been used to calculate the Gottfried sum rule. The experimental value of 0.24[10] disagrees significantly with respect to the quark-parton model expectation of 1/3, providing strong evidence that SU(2) flavor symmetry is broken by the sea quark distributions of the nucleon. From the NMC[10] experimental values we see that 60% of the integral comes from data in the intermediate region of x_b (0.1 to 0.6) where the experimental errors are large. Hence a precise measurement in this region will better help define the discrepancy between theoretical predictions and experimental findings.

The extraction of the neutron structure function is quite well understood now, with a maximum correction of about 2% due to Fermi motion in deuterium[11] for $x_b < 0.7$.

Structure Functions inside Nuclei

The difference of quark distributions in free and bound nucleons can be due to the partial deconfinement of quarks in nuclei and related to such effects as: swelling of nucleons, formation of multiquark bags, Q^2 rescaling effect caused by the increase of the radius of confinement (see ref.[12–15]). Moreover the quark distribution in nuclei can be deformed due to Fermi motion and binding effects (see ref. [11,16,17]).

Recently, it has been argued that when relativistic effects are consistently taken into account by considering the so called flux factor in the normalization of the relativistic spectral function [15], the effects of nucleon binding energy E and kinetic energy T are strongly reduced. Also nucleonic correlations, which increase in a significant way E and T in comparison with Hartree-Fock models, are not able to explain definitively the data for $x_b \geq 0.5$, so that non-nucleonic degrees of freedom or bound nucleon modifications[11] should also be considered.

There are different models that postulate an increase of quark confinement radius inside the nucleus. For instance this can be explained by introducing quark deconfinement because of the admixture of multiquark states. In the framework of this model[12,13], the ratio of nuclear and deuterium structure functions can be written:

$$R_A = 2\frac{(1-w)F_{2N} + wF_{2B}}{F_{2D}}$$

where F_{2N} is the nucleon structure function corrected for the Fermi motion, F_{2D} is the deuteron structure function and F_{2B} is the cluster structure function and w the cluster relative probability; this probability increases from 10% in ^{4}He to 30% in ^{56}Fe.

Data are presently available for several nuclei from ^{4}He to ^{197}Au and the EMC effect is well evident for all. In particular in the region of $x_b \sim 0.5$ - 0.6 the size of this effect in ^{4}He is 40 to 50% of the effect in the heaviest target. Unfortunately no data are yet available on ^{3}He that might help to understand this behaviour in very light nuclei. Many nucleonic and non nucleonic interpretations are able to reproduce the data in heavy nuclei, but not one can be used to draw definite conclusions. It should be stressed, however, that those interpretations which are able to reproduce the data for heavy nuclei are generally parameter dependent as far as nuclear structure is concerned. Therefore a careful measurement in few body systems becomes essential. The fact that the ^{3}He

spectral function is exactly known and the one for ^{4}He can be computed much better than in heavier nuclei suggests that data from these two nuclei should provide a good tool for discriminating between different theories. It is also clear that the presence of a multiquark cluster state[13] can be easily checked comparing the results from the two Helium isotopes. It has also been shown that quark exchange between nucleons can be precisely evaluated and give an overall non-negligible effect of a few percent in the ratio R_A for a relative dilute nucleus like ^{3}He[19].

A systematic study of nuclear structure function is also needed to improve and complete SLAC data that are only partially separated with Rosenbluth plots. In fact the SLAC data, in the valence quark region, are not able to disentangle the A behaviour of the ratio $R_A = \sigma_A/\sigma_D$ between a power law $R_A = cA^\alpha$ and a proportionality to nuclear density $R_A = a(1 + b\rho(A))$[5] as suggested by multiquark state models. So a nuclear density fit could be better verified in light nuclei where the density changes very quickly and with a non monotonic law and in heavy nuclei where a saturation effect should appear. The Rosenbluth separation, which is presently available for only a few nuclei [20], allows one to determine the ratio $R_A^{lt} = \sigma_l/\sigma_t$ and helps to investigate possible nuclear medium effects by studying the difference $R_A^{lt} - R_D^{lt}$ as a function of x_b for various nuclei.

A new and interesting measurement is to study how u-quark and d-quark distributions are modified in bound nucleons by comparing results on nuclei with same A but different Z (like ^{48}Ca and ^{48}Ti) and same Z and different A (like ^{40}Ca and ^{48}Ca): in this way one can discriminate between standard nuclear models and multiquark models with a relative measurement of few % precision[18]. It is important to point out that whereas Q^2 scaling violations have been clearly shown in the measurements of the structure function F_2, no significant Q^2 dependence was ever found in the ratio of structure functions R_A, allowing us to perform this measurement in the region of modest values of Q^2.

New possibilites at CEBAF

An exact kinematic reconstruction, through a 0.1% measurement of the incoming and scattered electron energies E and E' and a scattering angle determination better then 1 mrad, is needed for a precise measurement of structure functions. A precise determination of the spectrometer acceptance and efficiency and a high π/e rejection factor (of the order of $10^4 : 1$) are also important.

All these requests should be satisfied by the HALL A HRS spectrometer at CEBAF. In comparison with the previous SLAC E139 experiment one can expect an increase in sensitivity of a factor greater than 100 due to solid angle, momentum acceptance and beam intensity.

The vertex reconstruction capability of HRS would allow a better rejection of cryogenic target wall backgrounds and, at least for solid targets, a simultaneous measurement on different nuclei that could minimize systematic errors in the ratio of structure functions and reduce time required to accumulate data.

It will be possible to measure the structure function $F_2(x_b)$ and $R^{lt}(x_b)$ on ^{1}H, ^{2}H,^{3}He, ^{4}He, ^{6}Li, ^{7}Li, ^{40}Ca, ^{48}Ca, ^{48}Ti and on a set of "standard" nuclei like C, Al, Fe, Cu, Sn, W, detecting the scattered electrons with one HRS spectrometer and using the other one at fixed angle for normalization purposes. It will be possible also to make use of both spectrometers for data taking to reduce the time required to accumulate data. For a Rosenbluth separation of the structure functions at least two beam energies would be required. It would be convenient to use the 5th and 4th beam recirculation

corresponding to 6 and 4.8 GeV respectively, for a beam of 6 GeV maximum energies. In this case, the available kinematic region is shown in fig. 1 and is defined approximately by the triangle between the line $W \geq 2$ GeV (resonance constraint), the line $Q^2 \geq 1$ GeV^2 (scaling constraint) and the line $\nu \leq 4.3$ GeV ($y_{max} = \nu_{max}/E_{min} = 0.9$ due to radiative correction constraint). The x_b range to be explored is 0.1 to 0.65 , where for each x_b point the maximum Q^2 (and ν) is selected to minimize possible higher twist effects in the ratio of structure functions. Target mass corrections can be taken into account considering the Nachtman scaling variable ξ instead of the Bjorken variable x_b.

For the propsed measurement several kind of target will be required:
- liquid hydrogen and deuterium targets, operating at 20 K;
- high pressure (70 Atm) ^{3}He and ^{4}He gas targets, operating at 10 K;
- solid targets for other nuclei.

All these targets have to operate with a beam current of 100 μA, which correspond to a power dissipation of about 500 Watt for an hydrogen or deuterium target of 15 cm. Therefore beam position rastering or direct cooling of the target will be necessary. To minimize the contributions due to radiative corrections in the ratio of the structure functions, all targets must have similar thicknesses of 1% to 2% of radiation length, X_o, (for comparison, target thicknesses of 2% X_o for light nuclei and 6% X_o for heavy nuclei were used in the SLAC E139 experiment). Up to three solid targets can be used simultaneously due to the 10 cm longitudinal acceptance of the spectrometer and the vertex reconstruction capability.

Using sets of solid targets simultaneously not only shortens the time necessary to accumulate data but also reduces the systematic errors between targets in each set.

To estimate the count rates we have assumed a 100 μA of beam current, a 1% X_o hydrogen target (total luminosity of about $2.3*10^{38}$ cm$^{-2}s^{-1}$), a 7.0 msr solid angle and a momentum bite $\Delta p/p$ of 10% for the spectrometer. Details on kinematic parameters and the counting rates can be found in Tables 1, 2 and 3 of LOI-93-009, moreover the total beam time needed to accumulate 0.5% statistics for each x_b experimental point for all the nuclei is around 300 hours, mainly due to angle and energy changes.

Conclusions

Unpolarized structure functions of free and bound nucleons can be measured with the CEBAF 6 GeV beam in the valence quark region. An improvement on the precision of actual data and the measurements on non isoscalar nuclei will provide a tool for discriminating the standard nuclear models from more exotic ones.

This physics program could be extended to future measurements of polarized structure functions when the polarization of the beam and of the targets becomes available. In particular, we point out that about 75% of the integral of the polarized structure function of the proton, $\int_0^1 g_1^p(x_b)dx_b$, which does not agree with the prediction of the Ellis-Jaffe sumrule, is determined in the region of intermediate x_b value ($0.1 \leq x_b \leq 0.7$) accessible with a 6 GeV beam and that the measured asymmetry A_1^p is almost Q^2 independent in the range 1 (GeV/c)$^2 \leq Q^2 \leq 100$ (GeV/c)^2.

References

1. J.J. Aubert et al., *Phys. Lett.* 123B (1983) 275
2. A.C. Benvenuti et al.,*Phys. Lett.* B189 (1987) 483

3. P.Amaudruz et al., CERN-PPE/91-52
4. M.R.Adams et al., *Phys. Rev. Lett.* 68 (1992) 3266
5. R.G. Arnold et al.,*Phys. Rev. Lett.* 52 (1984) 727
6. N. Bianchi and A. Saha, Spokespersons, CEBAF LOI-93-009 and N.Bianchi, Spokeperson, CEBAF LOI-91-008.
7. L. W. Whitlow, Ph. D. thesis , SLAC-357 (1990)
8. A.C. Benvenuti et al., *Phys. Lett.* B237 (1990) 599
9. D. Allasia et al., CERN-PPE/90-103
10. P. Amaudruz et al., *Phys. Rev. Lett.* 66 (1991) 2712
11. C. Ciofi degli Atti and S.Liuti, *Phys. Rev.* C 41 (1990) 1100; and *Phys. Rev.* C 44, Rapid Communications.
12. F.E.Close et al, Phys. Rev. D31 (1985) 1004
13. L.A. Kondratyuk and M.Zh.Shmatikov, Z. Phys. A 321(1985) 301
14. E.L.Berger et al., Ann. Rev. Nucl. Part. Sci. 37 (1987) 463
15. L.L.Frankfurt and M.I.Strikmann, Phys. Rep. 160 (1988) 236
16. A. Bodek et al., *Phys. Rev.* D23 (1981) 1071
17. S.V Akulinichev et al., *Phys. Rev. Lett.* 55 (1985) 2239
18. L.A. Kondratyuk, private communication.
19. P.Hoodbhoy and R.L. Jaffe *Phys. Rev.* D35 (1987) 113
20. S. Dasu et al., *Phys. Rev. Lett.* 60 (1988) 2591

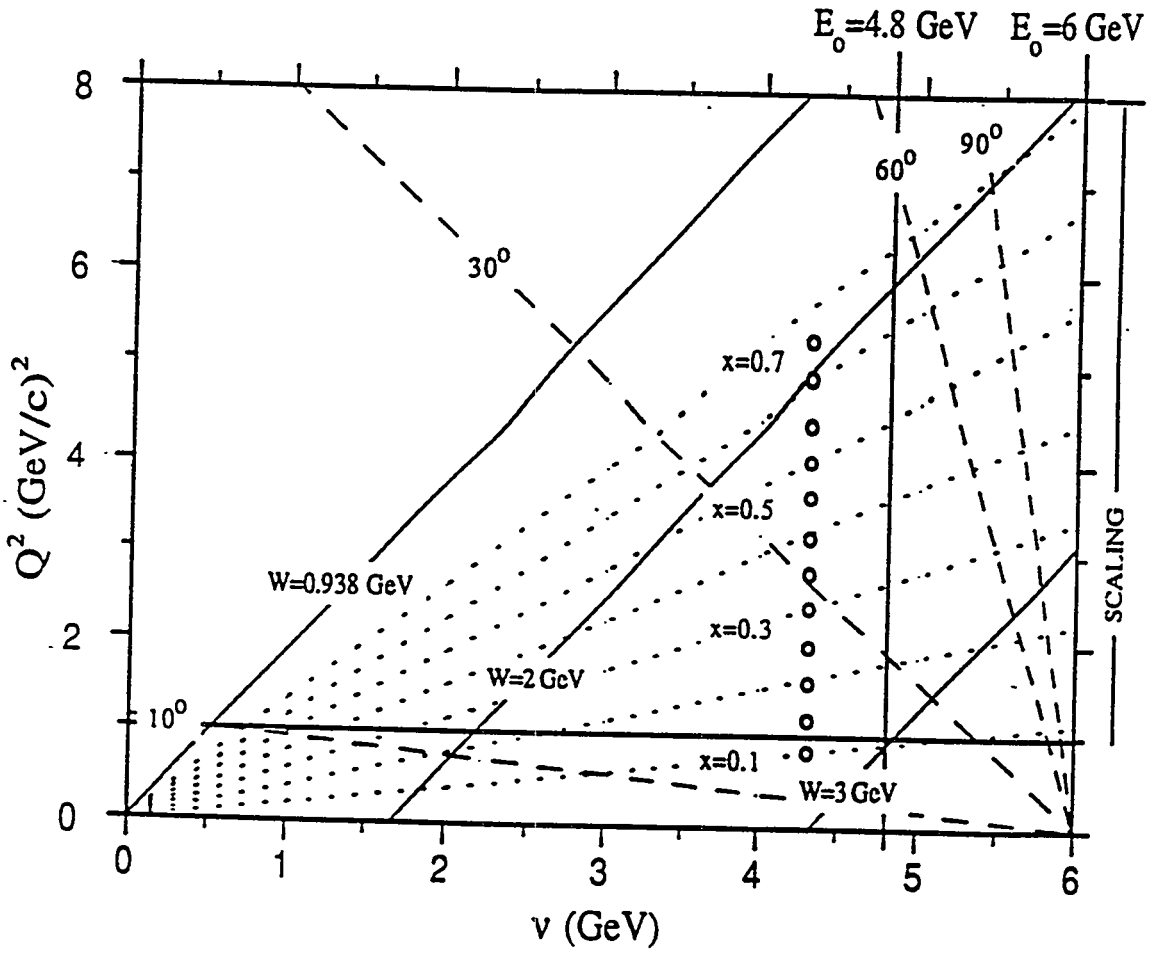


Figure 1. *Kinematic plane for inclusive electron scattering (e,e') with a 6 GeV electron beam. The circles are the kinematic data points for this proposal for measuring* F_{2A} *vs* x_b.

INELASTIC ELECTRON SCATTERING FROM A MOVING NUCLEON

SEBASTIAN E. KUHN
Old Dominion University, Norfolk, VA 23529

KEITH GRIFFIOEN
The College of William and Mary, Williamsburg, VA 23187

ABSTRACT

We propose to measure inelastically scattered electrons in coincidence with spectator protons emitted backwards relative to the virtual photon direction in the reaction $d(e, e'p_s)X$. In a simple spectator model, the backward proton has equal and opposite momentum to the neutron before it is struck, allowing us to study the dependence on kinematics and off-shell behaviour of the electron-nucleon inelastic cross section. If the photon couples to a quark in a 6-quark bag, a different dependence of the cross section on the kinematic variables (x, Q^2, and $\mathbf{p}_s$) can be observed. Our proposed experiment requires large acceptance and beam energies above 6 GeV. It is ideally suited for the CEBAF Large Acceptance Spectrometer (CLAS).

One of the currently fascinating questions in nuclear physics is "At what level does the quark-gluon picture supersede the nucleon-meson picture?" Clearly, when the wave functions of two nucleons overlap significantly, one can expect large changes in the internal structure of the nucleons. The chance of this occurring in nuclei is rather high. The probability of finding a nucleon inside a nucleus with internal momentum above the Fermi surface ($\geq$ 300MeV/c) is about 25% for heavy nuclei, and results primarily from 2-nucleon correlations[1]. Even in deuterium, approximately $3-4\%$ of the momentum-space wave function lies above 300 MeV/c and possibly 2% lies above 400MeV/c. By designing experiments that are sensitive to short-range correlations in nuclei, we can amplify the effects of microscopic degrees of freedom. We wish to concentrate our efforts on deuterium, the simplest nucleus, for which the interpretation of the data is easiest and realistic calculations exist[2]. In this case, the two baryons making up the correlation (np, $\Delta\Delta$, etc.) have equal and opposite internal momenta. By detecting a backward-going baryon with high momentum, we can ensure that the reaction occurred on a tightly correlated pair and we can measure its internal momentum. We wish to determine several things:

(a) Can we describe the scattering process in a spectator picture where the backward going nucleon is undisturbed by the reaction occuring on the correlated forward going nucleon? If the spectator picture is correct, we expect that the cross section will depend only on those variables that describe the free cross section, after a kinematical correction for the movement of the struck nucleon.[1]

(b) What is the correct description of the deuteron wave function? Does one need light cone wave functions? Can we directly measure the high-momentum tail of the deuteron wave function? One avenue to answer some of these questions would be to integrate the scattering cross section over large kinematic ranges in x and Q^2 at

fixed spectator momentum and then to study the dependence of the integrated cross section on the spectator momentum. The dependence on the direction of the spectator momentum, e.g., is quite different for light cone dynamics than for non-relativistic deuteron models.

(c) How are the nucleon form factors and structure functions modified for short-range nucleon-nucleon correlations? Within the spectator picture one could study off-shell elastic and transition form factors. One can compare resonance transition amplitudes to the free values to gain insight into possible deformations of nucleons inside tightly correlated pairs. Deep inelastic measurements address several issues including interpretations of the EMC effect, techniques for extracting the neutron structure functions from measurements on the deuteron, and the existence of 6-quark or $\Delta\Delta$ configurations.

Our experiment can be naturally extended to heavier nuclei, such as ^3He, ^4He, ^{12}C and ^{56}Fe, as described partially by the existing multi-hadron proposals for the CLAS detector [3]. Deuterium has originally been included in that proposal as a standard of comparison for experiments on complex nuclei. The unique perspective of the present proposal lies in the exclusive concentration on deuterium as the lightest nucleus and the emphasis on the highest available beam energies, enabling us to reach the scaling region. We believe that the fundamental mechanism of kinematic rescaling and any possible modifications of elastic and inelastic structure functions, as well as possible non-nucleonic configurations of correlated nucleons inside nuclei, must first be studied well in the relatively simple A=2 system. The interpretation of measurements on heavier nuclei is much more complicated, since final state interactions can influence the spectrum of spectators as well as produce additional backward-going nucleons which are difficult to separate experimentally from the spectator nucleons. Also, deuterium is the only nucleus where the center of mass of the correlated pair is guaranteed to be initially at rest in the laboratory frame.

The deep-inelastic scattering cross section on a nucleon is given by

$$\frac{d\sigma}{dxdy} = \frac{4\pi\alpha_{\rm EM}^2 mE}{Q^4}\left[1+(1-y)^2)\right]F_2(x,Q^2) = KF_2(x) \qquad (1)$$

in which m is the nucleon mass, E is the initial lepton energy, $y = \nu/E$, ν and $Q^2 = -q^2$ are the lab energy and the 4-momentum squared of the virtual photon, $x = Q^2/2k\cdot q$, k is the 4-momentum of the struck nucleon and $\alpha_{\rm EM}$ is the fine-structure constant. This form of the cross section makes the simplifying assumption that $R(x,Q^2) = \sigma_L/\sigma_T = 0$. For a nucleon at rest, $p\cdot q = m\nu$, and x becomes $x = x_{\rm Bj} \equiv Q^2/2m\nu$ (Bjorken-x). In the spectator model of deep-inelastic scattering[1], the virtual photon is absorbed on a quark in one nucleon (moving with momentum k), while the other nucleon is a spectator to the scattering (moving with momentum $\mathrm{p}_s = -\mathrm{k}$). If that second nucleon is truly a spectator, then it must be on-shell at the time of the scattering, with energy $E = \sqrt{m^2+k^2}$, in which m is the nucleon mass. Energy conservation requires that the other nucleon must be off-shell with energy $E^* = \sqrt{m^{*2}+k^2}$, where $E+E^* = 2m$ if we neglect the small binding energy

of the deuteron. Therefore, in this case $p \cdot q = E^* \nu - \mathbf{k} \cdot \mathbf{q}$. This can be rewritten as $p \cdot q = (2m - E)\nu - k_{\|} q = m\nu(2 - [E + k_{\|}(q/\nu)]/m)$. In the limit $q/\nu \to 1$, the second term on the right becomes $(\sqrt{m^2 + k^2} + k_{\|})/m \equiv \alpha$, the light-cone fraction of the momentum of the deuteron carried by the spectator nucleon. The variable α is normalized to have values from 0 to 2 (two nucleons). The approximation $q/\nu = \sqrt{1 - q^2/\nu^2} = \sqrt{1 + x_{\mathrm{Bj}} 2m/\nu} \approx 1$ becomes valid (to within 10%) if $x_{\mathrm{Bj}} < 0.4$ and $\nu > 4$GeV. Figure 1. shows that we can reach this kinematic region with CEBAF energies of $6 - 8$GeV.

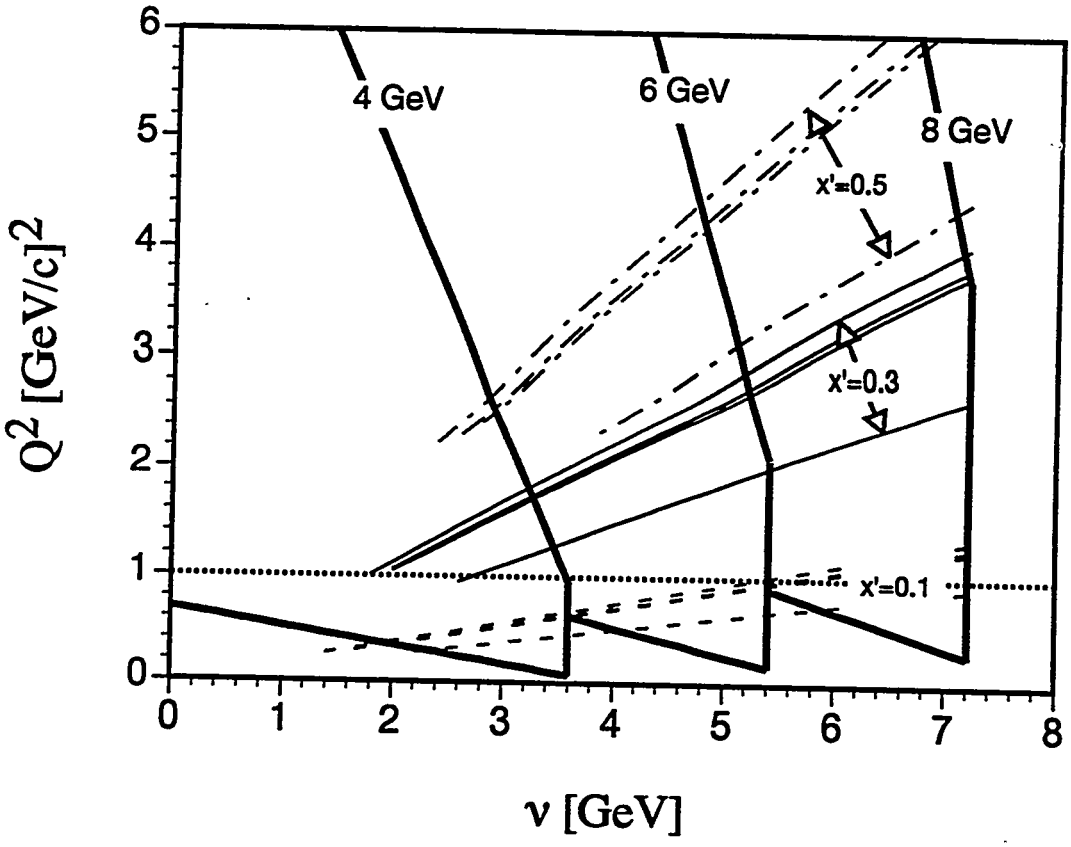


Fig. 1. Kinematics at CLAS for 4–8 GeV beams. Each kinematic range is limited by the physical detector acceptance on top and bottom and by the beam energy on the right. Four curves are shown for each value of $x_{\mathrm{true}} = 0.1$, 0.3 and 0.5. The upper curve in each case corresponds to deep inelastic scattering on a nucleon at rest, followed by three curves for scattering in coincidence with a spectator nucleon with momentum 0.3 GeV/c at 90° with respect to $\mathbf{q}$, 0.35 GeV/c at 90°, and 0.3 GeV/c at 150°. As the beam energy increases, the available kinematic range opens up. At 6 GeV, for example, one can easily satisfy the constraints that $\nu > 4$ GeV and make measurements between $0.2 < x < 0.5$. An additional 2 GeV would provide sufficient leverage to extend the range to about $0.1 < x < 0.5$ and to higher Q^2.

The implication of the spectator model is that $x \approx x_{\rm Bj}/(2-\alpha)$; the "true" x is related to the observed Bjorken-x by a factor involving the light-cone fractional momentum of the backward-going nucleon. Therefore, if the spectator model is correct, the measured structure functions tagged on the spectator will be essentially the structure functions of a free nucleon, rescaled by $x_{\rm Bj} \rightarrow x_{\rm Bj}/(2-\alpha)$. The cross section for deep inelastic scattering with coincident observation of a spectator nucleon becomes[4]

$$\frac{d\sigma_{\rm 2N}}{dxdyd\alpha d^2p_\perp} = \frac{4\pi\alpha_{\rm EM}^2 mE(2-\alpha)}{Q^4}\left[1+(1-y)^2)\right]F_2(\frac{x}{2-\alpha},Q^2)|\psi(\alpha,p_\perp)|^2 \qquad (2)$$

in which ψ is the momentum-space deuteron wave function expressed in terms of the light cone fraction α and the transverse momentum $p_\perp$.

At present, the existing data are sparse and do not allow us to investigate in detail the structure of the cross section (Eq. 2) as a function of all kinematic variables. The Big European Bubble Chamber (BEBC) collaboration has studied deep inelastic neutrino scattering in coincidence with the emission of a single backward-going nucleon[5]. They calculate the average value of the observed Bjorken-x both for their total data set ($< x_{\rm Bj} >$) and for several bins in the light cone fraction α of the backward-going nucleons ($< x_{\rm Bj} >_\alpha$). Since α and the "true" scaling variable x are uncorrelated, one expects a relation of the form

$$\frac{< x_{\rm Bj} >_\alpha}{< x_{\rm Bj} >} = 2-\alpha \qquad (3)$$

The BEBC data taken for deuterium and for neon indeed show this correlation. Unfortunately, this is not a conclusive proof for the validity of the spectator model. In fact, any object with baryon number $A = 2$ that fragments into a backward-going nucleon will produce a similar kinematic relationship[4]. Hence, for a better understanding of the light-cone structure of two close nucleons, it is crucial to map out the tagged structure functions, rather than to rely on gross averages. In heavier nuclei, particles in the backward direction coming from nucleon-nucleon correlations will be masked by nuclear reinteractions or cascading, even for events that contain only a single backward-going nucleon. Recent preliminary results from E665 at Fermilab bear this out for Xe[6].

In contrast to the spectator picture, we can imagine the opposite extreme, for which the two nucleons are kneaded into a 6-quark (6q) object. Although no more than 5% of the deuteron wavefunction could be due to 6q states (deduced from overlap arguments), above 0.3 GeV/c relative nucleon momentum a large fraction (even as much as 50–100%) of the wavefunction might be in a 6q configuration. Carlson and Lassila[4] have studied a model of deep inelastic scattering on a 6q cluster. In this case,

$$\frac{d\sigma_{\rm 6q}}{dxdyd\alpha d^2p_\perp} = KF_2^{(6)}(x)\frac{1}{2-x}D_{\rm N/5q}(\frac{\alpha}{2-x},p_\perp) \qquad (4)$$

in which $F_2^{(6)}(x)$ is the 6-quark structure function and $D_{\rm N/5q}(\frac{\alpha}{2-x},p_\perp)$ is the probability for a 5q object to fragment into a nucleon with ("apparent") light cone fraction α.

The authors of Ref. [4] have made the simple assumptions that $D_{N/5q}(z) \propto (1-z)^3$, that the 6q valence distribution is $V(x) \propto (1-x)^9 x^{1/2}$ and that the 6q sea distribution is $\bar{U}(x) \propto (1-x)^{11}$. They define a ratio

$$R = \frac{\sigma_{\text{measured}}}{K F_2(\frac{x}{2-\alpha})} \tag{5}$$

which in the spectator model becomes $R = (2-\alpha)|\psi(\alpha, p_\perp)|^2$. Obviously, the ratio R would be constant for fixed α and $p_\perp$. However, if one scatters from a 6q object, R will vary with x. In this case,

$$R = \frac{F_2^{(6)}(x) D_{N/5q}(z, p_\perp)}{(2-x)(2-\alpha) F_2(\frac{x}{2-\alpha})} \tag{6}$$

The solid line in Fig. 2 shows an example of the functional dependence of R on x for $\alpha = 1.4$.

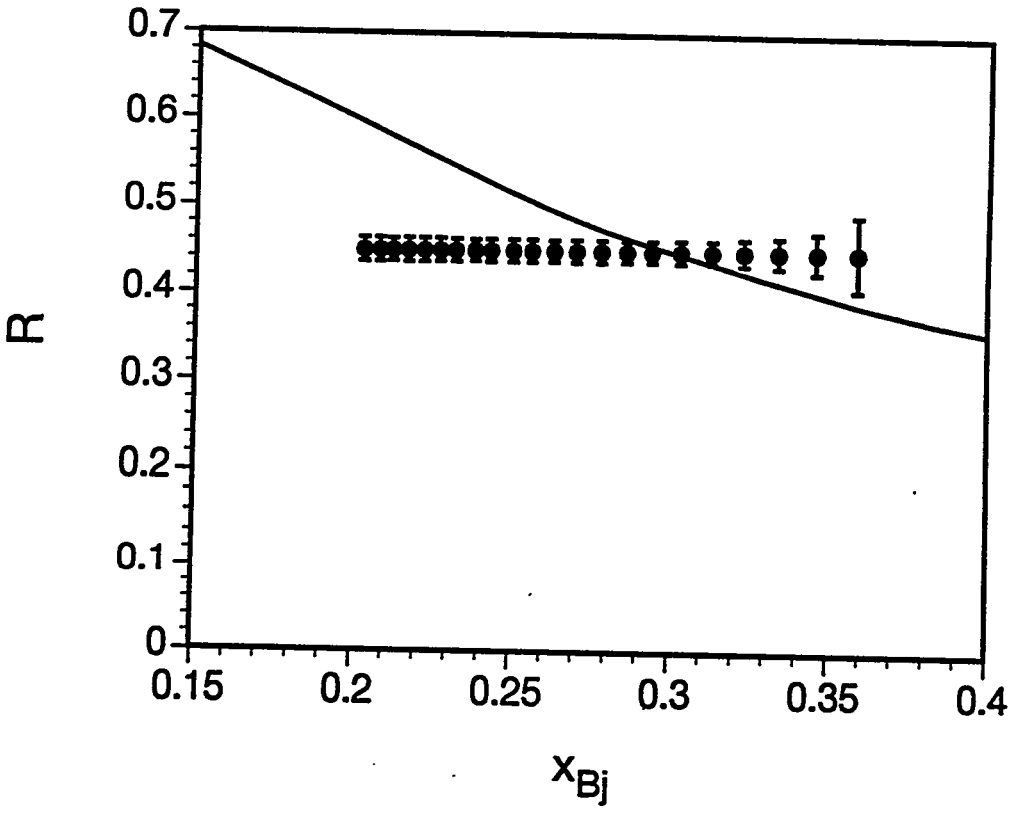


Fig. 2. Calculation of Carlson and Lassila for R in a 6q bag model (solid line), together with projected data obtained from CLAS using 16 days of running time on deuterium at luminosity $10^{34}\text{cm}^{-2}\text{s}^{-1}$. The error bars on these points are statistical. The data points have been plotted at an (arbitrary) constant value of R, corresponding to the spectator model expectation.

The true story in deuterium probably lies somewhere between the spectator and 6q extremes. However, these two models serve to provide a scale for the magnitude of the possible effect we can observe. If R is indeed flat with x one can perhaps set constraints on the 6q content of the deuteron. If R is not flat with x it will provide the first quantitative evidence for modification of the structure functions (beyond simple kinematics) when two nucleons get close to each other.

A common proposal for observing short-range correlation effects is to look at $x_{\rm Bj} > 1$ in deuterium. Clearly, for a fast-moving nucleon coming toward the electron, the light-cone fraction α approaches zero and $x_{\rm true} = x_{\rm Bj}/2$. Hence, as $x_{\rm Bj}$ approaches 2, one expects a significant enhancement of 6q objects if they exist. The problem with the $x > 1$ measurements is that there is no way to determine α and the data are by nature averaged over a number of true x-values for a fixed $x_{\rm Bj}$. Not only does the tagged structure function method provide similar information to the $x > 1$ measurements, it actually provides this information in much richer detail!

Because the tagged cross sections are typically small, the only way to do this experiment is with a high-duty-factor machine and a large acceptance spectrometer. Once CEBAF obtains 6–8 GeV beams, such a measurement will be possible using CLAS, as can be seen from Fig. 1. Although the overall luminosity at CLAS is low, the benefits of the large-acceptance spectrometer for both electron and backward-going proton far outweigh this liability. This experiment cannot be done in one of the other CEBAF halls. Figure 2 shows a projection for the quality of data one can expect from a tagged structure function measurement with CLAS. Due to the large acceptance of CLAS, one can collect data similar to those shown in Fig. 2 for many different bins in α and $p_\perp$ simultaneously. We are presently preparing a full proposal along these lines to the CEBAF PAC.

References

1. L.L. Frankfurt and M.I. Strikman, *Phys. Rep.* **76**, (1981) 215; *Phys. Rep.* **160**, (1988) 235; *Nucl. Phys.* **A497**, (1989) 155c.
2. G.D. Bosveld, A.E. Dieperink and A.G. Tenner, *Phys. Rev. C* **49** (1994) 2379.
3. K. Egiyan et al., *CEBAF proposal* **PR-89-036**.
4. C.E. Carlson and K.E. Lassila, *William and Mary Report* **WM-94-101**; see also elsewhere in these proceedings.
5. Matsinos, *et al.*, Z. Phys. C 44, (1989) 79.
6. K.A. Griffioen, E665 Collaboration, private communication.

Kaon Electroproduction

Pete Markowitz
Physics Department, University of Maryland
College Park, MD 20742, U.S.A.

ABSTRACT

The talk will focus on the physics which can be addressed by looking at semi-inclusive and exclusive channels in the DIS region. In particular, I will examine how this physics is reflected in the separated response functions.

1. Introduction

1.1. Definition of the Variables

Before discussing the physics, let me define the appropriate variables. The hadronic cross section can be expressed in terms of the following kinematical variables:

$$\begin{array}{cc} \gamma_v^2 = (e-e')^2 = -Q^2 & \nu = E - E' \\ \epsilon = [1 + 2\frac{\nu^2+Q^2}{Q^2}\tan^2\frac{\theta_e}{2}]^{-1} & M_X^2 = (e - e' + N - K)^2 \\ s = (\gamma_v + N)^2 = W^2 & t = (\gamma_v - K)^2 \\ x_B = Q^2/2M\nu & y = \nu/E \end{array}$$

The 4-momentum transfer squared, γ_v^2, is negative for electron scattering. ϵ is the longitudinal polarization of the virtual photon, while s is the square of the invariant mass of the hadronic system. ν is the energy transferred by the electron, making y the fraction of the initial energy which was tranferred. x_B cannot strictly be interpreted as the momentum of the struck quark, but is instead the variable given by the relationship in the table.

Of particular note is the Mandelstam variable t. t can be thought of as the momentum transferred to the remnant hadronic system. This is in comparison to Q^2, which is the mometnum transferred by the initial electron, and shared between the outgoing kaon and the remnant hadronic system.

1.2. The Cross Section

The electroproduction cross section can be expressed in terms of 4 response functions:

$$\frac{d^3\sigma}{de'd\Omega_e d\Omega_k} = \sigma_T + \epsilon\sigma_L + \epsilon\sigma_{TT}\cos 2\phi + \sqrt{2\epsilon(\epsilon+1)}\sigma_{LT}\cos\phi$$

where ϕ is the "out-of-plane angle" or the angle between the leptonic plane (defined by the incoming and outgoing electrons) and the reaction plane (defined by the

direction of the 3-momentum transfer, $\vec{q}$, and the outgoing kaon). The response functions can be defined as functions of the kinematical variables Q^2, t, and s.

2. The Kaon Form Factor

One of the subjects which can be addressed in kaon electroproduction is the Q^2-dependence of the kaon form factor. In order to get at this piece of physics, the t-channel diagrams, where the virtual photon is absorbed by a kaon (leaving behind a hyperon), must be separated from the u-channel (where the virtual photon is absorbed by a hyperon) and the s-channel (where the virtual photon is absorbed by a nucleon or nucleon resonance which decays into a kaon and a hyperon) diagrams.

The method chosen to maximize the t-channel contribution, while minimizing the s- and u-channel contributions is to examine the longitudinal response function as a function of t,[1] and to extrapolate to the kaon pole, similar to what is done in the case of the pion.[2] The difference comes in the mass of the spectatator baryon, which in this case is a hyperon, not a nucleon. The technique is a Chew-Low extrapolation in t:

$$(t-\mu)^2 \frac{d\sigma_L}{dt}|_{t=\mu^2} = N(\mu^2) F_K^2(Q^2)$$

The longitudinal cross section (as a function of t) is fit to a line and $F_K^2(Q^2)$ then extracted. With an 8 GeV beam energy, momentum transfers up to Q^2 of 4-5 $(\mathrm{GeV/c})^2$ can be reached.

3. The Isospin Content of the Nucleon

A long-standing question in kaon electroproduction is the ratio of the cross section for $\sigma(\Sigma^0)$ to $\sigma(\Lambda)$. Experimentally, the ratio $\sigma(\Sigma^0)/\sigma(\Lambda)$ goes to zero as x_B (or Q^2) increases.[5] There are two explanations proposed to explain this.

3.1. Possible t-channel Enhancement

The first explanation assumes that the longitudinal part of the cross section dominates at high Q^2. In this case the t-channel would be enhanced, since the main contribution to σ_L is from K^+-exchange and the coupling constant for the Λ is greater than that for the Σ^0 ($g^2_{pK\Lambda} >> g^2_{pK\Sigma^0}$). However, experimentally there is no evidence for the longitudinal response function dominating the cross section.[4,5] The errors are large, and better data are needed before this statement can be made conclusive however. CEBAF, even at 4 GeV, is well positioned to supply that data.

3.2. Isospin Content

The second explanation is given in termns of the quark-parton model.[6] In the quark-parton model, the struck quark is either a sea $\bar{s}$ quark (and a $u\bar{u}$-pair is created as the color string breaks) or the struck quark is a valence u quark (and a $s\bar{s}$-pair is created as the color string breaks).

Experimentally, inclusive scattering data has shown that the ratio of the neutron to proton structure functions in DIS, F_2^n/F_2^p goes to 1/4 as x_B goes to 1. This is intrepreted to mean that when the virtual photon, γ_v, hits a valence u-quark, the

remaining ud-quark pair is in an $I = 0$ state. This would favor $\Lambda(I = 0)$ production over $\Sigma(I = 1)$ production. However the argument depends on being in the DIS region; with a 6 GeV beam, CEBAF will be able to cover the range $0.2 < x_B < 0.7$ and $2 < Q^2 < 8$.

4. A Simplistic Parton Model

In the quark-parton model, the electroproduction of pseudoscalar mesons by transversely polarized virtual photons has been examined in the s-channel. For scattering followed by hadronization by vector gluons, the transverse-transverse interference part of the cross section, σ_{TT}, is strictly zero, and the part of cross section due to transversely polarized photons, σ_U, drops as one move out in t. In scattering by a transversely polarized virtual photon followed by hadronization by a scalar gluon it was found that the transverse-transverse interference piece, σ_P, is not equal to zero, and the transverse cross section σ_U initially rises as a function of t, before dropping at large values. This behavior is just due to helicity conservation.[4] Although the model uses wave functions for the quarks that are very simplistic, the basic conclusions are still valid for more complicated quark wavefunctions.

4.1. Pion Electroproduction Data

An example of this model can be found in the pion electroproduction data, where the ratio of π^+ electroproduction from the proton to π^- electroproduction on the neutron was measured.[5] The proton is described in terms of the valence quarks uud (charge 2/3, 2/3, -1/3) while the neutron is described as udd (charge 2/3, -1/3, -1/3). The π^+ (π^-) is a $\overline{u}d$ ($\overline{d}u$), meaning that for π^+ electroproduction, the virtual photon couples to the valence u quark, with charge 2/3. However for π^- electroproduction, the virtual photon couples to the valence d quark, with charge -1/3. The ratio of π^+ to π^- electroporduction should be $|2/3|^2 : |-1/3|^2 = 4:1$. As |t| increases, the experimental data do approach 4:1.

It is worth asking why this behavior should be seen as a function of t, which is after all inherently an exclusive quantity. The reasoning is that the data are for the cross section, where no L/T separation was performed. This means that as the absolute value of t increases, the longitudinal piece of the cross section dies away, leaving just the transverse piece showing the expected behavior. Experiments to measure the behavior of the separated L/T responses as a function of both t, Q^2, and W to map out the behavior are being planned for CEBAF.

4.2. Photoproduction Data

It is also worth asking whether or not this behavior is observed with real photons. The cross section for real photons is all transverse, and one might expect the photoproduction to also show this behavior; it does not. For real photons $Q^2 = 0$, meaning that $x_{Bj} = Q^2/2M\nu = 0$. The quark structure functions for the valence quarks peak at roughly $x_{Bj} = 0.3$, whereas the sea quarks peak at $x_{Bj} = 0$, and fall away to essentially zero by $x_{Bj} = 0.2$. Therefore real photons preferentially see the sea quarks, not the valence quarks. This experiment will measure between $0.2 \leq x_{Bj} \leq 0.5$, where scattering from valence quarks should dominate.[11,12]

The analogy between π^+/π^- (or $u\bar{d}/\bar{u}d$) in the case of kaons is the K^+/K^0 ratio (or $u\bar{s}/d\bar{s}$). The quark-parton model predicts that the ratio of the transverse cross section for $K^+\Sigma^0$ production on the proton to $K^+\Sigma^-$ production on the neutron is 1:2, reflecting the probability of finding the ud quarks in the proton in a I=1 state compared to the probablilty of finding the dd quarks in the neutron in a I=1 state. The important point here is that it is necessary to do an L/T separation to see the behavior of σ_U, the transverse part of the cross section.

Hall B at CEBAF is uniquely postioned to perform measurements of the K^0 cross sections, while all 3 halls are planning to measure the charged kaon production channels.

4.3. pQCD Photoproduction Predictions

There is also a perturbative QCD (pQCD) prediction for photoproduction of kaons.[7] The calculation is the leading twist, Born approximation helicity amplitudes for s-channel scattering from valence quarks. The cross section, plotted as a function of $\cos\theta$, the angle between the photon and the outgoing kaon (this is equivalent to t), shows a minimum for $\cos\theta \sim 0.4 - 0.5$, depending on the channel. The calculation is sensitive to the quark wavefunctions, which give a different behavior for the Λ channel versus the Σ channel (the dip for the Λ occurs around $\cos(\theta) = -0.5$, while the dip for the Σ occurs around $\cos(\theta) = -0.5$.) However the photoproduction data are not in perfect agreement with the calculation. At forward angles, the t-channel contributions come in, while at backward angles the u-channel contributions tend to shift the data from the theory. This prediction should hold more rigorously for the transverse part of the electroproduction cross section for the reasons given above ($0.2 \leq x_{Bj} \leq 0.5$ allows one to scatter predominantly from a valence quark, the L/T separation allows one to minimize the t-channel contribution, and the t-behavior will be mapped out by changing the kaon angle while keeping the electron arm fixed).

5. Transverse Momentum of the Quark

The longitudinal-transverse interference response function, σ_{LT}, has sensitivity to the quark's transverse momentum. If the lepton scatters off of a pointlike target, helicity conservation requires that for a spin-0 target, the transverse response function be zero ($\sigma_T = 0$) and the longitudinal response function be non-zero ($\sigma_L \neq 0$). This implies that the ratio of the longitudinal to transverse responses grows very large ($R = \frac{\sigma_L}{\sigma_T} \rightarrow \infty$). On the other hand if the lepton scatters off a spin-1/2 target, helicity conservation requires that the transverse response function be non-zero ($\sigma_T \neq 0$) and the longitudinal response function be zero ($\sigma_L = 0$). This would imply that the ratio would get very small ($R = \frac{\sigma_L}{\sigma_T} \rightarrow 0$).

From the single arm spectra we know that in the range of momentum transfers available at CEBAF the longitudinal response function is small but non-zero. There are two possible sources for these longitudinal amplitudes. The first is the initial (or primordial) transverse momentum of the struck quark.[9] In this case the longitudinal-

transverse response function would behave as:

$$\sigma_{LT} \sim -\frac{(2k_T/Q)\cdot(2-y)\cdot(1-y)^{1/2}}{[1+(1-y)^2]}.$$

However this is a purely kinematic effect. It would give a negative contribution to the cross section. This has never been measured and would require an exclusive reaction, since the response depends on the out-of-plane angle of the kaon. It would also require separation of the response functions. Hall A is ideally suited for such a measurement.

The second source of the longitudinal ampitudes comes from a higher-twist correction to the quark-parton model.[8] Here the prediction is that the longitudinal-transverse interference response would go as:

$$\sigma_{LT} \sim (k_T/Q)\cdot(1-y)^{1/2}$$

This would be a dynamic effect, and would give a positive contribution. The longitudinal-transverse response, σ_{LT}, can be extracted by examining the ϕ-dependence of the exclusive cross section. Here one does not need to go out of the plane of the floor, just to move left and right of the direction of the 3-momentum transfer.

5.1. Simulations

The feasibility of such experiments in Hall A has been studied using LEPTO.[10] There the reaction is described in terms of the string model. The string model evolves the reaction in 3 steps. First the formation of a quark-diquark pair, followed by the fragmentation of the quark-diquark pair into primary hadrons, which in turn decay into the observed particles. In this manner it contains u-, s-, and t-channel diagrams. The results of such simulations are consistent with being able to extract a value for σ_{LT} that is small but $\neq 0$.

6. Summary

In conclusion, in the DIS region only inclusive data have been taken thus far; no exclusive data are available (yet). Production of psuedoscalar mesons in the DIS region offers a new technique to probe the physics. However it is necessary to separate teh various response functions. These individual response functions are sensitive to different aspects of physics, as well as different reaction mechanisms. Because of this they offer a look at the basic underlying mechanisms. CEBAF at higher energies will be uniquely positioned to measure this physics with exclusive reactions.

1. Ji and Cotanch, *Phys. Rev.* **D41** (1990) 2319.
2. C.J. Bebek et. al., *Phys. Rev.* **D17** (1978) 1693.
3. C.J. Bebek et. al., *Phys. Rev.* **D15** (1977) 3082.
4. O. Nachtmann, *Nucl. Phys.* **B115** (1976) 61.
5. P. Brauel et. al., *Z. Phys.* **C3** (1979) 101.
6. J. Clemans, F.E. Close, *Nucl. Phys.* **B85** (1975) 429.
7. G.R. Ferrar, *Nucl. Phys.* **B349** (1991) 655.

8. E.L. Berger *Z. Phys.* C4 (1980) 289.
9. R.N. Cahn *Phys. Lett.* **B78** (1978) 269.
10. T. Sjojstrand, *Comp. Phys. Comm.* **39** (1986).
11. CCFR colloaboration, *Phys. Lett.***64** (1990) 1207
12. H. Deden etal., *Nucl. Phys.* **B85** (1975) 269.

Pion Content of the Nucleon in Polarized Semi-Inclusive DIS

W.Melnitchouk
Institute for Theoretical Physics, University of Regensburg, D-93040 Regensburg, Germany.

A.W.Thomas
Department of Physics and Mathematical Physics, University of Adelaide, S.A. 5005, Australia.

Abstract

An explicit pionic component of the nucleon may be identified by measuring polarized Δ^{++} fragments produced in deep-inelastic scattering (DIS) off polarized protons. The pion-exchange model predicts highly correlated polarizations of the Δ^{++} and target proton, in marked contrast with the competing diquark fragmentation process.

I. INTRODUCTION

Much has been learned about the internal structure of the nucleon from inclusive deep-inelastic lepton scattering since the first such experiments were carried out at SLAC in the late 1960s. These and many subsequent DIS experiments [1] were instrumental to the development of the quark-parton model of hadrons.

Successful as it has been in describing much of the DIS data in the perturbative region, a quark-parton based picture of the nucleon is not entirely complete — it is unable to explain the non-perturbative structure of the nucleon. A very good example of this is the deviation from the parton model prediction for the Gottfried sum rule seen in the recent NMC experiment [2]. The most natural explanation of this result is that there exists an excess of $\bar{d}$ quarks over $\bar{u}$ in the proton, something which is clearly impossible to obtain from perturbative QCD alone. A non-perturbative pionic cloud in the nucleon on the other hand offers a simple explanation of SU(2) flavor symmetry breaking in the proton sea [3].

The pion content of the nucleon has been investigated in previous studies of inclusive DIS [4], although only upper bounds on the average pion number were able to be extracted. In addition, since the pion contribution to the nucleon structure function appears at relatively small Bjorken x ($x \sim 0.1$), its signal is lost amongst the perturbative sea background. It is therefore a challenge to seek direct experimental confirmation of pionic effects in inclusive nucleon DIS.

The pertinent question is whether pions leave any unique traces in other processes which cannot be understood in terms of quarks and gluons alone. A possible candidate for this is semi-inclusive DIS, where a hadron is detected in the final state in coincidence with the scattered electron. We shall demonstrate that pions give rise to characteristic fragmentation distributions in comparison with the predictions of parton model hadronization. These differences are significantly enhanced when polarization degrees of freedom are considered. We focus on semi-inclusive polarized Δ^{++} electroproduction from a polarized proton, $e\vec{p} \to e'\vec{\Delta}^{++}X^{-}$. (The decay products of Δ^{+} or Δ^{0} include neutrals whose detection would be more difficult.)

Because the g_1 structure function of a pion is zero, an unpolarized electron beam will suffice for this purpose. The produced Δs will appear predominantly in the target fragmentation region, or backward hemisphere in the $\gamma^{*}p$ c.m. frame, and hence will appear slow in the laboratory frame. With the high luminosity beam available at CEBAF the rate of Δ^{++} production will generally be high. Even though the efficiency with which low momentum Δs can be accurately identified is lower

than for fast baryons produced in the forward $\gamma^* p$ c.m. hemisphere, their detection may still be feasible with the CEBAF Large Acceptance Spectrometer.

II. KINEMATICS OF TARGET FRAGMENTATION

We define our variables in the laboratory frame as follows: l, l' are the momentum four-vectors of the initial and final electrons, $P_\mu = (M; 0, 0, 0)$ and $p_\mu = (p_0; |\mathrm{p}| \sin\alpha \cos\phi,\ |\mathrm{p}| \sin\alpha \sin\phi,\ |\mathrm{p}| \cos\alpha)$ are the momentum vectors of the target proton and recoil Δ, respectively, and $q_\mu = (\nu; 0, 0, \sqrt{\nu^2 + Q^2})$ denotes the photon 4-momentum, defined to lie along the positive z-axis. Then $\nu = E - E'$ is the energy transferred to the target, $y = \nu/E = 1 - E'/E$ is the fractional energy transfer relative to the incident energy, and $Q^2 = -q^2 = 2MExy$ is minus the four-momentum squared of the virtual photon, with $x = Q^2/2P\cdot q$. With the CEBAF upgrade to $E \approx 8-10$ GeV, values of $x \approx 0.13-0.14$ can be reached in the deep inelastic region for $\nu \approx 8$ GeV and $Q^2 \approx 2$ GeV^2.

The four-momentum transfer squared between the proton and Δ is $t = (P-p)^2 = -p_T^2/\zeta + t_{max}$, which is bounded from above by $t_{max} = -(M_\Delta^2 - M^2\zeta)(1-\zeta)/\zeta$, where $\zeta = p\cdot q/P\cdot q$ is the light-cone fraction of the target proton's momentum carried by the Δ. In terms of t, the three-momentum of the produced Δ is given by

$$|\mathrm{p}| = \frac{1}{2M}\sqrt{(M^2 + M_\Delta^2 - t)^2 - 4M^2 M_\Delta^2}\ , \tag{1}$$

so that in the lab. frame the slowest Δs are those for which $t \to 0$, which occurs when $\zeta \to 1$. As the upper limit on ζ is $1-x$, slow Δ production also corresponds to the $x \to 0$ limit, and the slowest possible particles produced at $\zeta = 1$ (at $x = 0$) have momentum $|\mathrm{p}_{min}| = (M_\Delta^2 - M^2)/2M \approx 340$ MeV. For the pion-exchange process considered here, the peak in the differential cross section occurs at $|\mathrm{p}| \sim 600$ MeV. This corresponds to a total c.m. energy squared of the photon–proton system of $W^2 = (P+q)^2 \sim 14$ GeV^2, and a missing mass of $p_X^2 = (k+q)^2 \sim 0.8$ GeV^2.

In terms of the laboratory angle α between the Δ and γ^* directions, where

$$\cos\alpha = \frac{M_\Delta^2 + (1-2\zeta)M^2 - t}{\sqrt{(M_\Delta^2 - M^2 - t)^2 - 4M^2 t}}, \tag{2}$$

production of Δs will occur between $\alpha = 0$ and $\alpha_{max} = \cos^{-1}\left(\sqrt{1 - (M\zeta/M_\Delta)^2}\right) \simeq 50^\circ$ for $\zeta \to 1$.

For studies of the spin dependence of the fragmentation process, we require the target proton polarization to be parallel to the photon direction, with the spin of the produced Δ quantized along its direction of motion. Experimentally, the polarization of the produced $\vec{\Delta}^{++}$ can be reconstructed from the angular distribution of its decay products (p and π^+).

III. DYNAMICS OF PION EXCHANGE

The relevant process is illustrated in Fig.1, where the dissociation of a physical proton into a π^- and Δ^{++} is explicitly witnessed by the probing photon. In the pion-exchange model the differential cross section is

$$\frac{d^5\sigma}{dx dQ^2 d\zeta dp_T^2 d\phi} = \left(\frac{\alpha^2}{M\ E^2\ x^2\ Q^4\ \zeta}\right) \frac{f_{\pi N\Delta}^2}{16\pi^2 m_\pi^2} \frac{\mathcal{T}^{S\ s}(t)\ \mathcal{F}_{\pi\Delta}^2}{(t-m_\pi^2)^2}\ L_{\mu\nu}(l,q)\ W_\pi^{\mu\nu}(k,q) \tag{3}$$

where $L_{\mu\nu} = 2l'_\mu l_\nu + 2l'_\nu l_\mu - g_{\mu\nu}Q^2$ is the lepton tensor, and

$$W_\pi^{\mu\nu} = -\left(g^{\mu\nu} + \frac{q^\mu q^\nu}{Q^2}\right)\ W_{1\pi}\ +\ \left(k^\mu + \frac{k\cdot q}{Q^2}q^\mu\right)\left(k^\nu + \frac{k\cdot q}{Q^2}q^\nu\right)\ \frac{W_{2\pi}}{m_\pi^2} \tag{4}$$

describes the $\gamma^*\pi$ vertex. The pion structure function is extracted from Drell-Yan experiments [5].

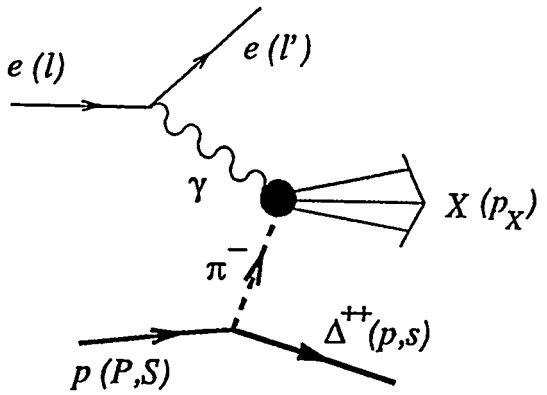


FIG. 1. Semi-inclusive deep inelastic scattering of an electron from a polarized proton target, with a polarized Δ^{++} in the final state.

For the $\pi N\Delta$ form factor in Eq.(3) we take the form suggested in Ref.[6] in an analysis of the pionic content of the proton in the infinite momentum frame,

$$\mathcal{F}_{\pi\Delta}(p_T^2,\zeta) = \left(\frac{\Lambda^2+M^2}{\Lambda^2+s_{\pi\Delta}}\right)^2 \tag{5}$$

where $s_{\pi\Delta} \equiv (m_\pi^2+p_T^2)/(1-\zeta)+(M_\Delta^2+p_T^2)/\zeta$. As discussed in Ref.[6], the formulation in the infinite momentum frame allows the use of the experimental structure function of the pion in Eq.(4).

The function $\mathcal{T}^{S\ s}(t)$ is obtained by evaluating the trace over the target nucleon spinor and the Rarita-Schwinger spinor-vector for the recoil Δ. Because it is emitted collinearly with the pion, production of Δ baryons with spin projection $\pm 3/2$ is forbidden, which leads to the selection rule:

$$\mathcal{T}^{S\ \pm\frac{3}{2}}(t) = 0. \tag{6}$$

The yield of spin projection $\pm 1/2$ states is given by

$$\mathcal{T}^{+\frac{1}{2}\ \pm\frac{1}{2}}(t) = \frac{1}{12M_\Delta^2}\left[(M-M_\Delta)^2-t\right]\ \left[(M+M_\Delta)^2-t\right]^2\ (1\pm\cos\alpha) \tag{7}$$

where α is also the angle between the polarization vectors S and s. Because the production of Δ baryons is limited to forward laboratory angles, the presence of the $(1\pm\cos\alpha)$ factor associated with the final state polarization will significantly suppress the $s=-1/2$ yield relative to that of $s=+1/2$ final states. This suppression leads to strikingly different predictions for the polarization asymmetry compared with those of the competing parton fragmentation process discussed below.

IV. BACKGROUNDS

At the large Q^2 and ν possible with an 8–10 GeV electron beam, the resonance backgrounds should not pose a major problem in identifying the required signal. Firstly, interference from quasi-elastic Δ^{++} production will not be present because of charge conservation. Secondly, the large $W(\sim 3-4$ GeV) involved means that interference from excited Δ^* states (with subsequent decay to Δ^{++} and pions) will be negligible. In addition, any such resonance contributions will be strongly suppressed by electromagnetic form factors at large Q^2 ($Q^2 \gtrsim 2$ GeV^2).

A potentially more important background will be that due to uncorrelated spectator fragmentation. Within the parton model framework the cross section for this process (assuming factorization of the x and ζ dependence) is proportional to [7] $\mathcal{F}_{p\uparrow}(x,Q^2)\ \widetilde{D}^s_{p\uparrow-q\uparrow\downarrow}(z,p_T^2)$, where $z=\zeta/(1-x)$ is

the light-cone momentum fraction of the produced baryon carried by the spectator system. The fragmentation function $\widetilde{D}(z,p_T^2)$ gives the probability for the polarized ($p^\uparrow$ minus $q^{\uparrow\downarrow}$) spectator system to fragment into a Δ^{++} with polarization s. The usual assumption is that the transverse momentum distribution of the Δ also factorizes, $\widetilde{D}^s_{p\uparrow-q\uparrow\downarrow}(z,p_T^2) = D^s_{p\uparrow-q\uparrow\downarrow}(z)\ \varphi(p_T^2)$, with $\int dp_T^2 \varphi(p_T^2) = 1$.

The function $\mathcal{F}_{p\uparrow}(x,Q^2)$ is proportional to the spin-weighted interacting-quark momentum distribution functions, $q^{\uparrow\downarrow}(x)$, where $\uparrow\downarrow$ denote quark spins parallel or antiparallel to the spin of the proton. For estimation purposes we consider the model for $q^{\uparrow\downarrow}(x)$ of Carlitz & Kaur [8]. The results change little if one uses the model of Schäfer [9], for example.

At large z the fragment Δ^{++} carries most of the parent system's momentum, and therefore contains both valence u quarks from the target proton. In our region of interest ($z \gtrsim 0.6$) by far the most important contributions to $D(z)$ come from the process whereby the Δ^{++} is formed after only one $u\bar{u}$ pair is created [10]. As a consequence DIS from valence u quarks will be unimportant. For scattering from sea quarks we assume the same fragmentation probabilities for $uuq\bar{q}$ spectator states as for uu (although at $Q^2 \simeq 2$ GeV^2 the sea constitutes at most $\sim 15\%$ of the cross section at $x \sim 0.1$). We thus parametrize the (very limited) EMC data [11] on unpolarized Δ^{++} muon production for $z \to 1$ as: $D_{uu}(z \to 1) = a(1-z)^b$, where $a \approx 0.68$ and $b \approx 0.3$.

For the spin dependence of the fragmentation process we follow the approach taken by Bartl et al. [12] in their study of polarized quark $\to$ baryon fragmentation. Namely, the diquark is assumed to retain its helicity during its decay, and the $q\bar{q}$ pair creation probability is independent of the helicity state of the quark q. At leading order this means that the produced baryon contains the helicity of the diquark, so that, for example, a $\Delta^{\Uparrow}$ or $\Delta^{\uparrow}$ can emerge from a $q^\uparrow q^\uparrow$ diquark, whereas a $\Delta^{\Downarrow}$ cannot. (Notation here is that $\Uparrow,\uparrow,\downarrow,\Downarrow$ represent $s = +3/2, +1/2, -1/2, -3/2$ states, respectively.)

The overall normalization of the spin-dependent fragmentation functions is fixed by the condition

$$\begin{aligned} q(x)\ D_{p-q}(z)\ +\ \bar{q}(x)\ D_{p-\bar{q}}(z)\ &= q^\uparrow(x)\ D_{p\uparrow-q\uparrow}(z)\ +\ q^\downarrow(x)\ D_{p\uparrow-q\downarrow}(z) \\ &+ \bar{q}^\uparrow(x)\ D_{p\uparrow-\bar{q}\uparrow}(z)\ +\ \bar{q}^\downarrow(x)\ D_{p\uparrow-\bar{q}\downarrow}(z) \end{aligned} \tag{8}$$

where $D(z) = \sum_{s=-3/2}^{+3/2} D^s(z)$. In relating the production rates for various polarized Δ^{++} we employ SU(6) spin-flavor wavefunctions, from which simple relations among the valence diquark $\to \Delta^{++}$ fragmentation functions, $D^s_{qq_{j(j_z)}}(z)$, can be deduced (the diquark state $qq_{j(j_z)}$ is labeled by its spin j and spin projection j_z). The leading functions are related by:

$$D^{\Uparrow}_{uu_{1(1)}}(z) = 3\ D^{\uparrow}_{uu_{1(1)}}(z) = \frac{3}{2} D^{\uparrow}_{uu_{1(0)}}(z) = \frac{3}{2} D^{\downarrow}_{uu_{1(0)}}(z), \tag{9}$$

with normalization determined from:

$$D^{\Uparrow}_{uu_{1(1)}}(z) = \frac{3}{4} D_{uu}(z). \tag{10}$$

(Note that this is true only when the spin projections of the diquark and Δ are in the same direction.) The non-leading fragmentation functions are those which require at least two $q\bar{q}$ pairs to be created from the vacuum, namely $D^{\Uparrow/\Downarrow}_{uu_{1(0)}}$, $D^{\downarrow/\Downarrow}_{uu_{1(1)}}$, $D^{\Uparrow/\uparrow/\downarrow/\Downarrow}_{ud_{0(0)}}$, $D^{\Uparrow/\uparrow/\downarrow/\Downarrow}_{ud_{1(0)}}$, and $D^{\Uparrow/\uparrow/\downarrow}_{ud_{1(1)}}$, and those which require 3 such pairs, $D^{\Downarrow}_{uu_{1(1)}}$ and $D^{\Downarrow}_{ud_{1(1)}}$. Except at very small z ($z \lesssim 0.2$) the latter functions are consistent with zero [10]. For the 2-$q\bar{q}$ pair fragmentation functions, we also expect that $D^{\Uparrow}_{uu_{1(0)}}(z) = D^{\Downarrow}_{uu_{1(0)}}(z)$. For $z \gtrsim 0.2$ the unpolarized model fragmentation functions of Ref.[10] requiring two $q\bar{q}$ pairs (e.g. $D_{ud}(z)$) are quite small compared with the leading fragmentation functions, $D_{ud}(z) \simeq 0.1\ D_{uu}(z)$. For spin-dependent fragmentation we therefore expect a similar behavior for those decay probabilities requiring two $q\bar{q}$ pairs created in order to form the final state with the correct spin and flavor quantum numbers. This then allows for a complete description of polarized fragmentation at large z in terms of only the 4 fragmentation functions in Eq.(9).

Finally, the p_T-integrated differential cross section for the electroproduction of a Δ^{++} with spin s can be written:

$$\frac{d^3\sigma}{dxdQ^2d\zeta} = \left(\frac{2\pi\alpha^2}{M^2E^2x(1-x)}\right)\left(\frac{1}{2x^2} + \frac{4M^2E^2}{Q^4}\left(1 - \frac{Q^2}{2MEx} - \frac{Q^2}{4E^2}\right)\right) \tag{11}$$
$$\times\left[\frac{4x}{9}\left(u_V^{\uparrow}D^s_{ud_{1(0)}} + 2\bar{u}^{\uparrow}\left(\frac{2}{3}D^s_{uu_{1(1)}} + \frac{1}{3}D^s_{uu_{1(0)}}\right) + u_V^{\downarrow}D^s_{ud_{1(1)}} + 2\bar{u}^{\downarrow}\left(\frac{2}{3}D^s_{uu_{1(1)}} + \frac{1}{3}D^s_{uu_{1(0)}}\right)\right)\right.$$
$$\left. + \frac{x}{9}\left(d_V^{\uparrow}D^s_{uu_{1(0)}} + 2\bar{d}^{\uparrow}\left(\frac{2}{3}D^s_{uu_{1(1)}} + \frac{1}{3}D^s_{uu_{1(0)}}\right) + d_V^{\downarrow}D^s_{uu_{1(1)}} + 2\bar{d}^{\downarrow}\left(\frac{2}{3}D^s_{uu_{1(1)}} + \frac{1}{3}D^s_{uu_{1(0)}}\right)\right)\right].$$

V. NUMERICAL RESULTS AND DISCUSSION

The differential cross section, $Q^2d^3\sigma/dxdQ^2d\zeta$, for the individual polarization states of the produced Δ^{++} (for DIS from a proton with $S = +1/2$) is shown in Fig.2, for $x = 0.14$, $Q^2 = 2$ GeV^2 and $E = 8$ GeV. The pion-exchange model predictions (solid curves) are for a form factor cut-off of $\Lambda = 800$ MeV, which gives $< n >_{\pi\Delta} \approx 0.02$ [6]. (For the same $< n >_{\pi\Delta}$ the cut-off in a t-dependent dipole form factor would be ~ 700 MeV.) The spectrum shows strong correlations between the polarizations of the target proton and Δ^{++}. In the quark-parton model (dashed curves) the correlations are significantly weaker, and the ratio of polarized Δs in this case is $s = +3/2 : +1/2 : -1/2 : -3/2 \approx 3 : 2 : 1 : 0$.

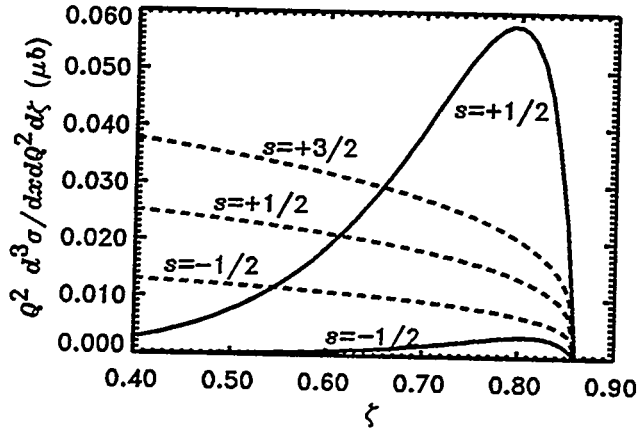


FIG. 2. Differential electroproduction cross section for various polarization states of the Δ^{++}. The π-exchange model, with cut-off mass $\Lambda = 800$ MeV, is shown by solid curves. The quark-parton model background (dashed curves) is estimated using the fragmentation function extracted from the unpolarized EMC data [12] and Eqs.(9) and (10).

The differences between the pion-exchange model and fragmentation backgrounds can be further enhanced by examining polarization asymmetries. In Fig.3 we show the difference $\sigma^+ - \sigma^-$, where $\sigma^{\pm} \equiv Q^2d^3/dxdQ^2d\zeta(s = \pm 1/2)$, as a fraction of the total unpolarized cross section. The resulting ζ distributions are almost flat, but significantly different for the two models.

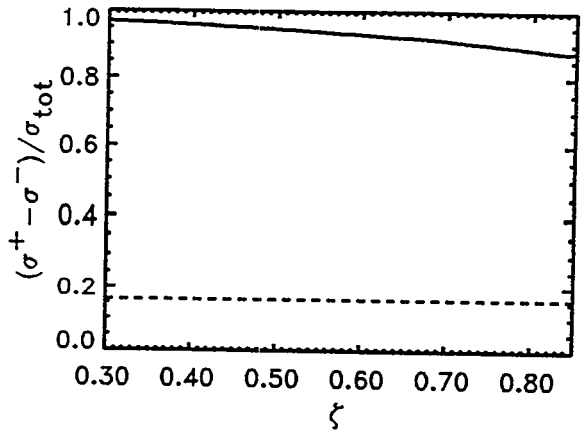


FIG. 3. Polarization asymmetry, with $\sigma^{\pm}$ as defined in the text, and $\sigma_{\rm tot}$ is the sum over all polarization states.

Of course the two curves in Fig.3 represent extreme cases, in which Δs are produced entirely via pion emission or diquark fragmentation. In reality we can expect a ratio of polarization cross sections which is some average of the curves in Fig.3. The amount of deviation from the parton model curve will indicate the extent to which the pion-exchange process contributes. From this, one can in turn deduce the strength of the $\pi N\Delta$ form factor. Unlike inclusive DIS, which can only be used to place upper bounds on the pion number, the semi-inclusive measurements could pin down the absolute value of $< n >_{\pi\Delta}$. A measurement of this ratio would thus be particularly useful in testing the relevance of non-perturbative degrees of freedom in high energy DIS process.

References.

[1] E.D.Bloom, et.al., *Phys.Rev.Lett.* **23** (1969) 930; M.Breidenbach, et.al., *Phys.Rev.Lett.* **23** (1969) 935; J.J.Aubert et al. (EM Collaboration), *Phys.Lett.* **123B** (1983) 275.
[2] P.Amaudruz et al. (New Muon Collaboration), *Phys.Rev.Lett.* **66** (1991) 2712.
[3] E.M.Henley and G.A.Miller, *Phys.Lett.* **B 251** (1990) 497; A.I.Signal, A.W.Schreiber and A.W.Thomas, *Mod.Phys.Lett.* **A6** (1991) 271; W.Melnitchouk, A.W.Thomas and A.I.Signal, *Z.Phys.* **A340** (1991) 85; S.Kumano and J.T.Londergan, *Phys.Rev.* **D44** (1991) 717.
[4] J.D.Sullivan, *Phys.Rev.* **D5** (1972) 1732; A.W.Thomas, *Phys.Lett.* **126B** (1983) 97.
[5] B.Betev, et.al. (NA10 Collaboration), *Z.Phys.* **C28** (1985) 15.
[6] W.Melnitchouk and A.W.Thomas, *Phys.Rev.* **D 47** (1993) 3794; A.W.Thomas and W.Melnitchouk, in: Proceedings of the JSPS-INS Spring School (Shimoda, Japan), (World Scientific, Singapore, 1993).
[7] R.D.Field and R.P.Feynman, *Nucl.Phys.* **B 136** (1978) 1; N.Schmitz, *Int.J.Mod.Phys.* **A3** (1988) 1997.
[8] R.Carlitz and J.Kaur, *Phys.Rev.Lett.* **D 38** (1977) 674; 1102.
[9] A.Schäfer, *Phys.Lett.* **B 208** (1988) 175.
[10] J. Levelt and P.J. Mulders, *Phys.Rev.* **D 49** (1994) 96.
[11] A.Bartl, H.Fraas and W.Majoretto, *Phys.Rev.* **D 26** (1982) 1061.
[12] M.Arneodo et al. (EM Collaboration), *Nucl.Phys.* **B 264** (1986) 739.
[13] J.F.Donoghue, *Phys.Rev.* **D 17** (1978) 2922; A.Bartl, H.Fraas and W.Majoretto, *Z.Phys.* **C 6** (1980) 335.

On the A-dependence of σ_L/σ_T: skeletons in the shadow

Joseph Milana
Nuclear Theory Group, Department of Physics
University of Maryland
College Park, Maryland 20742
milana@quark.umd.edu

Abstract:

A most counter–intuitve dependence in the differential cross–section in the shadowing regime is shown to result from a higher–twist nuclear enhancement in $R = \sigma_L/\sigma_T$ which severely complicates the unravelling from present data the corresponding dependence in Q^2 of the nuclear structure functions, $F_2^A(x, Q^2)$. Indeed, until precision measurements close this loophole, the extrapolations of the structure functions to either higher Q^2 or other processes (as is neccessary to address present data at FNAL or future experiments at RHIC) must be considered problematic. The contribution CEBAF can make in this regard by providing systematic determination of $R_A(x, Q^2)$ is thus emphasized.[1]

This talk is based on a recent paper that will be appearing soon (I hope) in Physical Review C.[2] Its purpose is to motivate an experiment CEBAF can and should do, especially if upgraded to higher energies. While providing information on nuclear structure that is interesting in itself, the added motivation is that precision results will have I believe, important impact on other high–energy experiments involving nuclear targets that have been, and will continue to be done all over the world.

Let me recall that for a Rosenbluth decomposition the double–differential cross–section for deep inelastic scattering (DIS) can be written in the lab. frame as:

$$\frac{d^2\sigma}{d\Omega dE'} = \Gamma\sigma_\perp(x, Q^2)[1 + \epsilon R(x, Q^2)]$$

in which the variables

$$\Gamma = \frac{\alpha E'}{4\pi^2 ME}\left(\frac{1}{x} - 1\right)\frac{1}{1-\epsilon}$$
$$\epsilon = \left[1 + (1 + \nu^2/Q^2)tan^2(\frac{1}{2}\theta)\right]^{-1}$$

and most importantly, R is the ratio of longitudinal to transverse polarization cross–sections of the virtual photon:

$$R(x, Q^2) = \frac{\sigma_L}{\sigma_\perp} = \frac{F_L(x, Q^2)}{2xF_1(x, Q^2)} = \frac{\left(1 + \frac{4x^2M^2}{Q^2}\right)F_2(x, Q^2)}{2xF_1(x, Q^2)} - 1.$$

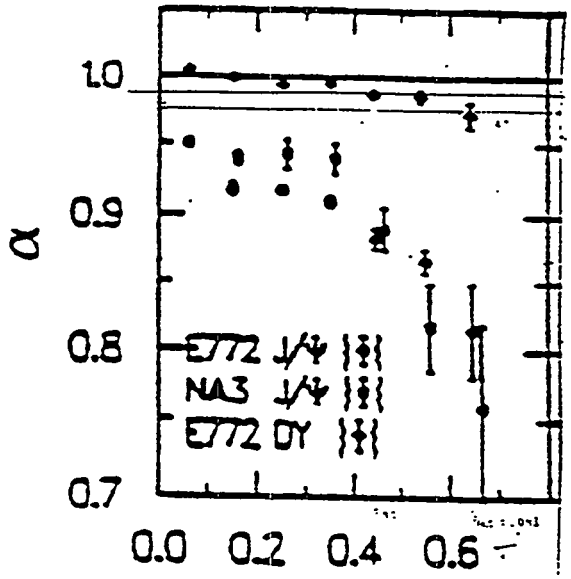
[1] presented: Workshop on CEBAF at Higher Energies, April 14–16, 1994.
[2] J. Milana, *On the A dependence of $R = \sigma_L/\sigma_T$ and the Q^2 dependence of Shadowing*, U. of MD PP #94-039 (1993).

Now, in the pure Bjorken scaling limit (also coincidentally, at $Q^2 = 0$ since for real photons $\sigma_L = 0$)

$$R_{Bj}(x) = 0$$

which follows by Helicity Conservation and is summarized by the Callan-Gross relation: $2xF_1(x) = F_2(x)$. However, $R(x, Q^2) \neq 0$ since pure Bjorken scaling is violated, both by pQCD corrections and due to higher–twist effects. Both of these corrections effectively give the struck quark a relative transverse momentum with respect to the center–of–mass frame defined by the virtual photon and proton so that $R(x, Q^2)$ is no longer tied to helicity–conservation (which is never violated on the quark level for massless quarks).

We now come to an interesting question, **What about a Nuclear Dependence to R?.** Beyond addressing potentially interesting questions of nuclear structure and the distribution/redistribution of quark degrees of freedom inside a nucleus, the determination of the nuclear dependence of R is crucial for understanding important unsettled issues in the Shadowing regime[3] regarding applications to other processes, *e.g.*:



- Drell–Yan production at FNAL,[4]
- J/ψ production at CERN and FNAL.[5]

[3]See also other recent work on a nuclear dependence to R in the shadowing region by: V. Del Duca, S. J. Brodsky and P. Hoyer, Phys. Rev. D46, 931 (1992); and also, N. N. Nikolaev and V. I. Zakharov, Z. Phys. C49, 607 (1991); V. Barone *et. al.*, Phys. Lett. B304, 176 (1993).

[4]D. M. Alde *et al.*, Phys. Rev. Lett. 64, 2479 (1990).

[5]J. Badier *et al.*, Z. Phys. C20, 101 (1983); D. M. Alde *et al.*, Phys. Rev. Lett. 66, 133 (1991).

As figure (1) indicates (reprinted from Alde *et al.*, ref. [5]) a distinct suppression develops in both these processes as a function of Feynman x. At large x_F, both these processes occur deeply in the shadowing regime of the nuclear target, however they also are occuring at large Bjorken x for the proton projectile where the stucuture functions are rapidly varying (roughly $\sim (1-x)^3$) and it is conceivable that the trends in the data are associated with projectile rather than target effects, especially since both the Drell–Yan and charmonium data are at much larger invariant masses than the associated measurements for DIS. [6]

Finally, I underscore the importance of our understanding shadowing by referring to studies of the Columbia, Duke, and Helsinki groups[7], where it is conceivable that nearly everything of interest to be seen at RHIC or the LHC will evolve from minijets calculable in pQCD. These minijets, *i.e.* jets with $p_\perp^2 \sim 2(\mathrm{GeV})^2$, are produced dominantly by gluon–gluon scatterings, occuring form gluon distribution functions evaluated deep within the shadowing regime of both of the colliding nucleii. A coherent understanding of shadowing in DIS is thus clearly neccessary.

The major issue at concern is, **What is the (large) Q^2 dependence of Shadowing?** We can rewrite the double–differential cross–section as:

$$\frac{d^2\sigma}{dxdQ^2} = \frac{4\pi\alpha_e^2}{Q^4}\frac{F_2(x,Q^2)}{x}\left[1 - \frac{Q^2}{2MEx} - \frac{Q^2}{4E^2} + \frac{Q^4}{8M^2E^2x^2}\left(\frac{1+4M^2x^2/Q^2}{1+R(x,Q^2)}\right)\right], \quad (1)$$

It is this double–differential cross–section that in fact is measured in DIS. In general we are interested in extracting the nuclear dependence of the structure functions $F_2(x,Q^2)$, which would, if leading twist, then provide information on the distribution of quarks inside a nucleus (easily) applicable to other processes. For most values of Bjorken x, the data taken at SLAC and CERN are over a range of large Q^2 for which R has been measured, is known to be small, and given fairly well by its value predicted by pQCD. However in the shadowing regime the situation is different. Here, not only has R never been actually measured (therefore requirng that we resort to an extrapolation, see [8] for a phenomenological fit to the world's data on $R(A=1)$ canonically used for this purpose), but by kinematic definitions and constraints, in order to probe small x with a fixed beam energy, one must lower Q^2.

We now come to the main question of this talk, **What about R_A?**

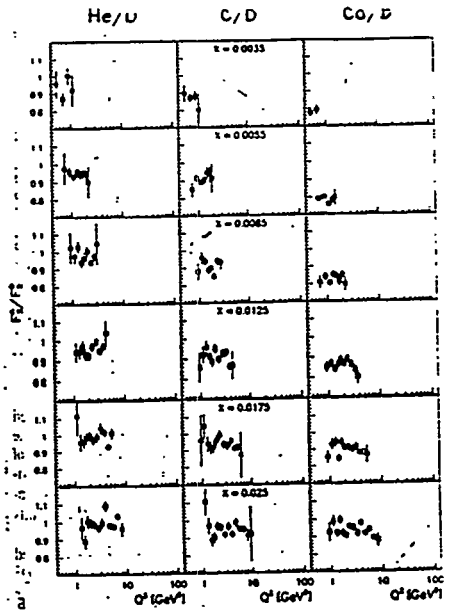
[6] S. Gavin and J. Milana, Phys. Rev. Lett. **68**, 1834 (1992); S. J. Brodsky, P. Hoyer, A. H. Mueller and W-K. Tang, Nucl. Phys. **B369**, 519 (1992).

[7] As a partial listing: R. C. Hwa and K. Kajantie, Phys. Rev. Lett. **56**, 696 (1986); J.-P. Blaizot and A. H. Mueller, Nucl. Phys. **B289**, 847 (1987); A. H. Mueller, Nucl. Phys. **A498**, 41c (1989); K. Kajantie, P. V. Landshoff, and J. Lindfors, Phys. Rev. Lett. **59**, 2527 (1987); K. J. Eskola, K. Kajantie, and J. Lindfors, Nucl. Phys. **B323**, 37 (1989); K. Geiger and B. Müller, Nucl. Phys. **B369**, 600 (1992); K. Geiger, Phys. Rev. D **47**, 133 (1993).

[8] L. W. Whitlow *et al.*, Phys. Lett. **B250**, 193 (1990). Beware, there is a typo in the first coefficent of the printed phenomenological formula.

Such a conjectured dependence was in fact once proposed by [9] to account for the initial discrepancies between the EMC and SLAC data for $x \approx .1$. Besides the ultimate experimental resolution, the shift used, $\Delta R \approx .15$, (taken Q^2 independent, to fit the wide range of Q^2 available at these x) does not seem to be supported by later experiments[10] at SLAC devoted to measuring ΔR. We're now though interested in ΔR at small x, for which Amaudruz *et al.*[11] is the sole source of experimental information. This data (as was that from SLAC) is consistent with a value for $\Delta R = 0$, but with such large error bars that the best one should probably safely conclude is that $\Delta R(x < .1) < .1$ (the situation for the SLAC data is slightly better so that reasonablely $\Delta R(x > .1) < .05$). However it should be emphasized that because of the experimental difficulty in measuring this quantity, a systematic double–binning in both x and Q^2 for $\Delta R(x, Q^2)$ in either data is lacking. The importance that CEBAF could hopefully improve upon this situation is of course the subject of this talk.

Some trivial observations upon R. First note that in (1), for fixed Q^2, the sensitivity to small x increases. Similarly note for fixed x and growing Q^2. Figure (2) displays the only data[12] for the double–differential cross–section (1) for some indicative values of Bjorken x in the shadowing regime.



Now for a surprise. A higher–twist nuclear enhancement in R is conjectured.

$$\begin{aligned} R^A &= R^{fit} + \Delta R \\ \Delta R &\sim \frac{1}{Q^2} \end{aligned} \tag{2}$$

The motivation for such a conjecture comes from a long history of higher twist calculations[13]

[9] I. A. Savin and G. I. Smirnov, Phys. Lett. **B145**, 438 (1984).
[10] S. Dasu *et al.*, Phys. Rev. Lett. **60**, 2591 (1988).
[11] P. Amaudruz *et al.*, Phys. Lett. **B294**, 120 (1992).
[12] P. Amaudruz *et al.*, Z. Phys. **C51**, 387 (1991).
[13] H. D. Politzer, Nucl. Phys. **B172**, 349 (1980); S. P. Lutrell and S. Wada, Nucl. Phys. **B197**, 290

in which the longitudinal structure function entering the definition of R is given by

$$F_L^{\tau=4}(x,Q^2) = \frac{4\Lambda^2}{Q^2} T_1(x),$$

where $T_1(x)$ is a new nucleon matrix element involving the transverese component of covariant derivative acting upon quark fields. In the limit one ignores that this is a covariant derivative, one obtains the intuitive parton picture result that $F_L^{\tau=4}$ is related to the average transverse momentum of the quarks inside a nucleus:

$$\lim_{g\to 0} \frac{4\Lambda^2 T_1(x)}{Q^2} = \frac{4}{Q^2}\int d^2k_\perp k_\perp^2 f(x,k_\perp^2) = 4\frac{\langle k_\perp^2\rangle}{Q^2},$$

where in the parton model $f(x,k_\perp^2)$ is related to $F_2(x)$ by

$$F_2^{\tau=2}(x) = x\int d^2k_\perp f(x,k_\perp^2).$$

A higher–twist nuclear enhancement to R is conjectured. From first principles $T_1(A)$ is both uncalculable and for the case of $A > 1$, a detailed nuclear–structure question. We know however that there is at the very least fermi–momentum, and thus using this to set the scale of a nuclear enhancement, I take therefore for a nuclear enhancement in R, an added transverse momentum for the quarks (ignoring the nontrivial caveat that parton intuition fails as $x \to 0$)

$$k_\perp = .3\text{GeV} \approx k_{fermi}.$$

Such an enhancement is consistent with the result that $\Delta R \leq .05$ for the larger Q^2 values (ones of interest). I also take in the curves to follow the effect to be x independent. The sensitivity in the ratio of nuclear to nucleon, double–differential cross–section to such an effect is shown in figure (3) for the CERN kinematics leading to figure (2). The various x values for each of the curves are labelled, and each curve cuts off at the kinematic upper bounds for Q^2 obtainable at the CERN runs. I urge comparison back to figure (2) where one sees that these effects are comparable in magnitude at the large Q^2 values to the total effect being measured.

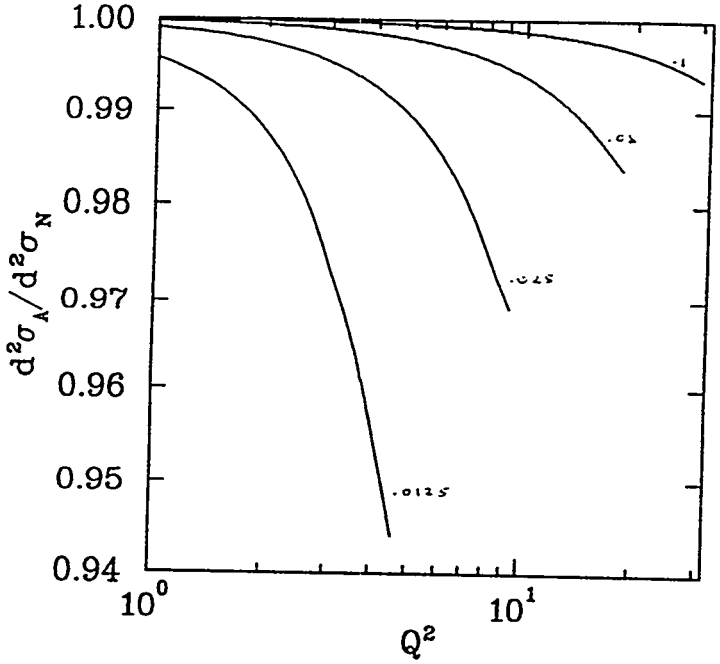
Let me summarize what is happening. First I note that for all curves, as Q^2 decreases the effect in figure (3) disappears, even though the shift in R *ala* (2) is increasing. Clearly this then is not the source of shadowing in general. Nevertheless kinematic factors in (1) are dominating so that as Q^2 increases the sensitivity to such a nuclear dependence to R increases, so that even though higher–twist (*i.e.* dropping as Q^{-2}) the effect is potentially significant in the observed rate. The key point to realize is that at the ends of phase–space, higher–twist effects cannot in general be ignored so that beyond x and Q^2, also crucial is the kinematic variable

$$y = \frac{Q^2}{2MxE} = \frac{\nu}{E},$$

(1982); R. L. Jaffe and M. Soldate, Phys. Rev. **D26**, 49 (1982); R. K. Ellis, W. Furmanski and R. Petronzio, Nucl. Phys. **B212**, 29 (1983); J. Qiu and G. Sterman, Nucl. Phys. **353**, 105 (1991).

the fractional energy loss experienced by the incoming lepton.

The conclusion therefore is that the shadowing regime is critically sensitive to $R_A(x,Q^2)$, and that we must get a handle on its nuclear dependence before unravelling $F_2^A(x,Q^2)$. Indeed, to put it more strikingly, one could claim that in fact NO data exists for the structure functions in the shadowing regime. If $R_A(x,Q^2)$ has the type of enhancement here conjectured, then the relatively flat curves in figure (2) could only be explained by a corresponding vanishing in $F_2^A(x,Q^2)$: i.e. its nuclear dependence would also be higher–twist!



We come finally to the question, **What can CEBAF do about this dilemma?**
First I note that, CEBAF

- cannot access (at large Q^2) the shadowing regime,

however, CEBAF

- CAN get precise measurement of $R_A(x,Q^2)$,

for range of x hopefully approaching the shadowing regime and a range of Q^2 for each x. This then would be informative, and highly suggestive if any nuclear enhancement is in fact seen for $x \to .1$. I end with a simple table showing the kinematic possibilities in this regard of an energy upgraded CEBAF.

E_{beam}	$\sim \nu_{max}$	$Q^2_{max} : x = .05$	$x = .1$	$x = .2$
6	5	...	1	2
10	9	...	1.8	3.6
15	14	1.4	2.8	5.6

TIME REVERSAL ODD FRAGMENTATION FUNCTIONS IN SEMI-INCLUSIVE DEEP INELASTIC LEPTON-HADRON SCATTERING

P.J. MULDERS
National Institute for Nuclear Physics and High Energy Physics (NIKHEF-K), P.O. Box 41882, NL-1009 DB Amsterdam, the Netherlands

and

J. LEVELT
Institut für Theoretische Physik, University of Erlangen-Nürnberg Staudtstrasse 7, D-91508 Erlangen, Germany

ABSTRACT

In semi-inclusive scattering of polarized leptons from unpolarized hadrons, one can measure a time reversal odd structure function. It shows up as a $\langle \sin\phi \rangle$ asymmetry of the produced hadrons. This asymmetry can be expressed as the product of a twist-three "hadron $\longrightarrow$ quark" profile function and a time reversal odd twist-two "quark $\longrightarrow$ hadron" fragmentation function. This fragmentation function can only be measured for nonzero transverse momenta of the produced hadron. Its appearance is a consequence of final state interactions between the produced hadron and the rest of the final state.

1. Leptoproduction of hadrons

In this paper we emphasize the importance of measuring the dependence on transverse momenta in electroproduction of hadrons and the possibility to measure some novel structure functions[1]. To be precise we investigate the process

$$e + H \longrightarrow e' + h + X, \tag{1}$$

where e and e' are the incoming and scattered electrons with momenta k and k', H is the hadronic target with momentum P, h is the produced hadron with momentum P_h and X is the unobserved rest of the final state. The differential cross section for this process is written as a product of a leptonic and hadronic tensor,

$$\frac{d\sigma}{dx_B\, dz\, dy\, d^2\boldsymbol{q}_T} = \frac{\pi\alpha^2\, y\, z}{2Q^4} L_{\mu\nu}\, 2M\mathcal{W}^{\mu\nu}, \tag{2}$$

where we have used the invariants expressed in the external momenta and the momentum q of the exchanged virtual photon, which is spacelike ($q^2 = -Q^2$),

$$x_B = \frac{Q^2}{2P\cdot q}, \quad z = \frac{P\cdot P_h}{P\cdot q} \approx -\frac{2P_h\cdot q}{Q^2}, \quad y = \frac{P\cdot q}{P\cdot k}, \tag{3}$$

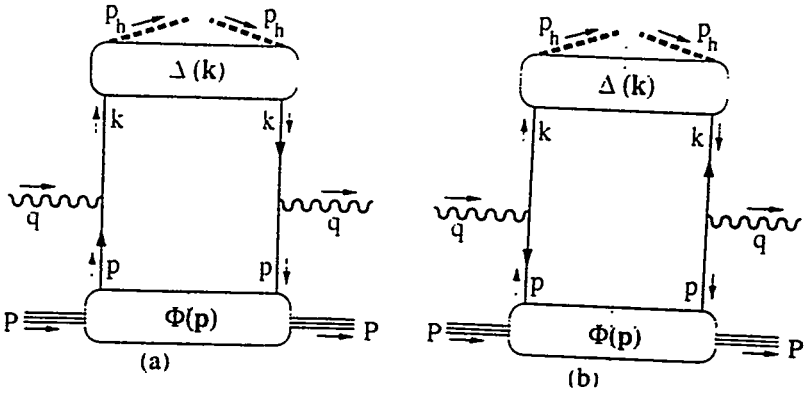


Figure 1: The Born terms in the expansion of the hadronic tensor.

and $\boldsymbol{q}_T$ is the transverse momentum of the photon in the frame in which the hadrons H and h are collinear. This translates to a perpendicular momentum of the produced hadron equal to $\boldsymbol{P}_{h\perp} = -z\boldsymbol{q}_T$ in the (more commonly used) frame in which the target hadron H and the photon are collinear. The leptonic tensor for polarized electrons with helicity $\lambda = \pm 1$ is of the form

$$L_{\mu\nu}(k,k',\lambda) = \left(2k_\mu k'_\nu + 2k_\nu k'_\mu - Q^2 g_{\mu\nu} + 2i\lambda\epsilon_{\mu\nu\rho\sigma}q^\rho k^\sigma\right). \tag{4}$$

and the (unpolarized) hadronic tensor is of the form

$$\begin{aligned} 2M\mathcal{W}_{\mu\nu}(q,P,P_h) &= \frac{1}{(2\pi)^4}\int \frac{d^3P_X}{(2\pi)^3 2P_X^0}(2\pi)^4\delta^4(q+P-P_X-P_h) \\ &\quad \times\langle P|J_\mu(0)|P_X,P_h\rangle\langle P_X,P_h|J_\nu(0)|P\rangle, \end{aligned} \tag{5}$$

where averaging and summation over spins is assumed. In all of our considerations we will keep all contributions of order $1/Q$, as it turns out that the time reversal odd structure function, that we investigate, contributes at the twist-3 level. It contains the product of a twist-3 profile function in the $H \to q$ part of the process and a time reversal odd twist-2 fragmentation function in the $q \to h$ part of the process. We will also not discuss any further the factorization of the process or the inclusion of radiative corrections. We assume that we can use the diagrammatic expansion for the hard process as outlined by Ellis, Furmánski and Petronzio (EFP)[2]. In this approach diagrams are separated in a hard scattering part and soft correlation functions[3].

The diagrammatic expansion of EFP is useful for deep inelastic scattering, because it in an appropriately chosen (color) gauge corresponds to an expansion in powers of Q^{-1}. This twist expansion as used here is discussed in refs[4,5,6]. The Born diagrams in this expansion are given in Fig. 1 and give[5]

$$2M\,\mathcal{W}_{\mu\nu}(q,P,P_h) = \frac{1}{2}\int d^4p\,d^4k\,\delta^4(p+q-k)\,\mathrm{Tr}\left(\gamma_\mu\Phi(p)\gamma_\nu\Delta(k)\right) + \left\{\begin{array}{c} q\leftrightarrow -q \\ \mu\leftrightarrow\nu \end{array}\right\}, \tag{6}$$

where the (soft) quark correlation functions are given by

$$\Phi_{ij}(p) = \frac{1}{(2\pi)^4}\int d^4x\, e^{ip\cdot x}\,\langle P|\overline{\psi}_j(0)\psi_i(x)|P\rangle, \tag{7}$$

$$\Delta_{ij}(k) = \sum_X \frac{1}{(2\pi)^4}\int d^4x\, e^{ik\cdot x}\,\langle 0|\psi_i(x)|P_h,X\rangle\langle P_h,X|\overline{\psi}_j(0)|0\rangle. \tag{8}$$

2. The twist analysis

In order to analyze the result it is useful to use lightcone coordinates for the external momenta P, P_h and q and the integration variables p and k. Using the representation $p = [p^-, p^+, \boldsymbol{p}_T]$ where $p^\pm = (p^0 \pm p^3)/\sqrt{2}$ we write in a frame where H and h are collinear

$$\begin{aligned}
P &= \left[\frac{x_B M^2}{A\sqrt{2}}, \frac{A}{x_B\sqrt{2}}, 0_T\right],\\
p &= \left[p^-, \frac{A}{\sqrt{2}}, \boldsymbol{p}_T\right],\\
q &= \left[\frac{Q^2}{A\sqrt{2}}, -\frac{A}{\sqrt{2}}, \boldsymbol{q}_T\right],\\
k &= \left[\frac{Q^2}{A\sqrt{2}}, k^+, \boldsymbol{k}_T\right],\\
P_h &= \left[\frac{zQ^2}{A\sqrt{2}}, -\frac{AM_h^2}{zQ^2\sqrt{2}}, 0_T\right],
\end{aligned} \tag{9}$$

This parametrization is consistent with $p + q = k$ and has been made under the assumption that the quark momenta are limited to a hadronic scale Λ of the order of a few hundred MeV. More precisely, p^2, $P\cdot p$, and k^2, $P_h\cdot k$ are of hadronic scale.

In the deep inelastic limit the process factorizes. For the $H \to q$ part one integrates over p^-. One can then analyze the Dirac content of the projections

$$\Phi^{[\Gamma]}(x_B, \boldsymbol{p}_T) = \frac{1}{2}\int dp^-\; Tr(\Phi\,\Gamma)\Big|_{p^+ = x_B P^+,\; \boldsymbol{p}_T}. \tag{10}$$

Using for Φ the constraints imposed by hermiticity, parity and time reversal invariance one obtains for an unpolarized hadron

$$\Phi^{[\gamma^+]} = f_1(x_B, \boldsymbol{p}_T), \tag{11}$$

$$\Phi^{[1]} = \frac{M}{P^+}\, e(x_B, \boldsymbol{p}_T), \tag{12}$$

$$\Phi^{[\gamma^i]} = \frac{p_T^i}{P^+}\, f^\perp(x_B, \boldsymbol{p}_T), \tag{13}$$

where f_1 is the well-known twist-2 quark distribution function, in which the $\boldsymbol{p}_T$-dependence is kept and e and $f^\perp$ are the twist-3 profile functions discussed in refs[4,5], respectively.

For the $q \to h$ part one can integrate over k^+ and analyze the Dirac content of the projections

$$\Delta^{[\Gamma]}(z, \boldsymbol{k}_T) = \frac{1}{4z} \int dk^+ \, Tr(\Delta\, \Gamma)\Big|_{k^- = P_h^-/z,\ \boldsymbol{k}_T}. \tag{14}$$

As the definition of Δ involves states $|P_h, X\rangle$, which are out-states, one cannot use constraints from time reversal invariance. As a consequence one obtains

$$\Delta^{[\gamma^-]} = D_1(z, -z\boldsymbol{k}_T), \tag{15}$$

$$\Delta^{[i\sigma^{i-}\gamma_5]} = \frac{\epsilon_T^{ij} k_{Tj}}{M_h} H_1^\perp(z, -z\boldsymbol{k}_T), \tag{16}$$

$$\Delta^{[1]} = \frac{M_h}{P_h^-} E(z, -z\boldsymbol{k}_T), \tag{17}$$

$$\Delta^{[\gamma^i]} = \frac{k_T^i}{P_h^-} D^\perp(z, -z\boldsymbol{k}_T), \tag{18}$$

$$\Delta^{[i\sigma^{ij}\gamma_5]} = \frac{M_h\, \epsilon^{ij}}{P_h^-} H(z, -z\boldsymbol{k}_T), \tag{19}$$

where D_1 is the well-known twist-2 quark fragmentation function of which the $\boldsymbol{k}_T$-dependence translates into a dependence on the transverse momenta of produced hadrons. Furthermore a time reversal odd twist-2 fragmentation function $H_1^\perp$ appears, which can only be measured when the dependence on the transverse momenta is measured, e.g. in azymuthal asymmetries. At the twist-3 level one finds the profile functions E (ref.[4]), $D^\perp$ (ref.[5]) and a time reversal odd function H.

One can gain insight in the nature of these time reversal odd functions by noting[7] that $|P_h, X; out\rangle = e^{2i\delta_{hX}} |P_h, X; in\rangle$ Bypassing complications of doing proper partial wave expansion, the constraints from time-reversal show that the functions D_1, E and $D^\perp$ are proportional to $\cos\delta_{hX}$, while the functions $H_1^\perp$ and H are proportional to $\sin\delta_{hX}$.

3. Results

The twist-2 functions are the ones that appear if one evaluates the result for the hadronic tensor in leading order. This yields

$$2M\, \mathcal{W}_{\mu\nu} = \left(\frac{q_\mu q_\nu}{q^2} - g_{\mu\nu} + \frac{\tilde{P}_\mu \tilde{P}_\nu}{\tilde{P}^2} \right) 2z\, I[f_1\, D_1], \tag{20}$$

where $\tilde{P} = P - (P\cdot q/q^2)\, q$, $\tilde{P}^2 = Q^2/4x^2$, and

$$I[f_1\, D_1] = \int d^2p_\perp\, d^2k_\perp\, \delta^2(\boldsymbol{p}_\perp + \boldsymbol{q}_T - \boldsymbol{k}_\perp)\, f_1(x_B, \boldsymbol{p}_\perp)\, D_1(z, -z\boldsymbol{k}_\perp). \tag{21}$$

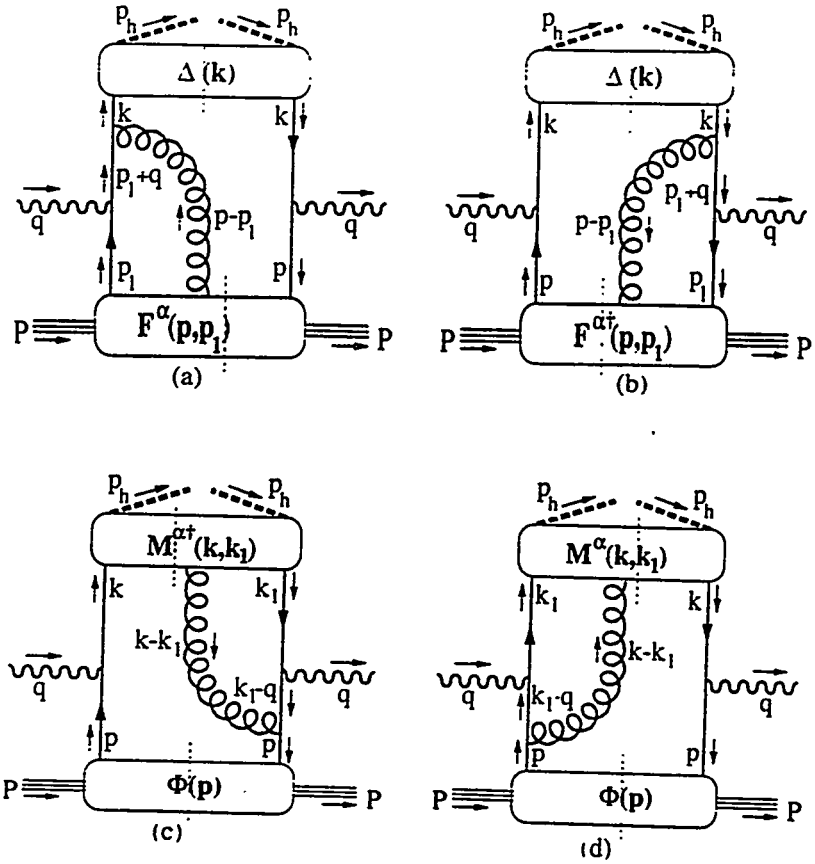


Figure 2: The contributions from quark - quark - gluon correlation functions in the expansion of the hadronic tensor. Only the quark part is shown.

We will consider the situation in which

$$f(x_B, \boldsymbol{p}_\perp) = f(x_B, 0)\, \exp(-R_H^2 \boldsymbol{p}_\perp^2), \tag{22}$$

$$D(z, -z\boldsymbol{k}_\perp^2) = D(z, 0)\, \exp(-R_h^2 \boldsymbol{k}_\perp^2). \tag{23}$$

In that case the above integral can be written as

$$I[f_1\, D_1] = \frac{\pi}{R_H^2 + R_h^2} \exp\left(-\frac{\boldsymbol{q}_T^2 R_H^2 R_h^2}{R_H^2 + R_h^2}\right) f_1(x_B, \mathbf{0}_T)\, D_1(z, \mathbf{0}_T). \tag{24}$$

Integrating over the perpendicular momenta of the produced hadron, i.e. over $\boldsymbol{q}_T$ one obtains the familiar factorized form $f_1(x_B)\, D_1(z)$, where $f_1(x_B) = \int d^2 p_T\, f_1(x_B, \boldsymbol{p}_T)$ is the lightcone momentum distribution and $D_1(z) = \int d^2 P_{h\perp} D_1(z,\ \boldsymbol{P}_{h\perp})$ is the fragmentation function. Finally it should be noted that everywhere the summation over quark flavors has been suppressed. Together with the antiquark part, it can easily be reinstated by adding a summation over flavors of quarks *and* antiquarks weighted with the charge squared (e_i^2) and labeling the functions as $f_1^{i/H}$ and $D_1^{h/i}$ respectively.

The Born contribution to $\mathcal{W}_{\mu\nu}$ also gives a contribution at subleading $\mathcal{O}(1/Q)$). These involve the twist-3 functions defined above. At the same order, however, also

contributions from diagrams with gluons, as shown in Fig. 2 for quarks, must be included. They give in addition to the result in Eq. 6 contributions that involve quark - quark - gluon correlation functions. These contributions can be rewritten in terms of the earlier defined (twist-3) projections of quark-quark correlation function.

The full (electromagnetically gauge invariant) result up to O(1/Q) reads

$$
\begin{aligned}
2M\,\mathcal{W}_{\mu\nu} \;=\; & \int d^2p_T\, d^2k_T\, \delta^2(\boldsymbol{p}_T + \boldsymbol{q}_T - \boldsymbol{k}_T) \\
& \times \Bigg[\left(\frac{q_\mu q_\nu}{q^2} - g_{\mu\nu} + \frac{\tilde{P}_\mu \tilde{P}_\nu}{\tilde{P}^2} \right) 2z\, f_1\, D_1 \\
& + \frac{(\tilde{P}_\mu p_{\perp\nu} + \tilde{P}_\nu p_{\perp\mu})}{Q^2}\, 8x_B z\, f^\perp\, D_1 \\
& + \frac{(\tilde{P}_\mu k_{\perp\nu} + \tilde{P}_\nu k_{\perp\mu})}{Q^2}\, 8z\, f_1 \left(\frac{1}{z} D^\perp - D_1 \right) \\
& + i\, \frac{(\tilde{P}_\mu k_{\perp\nu} - \tilde{P}_\nu k_{\perp\mu})}{Q^2}\, 8z\, \frac{M}{M_h} \left(x_B e - \frac{m}{M} f_1 \right) H_1^\perp \Bigg],
\end{aligned}
\tag{25}
$$

where $p_\perp$ is constructed from the vector that in the frame where the hadrons (H and h) are collinear is $p_T = [0, 0, \boldsymbol{p}_T]$ by subtracting the projection along q, i.e. $p_\perp = p_T + (\boldsymbol{p}_T \cdot \boldsymbol{q}_T/q^2)\, q$. This vector is orthogonal to q. Note, however that neglecting $1/Q^2$ contributions, the perpendicular components are the same, i.e. $\boldsymbol{p}_T = \boldsymbol{p}_\perp$.

In order to investigate the observable consequences of the various terms in the hadronic tensor, one needs to consider the contraction with the leptonic tensor. This gives

$$
L^{\mu\nu} \left(\frac{q_\mu q_\nu}{q^2} - g_{\mu\nu} + \frac{\tilde{P}_\mu \tilde{P}_\nu}{\tilde{P}^2} \right) = \frac{4Q^2}{y^2} \left(\frac{y^2}{2} + 1 - y \right), \tag{26}
$$

$$
L^{\mu\nu} \left(\frac{\tilde{P}_\mu p_{\perp\nu} + \tilde{P}_\nu p_{\perp\mu}}{Q^2} \right) = -\frac{4Q^2}{y^2} \frac{|\boldsymbol{p}_T|}{Q} \frac{(2-y)\sqrt{1-y}}{2x} \cos\phi_p, \tag{27}
$$

$$
L^{\mu\nu} \left(i \frac{\tilde{P}_\mu k_{\perp\nu} - \tilde{P}_\nu k_{\perp\mu}}{Q^2} \right) = -\frac{4Q^2}{y^2} \frac{|\boldsymbol{k}_T|}{Q} \frac{y\sqrt{1-y}}{2x}\, \lambda \sin\phi_k, \tag{28}
$$

where the azymuthal angles are those between the transverse vectors and the (lepton) scattering plane, e.g. $\boldsymbol{p}_T \cdot \boldsymbol{q}_T = |\boldsymbol{p}_T|\, |\boldsymbol{q}_T| \cos\phi_p$.

As the most general result one can consider the case where one measures the perpendicular direction of the struck quark from the jet direction ($\boldsymbol{p}_\perp$) and the momentum of one specific hadron (h) belonging to this jet, characterized by the lightcone momentum fraction z and the perpendicular momentum $\boldsymbol{p}_{h\perp}$. One obtains (using $\boldsymbol{k}_\perp = \boldsymbol{p}_\perp - \boldsymbol{P}_{h\perp}/z$)

$$
\frac{d\sigma^{(\ell + H \to \ell' + h + \text{jet} + X)}}{dx_B dy dz d^2\boldsymbol{P}_{h\perp} d^2\boldsymbol{p}_\perp} = \frac{4\pi\alpha^2\, s}{Q^4} \Bigg\{ \left(\frac{y^2}{2} + 1 - y \right) x_B f_1\, D_1
$$

$$+ 2(2-y)\sqrt{1-y}\,\cos\phi_h\,\frac{|\boldsymbol{P}_{h\perp}|}{zQ}\left[x_B f_1\,\left(\frac{1}{z}D^\perp - D_1\right)\right]$$
$$+ 2(2-y)\sqrt{1-y}\,\cos\phi_j\,\frac{|\boldsymbol{p}_\perp|}{Q}\left[-\frac{x_B}{z}f_1\,D^\perp + x_B\left(f_1 - x_B f^\perp\right)D_1\right]$$
$$+ 2y\sqrt{1-y}\,\lambda\,\sin\phi_h\,\frac{|\boldsymbol{P}_{h\perp}|}{zQ}\left[\frac{Mx_B}{M_h}\left(x_B e - \frac{m}{M}f_1\right)H_1^\perp\right]$$
$$- 2y\sqrt{1-y}\,\lambda\,\sin\phi_j\,\frac{|\boldsymbol{p}_\perp|}{Q}\left[\frac{Mx_B}{M_h}\left(x_B e - \frac{m}{M}f_1\right)H_1^\perp\right]\Bigg\}, \qquad (29)$$

where the $H \to q$ profile functions (f_1, $f^\perp$ and e) depend on x_B and $\boldsymbol{p}_\perp^2$, while the $q \to h$ profile functions (D_1, $D^\perp$ and $H_1^\perp$) depend on z and $(\boldsymbol{P}_{h\perp} - z\boldsymbol{p}_\perp)^2$.

The theoretically simplest results are the ones obtained by integrating over the momenta of produced hadrons[5]. Integrating over the perpendicular momenta one has

$$\frac{d\sigma^{(\ell+H\to\ell'+h+\text{jet}+X)}}{dx_B dy dz d^2\boldsymbol{p}_\perp} = \frac{4\pi\alpha^2 s}{Q^4}\Bigg\{\left(\frac{y^2}{2}+1-y\right)x_B f_1(x_B)\,D_1(z)$$
$$- 2(2-y)\sqrt{1-y}\,\cos\phi_j\,\frac{|\boldsymbol{p}_\perp|}{Q}\,x_B^2 f^\perp(x_B)\,D_1(z)\Bigg\}. \qquad (30)$$

This shows that the ratio $x_B f^\perp(x_B)/f_1(x_B)$ can be obtained most cleanly from the azimuthal $\langle\cos\phi_j\rangle$ asymmetry of the produced jet. Note that this ratio is an extension of the naive parton result of unity[8]. An estimate for $f^\perp$ using the bag model is given in ref[9].

The measurement of the time reversal odd fragmentation function $H_1^\perp$ is possible from the general cross section given above. However, the detection of a jet in the forward direction will be hard in view of the fact that one is interested in a subleading ($\propto 1/Q$). This makes it more realistic to consider $e + H \to e' + h + X$. Only convolutions of profile functions from the distribution and fragmentation part will appear in this case. We will again consider the transverse momentum dependence as in Eqs 22 and 23 and use the definition of $I[\,]$ as in Eq. 21. The result for the cross section for electroproduction of a hadron h up to $\mathcal{O}(1/Q)$ becomes

$$\frac{d\sigma^{(\ell+H\to\ell'+h+X)}}{dx_B dy dz d^2\boldsymbol{p}_\perp} = \frac{4\pi\alpha^2 s}{Q^4}\Bigg\{\left(\frac{y^2}{2}+1-y\right)x_B I[f_1 D_1]$$
$$+ 2(2-y)\sqrt{1-y}\,\cos\phi_h\,\frac{|\boldsymbol{P}_{h\perp}|}{zQ}\left(\frac{R_h^2 x_B}{R_H^2+R_h^2}I\left[f_1\left(D_1 - \frac{1}{z}D^\perp\right)\right] - \frac{R_H^2 x_B^2}{R_H^2+R_h^2}I[f^\perp D_1]\right)$$
$$+ 2y\sqrt{1-y}\,\lambda\sin\phi_h\,\frac{|\boldsymbol{P}_{h\perp}|}{zQ}\left(\frac{Mx_B}{M_h}\frac{R_h^2}{R_H^2+R_h^2}I\left[\left(\frac{m}{M}f_1 - x_B e\right)H_1^\perp\right]\right)\Bigg\}. \qquad (31)$$

The time reversal odd fragmentation function $H_1^\perp$ is a leading twist fragmentation function which appears as a consequence of the fact that the states $|p_h, X\rangle$ in the definition of Δ are out-states. This means that it is nonzero because of the final

state interactions of the outgoing hadron h. This makes it on the one hand a very interesting quantity to measure, although it appears to us difficult to give reliable estimates for this functions. This time reversal odd structure function appears in the cross section as part of a product that also contains the profile function e. This chirally odd function has been discussed in ref.[4] and an estimate using the bag model has been given.

In principle the extraction of the $\sin\phi_h$ asymmetry for pions does not seem to be extremely difficult. One does not need target polarization, while the result is proportional to the lepton helicity. It is important to emphasize once more that the $p_\perp$-dependence that we have discussed is the low-momentum range, say below 1 GeV. Here the $p_\perp$-dependence is dominated by the intrinsic transverse momentum of the profile functions, rather than by perturbative QCD processes[10,11] that dominate the high transverse momenta[12,13,14]. The fact that one deals with a twist-3 structure function furthermore requires not too large values for the momentum transfer Q. It is important, however, to have good particle identification and sufficient angular resolution in the forward direction.

4. Acknowledgement

This work is in part (P.J.M) supported by the foundation for Fundamental Research of Matter (FOM) and the National Organization for Scientific Research (NWO).

5. References

1. J. Levelt and P.J. Mulders, NIKHEF-94-P5 (1994), in preparation
2. R.K. Ellis, W. Furmanski, R. Petronzio, *Nucl. Phys.* **B212** (1983) 29.
3. J.C. Collins, D.E. Soper and G. Sterman in *Perturbative Quantum Chromodynamics*, ed. A.H. Mueller, World Scientific (1989)
4. R.L. Jaffe and X. Ji, *Nucl. Phys.* **B375** (1992) 527 and refs therein.
5. J. Levelt and P.J. Mulders, *Phys. Rev.* **D49** (1994) 96.
6. R. Tangerman and P.J. Mulders, NIKHEF-94-P1 (1994), subm. *Phys. Rev* **D**.
7. S. Gasiorowicz, *Elementary Particle Physics*, Wiley (New York), 1966
8. R. Cahn, *Phys. Lett.* **78B** (1978) 269.
9. J. Levelt and P.J. Mulders, NIKHEF-93-P8 (1993), to be publ. in proceedings of the Workshop on Exclusive Reactions at High Momentum Transfer, Elba, 24-26 June 1993.
10. G. Altarelli and G. Martinelli, *Phys. Lett.* **76B** (1978) 89.
11. R. D. Field, *Applications of Perturbative QCD*, Addison-Wesley (1989), chapter 4
12. M.R. Adams et al. (E665 collaboration), *Phys. Rev. Lett.* **72** (1994) 466.
13. J. Conrad, Ph.D. thesis, Harvard University (1992)
14. M.D. Baker, Ph.D. thesis, Massachusetts Institute of Technology (1993)

NUCLEON-NUCLEON CORRELATIONS AND MULTIQUARK CLUSTER EFFECTS IN SEMI-INCLUSIVE DEEP INELASTIC LEPTON SCATTERING OFF NUCLEI*

S. Simula
Istituto Nazionale di Fisica Nucleare, Sezione Sanità
Viale Regina Elena 299, I-00161 Roma , ITALY

ABSTRACT

Semi-inclusive deep inelastic lepton scattering off nuclei is investigated assuming that virtual boson absorption occurs on a hadronic cluster which can be either a two-nucleon correlated pair or a six-quark bag. The differences in the energy distribution of nucleons produced in backward and forward directions are analyzed both at x<1 and x>1.

The investigation of deep inelastic scattering (DIS) of leptons off nuclei can shed light on the origin of nuclear forces and the short range structure of hadronic matter. To this end semi-inclusive processes, in which, besides the scattered lepton, another particle is detected in the final state, can be of great relevance, providing information on, e.g.: i) the effects of the nuclear medium on quark and gluon distributions; ii) the relevance of exotic configurations at short nucleon-nucleon (NN) distances; iii) the mechanism of hadronization. The aim of this contribution is to analyze the energy distribution of nucleons produced in semi-inclusive DIS processes A(ℓ,ℓ'N)X off nuclei, assuming that the virtual boson absorption occurs on a hadronic cluster which can be either a correlated NN pair or a six-quark (6q) bag. The former case has been investigated in ref. [1] within the spectator mechanism, according to which, after lepton interaction with a quark belonging to a nucleon of a correlated NN pair, the recoiling nucleon is emitted and detected in coincidence with the scattered lepton. It has been shown that the treatment of nuclear effects requires a particular care, improving the two-nucleon correlation (2NC) model of ref. [2], which assumes that the correlated NN pair is at rest and predicts that the semi-inclusive nuclear structure function is directly proportional to the rescaled nucleon structure function $F_2^N[x/(2-z_2)]$, where $z_2=(E_2-p_2\cos\theta_2)/M$ is the light-cone momentum of the detected nucleon, θ_2 is the detection angle with respect to the three-momentum transfer q and $x=Q^2/2Mv$ is the Bjorken scaling variable. When the extended 2NC model is considered, such a proportionality is modified by the Fermi motion of the center of mass (c.m.) of the correlated pair in the medium [1]. Thus, within the extended 2NC model nuclear effects on backward and forward nucleon emissions in the semi-inclusive DIS processes ^{12}C(e,e'p)X have been investigated. The results of calculations are presented in fig. 1 at x<1 and in fig. 2 at x>1, assuming for the electron incident energy the value E_e = 8 GeV. It should be pointed out that a beam energy of at least ~ 8 GeV is a prerequisite for having sufficiently high values of Q^2 necessary to minimize

* Work done in collaboration with C. Ciofi degli Atti.

nucleon emissions arising from quasi-elastic scattering processes on a correlated NN pair. It should be reminded that at x>1 backward nucleon production is kinematically forbidden within the 2NC model (i.e., the correlated NN pair at rest) and it is strongly suppressed within the extended 2NC one, because only low-momentum components of the c.m. momentum distribution of the correlated NN pair contribute to the semi-inclusive nuclear response. The main results of the analysis of the spectator mechanism

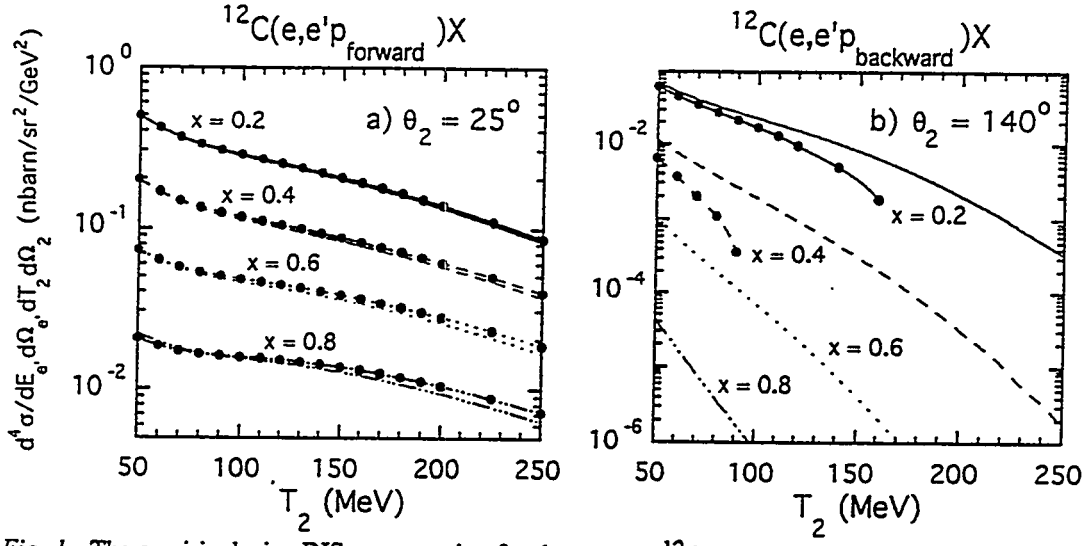


Fig. 1. The semi-inclusive DIS cross section for the process $^{12}C(e,e'p)X$ when the virtual photon is absorbed by a quark belonging to a nucleon of a correlated NN pair. T_2 is the kinetic energy of the detected proton emitted forward at $\theta_2=25^o$ (a) and backward at $\theta_2=140^o$ (b), when x<1. The curves without and with full dots represent the results obtained within the extended 2NC [1] and 2NC [2] models, respectively. Calculations have been performed assuming for the electron incident energy the value $E_e = 8$ GeV and for the electron scattering angle the values $\theta_{e'} = 45^o$ (a) and $\theta_{e'} = 80^o$ (b).

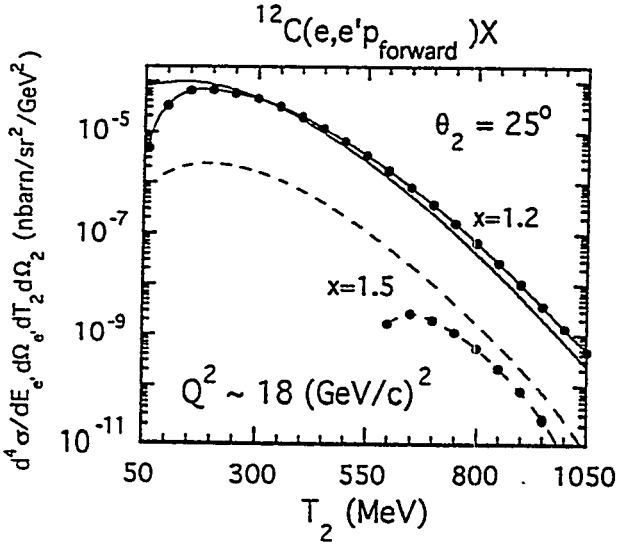


Fig. 2. The same as in fig. 1, but for protons emitted forward at $\theta_2=25^o$ and x>1. The electron incident energy and scattering angle are $E_e = 8$ GeV and $\theta_{e'} = 80^o$, respectively.

can be summarized as follows: i) backward emission at x<1 and forward emission at x>1 are sensitive to nuclear effects, whereas forward emission at x<1 is not; ii) at x<1 the momentum and energy dependencies of quark distributions in nuclei can be investigated, providing, e.g., a decisive test of various models of the EMC effect; iii) at x>1 forward emission is very sensitive to the high momentum components of nucleon light-cone momentum distributions in the medium, i.e., to the short-range structure of the two-nucleon system interacting with the incoming lepton.

A comparison of theoretical predictions with existing experimental data on single proton backward emission from neutrino (antineutrino) charged current interaction on neon nuclei [3], is shown in fig. 3. It can be seen that in single proton backward production nuclear effects arising from the Fermi motion of the c.m. of the correlated NN pair would reduce the role of competitive mechanisms, like intranuclear cascade or few-nucleon correlations, advocated in refs. [3] and [2], respectively.

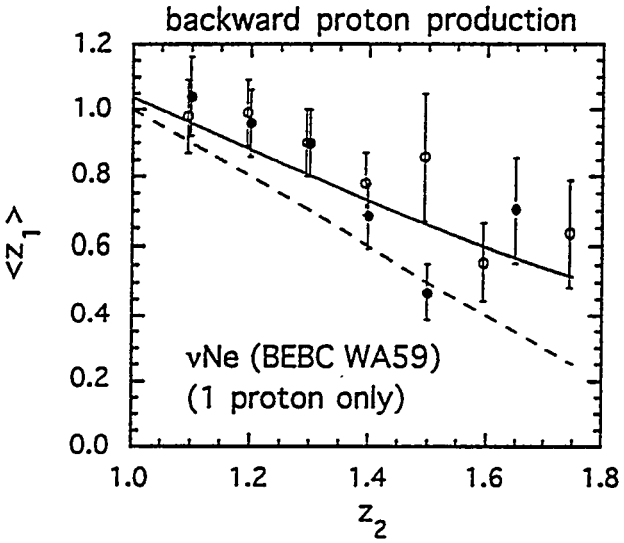


Fig. 3. The mean value of the light-cone momentum of the hit nucleon $\langle z_1 \rangle$, measured by the BEBC WA59 collaboration [3], versus the light-cone momentum z_2 of the detected proton, emitted in the backward hemisphere after neutrino (antineutrino) charged current interaction on neon nuclei. The solid and dashed lines represent the predictions of the extended 2NC [1] and 2NC [2] models, respectively. (After ref. [1])

The results presented could in principle be modified by mechanisms different from the spectator one. In ref. [1] the sensitivity of backward and forward nucleon emissions to the effects of the so-called target fragmentation of the hit nucleon and the final state interaction of the recoiling nucleon with the residual (A-2)-nucleon system, has been analyzed; it has been found that in the kinematics region of interest 0.3 GeV/c $\lesssim p_2 \lesssim$ 0.7 GeV/c, where the use of a non relativistic description of nuclear structure is well grounded, i) the effects of target fragmentation of the hit nucleon play a negligible role and do not affect at all backward nucleon emission, and ii) the contribution from the rescattering of the recoiling nucleon can modify the magnitude of the cross section without changing in a significant way its dependence upon the kinetic energy of the detected nucleon.

Let us now consider the possibility that the nucleons of a correlated NN pair can lose their identity at short separations; in particular, let us consider the extreme case in which the short-range structure of the hadronic cluster interacting with the incoming electron is entirely given by a 6q bag. The energy distribution of emitted nucleons can be obtained [4] assuming that the virtual photon interacts with a quark belonging to a 6q bag and the forward and backward nucleons are produced out of the penta-quark (5q) residuum. This

is the mechanism first proposed and applied to semi-inclusive DIS processes off the deuteron in ref. [5]. For complex nuclei the effects from the Fermi motion of the c.m. of the 6q bag have been taken care of by adopting the extended 2NC model, i.e., by using for the c.m. momentum distribution of a 6q bag the one of a correlated NN pair; this implies that the introduction of a 6q bag is assumed to modify only the intrinsic structure of a NN cluster at short separations. The relevance of nuclear effects on forward and backward nucleon emissions is presented in fig. 4 at x<1 and fig. 5 at x>1. By comparing

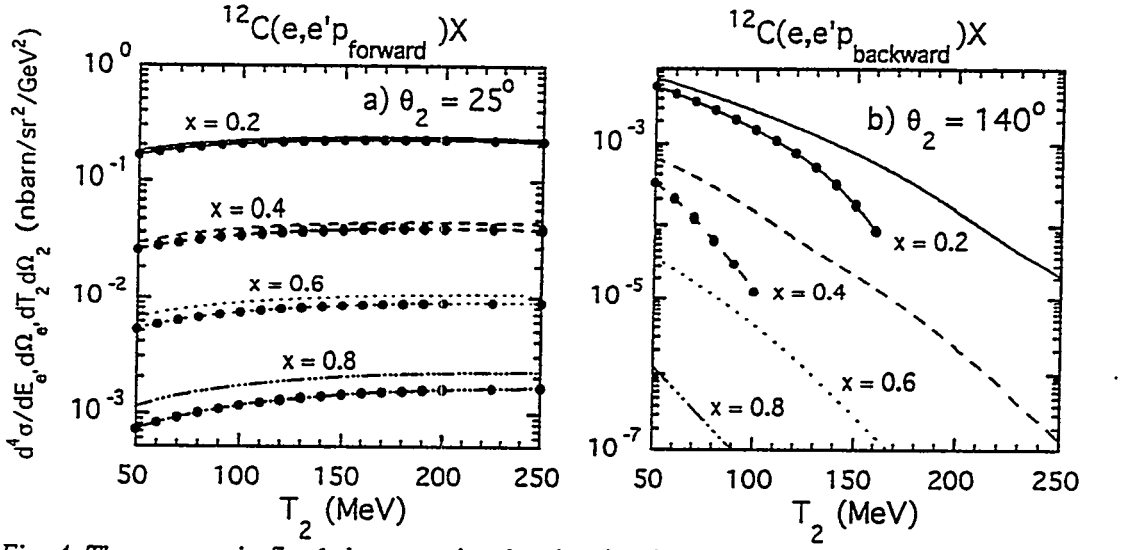


Fig. 4. The same as in fig. 1, but assuming that the virtual photon absorption occurs on a quark belonging to a 6q bag.

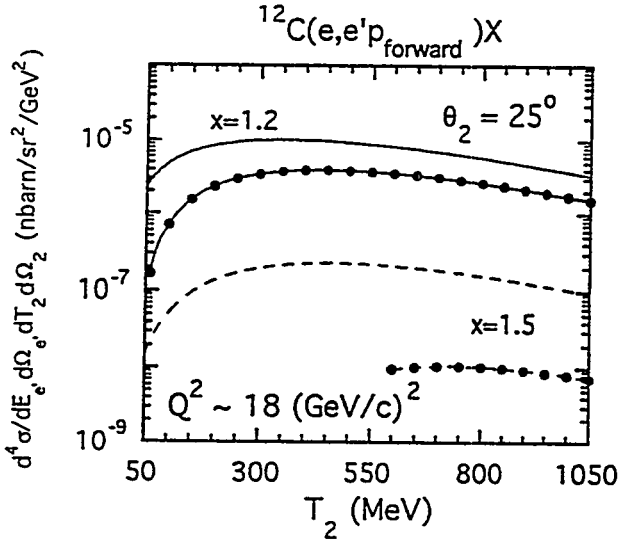


Fig. 5. The same as in fig. 2, but assuming that the virtual photon is absorbed by a quark belonging to a 6q bag.

the results shown in figs. 4-5 with the ones of figs. 1-2 it can clearly be seen that: i) the energy distributions of protons emitted backward at x<1 resulting from electron interaction with a quark belonging to a nucleon of a correlated NN pair or to a 6q bag,

are very similar, being the cross section dominated by the c.m. momentum distribution of the cluster interacting with the incoming electron (cf. figs. 4(b) and 1(b)); ii) forward emissions both at x<1 and x>1 arising from 6q bags strongly differ from those due to correlated NN pairs, being the cross section governed by the short-range structure of the cluster absorbing the virtual photon (cf. fig. 4(a) with fig. 1(a) and fig. 5 with fig. 2).

The effects of virtual photon absorption on a correlated NN pair and a 6q bag upon forward and backward proton emissions are compared in fig. 6 at x<1 and fig. 7 at x>1: it can clearly be seen that the effects from 6q bags are not expected to sharply modify the energy distribution of emitted protons when 0.3 GeV/c $\lesssim p_2 \lesssim$ 0.7 GeV/c (i.e., in the region of interest for the spectator mechanism); on the contrary, at higher values of p_2 ($\gtrsim$ 1 GeV/c) the presence of 6q bags may strongly affect the cross section both at x<1 and x>1.

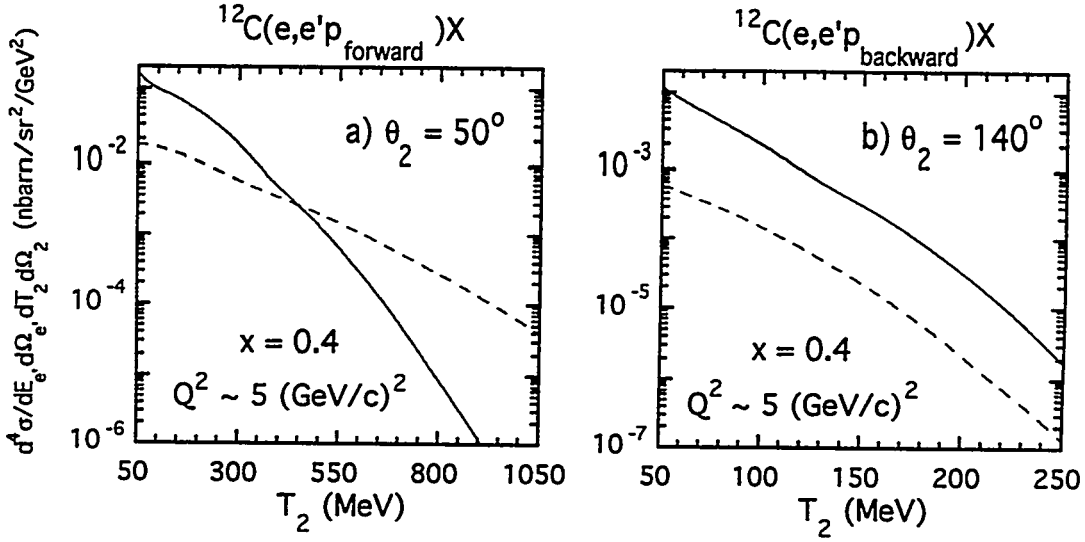


Fig. 6. The semi-inclusive DIS cross section for the process ^{12}C(e,e'p)X versus the kinetic energy T_2 of the detected proton, emitted forward at θ_2=50° (a) and backward at θ_2=140° (b), when x=0.4. The solid line is the contribution due to virtual photon absorption on a nucleon of a correlated NN pair, whereas the dashed line is the contribution resulting from virtual photon absorption on a quark belonging to a 6q bag.

In conclusion, forward and backward nucleon emissions in semi-inclusive DIS processes A(ℓ,ℓ'N)X off nuclei have been investigated assuming that virtual boson absorption occurs on a hadronic cluster which can be either a two-nucleon correlated pair or a six-quark bag. Nuclear effects have been taken care of by adopting the extended two-nucleon correlation model [1] which takes into account the binding and the motion of the center of mass of the hadronic cluster interacting with the incoming lepton. As for the effects of virtual boson absorption on a nucleon of a correlated NN pair, the main results of the analysis can be listed as follows: i) backward emission at x<1 and forward emission at x > 1 are sensitive to nuclear effects, whereas forward emission at x<1 is not (cf. figs. 1 and 2); as a matter of fact, a large part of the discrepancy between the predictions of ref. [2] and the experimental data on single proton backward production observed in neutrino and antineutrino charged-current interactions with neon nuclei ([3])

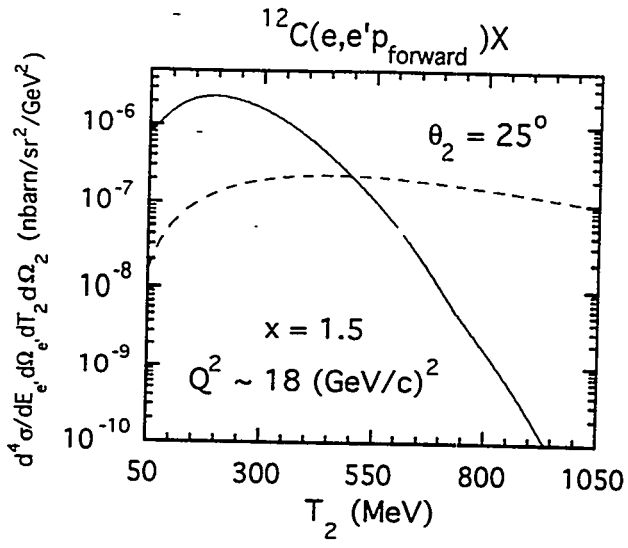


Fig. 7. The same as in fig. 6, but for protons emitted forward at θ_2=25^o and x=1.5.

can be ascribed to nuclear effects arising from the c.m. motion of the correlated NN pair rather than to intranuclear cascade or few-nucleon correlation effects (cf. fig. 3); ii) at x<1 the momentum and energy dependencies of quark distributions in nuclei can be investigated, providing, e.g., a decisive test of various models of the EMC effect; iii) at x>1 the cross section is mainly governed by the high momentum components of nucleon light-cone momentum distributions, i.e., by the short-range structure of the correlated NN pair. As for the effects from six-quark bags, the main conclusions are as follows: i) nuclear effects are not important in forward emission at x<1 but become relevant in backward emission at x<1 and forward emission at x>1 (cf. figs. 4 and 5); ii) the energy distribution of nucleons emitted in the backward hemisphere at x<1 resulting from virtual photon absorption on a 6q bag is similar to the corresponding one obtained when the virtual photon is absorbed by a 3q cluster (cf. fig. 6(b)), so that only forward emission (both at x<1 and x>1) appears to be the appropriate kinematics condition for studying multiquark configurations in nuclei, provided $p_2 \gtrsim 1$ (GeV/c) (cf. figs. 6(a) and 7).

REFERENCES

1. C. Ciofi degli Atti, S. Simula, Phys. Lett. **319B** (1993) 23.
2. L.L. Frankfurt, M.I. Strikman, Phys. Rep. **160** (1988) 235.
3. E. Matsinos et al., Z. Phys. **C44** (1989) 79.
4. S. Simula, to appear.
5. C.E. Carlson, K.E. Lassila, U.P. Sukhatme, Phys. Lett. **263B** (1991) 277;
   C.E. Carlson, K.E. Lassila, preprint WM-94-101, January 1994.
   C.E. Carlson, this Workshop.

PARITY VIOLATION IN DEEP INELASTIC SCATTERING AT CEBAF

PAUL SOUDER
Department of Physics, Syracuse University
Syracuse, New York 13244

ABSTRACT

A beam of polarized electrons at CEBAF with an energy of 8 GeV or more will be useful for performing precision measurements of parity violation in deep inelastic scattering. Possible applications include precision tests of the Standard Model, model-independent measurements of parton distribution functions, and studies of quark correlations.

1. Introduction

Experiments in deep inelastic scattering of leptons from nucleon targets during the past 25 years have been central in establishing the Standard Model, including the color SU(3) of QCD and the SU(2)×U(1) structure of the electroweak interactions. Given the maturity of the field and the fact that many facilities have energies available that are much higher than at CEBAF, one might ask if there is a role for CEBAF. The answer is that CEBAF, with its polarized beams, does have important contributions to make, especially at certain kinematic points. Two obvious areas are spin-dependent structure functions (discussed in another contribution by Z.-E. Meziani) and parity violation. Kinematics are available at sufficiently high Q^2 where experiments and theory can be cleanly compared. In addition, the theory of higher twist effects, relevant at lower Q^2, is being developed, and CEBAF would be ideal for the study of such effects. Spin-dependent effects have the potential to be sufficiently specific so that calculations might be tractable.

2. Theory

2.1. General Phenomenology

In deep inelastic scattering, an incident lepton of energy E is scattered at an angle θ with energy E'. Only the electron is detected. The relevant variables are $Q^2 = 4EE'\sin^2[\theta/2]$, $\nu = E - E'$ is the energy lost by the electron in the lab, and $M_X^2 = M^2 + 2M\nu - Q^2$ is the square of the missing mass of the hadron. For the scattering to be considered large, both Q^2 and M_X must be large. Normally the requirement is $M_X > 2$ GeV and Q^2 is sufficiently large so that the strong coupling constant of QCD α_s is small, which sets a lower limit on Q^2 in the range 1-5 $(\mathrm{GeV/c})^2$. Usually the scaling variables $x = Q^2/2M\nu$ and $y = [E - E']/E$ are

used. The variable x is interpreted as the fraction of the momentum of the nucleon carried by the struck quark. The kinematics is completely described by x, y, and Q^2.

The cross section is given by

$$\frac{d\sigma}{d\Omega dE'} = \frac{\alpha^2}{4E^2}\frac{\cos^2(\theta/2)}{\sin^2(\theta/2)}[W_2 + 2W_1\tan^2(\theta/2)] \tag{1}$$

where $\nu W_2 = F_2(x,Q^2)$ and $MW_1 = F_1(x,Q^2)$. Data are presented in terms of $F_2(x,Q^2)$ and $R(x,Q^2)$, where

$$R(x,Q^2) = \frac{\sigma_L}{\sigma_T} = \frac{F_2(x,Q^2)}{2xF_1(x,q^2)}\left[1+\frac{Q^2}{\nu^2}\right] - 1. \tag{2}$$

In terms of the Quark-Parton Model, $R \approx 0$ or $F_2(x) \approx 2xF_1(x)$. F_2 may be expressed in terms of quark momentum distribution functions $q_i(x,Q^2)$, where q_i=u, d, or s for up, down, or strange quarks as follows:

$$F_2(x) = x\left[\frac{4}{9}(u(x)+\overline{u}(x)) + \frac{1}{9}(d(x)+\overline{d}(x)) + \frac{1}{9}(s(x)+\overline{s}(x)) + \cdots\right]. \tag{3}$$

The cross section may be written:

$$\frac{d\sigma}{d\Omega dy} = \frac{4\alpha^2 EE'}{Q^4}F_2(1/y - 1 + y/2). \tag{4}$$

Based on the world data, including electromagnetic and weak (both charged and neutral current) scattering, the $q_i(x,Q^2)$ are known.[1]

2.2. Parity Violation

Parity violation in deep inelastic scattering was first studied at SLAC.[2] Indeed, this experiment was crucial in establishing that the Standard Model was indeed the correct theory instead of a number of alternatives consistent with experiments at that time. To discuss what further information might be obtained, I briefly describe the phenomenology. The idea is to measure a parity violating asymmetry $A = (\sigma_R - \sigma_L)/(\sigma_R + \sigma_L)$ where $\sigma_{L(R)}$ is the differential cross section for the scattering of left (right) helicity electrons. For deep inelastic scattering, the asymmetry may be determined in terms of the electroweak coupling constants in table I and the $q_i(x)$ as follows:[3]

$$A^{DIES} = Q^2\frac{G_F}{2\sqrt{2}\pi\alpha}\left[a(x) + \frac{1-(1-y)^2}{1+(1-y)^2}b(x)\right] \tag{5}$$

where

$$a(x) = \frac{\sum_i q_i(x)C_{1i}Q_i}{\sum_i q_i(x)Q_i^2} \qquad b(x) = \frac{\sum_i q_i(x)C_{2i}Q_i}{\sum_i q_i(x)Q_i^2}. \tag{6}$$

For an isoscalar target such as deuterium, this yields the simple result

$$a(x) = \frac{9}{5}\left[\frac{\tilde{\alpha} + \frac{1}{3}\tilde{\gamma}}{2} + \frac{2}{15}\frac{s(x) + \bar{s}(x) - c(x) - \bar{c}(x)}{D}\right] \approx \frac{9}{10}(\tilde{\alpha} + \frac{1}{3}\tilde{\gamma}) \tag{7}$$

$$b(x) = \frac{9}{5}\left[\frac{\tilde{\beta} + \frac{1}{3}\tilde{\delta}}{2}\frac{q(x) - \bar{q}(x)}{D} + \text{heavy quark terms}\right] \approx \frac{9}{10}(\tilde{\beta} + \frac{1}{3}\tilde{\delta}) \tag{8}$$

where

$$D(u) = u(x) + d(x) + \bar{u}(x) + \bar{d}(x) + \frac{2}{5}[s(x) + \bar{s}(x)] + \frac{8}{5}[c(x) + \bar{c}(x)] \tag{9}$$

$$q(x) = u(x) + d(x) + s(x) + c(x). \tag{10}$$

For the proton,

$$a(x) \approx \frac{3}{4}\left[\frac{6C_{1u}u(x) - 3C_{1d}d(x)}{u(x) + d(x)/4}\right] \approx \frac{-3}{40}\left[\frac{u(x) + 0.912d(x)}{u(x) + 0.25d(x)}\right] \tag{11}$$

$$b(x) \approx \frac{3}{4}\left[\frac{6C_{2u}u(x) - 3C_{2d}d(x)}{u(x) + d(x)/4}\right] \tag{12}$$

Constant	C_{iq}	Standard Model	$\sin^2\theta_W = 0.23$	SIP
$\tilde{\alpha}$	$C_{1u} - C_{1d}$	$-\rho(1 - 2\sin^2\theta_W)$	-0.54	-0.523
$\tilde{\gamma}$	$C_{1u} + C_{1d}$	$\frac{2}{3}\rho\sin^2\theta_W$	0.15	0.153
$\tilde{\beta}$	$C_{2u} - C_{2d}$	$-\rho(1 - 4\sin^2\theta_W)$	-0.08	-0.054
$\tilde{\delta}$	$C_{2u} + C_{2d}$	0.	0.00	-0.014
C_{1s}	C_{1s}	$\rho(\frac{1}{2} - \frac{2}{3}\sin^2\theta_W)$	0.35	0.338

Table I. Model independent electroweak coupling constants. Values are given in terms of the C_{iq} coupling constants, for the Standard Model in terms of ρ and $\sin^2\theta_W$, and numerically in the Standard Model for $\sin^2\theta_W = 0.23$. Last column, from Langacker's Standard Input Parameters (SIP),[4] gives more precise values including some radiative corrections.[5]

3. Experimental Capabilities at CEBAF

One obvious approach to performing a deep inelastic parity experiment at CEBAF is to use the methods proposed for the Hall A experiment designed to measure

parity violation in elastic scattering from hydrogen.[6] A possible kinematic point is $x = y$ =0.5 at E=8 GeV. The scattering angle is 20° and $Q^2 \approx 4(\mathrm{GeV/c})^2$. Given $F_2 = 0.117$ per nucleon, $d\sigma/d\Omega = 6.6$ nb/(GeV/c sr), which for a 2 g/cm^2 LD_2 target and a 100 μa beam implies an event rate $\approx 2 \times 10^4$/sec. If the beam polarization $P_e = 80\%$, $A^{PV} \approx 0.3\%$, and $\delta A/A = 2.5\%$ in 300 hours if the experiment is limited by statistics.

It may seem surprising at first glance that high resolution spectrometers are suitable for deep inelastic scattering, but for large values of x, only a small range of E' is available, and the spectrometers are a good match to the available kinematics. The most important systematic error will probably be the measurement of the beam polarization, and considerable effort is being devoted to that problem to meet the needs of approved experiments.

This is impressive precision. What might we learn here? For the deuteron at large x where the strange quarks are negligible, the parton distribution functions in the $a(x)$ term (see Eq. 7) cancel. The $b(x)$ terms are numerically small due to the small size of the vector electron coupling constants C_{2i}. Thus these kinematics might provide a clean measurement of the electroweak coupling constants as a test of the Standard Model,[7] although there is evidence that higher twist effects are more important at higher x.[8] The quantity $(\tilde{\alpha} + \frac{1}{3}\tilde{\gamma}) + 0.6(\tilde{\beta} + \frac{1}{3}\tilde{\delta})$ will be measured to 2.5% under the above assumptions. The unique feature of this experiment is that it is sensitive to the combination $(\tilde{\beta} + \frac{1}{3}\tilde{\delta})$.

It might be possible to design an apparatus specifically for parity violation studies at CEBAF which exploits the CW nature of the facility to achieve much greater solid angle and hence high precision measurements over a wide kinematic range. E' would be lower and the scattering angles larger. Substantial pions would be present, so coincident counting methods would be required.

4. Testing the Standard Model

A considerable amount of effort at high-energy facilities has yielded impressive precision data which for the most part supports the Standard Model. The question then arises as to how a facility such as CEBAF can compete. The argument is as follows. First, the most precisely measured quantity is the mass of the Z. However, this is a necessary input parameter to the theory, along with the fine structure constant α which is measured in atomic physics experiments and the Fermi constant G_F which is determined in *nuclear* physics experiments.

In order to *test* the theory, additional precise experiments must be performed. Examples include Γ_Z, the width of the Z, $A(Z \to b)$ at LEP, and A^{PV} at SLAC, M_W/M_Z (to be improved at Fermilab or LEP2), Cs parity violation (atomic physics), and R_ν, a ratio measured in neutrino experiments. Thus at the moment there are six precision tests, three involving the Z directly and two (Cs and R_ν) which determine the neutral weak current well below the Z pole, and M_W/M_Z.

These measurements set limits on possible extensions to the Standard Model. Possible extensions[4] that can be observed on the Z-pole include extra Z's that mix

with the known Z, S-type and T-type loops.[9] Physics that can best be observed off the Z include extra Z's that do not mix, leptoquarks, new heavy fermions, and composite structure of the fermions. Since different tests have different sensitivities to different modifications, it is useful to perform as many as possible. As a minimum, two independent tests both off and on the Z are needed.

At present, A^{PV} from SLAC(SLD)[10] implies $\sin^2\theta_W = 0.2290 \pm 0.0009 \pm 0.0004$, which differs by more than 2.5σ from the value $\sin^2\theta_W = 0.2322 \pm 0.0006$ obtained from asymmetries at LEP.[11] Should this discrepency persist with expected improvements in the data, the Standard Model will be demonstrated to be incomplete. Then the question of highest priority is which of the extensions to the Standard Model is correct. Many different precise measurements will be needed to settle the issue, and experiments at CEBAF might be crucial. Even if the discrepancy vanishes, the case for an experiment at CEBAF is still there, although it is more speculative. The kinematic point discussed above is unique among precision tests in that it is sensitive to the coupling constants $\bar{\beta}$ and $\bar{\delta}$, and for that reason alone the experiment is worthwhile.

5. Nucleon Structure

For the proton,

$$A_{PV} \propto \frac{u(x) + 0.921d(x)}{u(x) + 0.25d(x)} \tag{13}$$

and thus provides a measure of the ratio $u(x)/d(x)$, an interesting quantity at high x. The normal procedure is to measure

$$\frac{\sigma(P)}{\sigma(D)} \propto \frac{u(x) + 0.25d(x)}{u(x) + d(x)} \tag{14}$$

which has the same sensitivity to $u(x)/d(x)$ but different and perhaps larger systematic errors. This measurement takes advantage of the high x capabilities at CEBAF.

At low x, A_{PV} is sensitive to $s(x)$ as can be seen in Eq. 7 and also as emphasized by Bosted et al. in a proposal for SLAC.[12] A measurement of this sort might be practical at CEBAF, particularly if the energy limit is 10-12 GeV. For these kinematics, pion contamination is an important issue, and the CW nature of CEBAF can be exploited to allow counting techniques that have much better pion rejection than integrating techniques that must be used at SLAC. Information about structure functions has been obtained at CERN using the electroweak interference of muons.[13]

Another issue is the significance of higher twist corrections. For the experiments mentioned above, they are a nuisance, and kinematics must be chosen where they are believed to be negligible. However, there has been progress in calculating such terms; indeed this may be a vital frontier of QCD. Parity violation might be a technique that isolates specific operators that will enable useful studies whereas

cross sections contain so many amplitudes that they are much more difficult to untangle. For these studies, Q^2 values on the order of 1 $(\mathrm{GeV/c})^2$ are appropriate. Perturbative QCD is still useful as a baseline and yet the higher twist terms are of a significant size. This might develop into an important frontier of physics to be explored at CEBAF.

6. Conclusions

CEBAF has the potential to make significant contributions to the field of parity violation in deep inelastic scattering. Kinematic regions where y is large and $x > 0.1$ are accessible. Good physics can be done with apparatus already designed for the standard 4 GeV program, including the Hall A spectrometers, beam polarimeters, and the polarized beam. A new spectrometer designed could exploit the CW nature of CEBAF to significantly enhance the solid angle available. Such a facility might produce extremely precise data over a wide kinematic range.

7. References

1. A. D. Martin, W. J. Sterling, and R. G. Roberts, *Phys. Lett.* **B306** (1993) 145 .
2. C. Y. Prescott *et al.*, *Phys. Lett.* **B77** (1978) 347; C. Y. Prescott *et al.*, *Phys. Lett.* **B84** (1979) 524.
3. Our notation follows that of S. Bellucci, M. Lusignoli, and L. Maiani, *Nucl. Phys.* **B189** (1981) 329.
4. P. Langacker, M. Luo, and A. K. Mann, Rev. Mod. Phys. **64** (1992) 87.
5. W. J. Marciano, *Phys. Rev.* **D20** (1979) 274; W. J. Marciano and A. Sirlin, *Phys. Rev. Lett.* **46** (1981) 163, A. Sirlin, *Phys. Rev.* **D22** (1980) 971.
6. CEBAF proposal #PR-91-007, P. A. Souder and M. J. Finn, spokespersons.
7. J. D. Bjorken, *Phys. Rev.* **D18** (1978) 3239; L. Wolfenstien, *Nucl. Phys.* **B146** (1978) 477; E. Derman, *Phys. Rev.* **D19** (1979) 133; H. Fritzsch, Z. Phys. **C 1** (1979) 321.
8. M. Virchaux and A. Milsztajn, *Phys. Lett.* **B274** (1992) 221 .
9. M. E. Peskin and T. Takeuchi, *Phys. Rev.* **46** (1992) 381 .
10. Bruce Schumm, Aspen Winter Conf. (1994).
11. J. Lefrancoise, plenary talk at the Int. Europhysics Conf. on High Energy Physics, Marseille, 1993.
12. SLAC proposal E-149, P. Bosted, spokesperson.
13. A. Argento *et al.*, *Phys. Lett.* **120B** (1983) 245; A. Argento *et al.*, *Phys. Lett.* **140B** (1984) 142.

Working Group on Hadrons in the Nuclear Medium

Organizers: R. Ent & R. Milner

Working Group Report

on

Hadrons in the Nuclear Medium

R. Ent

CEBAF, Newport News, VA 23606

R. G. Milner

Masachusetts Institute of Technology

Cambridge, MA 02139

1. Introduction

This working group focussed on the subject of hadrons in the nuclear medium. It encompassed both the understanding of the nucleus itself in terms of its binding and its structure, and the use of the nucleus as a medium to probe QCD and the structure of hadrons. Both aspects were addressed during the workshop, though the emphasis tended towards the latter.

Almost inescapably this working group had some overlap with the other working groups, as the nucleus can also be used as a medium to probe the production and structure of vector mesons. Also, inclusive and semi-inclusive processes can be used as a probe of nuclear effects, for instance in the case of deep-inelastic scattering for $x > 1$.

In this summary report we will try to restrict ourselves to only those issues where the nuclear medium is important. To increase our understanding of the nucleus in terms of its binding and structure, we would like to know the effect of a dense nuclear medium on a nucleon, to know the non-nucleonic degrees of freedom needed to describe a nuclear system, and to understand the implications of the fact that a bound nucleon is necessarily off its mass-shell. The results of many lepton scattering experiments during the last two decades have raised these questions, but at this moment we have no definitive answers. The hope is that the well-known electron probe, with sufficient energy to probe the short-range properties of nuclei, can provide insight. Especially, we would like a conclusive answer to the question if, and to what extent, quark degrees of freedom are necessary to describe a nuclear system.

In the case of using the nucleus as a medium to investigate properties of QCD and hadronic wave functions, an electron probe with sufficient energy is mandatory. The high

energy electron enables us to either select or produce a hadron in a specific state. Furthermore, the strong interaction which this hadron sees as it exits the nucleus will depend on the hadronic wave function. Thus, the production rates we will measure for hadrons in principle will depend on their internal wave function. By varying both the momentum transfer given to produce the hadron, and the nuclear medium (nucleus), one can in principle probe the wave function of the produced hadron. A high-energy electron probe can be a unique microscope of these wave functions, with the only caveat that the energy and the luminosity have to be high enough!

The titles and speakers for the parallel talks in this session are given below. Though the Sections in this summary report will reflect closely the list of subjects addressed during the working group session, the text is only a personal viewpoint of the organizers on the importance of the physics issues which can be addressed with a high-energy electron beam. The two main issues addressed by several speakers were Color Transparency effects and Vector Meson Production. We will describe the former in Section 2, the latter in Section 3. Sections 4-6 will be devoted to the remaining subjects discussed in this session: Large Momentum Transfer (e,e'p) Scattering, Quark-Cluster Signatures and Parity Violation.

- G. Miller - Color Transparency
- M. Sargsyan - Effects of Short Range Correlations in Color Transparency
- G. Fang - ρ Production in Nuclei
- L. Frankfurt - Issues in Diffractive Vector Meson Production
- M. Kossov - Medium Modifications of Vector Mesons with Electroproduction
- R. Ent - A(e,e'p) at high Q^2
- J. van den Brand - Medium Modifications with Recoil Polarization
- C. Carlson - Quark Cluster Signatures in the Deuteron
- E. Beise - Parity Violation and Strangeness
- D. Beck - MEC at High Momentum Transfer
- N. Nikolaev - A and Q^2 Dependence of Diffractive Strangeness Electroproduction

We would like to thank all speakers for their excellent talks, and especially for their efforts and enthusiasm to try to answer our main question for them, "Does CEBAF need a beam energy higher than 4 GeV?". We also would like to thank all chairpersons for their help, and everybody who contributed to the lively discussions during and after the presentations.

2. Color Transparency

Color Transparency is the term given to the prediction that, at sufficiently large momentum transfers to a hadron, the strong interaction this hadron experiences as it traverses

the nuclear medium would be reduced. The arguments for this effect were originally formulated by Mueller and Brodsky in the context of Perturbative QCD,[1] however recent work suggests that this phenomenon also occurs in models with non-perturbative reaction mechanisms.[2]

Three prerequisites are needed for the existence of Color Transparency:[2] (i) large-momentum transfer scattering should predominantly take place via selection of color-singlet objects of small transverse size; (ii) the strong interaction of a color-singlet hadron is geometrical, thus smaller objects experience less interaction; (iii) the expansion of the selected "small" color-singlet hadron towards a physical hadron occurs on a length scale comparable with the "size" of the nuclear medium. The first condition has especially been the subject of interesting discussions. Perturbative QCD considerations of large-momentum transfer elastic electron-nucleon scattering conclude that the wave function of the recoiling proton has diminished transverse size. However, the momentum transfer at which Perturbative QCD becomes valid is still an open question, the debate concentrating on where soft non-perturbative processes can be neglected. Still, even in the case that the electron-proton scattering is completely due to these soft processes geometrical arguments suggest that scattering from small objects may be dominant at large enough momentum transfers. Thus models with non-perturbative reaction mechanisms can also give rise to Color Transparency.

The occurrence of Color Transparency can be verified by measuring observables which are related to the final- (and initial-) state interaction between the struck or produced hadron and the rest of the nuclear medium. One can either look for a disappearance of the absorption or deflection of hadrons, typically resulting in an increase of the reaction rates, or for the disappearance of a physics observable which is solely caused by final-state interactions. An example of the former is the standard (e,e'p) reaction, where one can measure the nuclear transparency T, i.e. the ratio of the measured cross sections with respect to the cross section expected in the absence of a nuclear medium. Examples of the latter are double rescattering observables (related to the deflection of hadrons on their way out of the nuclear medium) or induced polarization observables.

At this moment the only two experiments performed have been of the first kind, looking for a gradual change of the nuclear transparency as function of momentum transfer to the struck nucleon. At Brookhaven National Laboratory, Carroll *et al.* have determined the nuclear transparency by measuring simultaneous A(p,2p) and H(p,2p) reactions.[3] The results show an initial rise in the nuclear transparency, which has been interpreted as evidence of Color Transparency.[4] However, the data subsequently show a decrease in nuclear transparency at even higher energies. Ralston and Pire have suggested that this is related

to a known oscillation on the free nucleon-nucleon scattering cross section, explained in terms of Sudakov effects.[5] At this moment this decrease obscures a conclusive interpretation of these data in terms of Color Transparency.

At SLAC an A(e,e'p) experiment was performed by the NE18 collaboration using the Nuclear Physics Injector. Interpretation of the data should be greatly simplified by using the well-known electromagnetic probe. The results are well described in terms of standard nuclear physics calculations, without the inclusion of Color Transparency effects.[6] Results for the ^{12}C(e,e'p) reaction are shown in Fig. 1 together with some typical calculations. The results indicate that a momentum transfer squared of larger than 7 $(GeV/c)^2$ may be required for a conclusive observation of Color Transparency effects using this technique.

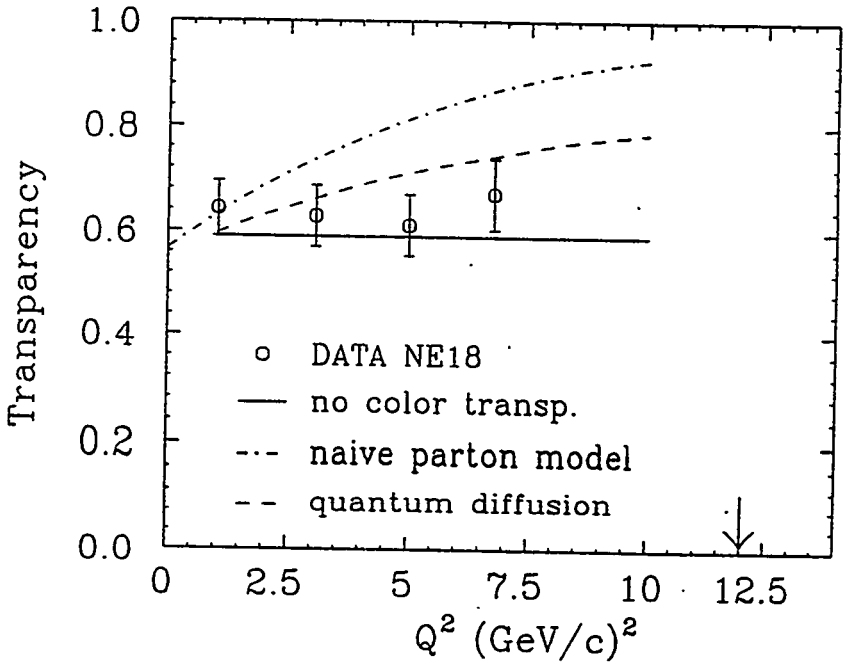


Figure 1: The measured transparency as a function of momentum transfer for the ^{12}C(e,e'p) reaction.[6] The solid line is a typical calculation not including Color Transparency effects. The dot-dashed and dashed lines correspond to the same calculations as shown in the NE18 Carbon paper, the dot-dashed being the naive parton model calculation of Ref. 7, the dashed the correlated-Glauber/quantum diffusion model of Ref. 8. The arrow indicates the maximum momentum transfer possible at CEBAF with a 8 GeV energy beam and existing Hall C spectrometers.

However, it must be kept in mind that theoretical predictions at this moment only suggest Color Transparency effects of order 10% on the nuclear transparency over this range of Q^2. The quality of the data can not rule out effects of order 5-10%, especially

because the conventional nuclear physics prediction of the nuclear transparencies (without the inclusion of Color Transparency effects) also varies by about 10%, depending on the assumptions made in the calculations. It seems that these uncertainties will have to be reduced before one can make any convincing claim about the existence or non-existence of Color Transparency effects in the A(e,e'p) reaction in this Q^2 range.

Thus we argue for the need to establish a more reliable baseline calculation of nuclear transparencies in a conventional nuclear physics framework. Also, in order to hunt for the possible small Color Transparency effects, one would like to see A(e,e'p) data at higher momentum transfer values (to boost any possible effect) and with higher statistical precision. Though still interesting to verify Color Transparency, one can argue whether the concept is still practical if we can not see it at momentum transfers lower than about 12-15 $(GeV/c)^2$. For these kind of momentum transfers a 8-10 GeV high luminosity beam would be sufficient. Fig. 2 shows the reduction of the effective struck nucleon-nucleon cross section in the case that Color Transparency effects set in as predicted by Nikolaev *et al.*.[9]

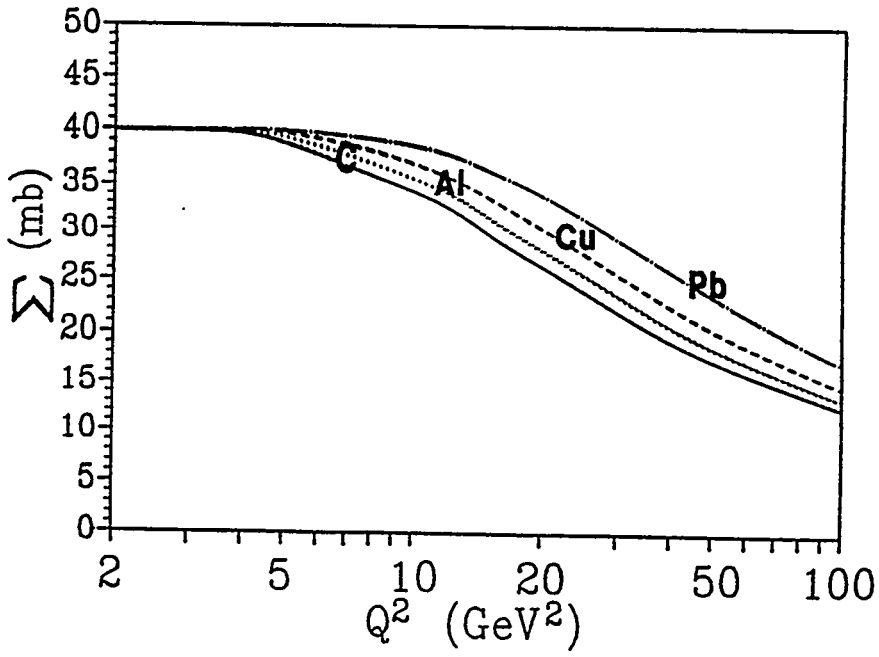


Figure 2: Effective cross section between the struck nucleon and a residual nucleon in the nuclear medium in the (e,e'p) reaction.[9] Color Transparency effects cause the reduction in cross section as a function of momentum transfer.

Sargsyan emphasized in his talk the need for high statistical precision and high resolution data, since the signature of Color Transparency effects may well vary for different

nuclear shells. Furthermore, by fixing regions in missing energy and missing momentum, uncertainties in nuclear structure can be reduced. One can select regions where the nuclear wave function has been well established in previous electron scattering experiments. Necessary assumptions about nuclear wave function and nucleon correlation effects were indeed a large contribution to the systematic uncertainty in the SLAC NE18 experiment.

The lack of a reliable baseline calculation might also hamper other experimental approaches to look for Color Transparency effects. In the case of an (e,e'pp) experiment as a probe of Color Transparency effects, one selects a kinematic region where events mainly originate from a double rescattering process. But, due to the lack of experimental data on the (e,e'pp) reaction, it is not a priori clear that one can select such a region. Even if one can, the conventional calculation of double rescattering may not be known well enough to interpret the data in terms of Color Transparency.

Still, the virtue of this method, as advocated in the talks of both Miller and Sargsyan, is that the signature of Color Transparency may be an appreciable fraction of the conventional expectation value, even at momentum transfers as low as 2-3 $(GeV/c)^2$. Also here a maximum momentum transfer of about 12 $(GeV/c)^2$ (or beam energy of about 10 GeV) seems sufficient, to both probe events with low and high relative transverse momenta between the two hadrons in the final state.

A similar method, probing the (e,e'Δ^{++}) reaction, was suggested by Miller. Here also the baseline calculation may be a problem. These experiments have never been performed before, which may make interpretation of the data in terms of Color Transparency difficult.

Alternatively, one can utilize polarization degrees of freedom. It has been suggested to look for the disappearance of induced response functions, for instance in the A(e,e'$\vec{p}$) reaction. Miller showed a calculation of $R_T{}^n$ in ^{208}Pb, where Color Transparency effects actually *increase* the induced response function.[10] The explanation given was that the induced response function was actually caused by a cancellation of many contributing orbitals, whereas the Color Transparency effects mainly showed up in the $1H_{11/2}$ orbital. This example, shown in Fig. 3, already shows how careful one has to be in looking for Color Transparency effects in induced polarization observables. Final-state contributions will show up in a complicated manner in these many-body response functions. However, because of this complexity, surprising effects may arise in these observables, which makes the experiments especially worthwile.

Recently, data on ρ and ϕ meson production from Fermilab experiment E665 also have been interpreted in terms of Color Transparency effects.[11] In this case the initial size of the vector meson is thought to be controlled by the momentum transfer squared Q^2. The E665 data were taken with such a high (muon) beam energy that the formation length

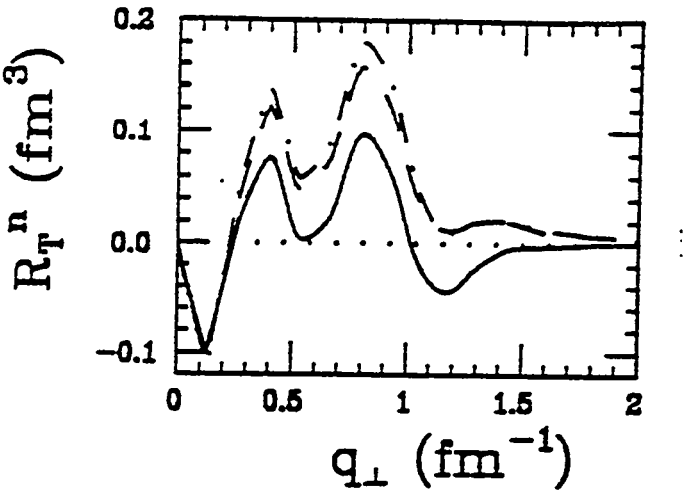


Figure 3: Normal-transverse response function for ^{208}Pb(e,e'p) at $Q^2 = 3.25$ (GeV/c)^2.[10] The solid line is DWIA, the dot-dashed and dashed lines are two models which include Color Transparency effects.

of the produced vector mesons (the time they need to expand to their proper size) is far larger than the nuclear radius. These data were shown by Fang. The momentum transfer dependence is in good agreement with a model calculation, including Color Transparency effects, by Nikolaev *et al.*.[12]

Fang remarked that a 10 GeV CEBAF beam should be sufficient to have formation lengths as large as the nuclear radius of medium-heavy nuclei. A 10 GeV CEBAF beam would also allow a momentum transfer high enough to select a small-size vector meson. Both Fang and Nikolaev remarked on the usefulness of a 10 GeV electron beam to study Color Transparency effects in ρ and ϕ production. Although an 8-10 GeV electron beam seems sufficient to start studying these interesting effects, a word of warning might be that this energy is only just enough to select both a small-size vector meson, and to have formation lengths comparable with the nuclear radius. Sophisticated theoretical calculations will therefore be required, and high-precision experiments on a light nucleus like ^{4}He are of highest priority.

3. Vector Meson Production

A CEBAF beam energy higher than 4 GeV opens up a unique window to study vector meson production. This was already partly addressed in the previous section. One idea behind vector meson production in a nuclear medium is to gain knowledge on the basic vector meson-nucleon interaction. However, depending on the experimental situation (beam energy, momentum transfer, produced vector meson, and radius of the nuclear medium) one may hope to obtain further information on the structure of the vector mesons,

and on properties of QCD.

Suppose a high energy electron beam produces a vector meson, for instance a ϕ, from a nuclear target. The ϕ will experience a strong ϕ-N interaction with the constituents of the nucleus, affecting the measured ϕ production rate. Thus, vector-meson production rates from different target nuclei inform us about the vector meson-nucleon interaction. However, a basic feature of QCD is that small size configurations interact at high energies with small cross sections with the nuclear medium. An example of this is the smallness of the ψ-N cross section, which has been interpreted as due to the smallness of a $c\bar{c}$ pair.[13]

Frankfurt discussed several distinctive signatures of color-coherent phenomena, reflecting this feature of QCD. One expects a large cross section for ϕ'-N, large non-diagonal $\phi + \mathrm{N} \rightarrow \phi' + \mathrm{N}$ transitions, small absorption probability of ψ', and production of ψ' in double rescattering processes. For the latter two processes a beam energy in excess of 10 GeV is a prerequisite.

Nikolaev showed the results of calculations for vector-meson production off nuclei. One of the ingredients of these calculations is a description of the evolution of the $s\bar{s}$ pair through the nuclear medium. This evolution is an overlap of both the internal dynamics (the internal wave function) of the $s\bar{s}$ pair and its interaction with the nuclear environment. The calculations for ρ, ρ', ϕ, and ϕ' production are expressed in terms of nuclear transparencies. Strong variations in dependencies on target nucleus, momentum transfer, and energy transfer show up amongst the various radial vector mesons. An example is shown in Fig. 4. The complex behaviour in the various production rates is related to the internal wave functions used for the various vector mesons, some of which have a node! This effect may be used to determine the radial structure (or at least the node position) of the vector mesons themselves. These measurements, and the theoretical interpretation, will benefit from a beam energy even higher than 10 GeV, but it is almost guaranteed that interesting effects will show up for high luminosity beams up to 10 GeV.

Increasing the beam energy would also open up possibilities to perform vector meson production experiments at both large energy transfer and large momentum transfer. As mentioned in the previous Section, large momentum transfer may also select a small spatial configuration of the $s\bar{s}$ pair in the initial state, enabling a search for Color Transparency effects. It may be difficult, though, to disentangle Color Transparency effects showing up in production rates from effects due to the radial structure of the vector mesons.

Kossov discussed an interesting idea to measure the properties of vector mesons in nuclear matter. Photoproduction of vector mesons near threshold can be used to measure the mass of vector mesons in the nuclear medium. The energy can be used to select the life time of the produced vector meson. For short enough life times, the decay will take place

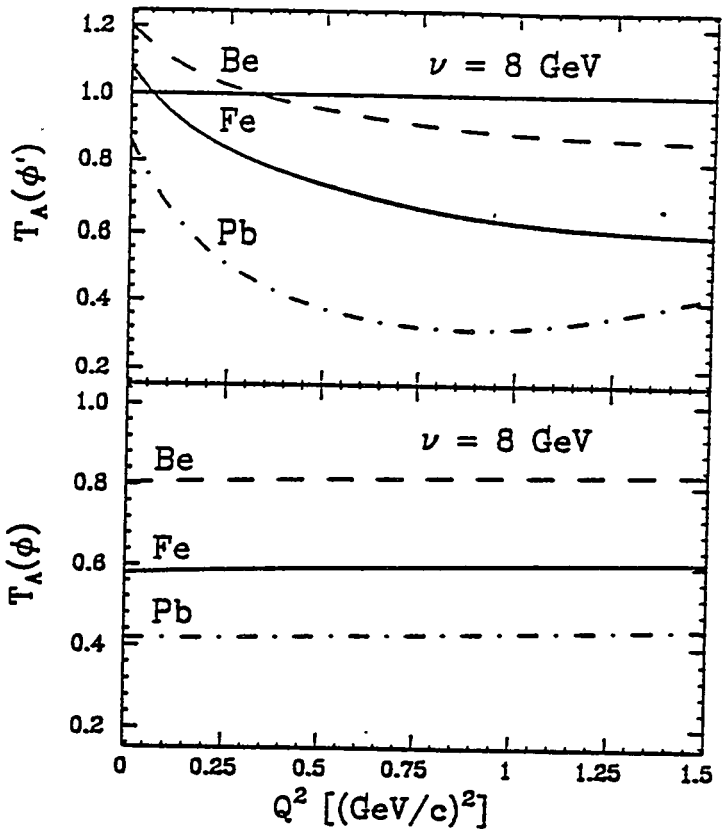


Figure 4: Momentum transfer dependence of the transparency ratio at an energy loss of 8 GeV for the ϕ' (upper figure) and ϕ (lower figure) mesons and for three different targets.

inside the nucleus. By selecting a purely electromagnetic decay mode, decay into e^+e^- pairs, properties of the vector mesons inside a nuclear field can be determined unobscured by the strong interactions in the decay channel.

During the workshop many interesting aspects of such a measurement were discussed. Is it possible to relate the measured mass of these vector mesons to the predictions of Brown and Rho,[14] who suggest that the mass of exchanged vector mesons in a nuclear system decreases with respect to their free mass? Here, the produced vector mesons hardly have time to interact with the nuclear system due to the relatively large values of the life time. However, the mass of the vector mesons may also be shifted when they decay virtually into pions, since the pion-nucleon interaction may be different inside a nuclear field. Though these experiments will be very hard to perform, probabilities for decay inside the nuclear field being small, and although modifications to free vector meson properties are likely to be small, they may prove very useful. A beam energy of 6 GeV seems well suited to study both these issues and the photoproduction of radially excited vector mesons.

4. Large Momentum Transfer (e,e'p) Scattering.

Recently the Virtual-Compton Scattering process has been the subject of consider-

able attention.[15] An electron scatters from a free proton, and causes the proton to emit a real photon. CEBAF combines both the capacity to measure the small cross section for this process and the excellent resolution required to distinguish this process from background processes (mainly emission of photons by the relativistic electrons and neutral pion production). This process can be seen as a powerful tool to study proton structure, complementary to the proton form factor measurements. Whereas the latter describes a fully on-shell nucleon, Virtual-Compton Scattering necessarily deals with a nucleon off its mass-shell, before emission of the real photon.

Van den Brand showed the strong sensitivity to the nucleon model used in the case of Virtual-Compton Scattering at large beam energies. Using polarization degrees of freedom in the ^{1}H($\vec{e}$,e'$\vec{p}$)γ reaction especially enhanced the sensitivity. Any nucleon model should not only be able to predict the proton form factors, but also the Virtual-Compton Scattering process.

A beam energy of about 8 GeV may be sufficient to access also the transition to hard scattering in the Virtual-Compton Scattering process, giving us information on the small scale non-perturbative structure of the proton.

These experiments will put high demands on the experimental resolutions required. To maintain at the higher energies a high resolution in invariant mass or in Bremsstrahlung photon emission angle, spectrometers with very good momentum and angular resolution are required.

Ent discussed the use of a high energy CEBAF beam in conjunction with the (e,e'p) reaction. During the last decades single-particle properties have been quite extensively investigated with the (e,e'p) reaction.[16] One of the surprising observations was the violation of the spectroscopic sum rule. Recently, possible explanations for this effect have been given, in which strong correlations among the nucleons in the nucleus shift strength up to very large missing energies.[17]

At large momentum transfers the hypothesis that the missing spectroscopic strength observed in (e,e'p) reactions will show up at large binding energies can be most readily checked. Final-State Interaction effects should become easier to calculate as the final-state proton-nucleon interaction is becoming essentially constant.

If the probability to find nucleons with high momentum and large binding energies is indeed significant, this would increase the average removal energy compared to previous calculations to about 70 MeV.[18] This large value of the average removal energy and high-momentum components has significant consequences in describing the nuclear dependence observed in deep-inelastic scattering (EMC effect[19]). The present theoretical belief is that a large part of the observed EMC effect can be explained by nucleon contributions only.

A measurement of the (e,e'p) reaction at large momentum transfers may constrain the nucleon contributions, and the need to include non-nucleonic components in the nuclear description.[20]

The kinematic freedom one has in the coincident (e,e'p) reaction can also be utilized to clarify the need to include relativistic effects in our description of the nuclear system. The presence of a lower component in the Dirac bound-state wave function may be apparent even at the Plane-Wave Impulse Approximation level.[21]

A CEBAF beam with energy between 4 and 8 GeV will be very suitable for investigating the (e,e'p) reaction in detail, providing information on nucleon models and the need to include non-nucleonic degrees of freedom in the description of nuclei.

5. Quark-Cluster Signatures

We typically describe a nucleus in a nucleonic framework as a set of protons and neutrons bound together by the strong interaction, mediated by the exchange of mesons. Of course we think that the real strong interaction occurs between the quarks (and gluons), confined in the nucleons, mediated by the exchange of gluons. Until now we do not have any clear signatures of the need to take these underlying quark degrees of freedom in the *description* of nuclei. As mentioned in the previous Section, some authors claim the EMC effect can only be explained fully if one includes non-nucleonic degrees of freedom, but this view is still controversial. Signatures for these underlying quark degrees of freedom might arise from a hunt for quark-exchange effects, or for 6q bags. The latter case distinguishes itself from a description in terms of two nucleons if the 6 quarks reorganize themselves in just one (antisymmetric) colorless state.[22]

Carlson described the possibility to look for the presence of 6q bags in nuclei by observing fast backward protons produced by high energy electron scattering off deuterium. He expressed the cross section of this reaction both in terms of nucleons and in terms of quarks, assuming the deep-inelastic scattering region has been reached ($Q^2 > 1$ (GeV/c)^2, $W > 2$ GeV). Carlson showed that for a CEBAF beam energy larger than 4 GeV an appreciable window to look for 6q bags will exist. A more conservative guess when these effects would play a role (looking only at fast backward protons with momenta larger than about 450 MeV/c), still shows an appreciable window for a beam energy between 6 and 10 GeV. If these 6q bags exist, it is likely that only the clean electromagnetic probe will be able to verify their existence conclusively.

6. Parity Violation

An important part of CEBAF's present scientific program is parity violation

experiments.[23,24] These experiments look at elastic scattering from the proton and ^{4}He, to probe strange quark effects in the hadronic systems.

Beise looked into the possibility to use a higher energy electron beam to measure the strangeness form factor at large values of the momentum transfer. Though it is very appealing to add a larger momentum transfer range to the measurements, the rate drops so fast as a function of momentum transfer that one would like to wait for the first round of CEBAF experiments first before embarking on such a program. Still, given the relevance of these experiments, we note the need for a small scattering angle, high momentum spectrometer. For instance, for a beam energy of 10 GeV and a scattering angle of 10 degrees, it seems possible to perform such measurements up to $Q^2 = 2$ (GeV/c)^2.

Beck discussed the possibility to measure parity-violating pion electroproduction. Such measurements might give access to the flavor dependence of meson production. A transition from pion production independent of the flavor of the struck quark at low momentum transfer, to production dependent on the flavor at high momentum transfer, is expected. The argument for the latter originates from the probability of producing leading pions being dependent on the flavor of the struck quark, as observed in deep-inelastic scattering experiments. These kind of measurements would become possible (with statistical uncertainties of the order of 10%) for an 8 GeV electron beam.

7. Conclusions

With respect to the areas covered by this Working Group, the two main topics of research which would open up with a CEBAF beam energy of 8-10 GeV are a precise study of Color Transparency effects, and a study of vector meson production.

When looking for the onset of Color Transparency, a major emphasis should be on high precision and high resolution (e,e'p) data at large momentum transfer. For the standard (e,e'p) reaction a reliable conventional nuclear physics baseline calculation seems possible, enabling one to look for possible small Color Transparency effects. Double rescattering experiments like (e,e'pp) and polarization experiments like (e,e'$\vec{p}$) are also of interest. Color Transparency effects may show up in these observables at lower values of momentum transfer, but it will be more difficult to obtain a reliable conventional nuclear physics baseline calculation.

Only limited data exist on lepton-induced vector meson production. A CEBAF beam energy higher than 4 GeV would open up a unique window to study the mechanism of these processes, and the properties of vector mesons. Calculations show a complex behaviour in production of various vector mesons off nuclei, related to the radial wave function of these vector mesons. At high energies these data may also give access to a possible onset

of Color Transparency effects.

A beam energy larger than 6 GeV may also solve a longstanding question of nuclear physics: whether there exists a need to include non-nucleonic degrees of freedom in our description of a nucleus. Measurements of the A(e,e'p) reaction at large values of the momentum transfer may inform us what part of the EMC effect can be explained only by including non-nucleonic degrees of freedom. Also, experiments looking for fast backward protons can show the possible existence of 6q bags. Measurements of Virtual-Compton Scattering may be used both as a check of our understanding of the (e,e'p) reaction, and as a test of the small-scale non-perturbative structure of nucleons.

Though interesting parity violation experiments seem possible with a higher energy CEBAF beam, e.g. measurements of the strangeness form factor at higher momentum transfer and of the flavor dependence of meson production, these studies would really benefit from even higher beam energies than 10 GeV.

References

1) A. Mueller, *Proceedings of the Seventeenth Recontre de Moriond on Elementary Particle Physics,* (Les Arcs, France 1982) edited by J. Tran ThanVan (Editions Frontieres, Gif-sur-Yvette, France 1982); S. J. Brodsky, in Van (Editions Frontieres, Gif-sur-Yvette, France 1982); S. J. Brodsky, in *Proceedings of the Thirteenth International Symposium on Multiparticle Dynamics* (Volendam, The Netherlands 1982) edited by W. Kittel *et al.*, (World Scientific, Singapore 1983).
2) L. Frankfurt, G. A. Miller, M. Strikman, Comments Nucl. Part. Phys., **21**, 1 (1992) and references therein.
3) A. S. Carroll *et al.*, Phys. Rev. Lett. **61**, 1698 (1988).
4) S. J. Brodsky and G. F. De Teramond, Phys. Rev. Lett. **60**, 1924 (1988).
5) J. P. Ralston and B. Pire, Phys. Rev. Lett. **65**, 2343 (1990).
6) N. C. R. Makins *et al.*, Phys. Rev. Lett. **72**, 1986 (1994)
7) G. Farrar, H. Liu, L. L. Frankfurt, and M. I. Strikman, Phys. Rev. Lett. **61**, 686 (1988).
8) O. Benhar *et al.*, Phys. Rev. Lett. **69**, 881 (1992).
9) N. Nikolaev *et al.*, Nucl. Phys. **A567**, 781 (1994).
10) W.R. Greenberg and G.A. Miller, Phys. Rev. C **49**, 2747 (1994), and W.R. Greenberg,

private communications.
11) G.Y. Fang, FERMILAB-93-305.
12) N. Nikolaev *et al.*, Phys. Lett. **B309**, 179 (1993).
13) L. Frankfurt and V. Khose, JETP Lett. 1976; L. Frankfurt and M. Strikman, Prog. Part. Nucl. Phys. 1990.
14) G.E. Brown and M. Rho, Phys. Rev. Lett. **66**, 2720 (1991).
15) CEBAF experiment 93-050, P.Y. Bertin, G. Fournier, and C.E. Hyde-Wright, spokespersons; CEBAF proposal 94-011, J.F.J. van den Brand, H.J. Bulten, and R. Ent, spokespersons.
16) L. Lapikás, Nucl. Phys. **A553**, 297c (1993).
17) R. Schiavilla *et al.*, Nucl. Phys. **A473**, 267 (1987); B.E. Vonderfecht et al., Nucl. Phys. **A503**, 1 (1989); M. Baldo et al., Phys. Rev. C **41**, 1748 (1990).
18) A.E.L. Dieperink and G.A. Miller, Phys. Rev. C **44**, 866 (1991).
19) J.J. Aubert *et al.*, Phys. Lett. **B123**, 275 (1983).
20) L. Frankfurt, G.A. Miller, and M. Strikman, Phys. Rev. Lett. **68**, 17 (1992).
21) S. Gardner and J. Piekarewicz, FSU-SCRI-94-01 and submitted to Phys. Rev. C; S. Gardner, private communications.
22) P. González and V. Vento, Few-Body Systems **2**, 145 (1987).
23) M.J. Musolf *et al.*, Phys. Rep. **239**, 1 (1994).
24) CEBAF experiment 91-004, E. Beise, spokesperson; CEBAF experiment 91-010, J.M. Finn and P. Souder, spokespersons; CEBAF experiment 91-017, D. Beck, spokesperson.

Color Transparency Experiments at Higher Energies

B. W. Filippone

California Institute of Technology, Pasadena, California 91125

Abstract

The phenomena of Color Transparency has recently attracted a significant amount of theoretical (and experimental) interest. With an increase in the CEBAF beam energy to 8 - 10 GeV, important new data on the process could become available. The present status of the experiments and future prospects at CEBAF are discussed.

INTRODUCTION

As there are several contributions to this workshop [1] that deal, at least in part, with the theoritical aspects of Color Transparency, I will only briefly review the physics. It was Mueller and Brodsky [2] who first proposed that in wide angle exclusive processes, the soft initial and final state interactions (ISI and FSI) of hadrons in nuclei should vanish at high energies. This effect, originally based on arguments using perturbative QCD, was called "Color Transparency" (CT), in reference to the disappearance of the color forces between the hadrons in nuclei. Some recent models of CT predict significant effects for Q^2 as low as $5\,(\mathrm{GeV/c})^2$ [3–7].

The main physics issues that play a role in experimental observables are:

1. Formation of a special state at high momentum transfer (Q^2) (eg. small interquark separation).

2. Vanishing of hadronic interactions for this special state (eg. color screening in a compact color singlet state).

3. Evolution of this special state back into a "normal" hadron in a characteristic time [eg. in the rest frame of the particle $t_c^0 \sim 1/\Delta M$ with $\Delta M \sim$ GeV. Then in the lab frame $t_c^L \sim (0.3 - 1 fm/c/GeV)E_h$, where E_h is the hadron energy in the lab.]

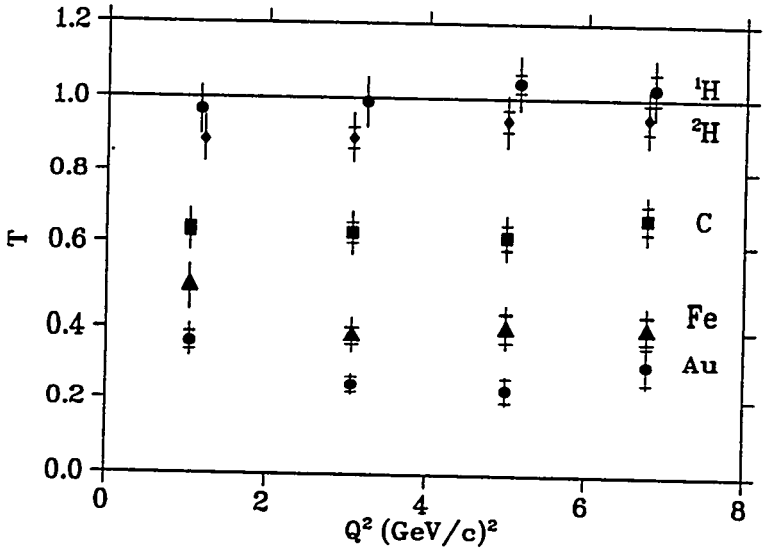
The experimental signatures of CT rely on explioting this features. For example, the appearance of CT with increasing energy can be tested by measurement of the nuclear transparency T, the ratio of the measured cross section to the cross section expected in the limit of complete CT (*i.e.*, no ISI or FSI). At low energies, $T < 1$ because of absorption or deflection of the hadrons by ISI and FSI with the nucleus. As the energy increases, and if CT effects begin to dominate the scattering, T should increase to unity. An alternative approach is to select a process that at low energies is known to be dominated by final state interactions (eg. final-state induced polarization) and look for the disappearance of these processes as the energy is increased. In this contribution, I will discuss the previous experiments, the present approved experiments, and the possible future experiments that could be done at CEBAF with higher energies.

PREVIOUS EXPERIMENTS

The first experimental suggestion of CT occurred in high energy $A(p, 2p)$ reaction studies at Brookhaven National Laboratory (BNL) by Carroll *et al.* [8], where some indications of an increasing transparency with Q^2 was observed. However, because of a measured decrease in T at even higher energies, these data could not be taken as an unambiguous signal of CT. Ralston and Pire [7] suggested that the maximum in T is due to a soft process that interferes with the perturbative QCD amplitude in free proton-proton scattering but is suppressed in the nuclear environment.

Another recent experiment, using an electromagnetic probe, has recently published their first results. Experiment NE18 [9,10], performed at SLAC, studied the $A(e,e'p)$ reaction as a function of momentum transfer up to $Q^2 = 7$ (GeV/c)^2. Measurement of the electron and proton in coincidence allows reconstruction of the "missing" energy $E_m \equiv \nu - E'_p + M_p - K_{A-1}$ and missing momentum $\mathbf{p}_m \equiv \mathbf{p}' - \mathbf{q}$ not accounted for in the detected particles. Here $q = (\nu, \mathbf{q})$ is the virtual photon four-momentum transfer ($Q^2 = -q^2$), $p' = (E'_p, \mathbf{p}')$ is the four momentum of the detected proton, and K_{A-1} is the kinetic energy of the recoiling $A-1$ system.

Figure 1 shows the measured transparency for $A(e,e'p)$ from this experiment.



i. 1 Nuclear transparency vs. momentum transfer. The inner error bars .e statistical and the outer error bars are the statistical and systematic errors added in quadrature.

Color Transparency is expected to produce an increase in T with increasing Q^2 for the nuclear targets. There is no statistically significant evidence of such an increase in the measured Q^2 range. The rise in the value of T at $Q^2 = 1\,(\mathrm{GeV/c})^2$ for Fe and Au is at least partially due to the smaller nucleon-nucleon total cross section at momenta $\simeq 1\,\mathrm{GeV/c}$, as has been suggested in Reference [6]. For $Q^2 \geq 3\,(\mathrm{GeV/c})^2$ the magnitude of the measured T is within the range of the existing Glauber model calculations (i.e., no CT effects) which

predict an essentially constant value for T [3–6,17–19]).

A new analysis from Fermilab E665 [12] also is interesting in the context of Color Transparency. In this experiment vector mesons (ρ's and ϕ's) are detected in coincidence with scattered muons from several nuclear targets. At the kinematics of the experiment the process is dominated by the fluctuation of the virtual photon into a vector meson which then "quasielastically" scatters either from the entire nuclues or from individual nucleons. Both of these processes show a suggestion of a Q^2 dependence that is consistent with CT [12]. In this experiment the evolution time of the small state back into a "normal" hadron is not important as the energy is so large (several hundred GeV) that the evolution certainly takes place outside the nucleus. Full results from this analysis are expected shortly.

APPROVED FUTURE EXPERIMENTS

The $A(p,2p)$ experiments at BNL are being improved and continued with experiment E850 [13]. For this experiment the collaboration has built a new large solid angle spectrometer to allow measurement of the momentum of both final-state protons. In the original experiment the momentum of only one of the protons was measured, preventing the extraction of missing energy information. The new experiment will take significantly more data in the energy range of the previous experiment ($Q^2 = 3 - 10$ (GeV/c)^2) and also extend the Q^2 range up to 20 (GeV/c)^2. This experiment has recently begun initial checkout of the spectrometer and shortly hopes to begin data taking.

At CEBAF there are 3 experiments that will provide some information on CT:

- E91-006 [14]: ^{12}C, ^{16}O $(e,e'\vec{p})$; $Q^2 = 1 - 4$ (GeV/c)^2

Searching for the vanishing of final-state induced recoil polarization.

- E91-007 [15]: $A(e,e'p)$; $Q^2 = 6$ (GeV/c)^2

Similar to the SLAC kinematics, but with much higher statistics. Able to study transparency for different nuclear shells.

- E91-013 [16]: $A(e,e'p)$; $Q^2 = 1 - 4$ (GeV/c)^2 (GeV/c)^2

Will provide a high statistics benchmark in a region where CT effects are likely to be small to allow comparison with future higher Q^2 data.

While these experiments will provide improved data in the Q^2 range of the SLAC experiment NE18 (eg. the ability to separate individual nuclear shells) higher energy is clearly needed to improve our understanding of this process.

POSSIBLE HIGH ENERGY EXPERIMENTS AT CEBAF

There are several obvious extensions of previous experiments that would be possible with higher energy beam at CEBAF. There are also several new types of experiments that could utilize the unique capabilities at CEBAF. Examples include:

- $A(e,e'p)$; $Q^2 = 12 - 16$ (GeV/c)^2.

Using the spectrometers available in Hall C and an 8 GeV beam, an experiment is possible up to $Q^2 = 12$ (GeV/c)^2 as shown in Table I. With such a configuration a 5% measurement on several nuclear targets would be possible with about 1 month of beam time. With 10 GeV and a new small-angle high-momentum spectrometer, the measurements could be extended up to $Q^2 = 16$ (GeV/c)^2.

- $A(e,e'p)$ at large perpendicular momentum [20]

By measuring in a kinematic region where simple quasielastic scattering is small (large p_m), most of the rate is from final-state rescattering. Since this process is dominated by final-state effects, a significant reduction in the rate as a function of Q^2 could be a signature of CT effects. However the rate in this kinematic region is extremely small.

- $A(e,e'\rho)$, $A(e,e'\rho N)$

Measurements of these processes in Hall B could be an important extension [21] of the E665 data at Fermilab. Information on evolution time of the small state would be possible with the much lower energy transfers (even with higher energies at CEBAF!).

- $A(e,e'\pi)$ at high Q^2

With proper choice of kinematics (E_π near ν) a "quasielastically" scattered pion can be produced in the nucleus. The experiment is then similar to $A(e,e'p)$. However at the larger momentum transfers there is a physics background due to quark fragmentation that must be corrected for.

•$A(e,e'\vec{p})$ at high Q^2

Extension of the proposed measurements from CEBAF E91-006 to high momentum transfer.

•$A(e,e'2N)$ at high Q^2

By selecting kinematics where this process is dominated by the final state rescattering of a struck nucleon, this process could be studied as a function of momentum transfer. Such a program has recently been proposed for Hall B [22] at lower Q^2.

In summary, experimental information on Color Transparency is clearly at an early stage. It is also clear that high energies and momentum transfer are the most direct route to improving our understanding of this process. A CEBAF beam of 8 or 10 GeV could certainly provide important input to this problem.

This work was supported in part by the National Science Foundation.

REFERENCES

[1] See eg. N. Nikolaev (contribution to this workshop) and S. Brodsy (contribution to this workshop).

[2] A. H. Mueller, in *Proceedings of the XVII Rencontre de Moriond, 1982*, edited by J. Tran Thanh Van (Editions Frontieres, Gif-sur-Yvette, France, 1982), p. 13; S. J. Brodsky, in *Proceedings of the Thirteenth International Symposium on Multiparticle Dynamics*, edited by W. Kittel, W. Metzger, and A. Stergiou (World Scientific, Singapore, 1982), p. 963.

[3] G. R. Farrar *et al.*, Phys. Rev. Lett. **61**, 686 (1988).

[4] B. K. Jennings and G. A. Miller, Phys. Rev. D **44**, 692 (1991).

[5] O. Benhar *et al.*, Phys. Rev. Lett. **69**, 881 (1992).

[6] L. L. Frankfurt, M. I. Strikman, and M. B. Zhalov, preprint 1993.

[7] J. P. Ralston and B. Pire, Phys. Rev. Lett. **61**, 1823 (1988).

[8] A. S. Carroll *et al.*, Phys. Rev. Lett. **61**, 1698 (1988).

[9] N.C.R. Makins *et al.*, Phys. Rev. Lett. **72**, 1986 (1994).

[10] T. G. O'Neill, *et al.*, 1994, (submitted for publication).

[11] T. G. O'Neill, Ph.D. thesis, 1994 (unpublished).

[12] G. Fang (contribution to this workshop).

[13] AGS exp. 850, A. S. Carroll and S. Heppelman, spokespersons.

[14] CEBAF experiment 91-006, A. Saha, spokesperson.

[15] CEBAF experiment 91-007, R. Milner, spokesperson.

[16] CEBAF experiment 91-013, D. Geesaman, spokesperson.

[17] A. Kohama, K. Yazaki, and R. Seki, Nucl. Phys. **A536**, 716 (1992).

[18] A.S. Rinat and B. K. Jennings, Preprint 1993.

[19] N.N. Nikolaev *et al.* Nucl. Phys. **A567**, 781 (1994).

[20] N. Nikolaev, private communication.

[21] G. Fang, private communication.

[22] M. Strikman, private communication.

TABLES

TABLE I. Possible kinematics for a high energy color transparency experiment at CEBAF. For the $Q^2 = 6-12\,(\mathrm{GeV/c})^2$ points the HMS and SOS spectrometers of Hall C would be suitable. For the $Q^2 = 16\,(\mathrm{GeV/c})^2$ point, a new high-momentum/small-angle spectrometer would be required.

Q^2	E	E'	θ_e	P_p	θ_p	Rate
$(\mathrm{GeV/c})^2$	(GeV)	(GeV)	(deg)	(GeV/c)	(deg.)	(1/hr)
6.0	4.70	1.50	55.0	4.03	17.8	320
8.0	5.76	1.50	57.5	5.12	14.3	100
10.0	6.83	1.50	59.2	6.20	12.0	40
12.0	7.90	1.50	60.4	7.27	10.3	10
16.0	10.00	1.50	62.1	9.39	8.1	1

KFA-IKP(Th)-1994-20
1 June 1994

Color transparency after the NE18 and E665 experiments: Outlook and perspectives at CEBAF.*

J.Nemchik[1,3], N.N.Nikolaev[2,3] and B.G.Zakharov[2]

[1)]*Institute of Experimental Physics, Slovak Academy of Sciences, Watsonova 47, 043 53 Kosice, Slovak Republik*
[2)]*L.D.Landau Institute for Theoretical Physics, GSP-1, 117940, ul.Kosygina 2, V-334, Moscow, Russia*
[3)]*IKP(Theorie), KFA Jülich, D-52425 Jülich, Germany*

ABSTRACT

CEBAF is a high-luminocity factory of virtual photons with variable virtuality Q^2 and transverse size. This makes CEBAF, in particular after the energy upgrade to (8-12)GeV, an ideal facility for uncovering new phenomena, and opening new windows, at the interface of the perturbative and nonperturbative QCD. We discuss color transparency as the case for a broad program on electroproduction of vector mesons ρ^0, ω^0, ϕ^0 and their radial excitations ρ', ω', ϕ' at CEBAF. We also comment on the second generation of experiments on color transparency in $^4He(e,e'p)$ scattering, which are also feasible at CEBAF.

In 1994, we can make more reliable projections into future because our understanding of the onset of color transparency has greatly been augmented by two experiments completed in 1993:
i) no effect of CT was seen in the SLAC NE18 experiment on $A(e,e'p)$ scattering at virtualities of the exchanged photon $Q^2 \lesssim 7$ GeV^2,
ii) strong signal of CT was observed in the FNAL E665 experiment on exclusive ρ^0-meson production in deep inelastic scattering in the same range of Q^2.

We discuss the impact of these observations on the CEBAF experimental program. We argue they both are good news, both were anticipated theoretically, and both rule in the correct QCD mechanism of the onset of CT.

*) Presented by NNN at the Workshop on CEBAF at Higher Energies CEBAF, 14-16 April 1994

1 Introduction

The fundamental prediction of QCD is that the quark configurations with small transverse size $\vec{r}$ have small interaction cross section [1], which was dubbed *color transparency* (CT) [2]. Looking for CT is long discussed as the case for the high-luminocity, high-duty cycle, (10-20) GeV electron facility, which is well documented in the ELFE project [3] (ELFE = European Laboratory for Electrons). In the meantime, the good news from CEBAF is a possibility of the (8-12)GeV upgrade, which opens exciting possibilities of doing CT physics at CEBAF.

CEBAF is a high-luminocity factory of virtual photons. Higher energy means a higher virtuality Q^2 of photons, and higher Q^2 means that smaller sizes are becoming accessible reaching eventually into the perturbative QCD region. Higher energy also means longer lifetime of these small-size states. However, from the very start, we must emphasize that as far as CT physics is concerned, the *purely perturbative* region lies well beyond the kinematical range of CEBAF experiments on *exclusive* processes, even after the (8-12)GeV energy upgrade. Testing the *purely perturbative* QCD to few decimal places is a task of *inclusive* experiments at superhigh energy facilities like LEP or HERA. Even at LEP and HERA, the predictive power of the *purely perturbative* QCD rapidly deteriorates when the *exclusive* processes are considered. The real task of the CEBAF experiments is *to uncover new QCD phenomena in exclusive reactions at the interface of the perturbative and nonperturbative QCD.* Very conservative conclusion of this overview is that the energy-upgraded CEBAF shall do the job.

Before jumping into conclusions on the feasibility of CT physics at CEBAF, one must recall and critically summarize the results of the two CT experiments completed in 1993:

- The $A(e,e'p)$ reaction on the D, C, Fe and Au targets was studied by the SLAC NE18 collaboration with the negative result: no CT effects are seen at $Q^2 \leq 7$ GeV^2 [4].
- The FNAL E665 experiment [5] on exclusive production of the ρ^0 mesons in deep inelastic scattering of muons on nuclei produced a solid evidence for CT in precisely the same range of Q^2 as explored in the NE18 experiment.

The early history of CT focused on the quasielastic $A(e,e'p)$ scattering of electrons on nuclei. A number of predictions of precocious CT at low Q^2 were published (for the review and references see [6]), and the failure to confirm this precocious CT in the NE18 experiment considerably dampened the whole subject of CT. Fortunately, more consistent treatment rather *predicted* a very slow onset of CT in the $A(e,e'p)$ scattering [7,8]. As a matter of fact, the NE18 results do perfectly confirm the correct theory and rule in the mechanism of CT, which is alive and well, and we can joyfully recite Mark Twain's telegram to the Associated Press: **"The reports of my death were an exaggeration".**

The parallel development was a theory of CT in (virtual) photoproduction of vector mesons $\gamma^* N \to VN$. From the theoretical point of view, this is a much cleaner case, with a well understood shrinkage of the transverse size of the virtual photon with the increase of Q^2 [9,10]. The prediction [9], not a postdiction, of the precocious onset of CT was confirmed by the FNAL E665 experiment [5], which put the CT physics in the right perspective.

The strong point which we wish to make in this review is that after the energy upgrade, CEBAF experiments on exclusive electroproduction of vector mesons can significantly contribute to our understanding of the onset of CT. Furthermore, the experiments on production of the radially excited vector mesons will open an entirely new window not only on the

mechanism of CT, but also on the quark structure and poorly known spectroscopy of radial excitations. In the $A(e,e'p)$ sector, we comment on the potential of experiments on the ^4He target, in which the onset of CT is sooner than for any other nucleus owing to the small size of the ^4He nucleus.

In this contribution to the Workshop on CEBAF at Higher Energies we concentrate on the recent experimental and theoretical developments, for the earlier reviews on the subject see [3,11-14].

2 CT in exclusive production of vector mesons

2.1 CT and dipole cross section

In order to be quantitative, let us set up the theoretical framework, which is the lightcone dipole-cross section representation [15]. Mesons can be viewed as color dipoles. The distribution of the transverse size $\vec{r}$ of color dipoles in the meson is given be the $q\bar{q}$ wave function $\Psi(z,\vec{r})$, where z is the fraction of meson's momentum carried by the quark. This mixed $(z,\vec{r})$ lightcone representation is custom tailored for description of CT. By the Lorentz-dilation, in the high-energy scattering the dipole size $\vec{r}$ becomes as good a conserved quantum number as an angular momentum. The fundamental quantity which describes all the scattering processes, is the dipole cross section $\sigma(\nu,r)$ for interaction of the color dipole of size r with the target nucleon. Of course, apart from the $q\bar{q}$ Fock state, the lightcone hadrons contain the higher $q\bar{q}g....$ Fock states. The effect of gluons in the *projectile* dipole brings in the dependence of $\sigma(\nu,r)$ on energy ν, which can be related to the gluon structure function $G(x,q^2)$ of the *target nucleon* [16,17]. Specifically, at small r, the dipole cross section is $\propto r^2$,

$$\sigma(\nu,r)=\frac{\pi^2}{3}r^2\alpha_S(r)G(x,q^2) \tag{1}$$

where $q^2=A_0/r^2$ with $A_0\approx 10$ [18], and $x=q^2/2m_p\nu$. This CT property $\propto r^2$ derives from the decoupling of gluons from a very small color dipole. At large $r\gtrsim 1$f, the dipole cross section saturates because color forces do not propagate beyond the confinement radius. At high energy, the dipole cross section is a solution of the generalized BFKL equation [19] and describes, for instance, structure functions of deep inelastic scattering at HERA [20]. For any $q\bar{q}$ state, the total cross section of interaction with the target nucleon equals

$$\sigma_{tot}=\int_0^1 dz\int d^2\vec{r}\,\sigma(\nu,r)|\Psi(r,z)|^2\,. \tag{2}$$

The dipole cross section is a universal function of r, the dependence on the process is only contained in the wave function of the $q\bar{q}$ state. Fig. 1 shows qualitatively, how the dipole cross section is probed in different processes:

- The total pion-nucleon cross section $\sigma_{tot}(\pi N)$ and the real photoabsorption cross section probe the region $r\gtrsim 1$f.
- The $\sigma_{tot}(J/\Psi N)\approx$(5-6)mb comes from $r\sim R_{J/\Psi}\approx 0.45$f.
- The real photoproduction of the open charm probes the region of $r\sim 1/m_c\approx 0.15$f.
- The proton structure function $F_2(x,Q^2)$ receives contribution from $1/\sqrt{Q^2}\lesssim r\lesssim 1$f, and CT property of the dipole cross section is crucial for the Bjorken scaling [12,15,17].

- The scaling violations in $F_2(x,Q^2)$ are dominated by the contribution from $r \sim 1/\sqrt{Q^2}$.

In CT experiments one looks for a weak intranuclear final (and initial) state interactions, which will be the case if the nuclear production amplitude is dominated by the dipole cross section at small r such that $\sigma(\nu,r)$ is much smaller than the free-nucleon cross section. Whether the particular exclusive reaction is selective of such a small r or not, requires the case-by-case study.

2.2 How CT is tested in leptoproduction of vector mesons?

The exclusive (elastic) production $\gamma^* p \to Vp$ ($V = \rho^0, \phi^0, J/\Psi, ...$) is an ideal laboratory for testing CT ideas [9,10,12,21-24]. The forward production amplitude equals

$$M = \langle V|\sigma(\nu,r)|\gamma^*\rangle = \int_0^1 dz \int d^2\vec{r}\,\sigma(\nu,r)\Psi_V^*(r,z)\Psi_{\gamma^*}(r,z) \tag{3}$$

Here $\Psi_{\gamma^*}(r,z)$ is the wave function of the $q\bar{q}$ fluctuation of the photon, which at high energy ν is formed at a large distance (the coherence length)

$$l_c = 2\nu/(Q^2 + m_V^2) \tag{4}$$

in front of the target nucleon. The most important feature of $\Psi_{\gamma^*}(r,z)$ as derived in [15] is an exponential decrease at large size

$$\Psi_{\gamma^*}(r,z) \propto \exp(-\varepsilon r), \tag{5}$$

where

$$\varepsilon^2 = m_q^2 + z(1-z)Q^2 \tag{6}$$

and m_q is the quark mass. Therefore, the amplitude (3) recives the dominant contribution from $r \sim r_S \approx 3/\varepsilon$. In the nonrelativistic quarkonium $z \approx \frac{1}{2}$, $m_V \approx 2m_q$, and we conclude that the vector meson production amplitude probes the dipole cross section at the scanning radius r_S given by [9,10,23]

$$r_S = \frac{6}{\sqrt{m_V^2 + Q^2}}. \tag{7}$$

The scanning phenomenon is qualitatively illustrated in Fig. 2. If the scanning radius $r_S \lesssim R_V$, where R_V is the radius of the vector meson, then for the (T) transverse and (L) longitudinal mesons

$$M_T \propto r_S^2 \sigma(r_S) \propto \frac{1}{(Q^2 + m_V^2)^2} \tag{8}$$

$$M_L \approx \frac{\sqrt{Q^2}}{m_V} M_T \propto \frac{\sqrt{Q^2}}{m_V} \frac{1}{(Q^2 + m_V^2)^2} \tag{9}$$

This prediction [10] of the dominance of the longitudinal cross section agrees with the E665 [5] and the NMC [25] data. Compared to the vector dominance model, the predicted amplitudes contain extra $(Q^2 + m_V^2)$ in the denominator, the origin of which is precisely in CT property $\sigma(r_S) \propto r_S^2$.

The scanning radius r_S decreases, and the virtual photon shrinks, with increasing Q^2. Notice, however, the large numerical factor in Eq. (7), for which the onset of small-size dominance requires very large Q^2. Remarkably, this large factor derives precisely from CT

property of the dipole cross section. Because of this large scanning radius, the vector meson production probes the gluon structure function $G(x,q^2)$ at [23]

$$q^2 \sim 0.2(Q^2 + m_V^2) \tag{10}$$

The emergence of this very low factorization scale was not noticed in [26].

Because of a large scanning radius, the simple nonrelativistic approximation remains viable in quite a broad range of Q^2, and the production amplitude can be calculated using the constituent quark wave functions of vector mesons. For the same reason of large r_S, the asymptotic predictions [10] $\sigma_T \propto 1/Q^8$ and $\sigma_L \propto 1/Q^6$, can not readily be tested at $Q^2 \lesssim (10-20)\mathrm{GeV}^2$ studied sofar.

In the conventional quark model, the radii of the ρ and π mesons are about identical. Once the radius of the ρ^0 is specified, further predictions [23,27] for the ρ^0 production cross section do not contain any adjustable parameters. They are presented in Fig. 3. We use the low-energy dipole cross section of Ref. [15]. Shown is the combination of the longitudinal and transverse cross sections as measured by the NMC collaboration. The agreement with the recent NMC data [25] is excellent. This agreement in a broad range of Q^2 shows we have a good understanding of the dipole cross section from the hadronic scale $r \sim$(1-2)f down to the smallest dipole size $r \sim 0.3$f achieved in the NMC experiment at $Q^2 \sim 20\mathrm{GeV}^2$. Over this range of radii r, the dipole cross section drops by approximately one order in magnitude, and this agreement of the total production rate with experiment is by itself a very important test of CT. Similar calculations [23] give an excellent description of the J/Ψ production and of the real photoproduction of the ρ^0 at HERA.

2.3 CT in exclusive production on nuclei

Having tested CT property of the dipole cross section in the production on free nucleons, now we turn our attention to the production on nuclei. The $q\bar{q}$ pair produced on the target nucleon, recombines into the observed vector meson with the recombination (formation) length

$$l_f = \frac{\nu}{m_V \Delta m}, \tag{11}$$

where Δm is the typical level splitting in the quarkonium. At high energy ν both l_c and l_f exceed the radius R_A of the target nucleus, which greatly simplifies the theoretical analysis. The E665 data [5] correspond to this situation. In this high-energy limit, nuclear transparency for the incoherent (quasielastic) production on a nucleus $\gamma^* A \to V A^*$ equals [12,22] (we suppress the energy-dpendence of $\sigma(\nu,r)$)

$$T_A = \frac{\sigma_A}{A\sigma_p} = \frac{1}{A}\int d^2\vec{b}T(b)\frac{\langle V|\sigma(r)\exp\left[-\frac{1}{2}\sigma(r)T(b)\right]|\gamma^*\rangle^2}{\langle V|\sigma(r)|\gamma^*\rangle^2}$$
$$= 1 - \Sigma_V \frac{1}{A}\int d^2\vec{b}T(b)^2 + \dots, \tag{12}$$

where

$$T(b) = \int dz n_A(b,z) \tag{13}$$

is the optical thickness of a nucleus at the impact parameter b and $n_A(b,z)$ is the nuclear matter density. In the quasielastic production one sums over all excitations and breakup of

the target nucleus. The total cross section of the coherent (elastic) production $\gamma^* A \to V A$, when the target nucleus remains in the ground state, equals [22]

$$\sigma_{coh}(VA) = 4\int d^2\vec{b}\left|\langle V|1-\exp\left[-\frac{1}{2}\sigma(r)T(b)\right]|\gamma^*\rangle\right|^2$$
$$= 16\pi\left.\frac{d\sigma(\gamma^* N\to VN)}{dt}\right|_{t=0}\int d^2\vec{b}T(b)^2\left[1-\frac{1}{2}\Sigma_V T(b)+...\right]. \qquad (14)$$

In Eqs. (12,14) we have explicitly shown the leading terms of final state interaction (FSI). The strength of FSI is measured by the observable [12]

$$\Sigma_V = \frac{\langle V|\sigma(r)^2|\gamma^*\rangle}{\langle V|\sigma(r)|\gamma^*\rangle}. \qquad (15)$$

Evidently, the matrix element in the numerator of (14) is dominated by

$$r\sim r_{FSI}=\frac{5}{3}r_S = 10\sqrt{Q^2+m_V^2}, \qquad (16)$$

which gives an estimate [10,23]

$$\Sigma_V \approx \sigma(r_{FSI}) \qquad (17)$$

CT and/or weak FSI set in when $r_{FSI}\ll R_V$, i.e., when $\Sigma_V \ll \sigma_{tot}(VN)$. In this regime of CT, the Σ_V is insensitive to the wave function of the vector meson, so that predictions of FSI effects are less model independent than predictions for the total production cross section. The large value of r_{FSI} Eq. (16) implies that FSI only slowly vanishes with the increase of Q^2, and this slow onset of CT is driven by the very mechanism of CT.

2.4 The E665 experiment [5]: the decisive proof of CT

Our predictions [9,10] for nuclear effects in the coherent and incoherent exclusive ρ^0 production are compared with the E665 data in Figs. 4-7. In Fig. 4 we show nuclear transparency for the incoherent production. Nuclear attenuation is very strong at small Q^2 and gradually decreases with Q^2. The effect is particularly dramatic for the heavy nuclei (Ca, Pb), and leaves no doubts the E665 observed the onset of CT. The predicted Q^2 dependence of nuclear transparency for the forward coherent production on nuclei $T_A^{(coh)} = (d\sigma_A^{(coh)}/A^2 d\sigma_N)|_{t=0}$ is shown in Fig. 5. We predict a rise of $T_A^{(coh)}$ with Q^2 towards $T_A^{(coh)}=1$ for vanishing FSI. The predicted Q^2 dependence of the coherent production cross section relative to the cross section for the carbon nucleus is presented in Fig. 6. In the regime of vanishing FSI,

$$R_{coh}^{(CT)}(A/C) = \frac{12\sigma_A}{A\sigma_C}\approx\frac{AR_{ch}(C)^2}{12R_{ch}(A)^2}, \qquad (18)$$

which gives $R_{coh}^{(CT)}(Ca/C)=1.56$ and $R_{coh}^{(CT)}(Pb/C)=3.25$. Here $R_{ch}(A)$ is the charge radius of a nucleus. The observed growth of the Pb/C ratio with increasing Q^2 gives a solid evidence for the onset of CT.

The (approximate) A^α parametrization is a convenient short-hand representation of the A-dependence of nuclear cross sections, although the so-defined exponent α slightly depends on the range of the mass number A used in the fit. Then, Eq. (12) predicts that $\alpha_{inc}(Q^2)$ tends to 1 from below, as Q^2 increases. In the limit of vanishing FSI Eqs. (14,18) predict

$\sigma_{coh} \sim A^{4/3}$, so that $\alpha_{coh}(Q^2)$ tends to $\approx \frac{4}{3}$ from below as Q^2 increases (more accurate analysis shows that the no-FSI cross section in the $C-Pb$ range of nuclei has the exponent $\alpha_{coh} \approx 1.39$). The agreement between the theory and the E665 fits is good (Fig. 7). Both the $\alpha_{coh}(Q^2)$ and $\alpha_{inc}(Q^2)$ rise with Q^2, which is still another way of stating that the E665 data confirm the onset of CT. Even at the highest $Q^2 \sim 10$ GeV^2 of the E665 experiment, the residual nuclear attenuation is still strong, confirming our prediction of large value of r_{FSI} Eq. (16).

2.5 Scaling properties of nuclear attenuation: electroproduction of the ρ^0 *vs.* the real photoproduction of the J/Ψ

Eq. (16) in conjunction with Eq. (7) suggests that nuclear attenuation approximately scales with $(Q^2 + m_V^2)$. Specifically, we predict identical nuclear transparency in the real photoproduction ($Q^2 = 0$) of the J/Ψ and electroproduction of the ρ^0 at $Q^2 \approx m^2_{J/\Psi} - m^2_\rho$, which nicely agrees with the experiment:

For the ρ^0 production at $\langle Q^2 \rangle = 7$ GeV^2 the E665 experiment gives $T_{Pb}/T_C = 0.6 \pm 0.25$. This can be compared with the NMC result $T_{Sn}/T_C = 0.7 \pm 0.1$ for the real photoproduction of J/Ψ in the similar energy range [28]. Similar scaling law holds for the coherent production of the ρ^0 and the J/Ψ. In the regime of vanishing FSI Eq. (12) gives [10,22] $R_{coh}(Sn/C) = 2.76$, $R_{coh}(Fe/Be) = 2.82$, $R_{coh}(Pb/Be) = 4.79$. The experimental data on the real photoproduction of J/Ψ give $R_{coh}(Sn/C) = 2.15 \pm 0.10$ in the NMC experiment [29] and $R_{coh}(Fe/Be) = 2.28 \pm 0.32$, $R_{coh}(Pb/Be) = 3.47 \pm 0.50$ in the Fermilab E691 experiment [30]. These data have successfully been described [22] in the discussed framework using the dipole cross section [15]. In all cases the observed $\sim 30\%$ departure of the observed ratios for the J/Ψ from predictions for vanishing FSI is of the same magnitude as in the highest Q^2 bin of the E665 data on the ρ^0 production (Fig. 6). This scaling relationship between production of different vector mesons [10] provides a very important cross check of the mechanism of CT.

Regarding the statistical accuracy of the data, the potential of the FNAL and CERN muon scattering experiments is nearly exhausted. Now we shall discuss what new can be done at CEBAF assuming the energy range $\nu \lesssim (8-10)$GeV and $Q^2 \lesssim (4-6)$GeV^2.

3 What next: Vector mesons at CEBAF

3.1 Two scales: the coherence length and the formation length

The coherence length l_c and the formation length l_f control the two different aspects of nuclear attenuation. The formation length tells how rapidly the electropoduced $q\bar{q}$ state evolves into the observed hadron. For the ρ^0 production,

$$l_f \sim 0.4\text{f} \cdot \left(\frac{\nu}{1\text{GeV}}\right). \tag{19}$$

In the low energy limit of $l_f \ll R_A$ we have an instantaneous formation of the final-state hadron, which then attenuates with the free-nucleon cross section and CT effects are absent. At high energies $l_f > R_A$, the formation of the observed hadron takes place behind the nucleus, and CT becomes possible. For the observation of the fully developed CT one needs

$$\nu \gtrsim (3-4) \cdot A^{1/3}\,\text{GeV}. \tag{20}$$

CT effects already start showing up, though, if $l_f \gtrsim l_{int}$, where the interaction length, or the mean free path, equals

$$l_{int} = \frac{1}{n_A \sigma_{tot}(VN)} \approx 2\text{f} \cdot \left(\frac{30mb}{\sigma_{tot}(VN)} \right) . \tag{21}$$

Therefore, purely kinematically, CT effects are within the reach of CEBAF experiments after the $8 - 12$GeV energy upgrade. Notice, that the formation length l_f does not depend on the photon's virtuality Q^2.

On the other hand, the coherence length l_c tells at which distance from the absorption point the pointlike photon becomes the hadronlike $q\bar{q}$ pair. If $l_c \gtrsim R_A$, then the whole thickness of the nucleus contributes to attenuation of the $q\bar{q}$ pair. Changing the virtuality of the photon Q^2 and/or reducing the photon's energy ν, one can make $l_c \ll R_A$. In this case, the incoming photon is absorbed approximately uniformly over the volume of the target nucleus, and attenuation of the produced $q\bar{q}$ pair will take place over half of the total thickness of the nucleus. In the practically interesting cases of $Q^2 \gg m_V^2$ for the light mesons, or in the real and virtual photoproduction of heavy quarkonia J/Ψ, Υ we have $l_c \ll l_f$. If $l_f \gtrsim R_A$, but $l_c \ll R_A$, then nuclear transparency equals

$$T_A = \frac{1}{A} \int d^2\vec{b} dz n_A(b,z) \frac{\langle V|\sigma(\rho) \exp[-\frac{1}{2}\sigma(\rho) t(b,z)]|\gamma^*\rangle^2}{\langle V|\sigma(\rho)|\gamma^*\rangle^2} \tag{22}$$

where $t(b,z)$ is the partial optical thickness of the nucleus

$$t(b,z) = \int_z^\infty dz' n_A(b,z') . \tag{23}$$

Notice, that $t(b,z) < T(b)$, and compared to the high-energy limit (12), here the attenuation effect in the nuclear matrix element is weaker. Consequently, a correct treatment of the coherency effects leads to a prediction [9,12,21,22] of the increase of nuclear attenuation with increasing energy ν:

$$T_A(l_c \gtrsim R_A) < T_A(l_c \ll R_A) \tag{24}$$

The energy dependence of the nuclear transparency is given by an approximate interpolation formula

$$T_A(\nu) \approx T_A(lc << R_A) + G_A(\kappa)^2 [T_A(l_c > R_A) - T_A(l_c << R_A)] \tag{25}$$

where $G_A(\kappa)$ is the charge form factor of the target nucleus and κ is the longitudinal momentum transfer in the transition $\gamma^* N \to VN$:

$$\kappa = \frac{1}{l_c} = \frac{Q^2 + m_V^2}{2\nu} . \tag{26}$$

The predicted energy dependence of nuclear transparency [22] is in excellent agreement with the NMC data on the real photoproduction of the J/Ψ [28] shown in Fig. 8. The NMC data rule out the widely discussed models of "quantum" and "classical" diffusion by Farrar, Frankfurt and Strikman [31], which has also predicted the precocious CT in the $A(e,e'p)$ scattering (for the review see [6]).

CT effects already start showing up, though, if $l_f \gtrsim l_{int}$, where the interaction length, or the mean free path, equals

$$l_{int} = \frac{1}{n_A \sigma_{tot}(VN)} \approx 2\text{f} \cdot \left(\frac{30mb}{\sigma_{tot}(VN)} \right) . \tag{21}$$

Therefore, purely kinematically, CT effects are within the reach of CEBAF experiments after the $8 - 12$GeV energy upgrade. Notice, that the formation length l_f does not depend on the photon's virtuality Q^2.

On the other hand, the coherence length l_c tells at which distance from the absorption point the pointlike photon becomes the hadronlike $q\bar{q}$ pair. If $l_c \gtrsim R_A$, then the whole thickness of the nucleus contributes to attenuation of the $q\bar{q}$ pair. Changing the virtuality of the photon Q^2 and/or reducing the photon's energy ν, one can make $l_c \ll R_A$. In this case, the incoming photon is absorbed approximately uniformly over the volume of the target nucleus, and attenuation of the produced $q\bar{q}$ pair will take place over half of the total thickness of the nucleus. In the practically interesting cases of $Q^2 \gg m_V^2$ for the light mesons, or in the real and virtual photoproduction of heavy quarkonia J/Ψ, Υ we have $l_c \ll l_f$. If $l_f \gtrsim R_A$, but $l_c \ll R_A$, then nuclear transparency equals

$$T_A = \frac{1}{A} \int d^2\vec{b} dz n_A(b,z) \frac{\langle V|\sigma(\rho) \exp[-\frac{1}{2}\sigma(\rho) t(b,z)]|\gamma^*\rangle^2}{\langle V|\sigma(\rho)|\gamma^*\rangle^2} \tag{22}$$

where $t(b,z)$ is the partial optical thickness of the nucleus

$$t(b,z) = \int_z^\infty dz' n_A(b,z') . \tag{23}$$

Notice, that $t(b,z) < T(b)$, and compared to the high-energy limit (12), here the attenuation effect in the nuclear matrix element is weaker. Consequently, a correct treatment of the coherency effects leads to a prediction [9,12,21,22] of the increase of nuclear attenuation with increasing energy ν:

$$T_A(l_c \gtrsim R_A) < T_A(l_c \ll R_A) \tag{24}$$

The energy dependence of the nuclear transparency is given by an approximate interpolation formula

$$T_A(\nu) \approx T_A(lc << R_A) + G_A(\kappa)^2 [T r_A(l_c > R_A) - T r_A(l_c << R_A)] \tag{25}$$

where $G_A(\kappa)$ is the charge form factor of the target nucleus and κ is the longitudinal momentum transfer in the transition $\gamma^* N \to VN$:

$$\kappa = \frac{1}{l_c} = \frac{Q^2 + m_V^2}{2\nu} . \tag{26}$$

The predicted energy dependence of nuclear transparency [22] is in excellent agreement with the NMC data on the real photoproduction of the J/Ψ [28] shown in Fig. 8. The NMC data rule out the widely discussed models of "quantum" and "classical" diffusion by Farrar, Frankfurt and Strikman [31], which has also predicted the precocious CT in the $A(e,e'p)$ scattering (for the review see [6]).

3.2 Quantum evolution and energy dependence of FSI.

If $l_f < R_A$, the frozen-size approximation is no longer applicable, and spatial expansion of the $q\bar{q}$ pair during its propagation inside a nucleus becomes important. The consistent path-intergal description of the spatial expansion effects was developed in [21]. Interaction of the $q\bar{q}$ pair with the nuclear matter can be described by the optical potential $V_{opt}(r) \propto \sigma(r)n_A(b,z)$, which adds to the confining $q\bar{q}$ potential $U(r)$. The longitudinal distance z plays the role of time. The path integral technique provides a systematic procedure for calculating the evolution kernel $\mathcal{K}(r',r,t)$ in the combined potential $U(r) + V_{opt}(r)$. The particularly elegant exact solution for the evolution kernel is found for the harmonic oscillator $U(r) \propto r^2$ and $\sigma(r) \propto r^2$ [21].

The resulting predictions for the energy dependence of nuclear transparency T_A for the production of different vector mesons are shown in Figs. 9,10. The salient features of T_A are [9,21,22]:

- At small Q^2, nuclear transparency for the ρ^0 and the J/Ψ decreases with energy ν, starting at the value given by Eq. (22) and levelling off at the value given by Eq. (12). This decrease is due to the increase of the coherence length l_c, discussed in section 3.1.

- At larger Q^2, the trend changes: T_A first increases with Q^2, and then decreases for the same reason of the rise of the coherence length l_c. In agreement with Eqs. (25,26), the larger is Q^2, the higher is the energy ν at which the levelling off of T_A takes place.

- For the Υ production, nuclear transparency T_A starts increasing with energy at all values of Q^2, in close similarity to the J/Ψ production at large Q^2, and in agreement with our conclusion that nuclear attenuation scales with $(Q^2 + m_V^2)$, see section 2.5. For instance, we predict $T_A(J/\Psi, Q^2 = 100\text{GeV}^2) \approx T_A(\Upsilon, Q^2 = 0)$.

- The radial excitations Ψ', Υ' have larger size, and larger free-nucleon cross section thereof, than the ground states J/Ψ and Υ, respectively. Nonetheless, the radial excitations are predicted to have weaker nuclear attenuation, which is a completely counterintuitive result.

- At last but not the least, for the ρ^0 production we predict very rich pattern of the ν and Q^2 dependence precisely in the kinematical range of CEBAF. CT effects are large and can readily be observed at CEBAF. The ρ' production will be treated in section 3.7.

These properties of nuclear transparency can best be understood in terms of the interplay of CT with the node effect.

3.3 CT and the node effect: antishadowing phenomenon.

The wave function of the radial excitation $V'(2S)$ has a node. For this reason, in the V' production amplituide there is the node efffect - cancellations between the contributions from r below, and above, the node. The product $\sigma(r)\Psi_{\gamma^*}(z,r)$ acts as a distribution, which probes the wave function of the $V(1S)$ and $V(2S)$ states at the scanning radius $\sim r_S$ [9,10,12] and the node effect evidently depends on the scanning radius r_S, see Fig. 2.

If the node effect is strong, even the slight variations of r_S lead to an anomalously rapid variation of the $V'(2S)$ production amplitude, which must be contrasted to the smooth Q^2

and r_S dependence of the $V(1S)$ production amplitude. Evidently, the stronger is the node effect and the smaller is the $V'(2S)$ production amplitude, the higher is the sensitivity to the model for the $V'(2S)$ wave function, and in some cases only firm statement will be the fact of the strong suppression of the $V'(2S)$ production.

For the real photoproduction of the Ψ', the calculations in [21] gave $\sigma(\gamma N \to \Psi' N)/\sigma(\gamma N \to J/\Psi N) = 0.17$, which is in excellent agreement with the NMC result $0.20 \pm 0.05(stat) \pm 0.07(syst)$ for this ratio [29]. In this case the node effect is already rather strong for the fact that the scanning radius $r_S(Q^2 = 0)$ is rather close to the J/Ψ radius $R_{J/\Psi}$. For the Υ', the scanning radius is substantially smaller than R_Υ, which is realtively large for the small strong coupling $\alpha_S(R_\Upsilon)$. For the light mesons, the scanning radius r_S is larger and, at small Q^2, the node effect is much stronger, see section 3.7.

Because r_{FSI} is larger than r_S, the node effect in the strength of FSI given by Eq. (15) becomes stronger. For the J/Ψ, one finds the **overcompensation:** $\langle V|\sigma(r)^2|\gamma\rangle < 0$, which leads to $\Sigma_V < 0$ and to the antishadowing phenomenon $T_A > 1$ shown in Fig. 10 . For the Υ', we find the **undercompensation:** $\langle V|\sigma(r)^2|\gamma\rangle > 0$, which leads to $\Sigma_V > 0$ and to the shadowing $T_A < 1$. None the less, the node effect shows up: for the Υ' with its large radius, nuclear attenuation is weaker than for the Υ ! With increasing Q^2, when $r_{FSI} \ll R_V$, the node effect becomes negligible, and the $V(1S)$ and $V'(2S)$ states will have identical nuclear attenuation, see Fig. 10.

3.4 The interplay of CT, of the node effect and of quantum evolution

Of course, the Ψ' has a larger radius and larger free-nucleon cross section $\sigma_{tot}(\Psi' N) \sim(2.5\text{-}3)\sigma_{tot}(J/\Psi N)$. How come, then, that in the real photoproduction $\Sigma_{\Psi'} < 0$ and we find the antishadowing of the strongly interacting Ψ' alongside with shadowing for the J/Ψ?

Although the above derivation of antishadowing was (deceptively) simple, still another look at antishadowing and the variation of energy dependence of nuclear transparency with Q^2 is in order [9]. Let us consider for simplicity the J/Ψ, Ψ' system. The numerator of the strength of FSI Σ_V can be expanded in terms of the complete set of intermediate states $|i\rangle >$ of charmonium

$$\langle V|\sigma(\rho)^2|\gamma^*\rangle = \sum_i \langle V|\sigma(\rho)|V_i\rangle\langle V_i|\sigma(\rho)|\gamma^*\rangle\,. \tag{27}$$

In terms of this expansion, antishadowing of the photoproduction of the Ψ' comes from the destructive interference of the two dominant intermediate states: the direct, VDM-like rescattering

$$\gamma^* \to \Psi' \to \Psi' \tag{28}$$

and the off-diagonal rescattering

$$\gamma^* \to J/\Psi \to \Psi' \tag{29}$$

(there is a small contribution from other intermediate states too).

Then, for the Ψ' production, the strength of FSI is given by

$$\Sigma_{\Psi'} = \sigma_{tot}(\Psi' N) + M(J/\Psi N \to \Psi' N)\cdot\frac{M(\gamma^* N \to J/\Psi N)}{M(\gamma^* N \to \Psi' N)}\,. \tag{30}$$

Because of the interplay of CT and the node effect, we have $M(\gamma^* N \to J/\Psi\, N)/M(\gamma^* N \to \Psi' N) \gg 1$. For the same interplay of CT and the node effect, there is an *overcompensation* in the amplitude of the off-diagonal transition

$$M(J/\Psi\, N \to \Psi' N) < 0\,, \tag{31}$$

and numerically this amplitude is not very small, $M(J/\Psi\, N \to \Psi' N) \sim -\sigma_{tot}(J/\Psi\, N)$. Consequently, the second, negative valued, off-diagonal term in $\Sigma_{\Psi'}$ takes over the $\sigma_{tot}(\Psi' N)$ (the higher intermediate states also slightly contribute to the antishadowing effect).

What happens with increasing Q^2 is very simple: The scanning radius r_S decreases with Q^2 and the node effect become weaker, the ratio of amplitudes $M(\gamma^* N \to J/\Psi\, N)/M(\gamma^* N \to \Psi' N)$ decreases with Q^2 and tends to approximately unity, whereas $\sigma_{tot}(\Psi' N)$ and $M(J/\Psi\, N \to \Psi' N)$ do not depend on Q^2. As a result, the off-diagonal contribution in Eq. (30) becomes small, and at large Q^2 the antishadowing of Ψ' changes to the shadowing.

Similarly, for the J/Ψ production

$$\Sigma_{J/\Psi} = \sigma_{tot}(J/\Psi\, N) + M(J/\Psi\, N \to \Psi' N) \cdot \frac{M(\gamma^* N \to \Psi' N)}{M(\gamma^* N \to J/\Psi\, N)}\,. \tag{32}$$

In this case, for the real photoproduction the off-diagonal contribution is small because of $M(\gamma^* N \to J/\Psi\, N)/M(\gamma^* N \to \Psi' N) \gg 1$, which is a consequence of CT. Therefore, for this numerical reason, for the real photoproduction we find

$$\Sigma_V \approx \sigma_{tot}(J/\Psi\, N) \tag{33}$$

which explains why the predicted nuclear attenuation of the J/Ψ is marginaly similar [21,22] to the vector dominance model estimates. With increasing Q^2, the off-diagonal term in (32) increases and starts camcelling the term $\sigma_{tot}(J/\Psi\, N)$, thus depleting $\Sigma_{J/\Psi}$ and leading to CT effect.

Consider now the J/Ψ and Ψ' photoproduction at a finite energy. The intermediate J/Ψ and Ψ' have different masses m_1 and m_2 and propagate with momenta which differ by

$$\kappa_{21} = \frac{m_2^2 - m_1^2}{2\nu} \approx \frac{1}{l_f} \tag{34}$$

If the production and rescattering points are a distance $\Delta z = z_2 - z_1$ apart, then the off-diagonal contribution to the rescattering amplitude acquires the phase factor $\exp[i\kappa_{21}(z_2 - z_1)]$ with respect to the elastic rescattering contribution [32,33]. Upon the integration over $z_{1,2}$, the effect of this phase factor is

$$\langle \exp[i\kappa_{21}(z_2 - z_1)] \rangle = G_A^2(\kappa_{21})\,, \tag{35}$$

and the off-diagonal contributions to Σ_V will enter with the suppression factor $G_A(\kappa_{i1})^2$ (for the detailed analysis see [7,8,9,13])

$$\Sigma_{\Psi'} = \sigma_{tot}(\Psi' N) + M(J/\Psi\, N \to \Psi' N) \cdot \frac{M(\gamma^* N \to J/\Psi\, N)}{M(\gamma^* N \to \Psi' N)} G_A^2(\kappa_{12})\,. \tag{36}$$

$$\Sigma_{J/\Psi} = \sigma_{tot}(J/\Psi\, N) + M(J/\Psi\, N \to \Psi' N) \cdot \frac{M(\gamma^* N \to \Psi' N)}{M(\gamma^* N \to J/\Psi\, N)} G_A^2(\kappa_{12})\,. \tag{37}$$

Evidently, at low energy such that $\kappa_{12}R_A \gtrsim 1$, i.e., at $l_f \ll R_A$, the nuclear form factor vanishes $G_A(\kappa_{12})^2 \ll 1$. Only the diagonal contributions to Σ_V survive, and CT effects which come from the off-diagonal terms in Σ_V, vanish at low energy. For instance, for the Ψ' one starts with the shadowing $T_A < 1$, which with increasing energy and the opening of the off-diagonal channels, changes to the antishadowing. For the J/Ψ and ρ^0, at small energy there is a competition of CT effect which rises with energy, and of the effect of growth of the coherence length. The latter takes over at small Q^2, whereas at larger Q^2 the opening of the off-diagonal transitions leads to a rapid near-threshold rise of nuclear transparency. For the ρ^0 production, nuclear transparency T_A is a lively function of energy ν and Q^2 in precisely the kinematical region accessible at CEBAF.

3.5 Measuring the J/Ψ-nucleon cross section at CEBAF

The smallness of the off-diagonal rescattering in the real photoproduction of the J/Ψ, see Eqs. (33), (37), leads to an important prediction [9,22] that nuclear attenuation allows to evaluate $\sigma_{tot}(J/\Psi N)$ using the conventional VDM formulas. This suggestion was carried over in an analysis [34] of the data [29,30] on the coherent photoproduction on nuclei with the result $\sigma_{tot}(J/\Psi N)$ ~(5-7)mb. The CEBAF experiments will allow measurement of this cross section at low energy, although being very close to the threshold requires a good understanding of the Fermi-smearing effects.

For the Ψ' photoproduction at low energies, the off-diagonal transitions (29) are non-negligible even close to the threshold, and for the Ψ' the VDM prediction for nuclear shadowing breaks down completely: T_A is always larger than the VDM prediction.

3.6 The coherence and formation lengths revisited: Vanishing nuclear shadowing in inclusive DIS at CEBAF coexists with lots of CT in exlusive production at CEBAF

Above we have repeatedly emphasized that the onset of CT is entirely controlled by the formation length l_f, which does not depend on Q^2. The onset of CT is quantified by Eqs. (36,37), in which the formation length enters via the nuclear form factor $G_A(\kappa_{12})$, where κ_{12} is the longitudinal momentum transfer in the off-diagonal transition $V_1N \to V_2N$.

At large Q^2 we have $l_c \ll l_f$ and much larger longitudinal momentum transfer κ Eq. (26) in the transition $\gamma^*N \to VN$. However, because $\kappa \gg \kappa_{12}$, this momentum transfer is approximately the same for all intermediate states. At $l_c \ll R_A$, the corresponding overall phase factor simply drops out from the incoherent production cross section. Neither does this phase factor affect T_A dramatically in the transient regime of $l_c \sim R_A$, see Eq. (25). In the coherent production on nuclei, the major effect of the momentum tranfer κ is that the nuclear production amplitude acquires the overall factor $G_A(\kappa)$, which significantly suppresses the coherent production amplitude but does not affect the nuclear attenuation properties.

As we discussed in section 2.2, the vector meson production on the free nucleon probes the gluon distribution in the target proton. Stretching the so-called factorization theorems, one can be tempted to conclude that nuclear attenuation in the production of vector mesons is given by the nuclear shadowing of gluon structure function [26]. Indeed, exclusive electroproduction of vector mesons is the typical diffraction dissociation of the photon $\gamma^*N \to XN$, and virtual diffractive transitions $\gamma^* \to X \to$ in the nuclear forward Compton scattering

amplitude are precisley the source of nuclear shadowing [15]. But, subtle is the nuclear shadowing!

The mere definition of the shadowed nuclear parton distributions is only useful provided that the shadowing term by itself satisfies the conventional evolution equations. To a certain approximation, this is the case [17]. However, there are no theorems on the universality of these shadowing corrections in all hard scattering processes and shadowing corrections may defy the factorization theorems [16]. Here we present simple arguments, essentially of kinematical origin, why the factorzation theorems must be taken with the grain of salt.

The contribution of the intermediate state X to the nuclear Compton scattering amplitude contains the excitation $\gamma^* N \to XN$ on one nucleon and the de-excitation $XN \to \gamma^* N$ on another nucleon. In both transitions there is a longitidunal momentum transfer κ Eq. (26). Consequently, the corresponding contribution to nuclear shadowing in the structure function will enter with the suppression factor $G_A(\kappa)^2$. The onset of nuclear shadowing requires $l_c \gtrsim R_A$, so that the larger is Q^2, the higher energy is required for the onset of nucler shadowing. In the opposite to that, nuclear attenuation and CT effects in the nuclear electroproduction of vector mesons only requires $l_f \gtrsim l_{int}, R_A$, and this condition does not depend on Q^2 and does not require $l_c \gtrsim R_A$. For instance, there will be **no nuclear shadowing in the inclusive electroproduction on nuclei** in the kinematical range of the CEBAF experiments, but **lots of CT effects in the exclusive production of vector mesons on nuclei** at CEBAF. We wish to emphasize this simple, but important, point in view of the opposite claims made to this effect by Frankfurt and Strikman at this Workshop.

3.7 Anomalous electroproduction of radial excitations ρ', ϕ' : CEBAF's new window at CT

For the light vector mesons, at small Q^2 the scanning radius $r_S \sim R_V$, and there is an exciting, and most likely, possibility of the *overcompensation* already in the free-nucleon production amplitude:$M = \langle V'|\sigma(r)|\gamma^*\rangle < 0$. The ρ' production on nuclei is indispensable for testing the node effect and Q^2 dependence of the scanning radius r_S, because nuclear attenuation gives still another handle on the scanning radius [9,13,27]. For the sake of simplicity, we discuss the quasielastic (incoherent) ρ' production on nuclei assuming that $l_f \gtrsim R_A$. Extension to lower energies and to the coherent production is straightforward and the prediction [13,27] of the anomalous Q^2 and A dependence persists in these cases too.

The A-dependence of the node effect comes from the nuclear attenuation $\exp[-\frac{1}{2}\sigma(r)T(b)]$ in the nuclear matrix element $M_A(T) = \langle V|\sigma(r)\exp\left[-\frac{1}{2}\sigma(r)T(b)\right]|\gamma^*\rangle$. The possibility of the A-dependent node effect effect in hadronic diffraction production on nuclei $hA \to h^*A$ was pointed out in [35].

Firstly, consider the Q^2 dependence of the ρ'/ρ^0 ratio on the free nucleon. Increasing Q^2 and decreasing the scanning radius r_S, one will bring the ρ' production on the free nucleon to the exact node effect, and the ρ'/ρ^0 ratio takes the minimum value at a certain finite Q^2, see Fig. 11. Because of the r-dependence of the attenuation factor, in the nuclear amplitude the node effect will be incomplete. Consequently, as a function of Q^2, nuclear transparency T_A will have a spike $T_A \gg 1$ at a finite value of Q^2 [9].

Secondly, consider the ρ' production on nuclei at a fixed value of Q^2 such that the free nucleon amplitude is still in the overcompensation regime. Increasing A and enhancing the importance of the attenuation factor $\exp[-\frac{1}{2}\sigma(r)T(b)]$, we shall bring the nuclear amplitude to the nearly exact compensation regime. Therefore, the ρ'/ρ^0 production ratio, as well as

nuclear transparency for the ρ' production, will decrease with A and take a minimum value at a certain finite A. With the further increase of A, the undercompensation regime takes over, and we encounter very counterintuitive situation: nuclear transparency for the ρ' is larger for heavier, more strongly absorbing nuclei! This situation is illustrated in Fig. 12a and must be contrasted with a smooth and uneventful decrease of transparency for the ρ^0 production on heavy nuclei.

With the further increase of Q^2 one enters the pure undercompensation regime for all the targets. Nuclear undoing of the node effect enhances M_A and nuclear transparency T_A, whereas the overall attenuation factor $\exp[-\frac{1}{2}\sigma(r)T(b)]$ decreases M_A and T_A. Of these two competing effects, the former remains stronger and we find antishadowing of the ρ' production in a broad range of A and Q^2, see Figs. 12c-12e. Typically, we find a nuclear enhancement of the ρ'/ρ^0 production ratio on heavy targets by one order in the magnitude with respect to the free nucleon target. This makes leptoproduction on nuclei the ρ' factory, and the ρ' production experiments at CEBAF can contribute much to the poorly understood spectroscopy of the radially excited vector mesons. Only at a relatively large $Q^2 \gtrsim 2\text{GeV}^2$, the attenuation effect takes over, and nuclear transparency for the ρ' production will start decreasing monotonically with A (Fig. 12f). Still, this decrease is much weaker than for the ρ^0 meson. At very large Q^2, when the node effect disappears because of the small scanning radius r_S, nuclear transparency for the ρ^0 and the ρ' production will become identical. This pattern repeats qualitatively the one studied for the J/Ψ and Ψ' mesons in sections 3.3 and 3.4 .

The above presented results refer to the production of the transversely polarized ρ^0 and ρ' mesons. Accurate separation of the transverse and longitudinal cross section can easily be done in the high statistics CEBAF experiments. Here we only wish to mention the interesting possibility that for the longitudinally polarized ρ' mesons, the exact node effect is likely to take place at a value of Q^2 larger than for the transverse ρ', so that polarization of the produced ρ' can exhibit very rapid change with Q^2.

The numerical predictions are very sensitive to the position of the node in the wave function of the $\rho'(2S)$. It is quite possible that the dip of nuclear transparency T_A will take place for targets much heavier than in Figs. 12a,12b, and disappearance of the node effect and the onset of the more conventional nuclear shadowing $T_A < 1$ for the ρ' production like in Fig. 12f only will take place at much larger Q^2. Also, the possibility of the undercompensation at $Q^2 = 0$ can not be excluded. However, the strikingly different A-dependence of the incoherent ρ^0 and ρ' production on nuclei persists in such a broad range of Q^2 and of the scanning radius r_S, that the existence of the phenomenon of anomalous A and Q^2 dependence of the ρ' preduction is not negotiable. It is a direct manifestation of the color-transparency driven Q^2 dependence of the scanning radius and, as such, it deserves a dedicated experimental study.

The case of the ϕ^0 and $\phi'(1680)$ production was studied in [24] using the path integral technique [21] modified to include corrections for the departure from the $\propto r^2$ dependence of the dipole cross section $\sigma(r)$. Corrections to the ϕ^0 production are negligible, corrections to the ϕ' production do not exceed 10%. Because of the smaller radius of the ϕ^0, ϕ', the numerical predictions are more reliable than for the ρ'. On the free nucleon, we find undercompensation for the transverse ϕ' production. There is much similarity to the J/Ψ, Ψ' system, but the node effect is stronger than for the charmonium. In the nuclear production of the ϕ', the antishadowing effect shown in Fig. 13 gradually builds up with increasing energy, and numerically is much stronger than for the Ψ'. Nuclear attenuation of the $\phi'(1680)$

is weaker than for the ϕ^0 starting already at low energy (Fig. 14). Because of the large mass and small radius of the ϕ^0, nuclear transparency for the ϕ^0 production only weakly depends on Q^2 at CEBAF, but for the $\phi'(1680)$ production the predicted Q^2 dependence is quite strong (Fig. 15) and can easily be measured at CEBAF. Here the larger Q^2 and smaller scanning radius r_S predict increasing attenuation of the $\phi'(1680)$. However, for the lead target we expect the onset of increasing nuclear transparency at already moderate $Q^2 \gtrsim 1 GeV^2$.

Few more comments about the possibilities of CEBAF are worth while. Because of the strong suppression of the ρ'/ρ^0 and ϕ'/ϕ^0 production ratio by the CT and node effects, the high luminosity of CEBAF is absolutely crucial for high-statistics experiments on the ρ', ϕ' production. Notice, that the most interesting anomalies in the A and Q^2 dependence take place near the minimum of the ρ' production cross section. Furthermore, the observation of the ρ' production requires detection of its 4-pion decays, and here one can take advantage of the CLAS multiparticle spectrometer available at CEBAF.

4 FSI and nuclear transparency in $A(e,e'p)$ scattering

4.1 Multiple-scattering expansion for the nuclear spectral function

We are interested in $A(e,e'p)$ scattering at large Q^2 >(1-2)GeV^2, when the struck proton has the kinetic energy $T_{kin} \approx Q^2/2m_p \gtrsim$(0.5-1)GeV. Such a proton has the free nucleon total cross section $\sigma_{tot}(pN)$ ≈40mb. The corresponding mean free path in the nuclear medium $l_{int} \sim$ 1.5f is short and implies strong FSI and strong nuclear attenuation of struck protons. At large Q^2 this FSI is expected to vanish by virtue of CT. One needs first a reliable formalism for description of FSI of the struck proton, and the coupled-channel generalization [7,8,36,37] of the Glauber's multiple scattering theory [38] provides the necessary framework.

The quantity measured in the ideal $A(e,e'p)$ scattering is the spectral function $S(E_m,\vec{p}_m)$ as a function of the missing energy E_m and missing momentum $\vec{p}_m = (p_{m,z},\vec{p}_\perp)$, for the kinematics see Fig. 16. The discussion greatly simplifies if the measured cross section is integrated over the sufficiently broad range of the missing energy E_m, when the closure can be applied [7,8,36]. We assume this is the case. If the plane-wave impulse approximation (PWIA) were applicable, then one would have have measured the single-particle momentum distribution $n_F(\vec{p}_m)$ ([39], for the recent review see [40]), which is related to the one-body nuclear density matrix $\rho_1(\vec{r},\vec{r}')$ as

$$d\sigma_A \propto n_F(\vec{p}_m) = \frac{1}{Z}\int dE_m S_{PWIA}(E_m,\vec{p}_m) = \int d\vec{r}'d\vec{r}\,\rho_1(\vec{r},\vec{r}')\exp[i\vec{p}_m(\vec{r}'-\vec{r})]\,. \qquad (38)$$

In this case the missing momentum $\vec{p}_m$ is precisely the intranuclear momentum of the struck proton.

PWIA is the theorists dream. The PWIA spectral function is what theorists do calculate in their models, in the real life the outgoing proton can not be described by the plane wave. At large $Q^2 \gtrsim 1$GeV^2, FSI of the struck ptoton can be treated in the Glauber approximation. The FSI modifies Eq. (38) [36,37]:

$$d\sigma_A \propto \frac{1}{Z}\int dE_m S(E_m,\vec{p}_m) =$$

$$\int d\vec{r}'d\vec{r}\,\rho_1(\vec{r},\vec{r}')\exp[i\vec{p}_m(\vec{r}'-\vec{r})]\cdot\exp\left[t(\vec{b},max(z,z'))\xi(\vec{\Delta})\right]$$
$$\cdot\exp\left[-\frac{1}{2}(1-i\alpha_{pN})\sigma_{tot}(pN)t(\vec{b},z)-\frac{1}{2}(1+i\alpha_{pN})\sigma_{tot}(pN)t(\vec{b}',z')\right], \qquad (39)$$

where $\vec{r}=(\vec{b},z)$, $\vec{r}'=(\vec{b}',z')$, $\vec{\Delta}=\vec{r}-\vec{r}'$, α_{pN} denotes the ratio of the real to imaginary parts of the forward proton-nucleon scattering amplitude and

$$\xi(\vec{\Delta})=\int d^2\vec{q}\;\frac{d\sigma_{el}(pN)}{d^2\vec{q}}\;\exp(i\vec{q}\vec{\Delta}). \qquad (40)$$

The derivation of attenuation factors in (39) uses the independent particle model. The effect of two-nucleon correlations in nuclear attenuation was studied in detail in [41] and found to be negligible.

FSI leads to the four important effects [13,36,37]

- Firstly, as a result of the phase factor in the integrand of (39) which is of the form $\exp[i\frac{1}{2}\sigma_{tot}(pN)\alpha_{pN}n_A(b,z)(z-z')]$ the spectral function $S(k_\perp,k_z)$ is probed at a shifted value of the longitudinal momentum with

$$k_z-p_{m,z}=\Delta p_{m,z}\sim\frac{1}{2}\sigma_{tot}(pN)\alpha_{pN}n_A\approx\alpha_{pN}\cdot 35\,(\mathrm{MeV/c}). \qquad (41)$$

  In the kinematical range of the NE18 experiment $\alpha_{pN}\sim-0.5$ [42] and $\Delta p_{m,z}\sim-20$ MeV/c is quite large. This shift makes the measured $p_{m,z}$ distribution strongly asymmetric about $p_{m,z}=0$.

- Secondly, the factor $\exp\left[t(\vec{b},z)\xi(\vec{\Delta})\right]$ in Eq. (39) leads to a broadening of the $p_\perp$ distribution. The multiple elastic-rescattering expansion for the $(E_m,p_{m,z})$-integrated spectral function reads

$$f_A(\vec{p}_\perp)=\frac{1}{Z}\int dE_m\,dp_{m,z}\;S(E_m,p_{m,z},p_\perp)=\sum_{\nu=0}^{\infty}W^{(\nu)}n^{(\nu)}(\vec{p}_\perp). \qquad (42)$$

  Here the $p_\perp$-distribution in the ν-fold rescattering $n^{(\nu)}(\vec{p}_\perp)$ equals

$$n^{(\nu)}(\vec{p}_\perp)=\int d^2\vec{s}\;\frac{B}{\nu\pi}\exp\left(-\frac{B}{\nu}s^2\right)n_F(\vec{p}_\perp-\vec{s}) \qquad (43)$$

  where B denotes the diffraction slope for elastic pN scattering, $d\sigma_{el}(pN)/dt\propto\exp(-B|t|)$, and

$$W^{(\nu)}=\frac{1}{A}\int dzd^2\vec{b}\;\;n_A(\vec{b},z)\exp\left[-\sigma_{tot}(pN)t(\vec{b},z)\right]\frac{[t(\vec{b},z)\sigma_{el}(pN)]^\nu}{\nu!} \qquad (44)$$

  gives the probability of having ν elastic rescatterings.

- Thirdly, FSI introduces the attenuation effect. Namely, whereas in the PWIA one has $\int d^3\vec{p}_m\,n_F(p_m)=1$, with allowance for FSI

$$T_A=\frac{1}{Z}\int dE_m\,d^3\vec{p}_m\,S(E_m,\vec{p}_m)=\int d^2\vec{p}_\perp\,f_A(p_\perp)$$
$$=\sum_{\nu=0}W^{(\nu)}=\frac{1}{A}\int dzd^2\vec{b}\;\;n_A(\vec{b},z)\exp\left[-\sigma_{in}(pN)t(\vec{b},z)\right]<1. \qquad (45)$$

In the completely integrated nuclear spectral function (45), nuclear attenuation is given by $\sigma_{in}(pN)$ [7]. This result is self-obvious: elastic rescatterings only deflect, but do not absorb, the struck proton, and the effect of deflection is not relevant for the full 4π acceptance.

- On the other hand, the forward peak of $f_A(p_\perp)$ at $\vec{p}_\perp = 0$ is dominated by $W^{(0)}$, which is also given by Eq. (45) but with $\sigma_{in}(pN)$ substituted by $\sigma_{tot}(pN)$. In this case elastic rescatterings also contribute to the observed attenuation.

The further discussion will be centered on: (1) how CT affects the integrated T_A and forward (the in-parallel kinematics) $W^{(0)}$ nuclear transparency; (2) why the onset of CT in $A(e,e'p)$ scattering is so slow; (3) the theoretical interpretation of the nonobservation of CT in the NE18 experiment; (4) the discussion of feasibility of CT studies at CEBAF.

4.2 FSI effect dominates at large transverse missing momenta

Measuring the spectral function at large missing momenta p_m is of great interest, because large p_m are expected to give a direct handle on the short-range correlations (SRC) of nucleons, which is widely discussed for 30 years since seminal works by Gottfried and Srivastava [43]. Our important finding [36] is that in the transverse kinematics, the FSI effect completely takes over the SRC effect.

The global effects of rescatterings are summarized in Table 1. Here we present, for different values of Q^2, the fractions $P^{(\nu)} = W^{(\nu)}/T_A$ of the ν-fold rescatterings, the nuclear transparency $W^{(0)}$ for quasifree knockout in parallel kinematics $p_\perp = 0$, the total transparency T_A and the average number of secondary rescatterings $\langle\nu\rangle$. The Q^2 dependence of $1 - W^{(0)}$ is reminiscent of the energy dependence of $\sigma_{tot}(pN)$, which is nearly flat at the kinetic energy $T_{kin} \approx Q^2/2m_p \gtrsim 0.5$ GeV [42]. The Q^2 dependence of $1 - T_A$ repeats the energy dependence of $\sigma_{in}(pN)$, which rises rapidly up to $T_{kin} \sim 1.5$ GeV and then approximately levels off [42]. The Q^2 dependence of the difference of the total and forward transparency $T_A - W^{(0)}$ and of the multiplicity of secondary rescatterings $\langle\nu\rangle$ repeats the energy dependence of the elastic cross section $\sigma_{el}(pN) = \sigma_{tot}(pN) - \sigma_{tot}(pN)$, which steadily decreases with T_{kin} [42]. The difference between $W^{(0)}$ and T_A is a convenient measure of the strength of rescatterings, and in the CEBAF range of Q^2 this difference is very large.

For our numerical estimates of the $p_\perp$-distribution we use a simple, yet realistic, parameterization of the SPMD [44]

$$n_F(\vec{k}) \propto \exp\left(-\frac{5}{2}\frac{k^2}{k_F^2}\right) + \epsilon_0 \exp\left(-\frac{5}{6}\frac{k^2}{k_F^2}\right), \qquad (46)$$

where $\epsilon = 0.03$ and the value of the Fermi-momentum k_F has been taken from Ref. [39]: $k_F(C) = 221\,\mathrm{MeV/c}$ and $k_F(Pb) = 265\,\mathrm{MeV/c}$. This parameterization is consistent with the results from the y-scaling analysis [45]. The steeply decreasing first term corresponds to the mean-field component of the SPMD, while the second term describes the SRC tail. In Fig. 17 we present our predictions for $f_A(\vec{p}_\perp)/T_A$ for the $^{12}C(e,e'p)$ and $^{208}Pb(e,e'p)$ reactions at $Q^2 = 1, 2, 4$ $(\mathrm{GeV/c})^2$, respectively. The FSI contribution to $f_A(\vec{p}_\perp)$ starts to dominate over the PWIA component $P^{(0)}n_F(p_\perp)$ already at $p_\perp \gtrsim 350$ MeV/c for carbon and $p_\perp \gtrsim 300$ MeV/c for lead, which is precisely the region thought of being dominated by the SRC tail in the single-particle momentum distribution.

An obvious signal of rescattering is the multinucleon emission (MNE). Rescatterings are not imperative for MNE, but rescatterings leading to $p_\perp \gtrsim k_F$ are necessarily followed by MNE. The contribution of rescatterings to MNE is characterized by the average number of secondary rescatterings $\langle \nu(p_\perp) \rangle$, which is very large (Table 1). Evidently, the strength of MNE coming from the rescattering mechanism must be the same in the longitudinal and transverse cross sections, which is a strong prediction. Presently, it can not be tested for the lack of the experimental data on large transverse missing momenta $p_\perp \gtrsim k_F$ taken at $Q^2 \gtrsim$(1-2)GeV^2, which is the domain of the forthcoming CEBAF experiments. This FSI driven MNE contributes significantly to the spectral function at large missing energy E_m. Namely, the contribution ΔE_m to the missing energy E_m from the kinetic energy of the recoil nucleons can be estimated as

$$\Delta E_m \approx \left\langle \frac{\vec{s}^2}{2m_p} \right\rangle = (1+\epsilon_0)\frac{k_F^2}{5m_p} + \frac{p_\perp^2}{2m_p}. \tag{47}$$

Incidentally, the SRC mechanism leads to a similar relationship between ΔE_m and $p_\perp$. The rescattering effect dominates the tail of the missing-energy distribution

$$\frac{df_A}{dE_m} \propto \exp\left(-\frac{E_m}{E_0}\right), \tag{48}$$

where the slope

$$E_0 \approx \frac{1}{2Bm_p} \approx \frac{8\pi\sigma_{el}(pN)}{m_p\sigma_{tot}(pN)^2}. \tag{49}$$

The definitive signature of the FSI mechanism is a strong Q^2 dependence of the slope E_0, which decreases from $E_0 \sim 250$ MeV at $Q^2 \sim 1$ (GeV/c)^2 down to $E_0 \sim 90$ MeV at $Q^2 \sim 6$ (GeV/c)^2. Such a large value of E_0 shows that in order to exhaust the closure, one has to integrate up to very large $p_\perp$ and very large missing energies $E_m \gtrsim E_0$.

4.3 Rescattering effect in $d(e,e'p)$

The rescattering effect is quite strong even in such a diluted target as the deuteron. The momentum distribution $f_d(\vec{p})$ of the observed protons equals [37]

$$f_d(p_{m,z},\vec{p}_\perp) = \left|\phi_d(p_{m,z},\vec{p}_\perp) - \frac{\sigma_{tot}(pn)}{16\pi^2}\int d^2\vec{k}\,\phi_d(p_{m,z},\vec{p}_\perp-\vec{k})\exp\left(-\frac{1}{2}B\vec{k}^2\right)\right|^2. \tag{50}$$

Here $\phi_d(\vec{k})$ is the momentum-space wave function of the deuteron, and gives the undistorted single-particle momentum distribution, the second term describes the rescattering effect. The measured transparency T_d depends on the acceptance p_{max}:

$$T_d = \frac{\int^{p_{max}} d^2\vec{p}_\perp f_d(\vec{p}_\perp)}{\int^{p_{max}} d^2\vec{p}_\perp \phi_d(\vec{p}_\perp)^2} \tag{51}$$

The attenuation effect $T_d < 1$ comes from the interference of the undistorted and rescattering terms in (50). If $R_d^2 p_{max}^2 \gg 1$, but $Bp_{max}^2 \ll 1$, which is the case for the NE18, then

$$1 - T_d \sim \frac{\sigma_{tot}(pn)}{2\pi R_d^2} \sim 0.07, \tag{52}$$

which is about twice the Glauber shadowing effect in the $\sigma_{tot}(Nd)$. Our prediction for T_d is shown in Fig. 18 and the agreement with the NE18 data [4] is good.

At still larger values of $p_\perp$, the spectral function will be entirely dominated by square of the rescattering term in (50), cf. Eqs. (42,43),

$$f_d(p_{m,z},p_\perp) \sim \frac{\sigma_{el}(pn)}{4\pi R_d^2}|\phi_d(p_{m,z})|^2 B\exp(-Bp_\perp^2) \tag{53}$$

It exhibits features of the rescattering contribution to the spectral function which are common to all the nuclei:

- The $p_\perp$ distribution has the broad tail with the small slope, which is the diffraction slope of the pN elastic scattering.
- The longitudinal momentum distribution is much narrower and is given by the PWIA single-particle momentum distribution.

In the opposite to that, the SRC effect in the single-particle momentum distribution is an isotropic function of the missing momentum $\vec{p}_m$, which must enable the experimental separation of the isotropic SRC effect from the sideways contribution from FSI.

4.4 The theoretical interpretation of the NE18 data $A(e,e'p)$ scattering

The most important conclusion from the above discussion is that the distortion effects make absolutely illegitimate a factorization of the measured spectral function $S(E_m,\vec{p}_m)$ into the PWIA spectral function $S_{PWIA}(E_m,\vec{p}_m)$ and an attenuation factor which is independent of the missing energy and momentum. In order to disentangle the genuine attenuation effect from the distortion effects, one can define nuclear transparency T_A as the ratio of the experimentally measured, and the theoretically calculated PWIA, cross sections integrated over the experimental acceptance domain $D(NE18)$ in the $(E_m,p_{m,z},p_\perp)$ space:

$$T_A(NE18) = \frac{\int_{D(NE18)} dE_m\, dp_{m,z}\, dp_\perp S(E_m,p_{m,z},p_\perp)}{\int_{D(NE18)} dE_m\, dp_{m,z}\, dp_\perp S_{PWIA}(E_m,p_{m,z}+\Delta p_{m,z},p_\perp)} \tag{54}$$

In order to eliminate the spurious effect in $T_A(NE18)$ due to the FSI generated asymmetry of the nuclear spectral function, we strongly advocate including the effect of the shift (41) in the calculation of the PWIA cross section. It was not included in the NE18 analysis. The effect of the shift (41) on T_A depends on the $p_{m,z}$-acceptance. It vanishes for the wide $p_{m,z}$-acceptance. For the narrow acceptance centered at $p_{m,z}=p^*$, the longitudinal asymmetry effect can be evaluated as

$$\frac{T_A(\Delta p_{m,z})}{T_A(\Delta p_{m,z}=0)} \approx 1+\frac{5}{2}\cdot\frac{(\Delta p_{m,z}+p^*)^2-(p^*)^2}{k_F^2} \tag{55}$$

and can be quite strong at large p^*. At $p^*=0$, which is approximetely the case in the NE18 experiment, the asymmetry effect enhances T_A by $\lesssim 2\%$ and is still within the error bars of the NE18 experiment.

The difference between $\sigma_{tot}(pN)$ and $\sigma_{in}(pN)$, and between $W^{(0)}$ and T_A thereof, is very large at moderate energies. $T_A(NE18)$ includes partly the elastically rescattered struck

protons. Since the diffraction slope B rises with the proton energy, the higher is Q^2 the larger is the fraction of the elastically rescattered struck protons included in $T_A(NE18)$. In Fig. 18 we present our predictions [38] for T_A, $W^{(0)}$ and $T_A(NE18)$ in which the $p_\perp$ integration for heavy nuclei is extended up to $p_{max} = 250\,\mathrm{MeV/c}$ as relevant to the NE18 situation [4]. We find very good quantitative agreement with the NE18 data. The principle conclusion from this comparison is that there is no large signal of CT in the $A(e,e'p)$ scattering at $Q^2 \leq 7$ GeV^2.

For the ^{12}C target we also show the effect of CT which is still small even at the largest Q^2 of the NE18 experiment (Fig. 18b), which must be contrasted with large CT effect in the E665 experiment. What makes the onset of CT in exclusive vector meson production and $(e,e'p)$ scattering so much different?

5 The onset of CT in $A(e,e'p)$ scattering

5.1 The ejectile state has a large size

The $(e,e'p)$ scattering can be viewed as an absorption of the virtual photon by the target proton, which leads to the formation of the ejectile state $|E\rangle$, which then is projected onto the observed final state proton. In the $A(e,e'p)$ scattering, this ejectile state propagates in the nuclear medium before evolving into the observed proton. The strength of FSI depends on what is the transverse size and the interaction cross section of the ejectile state.

In the exclusive production of vector mesons, the wave function of the ejectile state equals [9,21]

$$\Psi_E(r) \propto \sigma(r)\Psi_{\gamma^*}(r) \tag{56}$$

Because of CT, in this case the ejectile wave function $\Psi_E(r)$ has a hole at $r = 0$, but at large Q^2 the decrease of the wave function of the photon (5) takes over and $\Psi_E(r)$ has a small size $\sim r_S$. Notice, that in terms of the ejectile state $|E\rangle$ the strength of FSI can be rewritten as $\Sigma_V = \langle V|\sigma(r)|E\rangle/\langle V|E\rangle$.

The wave function of the ejectile state in the quasielastic scattering of electrons is much simpler. It can be found in any textbook in quantum mechanics and/or nuclear/particle physics. Indeed, the charge form factor $G_{em}(Q)$ of the $q\bar{q}$ "proton" can be written as (here the $\vec{r}$-plane is normal to the momentum transfer $\vec{Q}$):

$$G_{em}(Q) = \langle p|E\rangle = \int dz d^2\vec{r}\,\Psi_p^*(z,r)\Psi_E(\vec{r},z) = \int dz d^2\vec{r}\,\Psi_p^*(z,r)\exp\left(\frac{i}{2}Qz\right)\Psi_p(\vec{r},z). \tag{57}$$

Therefore, the ejectile wave function

$$\Psi_E(\vec{r},z) = \exp\left(\frac{i}{2}Qz\right)\Psi_p(\vec{r},z). \tag{58}$$

Because $|\Psi_E(\vec{r},z)|^2 = |\Psi_p(\vec{r},z)|^2$, the ejectile wave packet has the transverse size **identical** to the size of the proton [46,13]. This result is readily generalized to the three-quark proton and to the relativistic lightcone formalism. The often made statement that the ejectile has a small size $\propto 1/\sqrt{Q^2}$ is quite misleading. The small size only is believed to gradually appear when the ejectile wave function is projected at very large Q^2 onto the observed proton [46,47], but one must bear in mind the well known warning by Isgur and Llewellyn Smith [48] that the onset of the small-size dominance in the charge form factor is very slow.

Even provided that the proton form factor is dominated by the small size contribution, it still would be erroneous to identify the size of the ejectile state with the region of r which contribute to the form factor of the proton. In the problem of interest it is the large-size ejectile state with the initial wave function (58) which starts propagating and having FSI in the nuclear medium, evaluations of CT effects in models which start with the ejectile of vanishing size must be taken with grain at salt.

5.2 Color transparency sum rules and vanishing FSI: conspiracy of hard and soft scattering

The ejectile state can be expanded in terms of the electroproduced states $|i\rangle$ and the form factors $G_{ip}(Q)$ of the $ep \to ei$ transitions:

$$|E\rangle = J_{em}(Q)|p\rangle = \sum_i |i\rangle\langle i|J_{em}(Q)|p\rangle = \sum_i G_{ip}(Q)|i\rangle \tag{59}$$

where $G_{ip}(Q)$ are the $ep \to ei$ transition form factors. Detailed description of how CT emerges in the coupled-channel multiple scattering theory is given in [7,8,13,46]. There is much similarity to the treatment of CT in the production of vector mesons. To the leading order in FSI,

$$T_A = 1 - \Sigma_{ep}(Q)\frac{1}{2A}\int d^2\vec{b}\,T(b)^2 + ..., \tag{60}$$

where the strength of FSI is given by

$$\Sigma_{ep}(Q) = \frac{\langle p|\hat{\sigma}|E\rangle}{\langle p|E\rangle} = \frac{1}{G_{em}(Q)}\sum_i \sigma_{pi}G_{ip}(Q) = \sigma_{tot}(pp) + \frac{1}{G_{em}(Q)}\sum_{i\neq p}\sigma_{pi}G_{ip}(Q). \tag{61}$$

Here $G_{em}(Q) = G_{pp}(Q)$ is the form factor of the elastic ep scattering, $\hat{\sigma}$ is the cross section or diffraction operator, which gives the forward diffraction scattering amplitudes $M(jp \to kp) = i\langle j|\hat{\sigma}|k\rangle = i\sigma_{jk}$. The normalization is such that $\sigma_{tot}(jN) = \sigma_{jj} = \mathrm{Im}M(jN \to jN)$. Weak FSI and/or CT effect only is possible if the off-diagonal contributions in Eq. (60) cancel the $\sigma_{tot}(pN)$, which comes from the conventional Glauber rescattering of the struck proton. Evidently, such a cancellation **requires a very special conspiracy** between the electromagnetic form factors of hard ep interaction, and amplitudes of soft, forward, diffractive hadronic transitions $ip \to pp$. Now we shall demonstrate that such a conspiracy takes place.

In QCD the (anti)quarks in the hadron always have the one-gluon exchange Coulomb interaction at short distances. This Coulomb interaction leads to a very special asymptotics of the form factor at $Q^2 >> R_p^2$ [46,47] (for the sake of simplicity we discuss the two-quark state in the nonrelativistic approximation)

$$G_{ik}(\vec{Q}) \propto \frac{V(\vec{Q})}{\vec{Q}^2}\Psi_i^*(0)\Psi_k(0) \tag{62}$$

Here $\Psi_i(0)$ are the wave functions at the origin, and $V(Q)$ is the one-gluon exchange quark-quark hard scattering amplitude. Making use of the QCD asymptotics (62) we find [13]

$$\Sigma_{ep}(Q) = \frac{1}{G_{em}(Q)}\sum_i \sigma_{pi}G_{ip}(Q) \propto \frac{1}{G_{em}(Q)}\frac{V(\vec{Q})}{\vec{Q}^2}\sum_i \sigma_{pi}\Psi_i^*(0)\Psi_p(0) \propto \sum_i \sigma_{pi}\Psi_i^*(0). \tag{63}$$

Remarkably, the *r.h.s.* of Eq. (63) vanishes by virtue of CT sum rules [7]. The proof goes as follows: The state of transverse size $\vec{r}$ can be expanded in the hadronic basis as $|\vec{r}\rangle = \sum_i \Psi_i(\vec{r})^* |i\rangle$ and the hadronic-basis expansion for $\sigma(r)$ reads as

$$\sigma(\rho) = \langle\vec{r}|\hat{\sigma}|\vec{r}\rangle = \sum_{i,k} \langle\vec{r}|k\rangle \langle k|\hat{\sigma}|i\rangle \langle i|\vec{r}\rangle = \sum_{i,k} \Psi_i^*(\vec{r})\Psi_k(\vec{r})\sigma_{ki} \tag{64}$$

By virtue of CT $\sigma(r=0)=0$, and we obtain the "CT sum rule" [7]

$$\sum_{i,k} \Psi_k(0)^*\Psi_i(0)\sigma_{ki} = 0\,. \tag{65}$$

Considering the matrix elements $\langle\vec{r}|\hat{\sigma}|k\rangle$ at $\vec{r}\to 0$, one readily finds a whole family of CT sum rules [7,13]

$$\sum_i \Psi_i(0)\sigma_{ik} = 0\,. \tag{66}$$

It is precisely the sum rule (66), which in conjunction with the QCD asymptotics of the electromagnetic form factors (62) ensures that the strength of FSI (61) vanishes and CT indeed takes place.

5.3 The onset of CT and the coherency constraint

As we learned in section 3.4, at finite energy only few intermediate states contribute coherently into Σ_V. The case of the Σ_{ep} is quite similar. From the kinematics of deep inelastic scattering

$$m_i^2 - m_p^2 = 2m_p\nu - Q^2 - 2\nu k_z\,, \tag{67}$$

where k_z is the longitudinal momentum of the target nucleon. Consequently, different components $|i\rangle$ of the ejectile wave packet (59) are produced with the longitudinal momenta differing by [7]

$$\kappa_{ip} = m_p\frac{m_i^2 - m_p^2}{Q^2} = \frac{m_i^2 - m_p^2}{2\nu}\,, \tag{68}$$

and acquire the relative phase $\kappa_{ip}(z_2 - z_1)$ during propagation from the (z_1) production to the (z_2) rescattering point. Then, repeating considerations which lead to Eqs. (36, 37), we find [7,8,13]

$$\begin{aligned}\langle p|\hat{\sigma}J_{em}|p\rangle &= \sum_i \langle p|\hat{\sigma}|i\rangle\langle i|J_{em}|p\rangle \\ \Longrightarrow \sum_i \langle p|\hat{\sigma}|i\rangle\langle i|J_{em}|p\rangle \exp[i\kappa_{ip}(z_2 - z_1)] &\Longrightarrow \sum_i \langle p|\hat{\sigma}|i\rangle\langle i|J_{em}|p\rangle G_A^2(\kappa_{ip})\end{aligned} \tag{69}$$

and

$$\Sigma_{ep}(Q) = \sigma_{tot}(pN) + \sum_{i\neq p} \frac{G_{ip}(Q)}{G_{em}(Q)}\sigma_{ip}G_A(\kappa_{ip})^2 \tag{70}$$

At small Q^2 such that

$$Q^2 \ll 2R_A m_p \Delta m \sim (3-5)\cdot A^{1/3}\mathrm{GeV}^2\,, \tag{71}$$

for all inelastic channels $G_A(\kappa_{ip}) \ll 1$, so that $\Sigma_{ep} = \sigma_{tot}(pN)$, and FSI measures the free-nucleon cross section. With increasing Q^2, for larger and larger number of inelastic intermediate states channels $G_A(\kappa_{ip}) \approx 1$, the CT sum rule (66) will be better saturated and $\Sigma_{ep}(Q) \to 0$.

5.4 What makes the onset of CT in $A(e,e'p)$ and vector meson production different?

In the vector meson production, it is the energy ν which controls the number of intermediate states which contribute coherently to Σ_V and the signal of CT. The virtuality Q^2 is an independent parameter, which controls the srength of destructive interference between the diagonal (elastic) and off-diagonal (inelastic) contributions to Σ_V. In the quasielastic scattering of electrons $Q^2 \approx 2m_p\nu$, and one can increase the energy ν only at the expense of very high Q^2.

There is one more fundamental difference between the two processes. Compare in more detail the $\Sigma_{J/\Psi}$ Eq. (36) and $\Sigma_{ep}(Q)$ Eq. (70). Notice, that $M(J/\Psi N \to \Psi' N) = \sigma_{J/\Psi\,\Psi'}$ and, in the generic case, the off-diagonal matrix elements σ_{ip} are typically smaller than the diagonal $\sigma_{ii} = \sigma_{tot}(i\,N)$. The difference comes from the two ratios

$$\frac{M(\gamma^* N \to \Psi' N)}{M(\gamma^* N \to \Psi' N)} \qquad \text{and} \qquad \frac{G_{ip}(Q)}{G_{em}(Q)}\,, \tag{72}$$

which play the identical role in Eqs. (36), (70), respectively. In the vector meson production, the ratio (72) increases with Q^2, which further enhances the off-diagonal contribution to $\Sigma_{J/\Psi}$ and the signal of CT thereof. In the case of $A(e,e'p)$ at large Q^2, the ratio $G_{ip}(Q)/G_{em}(Q)$ does not change with Q^2, see Eq. (62) and Stoler's review [49].

5.5 The realistic estimates of the signal of CT in $A(e,e'p)$ scattering

One needs to evaluate the off-diagonal contributions to Σ_{ep}. Let us accept the optimstic scenario that the form factor ratios $G_{ip}(Q)/G_{em}(Q)$ are precociously close to QCD asymptotic predictions (62), and concentrate on the off-diagonal diffraction production amplitudes σ_{ip}. The experimentally observed mass spectrum of the diffraction excitation of protons is shown in Fig. 19 (for the review see [50]). Because of the nuclear form factor $G_A(\kappa_{ip})$, the onset of CT signal starts with the contribution to Σ_{ep} from the low-mass states.

In the diffractive mass spectrum of Fig. 19 there is a prominent signal of excitation $pp \to (\pi N)p$ of the low-mass πN state, which dominates at $M^2 \lesssim 2\mathrm{GeV}^2$. Its origin is in the admixture of the $\pi(3q)$ Fock state in the lightcone proton [13,51]

$$|N\rangle = \cos\theta|3q\rangle + \sin\theta|3q+\pi\rangle\,, \tag{73}$$

where the mixing angle θ is related to the number of pions n_π in the nucleon as

$$\sin^2\theta = \frac{n_\pi}{1+n_\pi} \tag{74}$$

There is a mounting evidence for such a hybrid quark core-pion structure of the nucleon, coming from the violation of the Gottfried Sum Rule and the recent NA51 observation [52] of large $\bar{u}/\bar{d}$ asymmetry in the proton sea in the Drell-Yan production [53]. The diffractive excitation of the $N+\pi$ Fock component of the nucleon (known since long also as the Drell-Hiida-Deck process [50]), gives an excellent description of the πN mass spectrum. For the purposes of the present analysis it is important, that the πN state contributes to Σ_{ep} a term [13]

$$\Delta\Sigma_{ep}(\pi N) \approx -\sigma_{tot}(\pi N)\frac{n_\pi}{1+n_\pi} \approx -8\mathrm{mb} \tag{75}$$

This result can be interpreted as follows. The pion-baryon component of the nucleon has a large size and a rapidly decreasing form factor, so that only the baryonic $3q$ core of the nucleon contributes to the ejectile state (the detailed analysis of electromagnetic form factor of the hybrid proton is given in [51]). The interaction cross section of the $3q$ core stripped off of pions, is smaller that $\sigma_{tot}(pN)$ by precisely the amount (75). Notice, how the nonperturbative quark core-pion Fock component of the nucleon gives a unified description of

- the diffraction dissociation of nucleons in the soft diffractive scattering,
- the asymmetry of the quark-antiquark sea in protons as probed in deep inelastic scattering,
- the onset of color transparency in quasielastic scattering of electrons on nuclei.

Diffraction excitation of higher mass states comes from the excitation of the $3q$ core of the nucleon. In [7] we described interaction of the $3q$ core in a QCD approach based on the dipole cross section [15], qualitatively shown in Fig. 1. The resulting diffraction matrix σ_{ik} has the built-in CT property and satisfies CT sum rules. The proton and its excitations are described by the diquark-quark harmonic oscillator model. Within the model, diffraction dissociation is dominated by excitation of N^* states of the positive parity shells. We find a good parameter-free description [54] of the diffractive mass spectrum shown in Fig. 19, and rightfully expect the realistic estimate of CT effects in $\Sigma_{ep}(Q^2)$. The excess of the observed mass spectrum in the so-called triple-pomeron mass region $M^2 \gtrsim 10\text{GeV}^2$ is an effect of excitation of higher $qqqg_1..g_n$ Fock states [17], which was not included in [7]. However, in the practically accessible range of Q^2, CT effect is completely dominated by excitation of the πN states and resonances of the first excited positive-parity shell $L = 1$, with little contribution of states of higher shells $L \geq 2$.

The resulting predictions [54] for $\Sigma_{ep}(Q)$ are shown in Fig. 20. With increasing Q^2, the strength of FSI decreases much slower than $\propto 1/Q^2$: the increase of Q^2 by one order in magnitude from 5 to 50 GeV^2 is followed by decrease of $\Sigma_{ep}(Q)$ only by the factor 3 from 36mb to 12 mb, respectively. The CT effect in $T_A(Q^2)$ follows closely the variation of $\Sigma_{ep}(Q^2)$. The heavier is the nucleus, the larger Q^2 is needed for the onset of CT. The values of Q^2 studied by NE18 correspond to the threshold of CT for the carbon nucleus, already at $Q^2 \sim 20$ GeV^2 we predict a substantial CT effect.

6 CT in $A(e,e'p)$ scattering at CEBAF

6.1 $^4He(e,e'p)$ scattering: CEBAF's choice

The principal inhibitor of the precocious CT is the coherency constraint, quantified by the factor $G_A(\kappa_{ip})^2$ in the off-diagonal contribution to $\Sigma_{ep}(Q)$. In order to have large CT effect one must excite intermediate states of high mass m_i. The condition $\kappa_{ip}R_A \lesssim 1$ implies, that excitation of the same mass on different nuclei requires

$$Q^2 \gtrsim (m_i^2 - m_p^2)R_A m_p \tag{76}$$

Consequently, one can hope to relax the coherency constraint and enhance the CT effect going to lighter nuclei which have smaller radius and less steeply decreasing charge form factor $G_A(\kappa)$.

With allowance for the center-of-mass motion, for the light nuclei [13,54]

$$\Sigma_{ep}(Q^2) = \sigma_{tot}(pN) + \sum_{i\neq p} \sigma_{ip} \frac{G_{ip}(Q^2)}{G_{pp}(Q^2)} G_A^2(\frac{A}{A-1}\kappa_{ip}^2). \tag{77}$$

The factor $A/(A-1)$ in the nuclear form factor, which comes from the center-of-mass motion important in light nuclei, is the most unwelcome news. For the deuteron target, it makes the onset of CT slower than for the ^{12}C target. The ^3He nucleus has a size smaller than the ^{12}C nucleus, but the onset of CT in both cases will be equally slow, which makes the $^3He(e,e'p)$ reaction ill-suited for the search of CT effects at CEBAF. Only for the ^4He nucleus, the onset of CT will be sooner than for the ^{12}C nucleus, which makes ^4He the CEBAF's choice target.

In the $^4He(e,e'p)$ scattering, nuclear attenuation effect is typically $1-T_A \sim 0.25$ [55] and with the onset of CT it will decrease

$$1 - T_A \propto \eta = \frac{\Sigma_{ep}(Q)}{\sigma_{tot}(pN)}. \tag{78}$$

Our predictions [54] of η for $^4He(e,e'p)$ scattering are shown in Fig. 21. We also show the decomposition of the CT signal $1-\eta$ in terms of excitation of inelastic intermediate states. At $Q^2 \lesssim$(5-6)GeV^2 the signal of CT comes primarily from the πN intermediate states. In this case the reduction of $\Sigma_{ep}(Q)$ from $\sigma_{tot}(pN)$ =40mb measures how much the size of the quark core of the nucleon stripped off the pionic cloud, is smaller than the size of the physical proton. With the increasing Q^2, excitation of the intermediate nucleonic resonances starts contributing to the signal of CT and atkes over at $Q^2 \gtrsim$7GeV^2. The experimental observation of the CT predicted $\sim 20\%$ decrease of η at $Q^2 = 6$GeV^2, requires the measurements of T_A with $\lesssim 1\%$ statistical accuracy. This challenge can be met at CEBAF thanks to its high luminocity.

6.2 The signal of CT at large transverse missing momenta

The broadening of the $p_\perp$ distribution discussed in sections 4.1-4.3 is generated by FSI and must vanish in the CT regime. With allowance for inelastic intermediate states, the propability of ν-fold rescattering $W^{(\nu)}$ will still be given by Eq. (44) subject to the substitution [13;14]

$$\sigma_{el}(pN)^\nu \Longrightarrow \sigma_{el}(pN)^\nu \left[\frac{\langle p|\hat{\sigma}^\nu|E\rangle}{\langle p|E\rangle \sigma_{tot}(pN)^\nu}\right]^2. \tag{79}$$

In the case of $^4He(e,e'p)$ scattering, the tail of the $p_\perp$-distribution $f_A(p_\perp)$ will be dominated by single scattering term, which will be proportional to the factor

$$W_1 \propto \eta^2 = \left(\frac{\Sigma_{ep}(Q^2)}{\sigma_{tot}(pN)}\right)^2 \tag{80}$$

Our prediction [54] for the rescattering suppression factor η^2 is shown in Fig. 21. Here the CT effect is twice as large compared to nuclear transparency T_A. One has to pay a heavy price, though: very accurate theoretical calculation of the rescattering effect in the absence of CT is a must before one can claim the reliable experimental determination of this suppression factor and separation of the CT effect. Such a calculation must be very

accurate, indeed, because the magnitude and the $p_\perp$-dependence of the differential cross section of elastic pN scattering changes very rapidly over the range of Q^2 of the interest.

Furthermore, the rescattering component of $f_A(p_\perp)$ appears on the background from the short-range correlation effect, see Fig. 17, and very good understanding of this background is necessary for reliable determination of a small decrease of η^2 with the increase of Q^2. The coincidence detection of the recoil nucleon little helps in this respect: once the struck proton emerges with large $p_\perp \gg k_F$, it will always recoil against the second nucleon emitted with the momentum $\vec{p}_2 \approx -\vec{p}_m$, and one can not tell whether the large $p_\perp$ originated from the correlation of two nucleons at short distances, or from the rescattering process. For this reason, the theoretical interpretation of high-precision measurements of the Q^2 dependence of nuclear transparency T_A will be much easier, compared to the Q^2 dependence of the large-$p_\perp$ production and/or the $^4He(e,e'pp)$ reaction.

6.3 Fermi-motion and asymmetry effect in nuclear transparency

In the $(e,e'p)$ scattering, the longitudinal momentum k_z of the target nucleon is uniquely determined by the electron scattering kinematics:

$$x = \frac{Q^2}{2m_p\nu} = 1 + \frac{k_z}{m_p}. \tag{81}$$

By kinematics of the electroproduction Eq. (67), the different components of the ejectile wave packet are produced on the target nucleon having different longitudinal Fermi motion, see Eq. (68). Consequently, varying the Bjorken variable x, one can change the composition of the ejectile wave packet [8,56,57], which gives a new handle on the CT effect. A detailed theory of the effect is given in [8].

Following West, it is convenient to introduce the PWIA structure function

$$F_A(x) = \int d^3\vec{k}\frac{dn}{d^3\vec{k}}\,\delta(1+\frac{k_z}{m_p}-x) = \frac{1}{2\pi}\int dk_z\,\delta(1+\frac{k_z}{m_p}-x)\int dz\,\rho(0,z)\exp(ik_z z). \tag{82}$$

Then, the Fermi-motion effect is quantified by the x-dependent decomposition of the ejectile state

$$|E\rangle_{eff} = \sum_i G_{ip}(Q)|i\rangle\frac{F_A(x+\frac{1}{2}\Delta x_{ip})}{F_A(x)}G_A(\kappa_{pi}) \tag{83}$$

and the x-dependent strength of FSI

$$\Sigma_{ep}(x,Q^2) = \sigma_{tot}(pN) + \sum_{i\neq p}\sigma_{pi}\frac{G_{ip}(Q)}{G_{em}(Q)}\frac{F_A(x+\frac{1}{2}\Delta x_{ip})}{F_A(x)}G_A(\kappa_{ip})^2, \tag{84}$$

where

$$\Delta x_{ip} = \frac{\kappa_{ip}}{m_p} = \frac{m_i^2 - m_p^2}{Q^2}. \tag{85}$$

In their counterpart of (83), instead of $F_A(x_{Bj}+\frac{1}{2}\Delta x_{ip})/F_A(x)$ Jennings and Kopeliovich [56] give $\sqrt{F_A(x+\Delta x_{ip})/F_A(x)}$, which is incorrect.

The x-dependence of $\Sigma(x,Q^2)$ and of the transparency $T_A(x,Q^2)$ comes from the fact that the ratio $F_A(x+\frac{1}{2}\Delta x_{ip})/F_A(x)$ is asymmetric around $x=1$ [8,56,57]. It is smaller than unity at $x>1$, which suppresses the inelastic contribution to Σ_{ep} and hence reduces the

color transparency signal. For $x < 1$, on the other hand, transparency is enhanced. With $F_A(x)$ evaluated using the single-particle momentum distribution (46), we find the results shown in Fig. 22. At small Q^2 the Fermi motion effect is numerically small because the contributions from inelastic channels to $\Sigma_{ep}(x, Q^2)$ are supressed by $G_A(\kappa_{ip})^2$. At higher Q^2 these contributions increase and the x-dependence of $T_A(x, Q^2)$ becomes significant. The SRC component of $F_A(x)$ has a significant influence on the Fermi motion effect reducing the departure of the ratio $F_A(x + \frac{1}{2}\Delta x_{ip})/F_A(x)$ from unity in the region of x where $F_A(x)$ is dominated by this component. This is demonstrated by the dashed curves in Fig. 22, where $T_A(x, Q^2)$ is evaluated with $F_A(x)$ which includes only the mean-field component. $T_A(x, Q^2)$ has a peak and the signal of CT is maximized at $x \sim 0.8$.

We emphasize that the asymmetry of nuclear transparency about $x = 1$ is the CT effect. It is large and persists at large Q^2. Zooming at $x \sim 0.8$ will significantly enhance the chances of discovering CT at CEBAF. However, there is a strong background to this CT induced asymmetry, which comes from the effective shift of the missing momentum (41), which also generates the asymmetry in nuclear transparency. Namely, $x \sim 0.8$ corresponds to $\alpha^* \sim k_F$, and the FSI generated asymmetry (55) is as large as the CT effect shown in Fig. 22.

7 Conclusions

The E665 observation [5] of strong signal of CT in exclusive production of vector mesons is a major breakthrough in the subject of CT and paves the way for dedicated experiments on CT. The E665 effect was predicted [9] (not postdicted!), and the agreement betwen the theory and experiment is very good. The nonobservation of CT in the NE18 experiment [4] was also predicted [7,8] and is a good confirmation of theory. We have a good understanding of why the onset of CT in $A(e, e'p)$ and $\gamma^* A \to VA$, VA^* reactions is so strikingly different.

The purpose of this presentation was to make the strong case for a broad experimental program on electroproduction of light vector mesons ρ^0, ω^0, ϕ^0, ρ', ω', ϕ' at CEBAF. Here the principal benefit is the theoretically well understood shrinkage of the virtual photon which elastically produces the vector meson. Variations of the scanning radius are very strong already at $Q^2 \lesssim$(1-3)GeV^2, and the first-class CT experiments with large expected signal of CT can be performed at the energy-upgraded CEBAF [58]. CT in conjunction with the node structure of wave functions of radially excited vector mesons $V' = \rho', \omega', \phi'$ leads to a very rich pattern of anomalous A and Q^2 dependence of the V' production. This unique possibility of directly scanning the wave function of radial excitations at CEBAF must not be overlooked, and CEBAF is the unique facility which can do the job. Furthermore, the CEBAF experiments on radially excited vector mesons can contribute much to the spectroscopy of vector mesons, which presently leaves much to be desired [59]. Besides the above CT aspects, there is much interest in studies of nuclear modifications of properties of vector mesons in electroproduction on nuclei at CEBAF [60].

^4He emerges as CEBAF's choice target to search for CT in $A(e, e'p)$ scattering. The realistic, and conservative, estimates show that CT effect in the conventional transmission experiment can be observed at CEBAF. CT effect can be enhanced studying the asymmetry of nuclear transparency (the Fermi-motion effect) in the parallel kinematics. Here more theoretical work is needed to reliably calculate the background asymmetry originating from the more conventional final state interaction. CT effect aslo can be enhanced looking at large missing momentum in the transverse kinematics. Here a very accurate calculation of

the rescattering effect and of the background short-range correlation effect is needed for a realiable normalization of the cross section and extraction of CT effect.

Acknowledgements

NNN thanks N.Isgur, R.Milner and P.Stoler for invitation to this stimulating Workshop.

References

[1] A.B.Zamolodchikov, B.Z.Kopeliovich and L.I.Lapidus, *JETP Lett.* **33** (1981) 595; G.Bertsch, S.J.Brodsky, A.S.Goldhaber and J.R.Gunion, *Phys.Rev.Lett.* **47** (1981) 267.

[2] A.H.Mueller, *in: Proceedings of the XVII Rencontre de Moriond, Les Arcs, France.* Ed. Tranh Thanh Van, Editions Frontieres, Gif-sur-Yvette, 1982, p.13; S.J.Brodsky, *in: Proceedings of the XIII International Symposium on Multipartcile Dynamics, Volendam, Netherlands.* Eds. E.W.Kittel, W.Metzger and A.Stergion, World Scientific, Singapore, 1982, p. 963; S.J.Brodsky and A.H.Mueller: Phys.Lett. **B206** (1988) 685.

[3] N.N.Nikolaev and J.Speth, The ELFE Project: an Electron Laboratory for Europe, edited by J.Arvieux and E.De Sanctis, Editrice Compositori, Bologna (1993) pp.179-212.

[4] NE18 Collaboration: N.C.R.Makins et al., *MIT preprint* **LNS-93/11.**

[5] E665 Collaboration: G.Fang, Talk at the PANIC, Perugia, July 1993, and private communication.

[6] L.L.Frankfurt, G.A.Miller and M.I.Strikman, "Colour Transparency and Nuclear Phenomena", *Comments in Particle and Nuclear Physics* **21** (1992) 1 and referencesn therein; B.Jennings and G.A.Miller, *Phys.Lett.* **B236** (1990) 209; *Phys.Rev.* **D44** (1991) 692.

[7] N.N.Nikolaev, A.Szczurek, J.Speth, J.Wambach, B.G.Zakharov and V.R.Zoller, *Nucl.Phys.* **A567** (1994) 781.

[8] N.N.Nikolaev, A.Szczurek, J.Speth, J.Wambach, B.G.Zakharov and V.R.Zoller, *Phys.Lett.* **B317** (1993) 287.

[9] B.Z.Kopeliovich, J.Nemchik, N.N.Nikolaev and B.G.Zakharov, *Phys. Lett.* **B309** (1993) 179.

[10] B.Z.Kopeliovich, J.Nemchik, N.N.Nikolaev and B.G.Zakharov, *Phys. Lett.* **B324** (1993) 469.

[11] B.Z.Kopeliovich, *Sov.J.Part.Nucl.* **21** (1990) 117.

[12] N.N.Nikolaev, Quantum Mechanics of Color Transparency. *Comments on Nuclear and Particle Physics* **21** (1992) 41; N.N. Nikolaev, *High Energy Nuclear Reactions in QCD: Colour Transparency Aspects*, in Lecture Notes of 1992 RCNP Kikuchi School on Spin Physics at Intermediate Energies, 16-19 November 1992, edited by M.Fujiwara and M.Kondo, **RCNP-P-128**, Osaka University.

[13] N.N.Nikolaev, Color transparency: Novel test of QCD in nuclear interactions. *Surveys in High Energy Physics,* 1994, in press.

[14] N.N.Nikolaev and B.G.Zakharov, *Proceedings of the Workshop on Electron Nucleus Scattering*, Marciana Marina, Elba, 5-10 July 1993, edited by O.Benhar, A.Fabrocini and R.Schiavilla , World Scientific (1994) p.323.

[15] N.N.Nikolaev and B.G.Zakharov, *Z.f.Phys.* **C49** (1991) 607; **C53** (1992) 331.

[16] V.Barone, M.Genovese, N.N.Nikolaev, E.Predazzi and B.G.Zakharov, *Z. Phys.* **C58** (1993) 541; *Int.J.Mod.Phys A*, 8 (1993) 2779; *Phys.Lett.* **B326** (1994) 161.

[17] N.Nikolaev and B.G.Zakharov, The triple-pomeron regime and the structure function of the pomeron in the diffractive deep inelastic scattering at very small x, *Landau Inst. preprint* **Landau-16/93** and *Jülich preprint* **KFA-IKP(Th)-1993-17**, June 1993, to appear in *Z. Phys.* **C** (1994); The pomeron in the diffractive deep inelastic scattering, to appear in *JETP* **78(5)** (1994).

[18] N.N.Nikolaev and B.G.Zakharov, On determination of the large-$\frac{1}{x}$ gluon distribution at HERA, *Jülich preprint* **KFA-IKP(TH)-1994-12**, March 1994, to appear in *Phys. Lett.* **B** (1994).

[19] N.N.Nikolaev, B.G.Zakharov and V.R.Zoller, *JETP Letters* **59** (1994) 8; The BFKL and GLDAP regimes for the perturbative QCD pomeron, *Jülich preprint* **KFA-IKP(TH)-1994-02**, January 1994; *JETP* **78(6)** (1994); The spectrum and solutions of the generalized BFKL equation for total cross sections, *Jülich preprint* **KFA-IKP(TH)-1994-01**, January 1994, to appear in *Phys. Lett.* **B** (1994);

[20] N.N.Nikolaev and B.G.Zakharov, *Phys. Lett.* **B327** (1994) 149.

[21] B.Z.Kopeliovich and B.G.Zakharov: Phys.Rev. **D44** (1991) 3466.

[22] O. Benhar, B.Z. Kopeliovich, Ch. Mariotti, N.N. Nikolaev and B.G. Zakharov, *Phys.Rev.Lett.* **69** (1992) 1156.

[23] J.Nemchik, N.N.Nikolaev and B.G.Zakharov, Scanning the BFKL pomeron in elastic production of vector mesons at HERA, *Jülich preprint* **KFA-IKP(Th)-1994-17**, May 1994, submitted to *Phys. Lett.* **B.**

[24] O.Benhar, S.Fantoni, N.N.Nikolaev and B.G.Zakharov, Workshop at CEBAF at High Energies, 14-16 April 1994, CEBAF, and paper in preparation.

[25] NMC collaboration: A.Sandacz, private communication.

[26] S.J.Brodsky et al., SLAC-PUB-6412R (1994).

[27] J.Nemchik, N.N.Nikolaev and B.G.Zakharov, Anomalous A-dependence of diffractive leptoproduction of radial excitation $\rho'(2S)$,.*Jülich preprint* **KFA-IKP(Th)-1994-18**, May 1994, submitted to *Phys. Lett.* **B.**

[28] NMC Collaboration: C.Mariotti, *Proceedings of the Joint International Lepton-Photon Symposium and Europhysics Conference on High-Energy Physics*, 25 July - 1 August 1991, Geneva, editors S.Hegarty, K.Potter and E.Quercigh, World Scientific, v.1, p.154;

[29] P.Amaudruz *et al.*, *Nucl. Phys.* **B371** (1992) 533.

[30] M.D.Sokoloff et al., *Phys. Rev. Lett.* **57** (1986) 3003.

[31] G.N.Farrar, L.L.Frankfurt, K.F.Liu and M.Strikman, *Phys.Rev.lett.* **64** (1990) 2996; *Phys.Rev.Lett.* **61** (1988) 686.

[32] V.N.Gribov, *Sov.Phys.JETP* **29** (1969) 483; **30** (1970) 709.

[33] V.A.Karmanov and L.A.Kondratyuk, *JETP Letters* **18** (1973) 266.

[34] L.Lesniak, *Phys. Lett.* **B302** (1993) 140.

[35] N.N.Nikolaev, Color transparency: facts and fancy. *Int. J. Mod. Phys. E: Reports on Nuclear Physics* **3(2)** (1994).

[36] N.N.Nikolaev, A.Szczurek, J.Speth, J.Wambach, B.G.Zakharov and V.R.Zoller, Multiple scattering effects in the transverse-momentum dustributions from $(e, e'p)$ reactions, *Juelich preprint* **KFA-IKP(Th)-1993-29**, submitted to *Nucl. Phys.* **A**.

[37] N.N.Nikolaev, A.Szczurek, J.Speth, J.Wambach, B.G.Zakharov and V.R.Zoller, Theoretical interpretation of the NE18 experiment on nuclear transparency in $A(e, e'p)$ scattering, submitted to *Phys. Rev.* **C**.

[38] R.J.Glauber, in: *Lectures in Theoretical Physics*, v.1, ed. W.Brittain and L.G.Dunham. Interscience Publ., N.Y., 1959; R.J.Glauber and G.Matthiae, *Nucl. Phys.* **B21** (1970) 135.

[39] E.J.Moniz et al., *Phys.Rev.Lett.* **26** (1971) 445.

[40] S.Boffi, C.Giusti and F.D.Pacati, *Phys.Rep.* **226** (1993) 1.

[41] N.N.Nikolaev, A.Szczurek, J.Speth, J.Wambach, B.G.Zakharov and V.R.Zoller, *Phys.Lett.* **B317** (1993) 281.

[42] C.Lechanoine-LeLuc and F.Lehar, *Rev. Mod. Phys.* **65** (1993) 47.

[43] K.Gottfried, *Ann.Phys.* **21** (1963) 29; W.Czyz and K.Gottfried, *Nucl.Phys.* **21** (1961) 676; *Ann.Phys.* **21** (1963) 47; N.Srivastava, *Phys.Rev.* **135B** (1964) 612.

[44] H.Araseki and T.Fujita, *Nucl.Phys.* **A439** (1985) 681; K.Saito and T.Uchiyama, *Z.Phys.* **A322** (1985) 299.

[45] D.B.Day, J.S.McCarthy, T.W.Donnelly and I.Sick, *Ann.Rev.Nucl. Sci.* **40** (1990) 357; C.Cioffi degli Atti, E.Pace and G.Salme, *Phys.Rev.* **C43** (1991) 1155.

[46] N.N.Nikolaev, *JETP Lett.* **57** (1993) 85.

[47] I.M.Narodetsky, Yu.A.Simonov and F.Palumbo, *Phys.Lett.* **B58** (1975) 125; S.J.Brodsky and G.P.Lepage, in *Perturbative Quantum Chromodynamics*, editor A.H.Mueller, World Scientific, Singapore, 1989.

[48] N.Isgur and C.H.Llewellyn Smith, *Nucl. Phys.* **B317** (1989) 527; *Phys. Rev. Lett.* **52** (1984) 1080.

[49] P.Stoler, *Phys. Rev.* D44 (1991) 1973; *Phys. Rep.* **C226** (1993) 103.

[50] N.N.Zotov and A.V.Tzarev, *Sov. Phys. Uspekhi* **51** (1988) 121; G.Alberi and G.Goggi, *Phys. Rep.* **74** (1981) 1.

[51] N.N.Nikolaev, A.Szczurek, J.Speth, J.Wambach, B.G.Zakharov and V.R.Zoller, Pions in the lightcone nucleon and electromagnetic form factors, *Jülich preprint* **KFA-IKP(TH)-1993-35**, to appear in *Z. Phys.* **A** (1994).

[52] NA51 Collaboration: L.Kluberg, Workshop on Deep Inelastic Scattering and related problems, Eilat, February 6-9, 1994.

[53] N.N.Nikolaev, A.Szczurek, J.Speth, J.Wambach, B.G.Zakharov and V.R.Zoller, Pion content of the proton as seen in the Derell-Yan process, *Jülich preprint* **KFA-IKP(TH)-1993-35**, submitted to *Phys. Rev. Lett.* (1994).

[54] N.N.Nikolaev, A.Szczurek, J.Speth, J.Wambach, B.G.Zakharov and V.R.Zoller, Quark-hadron duality and color transparency sum rules for $A(e,e'p)$ scattering, paper in preparation.

[55] L.G.Dakhno and N.N.Nikolaev, *Nucl. Phys.* **A436** (1985) 653.

[56] B.Jennings and B.Z.Kopeliovich, *Phys. Rev. Lett.* **70** (1993) 3384.

[57] A.Bianconi, S.Boffi and D.E.Kharzeev, *Phys. Lett.* **B305** (1993) 3384; *Nucl. Phys.* **A565** (1993) 767.

[58] G.Fang, talk at the Workshop on CEBAF at Higher Energies, 14-16 April 1994, CEBAF.

[59] T.H.Bauer et al., *Rev. Mod. Phys.* **50** (1978) 261; A.Donnachie and H.Mirzae, *Z. Phys.* **C33** (1987) 407; A.Donnachie and A.B.Clegg, *Z. Phys,* **C45** (1990) 313, and refrences therein.

[60] M.Kossov, talk at the Workshop on CEBAF at Higher Energies, 14-16 April 1994, CEBAF.

Tables

Table 1. Probabilities $P^{(\nu)}$ for ν-fold rescatterings (in per cent) for the $(e, e'p)$ reaction on ^{12}C (upper block) and ^{208}Pb (lower block). In addition we show the nuclear transparency $W^{(0)}$ for quasifree knockout in the parallel kinematics, the nuclear transparency for the semi-exclusive reaction rate T_A and the average number of rescattering $\langle\nu\rangle$.

Q^2	0	1	2	3	4	$W^{(0)}$	T_A	$\langle\nu\rangle$
1	65.15	23.40	8.09	2.49	0.67	0.63	0.97	0.51
1.2	68.37	22.06	6.96	1.98	0.50	0.60	0.87	0.45
1.5	71.94	20.39	5.76	1.48	0.34	0.56	0.77	0.38
2	74.18	19.26	5.03	1.21	0.26	0.54	0.72	0.34
4	81.31	15.24	2.87	0.49	0.08	0.54	0.67	0.23
6	83.40	13.89	2.31	0.35	0.05	0.55	0.66	0.19
8	85.65	12.33	1.76	0.23	0.03	0.56	0.65	0.17
1	30.13	21.60	16.09	11.69	8.12	0.25	0.84	1.98
1.2	39.32	23.70	15.00	9.39	5.70	0.23	0.57	1.46
1.5	49.36	24.44	12.81	6.72	3.46	0.20	0.41	1.03
2	55.08	24.12	11.22	5.25	2.43	0.19	0.34	0.83
4	67.45	21.54	7.30	2.48	0.83	0.19	0.28	0.49
6	70.66	20.39	6.23	1.91	0.57	0.20	0.28	0.42
8	74.37	18.79	5.02	1.34	0.35	0.20	0.27	0.35

Figure captions:

Fig. 1 - Qualitative dependence of the universal dipole cross section $\sigma(r)$ on the dipole size r for scattering of the color dipole on the nucleon target. Different processes probe this universal dipole cross section at different r [12].

Fig. 2 - The qualitative pattern of Q^2-dependent scanning of the wave functions of the ground state V and the radial excitation V' of vector meson [9,27]. The scanning distributions $\sigma(r)\Psi_{\gamma^*}(r)$ shown by the solid and dashed curve have the scanning radii ρ_S differing by a factor 3. All wave functions are in arbitrary units.

Fig. 3 - Predictions [23] for the exclusive production of vector mesons ρ^0, ϕ^0 vs. the NMC data [25].

Fig. 4 - Predictions [10] of nuclear transparency $T_A = \sigma_A/A\sigma_N$ for the incoherent exclusive production of ρ^0 mesons vs. the E665 data [5].

Fig. 5 - Predictions [10] of nuclear transparency $T_A^{(coh)}/T_C^{(coh)} = [144 d\sigma_A/A^2 d\sigma_C]_{\vec{q}^2=0}$ for the forward coherent production of the ρ^0 mesons.

Fig. 6 - Predictions [10] of the Q^2 dependence of the ratio of cross sections $R_{coh}(A/C) = 12\sigma_A/A\sigma_C$ for coherent production of the ρ^0 meson vs. the E665 data [5]. The arrows indicate predictions for the complete CT (vanishing FSI).

Fig. 7 - Predictions [10] of the Q^2 dependence of exponents of parametrizations $\sigma_A(inc) \propto A^{\alpha_{inc}}$, $[d\sigma_A(coh)/dq^2]_{\vec{q}^2=0} \propto A^{\alpha_{coh}(\vec{q}^2=0)}$ and $\sigma_A(coh) \propto A^{\alpha_{coh}}$ vs. the E665 data [5].

Fig. 8 - Energy dependence of the ratio of transparency in quasielastic J/Ψ photoproduction on tin and carbon predicted [22] from Eq. (25) (shown by solid line) versus the NMC data [28] for the 200 and 280 GeV primary muons [34]. The dotted line shows the prediction of the classical expansion model by Farrar et al. [31].

Fig. 9. - The predicted Q^2 and ν—dependence of the nuclear transparency in the virtual photoproduction of the ρ^0-mesons [9].

Fig. 10 - The predicted Q^2 and ν-dependence of the nuclear transparency in the virtual photoproduction of the heavy quarkonia [9]. The qualitative pattern is the same from the light to heavy nuclei.

Fig. 11 - The Q^2 dependence of the $\rho'(2S)/\rho^0(1S)$ ratio of forward production cross sections, which exhibits a dip because of the exact node effect in the $\rho'(2S)$ production.

Fig. 12 - The Q^2 and A dependence of nuclear transparency for the $\rho^0(1S)$ and $\rho'(2S)$ electroproduction on nuclei.

Fig. 13 - Predictions [24] for the onset of antishadowing in the incoherent real photoproduction of radial excitation $\phi'(2S)$ opn nuclear targets.

Fig. 14 - Predictions [24] for nuclear transparency $T_A = \sigma_A/A\sigma_N$ in electroproduction of the $\phi^0(1S)$ and $\phi'(2S)$ on nuclei.

Fig. 15 - Predictions [24] for the CT and node-effect driven steep Q^2 dependence of nuclear transparency in the electroproduction of the $\phi'(2S)$ on nuclei.

Fig. 16 - The final-state interaction in quasielastic $(e, e'p)$ scattering. FSI regenerates the observed proton $|p\rangle$ from electroproduced intermediate states $|i\rangle$.

Fig. 17 - Predictions [36] for the transverse missing momentum distribution of struck protons from $^{12}C(e, e'p)$ (left hand side) and $^{208}Pb(e, e'p)$ reactions (right hand side) for different values of Q^2. The solid lines correspond to the full momentum distributions. The PWIA component of the missing momentum distribution ($\nu = 0$) is shown by the long-dashed line. The ν-fold rescattering contributions are represented by the short-dashed lines ($\nu = 1$), the dash-dotted lines ($\nu = 2$) and the dotted lines ($\nu = 3$) respectively.

Fig. 18 - Predictions [37] for the Q^2 dependence of nuclear transparency are compared with the NE18 data [4]. The dashed curve denotes the $p_\perp$-integrated nuclear transparency T_A; the dotted curve gives the nuclear transparency $W^{(0)}$ measured in parallel kinematics at $p_\perp = 0$; the solid curve represents the nuclear transparency $T_A(NE18)$ including the NE18 acceptance cuts [4]; the dot-dashed curve in panel b) shows the predicted [37] effect of the onset of CT.

Fig. 19 - The predicted [54] mass spectrum (the solid line) in the diffraction dissociation of protons $pp \to pX$ into state of invariant mass M. The data are taken from the compilation [50]. Contribution to the mass spectrum from excitation of the πN continuum is shown by the dotted line; contributions from excitation of resonances corresponding to the positive parity excited shells is shown by dashed lines.

Fig. 20 - Predictions [54] for the Q^2-dependence of the strength of FSI $\Sigma_{ep}(Q^2)$ in $^{12}C(e, e'p)$ reaction (left box) and of nuclear transparency T_A for different nuclear targets.

Fig. 21 - The top box: Predictions [54] for the Q^2 dependence of the scaled strength of FSI $\eta = \Sigma_{ep}(Q^2)/\sigma_{tot}(pN)$ in $^4He(e, e'p)$ reaction (the solid line). Shown separately are the contributions to $1 - \eta$ which is the signal of CT, from excitation of intermediate πN state (the dotted line) and from excitations of nucleonic resonances (the dashed line).
The bottom box: Predictions [54] for the CT effect in the rate of $^4He(e, e'p)$ reaction with high transverse missing momentum. The quantity shown is the relative strength of the elastic-rescattering tail in the $p_\perp$-distribution which is given by $\eta^2 = [\Sigma_{ep}(Q^2)/\sigma_{tot}(pN)]^2$

Fig. 22 - The predicted [8] dependence of nuclear transparency T_A (upper part) and of the observable $\Sigma_{ep}(x, Q^2)$ (lower part) on the Bjorken variable x for different values of Q^2 (in $(GeV/c)^2$) listed in the figure. The dashed curves are obtained if only the mean-field component of the single-particle momentum distribution (46) is retained in evaluation of $F_A(x)$ in Eq. (82). top results are for $^{12}C(e, e'p)$ scattering.

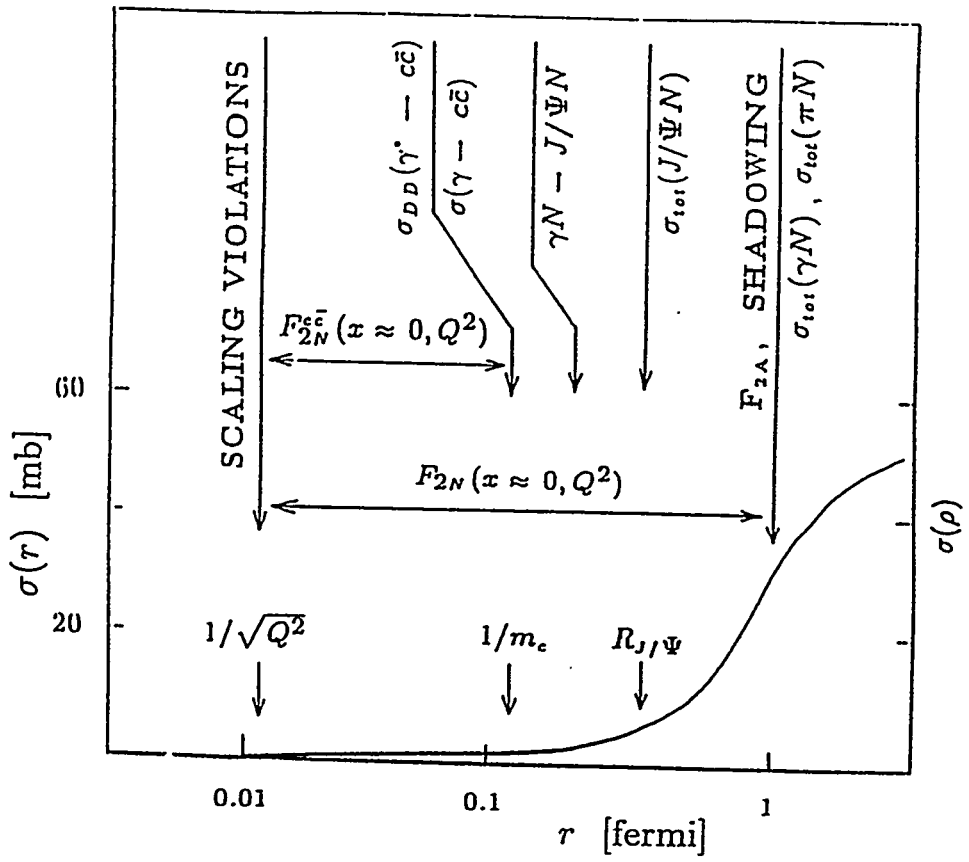

SCALING VIOLATIONS
$\sigma_{DD}(\gamma^* - c\bar{c})$
$\sigma(\gamma - c\bar{c})$
$\gamma N - J/\Psi N$
$\sigma_{tot}(J/\Psi N)$
F_{2A}, SHADOWING
$\sigma_{tot}(\gamma N)$, $\sigma_{tot}(\pi N)$
$F_{2N}^{c\bar{c}}(x \approx 0, Q^2)$
$F_{2N}(x \approx 0, Q^2)$
$\sigma(r)$ [mb]
60
20
$1/\sqrt{Q^2}$
$1/m_c$
$R_{J/\Psi}$
$\sigma(\rho)$
0.01
0.1
1
r [fermi]

Fig. 1

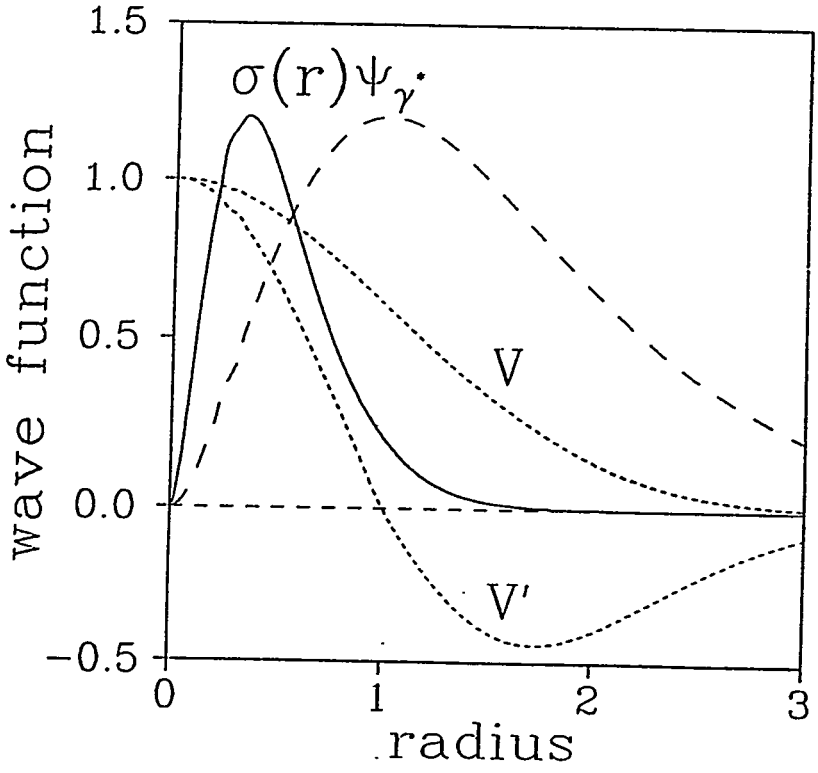

$\sigma(r)\psi_{\gamma^*}$
V
V'
wave function
1.5
1.0
0.5
0.0
−0.5
0
1
2
3
radius

Fig. 2

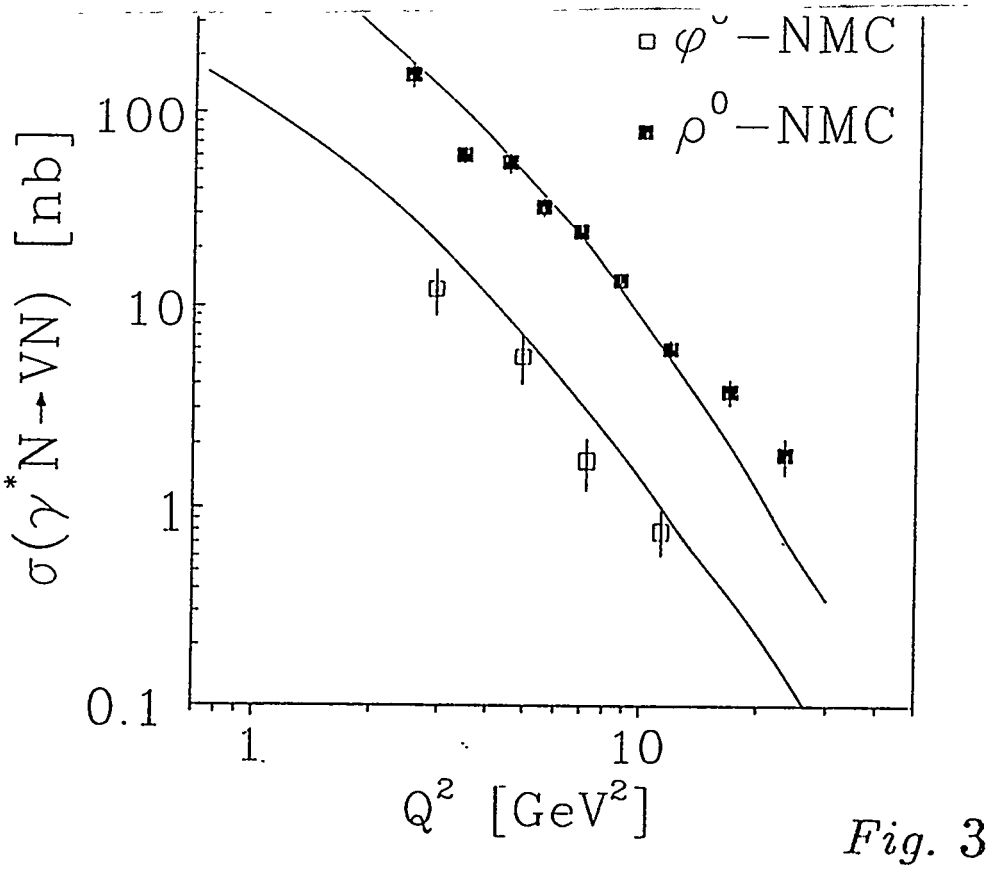

φ^0–NMC
ρ^0–NMC
$\sigma(\gamma^* N \to VN)$ [nb]
100
10
1
0.1
1.
10
Q^2 [GeV^2]

Fig. 3

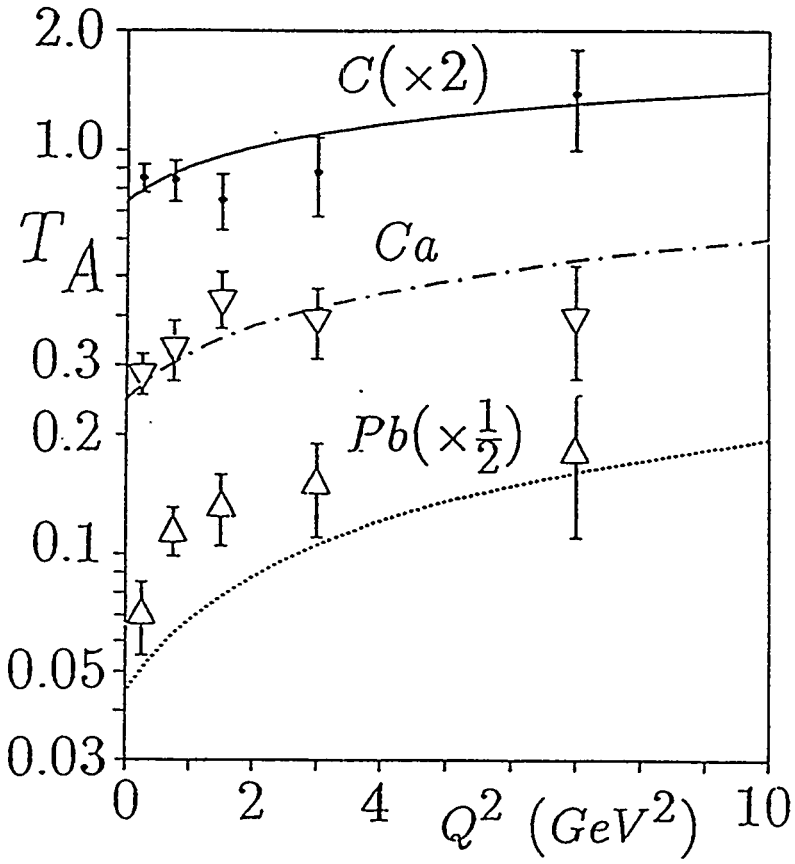

2.0
1.0
T_A
0.3
0.2
0.1
0.05
0.03
$C(\times 2)$
Ca
$Pb(\times \frac{1}{2})$
0
2
4
Q^2 (GeV^2)
10

Fig. 4

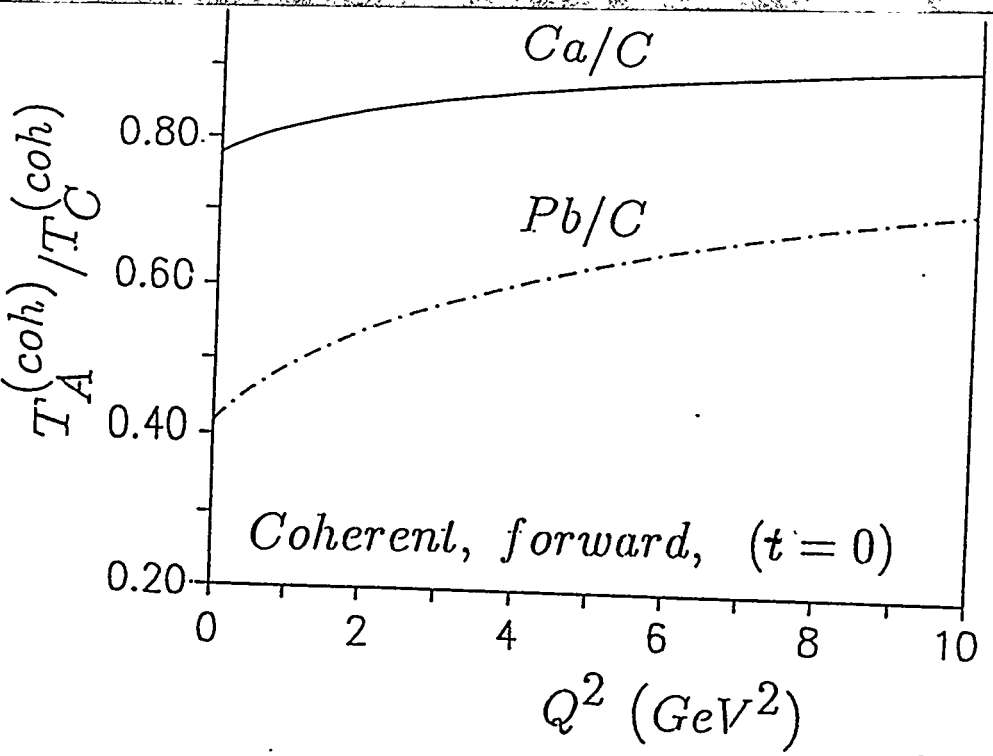

Ca/C
Pb/C
Coherent, forward, (t = 0)
$T_A^{(coh)}/T_C^{(coh)}$
0.80
0.60
0.40
0.20
0
2
4
6
8
10
Q^2 (GeV^2)

Fig. 5

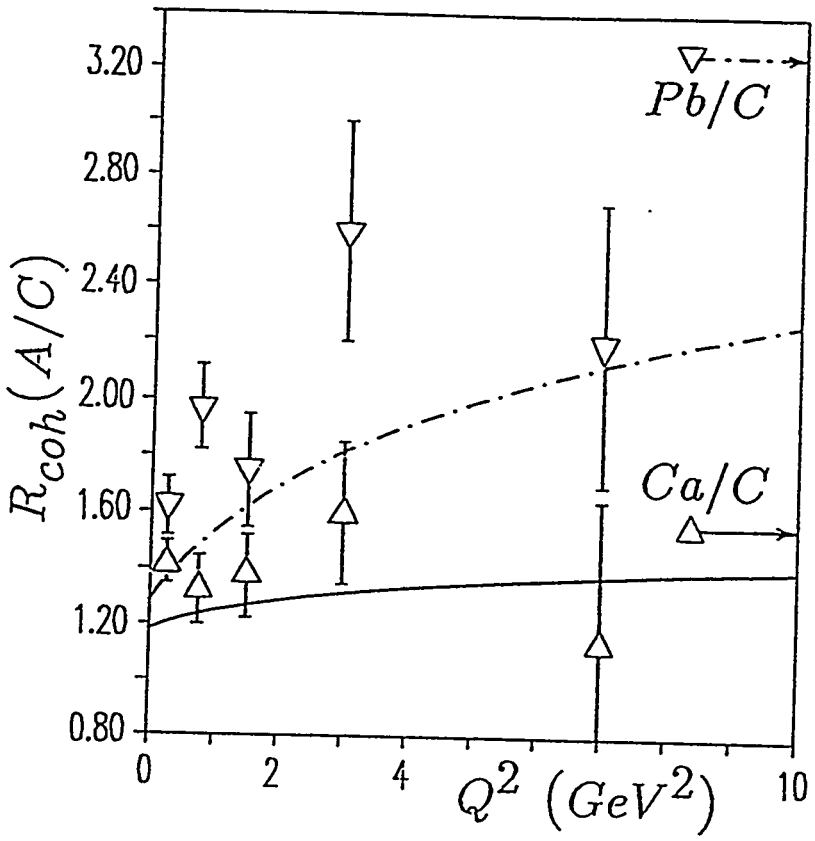

Pb/C
Ca/C
$R_{coh}(A/C)$
3.20
2.80
2.40
2.00
1.60
1.20
0.80
0
2
4
Q^2 (GeV^2)
10

Fig. 6

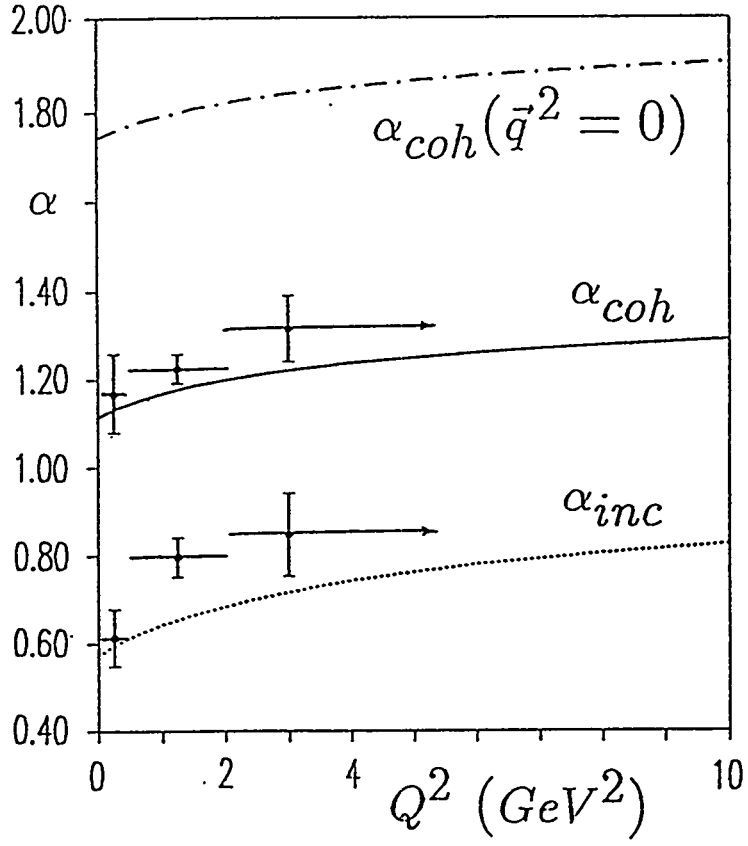

2.00
1.80
α
1.40
1.20
1.00
0.80
0.60
0.40
0
2
4
10
$Q^2\ (GeV^2)$
$\alpha_{coh}(\vec{q}^2 = 0)$
α_{coh}
α_{inc}

Fig. 7

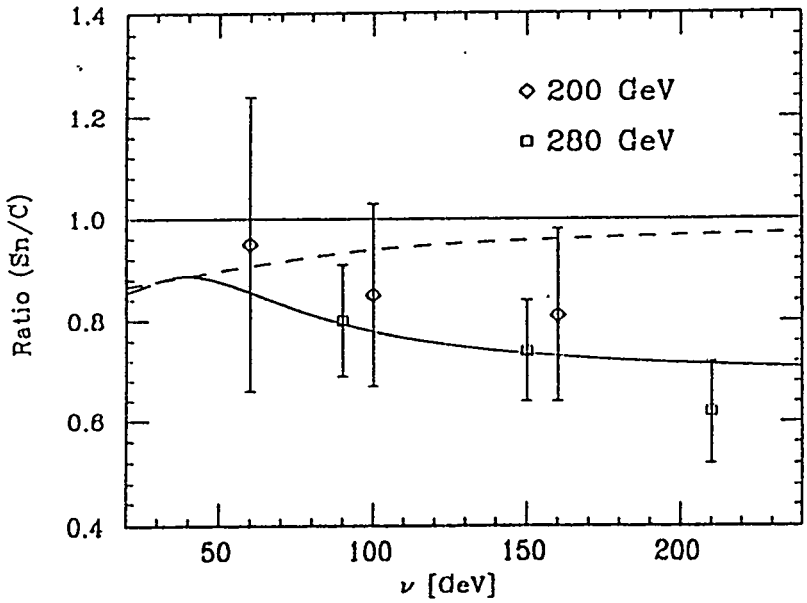

1.4
1.2
1.0
0.8
0.6
0.4
Ratio (Sn/C)
50
100
150
200
ν [GeV]
◇ 200 GeV
□ 280 GeV

Fig. 8

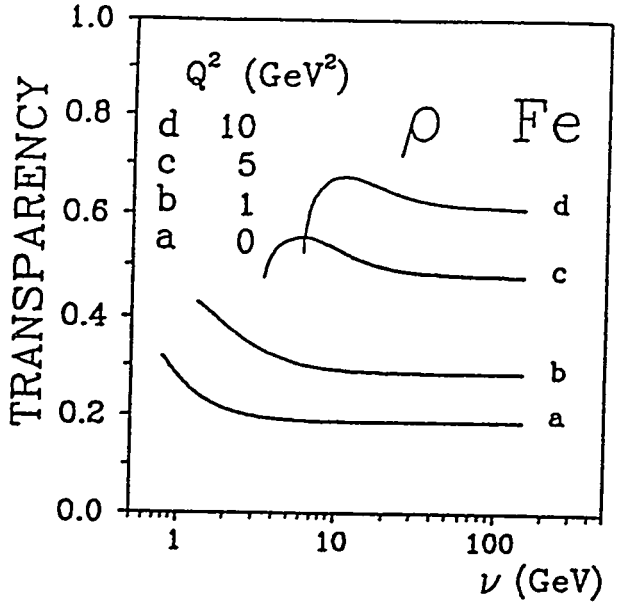

TRANSPARENCY
1.0
0.8
0.6
0.4
0.2
0.0
Q^2 (GeV^2)
d 10
c 5
b 1
a 0
ρ Fe
d
c
b
a
1
10
100
ν (GeV)

Fig. 9

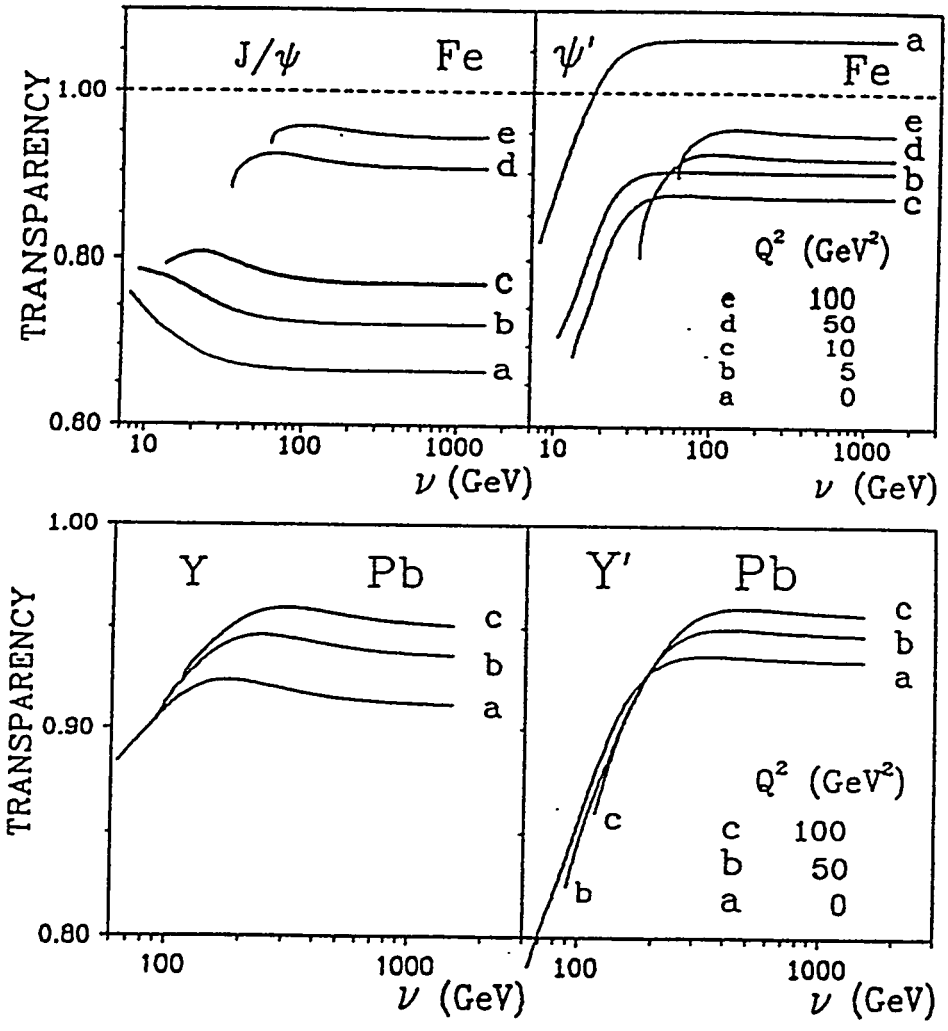

J/ψ Fe
ψ' Fe
TRANSPARENCY
1.00
0.80
0.80
e
d
c
b
a
Q^2 (GeV^2)
e 100
d 50
c 10
b 5
a 0
10
100
1000
ν (GeV)
Y Pb
Y' Pb
1.00
0.90
0.80
c
b
a
Q^2 (GeV^2)
c 100
b 50
a 0
100
1000
ν (GeV)

Fig. 10

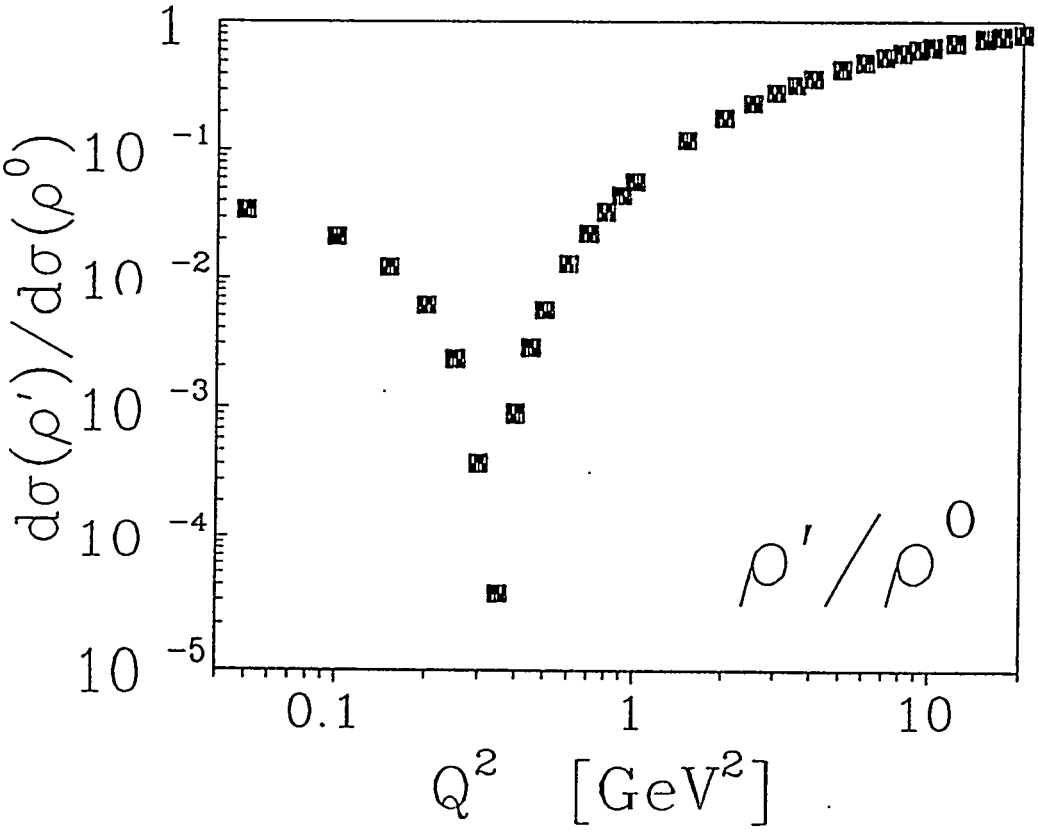


Fig. 11

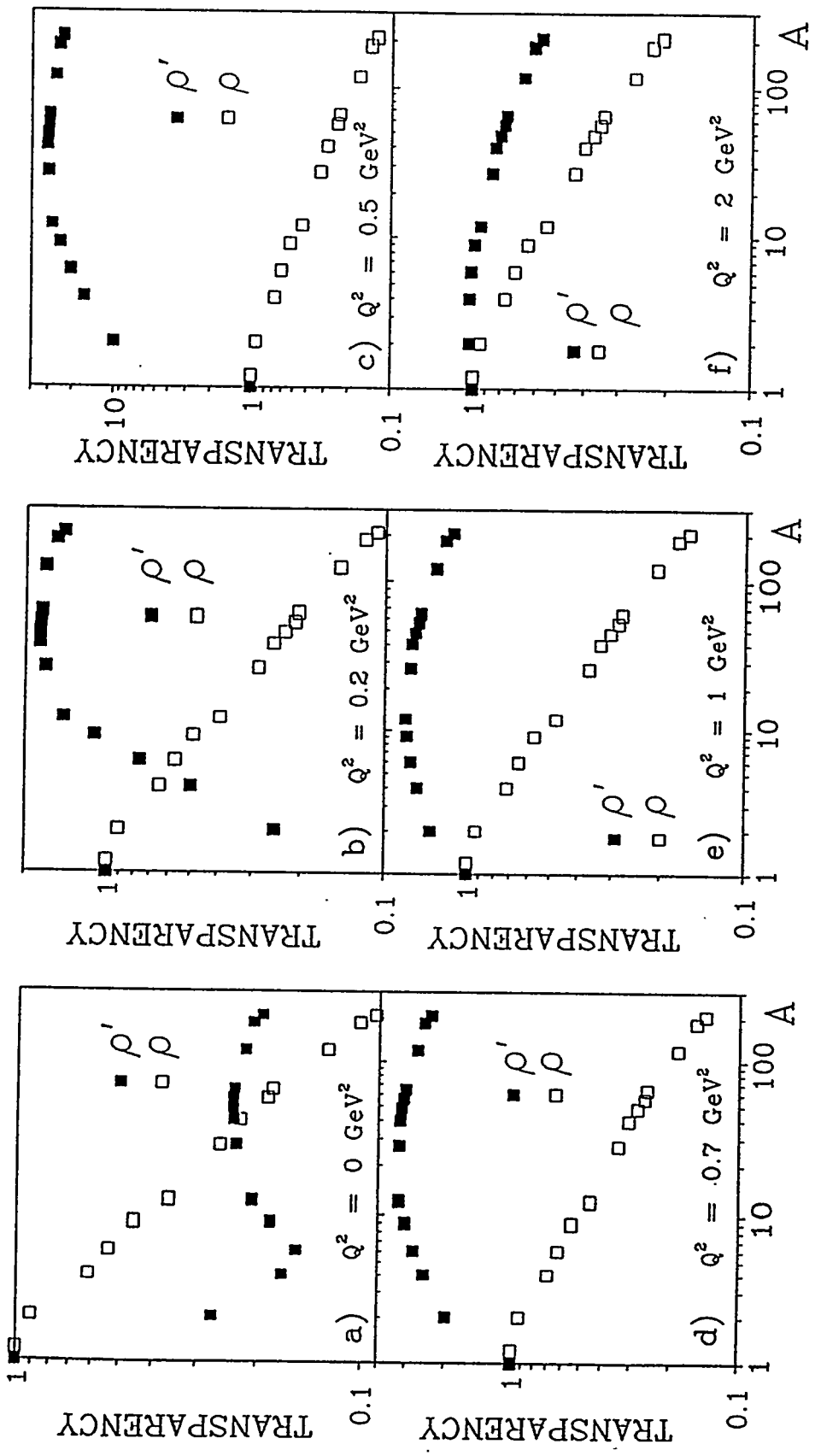

TRANSPARENCY
A
a) Q^2 = 0 GeV²
b) Q^2 = 0.2 GeV²
c) Q^2 = 0.5 GeV²
d) Q^2 = .07 GeV²
e) Q^2 = 1 GeV²
f) Q^2 = 2 GeV²
ρ
ρ'

Fig. 12

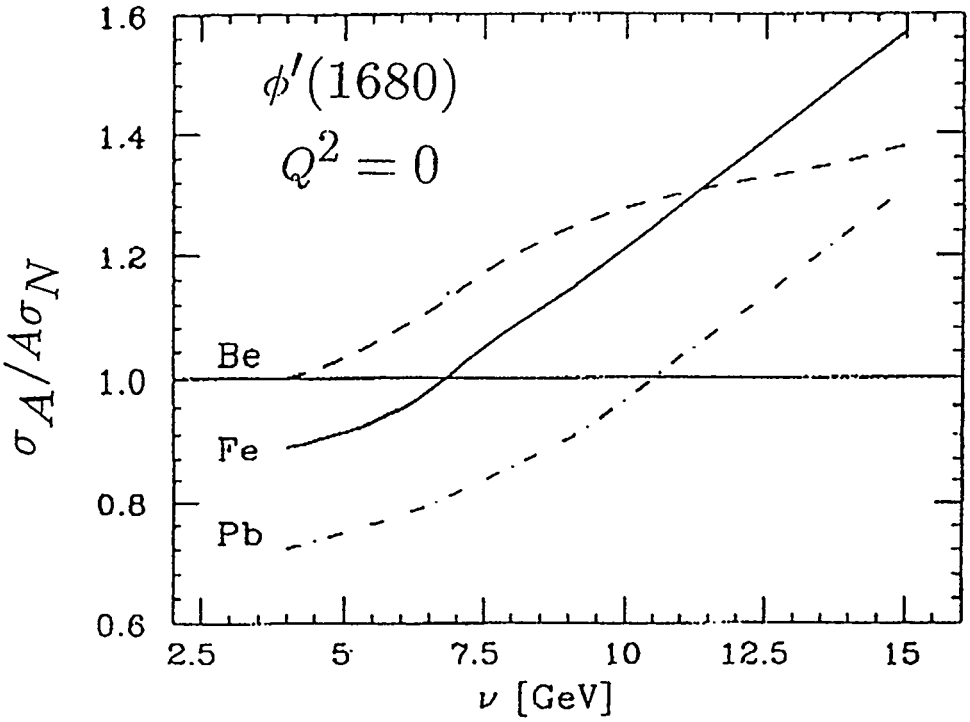

$\phi'(1680)$
$Q^2 = 0$
Be
Fe
Pb
$\sigma_A/A\sigma_N$
ν [GeV]
1.6
1.4
1.2
1.0
0.8
0.6
2.5
5
7.5
10
12.5
15

Fig. 13

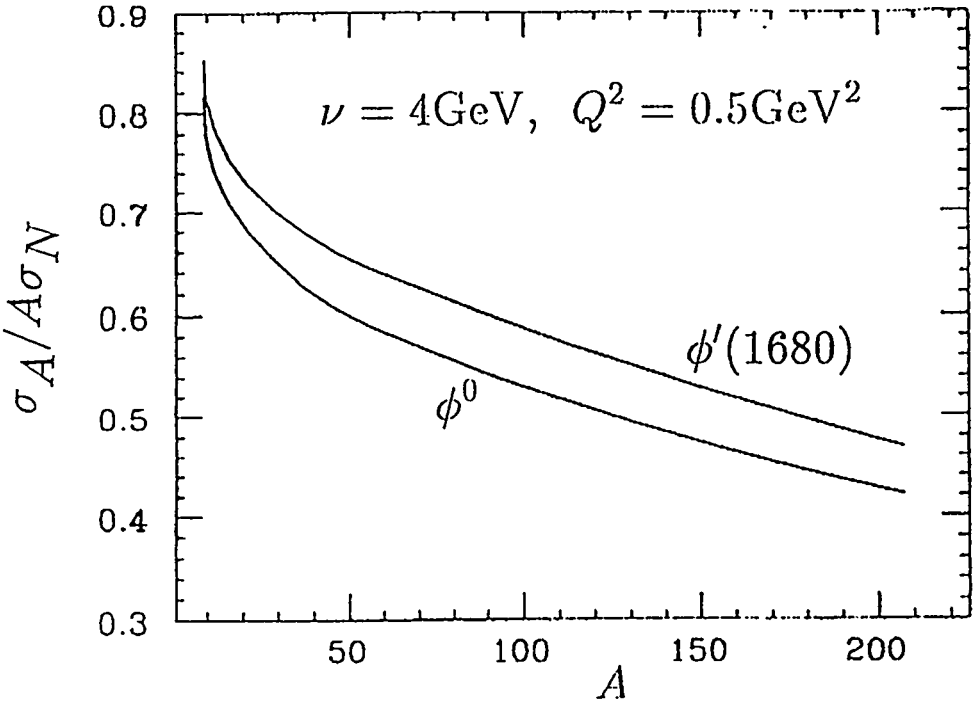

$\nu = 4\text{GeV}, \quad Q^2 = 0.5\text{GeV}^2$
$\phi'(1680)$
ϕ^0
$\sigma_A/A\sigma_N$
A
0.9
0.8
0.7
0.6
0.5
0.4
0.3
50
100
150
200

Fig. 14

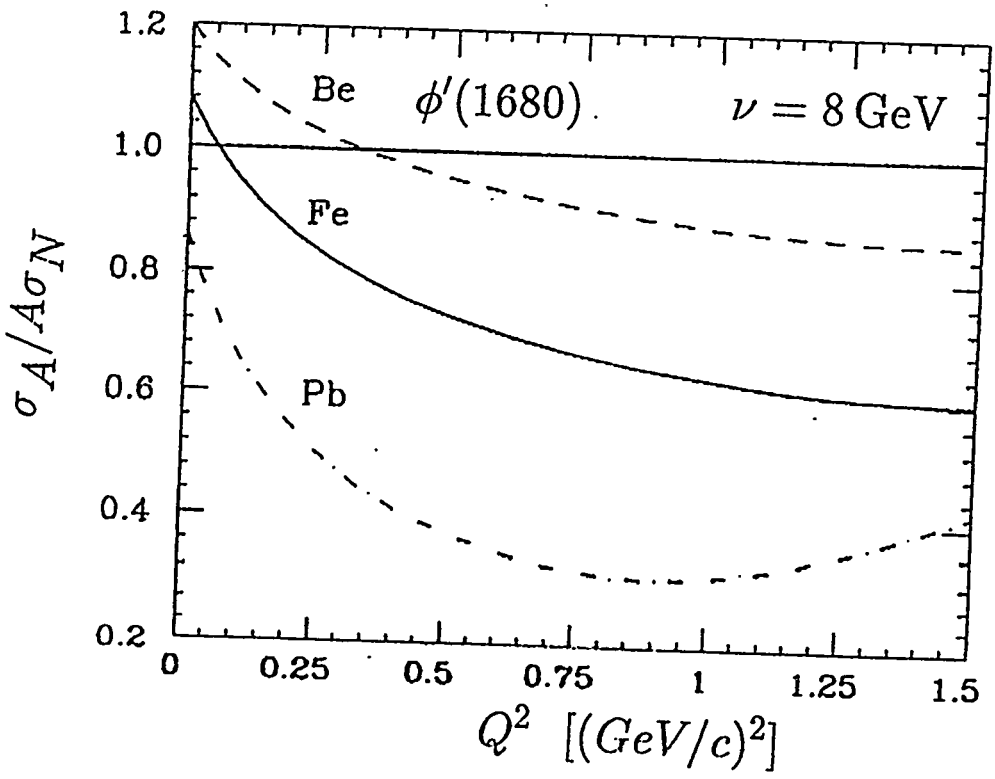

1.2
1.0
0.8
0.6
0.4
0.2
0
0.25
0.5
0.75
1
1.25
1.5
Be
$\phi'(1680)$
$\nu = 8\,\mathrm{GeV}$
Fe
Pb
$\sigma_A/A\sigma_N$
Q^2 $[(GeV/c)^2]$

Fig. 15

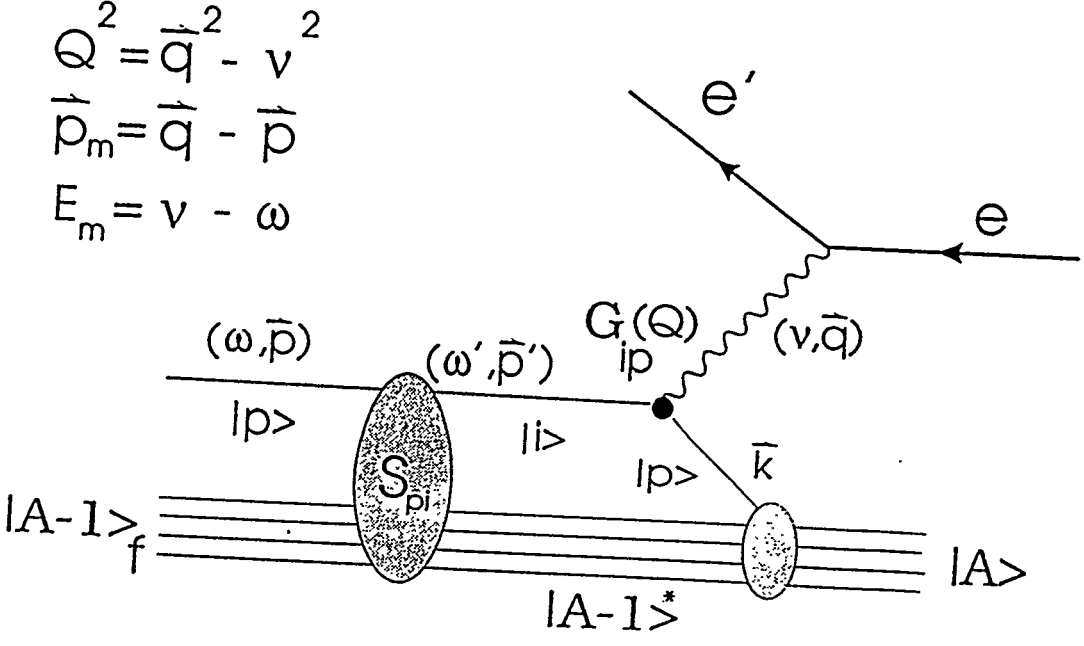

$Q^2 = \vec{q}^{\,2} - \nu^2$
$\vec{p}_m = \vec{q} - \vec{p}$
$E_m = \nu - \omega$
e'
e
$G_{ip}(Q)$
$(\nu,\vec{q})$
$(\omega,\vec{p})$
$(\omega',\vec{p}')$
|p>
|i>
|p>
$\vec{k}$
S_{pi}
|A-1>$_f$
|A>
|A-1*>
$\vec{p}_m$

Fig. 16

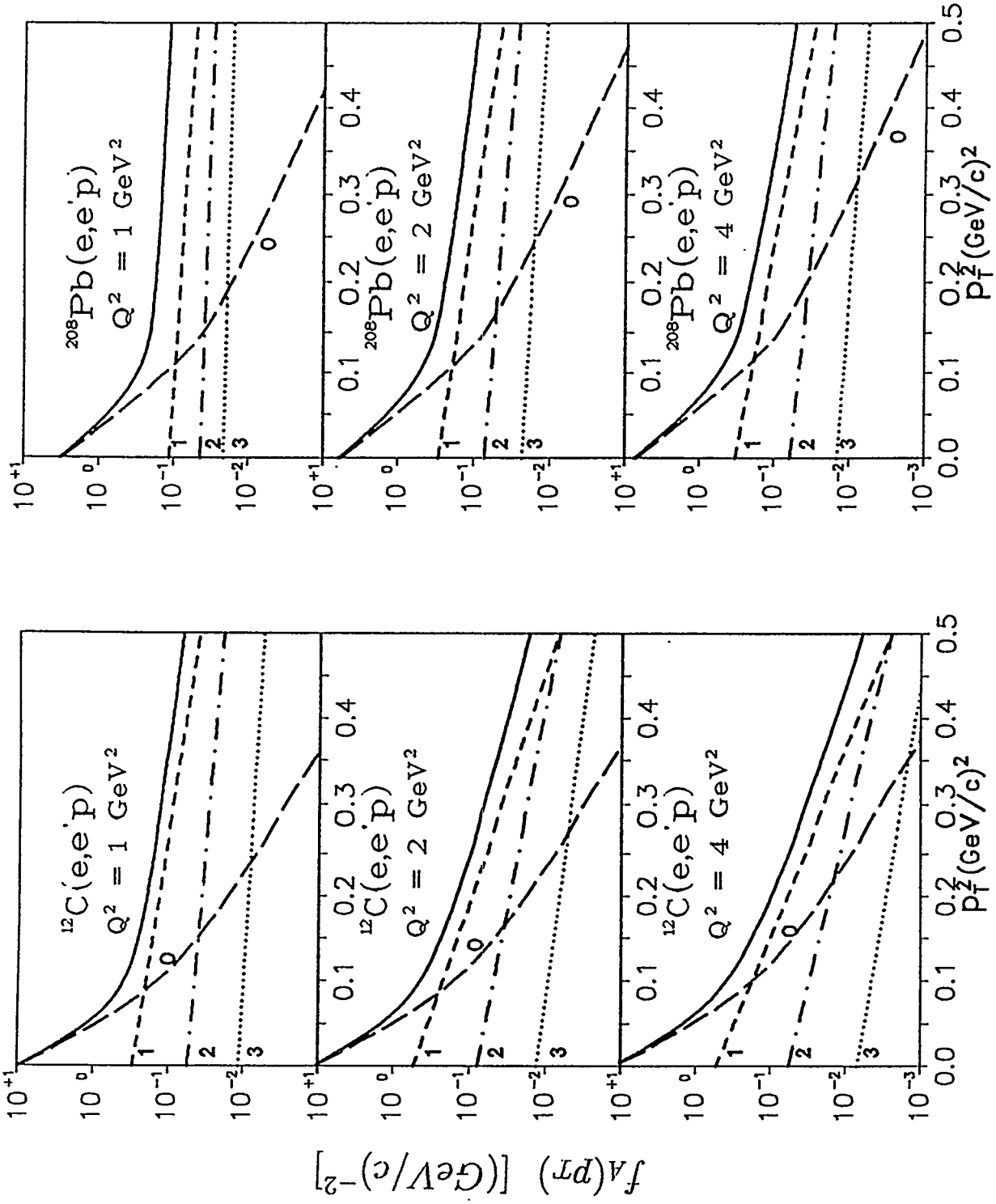

$f_A(p_T)$ $[(GeV/c)^{-2}]$
$^{12}C(e,e'p)$ $Q^2 = 1$ GeV^2
$^{12}C(e,e'p)$ $Q^2 = 2$ GeV^2
$^{12}C(e,e'p)$ $Q^2 = 4$ GeV^2
$^{208}Pb(e,e'p)$ $Q^2 = 1$ GeV^2
$^{208}Pb(e,e'p)$ $Q^2 = 2$ GeV^2
$^{208}Pb(e,e'p)$ $Q^2 = 4$ GeV^2
p_T^2 (GeV/c)^2
0
1
2
3

Fig. 1

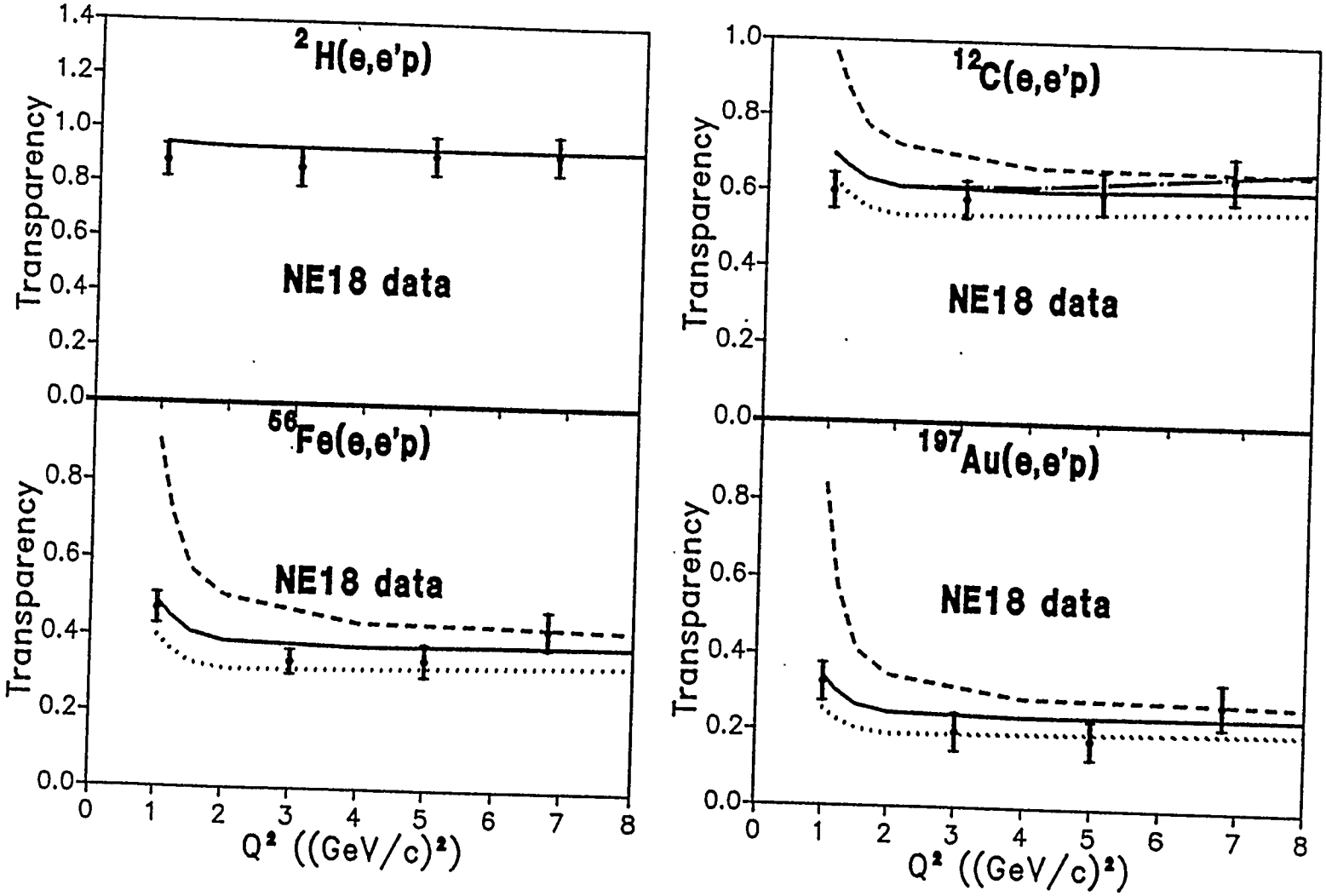

^{2}H(e,e'p)
NE18 data
^{56}Fe(e,e'p)
NE18 data
^{12}C(e,e'p)
NE18 data
^{197}Au(e,e'p)
NE18 data
Transparency
Q² ((GeV/c)²)

Fig. 18

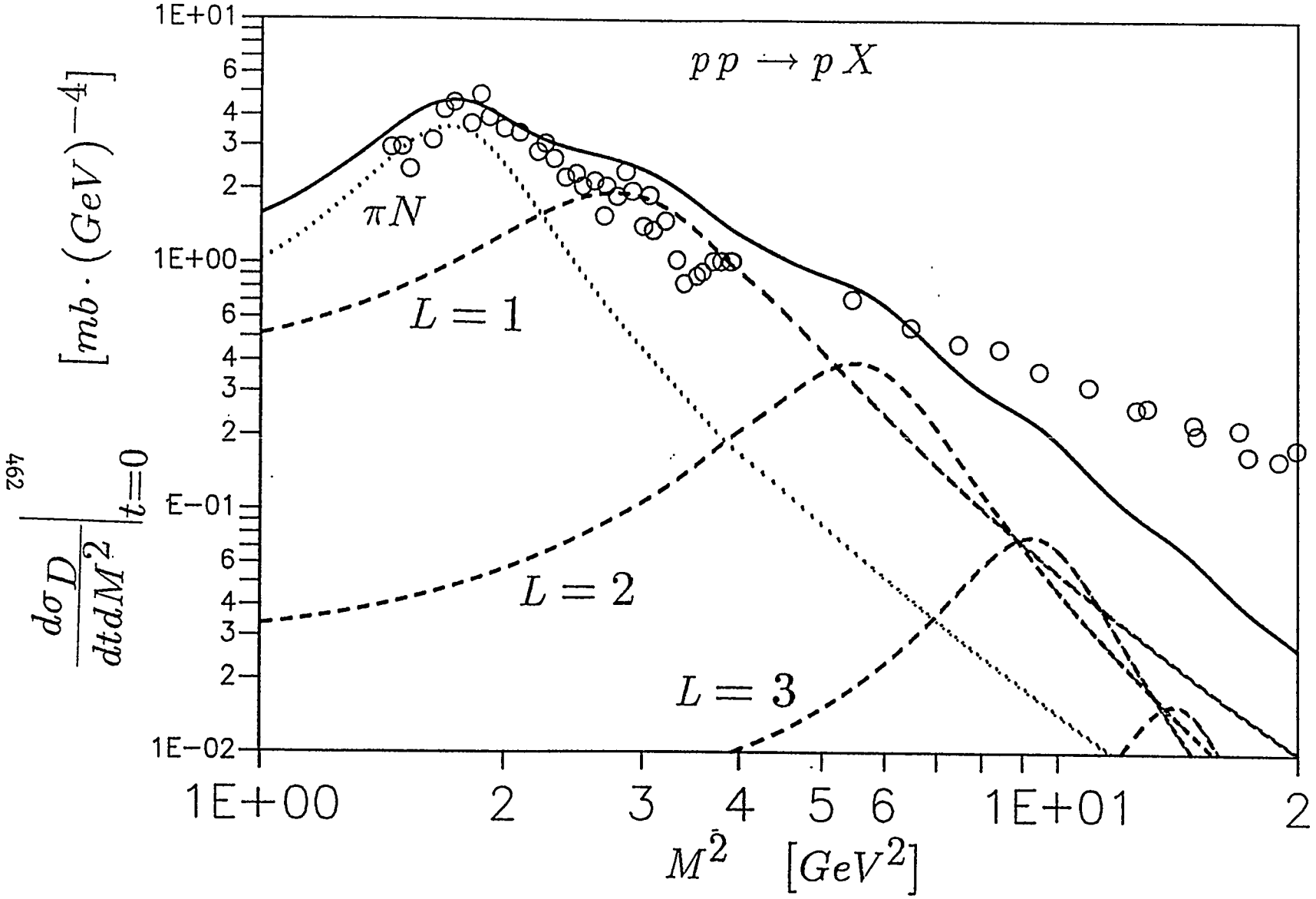
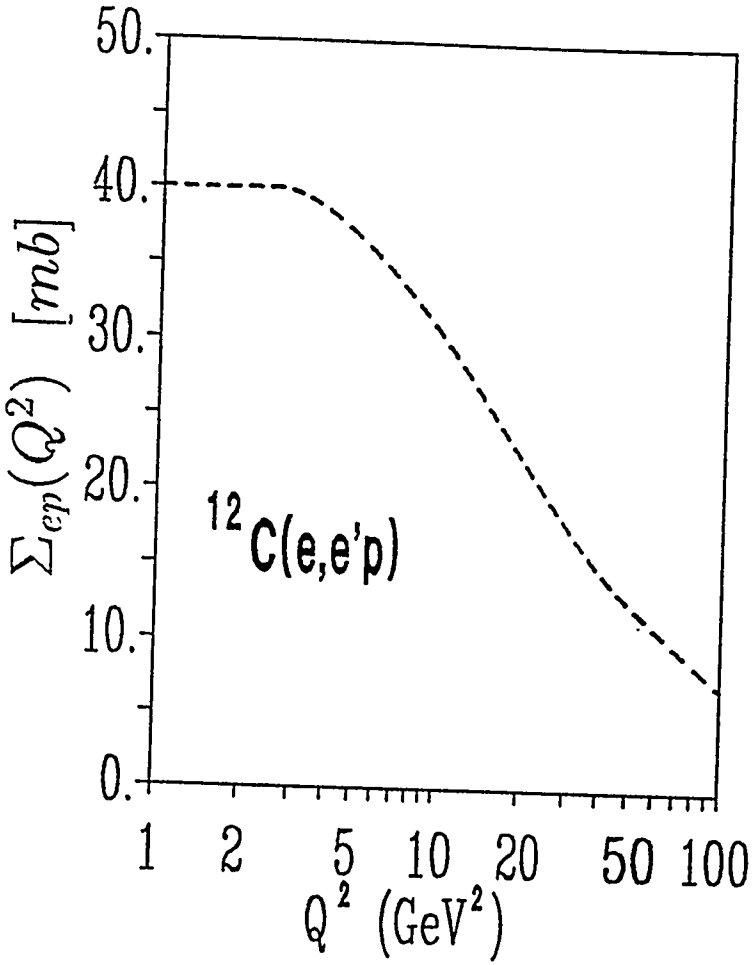

$pp \to pX$
πN
$L = 1$
$L = 2$
$L = 3$
$\left.\frac{d\sigma_D}{dtdM^2}\right|_{t=0}$
$[mb \cdot (GeV)^{-4}]$
462
1E+01
1E+00
1E-01
1E-02
1E+00
2
3
4
5
6
1E+01
M^2 $[GeV^2]$

Fig. 19


50.
40.
30.
20.
10.
0.
$\Sigma_{ep}(Q^2)$ [mb]
^{12}C(e,e'p)
1 2 5 10 20 50 100
Q^2 (GeV^2)

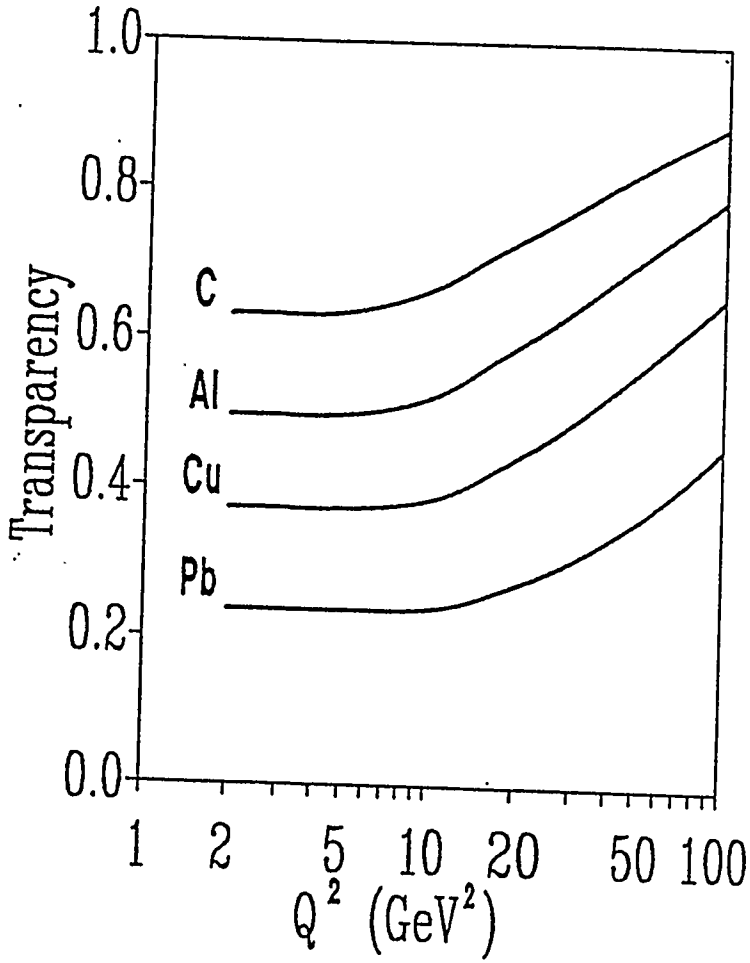

1.0
0.8
0.6
0.4
0.2
0.0
Transparency
C
Al
Cu
Pb
1 2 5 10 20 50 100
Q^2 (GeV^2)

Fig. 20

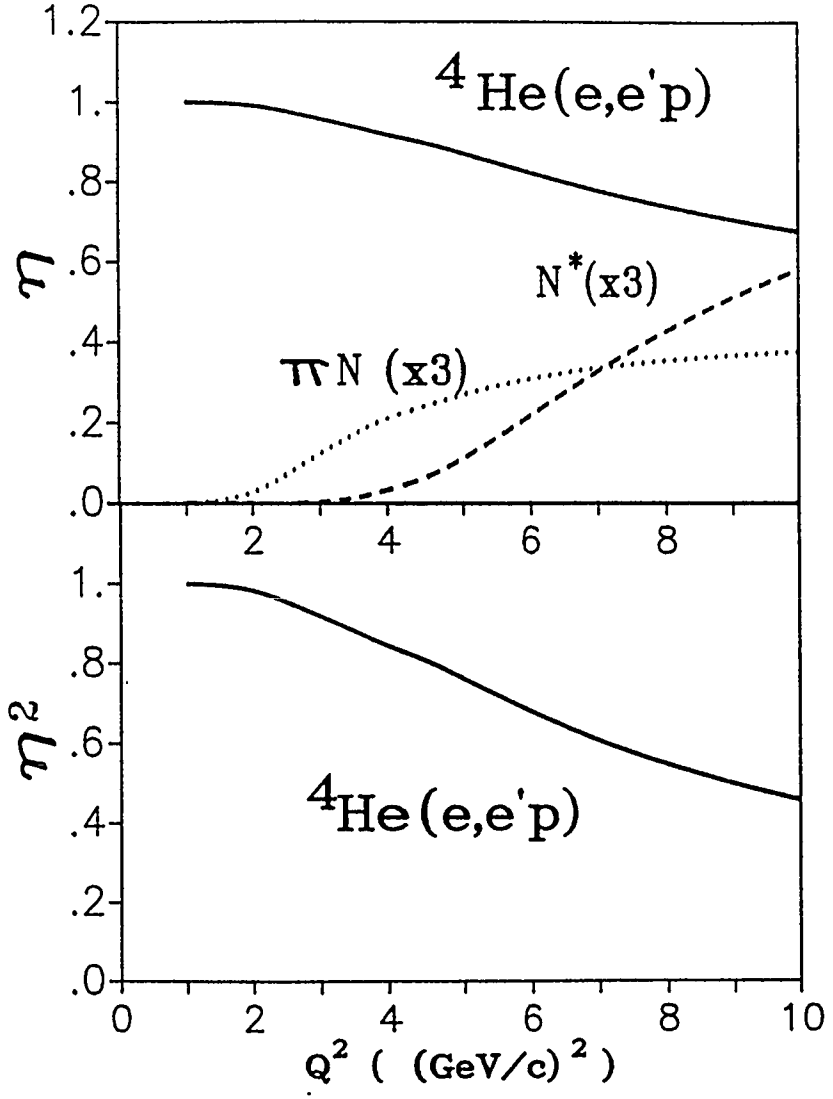

^{4}He(e,e'p)
N*(x3)
πN (x3)
η
^{4}He(e,e'p)
η²
Q² ((GeV/c)²)

Fig. 21

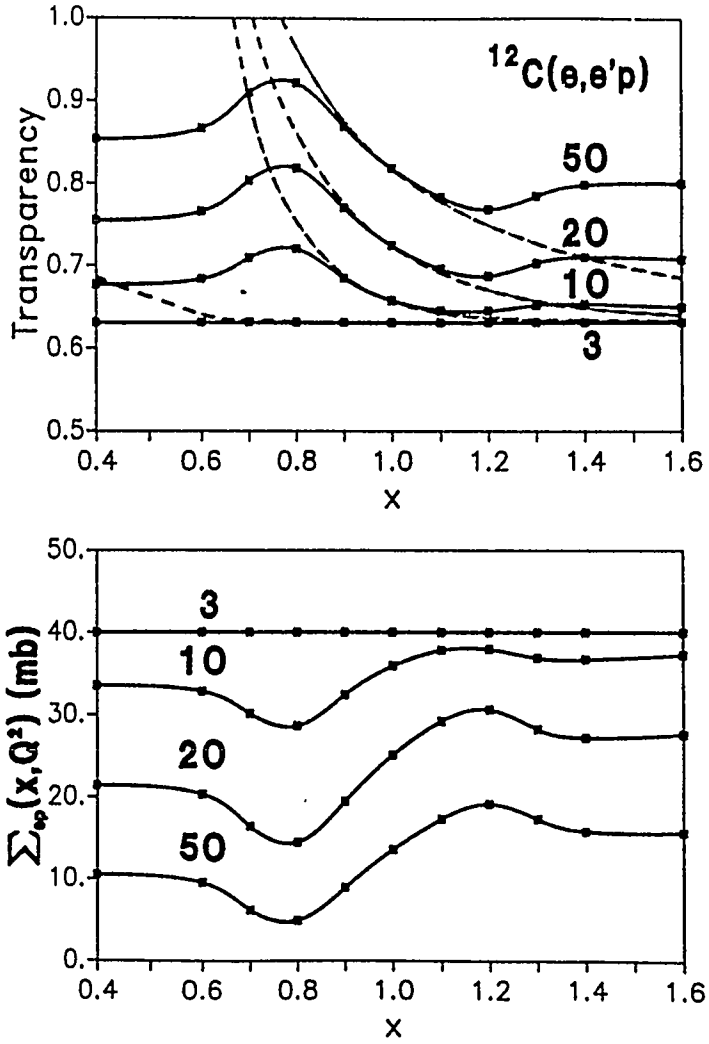

^{12}C(e,e'p)
Transparency
50
20
10
3
x
3
10
20
50
Σ_ep(x,Q²) (mb)
x

Fig. 22

Meson Exchange and Neutral Weak Currents

D. H. Beck
Nuclear Physics Laboratory
University of Illinois
Urbana, IL 61801

Abstract

Measurements of parity-violating electron scattering asymmetries to determine weak neutral currents in nuclei will be effected by the presence of meson exchange currents. Present low momentum transfer calculations, based on a flavor independent framework, show these effects to be small. In general, however, as the momentum transfer increases to values typical of deep-inelastic scattering, fragmentation functions show a clear flavor dependence. It is suggested that a good experimental starting point for understanding the flavor dependence of meson production and exchange currents is the Q^2 dependence of parity-violating asymmetry in inclusive single pion electroproduction. A CEBAF facility with doubled energy is necessary to approach momentum transfers where this process begins to scale.

1 Introduction

CEBAF is expected to be well suited to measuring electron scattering parity-violating asymmetries based mainly on the high beam quality anticipated. It would provide extended opportunities in this area if the energy is doubled. One of the amusing questions related to measurement of neutral weak currents in nuclei is the effect that meson exchange currents (MEC) might have. I argue in the following that a possible starting point is to look at the Q^2 dependence of single pion production asymmetries to determine the this neutral weak transition current.

Present calculations of MEC effects in electron scattering asymmetries from nuclear targets show that the effects are small [Mu94, Mu93]. The meson production framework here is effectively flavor independent. For example, for a pion exchange current, the important factors in the amplitude are

$$F_q^1(Q^2) \cdot f_{\pi NN}: \quad q = u,\ d,\ s; \tag{1}$$

i.e. the production is the product of the amplitude of finding a quark of flavor q in the nucleon and of the (flavor independent) amplitude of a nucleon producing a pion This is possible since, at low momentum transfer, the probability of producing a (virtual) meson may be independent of the flavor of quark 'struck' by the photon. In simple classical terms, the energy transferred to the nucleon is equilibrated before the meson is emitted (the 'interaction time' being relatively long).

At higher momentum transfer, however, this is not the case. It is observed in deep-inelastic scattering that the probability of producing a given meson does depend on the flavor of the struck quark. For example, the probability of producing leading ($E_\pi/\nu = z > 0.5$) pions depends on the flavor of the struck quark via [Cl79]

$$f_q(x) \cdot D_q^h(z): \quad q = u,\ d,\ s,\ \ldots; \quad h = \pi^\pm,\ \pi^0,\ \ldots \tag{2}$$

where the $D_q^h(z)$ are the so-called fragmentation functions. In particular it is observed that

$$\frac{D_u^{\pi^+}(z)}{D_d^{\pi^+}(z)} = 3 - 8 \tag{3}$$

depending on the value of z. Again this is plausible a result; from a simple point of view it is reasonable to expect that it is more likely a π^+ will be produced if it is a u quark rather than a d quark that is struck by the photon.

The comparison of the neutral weak and the electromagnetic currents in elastic parity-violation asymmetry measurements allows separation of the contribution of the quark flavors to the elastic form factors. This method also provides a possible method of 'tagging' the flavor of the struck quark in inelastic reactions. In this way it may be possible to measure the Q^2 dependence of single pion production asymmetry in an *inclusive* measurement (inclusive electron scattering between one and two pion threshold) and determine whether the limits described above are valid.

It is important to note some potential difficulties in this argument. At low momentum transfer, it should be straightforward to calculate the asymmetry in the Musolf, et al. framework. At high momentum transfer, the situation is not so clear. The choice of single pion production violates the canonical assumptions about the deep-inelastic scattering regime since the present measurement has $W = 1.1 - 1.2$ GeV rather than $W > 2$ GeV. However, even in the resonance region, there is an 'average' scaling closely related to the Bjorken scaling of weakly interacting quarks at large W and Q^2. This 'local duality' picture was first noted by Bloom and Gilman [Bl70, Bl71] and placed on a QCD footing by Georgi and Politzer [Ge76] and De Rújula, Georgi and Politzer [De77]. Recently published measurements [Bo94] suggest that the inclusive structure functions integrated from threshold over the $\Delta(1232)$ peak begin to scale at values of Q^2 between 8 and 10 GeV^2. It is therefore important to go as high in Q^2 as possible to approach the regime where quarks interact weakly.

An energy-doubled CEBAF can provide this capability. It would appear that with such a facility experiments may be feasible out to about $Q^2 = 5$ GeV^2 (see Section 3). Modeling the response at high Q^2 requires further consideration.

2 Formalism

For inelastic scattering, the explicit separation of the flavor dependent currents which is possible in the elastic case, is not, in general, possible because the transition currents are complex. The general form of the asymmetry for inclusive inelastic scattering may be written as [Do86, Mu94a]

$$A = a\left(A^{SM} + A^0 + A^A\right) \tag{4}$$

where

$$a = -\frac{G_\mu Q^2}{\alpha\pi\sqrt{2}}, \tag{5}$$

$$A^{SM} = \frac{1}{2} - \sin^2\theta_W, \tag{6}$$

$$A^0 = \frac{1}{4}\frac{v_L r_V^{L0} + v_T r_V^{T0}}{v_L R^L + v_T R^T}, \text{ and} \tag{7}$$

$$A^A = \left(1 - 4\sin^2\theta_W\right)\frac{v_T' r_A^{T'}}{v_L R^L + v_T R^T}. \tag{8}$$

There are a number of points to note about the asymmetry. The asymmetry has an overall factor of Q^2 offsetting, to some extent, cross sections which are falling with Q^2. There is a Standard Model term, A^{SM} which depends only on $\sin^2\theta_W$. The remaining two terms in the asymmetry are the flavor singlet A^0 (see [Ka88]), and the (target) axial vector A^A. These terms contain the product of electromagnetic and neutral weak current transition matrix elements in the reduced response functions r_I^J (see below). The v's are the usual kinematic factors [Do86] and the denominators of A^0 and A^A are proportional to the unpolarized cross section. The term A^A is suppressed by the accidental cancellation in $\left(1 - 4\sin^2\theta_W\right)$. We note the usual result that in the absence of flavor singlet and target axial vector contributions, the asymmetry depends only on the Standard Model.

The reduced response functions are labeled as follows. Subscripts denote the type of target neutral weak current – either vector (V) or axial vector (A). The superscripts denote the relevant photon polarization components (either longitudinal, L, transverse, T or 'transverse prime', T') and the flavor singlet structure functions have an additional 0 superscript as a reminder. The structure of the longitudinal response function is simplest

$$r_V^{L0} = \left\langle J_0^0\right\rangle^* \left\langle J_0^\gamma\right\rangle. \tag{9}$$

Here J_0^0 is the flavor singlet (equal weightings for u, d and s quarks) transition charge density and J_0^γ is the ordinary electromagnetic transition charge density. The longitudinal response is simple, because, if it could be separated experimentally, the ratio to the ordinary longitudinal response is

$$\begin{aligned} \frac{r_V^{L0}}{R^L} &= \frac{\langle J_0^0 \rangle^* \langle J_0^\gamma \rangle}{\langle J_0^\gamma \rangle^* \langle J_0^\gamma \rangle} \\ &= \frac{\langle J_0^0 \rangle^*}{\langle J_0^\gamma \rangle^*} \end{aligned} \tag{10}$$

which is real. Thus the relative magnitudes of the singlet and electromagnetic currents could be determined – no phase enters in this case. This is to be compared with the case of pion production from p and n where a relative phase is required to determine this ratio (with the further assumption that only u and d contribute).

The transverse responses are not as simple. For example,

$$r_V^{T0} = \left\langle J_+^0 \right\rangle^* \left\langle J_+^\gamma \right\rangle + \left\langle J_-^0 \right\rangle^* \left\langle J_-^\gamma \right\rangle \tag{11}$$

where, for comparison, the electromagnetic transverse response is

$$R^T = \left\langle J_+^\gamma \right\rangle^* \left\langle J_+^\gamma \right\rangle + \left\langle J_-^\gamma \right\rangle^* \left\langle J_-^\gamma \right\rangle. \tag{12}$$

In comparison to the case of the transition charge responses, the ratio of the transverse responses is more complicated.

At low momentum transfers it should be straightforward to calculate the asymmetry for inclusive single pion electroproduction using the same framework as in the consideration of MEC [Mu94, Mu93]. In the high Q^2 limit, a simple guess as to the approximate magnitude of the flavor singlet term can be made as follows. It is observed that as x nears 1, the ratio $d(x)/u(x)$ tends to zero [Cl79]. This is the well known statement that if a quark carries all the momentum of a proton in the infinite momentum frame, it will be a u quark. The region where x is near 1 is precisely the region of the single pion electroproduction. Assuming that the transverse responses dominate, that the + and − components of the currents are equal and neglecting the phases, the ratio of the reduced electroweak and electromagnetic structure functions is given by (u) quark electromagnetic charges and SU(3) factors (for the flavor singlet current)

$$A^0 \cong \frac{1}{4}\frac{r_V^{T0}}{R^T} \sim \frac{1}{4}\frac{\frac{1}{3}\cdot\frac{2}{3}+\frac{1}{3}\cdot\frac{2}{3}}{\frac{2}{3}\cdot\frac{2}{3}+\frac{2}{3}\cdot\frac{2}{3}} \tag{13}$$

$$= \frac{1}{4}\cdot\frac{1}{2} \tag{14}$$

This is to be compared to A^{SM} which is approximately 1/4; therefore, the flavor singlet piece could change the asymmetry by the order of 50% in the high momentum transfer limit (neglecting the contribution of the axial vector term because of the prefactor).

Table 1: Uncertainties expected for set of single pion electroproduction asymmetries based on a one month running time.

E_{inc} (GeV)	Q^2 (GeV^2)	A	$\Delta A/A$ (%)
1.0	0.09	7.73×10^{-6}	7.4
4.0	1.44	1.29×10^{-4}	4.4
8.0	4.93	4.43×10^{-4}	15.0

3 Experiment

A very rough estimate was made of the uncertainties that might be expected in a set of experiments that could be performed at an energy-doubled CEBAF facility. The cross section parameterization of Brasse, et al. [Br76] was used to determine the average cross section for a range of final electron energies of 100 MeV centered at $W = 1.15$ GeV. A large acceptance spectrometer with a 100 msr solid angle acceptance centered at a scattering angle of 20° is assumed. The luminosity was taken to correspond to a 40 μA beam on a 20 cm long LH_2 target giving $\mathcal{L} = 2 \times 10^{38}$ cm^{-2}s^{-1}. A nominal beam polarization of 50% was also assumed.

The resulting uncertainties are shown in Table 1 for a running time of one month per point. The value of the asymmetry is $A = a \cdot A^{SM}$ (i.e. assuming A^0 and A^A are zero). Even at the highest momentum transfer a reasonable measurement is possible given the possible size of the effects estimated above.

4 Summary

A measurement of the parity-violating asymmetries in inclusive single pion electroproduction is proposed. The goal of the measurement is to learn about the flavor dependence of meson production effectively by comparing the electroweak interference structure functions to the corresponding electromagnetic ones. It might be expected that the process will proceed from being independent of the flavor of the quark 'struck' by the photon at low Q^2 to being dominated by a single flavor at high momentum transfers. Such measurements would also inform the calculations of meson exchange current effects on parity-violation experiments with nuclear targets. A simple estimate suggests that changes from the Standard Model asymmetry are on the order of 50% at high momentum transfer. Estimates of the exper-

imental uncertainties possible with an energy-doubled CEBAF facility are roughly 15% at the same momentum transfer.

This work is supported in part by NSF grants PHY93-10871 and PHY92-57057 (NSF Young Investigator).

References

[Bl70] E. D. Bloom and F. J. Gilman, Phys. Rev. Lett. **25** (1970) 1140.

[Bl71] E. D. Bloom and F. J. Gilman, Phys. Rev. D **4** (1971) 2901.

[Bo94] P. Bosted, et al. Phys. Rev. D **49** (1994) 3091.

[Br76] F. W. Brasse, et al. Nucl. Phys. **B110** (1976) 413.

[Cl79] F. E. Close, *Quarks and Partons*, Academic Press (London) 1979.

[De77] A. De Rújula, H. Georgi and H. D. Politzer, Ann. Phys. **103** (1977) 315.

[Do86] T. W. Donnelly and A. S. Raskin, Ann. Phys. **169** (1986) 247.

[Ge76] H. Georgi and H. D. Politzer, Phys. Rev. D **14** (1976) 1829.

[Ka88] D. Kaplan and A. Manohar, Nucl. Phys. **B310** (1988) 527.

[Mu94] M. J. Musolf, R. Schiavilla and T. W. Donnelly, preprint CEBAF- TH-94-10, April 1994.

[Mu94a] M. J. Musolf, et al. Phys. Rep. **239** (1994) 1; and references therein.

[Mu93] M. J. Musolf and T. W. Donnelly, Phys. Lett. **B318** (1993) 263.

Diffractive electroproduction of $s\bar{s}$ mesons off nuclei at CEBAF energies

O.Benhar[1], S. Fantoni[2], N.N.Nikolaev[3,4] and B.G.Zakharov[3]

[1]*INFN Sezione Sanità. Physics Laboratory, Istituto Superiore di Sanità. Viale Regina Elena, 299. I-00161 Roma, Italy*
[2]*Interdisciplinary Laboratory, SISSA, and INFN, Sezione di Trieste. Via Beirut, 4. I-34014 Trieste, Italy*
[3]*L.D.Landau Institute for Theoretical Physics, GSP-1, 117940. Ul. Kosygina 2, V-334 Moscow, Russian Federation*
[4]*IKP (Theorie), KFA Jülich. D-52425 Jülich, Germany*

Abstract

We discuss diffractive incoherent electroproduction of $s\bar{s}$ mesons off nuclear targets at beam energies that are expected to be available at CEBAF (5-8 GeV). The Q^2 and target mass dependence of the ϕ and ϕ' transparency ratios has been studied within a theoretical approach in which the propagation of the $s\bar{s}$ pair trhough the nuclear medium is described in terms of the quantum mechanical evolution operator. We predict a complex pattern of nuclear effects, whose experimental study may provide information on several issues relevant to the understanding of QCD, both in the perturbative and nonperturbative regimes.

Introduction

The subject of nuclear effects in the diffractive photo- and leptoproduction of vector mesons off nuclear targets has recently attracted much attention [1, 2, 3, 4, 5]. In these processes a fluctuation of the (real or virtual) photon gives rise to a $q\bar{q}$ pair that travels through nuclear matter evolving to develop the vector meson detected in the final state.

The study of these reactions provides information on the structure of the hadrons and their interaction with the hadronic medium, thus sheding light on many important issues of QCD, both in the perturbative regime, relevant to the production of the pointlike $q\bar{q}$ state, and in the nonperturbative one, corresponding to the formation of the observed vector meson. Of particular relevance is the possibility of extracting clearcut evidence and reaching a quantitative assessment of the much debated issue of colour transparency (CT) (for recent reviews on CT see refs. [6, 7]).

The crucial requirement for CT to set in is that the reaction amplitude be dominated by contributions from $q\bar{q}$ pairs with small transverse size r_S, with [4, 5]

$$r_S = \frac{6}{\sqrt{Q^2 + m_V^2}}. \tag{1}$$

Eq.(1) clerly show that increasing Q^2 r_S decreases, implying weaker nuclear attenuation. A signal of the onset of CT, i.e. vanishing attenuation, in the diffractive leptoproduction of ρ mesons has been recently provided by the Q^2 dependence of the data from the FNAL E665 experiment [5, 8]

The $c\bar{c}$ and $s\bar{s}$ systems have the obvoius advantage, with respect to the light vector mesons, that the heavier masses of the strange and charm quarks make the theoretical description of both the initial and final states easier and more reliable. The coherent and incoherent production of $c\bar{c}$ mesons, J/ψ and ψ' , has been recently discussed [2, 3] within a fully consistent quantum mechanical approach, originally proposed in ref. [2]. The results, in good agreement with the J/ψ production data taken by the New Muon Collaboration (NMC) at CERN [9] and the E691 experiment at FNAL [10], indicate that CT produces a complex pattern of nuclear effects, contraddicting the naive expectation, based on the use of semiclassical approximations, that in the incoherent processes nuclear shadowing vanishes at high energy.

It has to be pointed out, however, that the kinematical regions covered

by both the NMC and E691 correspond to very high energies of the produced J/ψ in the lab frame, implying that, due to the Lorentz time dilation, the final state vector meson is formed way beyond the target. Studying the energy and target mass dependences in a different kinematical regime, corresponding to much shorter formation times, would provide important complementary information. Thanks to the beam energies and luminosity expected to be available and to the lighter mass of the strange quark, CEBAF will provide the ideal experimental conditions to study this kinematical domain measuring the electroproduction of $s\bar{s}$ mesons. More specifically, CEBAF energies will make it possible to study how intranuclear attenuation affects the evolution of the $s\bar{s}$ system from the small size of eq. (1) to the hadronic size of the ϕ and ϕ' mesons.

Space-time picture of diffractive vector meson electroproduction

We will focus on the process:

$$e + A \rightarrow e' + A^* + V, \tag{2}$$

where V denotes any $s\bar{s}$ vector meson (ϕ , ϕ' ...). Since we are interested in incoherent production, we will only consider processes in which the target nucleus makes a transition to an excited state. In addition, we require the elementary production process to be elastic:

$$\gamma^* + N \rightarrow N + V, \tag{3}$$

where γ^* is the exchanged virtual photon transferring energy ν and momentum $q = (Q^2 + \nu^2)^{(1/2)}$ to the target. As a consequence, we will restrict ourselves to the kinematical domain corresponding to $z = E_V/\nu = 1$, E_V being the energy of the produced vector meson in the lab frame.

As firstly pointed out in ref. [1], the process defined in eqs. (2) and (3) is characterized, in the lab frame, by two different length scales: the coherence length, i.e. the lifetime of the $s\bar{s}$ fluctuation of the virtual photon before an interaction with the target is required, defined as:

$$l_c = \frac{2\nu}{Q^2 + (2m_s)^2}, \tag{4}$$

and the time needed to develop the detected vector meson after the interaction has occurred, called formation time:

$$l_f = \frac{\nu}{2m_s \Delta E}. \tag{5}$$

In eq.(5), ΔE is a typical level splitting in the spectrum of the $s\bar{s}$ system. Taking $\Delta E = m_{\phi'} - m_{\phi}$ one gets $l_f \sim 0.3\nu$ (fm/GeV), showing that CEBAF energies correspond to $l_f \lesssim R_A$, R_A being the target radius, i.e. to the regime in which most of the evolution and the spatial expansion of the $s\bar{s}$ pair takes place within the target.

Calculation of the transparency ratio

The transparency ratio is defined as:

$$T_A(V) = \frac{1}{A}\frac{d\sigma(e + A \to e' + A^* + V)}{d\sigma(e + N \to e' + N + V)} = \frac{1}{A}\frac{\int d^3r \rho_A(\mathbf{r}) |\langle V|U|i\rangle|^2}{|\langle V|U|i\rangle|^2}. \tag{6}$$

Besides the target density ρ_A, the ingredients entering eq.(6) are:

- the initial state $|i\rangle = \sigma|\gamma\rangle$, where $|\gamma\rangle$ denotes the $s\bar{s}$ component of the virtual photon, whose calculation within perturbative QCD is discussed in ref. [11], and σ is the cross section describing the interaction between the $s\bar{s}$ pair and the target nucleons. In our calculations we have used σ resulting from the two-gluon approximation, as described in ref. [2]. As a function of the $s\bar{s}$ separation in the impact parameter plane, ρ, the cross section is characterized by a ρ^2 dependence at small ρ, responsible for the occurrence of CT, followed by a saturating behaviour at larger distances.

- the evolution operator U describes the evolution of the $s\bar{s}$ pair travelling through nuclear matter. It takes into account both the internal dynamics of the $s\bar{s}$ pair and its interaction with the medium. Assuming that the internal motion can be described by the harmonic oscillator model and neglecting the deviation of $\sigma(\rho)$ from the ρ^2 behaviour, U can be written in closed form [2]. The effect of the inclusion of the correct large ρ dependence of σ can then be estimated using standard perturbation theory [12].

- the final state $|V\rangle$, describing the observed vector meson. In the calculations we have used nonrelativistic harmonic oscillator wave functions.

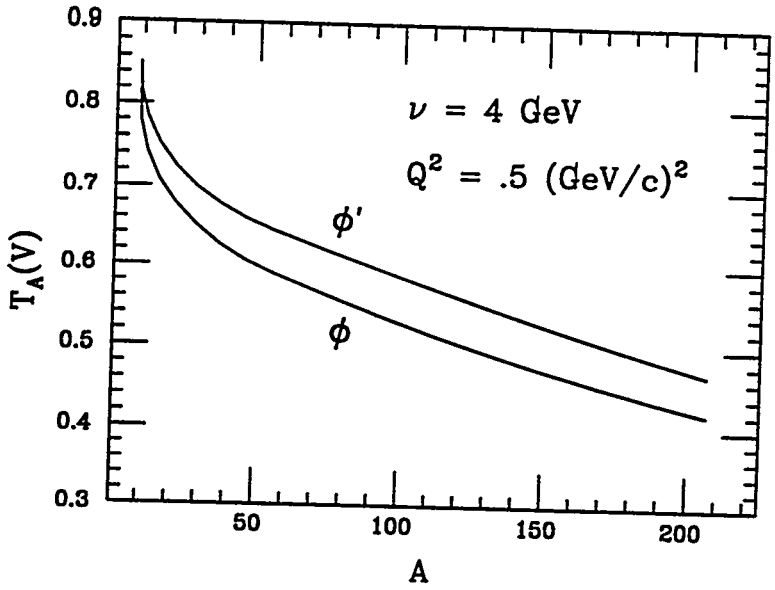


Figure 1: Target mass dependence of the transparency ratio at $\nu = 4\ GeV$ and $Q^2 = .5(GeV/c)^2$ for the ϕ and ϕ' mesons.

The target mass dependence of the transparency ratio at $\nu = 4\ GeV$ and $Q^2 = .5\ (GeV/c)^2$ is illustrated in fig. 1 for both the ϕ and the ϕ' mesons. The most striking feature of the results is the fact that, in spite of its larger size, the ϕ' is consistently less absorbed than the ϕ . This effect, which has been also predicted to occur for the $c\bar{c}$ mesons J/ψ and ψ' [2, 3], as well as for the light mesons ρ and ρ' [4, 5], has to be ascribed to the presence of a node in the wave function of the radial excitations ϕ' , ψ' and ρ' , leading to a suppression of nuclear shadowing or even to antishadowing , i.e. to $T_A(\phi') > 1$, as shown in fig. 2. At small Q^2 ($Q^2 \lesssim m_\phi^2$) the scanning radius r_S, defined in eq.(1), is close to the position of the node in the ϕ' wave function. This leads to strong cancellations in the ϕ' production amplituide, whose dependence upon r_S is very strong. As a consequence, the nuclear transparency $T_A(\phi')$ exhibits a very steep Q^2 behaviour, changing from antishadowing to shadowing over a rather narrow range of Q^2 which can be spanned at CEBAF. On the other hand, the predicted Q^2 dependence of the nuclear transparency

for ϕ production is rather weak, due to the absence of nodes in the ϕ wave function.

Experimental evidence of "anomalous" nuclear effects for a radial excitation has been recently provided by the FNAL E772 experiment [13]. The E772 data for J/ψ and ψ' production in proton-nucleus collisions at 800 GeV show that the two mesons have strong and identical nuclear attenuation.

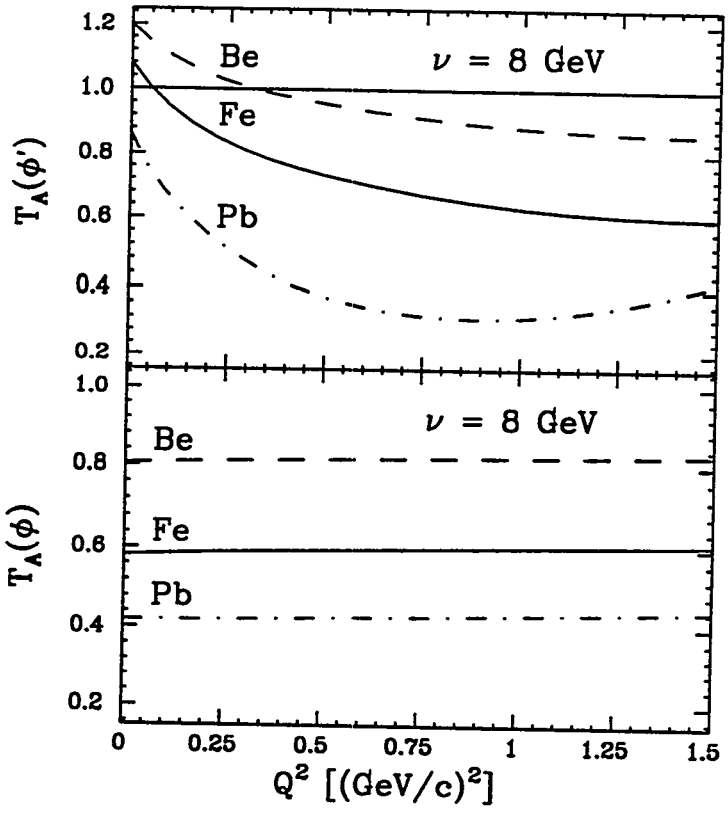


Figure 2: Q^2 dependence of the transparency ratio at $\nu = 8$ GeV for the ϕ (lower figure) and ϕ' (upper figure) mesons and for three different targets.

Conclusions

The results presented in this paper show that diffractive electroproduction

of $s\bar{s}$ mesons off nuclei at CEBAF energies provides a wealth of information on the structure and the interaction of hadronic systems, linking the perturbative and nonperturbative regimes. The high luminosity and the capability of full reconstruction of the final state foreseen for the CLAS will allow for a thorough investigation of the nuclear effects predicted by the theoretical calculations, including the Q^2, ν and A dependences of the transparency ratios. Particular enphasis should be put on the measurement of the ϕ' yield. There is no experimental information available on the leptoproduction of radial excitations off nuclear targets, and a measurement of the ϕ' at CEBAF would represent the first clearcut test of the suppression of nuclear shadowing, or even antishadowing, predicted by the theoretical calculations.

Acknowledgements

O.B. and B.G.Z. wish to gratefully acknowledge the warm hospitality of the Interdisciplinary Laboratory of the International School for Advanced Studies, in Trieste, where part of the work described in this paper has been carried out.

References

[1] S.J. Brodsky and A.H. Mueller, Phys. Lett. **B 206**(1988)685.

[2] B.Z. Kopeliovich and B.G. Zakharov, Phys. Rev. D 44(1991)3466.

[3] O. Benhar, B.Z. Kopeliovich, C. Mariotti, N.N. Nikolaev and B.G. Zakharov, Phys. Rev. Lett. **69**(1992)1156.

[4] B.Z. Kopeliovich, J. Nemchick, N.N. Nikolaev and B.G. Zakharov, Phys. Lett. **B 309**(1993)179.

[5] B.Z. Kopeliovich, J. Nemchick, N.N. Nikolaev and B.G. Zakharov, Phys. Lett. **B 324**(1994)469.

[6] N.N. Nikolaev, Comments Nucl. Part. Phys. **21**(1992)41.

[7] L. Frankfurt, G.A. Miller and M. Strikman, Comments Nucl. Part. Phys. **21**(1992)1.

[8] G.Y. Fang *et al*, talk delivered at the PANIC 93 (Perugia, Italy, July 1993). Preprint FERMILAB-Conf-93/385 (1993).

[9] New Muon Collaboration, C. Mariotti, in Proceedings of the Joint International Lepton-Photon Symposium and Europhysics Conference on High Energy Physics, Vol. 1. Eds. S. Hegarty, K. Pottr and E. Quercigh (World Scientific, Singapore, 1991)p.154.

[10] M.D. Sokoloff *et al*, Phys. Rev. Lett. **57**(1986)3003.

[11] N.N. Nikolaev and B.G. Zakharov, Z. Phys. C **49**(1991)607, **53**(1992)331.

[12] O. Benhar, S. Fantoni, N.N. Nikolaev and B.G. Zakharov, to be published (1994).

[13] D.M. Alde *et al*, Phys. Rev. Lett. **66**(1991)133.

Medium Modifications with Recoil Polarization

J.F.J. van den Brand

Nationaal Instituut voor Kernfysica en Hoge Energiefysica
1009 DB Amsterdam, The Netherlands

R. Ent

CEBAF, Newport News, VA 23606

Abstract: We show that the virtual Compton scattering process allows for a precise study of the off-shell electron-nucleon vertex. In a separable model, we show the sensitivity to new unconstrained structure functions of the nucleon, beyond the usual Dirac and Pauli form factors. In addition, we show the sensitivity to bound nucleon form factors using the reaction ^{4}He$(\vec{e}, e'\vec{p})^3$H.

A nucleon embedded in a nucleus represents a complex system. Firstly, the bound nucleon is necessarily off-shell and in principle a complete understanding of the dynamical structure of the nucleon is required in order to calculate its off-shell electromagnetic interaction.[1] Secondly, one faces the possibility of genuine medium effects, such as for example quark-exchange contributions.[2,3] Furthermore, the electromagnetic coupling to the bound nucleon is dependent on the nuclear dynamics[4] through the self-energy of the nucleon in the nuclear medium.

In the last decade, many experiments have been performed in kinematic regimes where electron scattering from a bound nucleon is expected to be the dominant process. Large discrepancies are observed[5–7] when this data is analyzed using current operators based on the *free* nucleon observables. At the moment a precise explanation of the observations is not available.

Here, we argue that one should first understand the treatment of the full off-shell electromagnetic vertex of a single nucleon, before considering any interpretation of a bound nucleon. Virtual-Compton (VC) scattering from the proton offers the possibility to study the off-shell coupling without the obscurance due to nuclear-structure or strong interaction effects in the final state. As a following step polarization transfer experiments are an excellent tool in order to investigate the coupling of the virtual photon to a bound nucleon in more detail. Measurements of the D_{ll} and D_{lt} polarization transfer coefficients are sensitive probes of the bound nucleon form factors with minimal effects due to FSI and MEC. In addition, the influence of these reaction mechanism effects can be measured separately through a measurement of the induced asymmetry p_y^0.

Virtual-Compton Scattering

The general expression for scattering off a nucleon with both initial and final nuclear momenta off-shell was first given by Bincer.[8]

In case that only the final nucleon is taken off-shell, the general form can be reduced to a description in terms of four form factors $F_i^{\rho' \rho}(q^2, M^2, W^2)$, dependent on two scalars ($Q^2 = -q^2$ and W^2).[1] For the on-shell matrix element one can show the equivalence of $F_1^{++}(Q^2, M^2, M^2)$ and $F_2^{++}(Q^2, M^2, M^2)$ to the Dirac and Pauli form factors $F_1(Q^2)$ and $F_2(Q^2)$, respectively. In general the off-shell interaction cannot be extrapolated from the on-shell case and a dynamical model of the nucleon is required in order to calculate $F_1^{+\pm}(Q^2, M^2, W^2)$ and $F_2^{+\pm}(Q^2, M^2, W^2)$.

It is possible to study the half off-shell electron-nucleon vertex by using two-step reactions, such as Compton scattering or photopion production. Fig. 1 shows the lowest-order Feynman diagrams for the virtual Compton scattering reaction $eN \rightarrow eN\gamma$. The first two diagrams can be calculated to high precision using QED and are termed Bethe-Heitler contributions. The other two diagrams (termed VC contributions) can only be unambiguously calculated in the soft-photon limit, where the cross section is independent of nucleon-structure ambiguities. In general they involve a sum over all possible intermediate hadronic states. The calculation of the VC contribution requires either solving QCD or a realistic nucleon model to describe the dynamical behavior. This reaction is a sensitive probe of the nucleon wave function since both $F_1^{\pm}(Q^2, M^2, W^2)$ and $F_2^{\pm}(Q^2, M^2, W^2)$ contribute to the cross section. It may be possible to obtain phase information on the off-shell nucleon matrix elements due to the interference of the Bethe-Heitler and VC contributions.

In order to maximize the strong interaction effects in the reaction $eN \rightarrow eN\gamma$ one has to choose sufficiently large photon energies E_γ to invalidate the soft-photon approximation and select photon emission angles where radiation from the proton is dominant. An example of this is real Compton scattering where the leading corrections allow one to measure nuclear polarizabilities. The reaction allows mapping the observables versus Q^2 and the invariant mass of the intermediate hadronic state, given by

$$W^2 = M^2 + 2E_\gamma(E_p - p_z^f) \tag{1}$$

where p_z^f is the component of the outgoing proton momentum along the photon direction. Note that $W^2 > M^2$, so as E_γ increases the role of the Delta resonance becomes increasingly important.

Experimentally, the reaction $eN \rightarrow eN\gamma$ can be best approached by detecting a scattered electron in coincidence with a proton using high-resolution magnetic spectrometers,

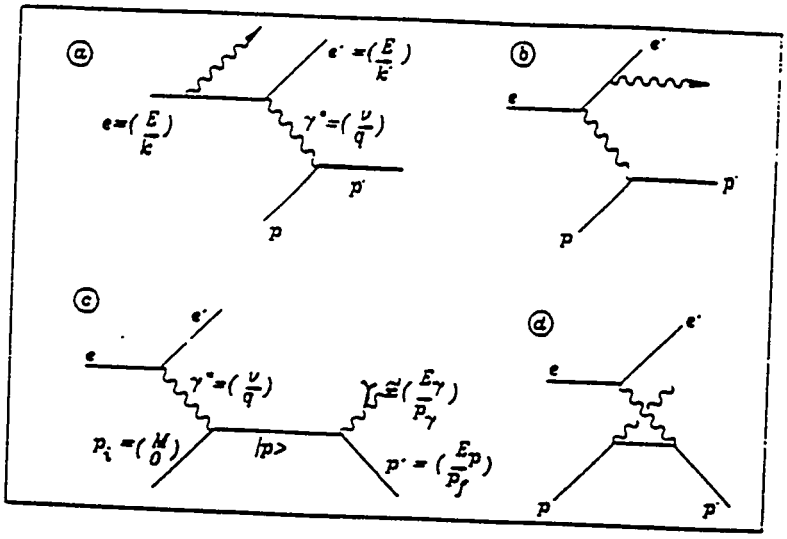


Figure 1. *Bethe-Heitler (a,b) and Virtual-Compton (c,d) contributions to the reaction* $e \rightarrow eN\gamma$.

xample available in Hall A at CEBAF. The measurement is complicated due to the fact an abundance of photons will be radiated by the incoming and scattered electrons.

To gain insight in the sensitivity of the VC scattering process to the nucleon structure, we extended the formalism by Mo and Tsai[9] to coincidence (e,e'p) reactions.[10] The treatment of order e^4 contributions to the virtual-photon correction involving the strong interaction is similar to that of Mo and Tsai. The formalism includes the complete half off-shell coupling allowing for a study of the dependence on various models of the nucleon. The model contains the approximation of separability which allows for only nucleon ediate states.

We have applied our model to the measurement of the reaction $ep \rightarrow ep\gamma$ at high y. Fig. 2 shows the probability, $P(\Theta_\gamma, E_\gamma)$, for photon emission for a kinematics with ') = 8.00 (6.65) GeV and $Q^2 = 2.52$ (GeV/c)^2 and for E_γ of 100 MeV. The radiated s section is defined as

$$\frac{d\sigma}{d\Omega_{e'} dE_\gamma d\Theta_\gamma} = \frac{d\sigma^{(ep)}}{d\Omega_{e'}} \frac{1}{E_\gamma} P(\Theta_\gamma, E_\gamma) \qquad (2)$$

where $\sigma^{(ep)}$ indicates the electron-proton cross section without any radiation. In addition, the predictions for the polarization transfer coefficients are shown. The dotted curve in Fig. 2 shows the result in the soft-photon limit, while the solid curve assumes F_2^{+-} equal to F_2^{++} (and F_1^{+-} equal to F_1^{++}). The other curves assume a W and Q^2 dependence estimated from the predictions of the one-pion loop model of Ref. 1, and only differ in the relative normalization of $F_2^{+-}(Q^2 = 0)$ to $F_2^{++}(Q^2 = 0)$. The dashed curve assumes a relative

normalization of $\approx \frac{M}{m_\pi}$ as given by Ref. 1, whereas the dotdashed curve assumes a relative normalization of $\approx \frac{2M}{m_\pi}$ as derived from dispersion relations.[11] The figure shows that in this kinematic region one is sensitive to the unconstrained form factors F_2^{+-} which measure the anomalous magnetic moment of an off-shell proton. The results clearly indicate the sensitivity to the nucleon model used in the calculations.

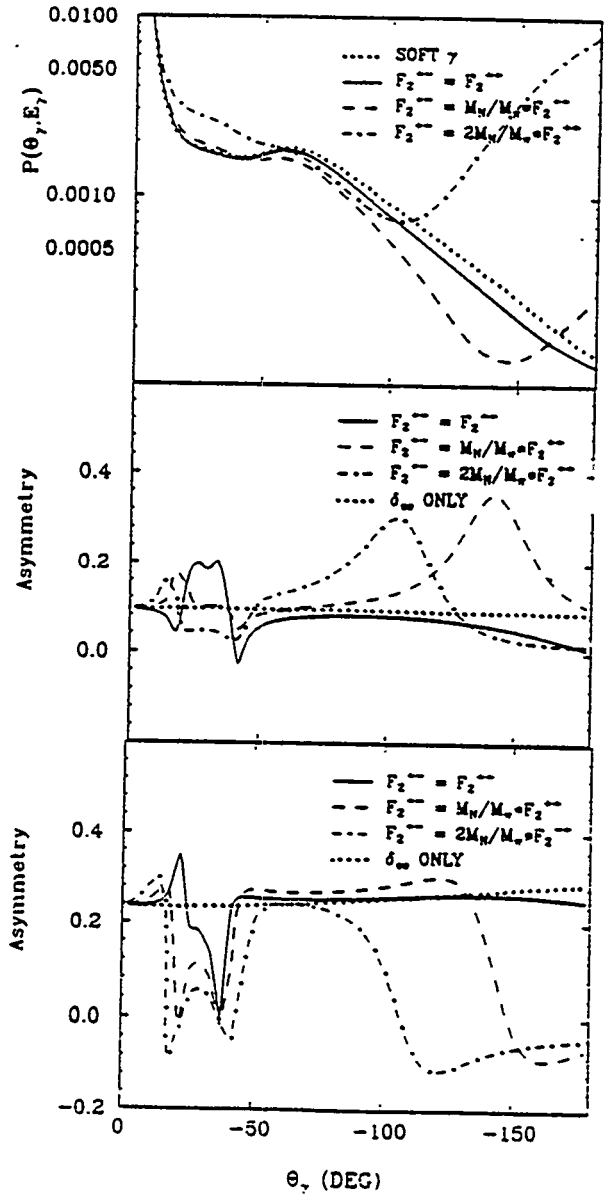


Figure 2. *Probability distribution (top) for the emission of photons of 100 MeV energy in the reaction $^1H(e,e'p)$, and angular distribution for the polarization transfer coefficients (middle: D_{lt}, bottom: D_{ll}). The various lines denote different nucleon models, as described in the text. A beam energy of 8.0 GeV and an electron scattering of 12.5° have been assumed.*

Polarization Transfer in the Reaction $^4He(\vec{e},e'\vec{p})^3H$

In exclusive (e,e'p) experiments on ^{4}He, ^{6}Li, ^{12}C and ^{40}Ca an anomalous ratio of transverse and longitudinal response functions has been observed.[12–15] Deviations from the value for a free proton have been interpreted as a signature of the modification of the virtual-photon proton coupling in a dense many-body quantum system. It has been argued that before considering such explanations one must be extremely cautious with the treatment of reaction-mechanism effects. It is well known that one has to incorporate correction factors associated with final-state interaction (FSI) and meson-exchange currents (MEC) effects for a complete description of the spin-averaged (e,e'p) cross section. Especially the spin-orbit field may be responsible for the relative enhancement of the transverse part of the cross section.[16,17] Apparently, the effects of a possible medium modification of the virtual photon-proton coupling are so intertwined with reaction mechanism effects as FSI and MEC, that the recently performed (e,e'p) studies do not permit a clear interpretation.

The ^{4}He atomic nucleus is an ideal candidate for a more detailed study of the anomalous ratio found. If the electromagnetic properties of the proton change when it is embedded in the nuclear medium, then significant effects, if any, may be expected for this nucleus due to its high density. The signature of these effects is expected to become experimentally observable, because advanced microscopic calculations, including FSI and MEC effects, have become possible for the ^{4}He(e,e'p)^{3}H reaction.[18]

Recent experiments have been performed at Saclay to separate the structure functions for the (e,e'p) reaction on the few-body nuclei.[15,19] Whereas the ratio of longitudinal to transverse structure functions at high momentum transfer seems to be understood for the ^{2}H(e,e'p) and ^{3}He(e,e'p) reactions, a significant discrepancy remains for the ^{4}He(e,e'p) reaction, even after correcting the data for FSI and MEC effects.

In Fig. 3 the predicted polarization-transfer coefficients ($p'_x = \mathrm{h}D_{lt}$, $p'_z = \mathrm{h}D_{ll}$, with h the electron beam helicity) are shown versus missing momentum for the ^{4}He$(\vec{e},e'\vec{p})^3$H reaction. Also the normal component, p^0_y, is shown, which is helicity independent and should vanish in PWIA. The microscopic calculation, performed by Laget,[20] uses a correlated bound-state wave function for the four-body system[21] obtained with the variational Monte-Carlo (VMC) method. For the current operator its non-relativistic reduction including terms of order $1/M_p^3$ is used. It is seen that for p'_x and p'_z the deviations from PWIA due to charge-exchange, FSI and MEC effects are negligible for missing momenta below 300 MeV/c. The component p^0_y for this kinematical setting increases with increasing missing momenta. The results of the calculation suggest that a measurement of the spin vector of the ejected proton yields information on the form factors of the bound proton.

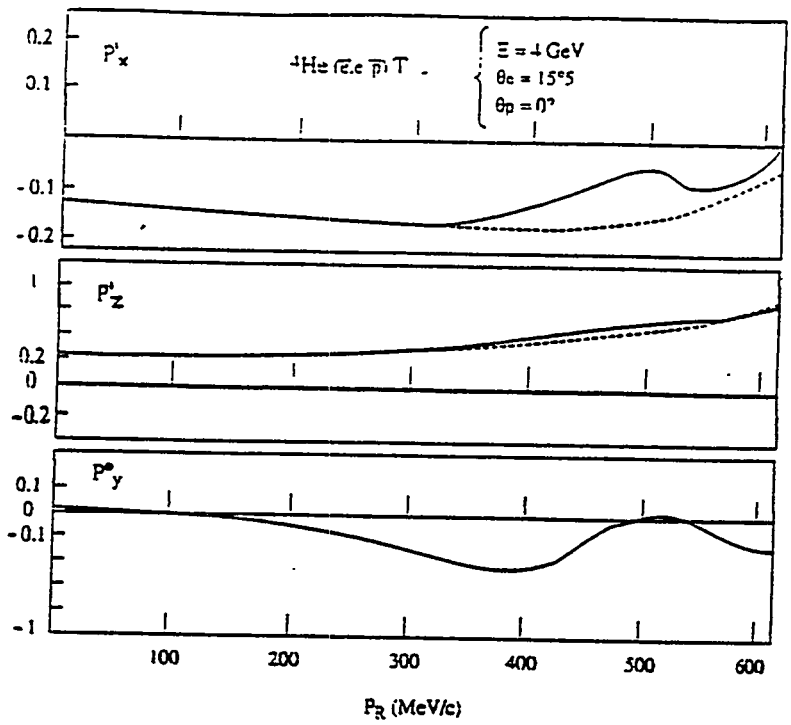


Figure 3. *The spin-transfer polarization p'_x, p'_z, and p^0_y of the reaction $^4He(\vec{e}, e'\vec{p})^3H$ calculated by Laget.[20] The dashed curve is the PWIA prediction, and the solid curve represents the results of the calculation including FSI and MEC effects.*

As shown in the figure the method is expected to be extremely insensitive to FSI and MEC effects. A higher energy beam energy at CEBAF would enable a gain in statistical precision of almost a factor of ten for measurements up to momentum transfers squared of 4 $(GeV/c)^2$, and would enable extension of these measurements up to about 7 $(GeV/c)^2$.

Summary

In summary, a measurement of the virtual Compton scattering cross section in the reaction $eN \rightarrow eN\gamma$ allows for a clean test of nucleon models. We have shown that this process will have sensitivity to new structure functions, beyond $F_1(Q^2)$ and $F_2(Q^2)$, which are required for a correct description of the off-shell vertex. Thus the ^{1}H(e,e'p)γ reaction may allow for a measurement of the off-shell behavior, free from obscurance due to nuclear-structure, final-state interaction and meson-exchange currents effects. Such measurements are crucial as a first step for our understanding of the electromagnetic interaction of a bound nucleon. Subsequently we discussed the sensitivity of measurements using the reaction $^4He(\vec{e}, e'\vec{p})^3H$ to the bound nucleon.

References

1. H.W.L. Naus and J.H. Koch, Phys. Rev. **C36**, 2459 (1987); Phys. Rev. **D44**, 3445 (1991).
2. L.Ya. Glozman, V.G. Neudatchin, I.T. Obukhovsky, and A.A. Sakharuk, Phys. Lett. **B252**, 23 (1990); Sov. J. Nucl. Phys. **55**, 1491 (1992).
3. P.J. Mulders, and A.E.L. Dieperink, Nucl. Phys. **A483**, 621 (1988).
4. W. Bentz *et al.*, Nucl. Phys. **A436**, 593 (1985).
5. P.J. Mulders in the Book *Modern Topics in Electron Scattering*, Eds. B. Frois and I. Sick, World Scientific (1991).
6. W. Bertozzi, R.W. Lourie, and E.J. Moniz in the Book *Modern Topics in Electron Scattering*, Eds. B. Frois and I. Sick, World Scientific (1991).
7. EMC Collaboration, J.J. Aubert *et al.*, Phys. Lett. **B123**, 275 (1983).
8. A.M. Bincer, Phys. Rev. **118**, 855 (1960).
9. L.W. Mo and Y-S. Tsai, Rev. Mod. Phys. **41**, 205 (1969).
10. D. Wasson, R. Ent, N. Makins, and R. Milner, to be published.
11. E.M. Nyman, Phys. Rev. **170**, 1628 (1970); Nucl. Phys. **A160**, 517 (1971).
12. G. van der Steenhoven *et al.*, Phys. Rev. Lett. **57**, 182 (1986); **58**, 1727 (1987).
13. D. Reffay-Pikeroen *et al.*, Phys. Rev. Lett. **60**, 776 (1988).
14. P.E. Ulmer *et al.*, Phys. Rev. Lett. **59**, 2259 (1987).
15. A. Magnon *et al.*, Phys. Lett. **222B**, 352 (1989).
16. T. Suzuki, Phys. Rev. C **37**, 549 (1988).
17. M. Kohno, Phys. Rev. C **38**, 584 (1988).
18. J.M. Laget, Nucl. Phys. **A497**, 391c (1989).
19. J.E. Ducret *et al.*, Nucl. Phys. **A553**, 697c (1993).
20. J.M. Laget, private communications.
21. R. Schiavilla *et al.*, Nucl. Phys. **A449**, 219 (1986).

SIGNATURES FOR QUARK CLUSTERING IN NUCLEI*

Carl E. Carlson[a] and K. E. Lassila[b]

[a]*Physics Department, College of William and Mary, Williamsburg, VA 23187*
[b]*Physics Department, Iowa State University, Ames, IA 50011*

ABSTRACT

As a signature for the presence of quark clusters in nuclei, we suggest sutudying backward protons produced by electron scattering off deuterons and suggest a ratio that cancels out much of the detailed properites of deuterons or 6-quark clusters. The test may be viewed as a test that the short range part of the deuteron is still a 2-nucleon system. We make estimates to show how it fails in characteristic and significant ways if the two nucleons at short range coalesce into a kneaded 6-quark cluster.

1. Introduction: What happens when nuclei get close?

1.1. The extreme cases: 6q or 2N.

When the constituents of the nucleus are far apart, a description in terms of neutrons and protons is accurate. The question is what happens to the material inside the nucleus when the pieces come close to each other. One view is that the pieces never come close to each other. A repulsive force keeps them apart. One may also suppose that even if the nucleons are pushed close together they maintain their nucleonic character and behave as recognizable neutrons and protons. This viewpoint we shall refer to as the two nucleon, or 2N, model for the behavior of nuclear material at short interparticle distances. (Note that it is not possible to put a neutron—three quarks in an S-state with the correct spin, isospin, and color—and precisely overlap it with a proton. The Pauli principle at the quark level prevents it.)

An alternative viewpoint is that if two nucleons come sufficiently close together, the quarks within them reorganize or mix into a new state where each quark is in the lowest energy spatial state, and the color-spin-flavor part of the quark wave function is uniquely fixed by the requirement that it be a totally antisymmetric colorless state of the desired spin and isospin. The six quarks may thus lie top of each other. This model of a quark cluster is also an extreme viewpoint, and we refer to it as a 6-quark or 6q model.

1.2. The 6q state: hidden color or collection of resonances?

When the six-quark state was first written down,[1] it led to the idea of "hidden color." The 6-q state is a color singlet overall, but if one selects three definite quarks, those quarks do not generally form a color singlet. For a 6-q state which has the quantum numbers of the deuteron, a given set of three quarks has a 20% chance of being a color singlet, divided as 9% probability of having the quantum numbers of a nucleon and 11% probability of having

*Presented by CEC.

those of the delta resonance. The remainder of the state can be written out as a collection of terms, 80% by probability, which have three quarks in a color octet coupled to another three quarks in a color octet. This part of the state was referred to as hidden color.

There is an alternative expression of the state which leads to a different vision of it nature.[2] One may write the state as a sum of product wave functions in which the quarks are always grouped into colorless quark triplets. For example, the first term consists of quarks 1, 2, and 3 in a color singlet with the quantum numbers of a nucleon with quarks 4, 5, and 6 also in a color singlet with the quantum numbers of a nucleon. The second term is similarly two factors, but now involving different quarks, say quarks 1, 2, and 4 in a color singlet with the quantum numbers of the nucleon and quarks 3, 5, and 6 in a similar state; and so on. There is no "hidden color." However, the state is not equivalent to a simple overlap of two nucleons. Additionally, the very same state could be expanded in term of delta-like objects, wherein every term consists of two factors, each having three overall colorless quarks with the quantum numbers of the delta. Some lessons are clear: we have to be careful in searching for such states by looking for phenomena dependent upon the hidden color or upon the delta-like components in the state.

1.3. Nuclear force at short range: repulsive at quark level?

It is "well known" that the nucleon-nucleon force is repulsive at short range. Clearly, the nucleon-nucleon scattering data, analyzed assuming that nucleons are the only degree of freedom. leads to a repulsive nucleon-nucleon potential. This, however, is a single channel analysis of a coupled channel problem. The other channels possible include what we may describe as hidden color channels, which disappear at long distances.

It is not difficult to devise a pedagogic coupled channel model which has only attractive potentials and yet mocks the nucleon-nucleon situation of having an apparent repulsive potential when viewed only in terms of one long distance channel.[3] More realistically, ref.[4] provides a coupled channel study of a nominally two nucleon system, with 2N interacting by meson exchance at long distances and having a 6-q cluster at short distances. The NN wave function diminishes at short range—an apparent repulsion—but a 6-q core comes into being. In a deuteron, the quark cluster core is 1–2% by probability yet still has a notable effect on the form factors.

Thus we learn that an apparently repulsive potential is not proof of an actual repulsion at short distances since we have a coupled channel situation. One cannot argue that a repulsive potential prevents the nucleons from ever coalescing into a 6-quark cluster. Arguments about formation of a 6q state have to be made on other grounds. We ourselves shall not here argue the question of possibility, but rather the question of proof: how we could know if a 6q cluster exists as part of the short range order of a nucleus?

2. Proposal for a distinctive signature.

Let us limit ourselves to the case of either having two reasonably unmodified nucleons or else of having a 6q state. We seek methods to experimentally distinguish them. We also limit ourselves to experiments off deuterons. Denser nuclei have a higher probability of having a

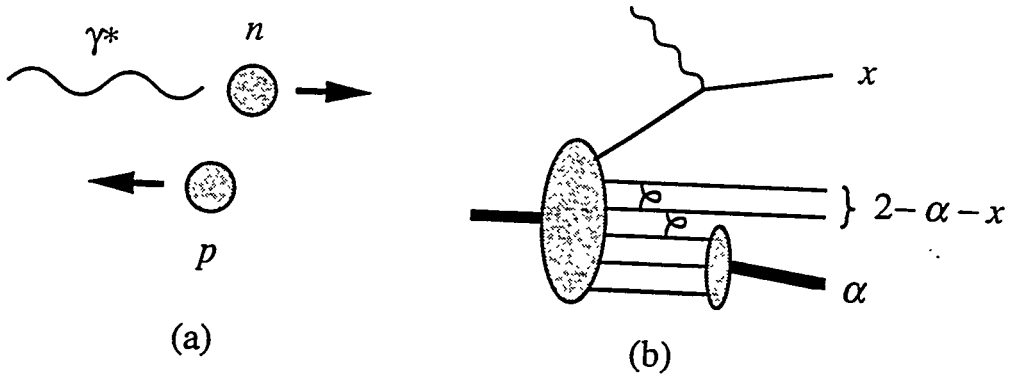


Fig. 1. Backward proton production in (a) 2N model, (b) 6q model.

6q state, but also have other nucleons around to disturb the free exiting of particles that scatter off a 2N correlation or 6q state.

One can find examples of data for which calculations using either a 2N correlation model or a 6q model show good agreement. It seems that plausible adjustments can often make calculations work out well. So as a general principle we will seek ratios of things where quantities that are not known without calcuation cancel out.

Next, when three quarks in a deuteron are far from the other three quarks, a description in terms of neutrons and protons works well. We need a tag that emphasizes the short range part of the deuteron. Consider electron-deuteron scattering reactions where protons emerge backward to the direction of the incoming beam, Fig. 1a. Whatever is struck by the probe goes forward. In a 2N view, a backward proton comes if the neutron was struck while its fermi momentum was forward. The bound state is broken and the proton emerges—backward—with whatever fermi momentum it had. The higher the backward momentum, the more the short distance part of the deuteron wave function is emphasized.

On the way to defining a suitable ratio, let us examine the cross section formula for $\gamma^* + d \to p(\text{backward}) + X$,

$$\sigma_{2N} \equiv \frac{d\sigma_{2N}}{dx\,dy\,d\alpha\,d^2p_T} = K\,F_{2n}(\xi)\cdot(2-\alpha)\,|\psi(\alpha, p_T)|^2\,, \tag{1}$$

where

$$K = \frac{4\pi\alpha_{em}^2 m_N E}{Q^4}\left(1+(1-y)^2\right). \tag{2}$$

We must state some kinematics: E is the incoming electron energy, x is $Q^2/2m_N E$, and y is the electron's energy loss given dimensionlessly as ν/E. We use light cone variables for the backward proton momentum, transverse components p_T and longitudinal component p^z (taken positive if backward) given using

$$\alpha = \frac{E_p + p^z}{m_N}. \tag{3}$$

The argument of the neutron structure function F_{2n} is the momentum fraction of the struck quark relative to the neutron. For a standing neutron, this is just x, but since the neutron has fermi momentum we must correct it to $\xi = x/(2-\alpha)$. Finally, we should mention that α lies between zero and 2, and that

$$0 \leq x \leq (2-\alpha). \tag{4}$$

Now we are in a position to define a ratio suitable for testing the 2N model. Let

$$R_1 = \frac{\sigma_{\text{meas}}}{K F_{2n}(\xi)}. \tag{5}$$

If the measured cross section is the cross section expected from the 2N model, then R_1 is simply the deuteron wave function squared (times $(2-\alpha)$). The test of the 2N model, however, does not require knowing the deuteron wave function. It is just to see if the ratio R_1 is independent of x for fixed α and p_T. Pictorially, we should see if we get a horizontal line on a plot like Fig. 2.

Of course, the test is not interesting unless the alternative gives a notably different result. Hence, our next job does involve some calculating to estimate what one expects for the 6q model, and show that R_1 is quite dependent on x in this case, again for fixed α and p_T.

For the 6q model, a diagram is shown in Fig. 1b, where a quark is knocked forward, and we speak of the remaining five quarks (of the leading fock component) as a "residuum." If x is large enough that the cross section is dominated by valence quarks, then

$$\sigma_{6q} \equiv \frac{d\sigma_{6q}}{dx dy d\alpha d^2 p_T} = Kx \sum_i e_i^2 V_i^{(6)}(x) \cdot \frac{1}{2-x} D_{p/5q}(z, p_T). \tag{6}$$

Here $V_i^{(6)}$ is the distribution function for a valence quark in a 6q cluster, the sum is over quark flavors, and $D_{p/5q}$ is the fragmentation (or recombination) function for the 5q residuum, i.e., the probability density per unit z and p_T for getting a proton from the residuum. The argument z is the fraction of the residuum's momentum going into the backward proton, or $z = \alpha/(2-x)$. For the quark distributions in a 6q cluster, we take some proposals of Lassila and Sukhatme made some time ago[5] in connection with the first EMC effect. For the fragmentation function we can use the counting rules to get $D_{p/5q} \propto (1-z)^3$. Supposing the data is dominated by the 6q cluster, and using the CTEQ quark distributions to get the denominator of ratio R_1, we get the curved lines of Fig. 2.

Between peak and minimum of the curves in Fig. 2 is at least a factor of two, so there is a clear distinction between the extemes. If the data lies inbetween, that is interesting also. It is evidence of something other than 2 nucleons in the nucleus.

3. The value of higher energy

Let us ask what is needed to validate our analysis. In writing the cross sections, we assumed we were in the scaling region, which requires that Q^2 is greater than 1 GeV^2 and that the final hadronic c.m. energy W for the equivalent one-nucleon reaction be greater than 2 GeV. The first of these puts a lower limit, and the second an upper limit, on x. For a given

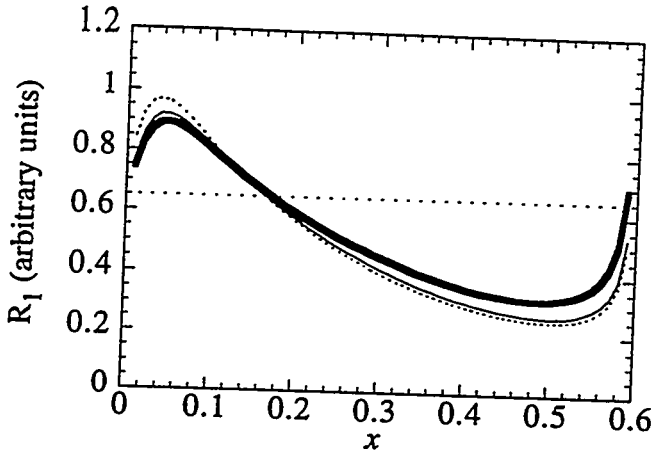


Fig. 2. Ratio R_1 for fixed $\alpha = 1.4$ (momentum 322 MeV for directly backward protons). 2N correlations lead to a horizontal line; 6q configurations lead to heavy, normal, or dotted curves from Lassila-Sukhatme parametrizations A, B, or C.

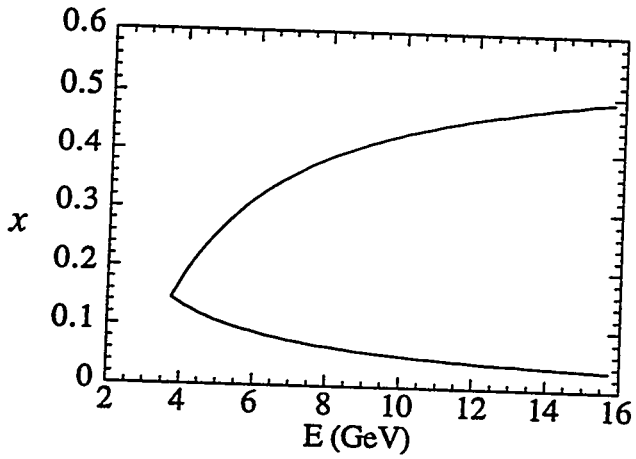


Fig. 3. The scaling window, calculated for $\alpha = 1.4$.

incoming electron energy E, the scaling window in x can be read off the plot in Fig. 3. The window is very narrow at 4 GeV, but opens out nicely and even at 8 GeV it nearly encompasses the maximum and minimum of the curves in Fig. 2.

Fig. 3 is drawn for $\alpha = 1.4$, which corresponds to 322 MeV backward proton momentum, if the proton comes straight backward. While we feel that is sufficient to be interesting, higher momentum still would be better, if the counting rate allows. For higher α, the scaling window shifts to higher incoming electron energy. For example, for $\alpha = 1.6$ or 458 MeV proton momentum straight back, the scaling window begins at $E = 5.5$ GeV and is quite well open beyond 10 GeV. So on energy we conclude that 8 GeV is good, but higher still would also be useful.

Our discussion here has been necessarily brief. More material may be found in.[6]

References

1. V. Matveev and P. Sorba, Il Nuovo Cimento **45A**, 257 (1978); A.P. Kobyshikin (Kobushkin in newer works by the same author), Yad. Fiz. **28**, 495 (1978) [Sov. J. Nucl. Phys. **28**, 252 (1978)].
2. P. González and V. Vento, Few-Body Systems **2**, 145 (1987).
3. F. Gross and W. Buck, private communication.
4. H. Dijk and B.L.G. Bakker, Nucl. Phys. **A494**, 438 (1989).
5. K.E. Lassila and U.P. Sukhatme, Phys. Lett. B **209**, 343 (1988).
6. C.E. Carlson, K.E. Lassila, and U.P. Sukhatme, Phys. Lett. B **263**, 277 (1991); C.E. Carlson and K.E. Lassila, Phys. Lett. B **317**, 205 (1993); C.E. Carlson and K.E. Lassila, Report WM-94-101 (submitted to Phys. Rev.).

Measuring Nuclear Transparency from Exclusive Vector Meson Production in Lepton-Nucleus Scattering

Guang Yin Fang
Harvard University, Cambridge, MA 02138

Abstract

Preliminary results on the measurement of nuclear transparencies from exclusive ρ^0 meson production from E665 at Fermilab are reported. The data were collected on hydrogen, deuterium, carbon, calcium, and lead targets with a mean beam energy of 470 GeV. Increases in the transparencies are observed in both coherent and incoherent production channels as the virtuality of the photon increases, as expected of color transparency. Ideas of systematic studies of color transparency in exclusive vector meson production at CEBAF are discussed.

1. Introduction

Exclusive electro-production of vector mesons from nuclei was suggested as a way of testing the idea of a "shrinking photon" before the advent of quantum chromodynamics (QCD).[1] The hadronic components of a virtual photon were conjectured to be smaller than the size of a normal hadron, thereby account for the point-like structure and diminished absorptions observed in photon-nuclei interactions at high Q^2.

More recently, exclusive vector meson production has been proposed as a way of testing the idea of color transparency by various authors.[2–5] According to perturbative QCD large momentum transfer exclusive processes select out small configuration hadrons. These small hadrons carry multiple color fields with decreasing strength, thus they experience diminished interactions while propagating through a nuclear medium.[6] Therefore, one expects the total cross section of a hard exclusive process that involves nucleons from a nucleus to be proportional to A, the total number of nucleons in the nucleus. Exclusive lepto-production of vector mesons at high energies provides an excellent venue for testing these ideas. In this case the initial size of the vector mesons is controlled by Q^2, the virtuality of the photon. At high energies both coherence length, $2\nu/(Q^2+m^2)$, and formation length, $\nu/m\delta m$, where m is the mass of the vector meson and δm is the typical mass splittings of the vector mesons, can be much larger than the size of the nucleus, thus ensuring that the produced vector mesons remain small and do not reach their normal sizes till long after they have left the nucleus. For example, in the kinematic region covered by the E665 data an exclusively produced $\rho 0$ meson typically carries about 120 GeV, leading to a coherent length of about 10 fermi and a formation length of more about 50 fermi at Q^2 of 5 GeV^2 which are larger than even the heaviest nuclei. Therefore one expects the nucleus to be highly transparent even at modest Q^2 values of a few GeV^2.

2. The E665 data

E665 is a deep inelastic muon scattering experiment at the Fermilab Tevatron designed with emphasis on final state hadron detection. The data used for the present analysis came from the 1990 run which was devoted to systematic studies of nuclear effect at high

energies. A detailed description of the E665 spectrometer can be found elsewhere.[7] Five targets were used for this measurement: liquid hydrogen and deuterium, each one meter long, and solid carbon, calcium and lead. The solid targets were longitudinally segmented into five equal pieces and distributed with equal separation over the full length of the liquid targets. The total muon flux collected was a bout $5 \cdot 10^{10}$ per target, corresponding to an integrated luminosity of about $3 \cdot 10^{35}$ per target.

The variables employed to describe exclusive vector meson production are defined as the following: $Q^2 = -(p_\mu - p'_\mu)^2$, $\nu = p \cdot q/m_p$, $x_{bj} = Q^2/2m_p\nu$, $t = (q - v)^2$, $t' = t - t_{min}$, $z_v = E_v/\nu$, where p_μ, p'_μ, q and v are the four momenta of the incoming muon, the outgoing muon, the virtual photon and the vector meson respectively, $-Q^2$ is the invariant mass of the virtual photon, ν is the energy lost by the muon in the laboratory frame, t is the the squared four momentum transfer between the vector meson and the nucleon, $\mid t_{min} \mid$ is the minimum $\mid t \mid$ allowed by the kinematics, z_v is the ratio of the energy carried by the vector meson to that lost by the muon and m_p is the proton mass.

Events accepted by the present analysis were required to have exactly two oppositely charged hadrons in the final state in addition to the scattered muon (the low energy recoil nucleon, with typical kinetic energy of less than .2 GeV, was not detected). Inclusive and combinatorial contaminations were suppressed by a cut $-1.5 \leq (z_v - 1)/\delta z_v \leq 3$ where δz_v is the error on z_v calculated from the measurement errors. Events from photon conversion were rejected using the calorimeter information by demanding that the energy and shower shape associated with the hadrons be inconsistent with that of an electron. The energy of both hadrons were required to be greater than 10 GeV to ensure that the particles were in well-understood regions of acceptance of the forward spectrometer. Events from exclusive ϕ meson production were removed by demanding that the invariant mass reconstructed with kaon hypothesis be greater than 1.05 GeV/c^2. Events from non-target interactions were subtracted statistically assuming that they were from carbon-like material. In addition, the following cuts were imposed on the final data samples used for the transparency analysis: $Q^2 \geq 0.1$ GeV^2, $\nu \geq 20$ GeV, $\delta\nu/\nu \leq 0.25$, $m_{\pi\pi} \leq 1.5$ GeV/c^2 and $\mid t \mid \leq 0.8$ GeV^2.

Exclusive production of vector mesons from a nuclear target has two components: coherent, corresponding to production off the nucleus as a whole, and incoherent, corresponding to production off individual nucleons in the nucleus. The slopes of the t' distribution of a diffractive scattering process measure the physical size of the scatterer. Therefore, for a nuclear target, one expects to see a $\mid t' \mid$ fall steeply initially, followed by a region with a much smaller slope. As examples, the observed t' distributions for hydrogen and calcium targets are shown in figures 1a and 1b respectively. Regions corresponding to coherent and incoherent production are clearly identifiable in figure 1b. In this measurement, events with $\mid t' \mid$ values greater than 0.1 GeV^2 were treated as incoherent (the same cut is used for all the targets). Contributions from coherent events to the incoherent samples were estimated by integrating the observed coherent exponential functions from 0.1 GeV^2 to infinity. The level of contaminations were less than 1% for all but the deuterium target for which the contamination is about 8%. Contributions from incoherent events to the coherent samples were subtracted by extrapolating the incoherent distributions down to $t = 0$ with a slope averaged over the observed incoherent slopes from all the targets.

The main source of background comes from events in which a ρ^0, or a pair of oppositely charged hadrons with $m_{\pi\pi}$ consistent with the ρ^0 mass, are produced through fragmentation with a sum of z values close to 1 and no other particles detected. A Lund-

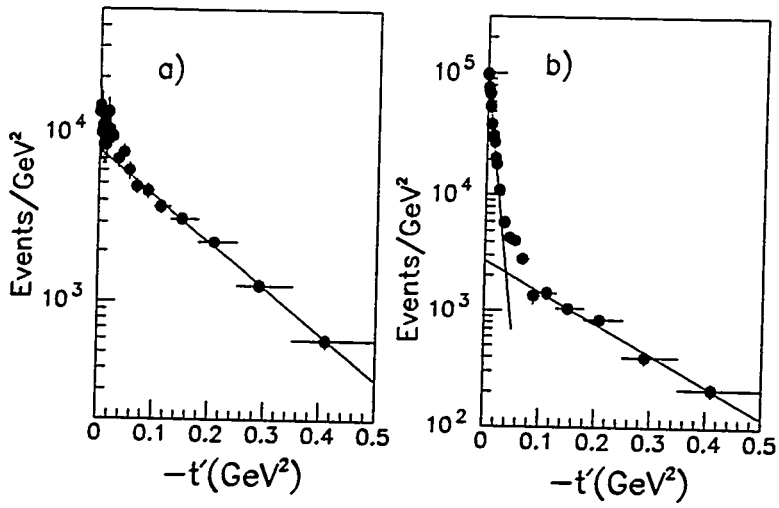


Figure 1: The observed t' distributions for a) hydrogen and b) calcium. The curve in a) is a fit to $N_n \cdot e^{-b_n|t'|}$ using only points between 0.08 and 0.5 GeV^2. The curves in b) are fits to $N_A \cdot e^{-b_A|t'|}$ using only the points between 0 and 0.02 GeV^2 and $N_n \cdot e^{-b_n|t'|}$ using only points between 0.08 and 0.5 GeV^2. The results from the fits: $b_n = 6.29 \pm .37$ GeV^{-2} from a, $b_n = 6.20 \pm 0.53$GeV^{-2} and $b_A = 100. \pm 6.0$GeV^{-2} from b.

based Monte-Carlo program was used to generate a sample of deep-inelastic events. These events were then subjected to the same analysis procedure as that used for the data. The surviving events were then normalized to the data by demanding that the number of total events from Monte Carlo sample in the background region equals to that of the data. The estimated background in the signal region were then subtracted.

The nuclear transparencies, defined as $(\sigma^A/A)/\sigma^H$, for incoherent ρ^0 production off deuterium, carbon, calcium and lead, versus Q^2 are shown in figure 2a. In figure 2b α is plotted as a function of Q^2. Here α is the power from a fit of the total production cross section σ^A, for a nucleus A, to the form NA^α. The transparencies for coherent ρ^0 production, defined as $(\sigma^A/A)/(\sigma^C/12)$, for calcium and lead are shown in figure 3a and the corresponding α plot is shown in figure 3b. Increases in α imply that more nucleons contribute to the production process, i.e., the nucleus become more transparent. For the case of complete transparency one expects that the coherent production cross section to be proportional to $A^{4/3}$ and the incoherent production cross section to be proportional to A. From these figures one sees that indeed, as Q^2 increases the transparencies for heavy targets all increase in both coherent and incoherent cases. This behavior in T agrees well with what is expected from the color transparency arguments. As Q^2 increases, the initial size of the produced mesons becomes smaller, and thus they experience weaker color field on the way out. Therefore, the attenuation due to final-state interactions becomes smaller and more mesons produced in the nuclear interior emerge intact. On the other hand, if we assume that the intermediate $q\bar{q}$ state and the produced ρ^0 mesons are of normal sizes Glauber multiple scattering theory would predict a Q^2 independent transparency.

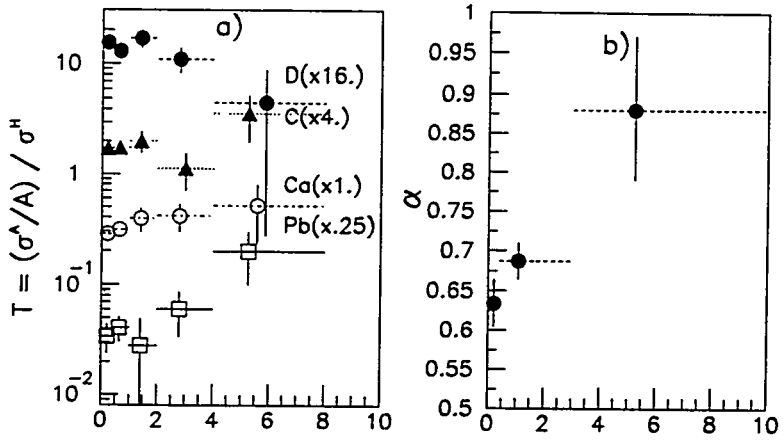


Figure 2: a) T vs Q^2, b) α vs Q^2 for incoherent ρ^0 production.

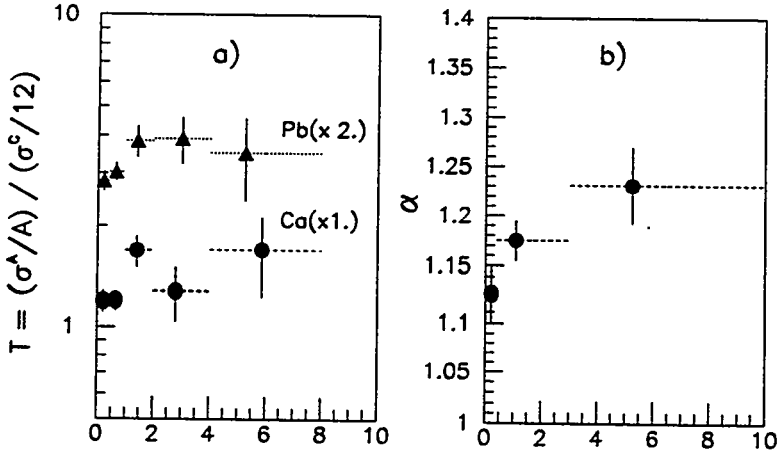


Figure 3: a) T vs Q^2, b) α vs Q^2 from coherent ρ^0 production.

Since the background subtraction relies on Monte Carlo input, any uncertainties in the input hadron z spectrum would affect the results. However detailed studies show that the dominant background are combinatorial. Thus only the pion z distributions that are important. Since the results from analyzing the Monte Carlo events reveal that the inclusive distributions match the data well we expect that the errors from this source to be small. Various studies on other potential sources of systematic errors have been performed and no statistically significant effect on the transparency measurements was found.

3. Studying color transparency at CEBAF

With the upgrade in beam energy and the superb machine properties CEBAF provides an unique facility for systematically studying color transparency. Extensive discussions on various processes can be found else where in these proceedings.[8] Here I will confine myself to the discussions of exclusive vector meson production.

In order to observe color transparency experimentally one needs not only a hard exclusive process that selects out small configuration hadrons but also high enough energy so that the small hadrons do not expand appreciably while propagating in the nuclear medium. Exclusive lepto-production of vector mesons can be used to extract information on these two aspects separately. Unlike in the case of an $(e, e'p)$ or fixed angle $(h, h'p)$ experiment, where the four momentum transfer and the energy carried by the hadrons are correlated, the Q^2 and energy can be varied independently in an exclusive vector production process. With enough luminosity one can, for example, perform measurements at fixed Q^2 with increasing energy, or at fixed (high) energy with increasing Q^2. The first case amounts to fixing the initial size of the hadron and measuring transparency as function of the travel time of the hadron inside the nuclear medium while the second case corresponds to fixing the travel time and measuring transparency as a function of the initial size of the the vector mesons. With these type of precision measurements on various targets one might gain detailed information on the dynamics of color transparency physics. In addition, one can perform measurements at fixed x_{bj} and increasing Q^2. Existent data on nuclear shadowing show very little Q^2 dependence. Fixing x_{bj} amounts to fixing effects associated with nuclear shadowing to the initial state virtual photons, thus allows one to derive transparency of the final state vector mesons.

One can also perform measurements similar to that of $(e, e'p)$ and $(h, h'p)$ interactions in exclusive vector meson production by measuring transparency at fixed (low) Q^2 and increasing t (here t is the four momentum transfer between the vector meson and the nucleon). In this case the initial state vector mesons should be similar to normal mesons. By selecting high t events one selects out small configurations the same way an $(e, e'p)$ or $(h, h'p)$ process does. However, unlike in the case of an $(ee'p)$ interaction t and energy in this case can be varied independently, thus allows one to measure transparency at fixed t with increasing energy. Depending on the setup one can perform truly exclusive (the recoil system is measured) or semi-exclusive (the recoil system is not measured) measurements. In the first case the value of the measured transparency will be dominated by the nucleon transparency since the nucleon will likely be at at lower energies. In the latter case one needs to take special care on backgrounds. As an example let us consider the case of 15 GeV ρ meson. At a t value of 3 GeV^2, corresponding to an initial size of about .15 fm at the point of interaction between the ρ meson and the nucleon, the outgoing ρ meson will still carries about 12 GeV. In terms of hadron energy this is equivalent to a Q^2 of about

25 GeV in an $(e, e'p)$ interaction.

How high an energy is necessary to pursue this type of physics? One way of making an estimate is to use the requirement that the coherence length of the interaction be larger than the size of the nucleus. Roughly speaking, only when the coherence length is large compared to the size of the nucleus can one be assured that the size of the vector meson produced at high Q^2 be small. Ignoring the mass of the vector mesons this requirement can be expressed approximately as $2\nu/Q^2 \geq 2R_A = 1.1A^{1/3}$, i.e., $\nu \geq 5.5 \cdot Q^2 \cdot A^{1/3}$ where ν is in GeV and Q^2 is in GeV^2. Clearly at moderate energies one should choose lighter targets. Using a helium target one should be able to observe sizable effects at about 10 GeV.

With the tremendous luminosity available at CEBAF one can produce high mass vector mesons (ρ', ρ'', ϕ, ϕ' ...) in unprecedented quantities. These states are predicted to have very distinctive features in their transparencies. Detailed study of these states will undoubtedly shed new light on the mechanism of color transparency.[4]

In summary, I have reported the preliminary results from E665 at Fermilab on measurements of nuclear transparencies in incoherent exclusive ρ^0 production off deuterium, carbon, calcium and lead and in coherent ρ^0 production off calcium and lead. Increases in the transparencies as Q^2 are observed, in agreement with the expectations of color transparency. Various options of pursuing systematic investigations on color transparency physics at CEBAF with higher beam energies are discussed.

I would like to thank Roy Holt and Nathan Isgur for inviting me to this exciting and stimulating workshop. I would also like to thank S.J. Brodsky, L.L. Frankfurt, A.H. Mueller, N.N. Nikolaev and M. Strikman for many stimulating discussions.

References

1. T.H. Bauer *et al.*, Rev. of Modern Phys. **50**, 261 (1978).
2. S.J. Brodsky and A.H. Mueller, Phys. Lett. **B206**, 685 (1988).
3. L.L. Frankfurt and M. Strikman, Phys. Rep. **160**, 235 (1988).
4. B.Z. Kopeliovich *et al.*, Phys. Lett. **B309**, 179(1993); B.Z. Kopeliovich *et al.*, Phys. Lett. **B324**, 469(1994).
5. S.J. Brodsky *et al.*, SLAC-PUB-6412, (1994).
6. A. H. Mueller, in Proceedings of the XVII Recontre de Moriond, Les Arcs, France, Ed. J. Tran Thanh Van, Editions Frontiers, Gifsur-Yvette, 1982, p. 13; S. J. Brodsky, in Proceedings of the XIII International Symposium on Multi-Particle Dynamics, Voldendam, Netherlands. Eds.E.W. Kittel, W. Metsger and A. Stergion, World Scientific, Singapore, 1982, p.963.
7. M. Adams *et al.*, Nucl. Inst. and Meth., **A291**, 533 (1990).
8. See discussions by A. Mueller, N.N. Nikolaev and many others in these proceedings.

COLOR COHERENT EFFECTS IN $(e, e'N)$ AND $(e, e'N, N(h))$ PROCESSES AT CEBAF

L. L. Frankfurt
Tel Aviv University, Ramat Aviv 69978, Israel, Tel Aviv, Israel,
on leave of absence from the St.Petersburg Nuclear Physics Institute, Russia

M. M. Sargsyan
Tel Aviv University, Ramat Aviv 69978, Israel, Tel Aviv, Israel,
also at the Yerevan Physics Institute, Yerevan 375036, Armenia

M. I. Strikman
Pennsylvania State University, University Park, PA 16802, USA,
also at the St.Petersburg Nuclear Physics Institute, Russia

ABSTRACT

The options for investigating color coherent effects and competing nuclear effects of nucleon-nucleon correlations in nuclei, nuclear shell effects in $(e, e'N)$ and $(e, e'NN(h))$ reactions are considered. We argue that extension of CEBAF energies to reach $Q^2 = 10\ GeV^2$ will allow systematical investigations of color coherent effects in nonperturbative regime of QCD and their interplay with nuclear effects.

1. Introduction

It is generally accepted now that color coherent phenomena in the collisions of high energy particles with nuclei provide promising new methods of investigating nonperturbative and perturbative QCD. The most celebrated example is the color transparency (CT) phenomenon - suppression of the final state interaction (FSI) in the quasiexclusive large angle reactions with nuclei [1,2].

The aim of original suggestion of CT[1,2] was to use the color screening effect (suppression of the interaction of small color singlets with hadrons) to establish an onset of the pQCD regime - to check at what Q^2 the elementary elastic reaction is dominated by the contribution of the small size configurations. Initial motivation for the dominance of small size configurations came from the analysis of the leading perturbative QCD diagrams which should dominate at sufficiently large momentum transfer. However the recent analysis [3] of the realistic models of nucleon and pion wave functions has found that the electromagnetic form factors of a nucleon, pion are dominated by smaller than average configurations already in the nonperturbative domain at $Q^2 \geq 2 - 3(GeV/c)^2$.

Hence it is necessary to search for the onset of CT in the $A(e, e'N), A(e, e'NN(h))$ processes at these moderate Q^2. One needs both dedicated high resolution experiments at intermediate Q^2 (see for example [4]) and theoretically unambiguous calculations of nuclear transparency within the *standard Glauber approximation*(GA) and with account for the *CT phenomena.* Such calculations should include effects of nu-

cleon correlations in nuclei, the nuclear shell effects when momentum of interacting nucleon is low ($\leq k_{Fermi}$), etc.

The practical problem in investigation of color transparency is that small size wave packet undergoes time evolution while passing through the nucleus. This evolution considerably slows down the onset of CT phenomena at the realistic values of Q^2. Therefore to investigate CT effects one needs to investigate carefully possible nuclear effects which can interfere with CT phenomena.

2. Nuclear Transparency in $(e, e'N)$ Reactions

The convenient quantity which characterizes the effects of FSI in $(e, e'N)$ processes (see e.g. Refs.[4,5,6,7]) is the ratio of the measured cross section of the $(e, e'N)$ reactions to the cross section calculated within the plane wave impulse approximation (PWIA):

$$T_A(Q^2, \vec{p}_i, \vec{p}_f, E_r) = \frac{\sigma^{EXP}(Q^2, \vec{p}_i, \vec{p}_f, E_r)}{\sigma^{PWIA}(Q^2, \vec{p}_i, E_r)} = \frac{\sigma^{FSI}(Q^2, \vec{p}_i, \vec{p}_f, E_r)}{\sigma^{PWIA}(Q^2, \vec{p}_i, E_r)}, \quad (1)$$

where $\vec{p}_f$ is the momentum of the registered nucleon, $\vec{q}$ is the transferred momentum, E_r is the removal energy, and $\vec{p}_i = \vec{p}_f - \vec{q}$. In the limit of complete nuclear transparency this ratio will approach unity. Corresponding theoretical quantity is the ratio of the cross section calculated with FSI to the cross section calculated within PWIA (see the right hand side of eq.(1)). To calculate the cross section of the semiexclusive $(e, e'N)$ reaction with final state interaction of knocked-out nucleon and residual nucleus, we can use the distorted wave impulse approximation (DWIA) where the cross section can be represented as follows:

$$\frac{d^6\sigma}{d\epsilon_2 d\Omega_2 d^3\vec{p}_f} = \sigma_{eN} \cdot S_A(\vec{p}_i, Em, \vec{p}_f), \quad (2)$$

where σ_{eN} is proportional to the cross section of electron scattering off a bound nucleon. If the specific shell is fixed the DWIA spectral function can be written as [8]:

$$S_A(\vec{p}_i, E_r, \vec{p}_f) = n_\alpha(E_r) \cdot \mid \Phi_\alpha(\vec{p}_i, \vec{p}_f) \mid^2, \quad (3)$$

where $n_\alpha(E_r)$ characterizes the strength of the α shell and $\Phi^2_\alpha(\vec{p}_i, \vec{p}_f)$ is the distorted momentum distribution of the nucleons for this shell. In the calculation of the $(e, e'N)$ cross section with final state interaction it is useful to classify the structure of FSI depending on whether the residual energy is fixed or not.

2.1. Coherent Final State Interaction

It is well known from the low energy studies that the cross section of exclusive $A(e, e'p)$ processes strongly depends on the value of removal energies E_r which characterizes the binding energy of the knocked-out proton and as well as the excitation energy of the residual $(A-1)$ nuclei. If the removal energy is fixed one cannot use

closure, the cross section depends on the momentum and removal energy (the spectral function).

If E_r is fixed and does not exceed the value characteristic for the nuclear shell excitations ($\leq 50 - 80MeV$) it is natural to decompose final state interaction over the number of collisions with nucleons in the nucleus. Calculations show that final state interaction of the knocked-out nucleons with the residual nucleus is dominated by the coherent rescattering off the $(A-1)$ residual nucleus.

To calculate this final state interactions we adopted the method developed by Moniz, Walecka, Nixon [9],[10] and Yennie [11], which allows to include the nucleon correlations in the conventional Glauber approximation [12].

Considering only coherent final state interaction of knocked-out nucleon with the residual $(A-1)$ nucleus for the distorted momentum distribution of the nucleons from shell α we obtain:

$$\mid \Phi_\alpha(\vec{p}_i,\vec{p}_f) \mid^2 = \left| \int d^3r_1 \Psi_\alpha(r_1) e^{-i\vec{p}_i\vec{r}_1} \times \left[e^{-\int\limits_{z>z_1} \Gamma(b_1-b)\tilde{n}(r)d^3r} \right] \right|^2, \qquad (4)$$

where the profile function $\Gamma^N(b)$ is expressed through the NN amplitude ($f^{NN} \approx i\frac{k}{\pi}\sqrt{\frac{d\sigma}{dt}}$) as:

$$\Gamma^N(b) = \frac{1}{2\pi i k} \int \exp(i\vec{k}_t\vec{b}) \cdot f^{NN}(\vec{k}_t) d^2k_t, \qquad (5)$$

and $\tilde{n}(r) = (A-1)\cdot\tilde{\rho}(r)$, where

$$\tilde{\rho}(r) = \rho(r)\left[1 + \frac{1}{2}g(r_1,r) - \frac{A-1}{2}\int\limits_{z_1} \Gamma(b_1-b')g(r,r')\rho(r')d^3r'\right]. \qquad (6)$$

The correlation function $g(r_i,r_j)$ is defined as:

$$\rho_2(r_i,r_j) = ((1+g(r_i,r_j))\cdot\rho(r_i)\cdot\rho(j). \qquad (7)$$

In the limit when correlations are neglected the derived equation (4) coincides with predictions of the Glauber model in the independent particle approximation. The interesting feature of eqs.(4-7) is that correlations affect the final state interaction in two opposite ways. Due to the second term in eq.(6) correlations decrease the effective nuclear densities ($g(r,r') < 0$) and therefore increase the transparency of the nuclear matter for knocked-out nucleon. This effect, mentioned in Ref.[13] reflects the presence of the hole around the scattered nucleon. The formulae for the second term has been suggested firstly in Ref.[5] within the optical model approximation. The third term in eq.(6) leads to the increase of the effective nuclear densities and the nuclear matter become more opaque for the knocked-out nucleon. Third term has been actually obtained in Refs.[9,11] for high energy hadron-nucleus scattering. In difference from Refs.[9,11] eq.(6) accounts for the difference in geometries of electron and hadron collisions with nuclei. Note that opposite effects of nucleon correlations

were discussed also in Ref.[14] for the particular case of cross section integrated over all internal nucleon momenta and summed over final states of residual nucleus.

2.2. Noncoherent (Summed) Final State Interaction

In this subsection we consider the cross section summed over the final states of the residual nucleus. Such cross section can be measured in an experiment which covers wide range of energies of recoil system. Representing the FSI by the sum of nonrescattering, single rescattering . . . etc. terms, the distorted spectral function can be written as:

$$S^{DWIA} = S^{(0)}(Q^2, p_i, p_f) + S^{(1)}(Q^2, p_i, p_f) + ...S^{(n)}(Q^2, p_i, p_f), \tag{8}$$

where we further will restricted by the contribution of nonrescattering and single rescattering terms. Adopting the prescription for including the nucleon correlations described in section 2.1 using the closure over the residual nuclear states we obtain:

$$S^{(0)} = \sum_\alpha n_\alpha(E_r) \left(\mid \Phi_\alpha(p_i, p_f) \mid^2 + \int\int d^3r_1 d^3r_1' \Psi_\alpha(r_1)\Psi_\alpha^+(r_1')e^{-i\vec{p}_i(\vec{r}_1-\vec{r}_1')} \right.$$
$$\left. \times \left[\int\limits_{z>z_1,z_1'} \Gamma(b_1-b)\cdot\Delta n^+(r_1',r)d^3r + \int\limits_{z>z_1,z_1'} \Gamma^+(b_1'-b)\cdot\Delta n(r_1,r)d^3r \right] \right). \tag{9}$$

Here

$$\Delta n(r_1, r) = \frac{\rho(r)}{2}\left[-g(r_1, r) + \int\limits_{z'>z1} \Gamma(b_1 - b')\cdot g(r, r')n(r')d^3r' \right] \tag{10}$$

and (in quasiclassical limit)

$$S^{(1)} = \sum_\alpha n_\alpha(E_r) \int d^3r_1 d^3r_1' \Psi_\alpha(r_1)\Psi_\alpha^+(r_1')e^{-i\vec{p}_i(\vec{r}_1-\vec{r}_1')} e^{-\int(\Gamma(b_1-b)+\Gamma^+(b_1'-b))\tilde{n}'(r)d^3r}$$
$$\times \left[\frac{1}{\pi}\int e^{-ik_t(b_1-b_1')}\frac{d\sigma}{dt}d^2k_t \cdot \tilde{T}_A'(0) - \int \Gamma(b_1-b)\tilde{n}'(r)d^3r \int \Gamma^+(b_1'-b)\tilde{\rho}'(r)d^3r \right], \tag{11}$$

where $\tilde{n}'(r) \equiv \tilde{n}(b_1, b_1', r) = (A-1)\cdot\tilde{\rho}'(b_1, b_1', r)$ and

$$\tilde{\rho}'(b_1, b_1', r) = \rho(r)\left[1 + \frac{g(r_1, r) + g(r_1', r)}{2} - \frac{A-1}{2} \int\limits_{z>z_1,z1'} \tilde{\Gamma}(b1-b')g(r, r')\rho(r')d^3r' \right] \tag{12}$$

The integral $\tilde{T}_A'(0) = \int \tilde{n}'(0, z)dz$ describes the actual number of the nucleons participating in rescatterings. $\frac{d\sigma}{dt}$ - is the NN elastic differential cross section.

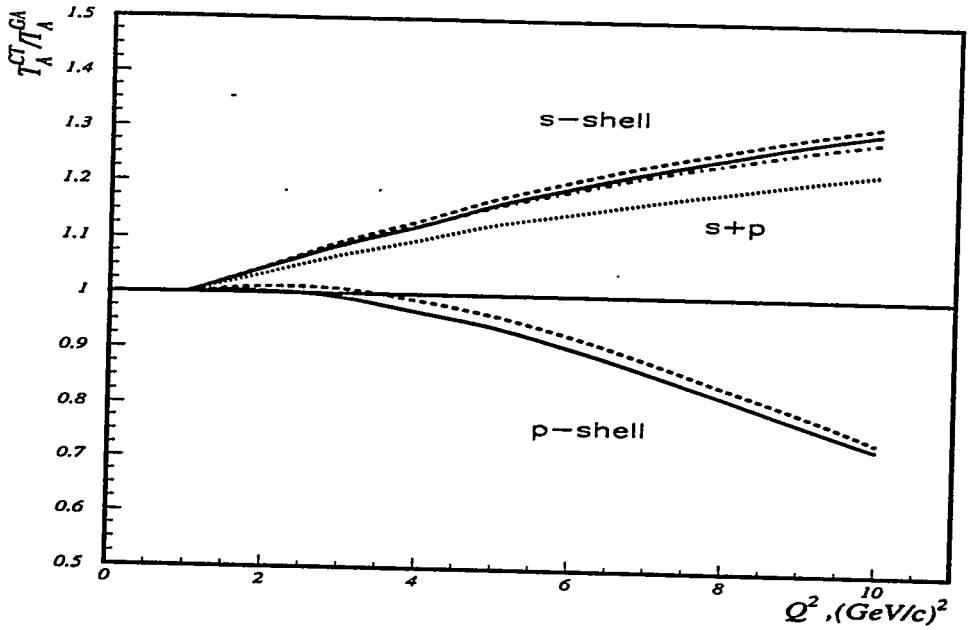


Fig. 1. Normalized CT calculation with and without nucleon correlations for different constraints on the energy of the final state described in the text.

The main result of eq.(9) is that if the sum over the final states of residual nucleus is performed nucleon correlations make the nucleus effectively more transparent (the Δn is positive at the range where $g(r)$ is negative) even if all rescattering contributions are neglected. (Although less transparent than according to the optical model calculations of Ref.[5]).

One can see from eq.(11) that correlations have a dual effect on the single rescattering. Firstly, they increase the forward rescattering since they reduce the contribution of subtracted term, the second term in the brackets of eq.(11). Secondly, they reduce contribution of the single rescattering at the large rescattering angles (where contribution from the subtracted term is negligible), since correlations decrease the actual number of nucleons for the struck nucleon to rescatter. Therefore the nuclear correlations steepen the angular distribution of the knocked-out nucleons.

2.3. Color Transparency Effects

To see how the above discussed effects interfere with the anticipated effects of color transparency (CT) we use the quantum diffusion model (QDM) [6] to account for the reduction of FSI for knocked-out proton due to CT effects. For this purpose we introduce the modified profile function eq.(5) with the modified NN scattering amplitude [15]:

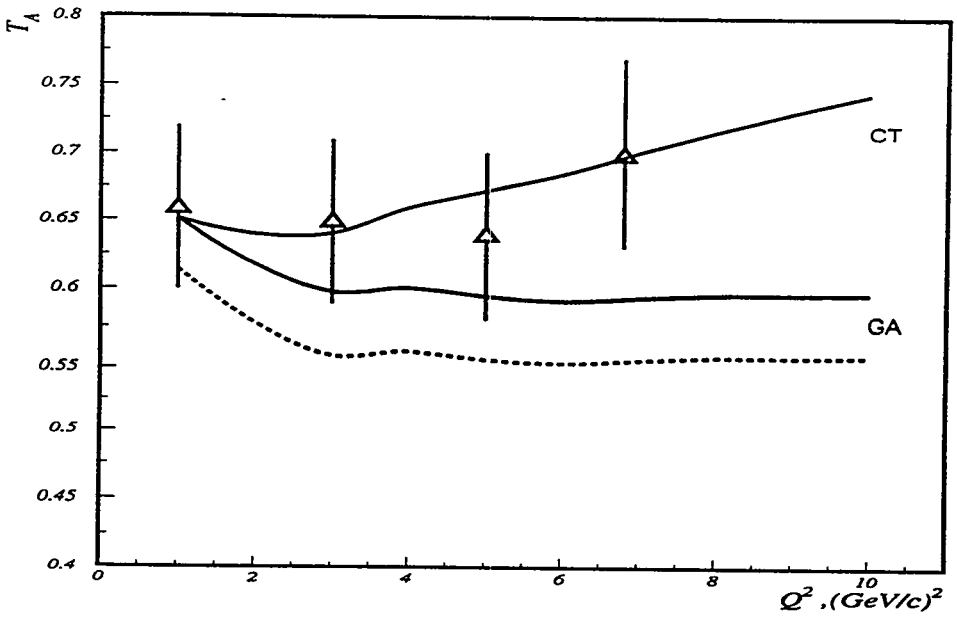


Fig. 2. Comparision with NE18[4] data. GA - Glauber approximation with (solid) and without (dashed) correlations. CT - QDM prediction for color transparency.

$$f^{NN}(k_t, Q^2, l) \approx i\frac{k}{4\pi}\sigma_{tot}(l, Q^2) \cdot e^{\frac{b}{2}t} \cdot \frac{G_N(t \cdot \sigma_{tot}(l, Q^2)/\sigma_{tot})}{G_N(t)} \qquad (13)$$

where b is the slope of elastic NN-cross section and $G_N(t)$ ($\approx (1 - t/0.71)^2$) is the Sachs form factor. The last factor in Eq. (13) accounts for the difference between form factors for point-like and average configurations, which is based on the observation that the t dependence of $d\sigma^{h+N\to h+N}/dt \sim G_h^2(t) \cdot G_N^2(t)$. We calculated the effective NN total cross section using the (QDM) predictions [6]:

$$\sigma_{tot}(l, Q^2) = \sigma_{tot}\left\{\left(\frac{l}{l_h} + \frac{< r_t(Q^2)^2 >}{< r_t^2 >}(1 - \frac{l}{l_h})\right)\Theta(l_h - l) + \Theta(l - l_h)\right\} \qquad (14)$$

where $l_h = 2p_f/\Delta M^2$, with $\Delta M^2 = 0.7\ GeV^2$. $\frac{<r_t(Q^2)^2>}{<r_t^2>} \approx \frac{1GeV^2}{Q^2}$ - is the average transverse size squared of the configuration produced in the interaction point.

In Fig.1 we present the results of the calculation of the effect of CT for ^{12}C. We plot the ratio of nuclear transparencies calculated with and without CT -T_A^{CT}, and T_A^{GA} for the case of coherent FSI of the struck nucleon from s and p shells with (solid line) and without (dashed line) correlations and for the case of noncoherent FSI with (dotted) and without (dott-dashed) correlations. One can see from inspection of Fig.1 that:

- When missing energy is fixed the contribution of correlations is minimal and T_A is more sensitive to the CT phenomena;

- Fixed nuclear shell and fixed internal momentum measurements will allow to search for different (even opposite) implications of Color Coherent phenomena. For examples at the fixed value of $p_i \approx 0$, the CT increases T_A for scattering from the s-shell while it decreases T_A for the scattering from the p-shell;

- The color transparency effect is sufficiently large starting from $Q^2 \sim 10(\frac{GeV}{c})^2$.

In Fig.2 we compare our calculations of $T_A(p_i = 0)$ with first experimental data of NE18[4] for the nuclear transparency in the $^{12}C(e, e'p)$ process. The data correspond to the wide range of removal energy and therefore approximation of noncoherent scattering is valid. This comparison should be considered as preliminary both because we did not include actual acceptance of the experiment and since the experimental analysis of data assumed that transparency does not depend on p_i and on the excitation energy. In any case it appears that the calculation with CT effects does not contradict to the experimental data although the experimental errors are large enough to allow definite conclusions.

It is worth emphasizing that eq.(11) shows that single rescattring term is more sensitive to the CT phenomena since it is proportional to the square of NN scattering amplitude. Therefore in the kinematics where considered processes is controlled mostly by the single rescatterings the color coherent effects are expected to be more prominent. One example of such processes is double scattering processes.

3. Nuclear Transparency in $(e, e'NN, e'NN^*(h))$ Reactions

In double scattering reactions $A(e, e'NN), A(e, e'NN^*(h))$ photon strucks a nucleon which experiences an additional rescattering off another nucleon. The NN rescatterings can be either elastic or inelastic. For inelastic channels main idea is to fix a specific reaction where final state cannot be produced in electroproduction off a single nucleon (for examples - $pp \to \Delta^{++}+N$)[16]. The measure of nuclear transparency in double scattering reactions as suggested in Ref.[17] is:

$$T_{resc} = \frac{\sigma(e, e'NN)}{\sigma(e, e'N)} \tag{15}$$

In the framework of Glauber approximation, the two proton decay (spectral) function for the $(e, e'pp)$ reaction off the light nuclei can be represented as follows:

$$\begin{aligned} D^{pp}(q, p_f, p_r) =& < \tilde{F}(p_f) >< \tilde{\chi}(p_r) > \cdot \Big\{ \Psi^2(p_i, p_r) - \\ & - \int \Psi(p_i, p_r)\Psi^+(\tilde{p}_i, \tilde{p}_r) f^{NN}(k_t) \frac{d^2k_t}{2\pi ik} + \\ & + \frac{1}{4} \int\int \Psi(\tilde{p}_i, \tilde{p}_r)\Psi^+(\tilde{p}'_i, \tilde{p}'_r) f^N(k_t) f^N(k'_t) \frac{d^2k_t d^2k'_t}{(2\pi)^2 kk'} \Big\} \end{aligned} \tag{16}$$

where $\Psi(p_i, p_r)$ is the two nucleon wave function of the nucleus and $\vec{p}_r$ is the momentum of rescattered slow proton. The factors $< \tilde{F}(p_f) >$ and $< \tilde{\chi}(p_r) >$ accounts for

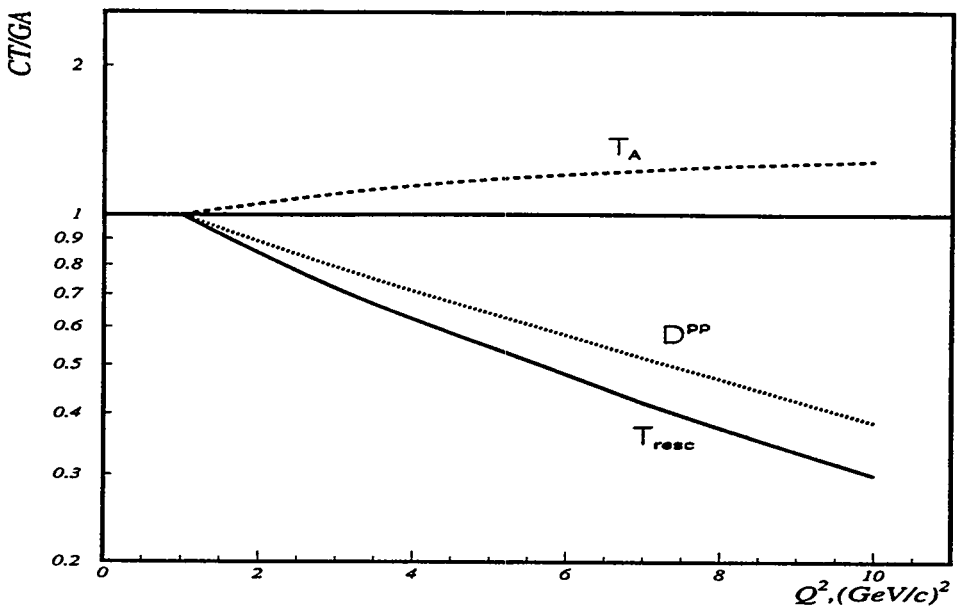


Fig. 3. CT effects at double scattering processes.

the residual final state interactions of fast and rescattered protons with slow spectator nucleons. The factorized form of this interactions is due to our approximation. A more sophisticated calculation is necessary (and we plan to perform it in the near future) which would include simultaneously soft and hard scatterings. Eq.(16) demonstrates that to isolate the rescattering term (third term in the equation) special kinematics is needed to suppress the Born and interference terms[15].

The main reasons that T_{resc} is more sensitive to the color coherent effects are:

- The analysis of eq.(16) shows [16] that for light nuclei and $Q^2 \sim 8-10\ (GeV/c)^2$ the NN scatterings occurs at the distances of $\sim 1-1.5\ fm$ from a point where small size object is produced in the $\gamma^* N$ scattering. At these distances the small size wave packet is still expanding and the NN scattering will occurs in the situation when one of nucleons is small;

- It is possible to select the particular channel for NN - scattering which is more sensitive to the size of scattered nucleon than in average[17] (for example $\sigma_{NN}^{elastic}$ $\sim$ $\sigma_{tot}(Q^2)^2$);

- In the double scattered processes when momentum transferred in the NN rescattering is not large ($\leq$ $0.7GeV^2$) the Color Coherent effects manifest themselves as a substantially stronger decrease of the cross section with Q^2 than within the Glauber approximation. The measured ratio T_{resc} defined in Eq.(15) is even more sensitive to CT, since the same (Coherent) effects in $(e,e'N)$ reaction leads to the increase of cross section as compared to GA. Besides this

ratio is easier to interpret since in the GA model it is practically constant for $Q^2 \geq 2(GeV/c)^2$ since the elementary NN amplitude weakly depends on the incident energy at $p_{inc} \geq 2GeV/c$;

- At $Q^2 \geq 10\ (GeV/c)^2$ it will be possible to select events where two baryons in final state have large relative transverse momenta ($\geq 1GeV/c$). In this kinematics Color Coherence leads to an increase of the double scattering cross section as compared to GA;

- In the double scattering processes the two-body densities of the nucleus are involved and therefore the reaction is more sensitive to the correlations between scattered nucleons in certain kinematical region.

In Fig.3 we illustrate the sensitivity of the double scattering processes to CT, in $(e, e'pp)$ reactions off ^4He, by comparing the predictions for T_A(dashed), D^{pp} (dotted) and T_{resc} (solid) in Quantum Diffusion model of CT normalized to the corresponding GA calculations.

References

1. A. Mueller, in *Proceedings of the 17 Rencontre de Moriond* edited by J. Tranh Thanh Van (Editions Frontieres, Gif-sur-Yvette, 1982), p.13.
2. S.J. Brodsky, in *Proceedings of the Thirteenth International Symposium on Multiparticle Dynamics*, edited by E.W. Kittel, W. Metzger, and A. Stergiou (World Scientific, Singapore, 1982), p.964.
3. L.L. Frankfurt, G.A. Miller, and M.I. Strikman, *Comments on Particle and Nuclear Physics*, v.**21** (1992) 1; L.Frankfurt, G. A. Miller, and M.Strikman, Nucl. Phys. *A555* (1993) 752.
4. N.C.R. Makins et al. *MIT preprint*, LNS-93/31, (1993).
5. O. Benhar *et al.* Phys. Rev. Lett., v.**69**, 881(1992).
6. G.R. Farrar, L.L. Frankfurt, H. Liu and M.I. Strikman, *Phys. Rev. Lett.* **61** (1988) 686.
7. L.L. Frankfurt, M.I.Strikman and M.Zhalov, *Phys. Rev. C*, 1994, in press.
8. S. Frullani and J. Mougey, *Advances in Nuclear Physics*, 14, Plenum Press, New York, 1984.
9. E.J.Moniz, G.D.Nixon, *Phys. Lett.* **30B** (1969) 393; E.J.Moniz, G.D.Nixon and J.D.Walecka, *Effect of Correlations on High-Energy Processes Using Nuclear targets* 1970.
10. E.J.Moniz, G.D.Nixon, *Ann.Phys.* **67** 68 (1971).
11. D.R.Yennie in *Hadronic Interactions of Electrons and Photons* ed. J.Cummings, D.Osborn, (1971) 321.
12. R.J.Glauber, *Lectures in Theoretical Physics*, Vol.1, p.315 eds. W.Brittain and L.G.Dunham, New-York, 1959.
13. L.L. Frankfurt, M.I.Strikman and M.Zhalov, *Nucl. Phys.*, **A515** (1990) 599.
14. N.N. Nikolaev, A. Szczurek, et al. *Phys. Lett.* **B317** (1993) 287.

15. K.Sh. Egiyan, L.L. Frankfurt, W.R. Greenberg, G.A. Miller, M.M. Sargsyan and M.I.Strikman, *Nucl. Phys. A*, 1994, in press.
16. L.Frankfurt, G.Miller, M. Strikman, Ann. Rev. of Nucl. Part. Phys., 1994, in press
17. K.Sh. Egiyan, L.L. Frankfurt, W.R. Greenberg, G.A. Miller, M.M. Sargsyan and M.I.Strikman, CEBAF preprint, PR-93-002, (1993).

Photoproduction of Vector Mesons off Nuclei

M.Kossov

CEBAF at Higher Energies Workshop

Vector mesons play an important role in photonuclear reactions because they carry the same quantum numbers as the incident photon. It has recently been suggested by G.E. Brown and M. Rho [1] that the mass of vector mesons could decrease with increasing baryon density. This phenomenon would provide a physical observable for chiral symmetry (χ^S) restoration at high baryon density, an essential non-perturbative phenomenon associated with the structure of quantum chromodynamics (QCD). According to the constituent quark model the difference between the mass of the valence quark (m_v) and the mass of the current quark (m_c) is expected to be proportional to the mean vacuum value of the quark condensate: $m_v - m_c \propto \langle\psi\psi\rangle_v$. The mass difference appears because of chiral symmetry breaking (χ^{SB}). QCD sum rule calculations [2] show that the value of this difference is about 300 MeV for all quarks. If the mean vacuum value differs from that for the hadron density in nuclei, then the constituent quark mass should be renormalized as follows: $m_v' = m_c + \frac{\langle\psi\psi\rangle_n}{\langle\psi\psi\rangle_v} \cdot 300MeV$, where the indices n correspond to nuclear matter and v to vacuum. The same conclusion was reached in a nuclear matter model based on quark degrees of freedom [3,4]. Using the symmetry properties of QCD in an effective Lagrangian theory, Brown and Rho [1] have found a scaling law for the vector meson masses at finite baryon density: $\frac{M_N^n}{M_N^v} = \frac{M_V^n}{M_V^v} = \frac{f_\pi^n}{f_\pi^v}$, where f_π is the $\pi \to \mu\nu$ decay constant playing the role of an order parameter for the chiral symmetry restoration. At nuclear density the value of f_π was found to be 15-20% smaller than in vacuum. In contrast to the constituent quark model, it was found that $\frac{M^n}{M} = (\frac{<q\bar{q}>_n}{<q\bar{q}>_v})^{1/3}$.

We propose to measure the properties of vector mesons in nuclear matter. The mass of vector mesons is predicted to change due to the chiral symmetry restoration at high baryon density. The photoproduction of vector mesons near threshold can be used to measure the mass of the vector mesons in nuclear matter. ρ-meson production at CEBAF energies (small boost) and off heavy nuclei is an ideal experiment for the measurements of the ρ-meson mass shift in nuclear matter. Another possibility is to measure the mass shift for narrow vector mesons. Because of the long $c\tau$, only a few percent of these vector mesons will decay inside the nucleus, but these events will be easier to separate from the events of vector mesons decaying outside of the nucleus.

There are no data for ϕ-meson photoproduction off nuclei in the $A(\gamma, e^+e^-)$ reaction. It has been predicted that the reduction in the ϕ-meson mass is dependent

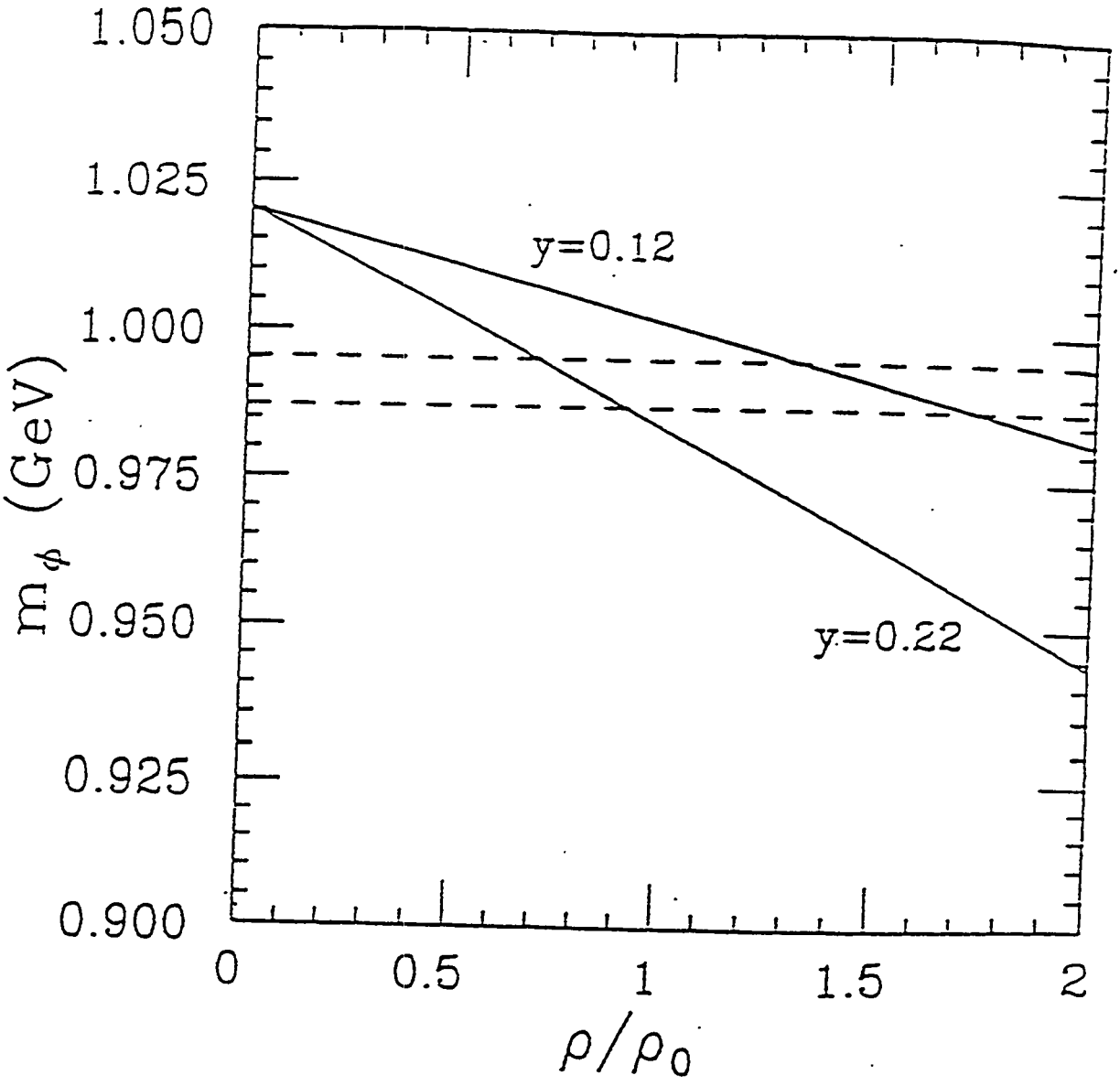


Fig.1.
ϕ-meson mass with two typical values of y (the strangeness content in the nucleon). Dashed lines indicate the K^0K^0 and K^+K^- threshold at $\rho=0$ which are the main decay modes of ϕ.

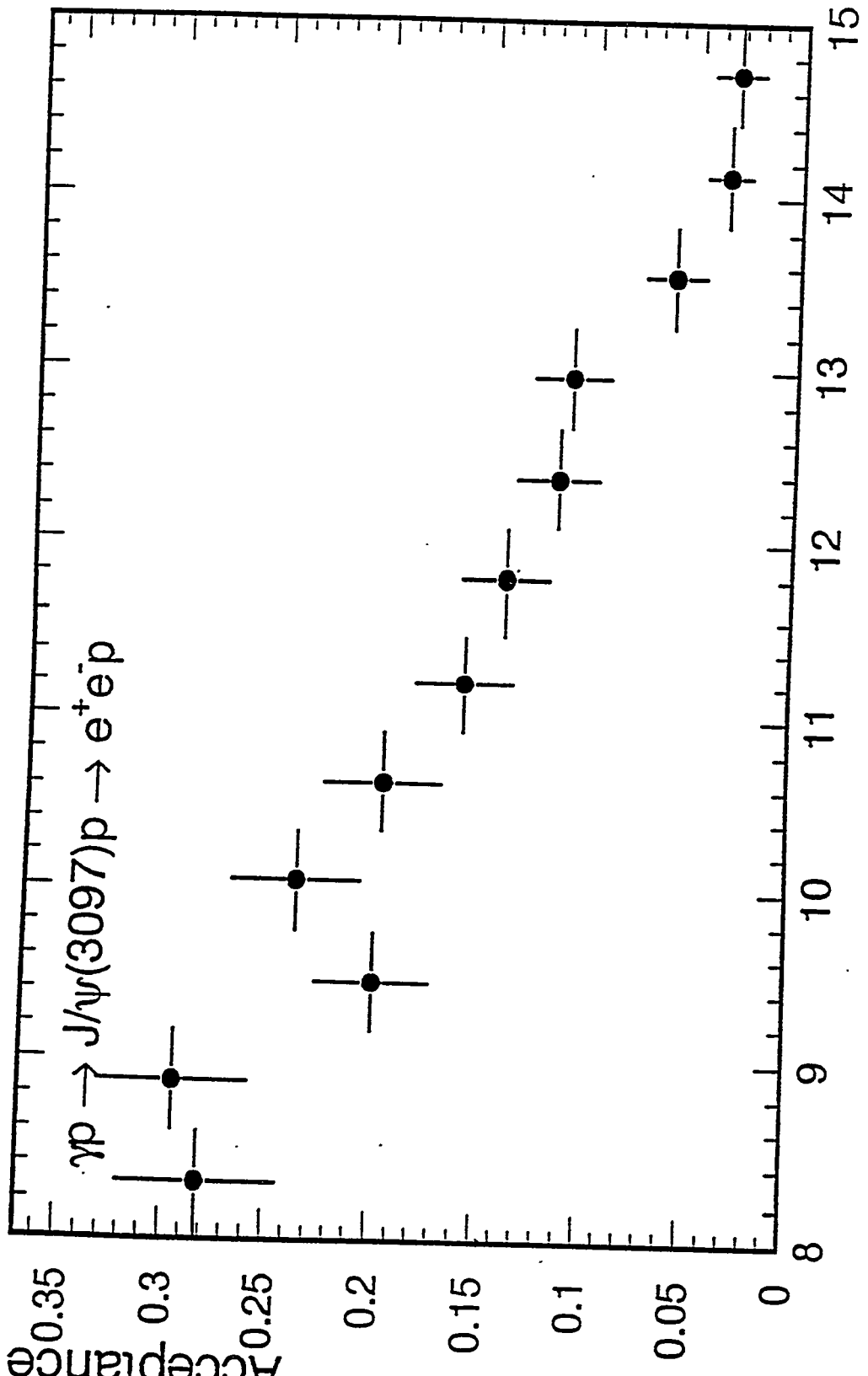


Fig.2. CLAS acceptance for $A(\gamma, J/\psi)X$ reaction.

on the amount of strangeness in the nucleon [5]. In Fig. 1 one can see the predicted mass shift for the ϕ-meson for two values of $y = \frac{2\langle s\bar{s}\rangle_N}{(\langle u\bar{u}\rangle_N + \langle d\bar{d}\rangle_N)}$.

The leptonic decays of vector mesons are the only way to measure the mass shift of vector mesons, because the hadronic decay mode is always disturbed in nuclear matter by final state interactions. We propose to measure the $A(\gamma, e^+e^-)A'$ reaction, which can be naturally triggered on by the CLAS detector. Electromagnetic calorimeter threshold, Cerenkov counter signal, ϕ symmetry, and p_t compensation define clear cuts for the separation of the reaction from the hadronic background. Small cross sections for secondary interactions of the incident photon and of the outgoing electrons with nuclear matter makes this reaction the ideal probe to test the properties of the dense central nuclear region without significant input and output distortions.

We propose to measure four nuclear targets simultaneously: deuterium, carbon, iron, and lead with a beam intensity of $5 \cdot 10^7$ tagged photons per second in the energy range 1.2-2.2 GeV ($E_o = 2.4$ GeV). Half magnetic field of the CLAS detector was found to be optimal for this photon energy range. Tagged photons are needed to isolate events with small energy transfer to the nucleus. To suppress the coherent vector meson production, which takes place essentially outside of the nucleus, one needs to detect the recoiling nucleon (proton or neutron).

Unfortunately, only one of the light vector mesons (ρ-meson) has a short $c\tau$ and will decay inside nucleus at CEBAF energies. That is why the measurements of the photoproduction of radially excited vector mesons ($\omega'(1390)$, $\rho'(1450)$, $\omega"(1600)$, $\phi'(1680)$, and $\rho"(1700)$) can be even more interesting task, because all of these vector mesons have a short $c\tau$ (about 1 fm, see Tab.1) and the low cross section of their production is compensated by a higher branching ratio for the e^+e^- decay. The optimal electron energy for the tagged photons with the energy range $E_\gamma = 3 - 5.7$ GeV is $E_o = 6$ GeV. This energy fits the limit of the photon tagger of the CLAS detector.

Table 1. The Characteristics of the Radially Excited Vector Mesons

Vector meson	Mass, MeV	$c\tau$, fm	Seen decay mode
ω'	1394	0.86	$\rho\pi$
ρ'	1465	0.63	$2\pi, 4\pi, e^+e^-$
ω''	1594	1.97	$\rho\pi, \omega\pi\pi, e^+e^-$
ϕ'	1680	1.3	$K\bar{K}^*, K\bar{K}, e^+e^-, K\bar{K}\pi$
ρ''	1700	0.84	$\rho\pi\pi, 4\pi, 2\pi, K\bar{K}^*, \eta\rho, K\bar{K}, e^+e^-$
J/ψ	3097.	2326. e^+e^- (6%)	

The CLAS detector with full magnetic field is efficient for the $\gamma \to e^+e^-$ reaction up to 12 GeV. As an example the Monte-Carlo simulation of the J/ψ photoproduction was made. The acceptance for the J/ψ-mesons is of the order of 30% (Fig.2).

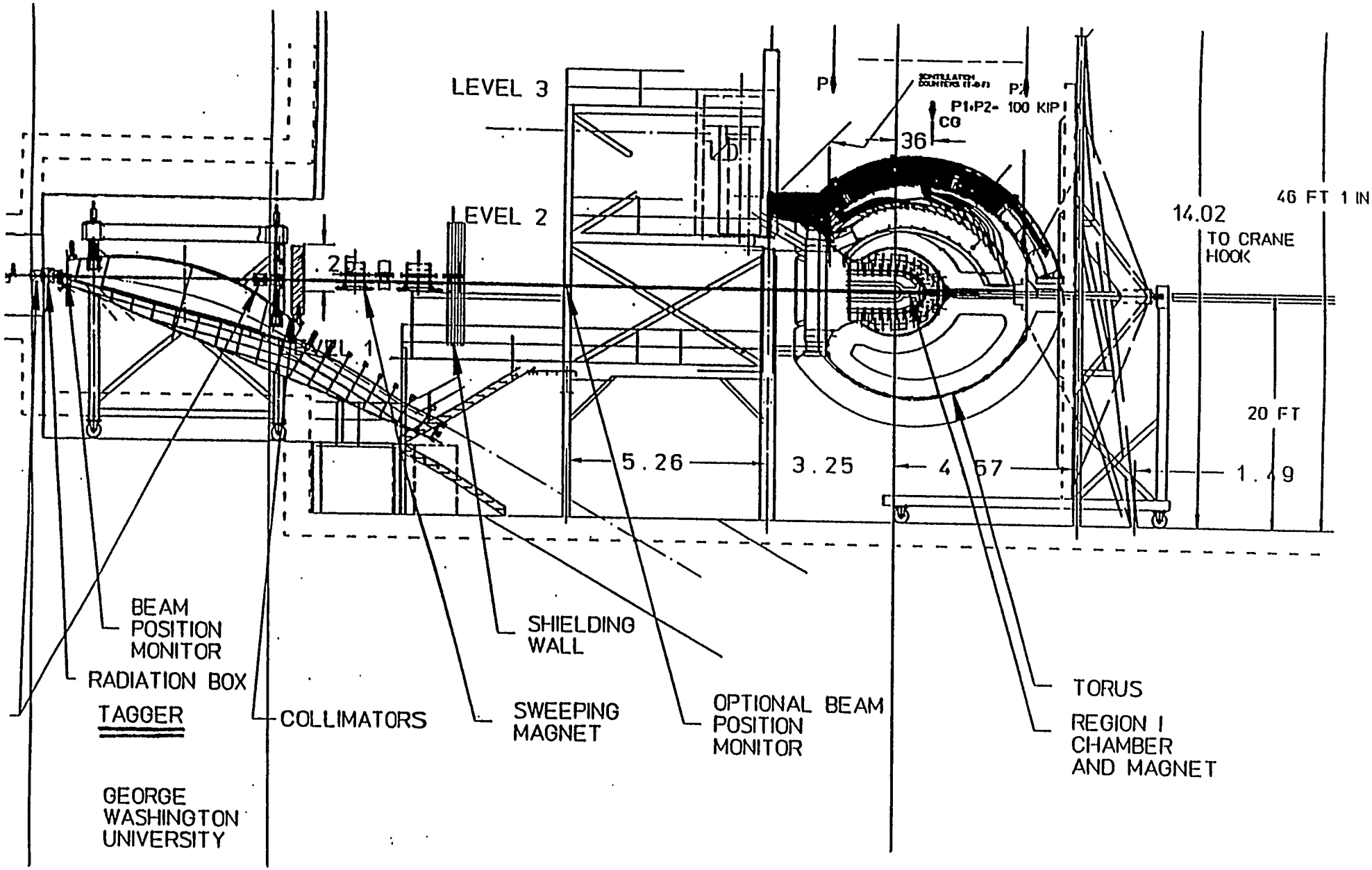


Fig.3. Tagger position in respect to the CLAS detector.

Taking into account the high branching ratio for the e^+e^- decay channel, the reaction becomes very sensitive to the J/ψ photoproduction off nuclei. Unfortunately, the mass shift physics cannot be expected (but can be measured) for the J/ψ mesons because of their very long life time (see Tab.1). But the other possible modifications of J/ψ-meson properties in nuclear matter can be successfully measured with the CLAS detector. One of the interesting measurements is the photoproduction of the J/ψ mesons below threshold. This physics can be investigated at CEBAF with an energy 8 GeV.

To make the tagged photon beam at the electron energy larger than 6 GeV, the photon tagger of the CLAS detector needs some modification (Fig.3): new path for the higher energy electrons should be made, the tagger itself should be moved deeper inside the alcove, and small superconducting magnet should be added to bend high energy beam into the existing beam dump. The tagger upgrade is the only upgrade of the CLAS detector which should be done to work at 12 GeV electron beam energy.

References

1) G.E. Brown and M. Rho, Phys. Rev. Lett. **66** (1991) 2720.

2) T.D. Cohen, R.J. Furnstahl, and D.K. Griegel, Phys. Rev. Lett. **66** (1991) 961.
E.G. Drukaev and E.M. Levin, Nucl. Phys. **A511** (1990) 679.

3) P.Y. Bertin and P.A.M. Guichon, Phys. Rev. **C42** (1990) 1133.

4) P.A.M. Guichon, Phys. Lett. **B200** (1988) 235.
P.A.M. Guichon, Nucl. Phys. **A497** (1989) 265c.

5) T. Hatsuda and Su H. Lee, Phys. Rev. **C46** (1992) R34.

COLOR TRANSPARENCY EFFECTS IN QUASI-ELASTIC NUCLEAR REACTIONS

GERALD A. MILLER
Physics Department FM-15, University of Washington
Seattle, Washington 98195, USA

ABSTRACT

Previous work on color transparency is reviewed briefly with an emphasis on aspects related to an upgrade of CEBAF.

1. Introduction

My CEBAF talk occurred shortly after submitting a lengthy review[1] on color transparency and the related issues of color fluctuations. Thus the reader is directed to that review for the details. Here I shall be concerned with presenting a brief outline and making a few summary points. The review contains many references, so the reference list here is short.

Usually initial and final state interactions cause absorptive effects which reduce the cross sections. If color transparency CT occurs, such interactions are suppressed at high enough Q^2. I discuss some well-known examples of possible reactions: (e,e'p), (p,pp), (e,e'pp) and (e,e'Δ^{++}). The experimental resolution must be good enough to insure that no extra pions are produced and the energy transfer to the recoil nuclear system is small ($\leq 70 - 100$ MeV). This requirement, stringent at high energies, has hindered progress in this field. New measurements at CEBAF and its higher energy version would be of high interest.

CT requires the production of a point-like configuration PLC in two-body reactions. Such PLC do not interact with the residual nucleus. However, even if a PLC is formed, it will expand as it moves through the nucleus[2-4]. One can express expansion effects in both quark and in hadronic bases. Such effects must be included in any realistic estimate of color transparency effects.

The CT idea is based on: small short-lived color singlet objects are produced in elastic hadronic reactions at high momentum transfer Q^2 (Sect. 2). Such objects have small interactions with nucleons. The small system is not an eigenstate so, unless its energy is very high, it expands and interacts as it moves through the nucleus, Sect. 3. In addition, careful calculations including various effects present in ordinary nuclear reactions are necessary, Sect. 4. A summary of the implications of color transparency for the proposal of extending CEBAF to higher energies is given in Sect. 5.

2. Is a small system made?

Perhaps the most interesting question is whether or not a small system is made in a high Q^2 hadronic exclusive process. The present postulate is that at high Q^2,

the matrix elements are dominated by components or configurations that behave as of smaller than average size. Such small-sized configurations or wave packets have been termed point-like configurations PLC.

If one considers asymptotically large values of Q^2, perturbative QCD holds and PLC are produced[6,7]. Eloquent criticisms of early pQCD calculations were put forward by Radyushkin[8] and Isgur and Lewellyn Smith[9].

But the pQCD arguments and the criticisms thereof were not complete because one must investigate the possible role of low momentum (soft) long wavelength gluons that are radiated as the colored quarks are accelerated. The effects of such radiation can be included via a form factor similar to that introduced by Sudakov, which decreases the probability for elastic scattering of a free fermion. However, for a color singlet system, the gluon radiation contributions cancel if the quarks and gluons making up the system are closely separated. Then significant contributions to the elastic form factor occur mainly for configurations of small size. The so-called Sudakov effects were known early on but numerical evaluations did not occur until recently with the work of Botts, Li and Sterman[10–13] and now others.

So far we have discussed pQCD calculations. But if one is interested in seeing how color transparency effects grow as Q^2 is increased from low values it is necessary to see if non-perturbative calculations also admit a PLC. Several different models have been examined using a new numerical criterion[14,15]. The result is that the form factor is dominated by PLC within many non-perturbative models. Furthermore, these effects set in at relatively low values of Q^2.

3. Time development

Suppose a *PLC* is produced in the interior of the nucleus. Any non-eigenstate undergoes time development. Here expansion occurs because the starting system is defined to be small. This expansion has been found to be a vital effect for intermediate energies, P_{lab} less than about 20 GeV/c.

We are concerned here with time development in nuclear quasielastic reactions. Consider the (e,e'p) reaction. The virtual photon is absorbed by a proton creating a high momentum object which is ejected from the nucleus. The old fashioned approach is to treat the ejectile as proton. Then the final state interactions are governed by the optical potential U^{opt}. If the proton wave function is computed from U^{opt}, the proton wave is said to be distorted (from the plane wave approximation). The use of such a wave function in computing cross sections is called the distorted wave impulse approximation DWIA, where the "impulse" refers to the use of the free nucleon-nucleon cross section.

But if the ejected object is a PLC, using U^{opt} is not appropriate. On the other hand, the ejectile expands as it moves through the nucleus, so that one can not simply neglect the soft final state interactions. The need to include this expansion was recognized by Farrar et al.[2] who argued that the square of the transverse size (and therefore the forward scattering amplitude) is roughly proportional to the distance travelled Z from the point of hard interaction where the PLC is formed.

The time development of the PLC can also be obtained by modeling the ejectile-nucleus interaction as $\hat{U} = -i\sigma(b^2)\rho(R)$, where b^2 represents the transverse separation of the quarks and $\rho(R)$ is the nuclear density at a distance R from the nuclear center. Then one can assume a baryonic basis and compute the relevant matrix elements of $\sigma(b^2)$. Jennings and Miller[3,4] solved the Lippman-Schwinger equation using an exponentiating procedure. Greenberg and Miller[5] showed that exponentiation is often a very accurate approximation. A more elaborate approach was taken later[16] by using measured matrix elements for deep inelastic scattering and diffractive dissociation. In this case, an approximate linear growth of the PLC cross section with distance is obtained.

Still another approach involves treating the baryon-nucleon amplitude in terms of a finite number of baryonic states. Then the baryon-nucleon T-matrix can be represented as an N by N matrix. The eigenvalues of such a matrix are an example of the Good-Walker diffractive eigenvalues[17]. The absence of interactions required for complete color transparency can only be obtained if the T-matrix has at least one state of eigenvalue 0, the PLC[18], but several different papers use two state models without satisfying this condition.

4. Relevant data

It is natural to consider the (e,e'p) and (p,pp) processes for color transparency searches. The first published experiment aimed at color transparency was the BNL (p,pp) work of Carroll *et al.*[19]. The only other one published is the SLAC (e,e'p) NE18 experiment[20]. We discuss each.

4.1. The BNL (p,pp) experiment

Proton beams of momenta p_L were 6, 10 and 12 GeV/c aimed at a target consisting of CH_2 interleaved with nuclei. The experimental setup used was that for proton hydrogen elastic scattering at a center of mass angle of 90°. For the hydrogen target, identifying an elastic scattering event requires detecting the outgoing momentum of one proton and the angle of the other. This is not sufficient for nuclear scattering because of the Fermi motion of the bound proton. However, information from veto counters was used to suppress inelastic events.

The data were originally plotted with an effective beam momentum, P_{eff}. It is better to use -k_z, the component of the momentum of the struck nucleon calculated in the plane wave impulse approximation. The z-axis is defined by the beam direction. The DWIA describes similar data at intermediate energies of E_p =1 GeV with accuracy of better than 20%. However the BNL data are considerably above the DWIA results, see Figs. 9 and 10 of Ref. [1].

The observed large value of the ratio of the cross section to its value in Born approximation indicated the presence of a large transparency effect, but the apparent drop at 12 GeV/c caused considerable discussion.[21,22] The color transparency models which include expansion effects naturally produce an increase of the transparency

consistent with the one observed in the BNL experiment at 6 and 10 GeV/c.

The possible nuclear results depend on the pp elastic scattering data. The energy dependence of the 90° angular distribution is of the form of $1/s^{10}$ R(s) where R(s) oscillates between 1 and 3 over the energy range of the BNL experiment. Ralston and Pire[22], suggested that the energy dependence is caused by an interference between an amplitude which produces a PLC, and a soft one which involves a large or blob-like configuration BLC. Another mechanism is that of Brodsky and de Teramond.[21] It is natural to discuss high Q^2 elastic proton-proton scattering in terms of configurations of different sizes. Separating the contributing configurations into two, a PLC and a BLC is only a simple first step.

Effects of the Fermi motion in treating the expansion process were evaluated[23,24,25], and big numerical effects were obtained. The result was that it became possible to construct a model[26] which is able to describe BNL data at all energies. The solid curves of Fig. 10 of Ref. [1] show the full calculation of Ref. [26] including the Ralston-Pire intereference effect. Keeping the experimental uncertainties in mind, the agreement between theory and experiment is rather good.

4.2. The SLAC (e,e'p) experiment

If color transparency effects observed at BNL are real they should be manifest in reactions other than (p,pp). Thus the recent measurement of the (e,e'p) reaction made at SLAC[20] and the possibility of future work at CEBAF are very exciting. The NE18 collaboration measured cross sections for ^{12}C, Fe and Ag targets for momentum transfers Q^2 of 1, 3, 5 and 6.8 GeV^2. We quote results presented recently[20] for ^{12}C. The available data and the related theory are shown in Fig. 11 of Ref. [1].

The NE-18 experiment has made a significant achievement in observing the quasi-elastic (e,ep') reaction at Q^2 between 1 and 7 GeV^2. One is now faced with the task of assessing the data. The results of Ref. [20] are that no significant rise of the transparency with Q^2 is seen. Early predictions depended on the unknown expansion rate. This is still unknown but is now better constrained by the (p,pp) data. One is now in a much better position to ask for the SLAC experiment: how large can one expect CT effects to be? One way to see is to compare the data with DWIA calculations, another way is to use models consistent with the BNL data to compute CT effects for the (e,e'p) reaction.

Relevant DWIA calculations must satisfy certain criteria: (1) compute the relevant observable T(A) according to the experimental acceptance; (2) use nuclear wave functions which reproduce the nuclear density and spectral function; (3) include the energy dependence of σ. Calculations satisfying these criteria are shown in Fig. 11 of Ref. [1] along with calculations including color transparency effects consistent with the BNL results.

The net result is that calculations which predict substantial color transparency effects for the (p,pp) reaction do not predict much color transparency in the regime of Q^2 available to the NE18 experiment. The (e,e'p) reaction is inherently simpler than the (p,pp) reaction so it is imperative to push the (e,e'p) measurements to

higher values of Q^2, say up to 12 or 15 GeV^2. Observing substantial effects would be possible.[16]

4.3. Rescattering vs. time development

The problem in looking for CT effects in experiments at Q^2 from about one to a few GeV^2 is that the assumed *PLC* expands rapidly while propagating through the nucleus. To observe CT at intermediate values of Q^2 it is necessary to suppress this expansion. If one studies a process where the produced system can **only** be produced by an interaction in the final state, a double scattering event, then the color coherent effects would be manifest as a decrease of the probability for final-state interactions with increasing Q^2. One could then observe an effect decreasing from the value expected without CT (Glauber-value) to zero. Thus, the measured cross section is to be compared with a vanishing quantity so that the relevant ratio of cross sections runs from 1 to infinity. The first calculations[27] show that substantial CT effects are observable in the (e,e'pp) reactions on $^{4,3}He$ targets. Such experiments can be done at CEBAF. It would be important to do these experiments at low Q^2, say 4 to 6 GeV^2 to establish the effects and then to confirm them by going to higher values of Q^2.

Another idea involves pionic degrees of freedom. Probing a nucleon at intermediate momentum transfers (Q^2 about a few GeV^2) may produce a small system without a pion cloud[14,15]. This cloud-stripping effect can be studied by considering processes that require a pion exchange to proceed. An example is the quasielastic production of the Δ^{++} in electron scattering - the $(e, e'\Delta^{++})$ reaction. The initial singly charged object is knocked out of the nucleus by the virtual photon and converts to a Δ^{++} by emitting or absorbing a charged pion. But pionic coupling to small-sized systems is suppressed, so this cross section for quasielastic production of Δ^{++}'s should fall faster with increasing Q^2 than the predictions of conventional theories. Calculations are now in progress [28]. This could be a new kind of transparency that involves pions, so the name "chiral transparency"[14] was invoked.

5. Spin Dependent Color Transparency

Bill Greenberg's thesis included a detailed study of effects which can be observed by measuring the polarization of the outgoing proton. I will discuss the principle results of this work[29].

Our procedure was to treat the vector nature of the photon and the spin of the proton and photon explicitly by describing the initial bound proton and the ejected wave packet as four-component Dirac spinors. Such effects, ignored in previous calculations, yield several results.

(1) The use of Dirac based optical potentials in the "standard calculation" (ignoring CT) leads to smaller cross sections than predicted before. This model dependence, which arises from the different radial form used in the optical potential, means that one must be wary of claims that color transparency can be observed by finding small

differences between data and the magnitude of a DWIA prediction.

(2) The normal component of the ejectile polarization, which vanishes in the limit of full CT, is found to approach zero very slowly as the energy increases. Finding color transparency by measuring the polarization of the outgoing proton will be very difficult at *any* forseeable energy.

(3) The presence of the $1H_{11/2}$ orbital, causes the normal-transverse response in ^{208}Pb to be sensitive to color transparency effects at quite low momentum transfers $\sim$ 1 GeV/c. There is a similar effect in ^{120}Sn.

(4) The four-component nature of our formalism, allows us to determine that our calculations are roughly consistent with current conservation, except when the momentum k_z of the struck nucleon is greater than about 150 MeV/c. Here the z direction is that of the virtual photon. More generally, we argue that attempts to enhance color transparency effects by measuring cross sections for large values of k_z are risky. One needs to check that the relevant predictions satisfy the current conservation.

6. Implications for CEBAF at higher energy

Studying the (e,e'p) reaction at high Q^2 represents an excellent opportunity to observe color transparency. One should not be discouraged by the NE18 results. Calculations which predict substantial color transparency effects for the (p,pp) reaction do not predict much color transparency in the regime of Q^2 available to the NE18 experiment. The (e,e'p) reaction is inherently simpler than the (p,pp) reaction so it is imperative to push the (e,e'p) measurments to higher values of Q^2, say up to 12 or 15 GeV^2. If the effect is not seen at 15 GeV^2, it can regarded as inconsequential.

Using double scattering reactions (e,e'pp) and (e,e'Δ^{++}) would allow a measurement of color transparency effects at modest values of Q^2, from 1 or 2 up to about 6 GeV^2. It would be important to do these experiments to establish the effects and then to confirm them by going to higher values of Q^2.

Observing color transparency in (e,e'$\vec{p}$) measurements would be very difficult at any momentum transfer. Such measurements are sensitive to interesting nuclear structure effects, but there is no urgent need to do these at higher energies.

7. Acknowledgments

The work discussed in my oral CEBAF presentation was done in collaboration with K.S. Egiyan, L. Frankfurt, W.R. Greenberg, B.K. Jennings, M.M. Sargsyan, and M.Strikman.

This work was supported in part by the USDOE.

8. References

1. L.L. Frankfurt, G.A. Miller and M. Strikman, "The Geometrical Optics of

Coherent High Energy Processes", U. Wa preprint DOE/ER/40427-06-N94; in press *Ann. Rev. Nucl. Part. Sci.* **44** (1994).
2. G.R. Farrar, H. Liu, L.L. Frankfurt & M.I. Strikman, *Phys. Rev. Lett.* **61** (1988) 686.
3. B.K. Jennings and G.A. Miller, *Phys. Lett.* **B236** (1990) 209.
4. B.K. Jennings and G.A. Miller, *Phys. Rev.* **D44** (1991) 692.
5. W.R. Greenberg and G.A. Miller, *Phys. Rev.* **D47** (1993) 1865.
6. S.J. Brodsky, G.P. Lepage, *Phys. Rev.* **D** (1980) 2157.
7. A.H. Mueller in *Proceedings of Seventeenth rencontre de Moriond, 1982* ed. J Tran Thanh Van (Editions Frontieres, Gif-sur-Yvette, France, 1982) Vol. I, p13.
8. G.P. Korchemski, A.V. Radyushkin, *Sov. J. Nucl. Phys.* **45** (1987) 910 and refs. therein.
9. N. Isgur and C.H. Llewellyn-Smith, *Phys. Rev. Lett.* **52** (1984) 1080 *Phys. Lett.* **B217** (1989) 535.
10. J. Botts and G. Sterman, *Nucl. Phys.* **B325** (1989) 62.
11. H-N Li *Phys. Rev.* **D48** (1993) 4243.
12. J. Botts and G. Sterman, *Nucl. Phys.* **B325**, 62 (1989).
13. H.-N. Li and G. Sterman, *Nucl. Phys.* **B381** (1992) 129.
14. L. Frankfurt, G.A. Miller, and M. Strikman, *Comments on Nuclear and Particle Physics* **21** (1992) 1.
15. L. Frankfurt, G.A. Miller, and M.Strikman, *Nucl. Phys.* **A555** (1993) 752.
16. B.K. Jennings and G.A. Miller, *Phys. Rev. Lett.* **70** (1992) 3619; *Phys. Lett.* **B274** (1992) 442.
17. M.L. Good and W.D. Walker, *Phys. Rev.* **120**, (1960) 1857.
18. L. Frankfurt, W. R. Greenberg, G. A. Miller and M. Strikman, *Phys. Rev.* **C46** (1992) 2547.
19. A.S. Carroll et al. *Phys. Rev. Lett.* **61** (1988) 1698.
20. N.C.R. Makins et. al. *Phys. Rev. Lett.* **72** (1994) 1986.
21. S.J. Brodsky & G.F. De Teramond, *Phys. Rev. Lett.* **60** (1988) 1924.
22. J.P. Ralston and B. Pire, *Phys. Rev. Lett.* **61** (1988) 1823.
23. S. Boffi, D.E. Kharzeev *Phys. Lett.* **B305** (1993) 1; *Nucl.Phys.* **A565** (1993) 767; **B325** (1994) 294.
24. B.K. Jennings and B. Kopeliovich, *Phys. Rev. Lett.* **70** (1993) 3384.
25. S. Gardner "Color transparency in (e,e'p) and the electroproduction of resonances" IU-NTC-92-27, Aug 1992.
26. B.K. Jennings and G.A. Miller, *Phys. Lett.* **B318** (1993) 7.
27. K.S. Egiyan, L.L. Frankfurt, W.R. Greenberg, G.A. Miller, M.M. Sargsyan, M.I. Strikman, Searching for Color Coherence Effects Via Double Scattering Events, 1993 preprint, in press *Nucl. Phys* **A**.
28. L. Frankfurt, T.-S.H. Lee, G. A. Miller and M.Strikman, in progress.
29. W.R. Greenberg and G.A. Miller, *Phys. Rev.* **C49** (1994) 2747; Erratum Phys. Rev. C; W.R. Greenberg, 1993 U. Wa. Ph. D. thesis. "Color Transparency in Quasi-Elastic (e,e'p) Reactions at Large Momentum Transfers"

Exclusive experiment on nuclei with backward emitted particles by electron-nucleus collision in ~10 GeV energy range

T. Saito and F. Takagi*

Laboratory of Nuclear Science, Tohoku University, Sendai 982, Japan
*Department of Physics, Tohoku University, Sendai 980, Japan

§1. Introduction

Since the evidence of strong cross section in proton-nucleus backward scattering was presented in the early of 1970 years, this phenomena have been interested from the point of view to be related to information on the short range correlation between nucleons or on high momentum components of the wave function of the nucleus.

In the analysis of the first experiment on protons from the carbon target under bombardment by 1.5-5.7 GeV protons, indications are found of an effect of analogous to scaling in high-energy interactions of elementary particles with protons.[1] Moreover it is found that the function $f(p^2)/\sigma_{tot}$, which describes the spectra of the protons and deuterons emitted backward from nuclei in the laboratory system, does not depend on the energy and the type of the incident particle or on the atomic number of the target nucleus.[2] In the following experiments the spectra of the protons emitted from the nuclei C, Al, Ti, Cu, Cd and Pb were measured in the inclusive reactions with incident particles of negative pions (1.55-6.2 GeV/c) and protons (6.2-9.0 GeV/c).[3] The cross section f is described by

$$f = E/p^2\, d^2\sigma/dp\, d\Omega = C \exp(-Bp^2),$$

where p is the momentum of hadron. The function f depends linearly on the atomic weight A of the target nuclei. The slope parameter B is independent of the target nucleus and of the sort and energy of the bombarding particles. The invariant cross section $\rho = f/\sigma_{tot}$ is also described by exponential $A_0 \exp(-A_1 p^2)$. ρ becomes independent of energy at initial particle energies ≥ 1.5 GeV for C nucleus and ≥ 5 GeV for the heaviest of the investigated Pb nuclei.

Inclusive cross sections for the production of protons, deuterons, and tritons were measured at 180° in the proton-nucleus interaction at 600 MeV and 800 MeV.[4] The cross sections are well fitted by exponential. Extremely large d/p and t/p ratios and large A and q^2 dependence of the relative cross sections are observed. Also inclusive spectra and angular distribution of protons emitted backwards in the interaction of 640 MeV protons with C, Be,

Al, Cu, and Pb nucleus were measured.[5] Spectra are fairly described by exponential. The parameters A_0 and A_1 of the invariant cross section (ρ) depend strongly on A for light nuclei, but weakly for A > 30.

Invariant cross sections for the production of protons by 400 GeV protons were measured for the Li, Be, C, Al, Cu, and Ta nuclei.[6] From comparison with observed results at other energies, little change in the shape of the cross sections in going from 8 to 400 GeV incident proton energy. However the shape of the inclusive cross section does not appear to follow a strict exponential in the kinetic energy. There is little difference in the strong A dependence of the cross sections in going from 8 to 400 GeV in contrast to the less pronounced variation with A at lower energies. There is less dependence of the shape of the cross sections on A at 400 GeV than 0.8 or even 3 GeV, but a dependence appears to persist. Another backward production of protons, deuterons, tritons, ^{3}He, ^{4}He, and pions in the interaction of 400 GeV protons with the nuclei were measured.[7] The cross section appear to depart from a strictly exponential dependence on the kinetic energy T. The near equality of the cross sections at 8.5 GeV and 400 GeV argues strongly against a back scattering mechanism. The cross sections have been measured above the kinematics limit -dinucleon scatter... that two particle correlations alone cannot account for the shape of the cross sections. A large A dependence persists at 400 GeV. It is borne out by the data that the ratio t/^{3}He should be proportional to N/Z. Also backward particles from proton-nucleus interactions using 200 GeV protons[8] and 28.5 GeV/c protons[9] were measured. In the case charged pions produced at 180° in 0.8-4.9-GeV proton -nucleus collisions both the slopes of the energy spectra and the π^-/π^+ ratios increase rapidly with primary energy up to ~3-4 GeV, where limiting values appear to be reached.[10] The dependence on A also changes over the energy range. Backward pions at these energies do not obey the scaling law.

These cumulative interactions have been also investigated using leptons. Energy spectra of photoprotons and photodeuterons were measured using the maximum energies of 700 MeV and 1200 MeV bremsstrahlung interacting with nuclei of Li, Be, C, Si, Cu , Ta and Pb. The measured spectra were well described by exponential.[11] Backward proton production in antineutrino-neon charged current interactions were measured. [12, 13] The cross section was found to be in agreement with previous results from backward-proton events obtained using hadron and γ beams.

The inclusive spectra in the backward direction show the following peculiarities. The differential cross section in the relativistic invariant representation

$\rho = E/(\sigma_{tot} p^2) d^2\sigma/(d\Omega\, dp)$

is well reproduced by the dependence

$\rho = A_0 \exp(-A_1 p^2)$

where ρ is the so-called structure function, σ_{tot} is the total cross section of the hadron-nucleus interaction and $d^2\sigma/(d\Omega\, dp)$ is the inclusive differential cross section for the production of particles with a momentum p and a total energy E. The parameters A_0 and A_1 depend only weakly on the kind and the energy of incident hadrons as well as on the mass number A of target nuclei.

§ 2. Theoretical interpretation for the cumulative interaction

A large number of cumulative experiments, namely backward-proton (hadron) production from inclusive reaction have been performed to study the collective behavior of the nucleons in the nuclear target. Since the backward protons cannot originate from interactions on free stationary nucleons, they indicate the presence of nuclear effects in the scattering process.

Recently, Kanki, Kinoshita, Sumiyoshi and Takagi[14] reviewed on multiparticle production in particle and nuclear collisions. According to their review, models for cumulative production are classified two category of short range nature and of long range one.

2.1 Models with short-range correlation

a. Nucleonic Fermi Motion

In this model an incident hadron interacts with an intranuclear nucleon which is moving backward with large momentum. The crucial point is the behavior of the high momentum tail of the nucleon momentum distribution in a nucleus. Amado and Woloshin[15] confirmed that data of 400-600 MeV protons (Ref. 4) cannot be explained if one uses the momentum distribution with a Gaussian tail given by Fermi model. In order to explain the data they used an alternative distribution function which behaves like $\exp(-\gamma k)$ at large momentum k.

b. Short range few nucleon correlation with spectator mechanism

In this model an incident hadron interacts with a system consisting a few correlated nucleon. In this case, the spectator mechanism is important for cumulative production of nucleons and heavier nuclear fragments.[16] N nucleon correlations in a nucleus A are broken by the incident hadron releasing one nucleon in the backward direction. The momentum spectrum of fast backward protons should reflect directly the momentum distribution of the correlated nucleons. Data for nucleon momentum distribution against Bjorken x are desirable. Measurements of backward neutrons are also important.

c. Fluctuons or few nucleon cluster

Burov et al.[17] proposed the existence of nuclear density fluctuations (fluctuons) at short distances in order to explain cumulative pion production at 8.4 GeV/c. A fluctuon of order k

is a system consisting of k overlapping nucleons concentrated in a volume $V_\xi = 4\pi r_\xi^3/3$. Burov et al. fitted the data by using the fluctuons of order k = 2, 3, 4 with r_ξ = 0.5~0.7 fm.

2.2 Models with long range correlations

a. Fireballs or clusters

The short range correlated few nucleon system are heavy objects. Another possibility of a heavy object is consider to be formed by some long range correlations during the reaction process. The simplest possibility is the fireball,[18] which may be produced as an intermediate state of h A collisions. The fireball model reproduces well both the p and θ dependence of observed cross sections but lacks the predictive power on the absolute magnitude of the cross sections and hence on the A-dependence.

b. Hot spots

Stelte and Weiner[19] analyze the cumulative effect in terms of a hot spot drifting in a nucleus. In this model, when an incident particle collide with a nucleus, an amount of the incident energy is deposited in a small region near the backward surface of the target nucleus. The small region is locally heated becoming a pre-equilibrium state (a hot spot) and at the same time the hot spot dissipates its energy in the surrounding nuclear medium. A good fit to 400 GeV data was obtained. Though this model may have some relevance to cumulative production in sub-GeV region, it may not be applicable to higher energies because the model seems incompatible with the participant-spectator picture or the tube picture of nondiffractive inelastic h A collisions at high energy.

c. Quark-parton models with collective tube

A group of nucleons contained in a tube region of a target nucleus is supposed to behave collectively and this collectivity may be due to a kind of long range correlations intimately related to quark confinement. A heavy object responsible for cumulative production is identified with the nuclear tube with mass $A_e m_N$ where A_e is the number of nucleons contained in the tube. A model for fragmentation of the tube is needed in order to calculate the cross sections of cumulative productions. In calculation the parton recombination model was used to describe the fragmentation of a collective tube which consists of $3A_e$ valence quarks, the associated sea quark-antiquark pairs and gluons. Calculations[20] predict that the absolute magnitude of the cross section for cumulative production increases considerably as E_{lab} increase from 8.4 GeV to several hundreds GeV.

d. Color flux tube

Kopeliovich and Niedermayer[21] proposed a following model. There may be such a process in which many-gluon-exchange takes place when an incident hadron h collides with a nucleus A producing "an internally color -excited" state A_e^* in the nucleus and a possibly excited color singlet hadron h*. If a color flux tube is stretched between many nucleons lying

along the beam direction, the nucleon on the fore end of the flux tube will be accelerated backward by the long range confining force and may be eventually emitted in the backward direction if color flux breaking takes place at an appropriate moment. They calculated the cross sections for h+d→p(180°) +X.

§3. Proposed experiment on nuclei with backward emitted particles by electron-nucleus collision in ~10 GeV energy range

Previous experiments are limited to the inclusive reaction. Exclusive reactions are powerful to investigate nuclear correlation such as short range correlation. Deep inelastic electron-nucleus collisions are unique probes in which electrons are pointlike particles with no structure and their interactions with hadrons or quarks are well described by electro-magnetic interaction. Thus one expects that electron-nuclear collision provides a particularly definite information for the mechanism of the cumulative reaction.

The subjects to be measured by the exclusive reaction at backward.

i) Two or three nucleons (pions) knock out
   momentum distribution of emitted particles
   angular correlation
   target mass dependence of the cross section
   incident energies dependence (1~10 GeV) of the cross section

ii) Cluster knock out
   momentum distribution of emitted particles
   angular distribution
   target mass dependence of the cross section
   incident energies dependence (1~10 GeV) of the cross section

iii) Multi-particles production
   same as ii)

Also it is important to take a data for the inclusive reaction and compare with previous hadron (lepton and γ) data.

References:

1) Yu. D. Bayukov et al., Sov. J. Nucl. Phys. 18, 639 (1974).
2) Yu. D. Bayukov et al., Sov. J. Nucl. Phys. 19, 648 (1974).
3) N. A. Burgov et al., Sov. J. Nucl. Phys. 24, 620 (1976).
4) S. Frankel et al., Phys. Rev. Rett. 36, 642 (1976).
5) V.I. Komarov et al., Phys. Lett. 69B, 37 (1977).

6) Y. D. Bayukov et al., Phys. Rev. C20, 764 (1979).
7) Y. D. Bayukov et al., Phys. Lett. 85B, 315 (1979).
8) G. Fujioka et al., J. Phys. Soc. Japan 39, 1131 (1975).
9) T. Hayashino et al., Lett. Nuovo Cim. 16, 71 (1976).
10) L. S. Schroeder et al., Phys. Rev. Lett. 43, 1787 (1979).
11) Yu. P. Antuf'ev et al., Sov. J. Nucl. Phys. 13, 265 (1971).
12) J. P. Berge et al., Phys. Rev. D18, 1367 (1978).
13) V. I. Efremenko et al., Phys. Rev. D22, 2581 (1980).
14) T. Kanki et al., Prog. Theo. Phys. Suppl. 97B (1989), references therein.
15) R. D. Amado and R. M. Woloshyn, Phys. Rev. Lett. 36, 1435 (1976).
16) For example, L.L. Frankfurt and M. I. Strikman, Phys. Lett. 69B, 93 (1977).
17) V. V. Burov et al., Phys. Lett. 67B, 46 (1977).
18) D. V. Anchishkin et al., Phys. Lett. 108B, 47 (1982).
19) N. Stele and R. Weiner, Phys. Lett. 103B, 275 (1981).
20) F. Takagi, Phys. Rev. D19, 2612 (1979); G. Berlad et al., Phys. Rev. D22, 1547 (1980).
21) B. Z. Kopeliovich and F. Niedermayer, Phys. Lett. 117B, 101 (1982).

EVIDENCE FOR SHORT RANGE CORRELATIONS FROM High Q^2 (e, e') REACTIONS

M. I. Strikman
Pennsylvania State University, University Park, PA 16802, USA,
also at the St.Petersburg Nuclear Physics Institute, Russia

L. L. Frankfurt
Tel Aviv University, Ramat Aviv 69978, Israel, Tel Aviv, Israel,
on leave of absence from the St.Petersburg Nuclear Physics Institute, Russia

D. B. Day
Institute of Nuclear and Particle Physics,
University of Virginia, Charlottesville, VA, USA

M. M. Sargsyan
Tel Aviv University, Ramat Aviv 69978, Israel, Tel Aviv, Israel,
also at the Yerevan Physics Institute, Yerevan 375036, Armenia

For many years now short-range correlations (SRC) in nuclei have been considered as an essential feature of the nuclear wave function.

At high energy $(e, e\prime)$ reactions, where $Q^2 > 1\ (GeV/c)^2$, $x = Q^2/2mq_0 > 1$ and $1\ GeV > q_0 > 300 \sim 400\ MeV$ the scattering from low momentum nucleons is kinematically suppressed and therefore the evidence of SRC expected to be more prominent. These reactions have been intensively investigated during the last decade or so at SLAC on both light and heavy nuclei [?,?,?,?,?]. The above kinematics allows one to compute the cross section through the processes local in space. To explain this we analyse the representation of the cross section as a Fourier transform of the commutator of electromagnetic currents and see that the major contribution in the cross section is given by the region of integration where

$$y_+(y_0 + y_3) \sim \frac{1}{q_-} < 1fm \ , \ y_-(y_0 - y_3) \sim \frac{1}{q_+} < 0.2fm \ , \ y_t^2 < \frac{1}{Q^2}.$$

This and analysis of the Green function of the struck nucleon indicate that significant FSI of the struck nucleon would occur only with nucleons which are very close to it[?]. It is easy to check that for our particular kinematics, the struck nucleon and its nearest neighbors in the initial state have large and comparable momenta in the final state while the rest of the nucleons which were at large distances from the struck nucleon in the initial state end up with small momenta [?,?].

Under these conditions the nonrelativistic spectral function containing the one

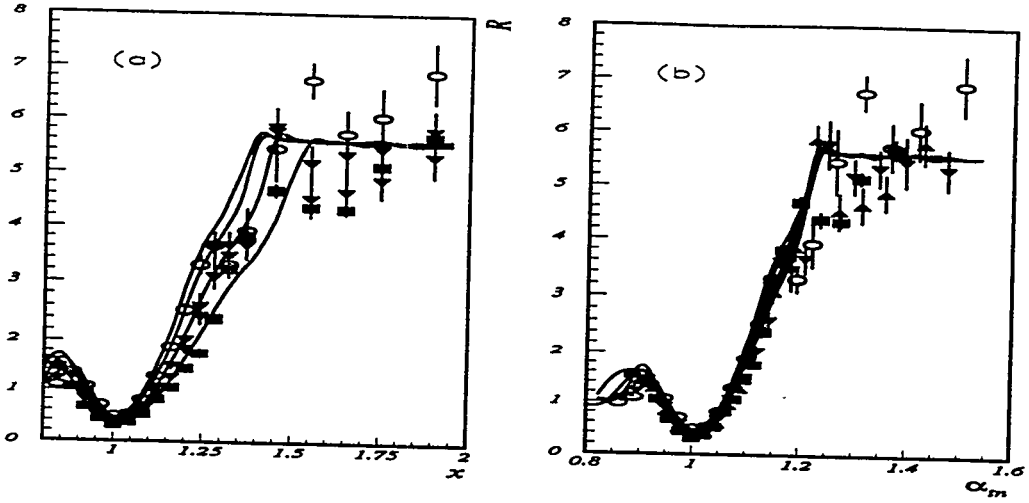


Fig. 1. Ratio $R = \frac{2}{A}\frac{\sigma_{Fe}(x,Q^2)}{\sigma_D(x,Q^2)}$ for different Q^2 ($(1.2 \div 2.9)(GeV/c)^2$).

nucleon with large momentum can be represented as the sum which includes of few (2, 3 ...) nucleon correlations. Therefore if we construct the ratio of the (e,e') cross sections as: $\frac{\sigma_{eA}}{\sigma_{ej}}\mid_{j-1<x\leq j}$, we expect that these ratios will reveal the scaling behaviour and FSI in large extent will be cancel out. In particular case one consider the relevance for scaling relations for contribution of two - nucleon correlation and use the prediction of few - nucleon correlation model:

$$\frac{2}{A}\frac{\sigma_A(x,Q^2)}{\sigma_D(x,Q^2)} = a_2(A)\mid_{1<x\leq 2}. \qquad (1)$$

To check this prediction experimentally we use the data for the deuteron and heavier nuclei which cover the (x,Q^2) range of interest here. As no single experiment includes both the deuteron and heavy nuclei at the same values of (x,Q^2) necessary to form the ratios in Eq. (1) we use the model independent procedure to fit the deuteron data to the kinematical region of heavy nuclei, which were obtained at identical energies and angles. Most of the deuteron Q^2 dependence is due to the elastic form factor and can be accounted for by an impulse model calculation of the cross section. We account to this dependence using the y-scaling model. One can see in Fig. 1a, where the ratios of $\frac{2}{A}\frac{\sigma^A(x,Q^2)}{\sigma^D(x,Q^2)}$ for ^{56}Fe, at four values of Q^2 (the similar ratios we get for ^3He, ^4He, ^{12}C , ^{27}Al , ^{197}Au) are presented, that Eq. (1) is well satisfied by the data.

The argument presented above in favor of Eqs. (1) was implicitly nonrelativistic.

But the kinematics under discussion are relativistic, so it is necessary to elaborate. It is well known that the cross sections of hard high–energy processes are expressed through the light–cone (LC) wave function of nuclei. Introducing the LC variables for the virtual photon and the struck nucleon, $q_{\pm} = q_0 \pm q_3$, $\alpha \equiv \frac{Ap_-^{int}}{p_-^A}$, $p_t \equiv p_t^{int} = -p_t^{rec}$ we were able to check that already at $Q^2 \sim 2-3\ (GeV/c)^2$ α does not depend on (m^{rec}, p_t). Consequently, one can integrate over the recoil mass at fixed α in the expression for the total cross section, which then can be expressed only in terms of α. In formal terms this result means that the cross section is expressed through the light-cone nucleon density matrix $\rho_A^N(\alpha, p_t)$ and therefore at large Q^2 and $x < 2$ this leads to the α_{tn} dependence for the ratio of cross sections in Eq. (1). Here α_{tn} is the light-cone variable for the interacting nucleon belonging to the correlated nucleon pair:

$$\alpha_{tn} = 2 - \frac{q_- + 2m}{2m}\left(1 + \frac{\sqrt{W^2 - 4m^2}}{W}\right). \qquad (2)$$

W is the invariant mass of the two nucleon system ($W^2 = -Q^- + 4q_0m + 4m^2$). This relation is reasonably satisfied by the data, as shown in Fig. 1b where we present σ_A/σ_D as a function of α_{tn} for ^{56}Fe.

Let us briefly comment on the utility of this analysis for the color transparency (CT) experiments. The idea that in the impulse approximation the ratio of the cross sections of $A(a, ap)$ and $D(a, ap)$ at fixed α integrated over p_t is equal to the ratio of the light-cone densities and therefore the off–shell effects are cancelled out to large extent. Therefore we can introduce the transparency as

$$T = \frac{\sigma^{(A(a,ap)}/\sigma^{D(a,ap)}\,|_{\alpha}}{\sigma^{A(e,e')}/\sigma^{D(e,e')}|_{x(\alpha)}},$$

where $x = \frac{Q^2}{2q_0m}$ can be calculated through $\alpha = \alpha_{tn}$ using Eq. (2). CT in this quantity may reveal itself at lower energies than for $(e, e'p)$ reactions in general, since uncertainties in the nuclear wave function are less important in this ratio.

CEBAF at higher energies would be in a unique position to check the scaling relations at $x < 2$ in more detail as well as to investigate their validity at $3 > x > 2$ where data currently are very limited.

It would be possible also to study the transition from the dominance of quasielastic

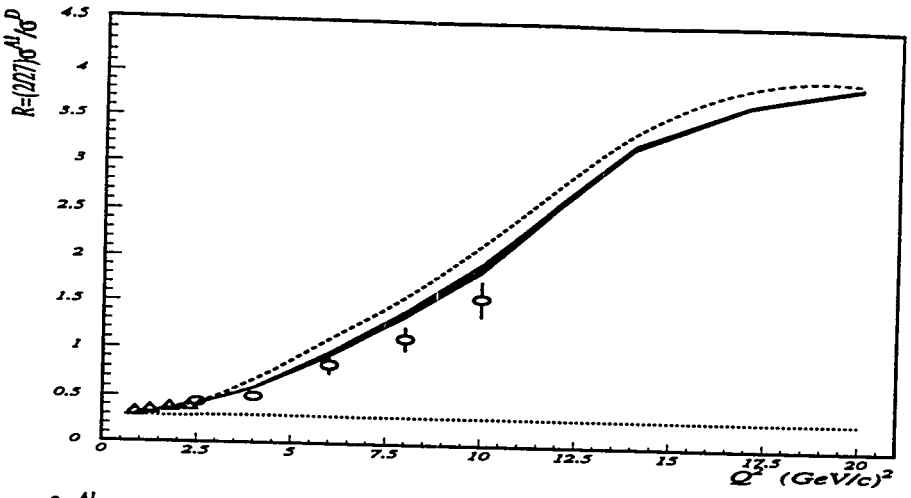


Fig. 2. $\frac{2\sigma^{Al}}{27\sigma^{D}}$ as a function of Q^2 for $x = 1$. Data from Refs.[?,?]. The hatched area a calculation including the inelastic channels and EMC effects with model uncertainties. The dashed line - same as above without EMC effect. The dotted line - only quasielastic scattering is considered.

reactions to the dominance of inelastic (deep inelastic) final states. In this region the ratio $\frac{\sigma^{A(e,e')}}{\sigma^{D(e,e')}}|_{x=const\geq 1}$ should substantially increase with Q^2. Current data support such a rise, see Fig.2, but they are clearly insufficient.

It is important to extend the measurements on the deuteron to the region of large $x > 1$ and $Q^2 \geq 2(GeV/C)^2$. The existing data seem to support presence of the suppression of the cross section in this kinematics as expected due to suppression of point-like configurations in bound nucleons [?]. It is also necessary to compare the d(e,e') and d(e,e'p) cross sections in these kinematics.

If the incident energy of the order of 10 GeV is reached it would be possible to start mapping parton distributions in nuclei at $x > 1$. Such measurements require Q^2 in the range between 10 and 20 $(GeV/c)^2$. Indeed according to the estimations of Ref.[?] $Q^2 = 10\ (GeV/c)^2$ is minimal Q^2 where leading twist is dominant ($\geq 80\%$ of the cross section for $A \geq 4$). Also one needs measurements at least up to $Q^2 = 20(GeV/c)^2$ to prove experimentally that the leading twist indeed dominates. It is worth emphasizing that measurements in this kinematics could provide new insight into the origin of the EMC effect. In fact, the recently released BCDMS data [?] at $x \geq 1$ indicates that quark distribution at $x > 1$ is strongly suppressed as compared to the expectations of the naive Fermi motion models, though it is consistent with the predictions of the

color screening model of the EMC effect [?].

References

1. S. Rock, R.G. Arnold, P.Bosted, B.T. Chertok, B. A. Mecking, I. Schmidt, Z.M. Szalata, R. C. York, and R. Zdarko., *Phys. Rev. Lett.* **49** (1982) 1139.
2. R.G. Arnold, D. Benton, P. Bosted, *et al. Phys. Rev. Lett.* **61** (1988) 806.
3. S. Rock, R.G. Arnold, P.E. Bosted, B.T. Chertok, B.A. Mecking, I. Schmidt, Z.M. Szalata, R.C. York, and R. Zdarko,*SLAC-PUB-5239*(1991).
4. D. Day, J.S. McCarthy, I. Sick, R.G. Arnold, B.T. Chertok, S. Rock, Z.M. Szalata, F. Martin, B.A. Mecking, and G. Tamas, *Phys. Rev. Lett.* **43** (1979) 1143.
5. D. Day, J.S. McCarthy, Z.E. Meziani, R. Minehart, R. Sealock, *et al. Phys. Rev. Lett.* **59** (1987) 427, D. H. Potterveld, *Ph. D. Thesis.* California Institute of Technology, unpublished, 1989.
6. L. L. Frankfurt, M. M. Strikman, D. B. Day and M. M. Sargsyan, *Phys. Rev.*, **C48** (1993) 2451.
7. L.L. Frankfurt and M.I. Strikman, *Phys. Rep.* **76** (1981) 215.
8. L.L. Frankfurt and M.I. Strikman, *Phys. Rep.* **160** (1988) 235.
9. A.C.Benvenuti et al (BCDMS), Preprint CERN-PPE/94-65, 1994.

Appendix A

CEBAF

The Continuous Electron Beam Accelerator Facility

Capabilities of Current CEBAF Experimental Equipment at Higher Energies

Hall A Future Capabilities with 8 - 10 GeV beams

Current Instrumentation and likely additions

- Pair of 4 GeV /c High Resolution Spectrometers.
  Septum for small angle capability.

- Target Systems: High Powered Cryogenic targets (1000 W)
  Waterfall ^{16}O target (t=5 mm)
  Polarized ^{3}He target

- Focal Plane Polarimeter in the Hadron HRS.

- Third arm detectors: Multi-Purpose Spectrometer
  Harp detector
  Neutron detectors

Physics Upgrades

Inclusive Studies

- Elastic Form Factors: p, n, ^{2}H, ^{3}He, ^{4}He:

Could use beams up to 7 GeV extending the Q^2 range to 2.5 $(GeV/c)^2$ for G_E^n and 6 $(GeV/c)^2$ for G_E^p using either a polarized target or measuring the recoil polarization.

- Deep Inelastic Scattering (DIS)

The intermediate scaling region ($0.1 < x_b < 0.7$) would be accessible at 8 to 10 GeV. Precise data using the 4 GeV/c spectrometer would allow one to disentangle between nucleonic and non-nucleonic effects (see LOI 93-007) and also study the A dependence of the so-called "EMC" effect.

Exclusive Studies (e,e'N) and (e,e'2N) Studies

- Separation of response functions
- Spectral Function Distributions, high momentum components
- Polarization Responses
- Color Transparency, hadronization.
- Kaon Electroproduction in DIS: Enhanced with small angle capability

A pair of 4 GeV/c spectrometers allows one to use a 7.2 GeV beam and achieve a Q^2 value of up to 6 $(GeV/c)^2$ in quasielastic kinematics.

A. Saha, BEAMTR12.DOC (April, 1994)

CLAS PERFORMANCE at HIGH ENERGY

Introduction. The CEBAF Large Acceptance Spectrometer (CLAS) is based upon an open, six-coil toroidal magnet. Tracking chambers are situated in the wedge-shaped sectors between adjacent magnet coils, followed by Cerenkov counters for electron identification, time-of-flight (TOF) counters for triggering and particle identification, and shower counters for the identification of electrons, gammas and/or neutrons.

The goal of the detector design is to obtain good momentum resolution with large acceptance for detecting all particles in an event. The toroidal geometry provides maximum $\int B \cdot dl$ at forward angles, consistent with fixed target events in which high momentum particles go forward. Table 1 summarizes the operational parameters of the CLAS.

Effect of Higher Beam Energy. Higher beam energy events tend to contain higher momentum secondaries which must be detected. Because the CLAS is a non-focusing spectrometer, there is no definite maximum momentum for detecting particles; however, there are angular regions where the acceptance is reduced, there is a degradation of the momentum resolution of the device and there are maximum momentum limits to the particle identification procedures.

The maximum energy of the tagged photon beam is limited by saturation in the tagging magnet. The field-current relation is linear up to 4 GeV; with proper calibration the magnet can be used with a 6 GeV incident electron beam.

Electron Acceptance. Figure 1 shows the accepted region in the Q^2, ν plane. Figure 1a is for a 4 GeV beam, 1b if for an 10 GeV beam. The main effect is an extension of the Q^2, ν range. However, there is a loss of acceptance at the higher energy for low Q^2 and high ν, due to in-bending electrons being swept into the forward non-instrumented 'hole' of the toroid.

Momentum Resolution. Figure 2 shows that the momentum resolution of the CLAS rises with increasing particle momentum. The two terms, one constant due to multiple scattering and one rising linearly with momentum due to measurement accuracy, are shown separately. For 10 GeV particles the momentum resolution is 0.4% at forward angles.

Hadron Acceptance. The effect of an energy increase on the hadron acceptance of the CLAS is different for photon experiments than those using an electron beam. The photon beam is directed down the detector axis, and the higher its energy the larger the fraction of the center of mass solid angle which is not accepted. An electron beam, though, is the source of a virtual photon which is emitted at larger laboratory angles for higher electron beam energies, for a given value of Q^2 and ν. Therefore, hadrons emitted along the virtual photon direction have increased acceptance.

Table 1: CLAS Operating Parameters

Magnetic Field	Toroidal	Six Superconducting Coils
	$\int B \cdot dl$	2.7 Tesla-m at Θ=10°
		0.7 Tesla-m at Θ=90°
Drift Chambers	3 Regions	Axial, Stereo Superlayers
	Sense Wires	34,000
	Θ Range	10–140°
	Φ Acceptance	50% at Θ=10°
		85% at Θ=90°
	Momentum Range	p $\geq$ 300 MeV/c (Θ=10°)
		p $\geq$ 100 MeV/c (Θ=90°)
	Momentum Resolution (FWHM)	0.5% (Θ=20°, p = 4 GeV/c)
		1.0% (Θ=90°, p = 1 GeV/c)
Particle Identification	TOF and dE/dx	3σ limits
	π/K	up to 2.0 GeV/c
	π/p	up to 3.0 GeV/c
	K/p	up to 3.5 GeV/c
Maximum Luminosity	Electron Beam	10^{34}cm^{-2}sec^{-1}
	Photon Beam	Flux = 5×10^{7}/sec

Figure 3 is a contour plot of the laboratory angle of K^+'s versus their center-of-mass angles, θ^* and ϕ^*, for Q^2=1, W=1.8. Particles with lab angles of 10° or less are not accepted, indicated by the hatched region. This region of no acceptance shifts with electron beam energy, reflecting the change of direction of the virtual photon.

So far we have considered the acceptance of a single hadron in the final state, which is approximately 60%. Access to higher masses with increased beam energy requires the detection of multiple hadrons to reconstruct the final state. In this case the event acceptance is the product of individual particle acceptances, which is small for large multiplicities.

Particle Identification. The limits of particle identification depend only the momentum of the detected particles. Higher beam energies produce higher energy secondaries. However, the secondary energies increase rather slowly with increasing beam energy. Figure 4 displays the particle identification capability of the CLAS. As an example, pions and kaons are separated at the 3.3σ level up to a momentum of 2.15 GeV/c.

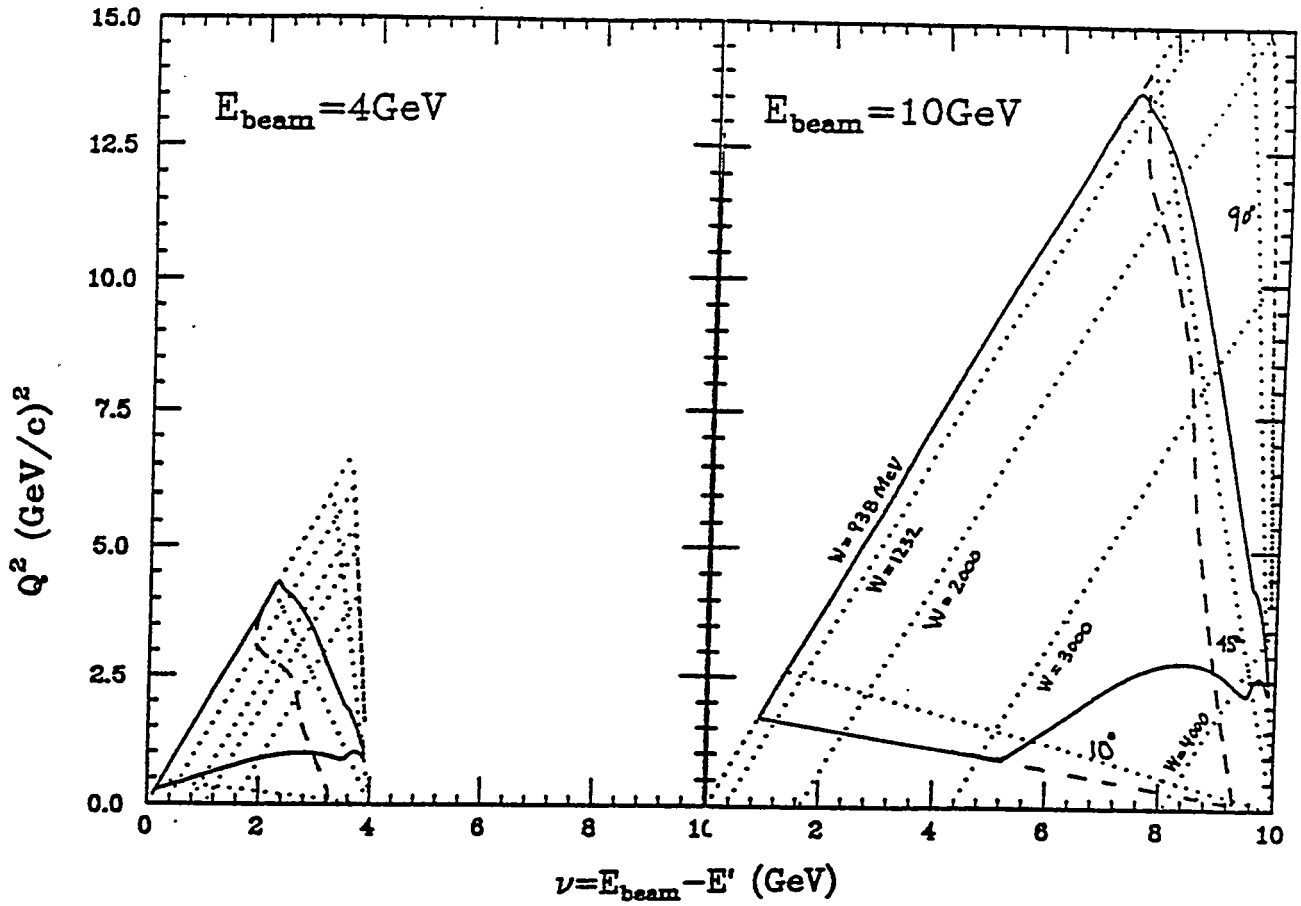


Figure 1: Electron Acceptance in the Q^2–ν plane. Dashed curve: negative particles outbending; solid curve: inbending.

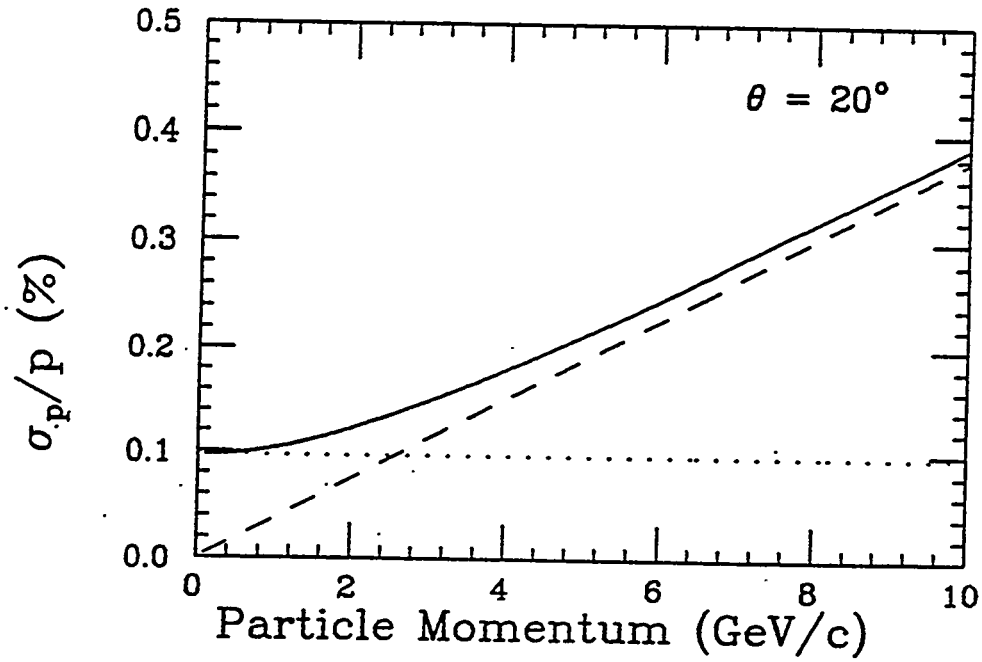


Figure 2: Momentum resolution showing the contributions from multiple scattering (dotted line) and measurement errors (dashed line).

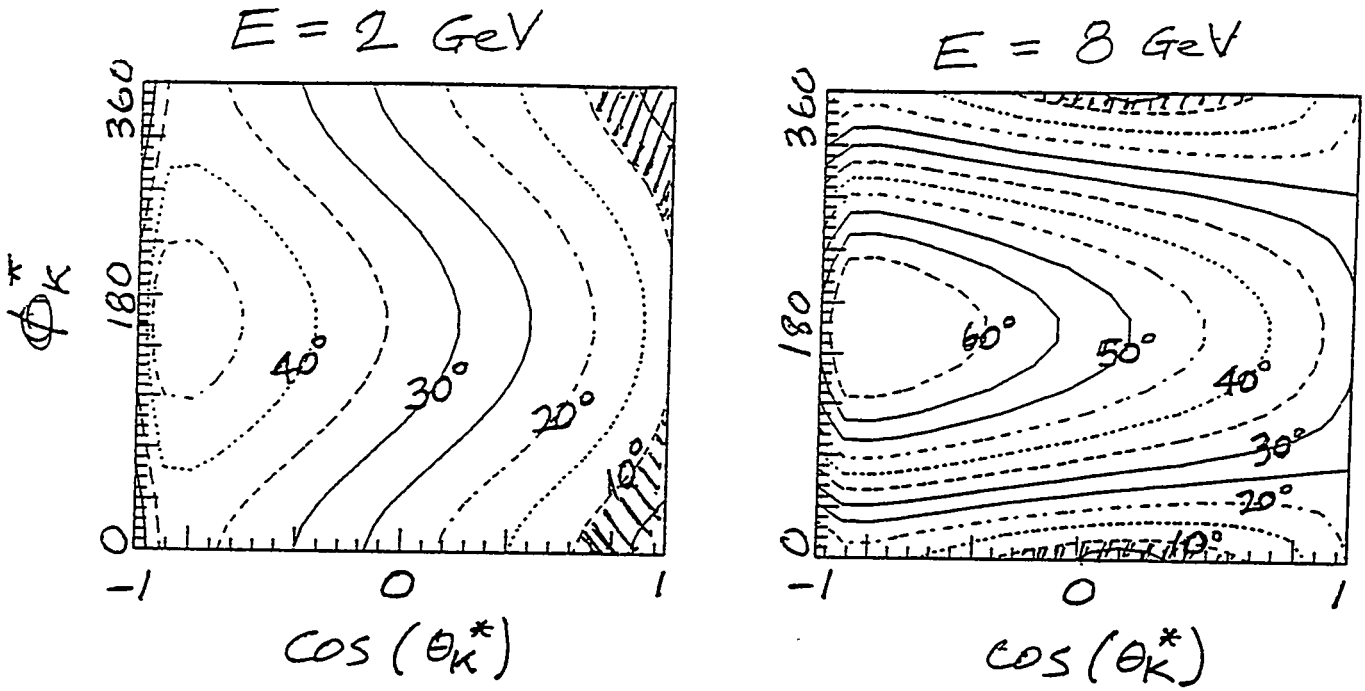


Figure 3: Contours of kaon laboratory angles plotted vs kaon angles in the hadronic center-of-mass for inclusive kaon production at Q^2=1, W=1.8. Kaons with lab angles of 10° or less are not accepted, indicated by the hatched region.

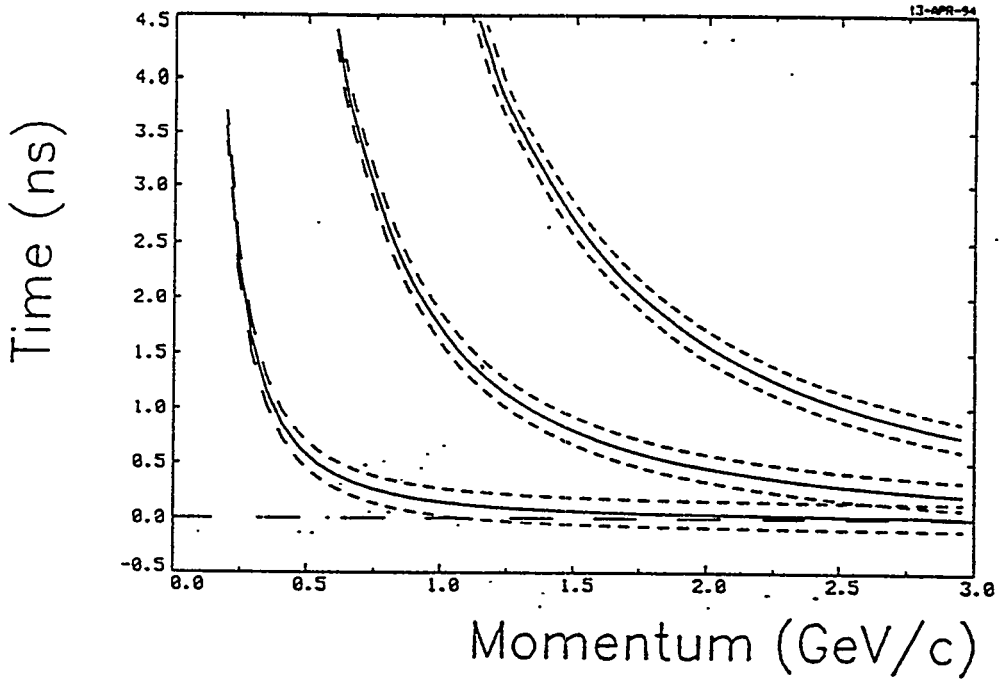


Figure 4: The flight time difference for protons, kaons and pions is shown as a function of momentum. The dotted lines are $\pm 1\sigma$ bands corresponding to a time resolution of 120 ps and a path length of 4.5 m.

Hall C Future Capabilities with ~8 to ~15 GeV Beams

Current & Likely Instrumentation and Capabilities

High Momentum Spectrometer $P^{max} = 7.4$ GeV, $\theta^{min} = 10°$

Second Arms

Short Orbit Spectrometer for $P^{max} = 1.8$ GeV, $\theta^{min} = 11.5°$

KSU neutron polarimeter & TOF array

UVA - Basel neutron TOF array

Enge 0° spectrometer

T_{20} spectrometer and deuteron polarimeter (proposed)

Stand Alone Spectrometers

G^0 spectrometer (proposed)

Current & Likely Beamline Hardware

Basel-UVa-CEBAF polarized target ($\vec{p}$,$\vec{D}$)

CEBAF cryo target (LH_2, LD_2, He) (200 watts---> ~400 watts)

Polarized target chicane magnets

Möller polarimeter ($P^{max} = 6$ GeV)

HNSS beam splitter

Hall C energy measurement system $P^{max} = 6$ GeV

Misc

1.5 MW of DC power and LCW for cooling are available at the pivot for use with do-it-yourself resistive magnetic spectrometers.

Strawman Upgrade Path

RHMS - "Really" High Momentum Spectrometer (10-15 GeV/c) (non-rotating small angle resistive spectrometer constructed using surplus magnets)

+

HMS - Higher Momentum Spectrometer - 7.4 GeV/c

Physics Examples: Survey of a few exclusive reactions assuming 10 GeV/c beam:

$d(\gamma p)n$	P_p (5°)	= 10.5 GeV/c	
$p(e,e'p)$	P_p (5°)	= 10.0 GeV/c,	P_e (5°) = 9.6 GeV/c
$d(e,e'd)$	P_d (5°)	= 9.8 GeV/c,	P_e (5°) = 10.6 GeV/c
$p(e,e'\pi^+)n$ @ $Q^2 = 5.0$,		$W = 2.5$	$P_\pi = 5.3$ GeV/c

Appendix B

Participants

Workshop on CEBAF at Higher Energies

Adams, G.	Rensselaer Polytechnic Institute
Ananyan, S.	William and Mary
Armstrong, C.	William and Mary
Asyran, G.	Yerevan Physics Institute
Arrington, J.	California Institute of Technology
Baker, O. K.	Hampton University & CEBAF
Barnes, T.	Oak Ridge Nat'l Lab & Univ of Tennessee
Beck, D.	University of Illinois
Beise, B.	University of Maryland
Bianchi, N.	Istituto Nazionale di Fisica Nucleare
Bimbot, L.	Rutgers University
Blok, H.	NIKHEF
Bowman, D.	Los Alamos National Laboratory
Breuer, H.	University of Maryland
Brodsky, S.	Stanford Linear Accelerator Center
Brooks, W.	CEBAF
Burkert, V.	CEBAF
Burtin, E.	CEBAF & University of South Carolina
Cardman, L.	CEBAF
Carlini, R.	CEBAF
Carlson, C.	William and Mary
Chang, C.C.	Univeristy of Maryland
Chant, N.	University of Maryland
Chen, J-P.	Massachusetts Institute of Technology
Chung, S-U.	Brookhaven National Laboratory
Coffman, D.	Cornell University
Cole, P.	George Washington University
Cords, D.	CEBAF
De Sanctis, E.	Istituto Nazionale di Fisica Nucleare
de Witt Huberts, P.	NIKHEF
Domingo, J.	CEBAF
Duncan, F.	University of Maryland
Eckhardt, R.	Ruhr University-Bonn
Ent, R.	CEBAF
Fang, G-Y.	Harvard University
Filippone, B.	California Institute of Technology
Frankfurt, L.	Tel Aviv University
Funsten, H.	William and Mary
Gai, Moshe	Yale University
Garibaldi, F.	Istituto Nazionale di Fisica Nucleare
Gilman, R.	Rutgers University

Participants (cont'd)

Giovanni, S.	Istituto Nazionale di Fisica Nucleare
Godfrey, S.	Carleton University
Gross, F.	William and Mary & CEBAF
Guidal, M.	CEN Saclay
Hansper, J.	Ruhr University-Bonn
Hovones, E.	Yerevan Physics Institute
Huber, G.	University of Regina
Hyde-Wright, C.	Old Dominion University
Iodice, M.	Istituto Nazionale di Fisica Nucleare
Isgur, N.	CEBAF
Jackson, H.	Argonne National Laboratory
Ji, C-R.	North Carolina State University
John, S.	CEBAF
Jones, C.	Argonne National Laboratory
Keppel, C.	Stanford Linear Accelerator Center
Kuhn, S.	Old Dominion University
Li, Z.	Christopher Newport University & CEBAF
Laget, J.	CEN Saclay
LeRose, J.	CEBAF
Lorenzon, W.	University of Pennsylvania
Mack, D.	CEBAF
Magahiz, R.	Carnegie-Mellon University
Margaziotis, D.	California State University-LA
Markowitz, P.	University of Maryland
McIntyre, J.	William and Mary
Mecking, B.	CEBAF
Melnitchouk, W.	University of Regenburg
Mestayer, M.	CEBAF
Meyer, C.	Carnegie-Mellon University
Michaels, R.	CEBAF
Miller, G.	University of Washington
Milner, R.	Massachusetts Institute of Technology
Miskimen, R.	University of Massachusetts
Mucifora, V.	Istituto Nazionale di Fisica Nucleare
Mueller, A.	Columbia University
Musolf, M.	Old Dominion University & CEBAF
Mukhopadhyay, N.	Rensselaer Polytechnic Institute
Mukhopadhyay, S.	California State University
Nanda, S.	CEBAF
Napolitano, J.	Rensselaer Polytechnic Institute

Participants (cont'd)

Nikolaev, N.	Landau Institute
Pang, A.	North Carolina State
Petratos, G.	Kent State University
Preedom, B.	University of South Carolina
Punjabi, V.	Norfolk State University
Potterveld, D.	Argonne National Laboratory
Radyushkin, A.	Old Dominion University & CEBAF
Roos, P.	University of Maryland
Rutt, P.	Rutgers University
Saha, A.	CEBAF
Saito, T.	Tohoku University
Sargsyan, M.	Tel Aviv University
Savkli, C.	University of Pittsburgh
Schoch, B.	University of Bonn
Schumacher, R.	Carnegie-Mellon University
Schafer, A.	University of Frankfurt
Silvano, S.	Istituto Nazionale di Fisica Nucleare
Sher, M.	William and Mary
Seth, K.	Northwestern University
Smith, E.	CEBAF
Souder, P.	Syracuse University
Stoler, P.	Rensselaer Polytechnic Institute
Strikman, M.	Pennsylvania State University
Swanson, E.	Massachusetts Institute of Technology
Taiuti, M.	Istituto Nazionale di Fisica Nucleare
Tung, T.-Y.	William and Mary
Voutier, E.	Institute des Sciences Nucleares
Walcher, T.	University of Mainz
Wang, K.	University of Massachusetts
Welsh, R.	William and Mary
Wise, J.	CEBAF
Wojtsekhowski, B.	Rensselaer Polytechnic Institute
Yang, J-C	Chungnam University